A MANUAL FOR THE

PREDICTION OF BLAST

AND

FRAGMENT LOADINGS

ON STRUCTURES

U. S. DEPARTMENT OF ENERGY

ALBUQUERQUE OPERATIONS OFFICE

AMARILLO AREA OFFICE

AMARILLO, TEXAS

November, 1980

Change 1 - 15 August 1981

	Report Documentation Page		*Form Approved* *OMB No. 0704-0188*

Public reporting burden for the collection of information is estimated to average 1 hour per response, including the time for reviewing instructions, searching existing data sources, gathering and maintaining the data needed, and completing and reviewing the collection of information. Send comments regarding this burden estimate or any other aspect of this collection of information, including suggestions for reducing this burden, to Washington Headquarters Services, Directorate for Information Operations and Reports, 1215 Jefferson Davis Highway, Suite 1204, Arlington VA 22202-4302. Respondents should be aware that notwithstanding any other provision of law, no person shall be subject to a penalty for failing to comply with a collection of information if it does not display a currently valid OMB control number.

1. REPORT DATE **15 AUG 1981**	2. REPORT TYPE	3. DATES COVERED **00-00-1981 to 00-00-1981**

4. TITLE AND SUBTITLE **A Manual for the Prediction of Blast and Fragment Loadings on Structures**	5a. CONTRACT NUMBER
	5b. GRANT NUMBER
	5c. PROGRAM ELEMENT NUMBER
6. AUTHOR(S)	5d. PROJECT NUMBER
	5e. TASK NUMBER
	5f. WORK UNIT NUMBER

7. PERFORMING ORGANIZATION NAME(S) AND ADDRESS(ES) **Department of Energy, Amarillo Energy Office,Amarillo ,TX,79101**	8. PERFORMING ORGANIZATION REPORT NUMBER
9. SPONSORING/MONITORING AGENCY NAME(S) AND ADDRESS(ES)	10. SPONSOR/MONITOR'S ACRONYM(S)
	11. SPONSOR/MONITOR'S REPORT NUMBER(S)

12. DISTRIBUTION/AVAILABILITY STATEMENT
Approved for public release; distribution unlimited

13. SUPPLEMENTARY NOTES

14. ABSTRACT

15. SUBJECT TERMS

16. SECURITY CLASSIFICATION OF:			17. LIMITATION OF ABSTRACT	18. NUMBER OF PAGES	19a. NAME OF RESPONSIBLE PERSON
a. REPORT **unclassified**	b. ABSTRACT **unclassified**	c. THIS PAGE **unclassified**	**Same as Report (SAR)**	**765**	

Standard Form 298 (Rev. 8-98)
Prescribed by ANSI Std Z39-18

DISCLAIMER

DISCLAIMER

Portions of this document may be illegible in electronic image products. Images are produced from the best available original document.

Page No.	# Change No. & Date	Page No.	# Change No. & Date
5-36 thru 5-39	1 - 15 Aug 81	6-57	1 - 15 Aug 81
5-40 thru 5-43	0 - 01 Nov 80	6-58 thru 6-91	0 - 01 Nov 80
5-44	1 - 15 Aug 81	6-92 thru 6-94	1 - 15 Aug 81
5-45 thru 5-47	0 - 01 Nov 80	6-95 thru 6-97	0 - 01 Nov 80
5-48	1 - 15 Aug 81	6-98	1 - 15 Aug 81
5-49	0 - 01 Nov 80	6-99 thru 6-110	0 - 01 Nov 80
5-50	0 - 01 Nov 80	6-111	1 - 15 Aug 81
5-51	1 - 15 Aug 81	6-112 thru 6-116	0 - 01 Nov 80
5-52	1 - 15 Aug 81	6-117	1 - 15 Aug 81
5-53 thru 5-59	0 - 01 Nov 80	6-118 thru 6-121	0 - 01 Nov 80
5-60	1 - 15 Aug 81	6-122	1 - 15 Aug 81
5-61 thru 5-72	0 - 01 Nov 80	6-123	0 - 01 Nov 80
5-73	1 - 15 Aug 81	6-124	1 - 15 Aug 81
5-74	0 - 01 Nov 80	6-125 thru 6-134	0 - 01 Nov 80
5-75	0 - 01 Nov 80	6-135	1 - 15 Aug 81
5-76	1 - 15 Aug 81	6-136 thru 6-139	0 - 01 Nov 80
5-77	0 - 01 Nov 80	6-140 thru 6-142	1 - 15 Aug 81
5-78	1 - 15 Aug 81	6-143	0 - 01 Nov 80
5-79	0 - 01 Nov 80	6-144	1 - 15 Aug 81
5-80 thru 5-82	1 - 15 Aug 81	6-145	0 - 01 Nov 80
5-83 thru 6-4	0 - 01 Nov 80	6-146	1 - 15 Aug 81
6-5	1 - 15 Aug 81	6-147	0 - 01 Nov 80
6-6 thru 6-8	0 - 01 Nov 80	6-148	1 - 15 Aug 81
6-9	1 - 15 Aug 81	6-149 thru 6-151	0 - 01 Nov 80
6-10 thru 6-13	0 - 01 Nov 80	6-152	1 - 15 Aug 81
6-14	1 - 15 Aug 81	6-153 thru 6-162	0 - 01 Nov 80
6-15	0 - 01 Nov 80	6-163 thru 6-165	1 - 15 Aug 81
6-16	1 - 15 Aug 81	6-166 thru 6-188	0 - 01 Nov 80
6-17	0 - 01 Nov 80	6-189 Blank	0 - 01 Nov 80
6-18	0 - 01 Nov 80	7-1 thru 7-3	0 - 01 Nov 80
6-19	1 - 15 Aug 81	7-4	1 - 15 Aug 81
6-20	0 - 01 Nov 80	7-5 thru 7-8	0 - 01 Nov 80
6-21	1 - 15 Aug 81	7-9	1 - 15 Aug 81
6-22 thru 6-24	0 - 01 Nov 80	7-10	0 - 01 Nov 80
6-25 thru 6-27	1 - 15 Aug 81	7-11	1 - 15 Aug 81
6-28 thru 6-36	0 - 01 Nov 80	7-12 thru 7-36	0 - 01 Nov 80
6-37 thru 6-40	1 - 15 Aug 81	7-37	1 - 15 Aug 81
6-41 thru 6-44	0 - 01 Nov 80	7-38 thru 8-5	0 - 01 Nov 80
6-45	1 - 15 Aug 81	8-6	1 - 15 Aug 81
6-46	1 - 15 Aug 81	8-7 thru 8-11	0 - 01 Nov 80
6-47 thru 6-54	0 - 01 Nov 80	8-12	1 - 15 Aug 81
6-55	1 - 15 Aug 81	8-13 thru 8-41	0 - 01 Nov 80
6-56	0 - 01 Nov 80	8-42	1 - 15 Aug 81

LIST OF EFFECTIVE PAGES

Total number of pages in this manual is 768, consisting of the following:

Page No.	# Change No. & Date	Page No.	# Change No. & Date
Title	1 – 15 Aug 81	4-90	1 – 15 Aug 81
A	1 – 15 Aug 81	4-91 thru 4-107	0 – 01 Nov 80
Foreword	0 – 01 Nov 80	4-108	1 – 15 Aug 81
Blank	0 – 01 Nov 80	4-109 thru 4-132	0 – 01 Nov 80
Preparation	0 – 01 Nov 80	4-133	1 – 15 Aug 81
Blank	0 – 01 Nov 80	4-134 thru 4-145	0 – 01 Nov 80
Acknowledgements	0 – 01 Nov 80	4-146	1 – 15 Aug 81
Blank	0 – 01 Nov 80	4-147 thru 4-173	0 – 01 Nov 80
i thru xxiii	0 – 01 Nov 80	4-174	1 – 15 Aug 81
Blank	0 – 01 Nov 80	4-175	1 – 15 Aug 81
1-1 thru 1-7	0 – 01 Nov 80	4-176	1 – 15 Aug 81
Blank	0 – 01 Nov 80	4-177 thru 4-179	0 – 01 Nov 80
2-1 thru 2-11	0 – 01 Nov 80	4-180	1 – 15 Aug 81
2-12	1 – 15 Aug 81	4-181	0 – 01 Nov 80
2-13	0 – 01 Nov 80	4-182	0 – 01 Nov 80
2-14	0 – 01 Nov 80	4-183	1 – 15 Aug 81
2-15	1 – 15 Aug 81	4-184	1 – 15 Aug 81
2-16	1 – 15 Aug 81	4-185	1 – 15 Aug 81
2-17 thru 2-23	0 – 01 Nov 80	4-186 thru 5-1	0 – 01 Nov 80
Blank	0 – 01 Nov 80	5-2	1 – 15 Aug 81
3-1 thru 3-19	0 – 01 Nov 80	5-3 thru 5-5	0 – 01 Nov 80
Blank	0 – 01 Nov 80	5-6	1 – 15 Aug 81
4-1 thru 4-19/20	0 – 01 Nov 80	5-7	0 – 01 Nov 80
4-21/22	0 – 01 Nov 80	5-8	0 – 01 Nov 80
4-23/24	0 – 01 Nov 80	5-9	1 – 15 Aug 81
4-25 thru 4-28	0 – 01 Nov 80	5-10	0 – 01 Nov 80
4-29	1 – 15 Aug 81	5-11	1 – 15 Aug 81
4-30	1 – 15 Aug 81	5-12	0 – 01 Nov 80
4-31 thru 4-42	0 – 01 Nov 80	5-13	1 – 15 Aug 81
4-43	1 – 15 Aug 81	5-14	0 – 01 Nov 80
4-44	0 – 01 Nov 80	5-15	1 – 15 Aug 81
4-45	1 – 15 Aug 81	5-16 thru 5-19	0 – 01 Nov 80
4-46	1 – 15 Aug 81	5-20 thru 5-25	1 – 15 Aug 81
4-47 thru 4-54	0 – 01 Nov 80	5-26 thru 5-28	0 – 01 Nov 80
4-55	1 – 15 Aug 81	5-29	1 – 15 Aug 81
4-56 thru 4-89	0 – 01 Nov 80	5-30 thru 5-35	0 – 01 Nov 80

Zero in the No. column indicates an original page.

LIST OF EFFECTIVE PAGES (Cont'd)

Page No.	# Change No. & Date
8-43.....................1 - 15 Aug 81
8-44 thru 8-60...........0 - 01 Nov 80
8-61 Blank...............0 - 01 Nov 80
A-1 thru A-24............0 - 01 Nov 80
A-25 Blank...............0 - 01 Nov 80
B-1 thru B-50............0 - 01 Nov 80
B-51 Blank...............0 - 01 Nov 80
C-1 thru C-6.............0 - 01 Nov 80
DD 1473 (Front)..........0 - 01 Nov 80
DD 1473 (Back)...........0 - 01 Nov 80

FOREWORD

The purpose of this manual is to provide Architect-Engineer (AE) firms guidance for the prediction of air blast, ground shock and fragment loadings on structures as a result of accidental explosions in or near these structures. Information in this manual is the result of an extensive literature survey and data gathering effort, supplemented by some original analytical studies on various aspects of blast phenomena. Many prediction equations and graphs appear in the manual, accompanied by numerous example problems illustrating their use.

The manual is complementary to existing structural design manuals and is intended to reflect the current state-of-the-art in prediction of blast and fragment loads for accidental explosions of high explosives at the Pantex Plant. In some instances, particularly for explosions within blast-resistant structures of complex geometry, rational estimation of these loads is beyond the current state-of-the-art, and tests or analyses to supplement existing data or analysis methods are recommended.

Although the manual is specific for the Pantex Plant, most prediction methods are general enough to apply to other safety structures used in high explosives operations.

This manual was prepared for the Department of Energy, Amarillo Area Office, Amarillo, Texas by Southwest Research Institute, San Antonio, Texas, under contract with the U. S. Army Engineer Division, Huntsville (USAEDH), Huntsville, Alabama.

Comments for corrections and improvements are invited from individuals or organizations in industry and the U. S. Government. Contact:

Department of Energy
Albuquerque Operations
Amarillo Area Office
Facilities and Maintenance Branch
P. O. Box 30030
Amarillo, Texas 79120

Phone: 806/335-1581, Ext. 2161

FTS No.: 572-2161

STATEMENT ON MANUAL PREPARATION

This manual was sponsored by the U. S. Department of Energy (DOE), Amarillo Area Office, to satisfy the need to provide a design tool for architect-engineer firms engaged in work for the Pantex Plant. The manual provides state-of-the-art information and example problems for blast and fragment load predictive techniques for structures at the plant.

At the request of the DOE Amarillo Area Office, the U. S. Army Engineer Division, Huntsville (USAEDH) undertook the development of the manual by providing contracting services as well as technical guidance.

Southwest Research Institute (SwRI), San Antonio, Texas, was contracted to prepare the manual. SwRI was selected for its renowned expertise in the field of blast engineering.

Mason & Hanger-Silas Mason Co., Inc. the Operating Contractor for the U. S. Department of Energy, Pantex Plant, provided input for development of manual scope, chapter formulation, and content. Technical review throughout all phases of preparation was conducted by the personnel from this agency.

ACKNOWLEDGEMENTS

CONTENTS

CONTENTS (continued)

CONTENTS (continued)

CONTENTS (continued)

CONTENTS (continued)

CONTENTS (continued)

CONTENTS (continued)

CONTENTS (continued)

ILLUSTRATIONS

ILLUSTRATIONS (continued)

ILLUSTRATIONS (continued)

ILLUSTRATIONS (continued)

ILLUSTRATIONS (continued)

ILLUSTRATIONS (continued)

ILLUSTRATIONS (continued)

ILLUSTRATIONS (continued)

ILLUSTRATIONS (continued)

TABLES

EXAMPLE PROBLEMS

CHAPTER 1

INTRODUCTION

1.1 PURPOSE AND OBJECTIVE

The purpose of this manual is to provide Architect-Engineer (AE) firms guidance for the prediction of air blast, ground shock and fragment loadings of structures as a result of accidental explosions in or near these structures.

The primary objective is to develop a manual which is complementary to existing structural design manuals and can be used (in combination with other manuals) by AE firms to design new buildings which are resistant to blast and fragmentation effects of an accidental explosion. Another objective is to aid in the assessment of the explosion-resistant capabilities of existing buildings at the Pantex Plant.

The manual is specific for new or existing facilities at the Pantex Plant. However, most data and prediction methods are presented in general terms and can be applied to other high explosive facilities if proper modifying factors are used.

1.2 SCOPE

1.2.1 Topics Covered in This Manual

These topics are:

- General considerations affecting blast, ground shock, and fragment hazards in high-explosive facilities

- Explosives and damage mechanisms

- Air blast from accidental explosions resulting in both internal and external blast loading of structures

- Air blast spalling of concrete walls

- Air blast hazards to personnel

- Cratering and ground shock, including effects on buildings, equipment, and personnel

- Fragmentation, including methods for predicting fragment characteristics, trajectories, dispersion and impact effects

- Hazards to personnel from fragments

- Explosive initiation by fragments, overpressures, heat, friction, crushing, pinching, etc.

- Dynamic properties of materials of construction

- Overview of dynamic structural analysis and design methods

Included in appendices are tables of properties of explosives, an extensive bibliography, and an SI metric conversion table.

Methods and procedures included in the manual are intended to be applied by an engineer with a working knowledge of structural dynamics, with the aid of, at most, a desk calculator. Example problems are included for all prediction graphs. Confidence levels for prediction methods are cited throughout and needs for design verification by proof tests or experimental research are identified where appropriate.

General theory or fundamental principles are given for each topic if needed, and advanced concepts and theories identified, but not rigorously treated in the manual.

1.2.2 Related Topics Covered in Other Manuals

The complementary nature of this manual requires its use in conjunction with other references (1.1-1.20), rather than as a single comprehensive manual, if one wishes to cover all aspects of loading from accidental explosions, response to and damage from such explosions, and design for resistance to or survival under accidental explosions. Related items which are not covered in depth in this manual, but are well treated in other general references, are the following:

- Basic physics of air blast

- Detailed analysis methods for elastic-plastic dynamics of structures

- Fundamental studies of cratering and ground shock

- Exterior* and terminal ballistics of fragments and accident missiles over wide ranges of missile and target properties

- Fundamentals of dynamic properties of materials

- Detonation physics

Two good general references on basic physics of air blast are Baker (Ref. 1.1) and Swisdak (Ref. 1.2). Both of these references also include

---

*Exterior ballistics is the science of flight of high-speed objects through the air.

extensive tables and graphs for prediction of blast wave properties for high explosives.

There are a number of good references which present detailed analysis methods for elastic and plastic dynamics of structures. We recommend Biggs (Ref. 1.3), Norris, et al. (Ref. 1.4), "Suppressive Shields" (Ref. 1.5), Crawford, et al. (Ref. 1.6), TM5-1300 (Ref. 1.7), or Cox, et al. (Ref. 1.8). All references present approximate methods for dynamic structural response which are well validated. Refs. 1.3 through 1.7 use essentially the same approximation methods, while Ref. 1.8 employs a somewhat different approach.

Cratering and ground shock from buried or ground contact explosions are covered in a number of references. Of these, good general references, available only for ground shock processes, are Richart, et al. (Ref. 1.9) and Barkan (Ref. 1.10). The reader is referred to Chapter 5 for cratering references, which are scattered throughout the literature.

Studies of flight and impact of fragments and missiles from accidental explosions and planned detonations are relatively few, particularly when the majority of the fragments are secondary ones such as pieces of equipment or structure which were at some distance from the explosive source. Similarly, there are few comprehensive references for impact effects of relatively massive secondary fragments or missiles. Refs. 1.11 and 1.12 have the most complete studies, but they refer to fragments from liquid propellant explosions and gas vessel bursts. The most complete study for secondary debris hazards from accidental HE explosions is contained in Chapter 6 of this manual.

There are many references giving dynamic properties of structural metals. Ref. 1.13 is a good general reference on this topic. On the other hand, there are few such references for dynamic properties of concrete, earth or gravel, and frangible materials which form a large part of structures at the Pantex Plant. Chapter 7 contains a distillation of data which are available for these materials.

The physics of detonation of high explosives has been studied for many years, both in the U. S. and abroad. There are several good reference texts on this subject, with perhaps the best and most readable being Johansson and Persson (Ref. 1.14). Other good references on this topic are an Army manual on principles of explosive behavior (Ref. 1.15), and a set of symposium proceedings on behavior and utilization of explosives in engineering design (Ref. 1.16). A good working knowledge of this topic is very useful in prediction of such topics as fragment velocities and masses, and explosive initiation by fragment impact.

There are also several general references which contain background material useful in more than one area related to this manual. TM5-1300 (Ref. 1.7) and "Suppressive Shields" (Ref. 1.5) certainly are in this category, but one can also glean much useful information from a summary report on research

during World War II in many aspects of ballistics (Ref. 1.17), and a translation of German ballistic research studies from the same era (Ref. 1.18). The minutes of explosives safety seminars for the Department of Defense Explosives Safety Board (DDESB) are also quite useful, and will be cited many times in the reference lists. The final general reference containing good background material appears in an unlikely source, the Annals of the New York Academy of Sciences, as the proceedings of a 1968 seminar on explosive safety topics (Ref. 1.19).

1.2.3 Organization

This manual is organized into eight chapters and supporting appendices. This first chapter serves as a brief introduction, and contains no technical details, but all following chapters are technically oriented.

Chapter 2 covers general considerations in explosive safety and design at the Pantex Plant. It covers the scope of explosive safety in a general way, describes general procedures for designing or evaluating buildings subjected to high explosive hazards, gives typical building configurations, and discusses impact of safety regulations and procedures on explosion-resistant design. The applicability and limits of applicability of the manual are noted.

Chapter 3 gives qualitative discussions of the predominant aspects of explosive hazards and damage mechanisms associated with accidental explosions. The effects are also limited to those which could conceivably occur from accidental explosion of HE or chemicals used in processing of HE at Pantex. This chapter serves as a preview of Chapters 4, 5, and 6.

Chapter 4 gives relatively detailed coverage of air blast from those classes of accidental explosions which could conceivably occur in the Pantex Plant. Topics covered include blast waves from single and multiple sources, effects of containment and venting, methods of predicting blast loads on structures for both internal and external explosions, air blast spalling of concrete walls, and air blast hazards to personnel.

Cratering and ground shock are covered in Chapter 5. Basic phenomena are discussed, and methods are given for prediction of explosive cratering, ground shock waves, and effects of ground motion on buildings, equipment, and personnel.

Chapter 6 covers fragmentation and its effects for explosions which could occur at Pantex. General phenomena are discussed, followed by methods for predicting fragment characteristics, flight, and impact effects. A special topic included in this chapter is the prediction of explosive initiation by fragment impacts.

Chapters 4, 5 and 6 are the longest and most detailed chapters in the manual, but they are supported by two relatively short chapters giving

detailed information. Chapter 7 gives data on dynamic properties of materials of construction which are or could be used in explosives facilities at the Pantex Plant while Chapter 8 gives an overview of design methods for structures typical at Pantex.

In each chapter giving prediction methods, there is a section with one or more example problems for each method. Each chapter also contains a list of symbols and a list of all references cited in the chapter.

Ancillary material included in the manual are appendices giving a set of unit conversion tables to and from SI metric units, explosive properties, and an extensive bibliography.

1.3 REFERENCES

1.1 Baker, W. E., Explosions in Air, University of Texas Press, Austin, Texas, 1973.

1.2 Swisdak, M. M., Jr., "Explosion Effects and Properties: Part I - Explosion Effects in Air," NSWC/WOL/TR 75-116, Naval Surface Weapons Center, White Oak, Silver Spring, Maryland, October 1975.

1.3 Biggs, J. M., Introduction to Structural Dynamics, McGraw-Hill Book Company, New York, New York, 1964.

1.4 Norris, C. H., Hansen, R. J., Holley, M. J., Biggs, J. M., Namyet, S. and Minami, J. V., Structural Design for Dynamic Loads, McGraw-Hill Book Company, New York, New York, 1959.

1.5 "Suppressive Shields Structural Design and Analysis Handbook," U. S. Army Corps of Engineers, Huntsville Division, HNDM-1110-1-2, 1977.

1.6 Crawford, Robert E., Higgins, Cornelius, J., Bultmann, H., "The Air Force Manual for Design and Analysis of Hardened Structures," Report No. AFWL-TR-74-102, Contract No. F29601-74-C-0018, Civil Nuclear Systems Corporation, Albuquerque, New Mexico, October 1974, Second Printing October 1976.

1.7 Structures to Resist the Effects of Accidental Explosions, Department of the Army Technical Manual TM 5-1300, Department of the Navy Publication NAVFAC P-397, Department of the Air Force Manual AFM 88-22, Department of the Army, the Navy, and the Air Force, June 1969.

1.8 Cox, P. A., Westine, P. S., Kulesz, J. J., and Esparza, E. D., "Analysis and Evaluation of Suppressive Shields," Edgewood Arsenal Contractor Report, ARCFL-CR-77028, Report No. 10, Contract No. DAAA15-75-C-0083, Edgewood Arsenal, Aberdeen Proving Ground, Maryland, January 1978.

1.9 Richart, F. E., Jr., Hall, J. R., Jr., and Woods, R. D., Vibrations of Soils and Foundations, Prentice-Hall, Inc., Englewood Cliffs, New Jersey, 1970.

1.10 Barkan, D. D., Dynamics of Bases and Foundations, McGraw-Hill Book Company, New York, New York, 1962.

1.11 Baker, W. E., Kulesz, J. J., Ricker, R. E., Bessey, R. L., Westine, P. S., Parr, V. B., and Oldham, G. A., "Workbook for Predicting Pressure Wave and Fragment Effects of Exploding Propellant Tanks and Gas Storage Vessels," NASA CR-134906, NASA Lewis Research Center, November 1975.

1.12 Baker, W. E., Kulesz, J. J., Ricker, R. E., Westine, P. S., Parr, V. B., Vargas, L. M., and Moseley, P. K., "Workbook for Estimating the Effects of Accidental Explosions in Propellant Handling Systems," NASA Contractor Report 3023, Contract NAS 3-20497, NASA Lewis Research Center, August, 1978.

1.13 Huffington, Norris J., Jr., (Ed.), Behavior of Materials Under Dynamic Loading, The American Society of Mechanical Engineers, New York, New York, 1965.

1.14 Johansson, C. H. and Persson, P. A., Detonics of High Explosives, Academic Press, London and New York, 1970.

1.15 U. S. Army Material Command, Engineering Design Handbook: Principles of Explosive Behavior, AMC Pamphlet AMCP 706-180, 1972.

1.16 "Behavior and Utilization of Explosives in Engineering Design and Biochemical Principles Applied to Chemical Medicine," Proceedings of the 12th Annual Symposium American Society of Mechanical Engineers, New Mexico Section, March 1972.

1.17 Office of Scientific Research and Development, "Effects of Impact and Explosion," Summary Technical Report, National Defense Research Committee, Washington, D.C., 1946. AD 221 586

1.18 Doering, W. and Burkhardt, G., "Contributions to the Theory of Detonation," Translation from the German as Technical Report No. F-TX-1227-IA (GDAM A9-T-4G), Headquarters, Air Material Command, Wright-Patterson AFB, Ohio, May 1949. AD 77863

1.19 "Prevention of and Protection Against Accidental Explosions of Munitions, Fuels, and Other Hazardous Mixtures," Annals of the New York Academy of Sciences, Vol. 152, Art. 1, October 1968.

1.20 "Fundamentals of Protection Design (Non-Nuclear)," Department of the Army Technical Manual, TM 5-855-1, Department of the Army, July 1965.

CHAPTER 2

GENERAL CONSIDERATIONS

2.1 INTRODUCTION

In designing buildings subject to high explosive hazards, an AE firm would normally divide this complex problem into a series of general steps or disciplines, as follows:

A. Develop Conceptual Building Designs

    1. Consider operations in buildings

    2. Determine types and quantities of explosives in each cell or unit.

B. Define the Explosion Environment

    1. Determine explosion source characteristics

    2. Determine air blast loads from single or multiple explosion sources

    3. Determine possible ground shock and/or cratering effects

    4. Determine characteristics of fragments from casings for explosive materials and nearby objects and structures.

C. Predict Building, Equipment, and Personnel Response

    1. Determine response to air blast loading

    2. Determine response to ground shock

    3. Determine response to fragment impact.

D. Perform Iterative Design to Provide Explosion Resistance

We will present in this manual data and design information which will aid an AE firm in all of these steps, with the exception of Step D, which should be readily available in other manuals. To assist in the planning of Step D, a flow chart is presented in Chapter 8 which provides a procedure for the analysis and design of structures (existing and new).

In many instances, quantities of explosives which can be present in various facilities at Pantex, the types of explosives or other hazardous materials which can be stored or worked on together, distances between

buildings and areas, and many other factors which impinge directly on blast-resistant building design are fixed or limited by existing safety, security and other regulatory requirements. At Pantex, some of the pertinent regulations or manuals in effect are:

1. ERDA Facilities General Design Handbook (Ref. 2.1)

2. Seismic Hazard and Building Structure Behavior at the Pantex Facility (Ref. 2.2)

3. Development of Design Basis Tornadoes and Design Manual for the Pantex Plant Site (Ref. 2.3)

4. AMCR 385-100, Safety Manual (Ref. 2.4)

5. TM 5-1300, Structures to Resist the Effects of Accidental Explosions (Ref. 2.5)

6. DOD Ammunition and Explosives Safety Standards (Ref. 2.6)

7. Pantex Plant Design Criteria Manual (Ref. 2.7)

Reference 2.1 in particular includes a number of other regulations and guides by reference, including References 2.4 and 2.5. This design criteria handbook also defines three high-explosive hazard classes, with decreasing potential for explosive accident as the class number increases. An AE firm involved in design of protective construction at Pantex should review this handbook, and the other references cited here, to insure compliance. Some of the implications of the regulations are discussed in this chapter.

The existing facilities at the Pantex Plant include many types, constructed or modified from 1944 to the present. There are a number of above-ground buildings, both with and without barricades; mounded, earth-covered buildings; shallow-buried buildings; storage igloos; and containment structures. These buildings have various designs for venting explosion pressures and varying degrees of blast resistance. Planned new designs cover the same spectrum of building types, barricading or lack of barricading, and venting or containment as do existing buildings. Examples are given later in this chapter.

References 2.1 through 2.9 are documents which establish criteria for design of structures to be resistant to explosions and natural phenomena. This manual is not a criteria document, nor is it a manual for structural design. Rather, it is a design aid for predicting blast and fragment loading from accidental explosions, and it is intended for use as a complement to other structures design manuals.

2.2 GENERAL PROCEDURE FOR DESIGN OR EVALUATION OF BUILDINGS SUBJECTED TO HIGH EXPLOSIVE HAZARDS

2.2.1 Determination of Explosion Source Characteristics

Potential accidental explosion sources at the Pantex Plant consist primarily of high explosives (HE), in one of several forms, and in various states and configurations. Because some explosives synthesis is done at Pantex, potentially explosive liquid chemicals are also present in some facilities. The state of the solid explosives can be pressed HE, bulk (loose) HE, or cast HE. Although most explosives are HMX-based, RDX-based, or TATB pressed explosives, older types of castable explosives such as TNT or Composition B are also present in some facilities. The older types are usually present in larger quantities of 100 to 500 pounds as single items. Chapter 4 and Appendix A give much more detail on types and properties of explosion sources. Air blast source characteristics for all types of explosives can be determined using these data.

2.2.2 Determination of Air Blast Loading

Once the type, quantity and configuration of the explosion sources are defined, the next step in the definition of the explosion environment is the definition of the air blast loading. The general phenomena and qualitative discussions of explosions are covered in Chapter 3, while much more detailed phenomenology of air blast is covered in Chapter 4. In particular, one first determines free-field blast wave characteristics for the specified explosion source or sources, and then determines actual internal and external blast loading on structures or parts of structures. Details of these procedures, with example problems, appear in Chapter 4.

2.2.3 Determination of Ground Shock and Cratering

In some accident scenarios at Pantex, coupling of the explosion to the ground may be efficient enough to develop significant ground shock or to cause craters to be formed. These include:

1. Explosion in an earth-covered storage igloo

2. Explosion in a strong, buried containment cell*

3. Surface explosion with explosive source in contact with floor or ground.

These three situations represent different degrees of coupling of the explosion to the ground. Each is discussed in detail in Chapter 5, and methods for prediction of ground shock and cratering effects are given in that chapter, together with a number of example problems.

---

*See Chapter 5, Section 5.1, for discussion of buried structures and containment.

2.2.4 Determination of Fragment Characteristics

Many accidental explosions cause extensive fragmentation, and the resulting high-speed fragments in turn cause much of the damage from the explosion. Those fragments which are generated by the casings or containers which surround explosive sources are termed primary fragments. Secondary fragments are formed by pieces of equipment near explosive sources and pieces of the structures in which the explosion occurred. The definition of the characteristics and impact effects of both primary and secondary fragments one could expect in explosions in Pantex facilities is a major topic in this manual. Chapter 6 covers this topic, and gives many graphs and formulas for prediction of fragmentation. Example problems are given in that chapter.

2.2.5 Determination of Building, Equipment, and Personnel Response to Blast Loading

Once the explosion environment is defined for a design basis explosion at Pantex, the first step in the prediction of building and equipment response is to determine response to air blast loading. This response can be toppling or translation, elastic structural response, or elastic-plastic response up to rupture or complete failure. We reiterate that this manual does not contain detailed procedures for such response prediction. But, Chapter 8 does give an overview of dynamic structural design and reviews various manuals and references which can be used for such design.

2.2.6 Determination of Building, Equipment, and Personnel Response to Ground Shock

Ground shock motions can be similar to seismic disturbances for surface structures, shallow-buried structures, building equipment, and personnel. Intense ground shocks can also displace and damage buried piping. These effects are treated at some length in this manual, because they are not readily available elsewhere. The detailed treatment, and a number of example problems, appear in Chapter 5.

2.2.7 Determination of Building, Equipment, and Personnel Response to Fragment Impact

Primary fragments from HE explosions are generally numerous, metallic, small (less than a pound in weight), and high velocity (up to 9,000 feet per second). They are efficient penetrators of most building materials, and efficient for killing or seriously wounding humans. Secondary fragments are usually relatively few, can be quite massive (up to tons in weight), are usually slower than primary fragments (hundreds of feet per second), and can consist of a variety of materials, including chunks of relatively weak materials such as wood or concrete. They are usually poor penetrators, but can cause damage to structures and humans by simple momentum transfer during impact. Much more is known about response to primary fragment impact than is known for secondary fragment impact.

Chapter 6 covers our current state of knowledge for predicting impact effects of both types of fragments. Terms commonly used in this field, such as penetration, perforation and spalling, are defined and procedures are given for determining impact effects on structures, people, and HE. A number of example problems on fragment impact effects appear in Chapter 6.

2.2.8 Iterative Design of Explosion-Resistant Buildings

An AE firm, in designing explosion-resistant buildings for the Pantex facility, will usually find that for most parts of the building, the limiting response to one or more of the explosion environment conditions will far outweigh other design considerations, such as response to seismic disturbances, and tornadic winds (Refs. 2.2, 2.3, 2.8, and 2.9) but the first design will often prove to be seriously overdesigned or underdesigned. The AE must then redesign, and check to determine whether the new design, which may now be optimized for air blast resistance, is adequate for ground shock, fragment impact resistance, and other design loadings. The detailed procedures for such iterative design are not given in this manual, but Chapter 8 gives a flow chart to indicate the steps an AE firm may have to follow during the iterative design process.

2.3 IMPACT OF SAFETY, SECURITY AND OTHER REGULATORY REQUIREMENTS ON BLAST-RESISTANT DESIGN

2.3.1 Typical Building Configurations

There are many types of buildings existing or planned for the Pantex Plant. Figure 2.1 gives an aerial view of the entire plant, and Figures 2.2 and 2.3 show the complexes of buildings in Zone 11 and Zone 12, respectively. One can see in these photos a number of above-ground buildings, both barricaded and unbarricaded; and also several types of earth-covered buildings.

2.3.1.1 Above-Ground Buildings

These are of four types:

- Unbarricaded

- Barricaded

- Controlled venting

- Vented

Most of the above-ground buildings in Zones 11 and 12 are multiple-bay buildings. The majority of buildings in both zones are wood or steel framed with clay tile, masonry block or brick walls and reinforced concrete, blast-resistant walls. Some of the blast-resistant buildings are vented.
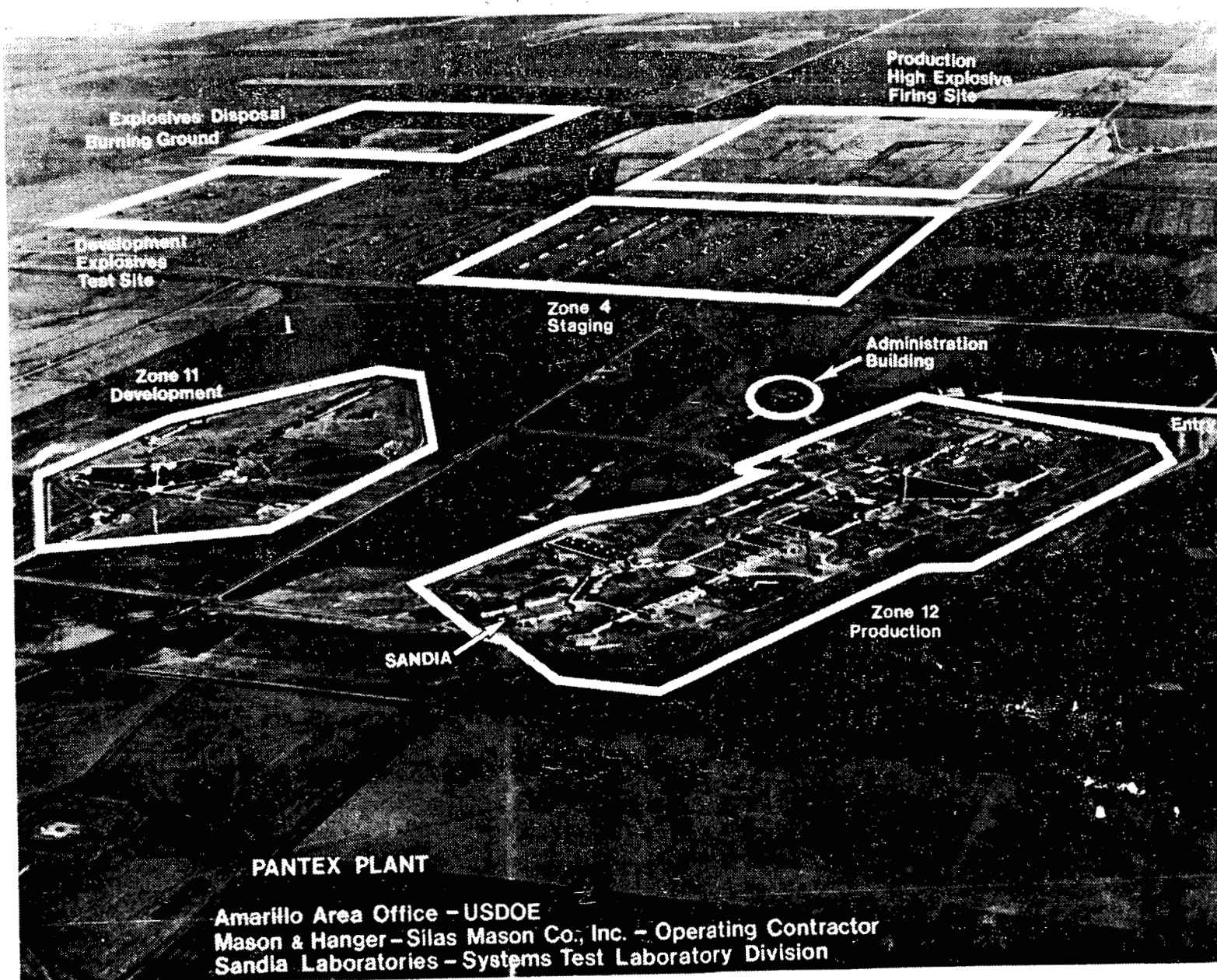
Figure 2.1 Aerial View of Pantex Plant
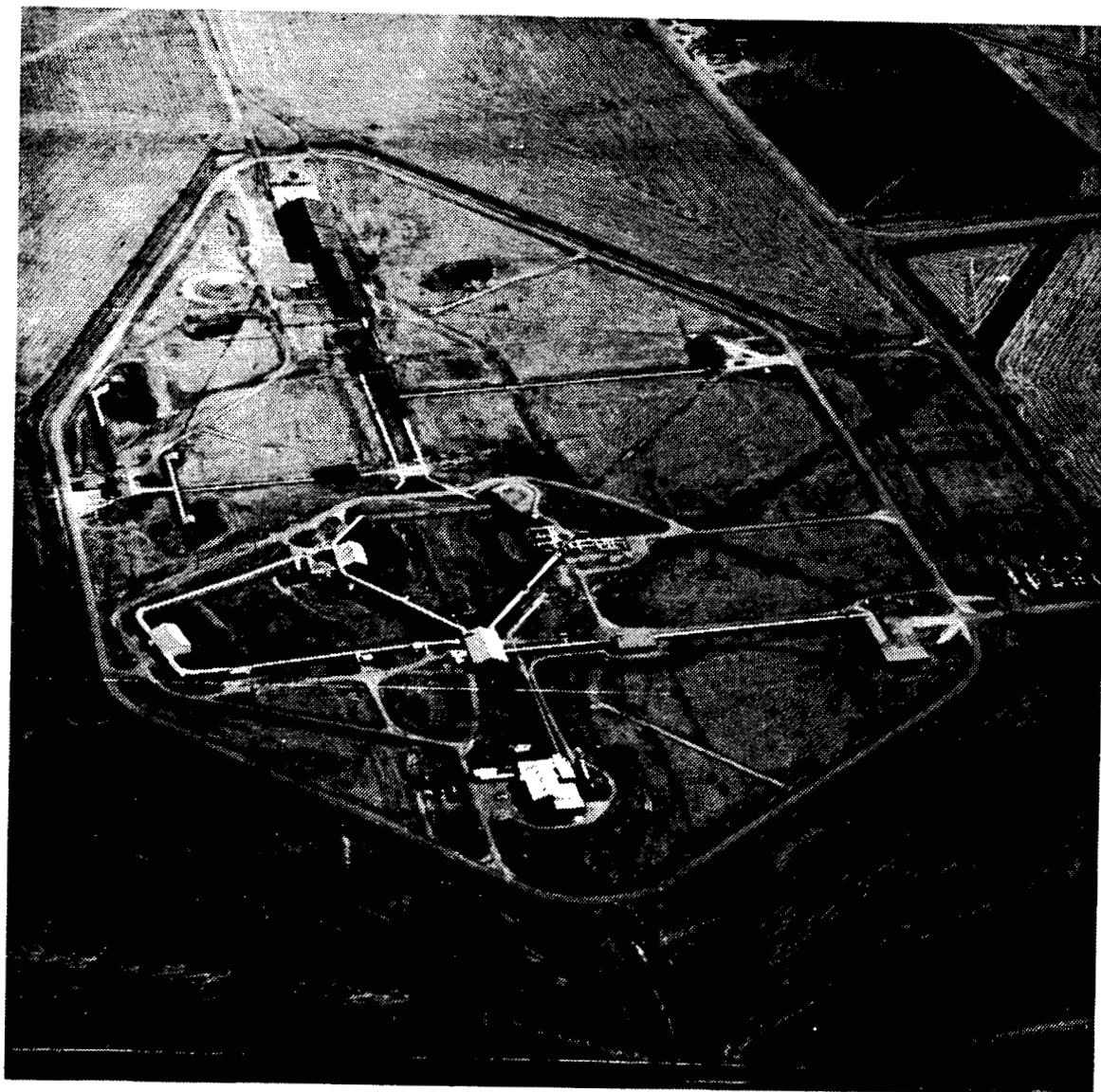
Figure 2.2 Aerial View of Zone 11, Pantex Plant
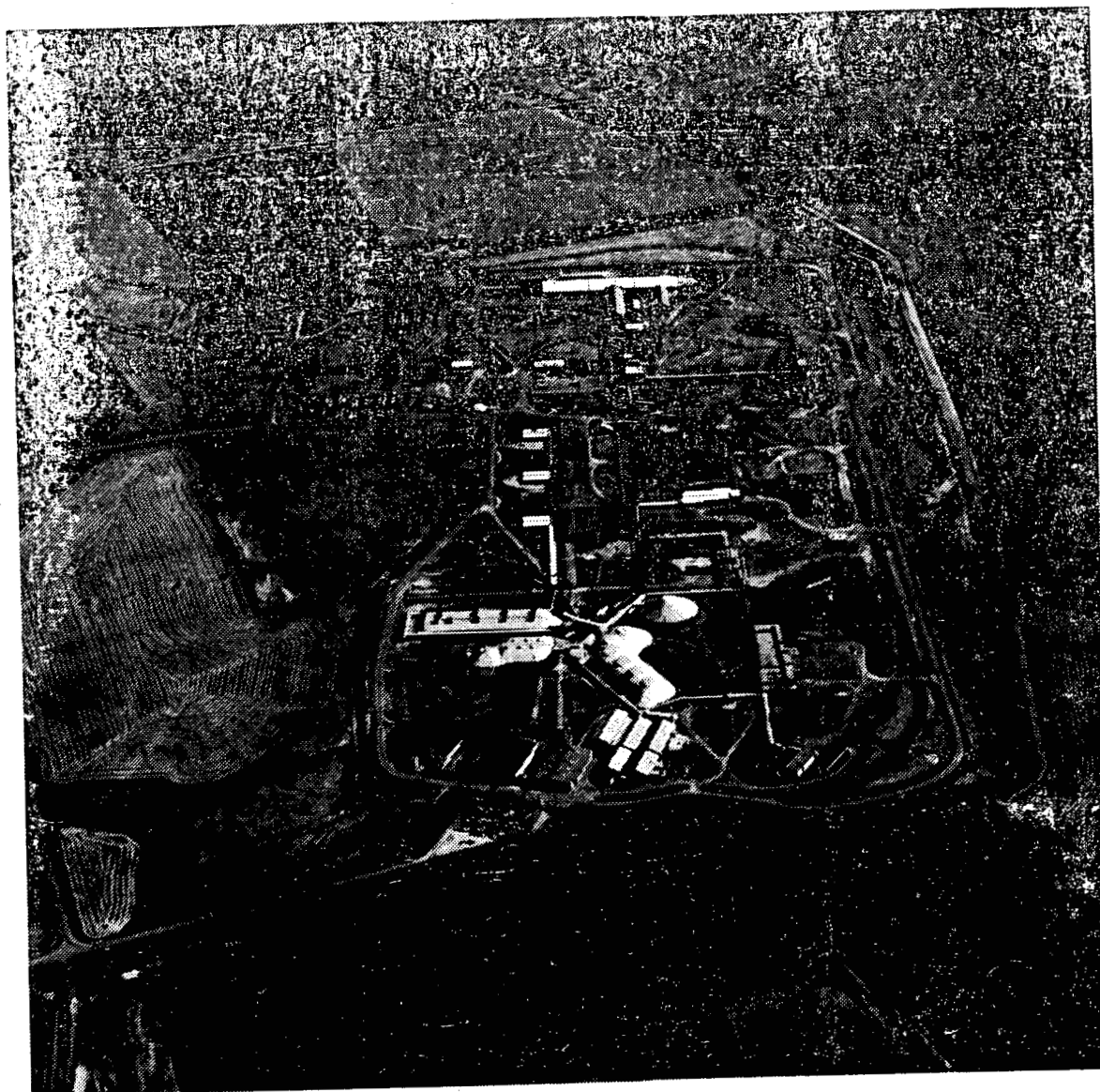
Figure 2.3 Aerial View of Zone 12, Pantex Plant

A typical unbarricaded building, used for testing with small quantities of HE, is Building 11-5, shown in Figure 2.4.

Figure 2.5 shows an above-ground barricaded building, Building 11-20. This multi-bay building is used for HE pressing, and has a double-revetted barricade placed on one side to arrest fragments and pieces of blowout panels in the event of an explosion in a bay.

Few of the existing buildings are designed for complete or nearly complete explosion containment, but a new design for a high explosives machining facility (Refs. 2.10 and 2.11) is essentially a containment structure, with minimal explosion venting and complete fragment containment being features of the design. Figure 2.6 is a plan view of the west sector of this facility.

2.3.1.2 Earth-Covered Buildings

These buildings are of three types:*

• Mounded structures

• Shallow-buried structures

• Underground structures

An example of a mounded structure is Building FS-11, Figure 2.7a. This building is used for gaging and has an explosive limit of 400 pounds.

In Zone 4 is a series of service magazines for storing various quantities of HE, up to 9,000 pounds in one bay. These magazines are examples of shallow-buried structures. They are visible in Figure 2.7b.

In Zone 12, there is a series of underground containment cells, or Gravel Gerties, designated Building 12-44. These cells have a reinforced concrete cylindrical wall and a roof of 17 feet or more of gravel, supported by a cable support system. Each cell and adjacent staging bays form one facility. Access is through equipment and personnel blast-resistant doors. There are presently seven such cell facilities located close to each other (Figure 2.8).

2.3.1.3 Venting Schemes

Many of the Pantex buildings employ some scheme for explosion venting. The most common types are relatively light roofs and outside walls in multi-bay explosion-resistant buildings. Some new designs will employ mazes

---

*The distinctions between these types of buildings are somewhat arbitrary. In Chapter 5, all are simply classed as buried structures.
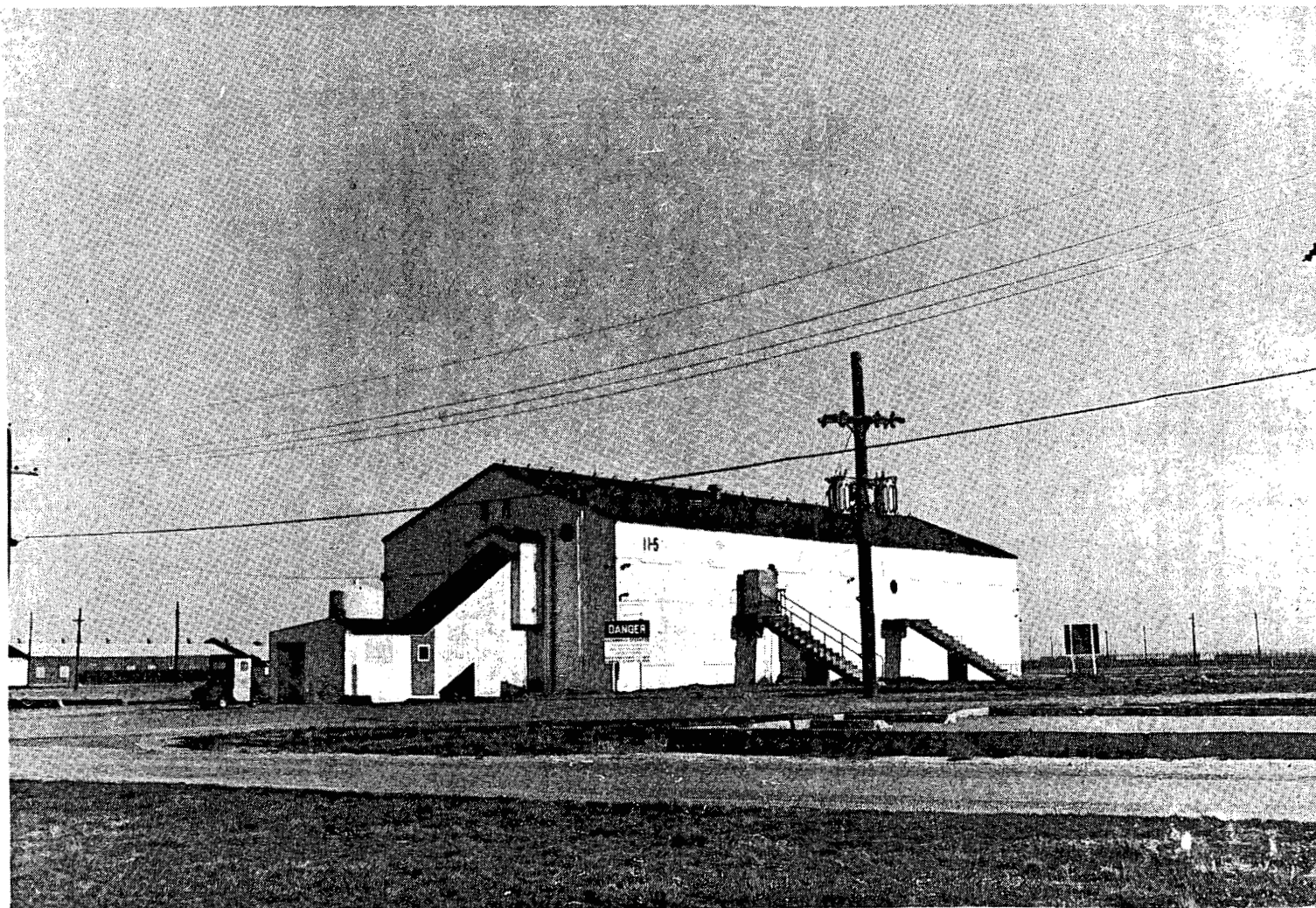
Figure 2.4   Typical Unbarricaded Above-Ground Building
at Pantex Plant, Building 11-5
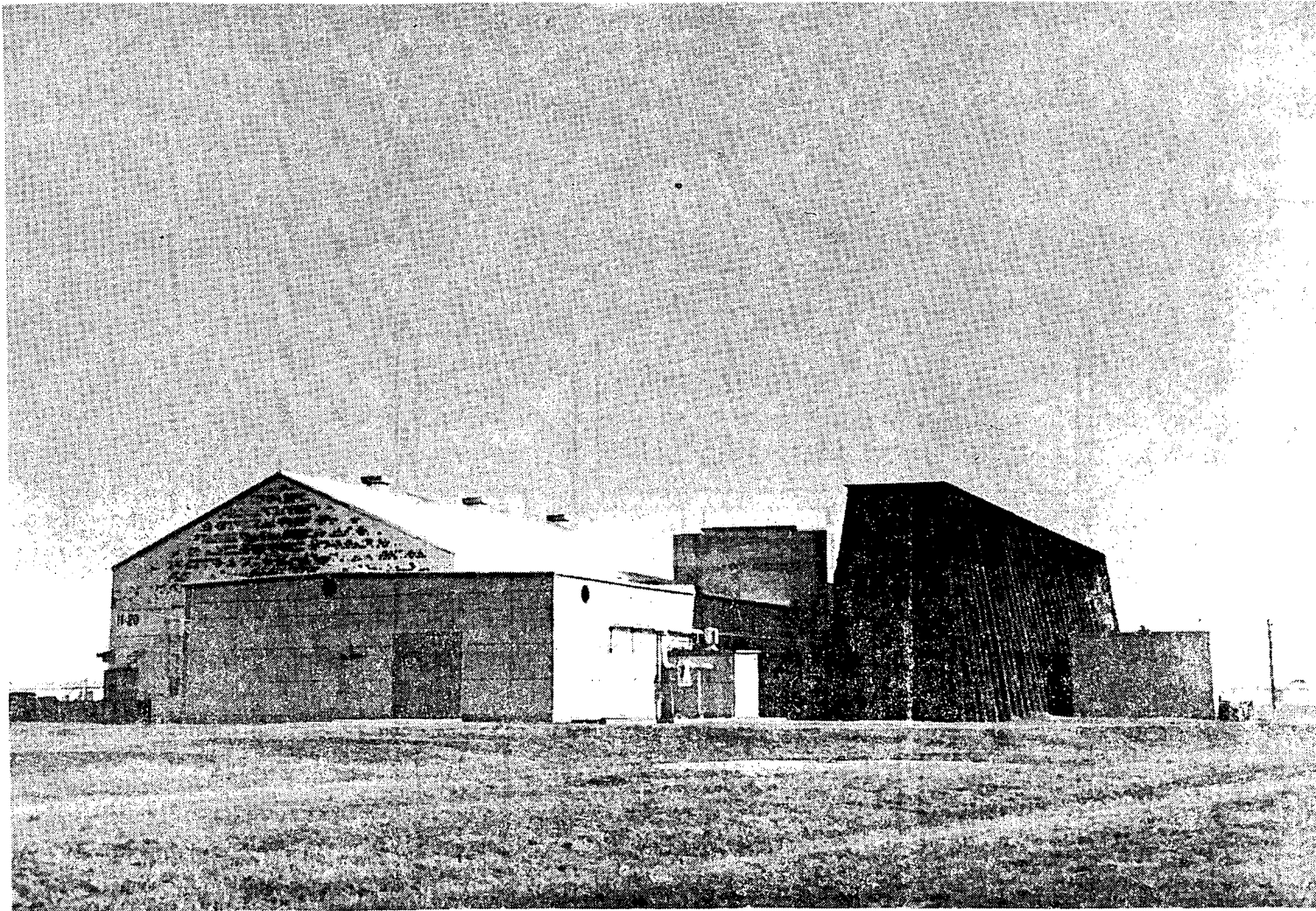
Figure 2.5 Typical Barricaded Above-Ground Building
at Pantex Plant, Building 11-20
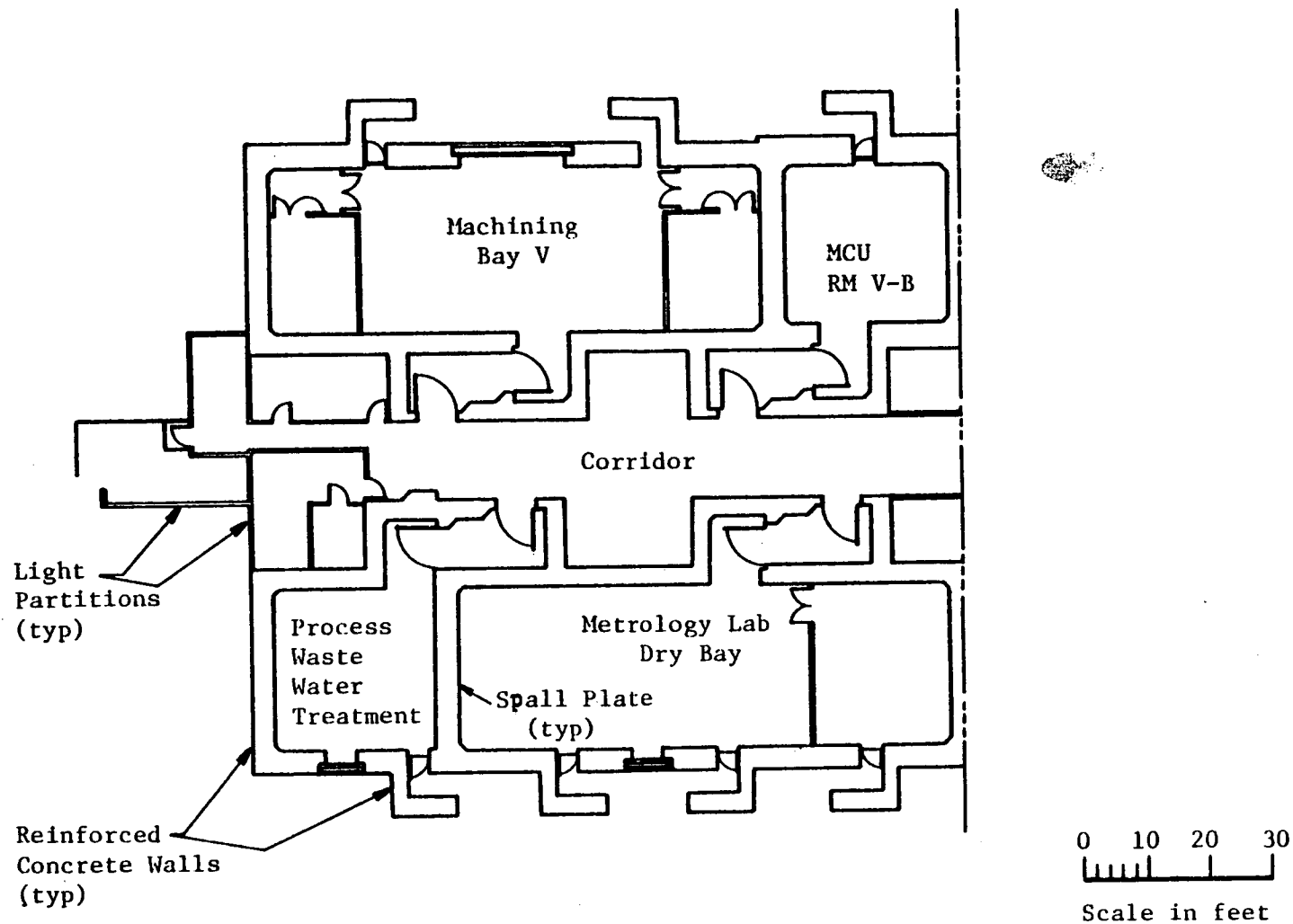
Figure 2.6 Plan View of West Sector for an Above-Ground Containment
Building at Pantex (New HE Development Machining Facility)
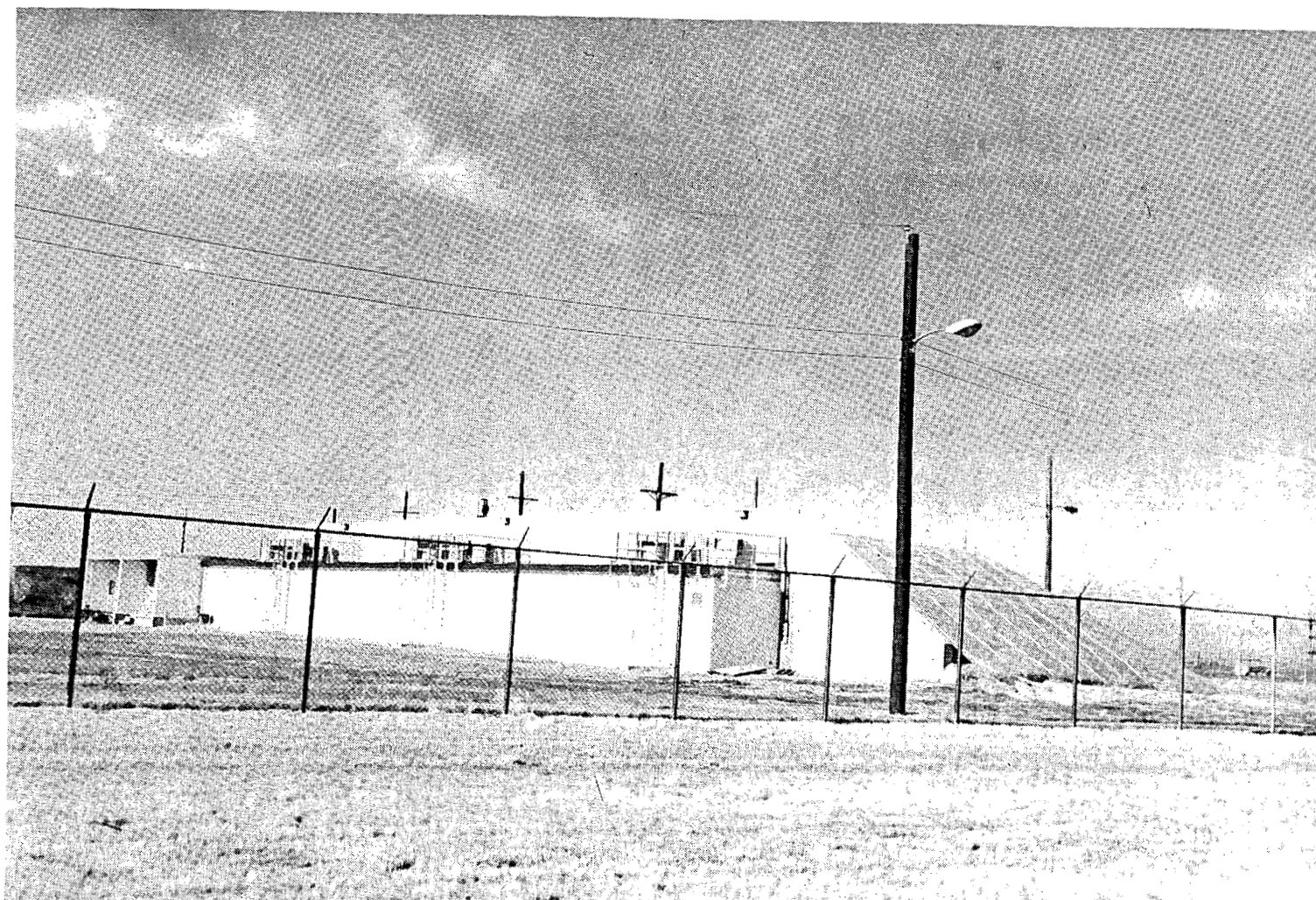
Figure 2.7a Typical Mounded Operations Structure at Pantex,
Building FS-11
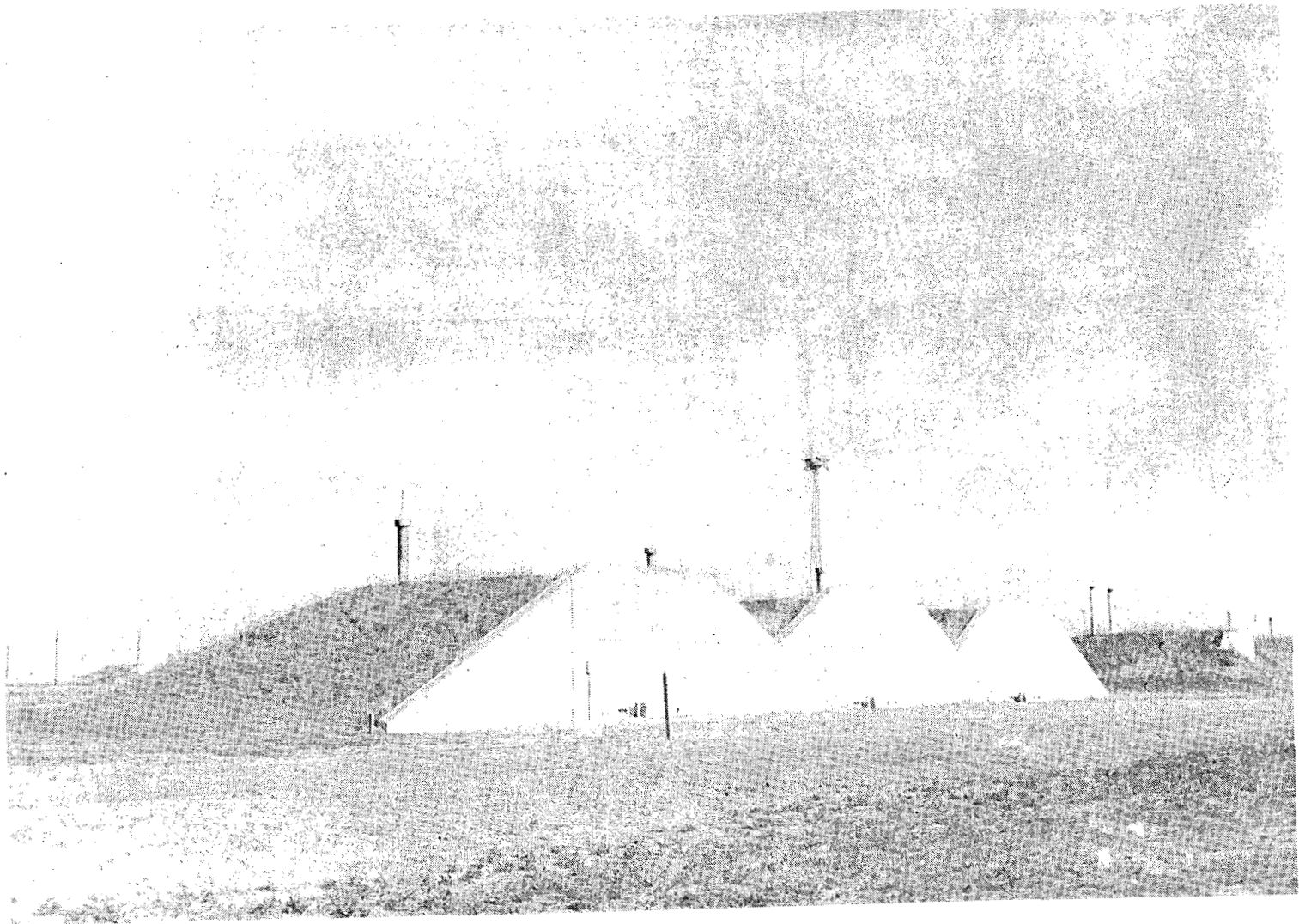
Figure 2.7b Typical Mounded Staging Structures at Pantex,
Buildings 4-101, 4-102, and 4-103
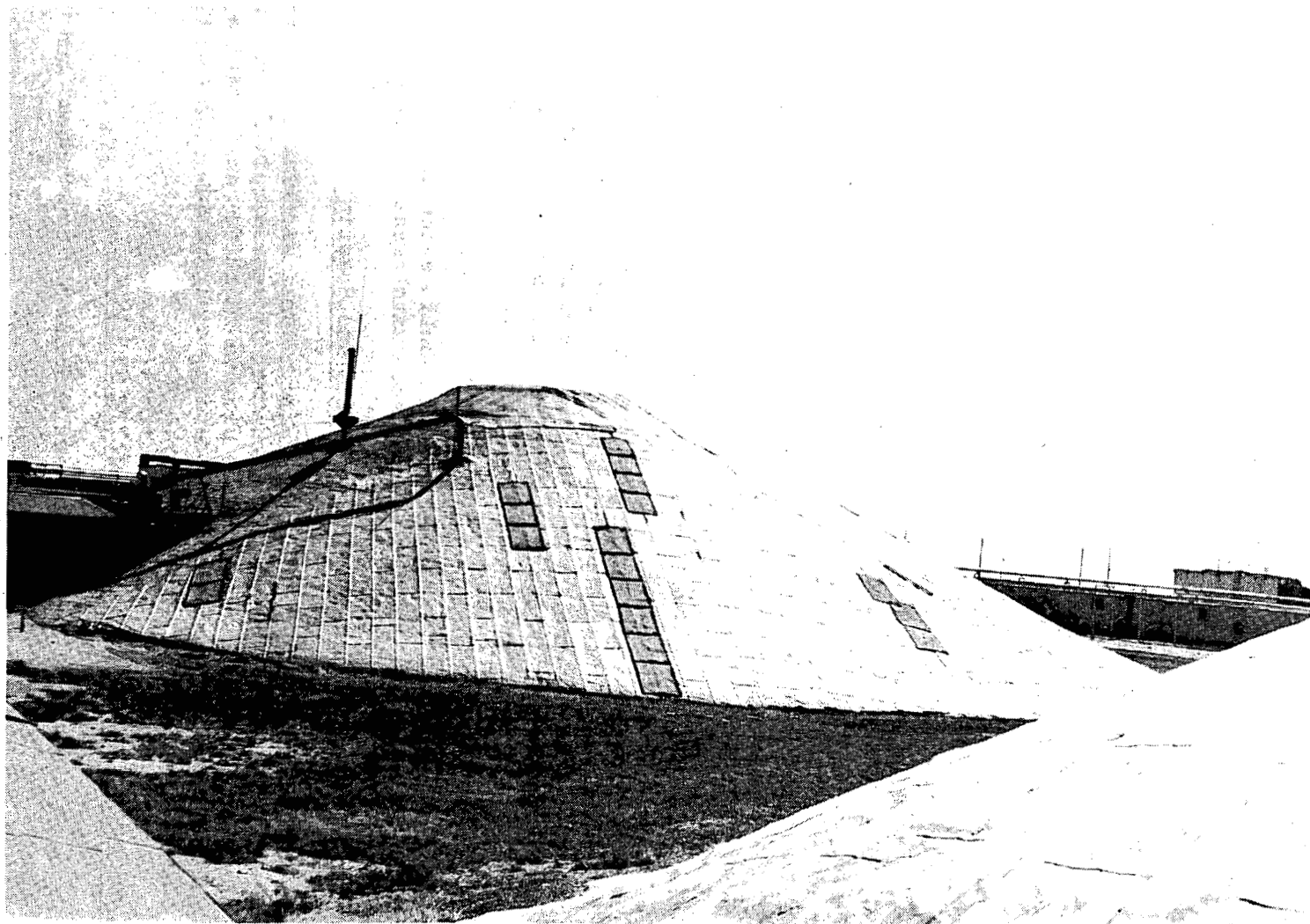
Figure 2.8   Typical Underground Structures at Pantex,
Building 12-44 (Gravel Gerties)

and open passageways for venting, and will use blast-resistant blowout covers over larger equipment openings. The Gravel Gertie structures are designed as containment buildings which should attenuate blast waves, as well as arrest fragments.

An old design for light, venting roof construction is shown in Figure 2.9, and a design for a light, venting wall panel in Figure 2.10. Maze venting in a new design is shown in Figure 2.11.

2.3.2 Impact of Blast and Fragment Safety Regulations on Design and Spacing

In most instances, proximity of explosive storage and handling facilities to each other, to inhabited buildings, to roadways, etc., is dictated by current explosives safety regulations such as AMCR 385-100 (Ref. 2.4), which gives quantity-distance standards. These standards are based partly on accident data, partly on limiting air blast overpressures, and partly on very approximate fragment safety distances. If one can prove by test or con-servative analysis that all fragments are contained in an explosive facility, safety distances can sometimes be drastically reduced. If one can prove by test or conservative analysis that blast pressures are completely contained or strongly attenuated, one can also reduce safety distances.

In the Pantex Plant, radiological safety considerations often must be considered together with explosives safety, because the HE is often present in close proximity to plutonium, or in the same assembly. Reference 2.1 specifies various types of protective design, dependent on the class of the explosion hazard (Class I being severe, Class II moderate, and Class III minimal hazard), whether HE is present alone or with plutonium, and whether the HE-Pu combination is cased or uncased. Table 2.1 summarizes these requirements.

An AE firm involved in design at Pantex should be certain to check References 2.1, 2.4 and 2.13 to assure compliance with these requirements.

2.3.3 Impact of Security Requirements on Design and Spacing

In an explosives facility like the Pantex Plant, security is necessarily very strict. Needs for surveillance, control of access, prevention of theft or sabotage, etc., may in many cases dictate facility configuration or spacing which may conflict with explosive safety requirements. The AE will be given guidance as required by DOE.

2.4 APPLICABILITY AND LIMITS OF APPLICABILITY OF MANUAL

This manual is specific for helping define blast, ground shock, and fragment hazards for the Pantex Plant. We reiterate that it is not a structural design manual, but should aid structural designers in defining their dynamic input loads for various facilities within the plant. Effects are emphasized in example problems for typical quantities of HE that would be present in various Pantex facilities.

Built-up Tar and Gravel Roof (20 year specification)
Over 1 inch Insulation Board, 2 inch Poured Perlited
Gypsum Deck and 1/2 inch Gypsum Board Form

High Gravel Guard. See
Cornice Det.

8B15 Purlins

8B15 Purlins

Concrete
Filled Haydite
Lintel Blocks
#5 Top and Bottom

4 inch Haydite
Block

2 inch
Styrofoam Insulation

Notch Concrete
Walls for Purlins

L3x3x4 Hangers
Weld to GI &
8B15 Purlins

6T 12.5
Runway Beam

6 WF 15.5 Col.

6 inch Haydite Block

Figure 2.9 Detail for Venting Roof Design (Building 11-14)
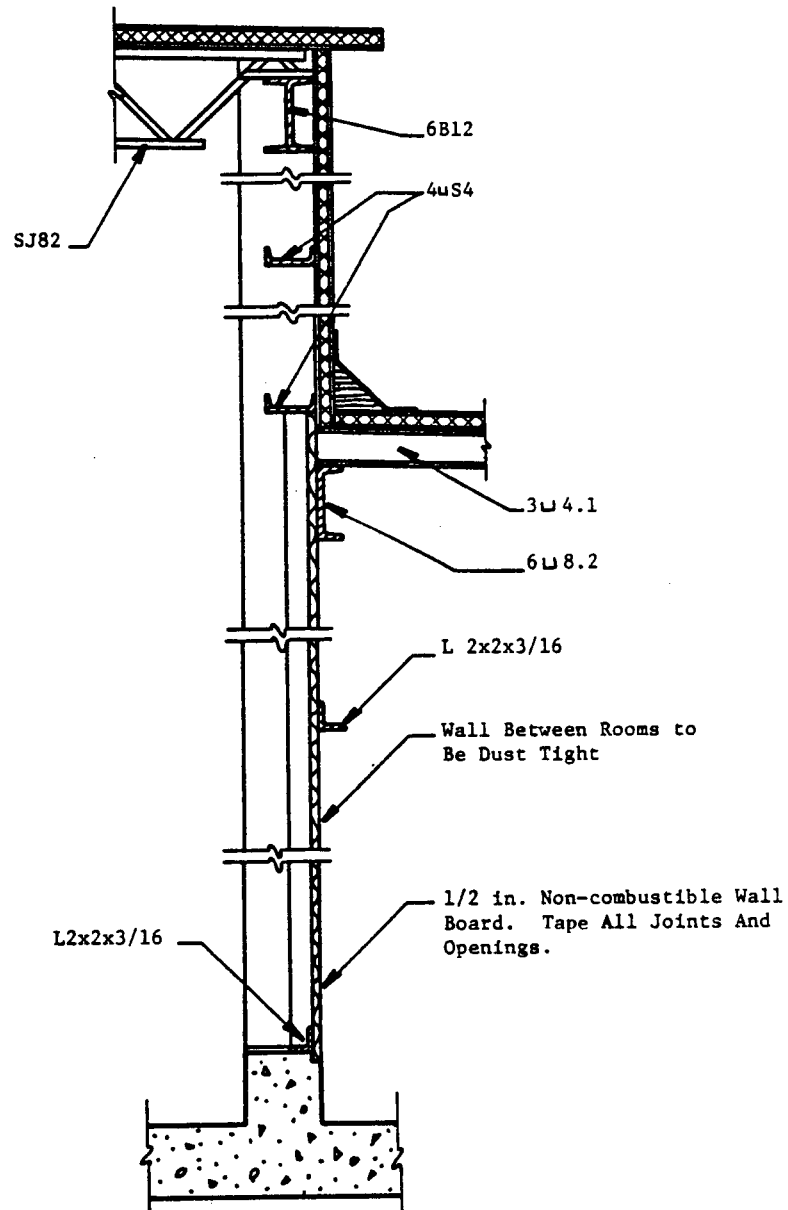
Figure 2.10   Detail of Venting Wall Panel (Building 11-20)

Labels in figure:
- 6B12
- 4uS4
- SJ82
- 3u4.1
- 6u8.2
- L 2x2x3/16
- Wall Between Rooms to Be Dust Tight
- L2x2x3/16
- 1/2 in. Non-combustible Wall Board.   Tape All Joints And Openings.
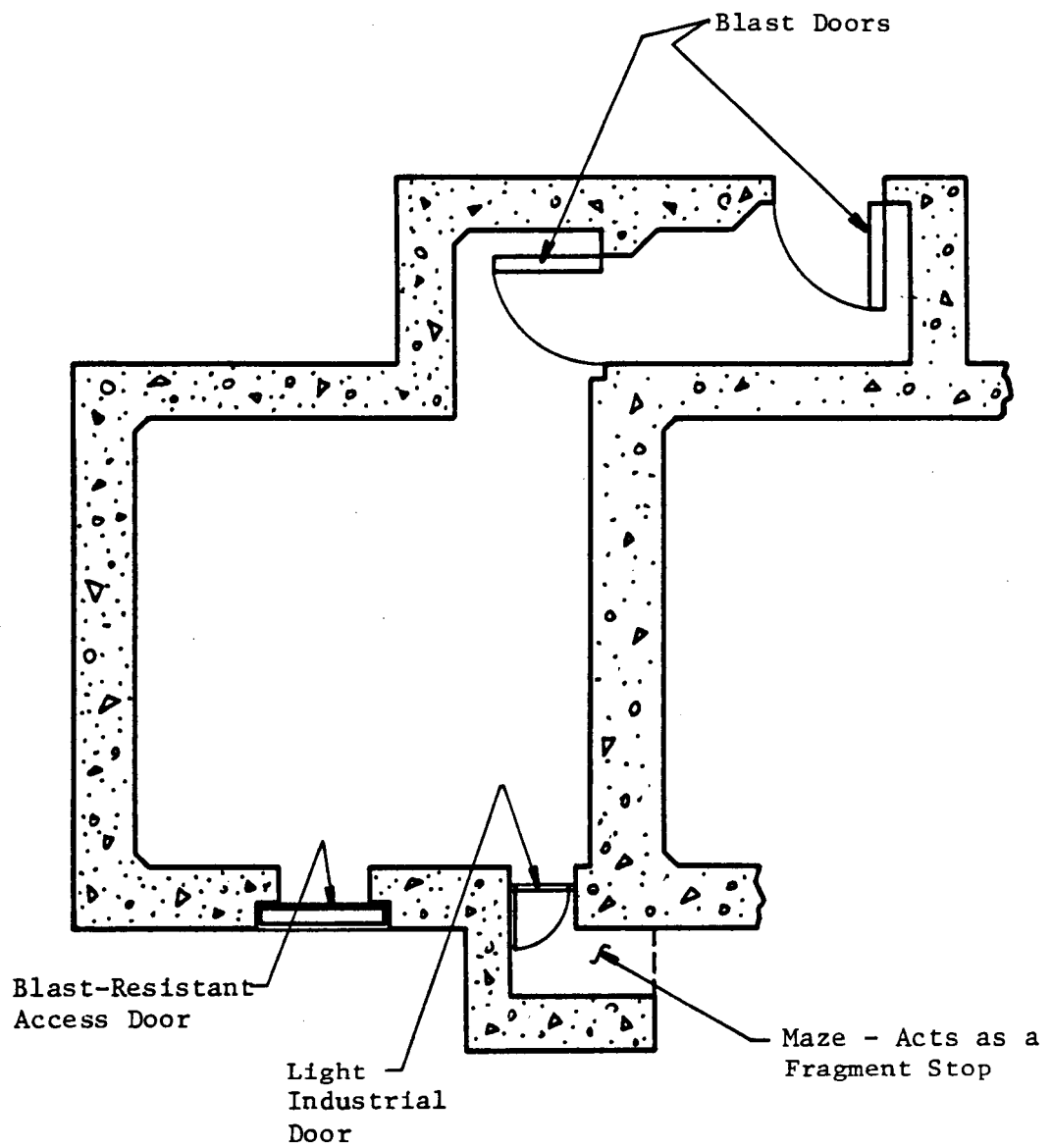
Figure 2.11   Plan View of New Design Containment
Bay with Maze Venting

Blast Doors

Blast-Resistant
Access Door

Light
Industrial
Door

Maze – Acts as a
Fragment Stop

Table 2.1 DOE Protective Design Requirements
By Type Of Activity (Ref. 2.1)

Protective Design Required	Class I HE			Class II HE			Class III HE			Support Area
	HE Only	HE-Pu Cased	HE-Pu Uncased	HE Only	HE-Pu Cased	HE-Pu Uncased	HE Only	HE-Pu Cased	HE-Pu Uncased	
AMCR 385-100 Requirements For Activity Involved	X	NOT PERMITTED	NOT PERMITTED	X	X	X	X	X	NOT PERMITTED	X
Explosion Protection For Personnel in Other Occupied Areas Including Adjacent Bays	X			X	X	X				
Explosion Protection For All Personnel (Remote Operation)	X									
Control of Plutonium In The Event of an Explosion						X				
High Level Protection From Natural Phenomena					X	X		X		
Normal Protection From Natural Phenomena	X			X			X			X
Radiological Considerations					X	X				

Type of Activity

Although this manual is specific for the Pantex Plant, much of the material is quite general and should be applicable to many high explosives facilities other than Pantex. But, AE firms are cautioned that it should be used outside of Pantex only if proper modifying factors are applied.

2.5 REFERENCES

2.1 "ERDA Manual Appendix 6301, Facilities General Design Criteria Handbook," ERDA, Division of Construction Planning and Support, March 1977.

2.2 URS/John A. Blume and Associates, Engineers, "Seismic Hazard and Building Structure Behavior at the Pantex Facility," prepared for U. S. ERDA, Amarillo Area Office, April 1976.

2.3 Department of Civil Engineering, Texas Tech University, "Final Report. Development of Design Basis Tornadoes and Design Manual for the Pantex Plant Site," prepared for U. S. AEC, Amarillo Area Office, August 1975.

2.4 AMCR 385-100, "Safety. Safety Manual," Department of the Army, Headquarters, U. S. Army Material Development and Readiness Command. (Basic document dated April 1970, but revisions through January 1977).

2.5 TM5-1300, Structures to Resist the Effects of Accidental Explosions, Department of the Army Technical Manual, 1969.

2.6 DOD 5154.45, "DOD Ammunition and Explosives Safety Standards," Department of Defense, Office of the Assistant Secretary of Defense (Manpower, Reserve Affairs and Logistics), January 1978.

2.7 "Pantex Plant Design Criteria Manual," (PDCM Vol. I & II), current edition.

2.8 URS/John A. Blume and Associates, Engineers, "Seismic Design of Buildings and Sprinkler Systems for the Pantex Facility," prepared for U. S. ERDA, Amarillo Area Office, April 1976.

2.9 Department of Civil Engineering, Texas Tech University, "Design Manual for Tornado Resistant Structures at the Pantex Plant Site," prepared for U. S. AEC, Amarillo Area Office, November 1974.

2.10 Booker Associates, Inc., "Title I Design Analysis, Volume I of II. Replacement of High Explosives Machining Facility," Pantex Plant, Amarillo, Texas, January 1979.

2.11 Booker Associates, Inc., "Title II Design Analysis, Volume II of IV. Structural Calculations. Replacement of High Explosives Machining Facility," Pantex Plant, Amarillo, Texas, September 1979.

2.12 Booker Associates, Inc., "Title II Design Analysis. Volume III of IV. More Structural Calculations. Replacement of High Explosives Development Machining Facility," Pantex Plant, Amarillo, Texas, September 1979.

2.13 "Interim Safety Criteria for the Design of Production Plant Explosive Facilities," Available from U.S. Department of Energy, Albuquerque Operations Office, Albuquerque, New Mexico.

CHAPTER 3

EXPLOSIVES AND DAMAGE MECHANISMS

3.1 INTRODUCTION

The topic of explosives and damage mechanisms is extensive, and we give in this chapter primarily qualitative discussions of the predominant characteristics and effects associated with accidental explosions. The effects are also limited to those which could conceivably occur at Pantex. This chapter serves as a preview of more detailed and explicit discussions and quantitative effects in Chapter 4, 5 and 6.

3.2 GENERAL ASPECTS OF EXPLOSIVE HAZARDS

3.2.1 Explosion Phenomena

Here we discuss the general characteristics of explosions of solid or liquid explosive materials, and of the air blast waves or ground shocks generated by such explosions, and their transmission through air or earth. Aspects covered are:

- Blast from bare explosives in air

- Air blast and ground shock from surface bursts

- Ground shock and cratering from buried explosives, including effects of air space around explosives

- Explosion of cased explosives, including blast and fragmentation.

3.2.1.1 Blast From Bare Explosives in Air

Bare, solid explosives must detonate to produce any explosive effect other than a fire. The term detonation refers to a very rapid and stable chemical reaction which proceeds through the explosive material at a speed D, called the detonation velocity, which is supersonic in the unreacted explosive.* Detonation velocities are of the order of 25,000 ft per sec for most high explosives. The detonation wave rapidly converts the solid or liquid explosive into a very hot, dense, high-pressure gas, and the volume of this gas which had been the explosive material then is the source of strong blast waves in air.

Only about one-third of the total chemical energy available in most high explosives is released in the detonation process. The remaining two-

---

*See Reference 3.1 or 3.2 for good general discussion of the detonation process.

thirds is released more slowly in explosions in air as the detonation products mix with air and burn. This afterburning process has only a slight effect on blast wave properties because it is so much slower than detonation.

When the detonation front reaches the surface of a bare explosive, it is transmitted into the surrounding air as an intense shock wave, which propagates outward at hypersonic speed.* The pressure, temperature, and density behind the shock front are very high, and there is also a strong outward flow of detonation products and air.* The shock front slows very rapidly as it diverges outward, and decays rapidly in strength (pressure), temperature, density, and outward flow. Eventually, the wave becomes so weak that it behaves like a sound wave. Then, the transmission speed is constant at sound speed (Mach 1), the changes in pressure and all other physical parameters from the ambient air are very small, and the wave can cause no damage. For an AE firm considering damaging effects of air blast waves at Pantex, this "far-field" regime is of little interest, except for possible blast wave focusing at great distances by inhomogeneous atmospheric effects.†

More complete discussion of air blast waves, definitions of terms, and prediction graphs and equations, all appear in Chapter 4. Reference 3.3 is a good general reference on this topic for background reading.

3.2.1.2 Air Blast and Ground Shock from Surface Bursts

An explosive source detonated on the ground surface will generate both intense air blast waves and also ground shock waves of moderate strength. The partitioning of the explosion energy between air and ground shock is, to some extent, determined by the characteristics of the surface in the immediate vicinity of the explosive and the explosive configuration. A heavily reinforced concrete slab will, for example, act as a better reflector than a soft bed of sand. But, any solid surface is a fairly efficient reflector, so the majority of the explosive energy drives the air blast wave. The effective energy for air blast will always be at least 1.7 times the energy for an explosion in "free-air" away from the ground (See Reference 3.4). In this manual, we do not present separate curves and formulas for air blast from surface explosions, but show in Chapter·4 how to use the free-air blast curves for this situation. Ground shock from surface explosions is discussed in more detail in Chapter 5.

---

*At the surface of TNT explosive detonated in air, the initial shock speed is about twenty-six times the speed of sound (Mach 26), and the initial flow velocity is about Mach 22.

†Focusing is not discussed in this manual.

3.2.1.3 Ground Shock and Cratering From Buried Explosives

An explosion from a buried explosive drives a wave into the ground which is called a ground shock. The characteristics of this wave are very different from an air blast wave. Initial pressures are much higher, but the wave velocity is very little more than the velocity of a compression wave (P wave) in a seismic disturbance. Particle velocities are low, and the time histories of velocity and displacement in the ground resemble seismic disturbances, with an initial strong pulse followed by several decaying, oscillating pulses. The character of the ground shock pulse is profoundly affected by the presence of the ground surface and by layering, or differences in soil properties, as it propagates outward from the explosion source. If the explosion occurs in an underground cavity with some air space around the explosive, the ground shock pulse can be drastically attenuated, compared to explosions in intimate contact with the soil.

A buried explosion will invariably form some kind of crater, or cavity in the ground. The type of crater is dependent on total explosion energy, depth of burial, and to a lesser extent, the type of soil. For shallow-buried explosions, the explosive gases vent through the ground surface, and there can be considerable ejecta thrown up and out, with some falling back into the crater. Below some burial depth, the explosive gases will not vent, and a more or less spherical cavity, called a camouflet, is formed.

Chapter 5 covers the topics of ground shock and cratering in some detail. Methods are given in Chapter 5 for prediction of ground shock characteristics for explosions which could occur in Pantex facilities, with a number of example problems. Methods are also given for prediction of cratering mode, and dimensions of craters, in the form of scaled curves. Cratering example problems also appear in Chapter 5.

3.2.1.4 Explosion of Cased Explosives

When an explosive is contained in a casing, the casing affects the blast wave generated by an explosion and provides a source of damaging, high-speed fragments. For a casing made of a ductile material, rapid expansion occurs when the very high pressure detonation products impinge on the inner surface of the casing. When the casing has expanded to about 1.5 times its original diameter, it ruptures into many fragments, and the explosion gases escape between the gaps in the fragments. The blast wave forms, and outruns the fragments for a time. But air shock speed decays much more quickly than fragment speed, and the fragments eventually pass through and outrun the blast wave.

The character of both the blast wave and the fragmentation are affected by overall geometry of the casing and explosive, the mass of each, and the casing materials. Thin, light casings can actually enhance the blast wave, for reasons that are not entirely clear, while heavy casings usually attenuate the blast. Fragment velocities, numbers, and mass distributions

are strongly affected by casing material and thickness. The fragments are usually numerous, and can have velocities as high as 9,000 ft per sec.

Chapter 6 is devoted to fragmentation, and gives methods for predicting fragment velocities and masses for cased explosives. Predictions for attenuation or enhancement of air blast by casings appear in Chapter 4. Example problems are given for prediction curves and equations in both chapters.

3.2.2 High Explosive Sensitivity

This discussion centers on those stimuli which can initiate violent reactions or detonations in high explosives and chemicals used in explosive processing. "Standard" tests for sensitivity are identified and discussed briefly.* The stimuli include:

- Shock initiation

- Impact initiation

- Thermal initiation

- Friction

- Static electric discharge.

3.2.2.1 Shock Initiation

High explosives can always be detonated by sufficiently strong shock waves, because this is their mode of initiation in normal use. In accidental explosions, the source of the strong shock can be a detonating explosive or high-speed fragments launched by an explosion. All secondary high explosives are relatively† insensitive to shock initiation, for safety in use, transportation, and storage.

The most commonly used test to determine shock sensitivity is the card gap test (See Refs. 3.5 and 3.6). The test arrangement is shown in Figure 3.1. A donor explosive charge is detonated, and drives a strong shock through a series of inert cards which fills a gap between the donor and an acceptor charge being tested. Detonation of the acceptor is assumed if the steel witness plate has a clean hole blown through it. The number of cards

---

*The word "standard" is in quotations because there are many variations of some of the tests, dependent on the agency which developed each test and on the agency or laboratory conducting the tests. Tests described may or may not accurately reflect those conducted at Pantex.

†Safe relative to primary or initiating explosives.

Engineers Special
Blasting Cap (J-2)

Wood Block

Pentolite Booster

Card Gap Cellulose
Acetate Cards
0.01 inch each

Propellant. or
Explosives Composi-
tion Sample

Cardboard Tube

Steel Tube

1/16 inch Air Gap Between
Steel Tube and Plate

3/8 inch
Witness Plate

Wood Stand

Ground

6-in. Min.
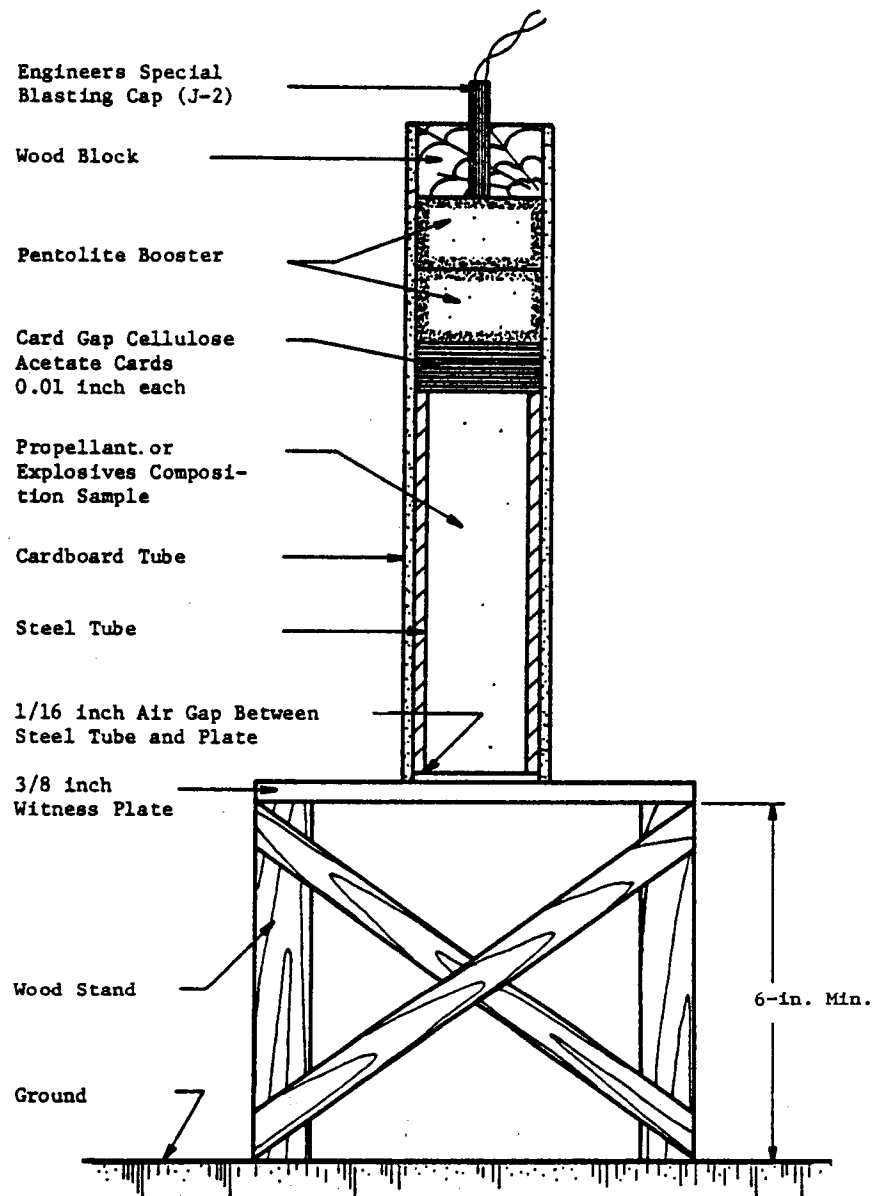
Figure 3.1 Card Gap Test Arrangement (Ref. 3.5)

is varied from test to test until limits are determined for detonation and no detonation.

An instrumented version of the card gap test is used to determine shock sensitivity for liquids (see Figure 3.2 and Ref. 3.7). Here, the detonation velocity in the liquid is measured by a resistance probe running the length of the tube used to contain the liquid. The resistance wire in the center of a very light, thin-walled aluminum tube is shorted by the collapsing tube, and gives a continuous measure of detonation or shock front location. If the velocity of the front continuously decays, there is no detonation. If it reaches and sustains a fixed, high value, detonation has occurred.

Another standard shock sensitivity test is the No. 8 blasting cap test (Ref. 3.5). A 2-inch cube of explosives is placed on a lead cylinder 1.5-inches in diameter by 4-inches high, which is in turn placed on a mild steel plate, 0.5-inches thick by 12-inches square. A No. 8 blasting cap is positioned with its flat end in contact with the center of the surface of the explosive cube opposite the lead cylinder. Mushrooming of the lead cylinder is considered evidence of detonation. The test is conducted a minimum of five times, or until detonation occurs.

3.2.2.2 Impact Initiation

The most common type of impact test for initiation is a drop weight test. There are a bewildering number of such tests, but all are similar in impacting a quite small sample of test material on an anvil or base with a relatively massive guided drop weight. Height of drop is varied in some systematic manner until an average height is obtained for achieving a violent reaction of the material.

Figure 3.3 shows a schematic of one drop weight impact test apparatus (Ref. 3.6). This test involves placing the sample on a fixed anvil in a restricted but unconfined state. The sample thickness is similar in dimension to that occurring in processing. A hammer of known contact area is positioned above the sample and the weight is raised to a predetermined height and dropped. Normally, sample initiation is detected by audible, visual, sensory means or by infrared analysis of selected decomposition products. A test is comprised of twenty "no initiation" trials at a given input and at least one initiation at the next higher interval (i.e., 25% greater energy input). The energy delivered to the sample is measured with a force gage.

A higher velocity and larger scale impact test is the Susan test (Ref. 3.8). The Susan Sensitivity test is a projectile impact test with the projectile shown in Figure 3.4. The weight of explosive in the projectile head is about 1 lb. The target is armor-plated steel. The results of the tests are expressed in terms of a "sensitivity" curve in which the relative "point-source detonation energy" released by the explosive as a result of the impact is plotted against the velocity of the projectile. The relative

① TEST CYLINDER, 304 STAINLESS STEEL, SCHED. 40
② CAP
③ FLANGES (BOLTS NOT SHOWN)
④ COOLANT JACKET, 20 GAUGE SHEET METAL, 1 in. FOAM INSULATION
⑤ BRASS DIAPHRAGM
⑥ THERMOCOUPLE, CHROMEL-CONSTANTAN
⑦ TEST GAS INLET
⑧ TEST GAS OUTLET
⑨ COOLING COIL FOR LIQUID NITROGEN
⑩ VELOCITY PROBE
⑪ BOOSTER WELL
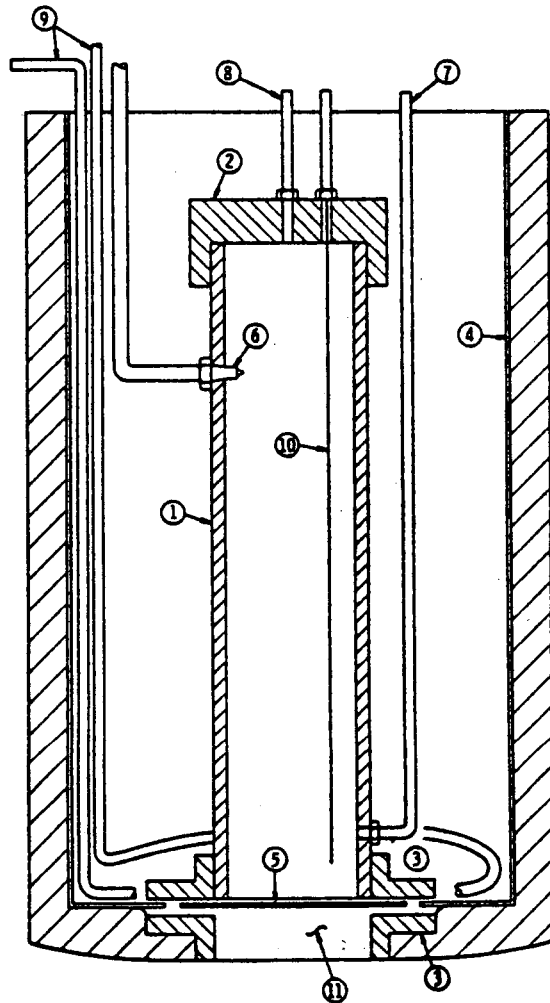
Figure 3.2 Schematic of Gap Test Apparatus for Liquids (Ref. 3.7)

RODS TO GUIDE WEIGHT

FALLING WEIGHT (VARIABLE MASS)
(STANDARD = 4.4 LBS.)

VARIABLE DISTANCE OF DROP

INTERMEDIATE HAMMER
(VARIABLE) (STANDARD = 2.7 LBS.)

GUIDE COLLAR

EXPLOSIVE SAMPLE

VARIABLE GAP DISTANCE

IMPACT ANVIL

FORCE GAGE

MOUNTING BASE

MACHINE BASE

CONCRETE
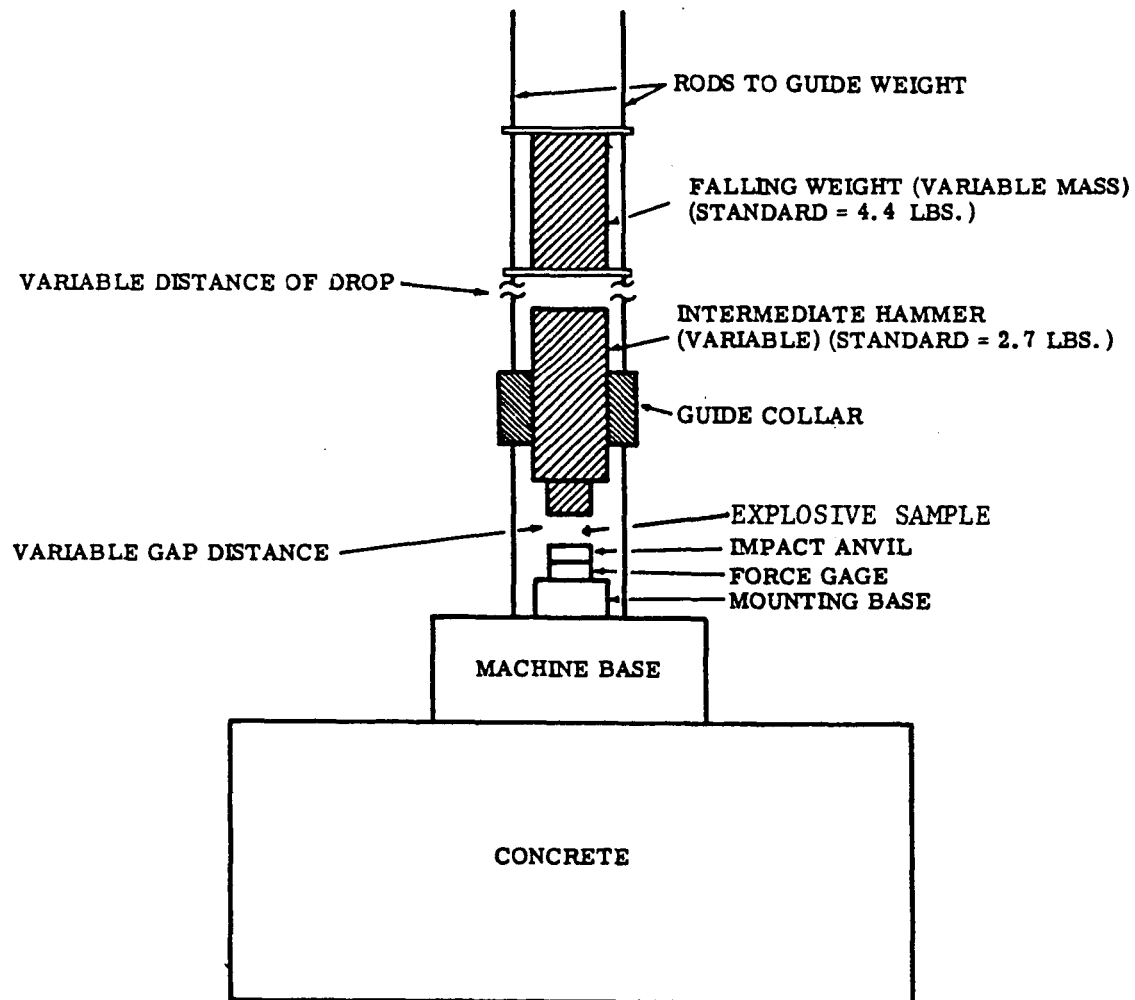
Figure 3.3   Schematic of a Drop-Weight Impact Test Machine (Ref. 3.6)

Leather cup seal

Aluminum cap

Steel body

High explosive head
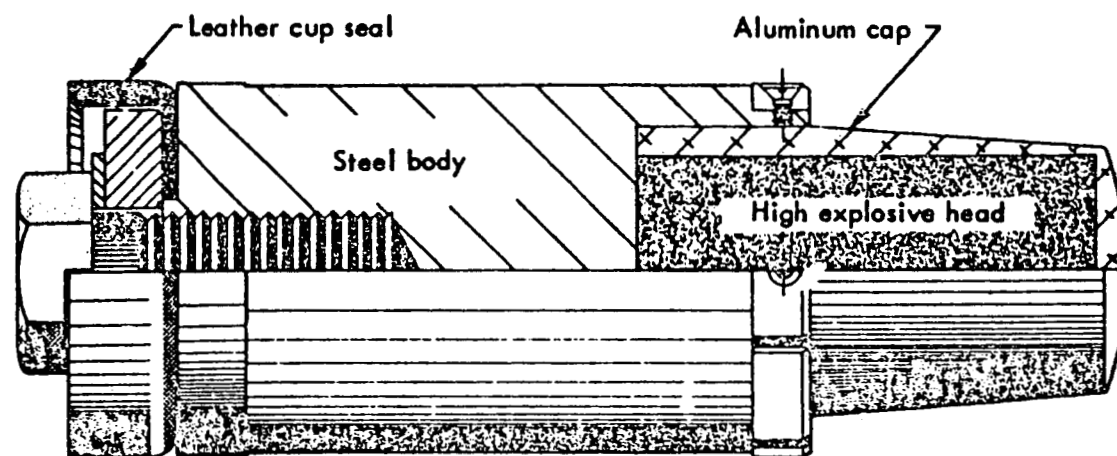
Figure 3.4   The Susan Projectile (Ref. 3.8)

point-source detonation energy can be derived from a transit-time measurement of the air shock from the point of impact to a pressure gauge 10 ft away. The results determined in this manner are somewhat subjective, particularly when the reaction level shows a large but relatively slow increase with time. The preferred way to get at the "point-source detonation energy" at present is to relate it to the overpressure measured 10 ft from the impact. This results in much more reproducible data and is not subject to many of the errors of the transit-time measurements.

The energy scale is set to range from zero for no chemical reaction to approximately 100 for the most violent detonation-like reactions (all explosive consumed) for the most energetic explosives. Less violent burning reactions that appear to consume all of the explosive can give values on the scale as low as 40; the energy equivalent of TNT fully reacted as a point source, would register at 70 on the scale. For each explosive considered, comments are made on the details of the impact process that seem to bear on the impact safety of an explosive. Remarks about probabilities of large reactions are relevant to unconfined charges in the 25-lb class. Smaller unconfined charges show a trend of decreasing reaction level as the charge size gets smaller.

3.2.2.3 Thermal Initiation

There are a number of standard tests of the thermal <u>stability</u> of explosives, which can also indicate sensitivity to thermal initiation. Several such tests, as described in Reference 3.8, follow.

Thermal changes in explosive materials can be measured in several ways, qualitatively and quantitatively. For high explosives (HE), one generally uses differential thermal analysis (DTA), thermogravimetric analysis (TGA) and tests (pyrolysis, CRT or vacuum stability) that measure the amount of gas evolved when an HE is heated for a stated period of time at elevated temperature. Heating rates are 10°C/min.

a. <u>Differential Thermal Analysis (DTA)</u>. In the usual DTA analysis, identical containers are set up (one containing the sample and the other containing a standard reference substance) in identical thermal geometries with temperature sensors arranged so as to give both the temperature of each container and the difference in temperatures between containers. The data are displayed as a DTA thermogram in which the temperature difference is plotted against the temperature of the sample. The standard reference material chosen is one whose thermal behavior does not change rapidly. Such a plot is almost a straight line if the sample also has no rapidly changing thermal behavior (or if it is very similar to the standard material). Excursions above and below a background line are due to endo- or exothermic (heat-absorbing or heat-releasing) changes. The DTA analyses permit interpretation for phase changes, decomposition and kinetic information, melting points, and thermal stability. Sample sizes are of the order of 20 mg.

b. **Pyrolysis.** The sample is placed in a pyrolysis chamber which is then flushed with helium. When the air has been swept out, the temperature of the chamber is raised at a constant rate. Gas evolution is measured as a function of temperature by a bridge formed by two thermal conductivity cells. Sample sizes are of the order of 10 mg.

c. **Thermogravimetric Analysis (TGA).** The objective in a TGA is to determine whether there are any weight changes in a sample, either when it is held at a fixed temperature or when its temperature is changed in a programmed linear fashion. The data are generally plotted as weight versus temperature or time or as weight change versus temperature or time. The TGAs are useful for only a limited number of physical property investigations, e.g., vaporization phenomena, but they are extremely useful for obtaining information on chemical properties such as thermal stability and chemical reactions. They are also useful for obtaining kinetic data. Sample sizes are of the order of 10 mg.

d. **LLL Reactivity Test (CRT).** The sample is heated at 120°C (393K) for 22 hours. A two-stage chromatography unit is used to measure the individual volumes of N_2, NO, CO, N_2O and CO_2 evolved per 0.25 g of explosive during this period. The test is used principally to determine the reactivity of explosives with other materials. When operated as a simple test of explosive stability, the results are expressed in terms of the sum of these volumes.

A crude thermal initiation test is specified in Reference 3.5, as follows:

"(1) Place a 2-inch sample on a bed of kerosene-soaked sawdust and ignite the sawdust with an electric match-head igniter. Perform this test twice.

(2) Place four 2-inch samples end to end in a single row in contact with each other on a single bed of kerosene-soaked sawdust and ignite the sawdust with an electric match-head igniter at one end.

(3) Record results under Ignition and Unconfined Burning Test."

The sample summary data sheet in Reference 3.5 shows that the results of this test are to be recorded under "Ignition and Unconfined Burning Test" as a did or did not explode. If burning only occurs, average burning time in seconds is recorded.

3.2.2.4 Friction

A standard friction test described in Reference 3.6 employs quite small samples of explosive material. The apparatus is shown schematically in Figure 3.5. This test simulates friction conditions occurring in the
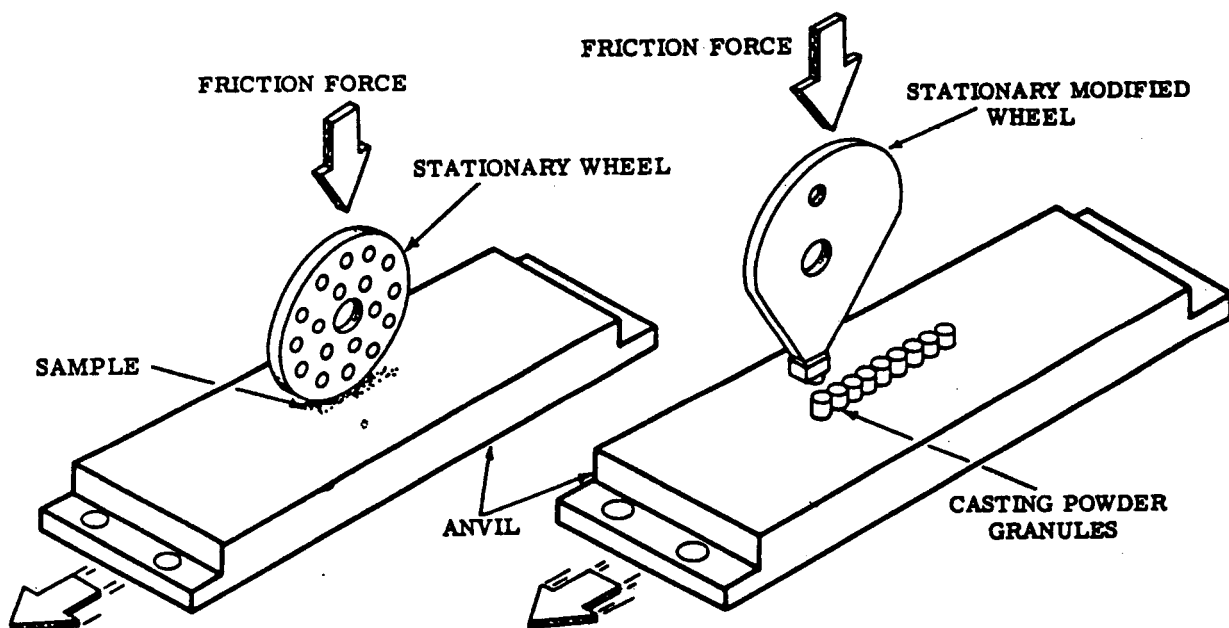
Figure 3.5   Schematic of Friction Test Apparatus (Ref. 3.6)

process when an explosive is subjected to a frictional force between moving components, such as in the mixer, or during disassembly, machining and material handling. The sample is placed on the anvil, a known force is applied hydraulically through a stationary wheel, and a pendulum is used to propel the sliding anvil at a known velocity perpendicular to the force vector. Normally, sample initiation is detected by audible, visual, sensory means or by infrared analysis of selected decomposition products. A valid test is comprised of 20 consecutive "no initiations" and at least one initiation at the next higher test interval. Force levels are decreased by 25 percent intervals, and velocity levels are reduced 1 ft per sec whenever an initiation is obtained at 10 lb force at a given velocity. Force is measured by hydraulic gauges and velocity by a sliding potentiometer.

A relatively large-scale test which can probably be classed as a friction test is the skid test used at Pantex and Lawrence Livermore Laboratory. A description from Reference 3.8 follows.

"Results from a sliding impact sensitivity test (skid test) with large hemispherical billets of HE have proved valuable for evaluating the plant-handling safety of HEs. The test was developed at AWRE in England.

In the LLL-Pantex version of this test, the explosive billet, supported on a pendulum device, is allowed to swing down from a preset height and strike at an angle on a sand-coated steel target plate. Impact angles employed are 14 deg (0.24 rad) and 45 deg (0.79 rad) (defined as the angle between the line of the billet travel and the horizontal target surface; the heights vary). The spherical surface of the billet serves to concentrate the force of the impact in a small area; the pendulum arrangement gives the impact both a sliding or skidding component as well as a vertical one. The results of the test are expressed in terms of the type of chemical event produced by the impact as a function of impact angle and vertical drop. Chemical events are defined as follows:

0   No reaction; charge retains integrity.

1   Burn or scorch marks on HE or target; charge retains integrity.

2   Puff of smoke, but no flame or light visible in high-speed photography. Charge may retain integrity or may be broken into large pieces.

3   Mild low-order reaction with flame or light; charge broken up and scattered.

4   Medium low-order reaction with flame or light; major part of HE consumed.

5   Violent deflagration; virtually all HE consumed.

6   Detonation

The sliding-impact test results are significant indications of plant-handling safety because the drop heights and impact angles used in the test are quite within the limits one might find for the accidental drop of an explosive billet. The test is used not only to evaluate the relative sensitivity of different explosives using the sand-coated target as a reference surface, but also to evaluate typical plant floor coverings, using LX-10 as a reference explosive."

3.2.2.5 Static Electric Discharge

A human can, in the low humidity environment which often prevails at Pantex, build up enough electrostatic charge to generate a significant electric spark on touching an electrically grounded object. A test to simulate this hazard and to determine the effect on a small explosive sample has been developed (Ref. 3.6).

The electrostatic test apparatus is shown in Figure 3.6. The sample to be tested is placed on a special holder which assures that electrostatic discharge will pass through the sample. A capacitor is charged with a 5000 volt potential. The discharge needle is lowered until a spark is drawn through the sample. Twenty consecutive failures at a given discharge energy level with one initiation at the next higher input constitutes an electrostatic discharge sensitivity test. A new sample is used for each trial.

Secondary high explosives are considered insensitive to static discharge from humans; they may be sensitive to discharges from equipment.

3.2.3 TNT Equivalence

When explosion sources consist of solids or liquids which are high explosives or similar energetic materials containing their own oxidants, all will generate blast waves which are quite similar in character. The strengths and durations of the waves may differ because the explosive materials may have different heats of detonation and combustion, and different densities. Because of the preponderance of measured blast data for TNT explosive, one can make an approximate conversion for other explosives equivalent weight or mass of TNT, based on comparative heats of detonation. These procedures are described in more detail in Chapter 4, while Appendix A includes TNT equivalence numbers for many explosives.

3.2.4 Venting Effects

An explosion occurring within a chamber which is vented, either with uncovered or lightly covered vent openings, will generate internal and external blast loads which can be affected by the degree and configuration of the vents.
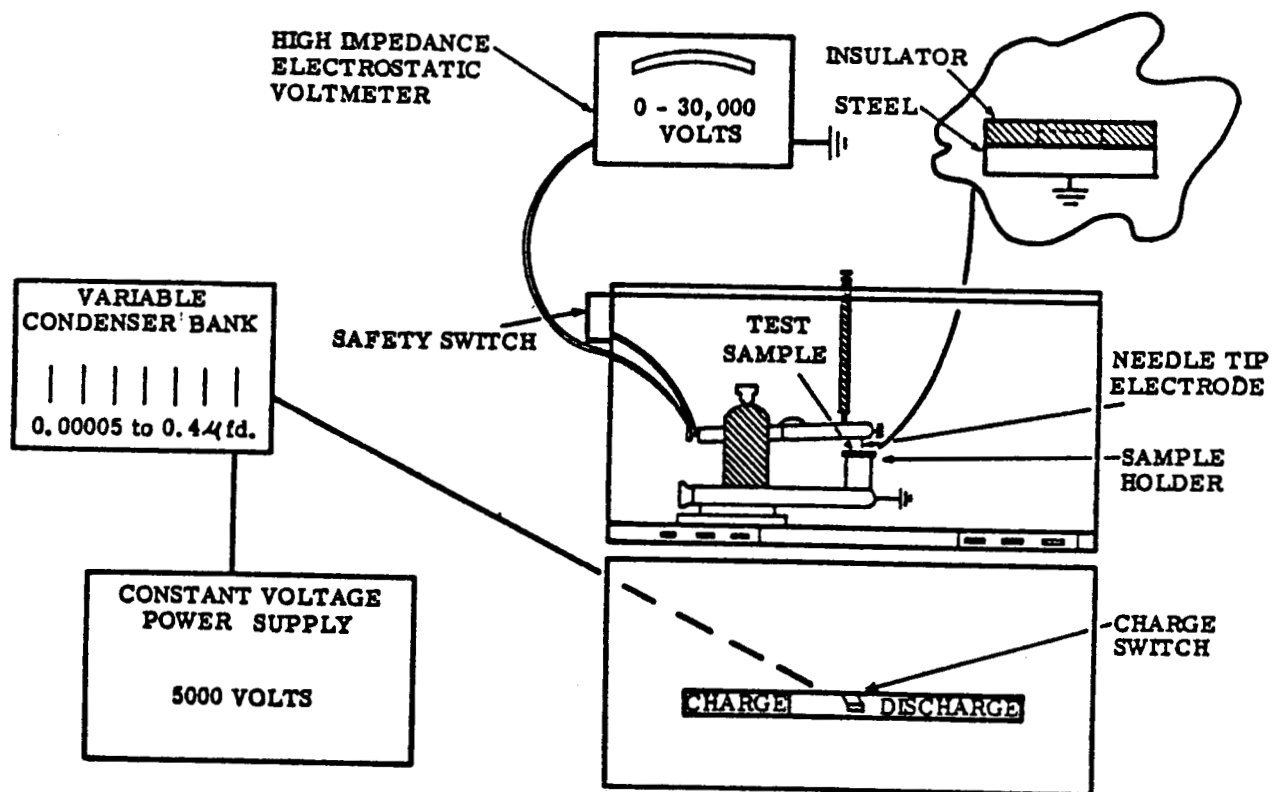
Figure 3.6 Electrostatic Discharge Spark Test Apparatus
(Ref. 3.6)

Within a vented enclosure, the initial air blast loading on the interior surfaces of the enclosure will be mostly unaffected by the vents if even very light vent closures are present. Open vents will have minimal effect on the first reflected internal shock load, but may somewhat attenuate later reflected shocks.

As shocks reverberate within a vented enclosure, they will dissipate after several reflections, but the thermal energy available from the explosion will heat the air and may cause a rise in gas pressure in the enclosure before venting can reduce this pressure.

The processes of shock reflection and subsequent gas pressure rise and decay are described in more detail in Chapter 4. This chapter also gives graphs and equations for predicting the shock and gas loads, and a number of example problems.

When an explosion occurs in a vented enclosure, the venting process can allow some escape of the initial blast wave, particularly if the vents are open. The shock emitted from the vents can be highly directional, and can be intense enough to damage nearby structures or injure people nearby. Directional venting is discussed in Chapter 4; but, for prediction for a variety of vented enclosure configurations, the majority of the prediction curves appear in Reference 3.9. An AE firm is referred to this reference for prediction of blast pressure and impulses outside directionally vented enclosures. For uniformly vented enclosures see Reference 3.10.

3.3 DAMAGE MECHANISMS

3.3.1 Air Blast Loading and Response

The blast wave generated by an explosion in air and being transmitted through the air is characterized primarily as noted earlier, by its transmission velocity U, by a peak overpressure P_s, by a positive phase duration t_d, and by a specific impulse i_s, which is the integral of the overpressure over the positive phase duration. When this wave interacts with any solid object or surface, it reflects from the surface, and diffracts around the object, producing pressure loads which vary rapidly in time, and loads which usually differ markedly from the free-field properties mentioned earlier. In this introductory chapter, we will not discuss these processes in detail, because they are discussed in Chapter 4. Prediction curves and example problems also occur in Chapter 4. Reference 3.3 also gives good general discussions of the reflection and diffraction processes. We merely note here that the blast wave properties important in structural loading are usually reflected overpressure P_r, reflected specific impulse i_r, peak drag pressure Q, and decay constant b, rather than the free-field properties.

Structures, equipment, and personnel loaded by air blast waves often respond to these rapidly varying pressures in a complex manner. Characteristic response times for these "targets" are very important in determining

which blast loading parameters govern response or damage. If the response times are <u>long</u> compared to loading time, specific impulse and the inertia (mass per unit area) of the target usually govern. If the response times are <u>short</u> compared to loading time, peak overpressure and loaded area dominate in determining response. If the response and loading times are similar, all of the parameters mentioned must be considered. The important facet of the response for an AE firm to remember is that these problems are <u>always</u> dynamic response problems, and only in isolated instances can the inertia of the structure and relative loading and response times be ignored.

This manual <u>does not</u> cover dynamic structural response in detail, but elements of such calculation are outlined in Chapter 8. The dynamic response and injury or death to personnel subjected to blast loading are discussed in some detail in Chapter 4, and prediction graphs for effects of blast waves on personnel are included in that chapter, together with example problems.

3.3.2 <u>Fragment Impact Effects</u>

The terms <u>primary</u> fragment and <u>secondary</u> fragment were defined in Section 2.2.4. Recall that primary fragments are usually small, numerous and have high velocity. They can cause damage to structures by penetration or perforation and injure or kill personnel by the same processes. They can also cause initiation of high explosive and consequent escalation of a minor explosive accident into a major one. These effects are discussed in Chapter 6.

Secondary fragments, on the other hand, are usually large, few in number, and have low velocity. They can also be of relatively weak, crushable material such as concrete or wood. They can penetrate or perforate light structures, but are much more apt to cause damage or injury by non-penetrating impact. The state of knowledge for impact effects of the larger and more crushable secondary fragments is poor, but such prediction methods and equations as are available are presented in Chapter 6.

As is true throughout this manual, Chapter 6 also gives example problems to illustrate use of all prediction methods.

3.3.3 <u>Cratering and Debris</u>

Close to buried explosions, the ground is violently displaced and craters are formed. For shallow burial, there can be considerable ejecta which rains down in the vicinity and back into the crater. Buried or surface structures located close to or within the crater radius, or directly over camouflets (deep, buried explosion cavities), can suffer severe damage by being violently displaced. Usually, one simply assumes destruction of any structure within the crater radius for a shallow-buried explosion. Graphs and equations for predicting cratering effects appear in Chapter 5, together with example problems.

3.3.4 Ground Shock

At distances from buried or surface explosions beyond crater radii, ground shock damage can occur to buildings, personnel, and equipment, including buried pipes. Ground shock pulses travel at seismic velocities and are characterized by transient displacements and velocities which look like heavily damped sine waves. Depending on the response time for the structure subjected to ground shock, either the peak velocity or the peak displacement in the ground shock wave may more nearly correlate with maximum response or damage. Response to ground shock waves is discussed in some detail in Chapter 5, with prediction equations and example problems given in that chapter.

3.4 REFERENCES

3.1 Johansson, C. H. and Persson, P. A., Detonics of High Explosives, Academic Press, London and New York, 1970.

3.2 Engineering Design Handbook, Principles of Explosive Behavior, AMCP 706-180, Headquarters, U. S. Army Material Command, Washington, D. C., April 1972.

3.3 Baker, W. E., Explosions in Air, University of Texas Press, Austin, Texas, 1973.

3.4 Kingery, C. N., "Air Blast Parameters Versus Distance for Hemispherical TNT Surface Bursts," BRL Report No. 1344, Aberdeen Proving Ground, Maryland, September 1966.

3.5 "Explosives Hazard Classification Procedures," Department of the Army Technical Bulletin TB 700-2, Department of the Navy Publication NavOrd Inst. 8020.3, Department of the Air Force Technical Order TO 11A-1-47, Defense Supply Agency Reg. DSAR 8220.1, May 19, 1967.

3.6 Hazards of Chemical Rockets and Propellants Handbook, Volume II, Solid Rocket Propellant Processing, Handling, Storage and Transportation, CPIA/194, May 1972, (AD 870 258).

3.7 Ribovich, J., Watson, R., and Gibson, F., "Instrumented Card-Gap Test," AIAA Journal, 6, 7, 1968, pp. 1260-1263.

3.8 Dobratz, Brigitta M., "Properties of Chemical Explosives and Explosive Simulants," UCRL-51319 Rev. 1, U. S. Atomic Energy Commission Contract No. W-7405-Eng-48, Lawrence Livermore Laboratory, University of California, Livermore, California, July 31, 1974.

3.9 Keenan, W. A., and Tancreto, J. E., Technical Report No. R828, "Blast Environment from Fully and Partially Vented Explosions in Cubicles," Civil Engineering Laboratory, Naval Construction Battalion Center, Port Hueneme, California, November 1975.

3.10 "Suppressive Shields Structural Design and Analysis Handbook," (1977), U. S. Army Corps of Engineers, Huntsville Division, HNDM-1110-1-2.

CHAPTER 4

AIR BLAST

4.1 INTRODUCTION

Almost by definition, any accidental explosion which occurs above ground drives an air blast wave into the surrounding atmosphere. This wave can interact with and load the walls of any containment structure; or can exit through venting panels and load nearby structures or other "targets" such as vehicles, humans, etc.; or can load nearby targets if it occurs in the open. It is often the primary source of damage from accidental explosions, and it is all-pervasive, interacting with everything in its path and even being heard as a "bang" or "boom" at distances too great to be damaging.

The Pantex Plant is used as a basis for this study. However, the materials presented are general enough to be applicable to facilities handling HE similar to the operations at Pantex.

The physics of air blast generation and interaction with targets is complex, and is the topic of voluminous literature. Some basic references on this topic for supplemental reading, which provide an understanding of basic air blast physics for single and multiple explosion sources and effects of containment and venting are listed below:

Reference	Topics Covered
4.1	Basic air blast physics and theory, computational methods, blast scaling, diffraction and reflection, experimentation, instrumentation, scaled-blast wave properties, blast transducers, photography, and data reduction methods
4.2	Scaled curves of blast wave properties
4.3	Blast environment within vented and unvented protective structures, blast waves outside vented structures
4.4	Blast physics for explosions in air, scaled blast wave properties
4.5	A compilation of scaled blast wave properties for bare, spherical Pentolite
4.6	General description of accidental explosions, and blast waves from such explosions

Reference	Topics Covered
4.7	Description of blast waves from nuclear weapons explosions

Many more references listed in the bibliography (Appendix B) will also be cited in this chapter.

This chapter:

(1) presents prediction graphs and methods for determining free-field and reflected blast wave properties, and the manner in which these basic properties can be applied to predicting time-varying loads on various structures typical of those in the Pantex Plant;

(2) contains data on properties of explosives which could be involved in accidents in the Pantex Plant;

(3) presents prediction methods for some damage effects which are directly related to air blast wave characteristics, including spalling of concrete walls and the damaging effects of air blast on humans; and

(4) provides illustrative example problems.

4.2 GENERAL

This section includes general information about the classes of explosions and explosives pertinent to potential accidents at the Pantex Plant. Table 4.1 gives the current mission of the Pantex Plant. All but one of the line items in this mission, manufacture of mock high explosive, involve some potential for explosive accidents.

4.2.1 Classes of Explosions Considered

Accidental explosions could, conceivably, occur in various operations so we first review these activities briefly.

In conducting their mission for new production, the Pantex staff receives potentially explosive and inert chemicals and unbonded or loose high explosives, mixes and presses the raw materials, conducts inspections, machines the pressed explosives, assembles explosives components into assemblies, does more inspections, and finally packages and ships the final product. This process flow is shown in Figure 4.1. The potential for chemical explosions exists at many stages of this process, including transport and storage of various quantities of high explosives and explosive chemicals, either in containers or bare or with some type of outer casing or container.

In performing their mission of weapons disposal, Pantex staff receives surplus weapons, inspects them, disassembles them, and disposes of the components. This process flow is shown in Figure 4.2. Until the high explosive

Table 4.1 Pantex Mission

- To manufacture high explosives (HE) and other components and, with supplied components, perform final assembly of nuclear weapons.

- To manufacture mock HE components and, with supplied components, perform final assembly of type units for DOE and DOD testing and training programs.

- To perform new material and stockpile laboratory tests, weapon modifications and repair work necessary on all existing weapons within the U.S. nuclear war reserve.

- To dispose of weapons which are surplus to stockpile requirements.

- To provide technical support in the field of high explosives and to fabricate explosive device components for the design agency laboratories.

- To maintain active portions of the plant facilities for the above activities.
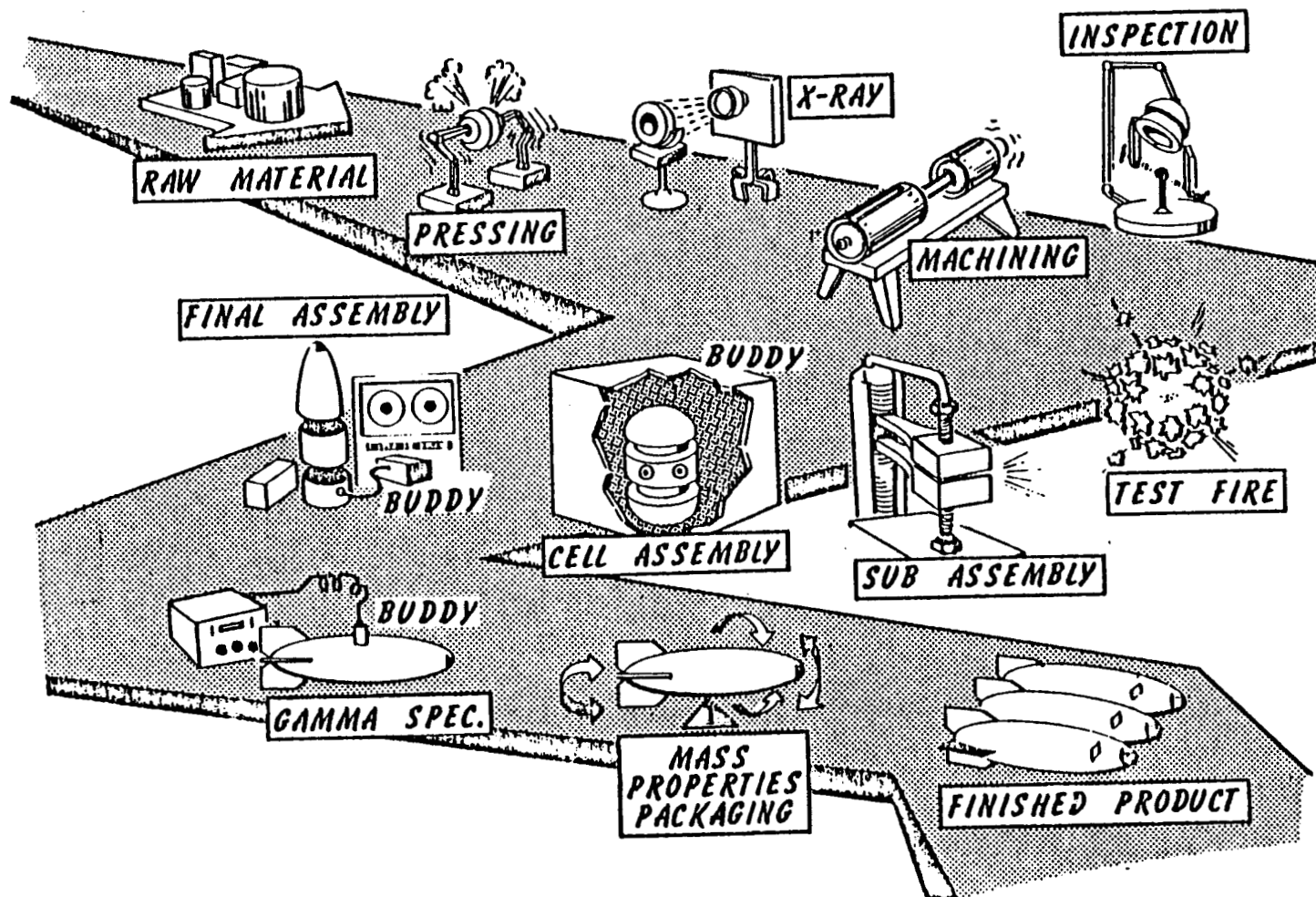
Figure 4.1 Pantex Plant New Production Process Flow

components have been disposed of by burning, there is the potential for accidental explosion during storage, transport and the operations shown in the figure.

Because the potential for accidental explosions in the Pantex Plant involves primarily high explosives, the classes of explosion we must consider in the manual are quite limited. From Reference 4.6, we see that there are many classes of accidental explosions, including such events as simple pressure vessel bursts, runaway chemical reactions in vessels, vapor cloud explosions, molten metal and water reactions, and finally munitions explosions. Even munition explosions often involve violent reactions of solid or liquid propellants which are not true high explosives. So, our task of defining explosion sources for potential accidents at Pantex is somewhat simpler than for accidental explosions in general. We can basically restrict ourselves to high explosive sources.

Elaborate safety precautions are taken at Pantex and other facilities which manufacture high explosives and munitions containing high explosives. Furthermore, only secondary (e.g., relatively insensitive) explosives are handled in potentially damaging quantities in such facilities. But in spite of all precautions and safety regulations, severely damaging explosive accidents have occurred at the Pantex Plant and similar facilities. The most serious accident at Pantex occurred in 1977 during an explosive machining operation in a bay of Building 11-14A (Ref. 4.8), with the detonation of two sizeable pieces of pressed high explosive. Three deaths and severe structural damage resulted. Probably the most spectacular explosion at a facility like the Pantex Plant occurred in 1963 at Medina Facility with detonation of 111,500 pounds of high explosive in a storage magazine (Ref. 4.71). There were no deaths or injuries, but damage at a distance (primarily broken windows) was extensive.

In explosive safety studies, there have been a number of tests simulating HE explosive accidents, on both full and model scale. These tests are too numerous to discuss in detail here, but we note that many are reported in the Minutes of the Explosives Safety Board (DDESB). Specific studies pertinent to this manual are cited in references in various chapters and in the bibliography.

4.2.2 Explosives Considered

This section includes a discussion of the types of high explosives and potential explosives which are or could be present within the Pantex Plant. A number of properties of these explosives are given in Appendix A.

4.2.2.1 Types of Explosives

Most of the types of explosive which could accidentally explode in the Pantex Plant are secondary high explosives which are solid at normal ambient temperatures. Also, all explosives fabrication involves pressing and machining rather than melt casting. So the explosives only exist in the solid

STOCKPILE SURPLUS

RECEIVING & INSPECTION

DISASSEMBLY (LIMITED TESTING)

RECOVERABLE MATERIAL

OTHER VENDORS

METAL COMP. DISP.

PADUCAH KY.

H.E. BURN

PANTEX

NUCLEAR COMP. RECYCLE TO DOE VENDORS

S.R.O.   R.F.   O.R.
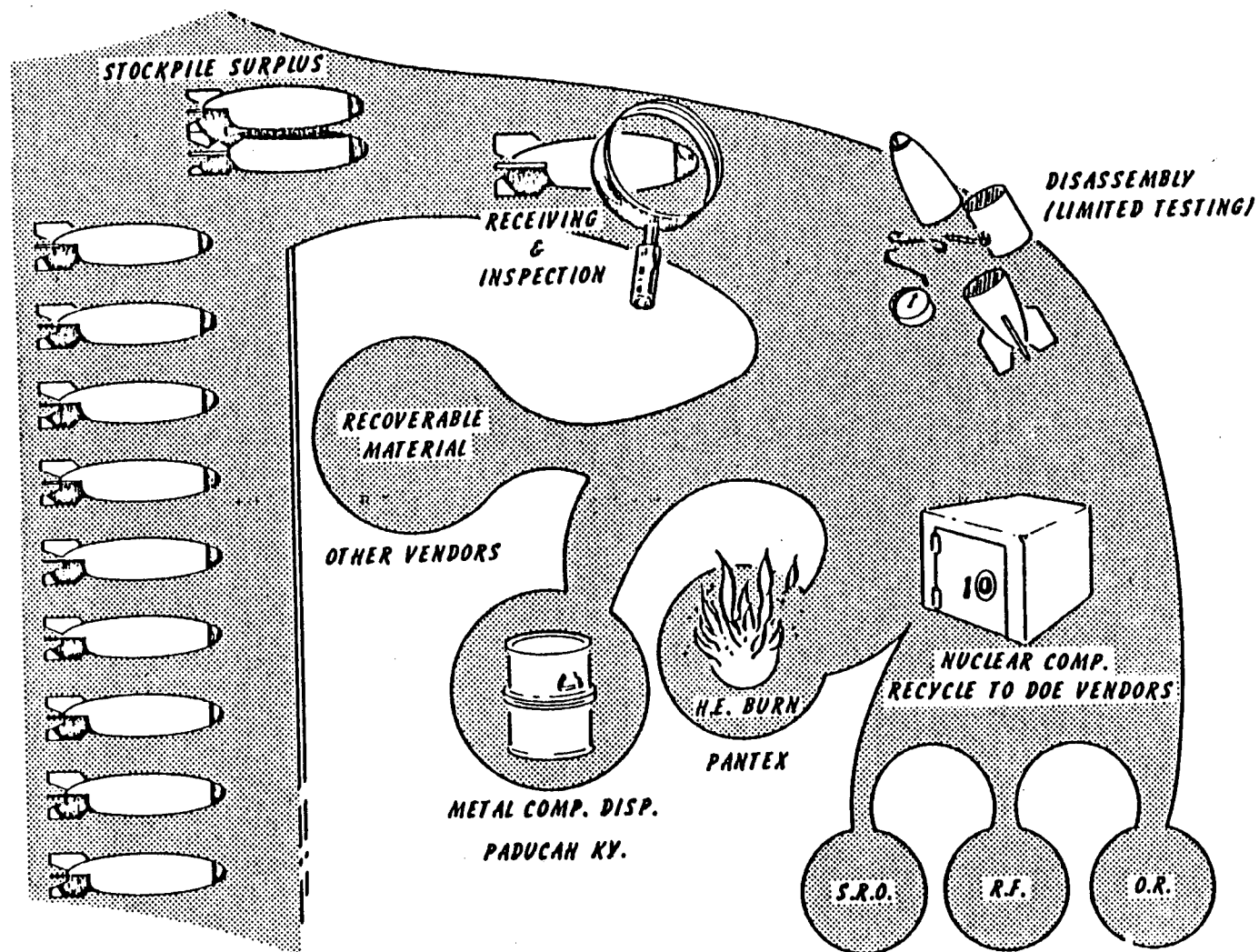
Figure 4.2   Pantex Weapons Disposal

state, regardless of their stage in the processes carried out in the plant. Although solid, the explosives can be in granular or flake form, either mixed with inert bonding materials or by themselves, or they can be consolidated by pressing. No primary explosives are processed in the facility. Some potentially explosive liquid and solid chemicals can be present in those parts of the plant devoted to explosive synthesis. In the plant, explosives, or hardware containing explosive components, are not normally married to other marginally explosive materials such as solid or liquid propellants.

These limitations on the operations and classes of explosives employed in the Pantex Plant narrow the list of materials we need to consider. But there is still an extensive list of high explosive chemical compounds or mixtures of these compounds which are handled in the plant. We give here tables of data available in several references for a number of these explosives and chemicals for ready reference. Primary data sources are References 4.9, 4.10 and 4.11. Because the data are rather voluminous, they are given in tables in Appendix A. The types of data are indicated in Table 4.2.

4.2.2.2 Geometry, Density and Casings

Explosives are present in the Pantex Plant in a wide variety of geometries. Densities range from the average density of loose, flake or granular explosive as it comes from a commercial manufacturer or from the in-house synthesis facility up to densities after pressing, which are close to crystal density for the HE. They can be bare, in light containers for transport about the plant; in packing containers for bulk HE, with one or more metal or other high strength outer casings in a weapon; or with several layers of strong outer casing when a weapon is in a shipping container. To some extent, these variations parallel the possible geometries, densities, and casing variations found in conventional HE weapons manufacture, transport and storage. One notable difference is that the primary damage mechanism for many conventional HE warheads involves high-speed fragmentation. This is not normally the case for the weapons at the Pantex Plant, so the primary fragment hazards should be less severe than at a LAP (Load, Assembly and Pack) plant for fragmentation ordnance.

4.3 BLAST WAVES FROM SINGLE AND MULTIPLE SOURCES

In accidental explosions involving HE, some stimulus usually initiates an explosion in one piece of HE. If this piece is isolated or shielded in some manner so that no other high explosives in the vicinity can be initiated by blast or fragments from the first explosion, then the blast waves come from a single explosion source. But high-speed primary or secondary fragments* can impact other nearby pieces of high explosive, or the intense air shock wave

---

*Fragmentation is discussed in detail in Chapter 6.

Table 4.2 Properties of Explosives and Explosive Chemicals

ITEM	PROPERTY

1   PHYSICAL PROPERTIES

        Common Name
        Chemical Name
        Formulation
        Color
        Physical State
        Theoretical Maximum Density
        Nominal Density
        Molecular Weight
        Melting Point
        Vapor Pressure
        Toxicity

2   CHEMICAL PROPERTIES

        Common Name
        Heat of Formation
        Heat of Detonation
        Heat of Combustion

3   SENSITIVITY AND INITIATION

        Common Name
        Drop Weight Test
        Skid Test
        Friction Pendulum Test
        Explosion Temperature
        Rifle Bullet Impact Test
        Susan Test
        Gap Test

4   MECHANICAL PROPERTIES

        Common Name
        Density
        Hugoniot Intercept
        Hugoniot Slope
        Range of Data

Table 4.2 Properties of Explosives and Explosive Chemicals (Con't)

ITEM	PROPERTY
5	THERMAL PROPERTIES

        Common Name
        Thermal Conductivity
        Thermal Expansion Coefficients
        Specific Heat
        Thermal Stability

| 6 | PERFORMANCE |

        Common Name
        Detonation Velocity
        Chapman-Jouget Detonation Pressure
        Explosive Energy
        Equation of State
        TNT Equivalence
        Critical Energy

from the first explosion can load these same pieces or low-speed skidding and impact can cause initiation and result in deflagration or detonation. The delay time between explosions of multiple sources can be so short that the entire sequence of explosions can be considered as a single simultaneous explosion. On the other hand, for widely separated sources, delays can be great enough that the sequential explosions can be considered to be separate events. In between is a "gray area" where the multiple explosions may or may not be treated as a single explosion.

Our understanding of single-source explosions and the available data and methods for prediction of blast waves characteristics is vastly superior to our knowledge and data for multiple-source explosions. Similarly, our knowledge of blast waves for spherical single sources is superior to our knowledge for other explosion source geometries.

For spherical single-source explosions, we present graphs of scaled compiled data which will allow prediction of many blast parameters, from the surface of the source out to distances where the blast wave is so weak that it is a sound wave. Close to cylindrical blast sources, we give some data on the effect of source geometry. Limited data on sequentially detonated and simultaneously detonated multiple sources are also presented. Implications of blast wave scaling are discussed, without proof.

4.3.1 Single Explosion Source

When a single, high explosive source is initiated by some stimulus, it may burn, deflagrate, or detonate. Detonation is by far the most severe reaction, so in this manual devoted to explosive safety hazards, we will henceforth assume that the explosive detonates.

The physical processes occurring in detonations in high explosives have been exhaustively studied, and are well described in general references such as 4.11 and 4.12. We will discuss these processes only insofar as they affect blast wave properties.

A detonation wave is a very rapid wave of chemical reaction which, once it is initiated, travels at a stable supersonic speed, called the detonation velocity, in a high explosive. Typically, detonation velocities for pressed or cast high explosives range from 22,000 - 28,000 ft/sec. As the detonation wave progresses through the condensed explosive, it converts the explosive within a fraction of a microsecond into very hot, dense, high pressure gas. Pressures* immediately behind the detonation front range from 2,700,000 - 4,900,000 psi.

The most important single parameter for determining air blast wave characteristics of high explosives is the total heat of detonation, E. This

---

*These pressures are called Chapman-Jouget, or CJ, pressures.

quantity is, in general, directly proportional to the total weight W or mass M of the explosive. Any given explosive has a specific heat of detonation, ΔH per unit weight or mass, which can be either calculated from chemical reaction formulas or measured calorimetrically (see References 4.11 and 4.12). So E equals $W \cdot \Delta H$ or $M \cdot \Delta H$, depending on units for ΔH. Values for ΔH for many explosives are given in tables in Appendix A.

If the detonating explosive is bare, the detonation wave propagates out into the surrounding air as an intense shock or blast wave, and is driven by the expanding hot gases which had been the explosive material. If it is encased, the detonation wave simply overpowers the casing material, and drives it outward at high velocity until the casing fragments. The high pressure gases then vent out past the casing fragments and again drive a strong blast wave into the surrounding atmosphere.

As the blast wave expands, it decays in strength, lengthens in duration, and slows down, both because of spherical divergence and because the chemical reaction is over, except for afterburning, as the hot explosion products mix with the surrounding air.

Good descriptions of the characteristics of air blast waves appear in References 4.1, 4.4, and 4.7. The description here is paraphrased from Reference 4.1.

As a blast wave passes through the air or interacts with and loads a structure or target, rapid variations in pressure, density, temperature and particle velocity occur. The properties of blast waves which are usually defined are related both to the properties which can be easily measured or observed and to properties which can be correlated with blast damage patterns. It is relatively easy to measure shock front arrival times and velocities and entire time histories of overpressures. Measurement of density variations and time histories of particle velocity are more difficult, and no reliable measurements of temperature variations exist.

Classically, the properties which are usually defined and measured are those of the undisturbed or side-on wave as it propagates through the air. Figure 4.3 shows graphically some of these properties in an ideal wave (Reference 4.1). Prior to shock front arrival, the pressure is ambient pressure p_o. At arrival time t_a, the pressure rises quite abruptly (discontinuously, in an ideal wave) to a peak value $P_s^+ + p_o$. The pressure then decays to ambient in total time $t_a + t_d^+$, drops to a partial vacuum of amplitude P_s^-, and eventually returns to p_o in total time $t_a + t_d^+ + t_d^-$. The quantity P_s^+ is usually termed the peak side-on overpressure, or merely the peak overpressure. The portion of the time history above initial ambient pressure is called the positive phase, of duration t_d^+. That portion below p_o, of amplitude P_s^- and duration t_d^- is called the negative phase. Positive and negative specific
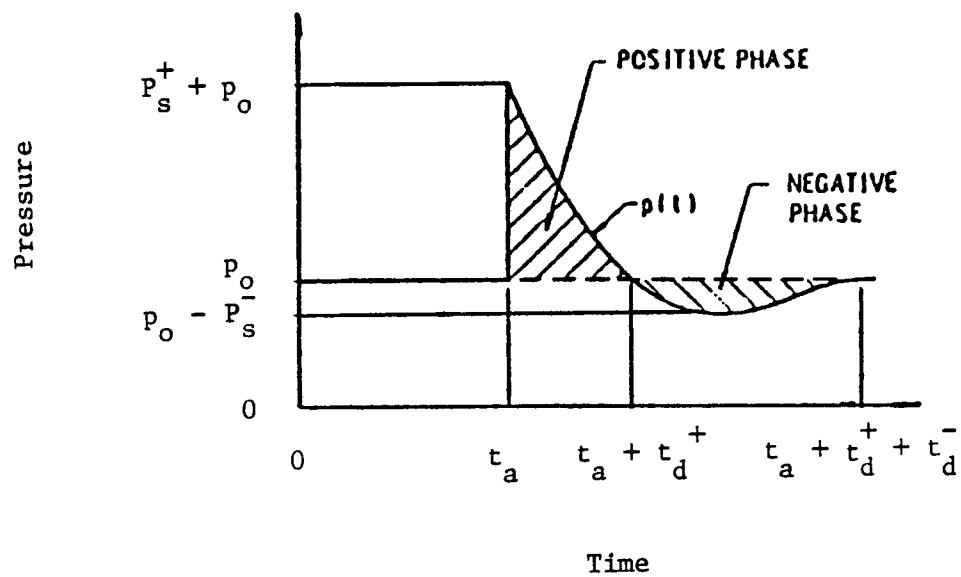
Figure 4.3   Ideal Blast Wave Structure

impulses*, defined by

$$i_S^+ = \int_{t_a}^{t_a + t_d^+} [p(t) - p_o]dt \qquad (4.1)$$

and

$$i_S^- = \int_{t_a + t_d^+}^{t_a + t_d^+ + t_d^-} [p_o - p(t)]dt \qquad (4.2)$$

respectively, are also significant blast wave parameters. These impulses are shown by the cross-hatched areas of Figure 4.3.

In most blast studies, the negative phase of the blast wave is ignored because $P_S^+ \gg P_S^-$ and $i_S^+ \gg i_S^-$, and only blast parameters associated with the positive phase are considered or reported. The positive superscript is then dropped and the parameters without superscripts represent the positive phase. The ideal side-on parameters almost never represent the actual pressure loading applied to structures or targets following an explosion. So a number of other properties are defined to either more closely approximate real blast loads or to provide upper limits for such loads. (The processes of reflection and diffraction will be discussed later in this chapter.) Properties of free-field blast waves other than side-on pressure which can be important in structural loading are:

Density ρ

Particle velocity u

Shock front velocity U

Dynamic pressure $q = \rho u^2/2$

Time constant b

---

*The units of i_S^+ and i_S^- are force times time divided by length squared, or pressure times time. They are, therefore, specific impulse or impulse per unit area, rather than true impulse, which has units of force times time.

Because of the importance of the dynamic pressure q in drag or wind effects and target tumbling, it is often reported as a blast wave property. In some instances drag specific impulse i_d, defined as

$$i_d = \int_{t_a}^{t_a + t_d} q\, dt = \frac{1}{2} \int_{t_a}^{t_a + t_d} \rho\, u^2\, dt \qquad (4.3)$$

is also reported.

Although it is possible to define the potential or kinetic energy in blast waves, it is not customary in air blast technology to report or compute these properties. For underwater explosions, the use of "energy flux density" is more common. This quantity is given approximately by

$$E_f = \frac{1}{\rho_o\, a_o} \int_{t_a}^{t_a + t_d} [p(t) - p_o]^2\, dt \qquad (4.4)$$

where ρ_o and a_o are density and sound velocity in water ahead of the shock.

At the shock front in free air, a number of wave properties are inter-related through the Rankine-Hugoniot equations. The two of these three equations most often used are (Reference 4.1):

$$\rho_s\, (U - u_s) = \rho_o\, U \qquad (4.5)$$

$$\rho_s\, (U - u_s)^2 + p_s = \rho_o\, U^2 + p_o \qquad (4.6)$$

In these equations, subscript s refers to peak quantities immediately behind the ideal shock front, and

$$p_s = P_s + p_o \qquad (4.7)$$

Scaling of the properties of blast waves from explosive sources is a common practice, and anyone who has even a rudimentary knowledge of blast technology utilizes these laws to predict the properties of blast waves from large-scale explosions based on tests on a much smaller scale. Similarly, results of tests conducted at sea level ambient atmospheric conditions are routinely used to predict the properties of blast waves from explosions detonated under high altitude conditions. It is not the purpose in this manual to review or derive laws for scaling of blast wave properties, which are adequately summarized in Reference 4.1. But, we will state the implications of the laws most commonly used.

The most common form of blast scaling is Hopkinson-Cranz or "cube-root" scaling. This law, first formulated by B. Hopkinson (Reference 4.13) and independently by C. Cranz (Reference 4.14), states that self-similar blast waves are produced at identical scaled distances when two explosive charges of similar geometry and of the same explosive, but of different sizes, are detonated in the same atmosphere. It is customary to use as a scaled distance a dimensional parameter,

$$Z = R/E^{1/3} \tag{4.8}$$

or

$$Z = R/W^{1/3} \tag{4.9}$$

where R is the distance from the center of the explosive source, E is the total heat of detonation of the explosive and W is the total weight of a standard explosive such as TNT. The correct equation, Equation 4.8 or 4.9, will be apparent in the problem. Figure 4.4 shows schematically the implications of Hopkinson-Cranz blast wave scaling. An observer located at a distance R from the center of an explosive source of characteristic dimension d will be subjected to a blast wave with amplitude P, duration t_d, and a characteristic time history. The integral of the pressure-time history is the impulse i. The Hopkinson-Cranz scaling law then states that an observer stationed at a distance λR from the center of a similar explosive source of characteristic dimension λd detonated in the same atmosphere will feel a blast wave of "similar" form with amplitude P, duration λt_d and impulse λi. All characteristic times are scaled by the same factor as the length scale factor λ. In Hopkinson scaling, pressures, temperatures, densities and velocities are unchanged at homologous times. Hopkinson's scaling law has been thoroughly verified by many experiments conducted over a large range of explosive charge energies. A much more complete discussion of this law and a demonstration of its applicability is given in Chapter 3 of Baker (Reference 4.1).
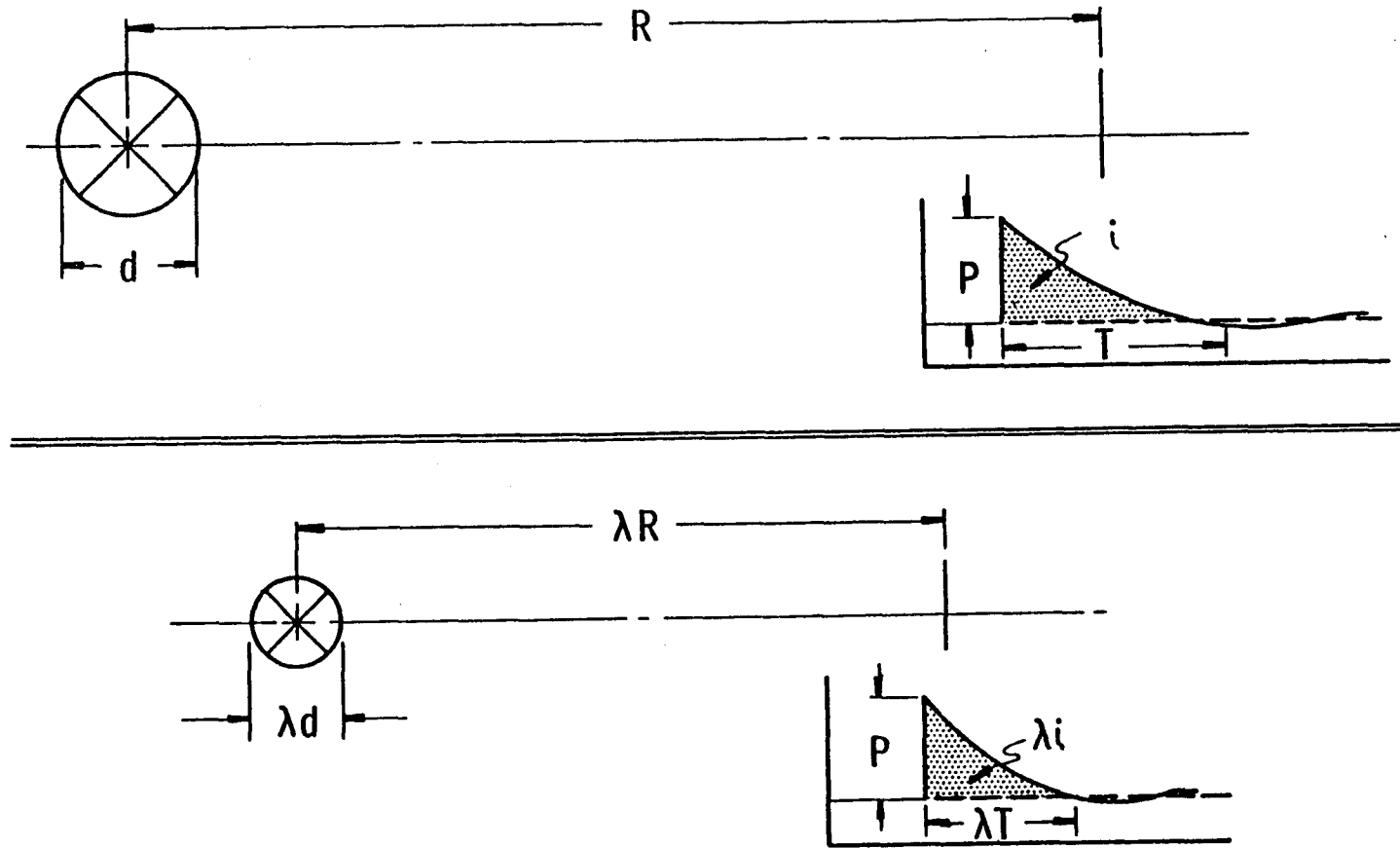
Figure 4.4 Hopkinson-Cranz Blast Wave Scaling

The blast scaling law which is almost universally used to predict characteristics of blast waves from explosions at high altitude is that of Sachs (Reference 4.15). Sachs' law states that dimensionless overpressure and dimensionless impulse can be expressed as unique functions of a dimensionless scaled distance, where the dimensionless parameters include quantities which define the ambient atmospheric conditions prior to the explosion. Sachs' scaled pressure is

$$\overline{P} = (P/p_o) \tag{4.10}$$

Sachs' scaled impulse is defined as*

$$\overline{i} = \frac{ia_o}{E^{1/3} p_o^{2/3}} \tag{4.11}$$

where a_o is ambient sound velocity. These quantities are a function of dimensionless scaled distance, defined as*

$$\overline{R} = R \left(\frac{p_o}{E} \right)^{1/3} \tag{4.12}$$

Both scaling laws apply to reflected blast wave parameters, as well as side-on parameters†.

4.3.1.1 <u>Spherical Geometry</u>

Most of the sources of compiled data for air blast waves from high explosives are limited to bare, spherical explosives in "free-air," i.e., distant from the nearest reflecting surface, or hemisphere in contact or nearly in contact with a good reflecting surface such as the ground. We present here scaled curves for a variety of side-on and normally reflected parameters. The curves are scaled according to the Hopkinson-Cranz (or cube-root) law, and are specific for spherical TNT explosive charges detonated under standard sea level conditions of p_o = 14.696 psi and a_o = 1116 ft/sec.

---

*Note that, if charge weight W is used instead of energy E, these parameters have dimensions.

†See Section 4.4.1.1 for a discussion of blast wave reflection.

The data are given in three large-scale curves, Figures 4.5, 4.6 and 4.7. All three curves employ weight-scaled distance, $Z = R/W^{1/3}$ as abscissae. The usage of "W" refers to TNT-equivalent weights. The subscript "TNT" will henceforth be dropped. Figure 4.5 presents the scaled form of the following parameters:

Peak side-on overpressure, P_s

Side-on specific impulse, i_s

Shock arrival time, t_a

Positive phase duration, t_d

These quantities have all been defined previously. Figure 4.6 presents the parameters:

Peak normally reflected overpressure, P_r

Normally reflected specific impulse, i_r

These quantities are defined in exactly the same manner as the corresponding side-on parameters, but are greater because of pressure enhancement caused by arresting flow behind the reflected shock wave. Durations t_d for the positive phases of normally reflected waves are essentially the same as for side-on waves. Figure 4.7 gives other parameters which are helpful in determining loads on drag-type objects. These quantities are:

Peak scaled particle velocity, $\overline{u}_s = u_s/a_o$

Peak dynamic pressure, Q

Scaled shock velocity, $\overline{U} = U/a_o$

Time constant for pressure decay, b

The quantities u_s and U have already been defined. The quantity Q is the maximum value for dynamic pressure q, i.e.,

$$Q = \rho_s u_s^2/2 \qquad\qquad (4.13)$$

where ρ_s is peak density immediately behind the shock front. The "time constant" b is determined from fitting data to the empirical modified Friedlander equation [See Chapter 1 of Baker (Reference 4.1)],

$$p(t) = p_o + P_s (1 - t/t_d) e^{-bt/t_d} \qquad\qquad (4.14)$$
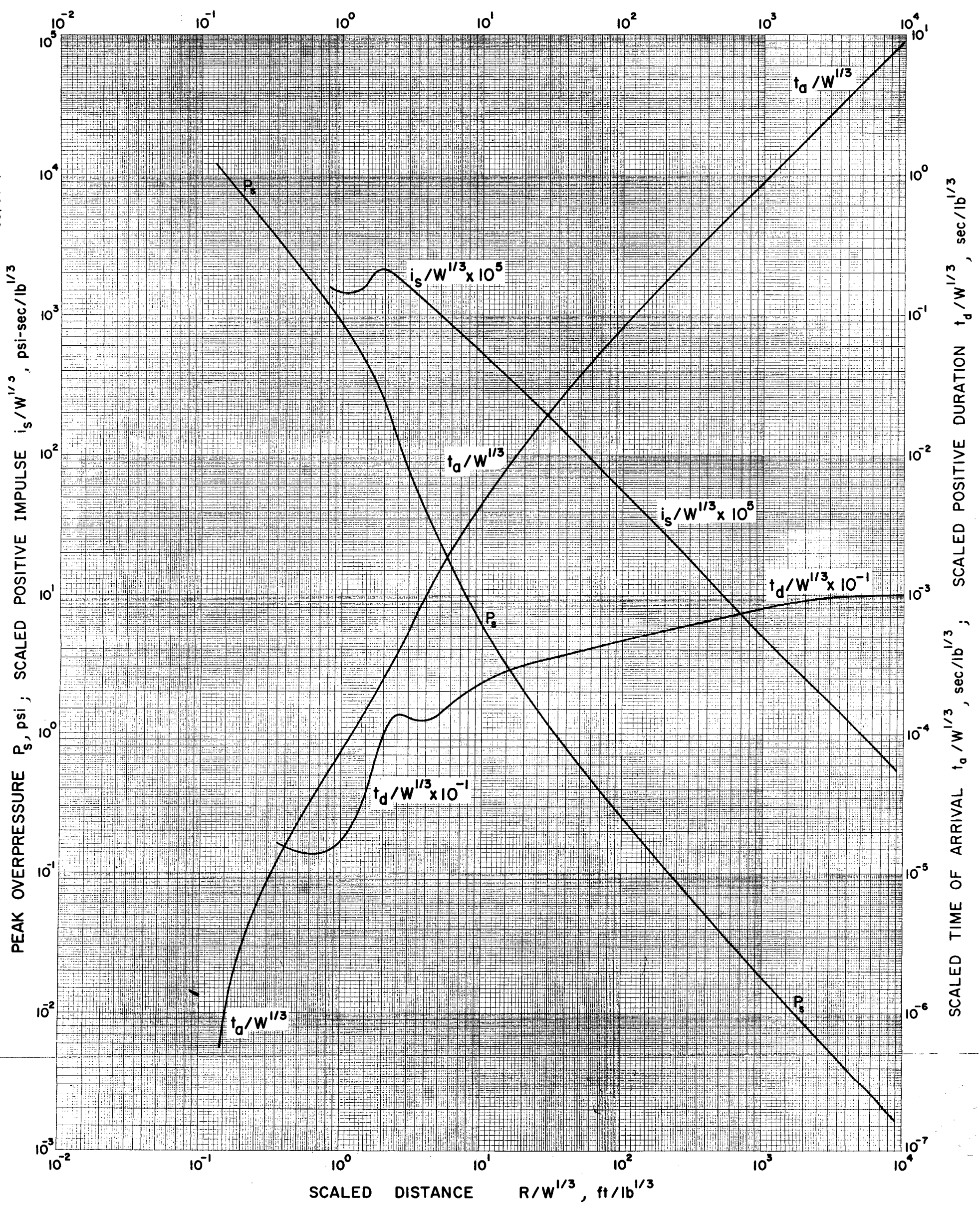
Figure 4.5 Side-On Blast Wave Properties for Bare,
Spherical TNT at Sea Level
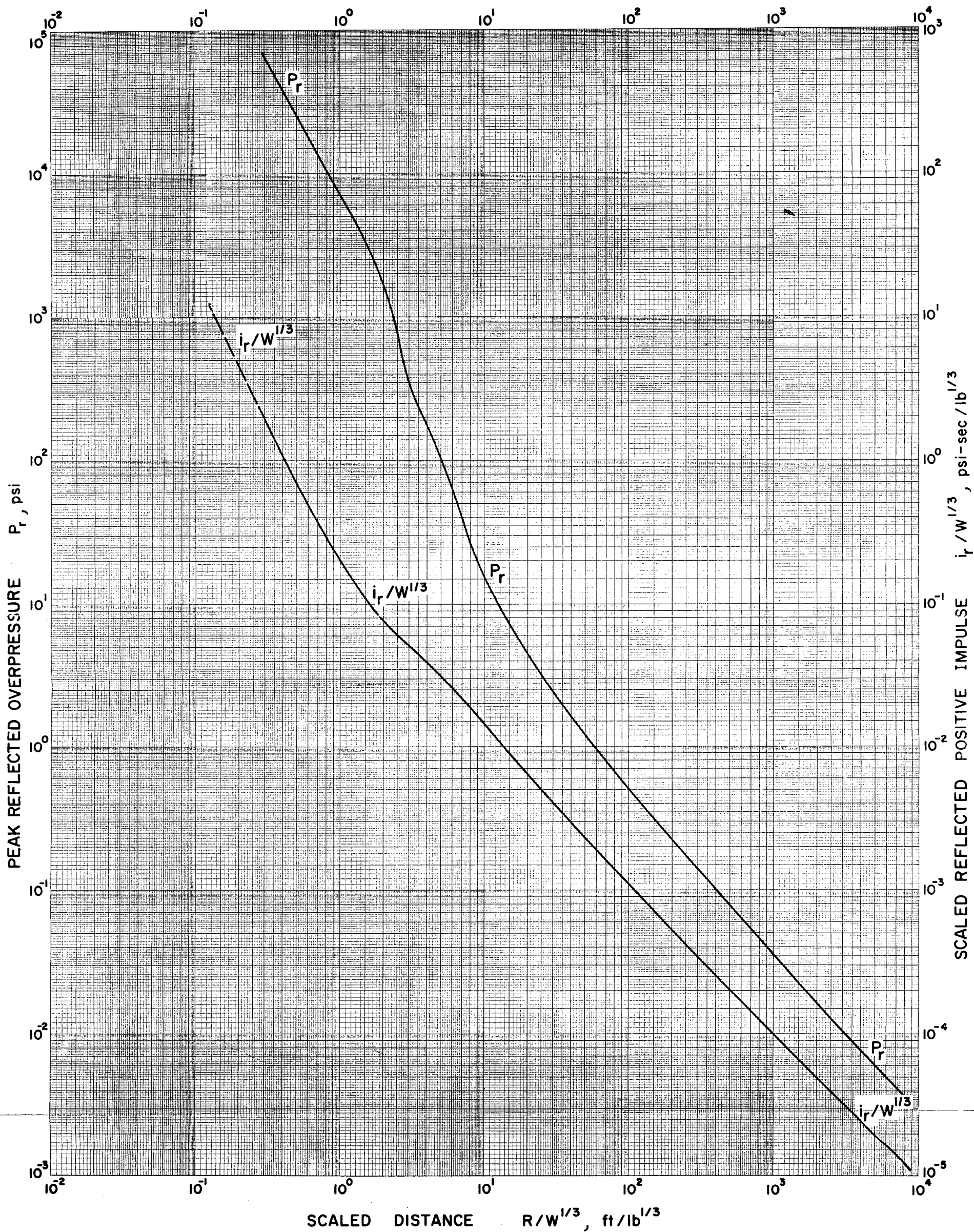
Figure 4.6   Normally Reflected Blast Wave Properties for
Bare, Spherical TNT at Sea Level

Figure 4.7 Blast Wave Properties For Drag And Diffraction Loading;
Bare, Spherical TNT At Sea Level

This equation approximates the positive phase in Figure 4.3. The method of fitting is described in Chapter 6 of Reference 4.1, but the numerical values for b in that reference are in error and have been recalculated correctly in plotting Figure 4.7.

The use of Figures 4.5, 4.6 and 4.7 is given in Section 4.8 in Example Problem 4.17.

One can use the curves in Figures 4.5, 4.6 and 4.7 for ground burst explosions* by adjusting the total charge weight W in the ground burst to account for blast wave strengthening due to ground reflection. For a perfect reflecting surface, the weight is simply doubled, i.e.,

$$W' = 2W \qquad\qquad (4.15)$$

For significant cratering, as normally occurs for high explosives detonated while resting on the ground, fits to data give a lower reflection factor. We suggest then that

$$W' = 1.8W \qquad\qquad (4.16)$$

These new effective weights are then used directly with Figures 4.5, 4.6 and 4.7 to predict blast wave properties for ground bursts. A more complete discussion of surface reflection is given later in this section.

a. Effect of Type of Explosive. Strictly speaking, Hopkinson-Cranz scaling and the curves in Figures 4.5, 4.6 and 4.7 are only valid for spherical TNT explosive. But the character of the blast waves from all condensed high explosives are remarkably similar. Work during World War II (Reference 4.16) gave two different equivalence factors based on comparisons of peak side-on overpressures and side-on specific impulses from a number of different explosives in existence then. The explosive Composition B (60% TNT, 40% RDX by weight) was used as a standard for this work. Swisdak (Reference 4.4) gives "TNT equivalence" curves for several high explosives based on air blast measurements, including a number of cast explosives with and without aluminum. He also gives average TNT equivalence numbers for overpressure and separate numbers for impulse. In a series of very careful free-air blast measurements

---

*TM 5-1300 has separate sets of air blast curves for air burst and ground burst. Those curves will yield essentially identical blast wave properties if one uses the reflection multipliers suggested here. Figures 4.5, 4.6 and 4.7 contain later data than comparable curves in TM 5-1300, and should supplant them.

of TNT and Composition B, Potter and Jarvis (Reference 4.17) found that they could use the equivalence factor 1.0 lb of Composition B = 1.5 lb of TNT over a rather wide range of overpressures.* For four plastic-bonded explosives, PBX-108, PBX-109, AFX-103 and AFX-702, Goodman and Giglio-Tos (Reference 4.18) determined equivalent weight factors compared to 50/50 Pentolite, using values obtained from overpressure and impulse measurements. There have been very few measurements of air blast for detonations of loose or granular high explosives. One can conservatively assume that this material is in its cast or pressed state, but the degree of conservatism is unknown.

In general, the equivalent weight factors found by comparing air blast data from different high explosives vary little with scaled distance, and also vary little dependent on whether peak overpressure or side-on impulse is used for the comparisons. So we feel that a single number to adjust for explosive type will yield quite adequate predictions for the purposes of this manual. (This procedure is used in References 4.3 and 4.12.) When actual comparative blast data exist, as in References 4.4, 4.17 or 4.18, these data can be used to determine a single number for TNT equivalence by averaging. When no such data exist, comparative values of heats of detonation ΔH for TNT and the explosive in question can be used to predict TNT equivalence. These values are given for various explosives in tables in Appendix A.

b. Modified Sachs' Scaling. Sachs' scaling law indicated by Equations 4.10, 4.11 and 4.12 can be used to predict the variation of blast wave properties with ambient conditions other than the sea-level conditions for which Figures 4.5, 4.6 and 4.7 were prepared. The Pantex Plant is located about 3500 ft above sea level, so the mean ambient conditions differ measurably from those at sea level. To apply Equations 4.10, 4.11 and 4.12, the ambient atmospheric pressure and sound velocity must be known. Since sound velocity is a function of temperature, it would suffice to know ambient pressure and temperature. An adequate estimate of their value can be obtained, provided the altitude is known, from Reference 4.19:

$$p = 14.6965 \left[\frac{288.15}{288.15 - 1.9812 \times 10^{-3}\ H} \right]^{-5.25588} \text{(psi)} \qquad (4.17)\dagger$$

---

*See Appendix A for present recommended value.

†Many significant figures are given in Reference 4.19 to allow calculation with fair accuracy over very large altitude changes. One should round to no more than four significant figures after calculation.

$$a = 65.77 \left[288.15 - 1.9812 \times 10^{-3} \, H \right]^{1/2} \, (\text{ft/sec}) \qquad (4.18)*$$

where H is altitude relative to sea level, in feet.

The equations represent the "U. S. Standard Atmosphere, 1976."

For the Pantex Plant located at an altitude of 3500 feet, p_0 and a_0 would have calculated standard values of 12.93 psia and 1103 feet per second, respectively, in contrast to the standard sea level values of 14.70 psia and 1116 feet per second.

All blast parameter values for bare, spherical HE can be determined from Figures 4.5 through 4.7 with the aid of Sachs' scaling law for atmospheric conditions other than those at sea level. The following computational procedure should be used:

1. Calculate Hopkinson-scaled distance,

$$Z = R/W^{1/3} \, \text{ft/lb}^{1/3}. \qquad (4.19)$$

2. Calculate a "corrected" Z* value to account for ambient atmospheric pressure p at altitude H:

$$Z* = Z(p/p_0)^{1/3}. \qquad (4.20)$$

3. Utilizing the proper blast parameter curve (Figures 4.5 through 4.7), find the blast parameter value corresponding to the Z* value.

4. Multiply the value obtained in (3) by the proper "correction factor" from Table 4.3 to obtain a blast parameter value adjusted to atmospheric conditions at altitude H.

Example problem 4.17 in Section 4.8 illustrates the above procedure for all blast parameters in Figures 4.5 through 4.7. This calculation shows that the corrections for the blast parameters side-on pressure and side-on specific impulse are less than 10 percent for all scaled distances. So, an AE firm need not formally apply this correction for design of Pantex facilities.

---

*Many significant figures are given in Reference 4.19 to allow calculation with fair accuracy over very large altitude changes. One should round to no more than four significant figures after calculation.

Table 4.3 "Correction Factors" for Blast Parameters
for Altitude Atmospheric Conditions

Parameter	Correction Factor[†]
Side-on overpressure, P_s	p/p_o
Reflected overpressure, P_r	p/p_o
Dynamic pressure, Q	p/p_o
Side-on specific impulse, i_s	$(p/p_o)^{2/3} \cdot \left(\dfrac{a_o}{a}\right)$
Reflected specific impulse, i_r	$(p/p_o)^{2/3} \cdot \left(\dfrac{a_o}{a}\right)$
Time of arrival, t_a	$\left(\dfrac{a_o}{a}\right)\left(\dfrac{p_o}{p}\right)^{1/3}$
Duration of overpressure, t_d	$\left(\dfrac{a_o}{a}\right)\left(\dfrac{p_o}{p}\right)^{1/3}$
Shock velocity, U	1
Peak particle velocity, u_s	1
Decay constant, b	1
Scaled distance, Z	$\left(\dfrac{p}{p_o}\right)^{1/3}$

[†]p and a are ambient atmospheric conditions at altitude H, while p_o and a_o are ambient atmospheric conditions at sea level.

$p_o = 14.6965$ psia

$a_o = 1116.4$ ft/sec

Equations 4.17 and 4.18 yield standard accepted estimates of the pressure and sonic velocity at an altitude H. The actual pressure and sonic velocity will vary about the standard accepted values according to local meteorological activity at time of explosion. Extreme meteorological activity (e.g., severe thunderstorms, abnormal temperature variations) could appreciably change the ambient atmospheric conditions from the standard accepted values at a given altitude. But, these variations are much less than the variation due to altitude alone, and no corrections need be made by an AE firm, if he also ignores altitude correction.

c. <u>Normal Reflection</u>. An upper limit to blast loads is obtained if one interposes an infinite, rigid wall in front of the wave, and reflects the wave normally. All flow behind the wave is stopped, and pressures are considerably greater than side-on. The pressure in normally reflected waves is usually designated $p_r(t)$, and the peak reflected overpressure, P_r. The integral of overpressure over the positive phase, defined in Equation (4.21), is the reflected specific impulse i_r. Durations of the positive phase of normally reflected waves are almost the same as for side-on waves, t_d. The parameter i_r has been measured closer to high explosive blast sources than have most blast parameters.

$$i_r = \int_{t_a}^{t_a + t_d} [p_r(t) - p_o] \, dt \qquad (4.21)$$

The Hopkinson-Cranz scaling law described earlier applies to scaling of reflected blast wave parameters just as well as it does to side-on waves. That is, all reflected blast data taken under the same atmospheric conditions for the same type of explosive source can be reduced to a common base for comparison and prediction. Sachs' law for reflected waves fails close to high explosive blast sources but it does apply beyond about ten charge radii.

The literature contains considerable data on normally reflected blast waves from high explosive sources, usually bare spheres of Pentolite or TNT [Goodman (Ref. 4.5), Jack and Armendt (Ref. 4.20), Dewey, et al. (Ref. 4.21), Johnson, et al. (Ref. 4.22), Jack (Ref. 4.23), Wenzel and Esparza (Ref. 4.24)]. So, from these sources, it is possible to construct scaled curves for P_r and i_r for specific condensed explosives over fairly large ranges of scaled distance. Figure 4.6 shows one such pair of curves. Measurements for reflected specific impulse extend in to smaller scaled distances, i.e., closer to the blast source, than do measurements of reflected pressure because a much simpler measurement technique suffices for specific impulse measurement [Johnson, et.al. (Ref. 4.22) and Dewey, et al. (Ref. 4.21)]. Furthermore, reflected specific impulses can be predicted in to the surface of a condensed spherical explosive source, using a simple formula applicable in the strong shock regime given by Baker (Ref. 4.25).

$$i_r = \frac{(2M_T E)^{1/2}}{4\pi R^2} \qquad (4.22)$$

where

$$M_T = M_E + M_A \qquad (4.23)$$

is total mass of explosive M_E plus mass of engulfed air M_A, and R is distance from the charge center. Very close to the blast source, $M_E \gg M_A$, and Equation (4.22) gives a simple $1/R^2$ relation for variation of i_r with distance, for strong shocks. This relation is also noted by Dewey, et al. (Ref. 4.21). Equation (4.22) is used to plot the dashed portion of the curve for scaled i_r in Figure 4.6.

Unfortunately, for explosive sources other than bare spheres of solid high explosives, very little data exist for normally reflected pressures and specific impulses. For shock waves weak enough that air behaves as a perfect gas, there is a fixed and well-known relation between peak reflected overpressure and peak side-on overpressure [Doering and Burkhardt (Ref. 4.26), Baker (Ref. 4.1)],

$$\overline{P}_r = 2\,\overline{P}_s + \frac{(\gamma + 1)\,\overline{P}_s^{\,2}}{(\gamma - 1)\,\overline{P}_s + 2\gamma} \qquad (4.24)$$

where

$$\overline{P}_r = P_r/p_o \qquad (4.25)$$

and

$$\overline{P}_s = P_s/p_o \qquad (4.26)$$

At low incident overpressures ($\overline{P}_s \to o$), the reflected overpressure approaches the acoustic limit of twice the incident overpressure. If one were to assume a constant $\gamma = 1.4$ for air for strong shocks, the upper limit would appear to be $\overline{P}_r = 8\overline{P}_s$. But, air ionizes and dissociates as sho strengths increase, and γ is not constant. In fact, the real upper limit

ratio is not exactly known, but is predicted by Doering and Burkhardt (Ref. 4.26) to be as high as 20. Brode (Ref. 4.27) has also calculated this ratio for normal reflection of shocks in sea level air, assuming air dissociation and ionization. His equation, given without noting its limits of applicability, is, for P_s in psi,

$$\frac{P_r}{P_s} = \frac{2.655 \times 10^{-3} P_s}{1 + 1.728 \times 10^{-4} P_s + 1.921 \times 10^{-9} P_s^{\ 2}} + 2 +$$

$$\frac{4.218 \times 10^{-3} + 4.834 \times 10^{-2} P_s + 6.856 \times 10^{-6} P_s^{\ 2}}{1 + 7.997 \times 10^{-3} P_s + 3.844 \times 10^{-6} P_s^{\ 2}} \qquad (4.27)$$

We have calculated this ratio, and have used Figure 4.5 to determine corresponding scaled distances, for a wide range of side-on overpressures. Results are tabulated in Table 4.4. They reach the proper low pressure asymptote of twice side-on peak overpressure, and agree remarkably well with the empirical fit to data for P_r in Figure 4.6. The ratio for the perfect gas, Equation (4.24) is also included for comparison. One can see that, above $P_s = 100$ psi and standard atmosphere conditions, the latter equation is increasingly in error and should not be used. Brode's equation gives a maximum reflection factor at the surface of a spherical HE charge at sea level of $P_r/P_s = 13.92$. Use of this formula is an improvement over predictions from TM 5-1300, and should be used in preference to that reference at small-scaled distances.

    d. Oblique Reflection. Although normally incident blast wave properties usually provide upper limits to blast loads on structures, the more usual case of loading of large, flat surfaces is represented by waves which strike at oblique incidence. Also, as a blast wave from a source some distance from the ground reflects from the ground, the angle of incidence must change from normal to oblique.

    There have been many theoretical studies of oblique shock wave reflection from plane surfaces, and some experiments. The general physical processes are well described in References 4.1, 4.16 and 4.28.

    We will summarize their work here and present curves which can be used to estimate some of the properties of obliquely reflected waves; usually shock front properties and geometry only.

Table 4.4 Normally Reflected Blast Wave Overpressures
for Standard Sea-Level Ambient Conditions

$R/W_{TNT}^{1/3}$, ft/lb$^{1/3}$	P_s, psi	P_r/P_s (Brode) Eq. (4.27)	P_r, psi Based On Eq. (4.27)	P_r/P_s † Perfect Gas Eq. (4.24)
33.64	1	2.055	2.055	2.058
11.88	5	2.250	11.25	2.278
7.765	10	2.478	24.79	2.532
3.612	50	3.862	193.1	3.962
2.793	100	4.930	492.8	4.958
1.425	500	7.565	3,783.0	(6.976)
0.8931	1,000	8.559	8,559.0	(7.440)
0.2611	5,000	11.96	59,800.0	(7.879)
0.1471	10,000	13.60	136,000.0	(7.939)
0.1272*	12,040	13.92	167,600.0	(7.949)

* Denotes scaled distance corresponding to surface of spherical TNT charge.

† Parentheses in this column indicate values which are too greatly in error
to be used.

Oblique reflection is classed as either <u>regular</u> or <u>Mach</u> reflection, dependent on incident angle and shock strength. Geometries of these two cases are shown in Figures 4.8 and 4.9. In regular reflection, the incident shock travels into still air (Region One) at velocity U, with its front making the angle of incidence α_I with respect to the wall. Properties behind this front (Region Two) are those for a free air shock. On contact with the wall, the flow behind the incident shock is turned, because the component normal to the wall must be zero, and the shock is reflected from the wall at a reflection angle α_R that is different from α_I. Conditions in Region Three indicate reflected shock properties. A pressure transducer flush-mounted in the wall would record only the ambient and reflected wave pressures (direct jump from Region One to Region Three) as the wave pattern traveled along the wall; whereas, one mounted at a short distance from the wall would record the ambient pressure, then the incident wave pressure, and finally the reflected wave pressure. Some interesting properties of this regularly reflected shock, given by Kennedy (Ref. 4.16) are as follows:

1. For a given strength of incident shock, there is some critical angle of incidence $\alpha_{extreme}$, such that the type of reflection described above cannot occur for $\alpha_I > \alpha_{extreme}$.

2. For each gaseous medium there is some angle α such that for $\alpha_I > \alpha´$ the strength of the reflected shock is greater than it is for head-on reflection. For air (approximated as an ideal gas with $\gamma = 1.40$), $\alpha´ = 39°23´$.

3. For a given strength of incident shock, there is some value for $\alpha_I = \alpha_{min}$ such that the strength of the reflected shock, P_r/p_o is a minimum.

4. The angle of reflection α_R is an increasing monotonic function of the angle of incidence α_I.

As noted in the discussion of regular oblique reflection, there is some critical angle of incidence, dependent on shock strength, above which regular reflection cannot occur. In 1877, Ernst Mach showed that the incident and reflected shocks would coalesce to form a third shock. Because of the geometry of the shock fronts, they were termed the Mach V or Mach Y, with the single shock formed by the coalesced incident and reflected shocks normally called the Mach stem. The geometry of Mach reflection is shown in Figure 4.9. In addition to the incident and reflected shocks I and R, we now have the Mach shock M; the junction T of the three shocks is called the triple point. In addition, there is also a slipstream S, a boundary between regions of different particle velocity and different density, but of the same pressure. When α_I in Figure 4.8 exceeds $\alpha_{extreme}$, the Mach wave M is formed at the wall and grows as the shock systems move along the wall with the locus of the triple point being a straight line AB.
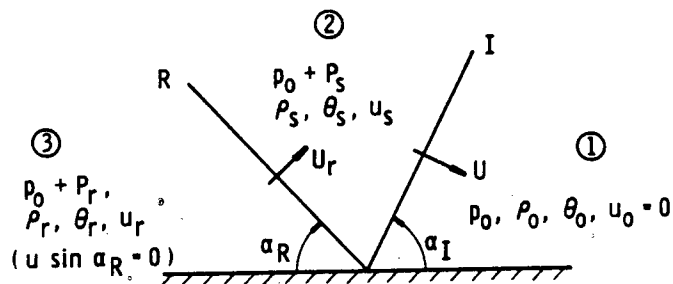
Figure 4.8 Regular Oblique Reflection Of A Plane Shock
From A Rigid Wall (Reference 4.16)
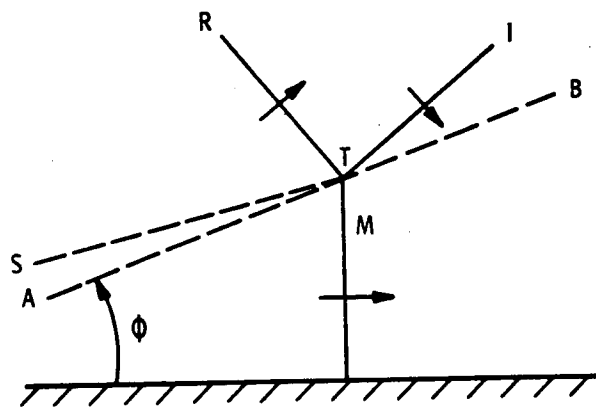
Figure 4.9 Mach Reflections From A Rigid Wall
(Reference 4.16)

Harlow and Amsden (Ref. 4.28) present a resume of theory and experiment on regular reflection and the limit of regular reflection (which is also the start of Mach reflection). Two useful curves from their paper are given here. Figure 4.10 gives angle of reflection α_R as a function of angle of incidence α_I in the regular reflection regime. The parameter ξ is defined as

$$\xi = \frac{P_o}{P_s + P_o} \qquad (4.28)$$

[Harlow and Amsden (Ref. 4.28) call ξ the shock strength, but it is, in fact, the inverse of the shock strength.] Inverting Equation (4.28) we also have the relation

$$\bar{P}_s = \frac{P_s}{P_o} = \frac{1}{\xi} - 1 \qquad (4.29)$$

A set of curves from the literature (Ref. 4.7) is included as Figure 4.11 to allow prediction of reflected peak pressure for oblique shocks. These curves give P_r/P_s as a function of P_s and α_I for incident shock overpressures P_s up to 50 psi.

There are some recent data for strong blast waves reflected from a nearby wall which include both normal and oblique reflections (Refs. 4.24 and 4.43). The test arrangement includes a number of flush-mounted pressure transducers in the wall. The data are shown in Figures 4.12 and 4.13. In these figures, X is the horizontal distance from the normal to the wall through the charge center and R is standoff, measured to the charge center (See Figure 4.14). These data are at much greater pressures than the data in Figure 4.11, but do not cover all shock front obliquities. There are curves given as Figure 4-6 in TM 5-1300 which show reflection factors for both strong and weak shocks as a function of obliquity. The lower curves in that figure agree well with Figure 4.11, but the origin of the curves for strong shocks is not known. The sharp drops in all of the upper curves in that figure at $\alpha_I = 45°$ do not agree with the data in Figure 4.12.

The AE is cautioned that there are significant data gaps in prediction of pressures and impulses for oblique reflections, and that additional experiments and code calculations are needed to fill these gaps. In a specific problem at Pantex, DOE will provide guidance.

e. Effect of Casing on Air Blast. Because of fragility and initiation sensitivity, most HE in weapon systems is encased in a tough, exterior shell or case. Experimental data indicate that blast parameters of cased HE
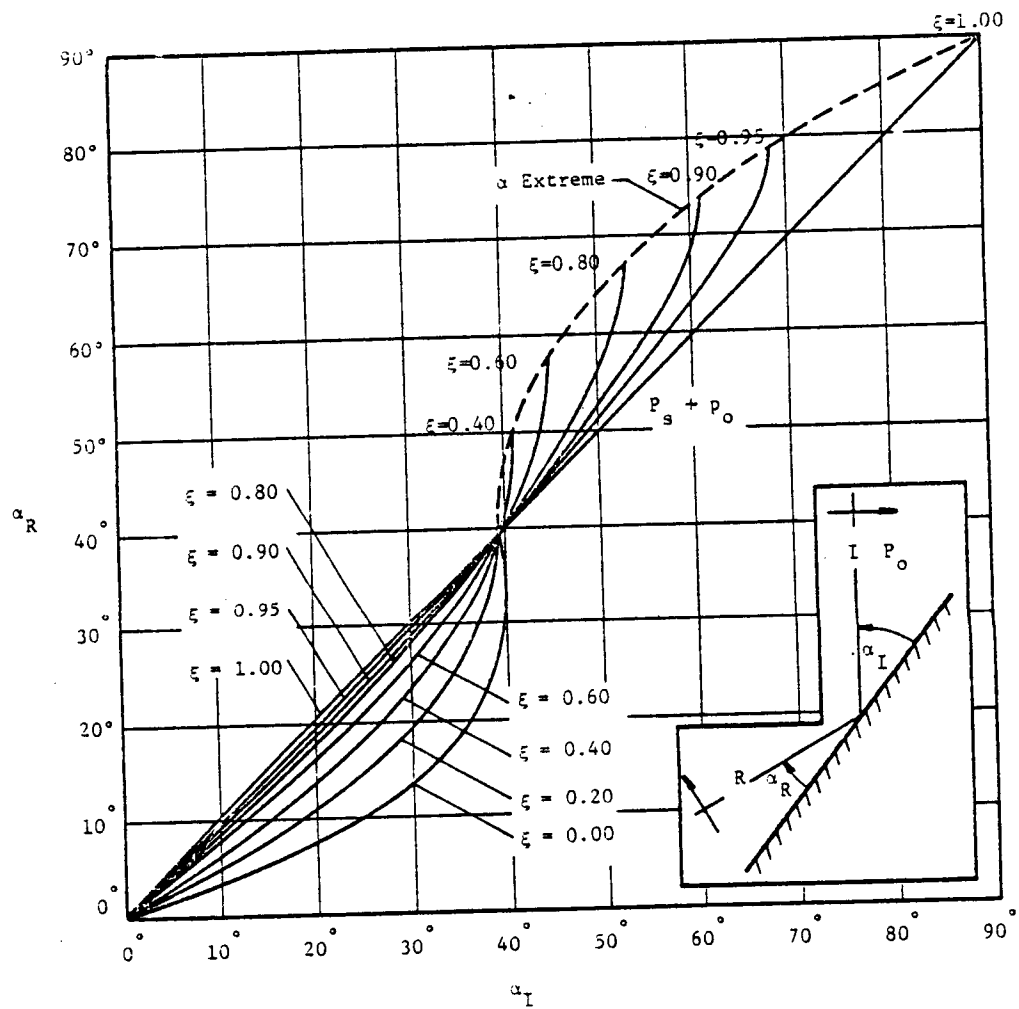
Figure 4.10 Angle of Incidence versus Angle of Reflection
for Shocks of Different Strengths Undergoing Regular Reflection
(Reference 4.28)
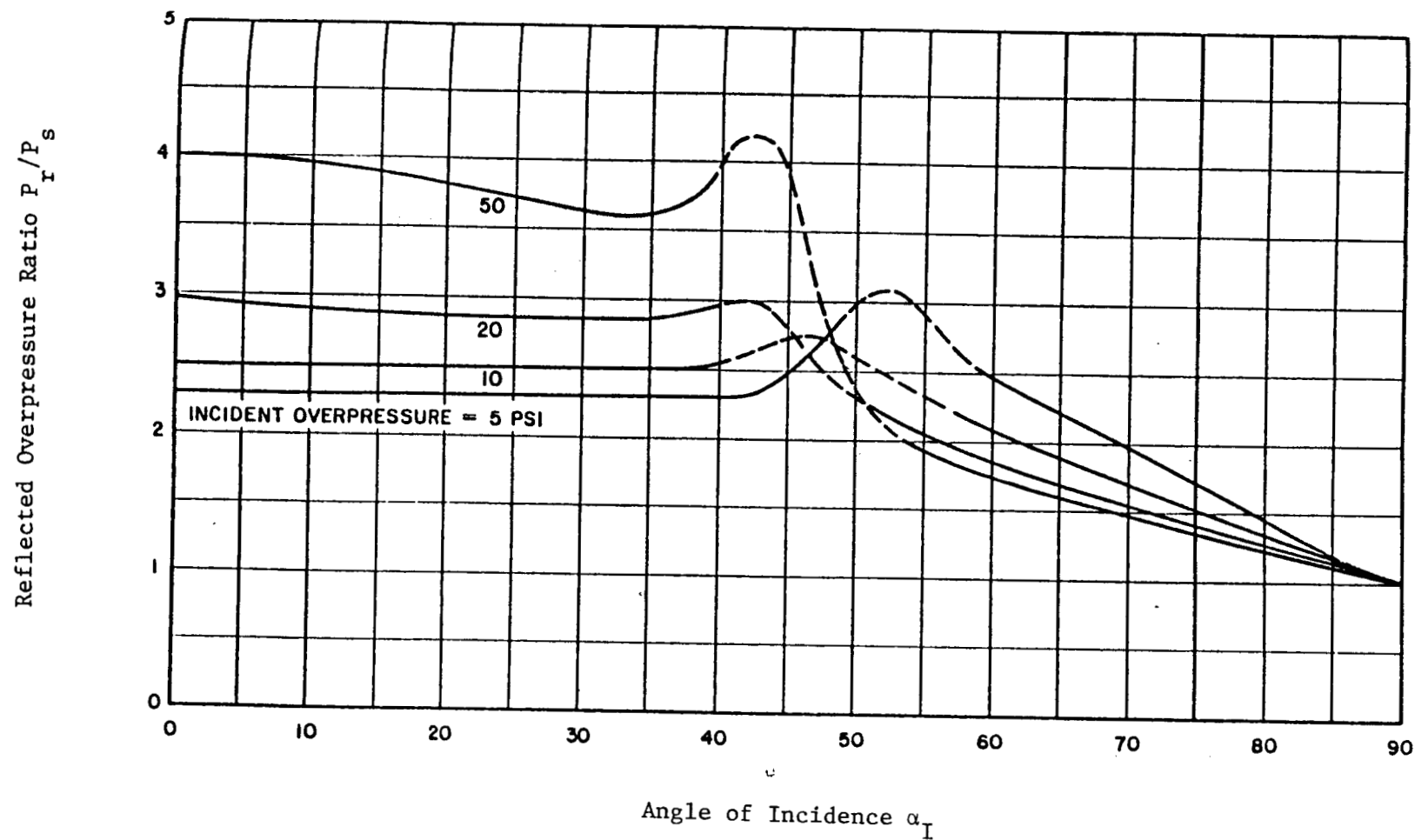
Figure 4.11   Reflected Overpressure Ratio as Function of Angle of Incidence
for Various Side-On Overpressures (Reference 4.7)

100,000
50,000
20,000
10,000
5,000
2,000
1,000
500
200
100

Peak Reflected Overpressure P_r, psi

Line	Z $(ft/lb^{1/3})$
1	0.3
2	0.6
3	0.8
4	1.3
5	1.5
6	1.6
7	3.0

0   1   2   3   4   5
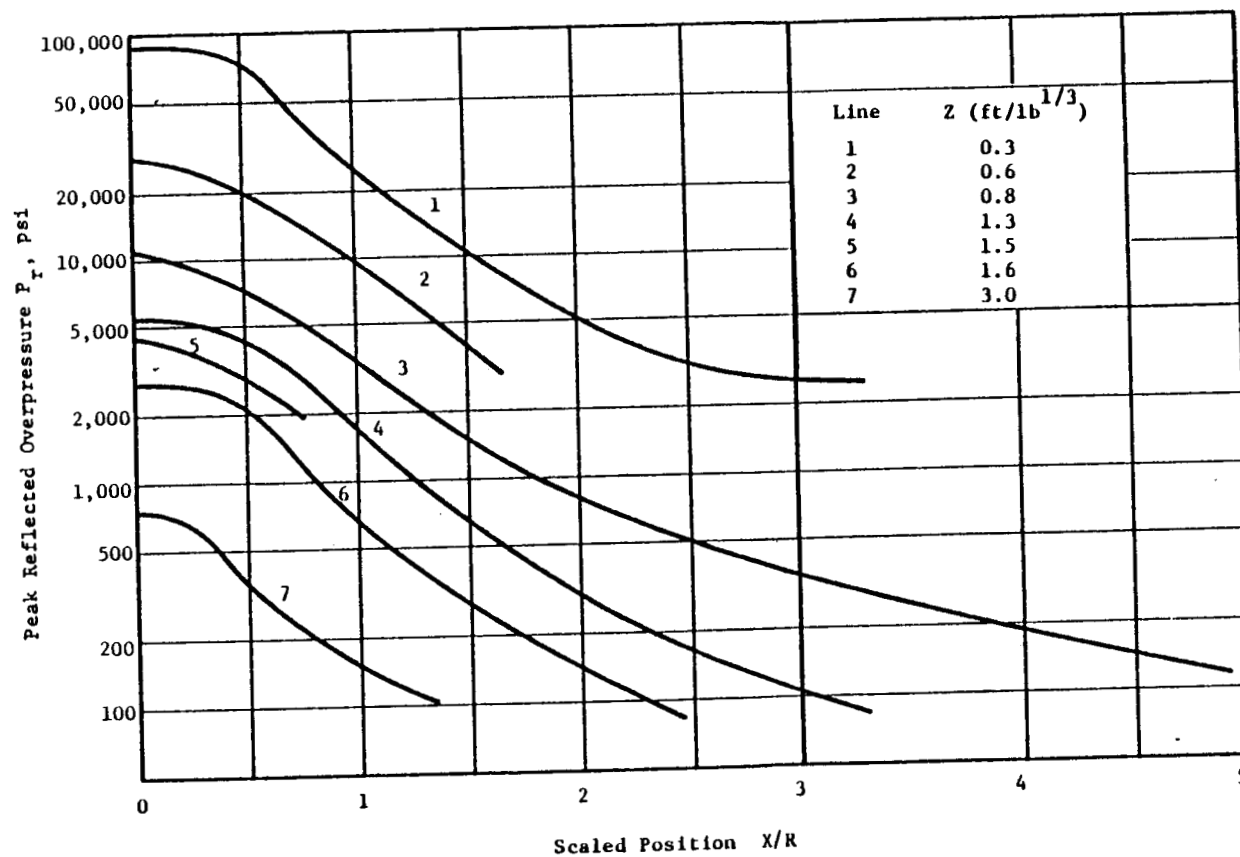
Scaled Position X/R

Figure 4.12   Peak Overpressure versus Scaled Position for Different Scaled
Distances for Single Charge (Reference 4.43)
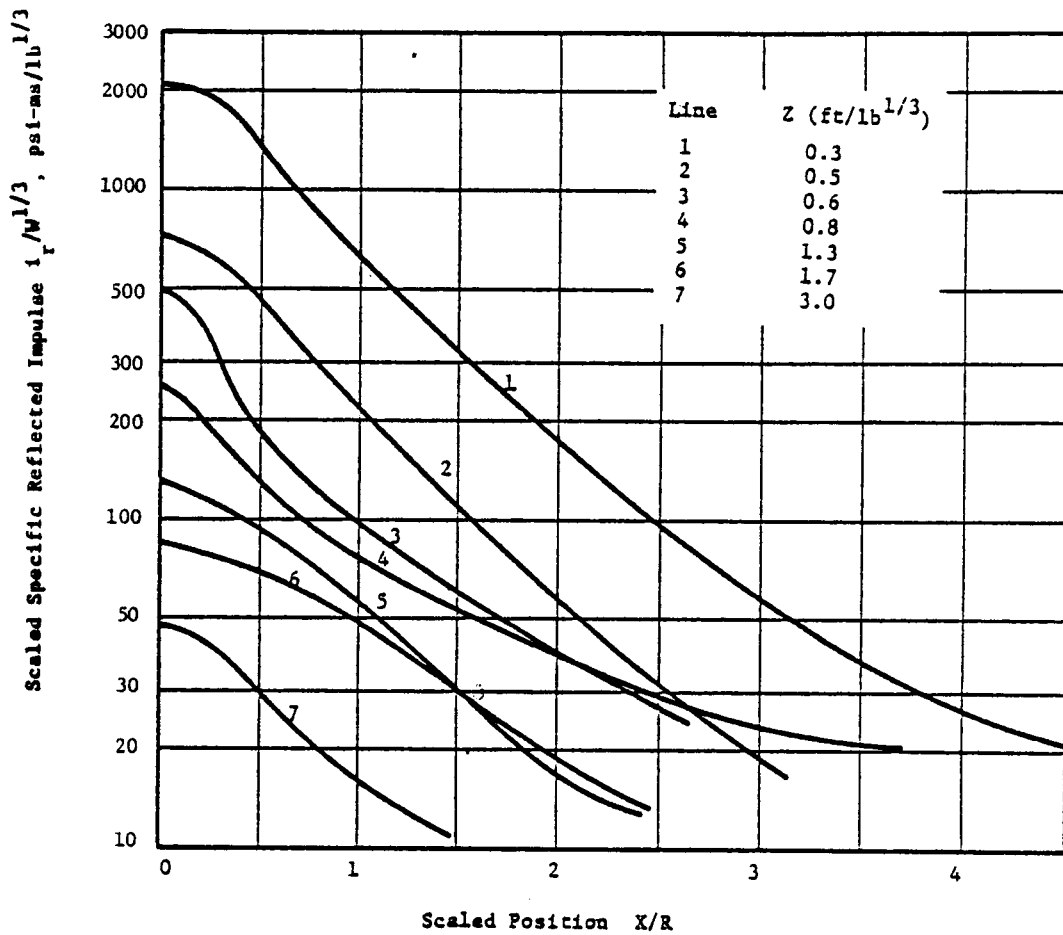
Figure 4.13   Scaled Specific Impulse versus Scaled Position
for Different Scaled Distances for Single Charge
(Reference 4.43)
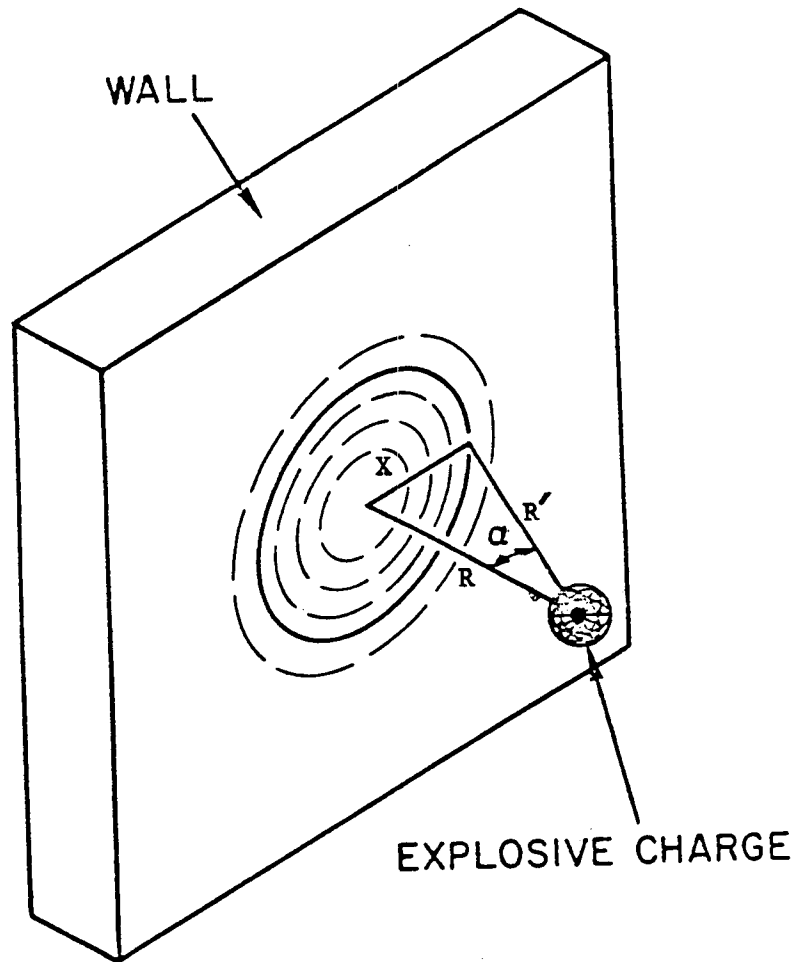
Figure 4.14 Explosive Charge Loading on a Wall as a Function of Position

are significantly different from those determined for bare charges, as obtained from Figures 4.5 through 4.7. The addition of casing to an explosive charge changes the functional format of the blast parameters; no longer are they simply a function of scaled standoff ($R/W^{1/3}$), but they become functions of other variables. Additional variables which could be important, besides standoff distance R and charge weight W are:

1. case weight, W_c,

2. case material properties such as toughness and density,

3. case thickness,

4. explosive properties such as detonation velocity and density.

Charge shape and ambient atmospheric conditions could also be important; however, these variables complicate the analysis and are treated in separate sections. The cased charges discussed in this section will, therefore, be assumed spherical in shape with mean sea level atmospheric conditions. The addition of a large number of independent variables to the functional format for blast parameters has the undesirable effect of increasing the difficulty of determination of the contribution of any single variable. The net result is the need for a large amount of experimental data of the "proper" type, that is, in a test matrix in which the contribution of each variable is investigated systematically. With such a large number of variables, assumptions have been made by various investigators to simplify matters. One approach is to assume that the only variable significantly contributing to the blast parameters other than charge weight W and standoff R, is casing weight, W_c. An equivalent bare charge weight, W', can then be defined. An equivalent scaled distance,

$$Z' = R/(W')^{1/3} \qquad (4.30)$$

is calculated and the blast parameters are obtained as previously described from Figures 4.5 through 4.7. Various functional formats for determination of W' have been suggested by different investigators (Ref. 4.30), with Equation (4.31) giving the best fit for steel-cased explosives.

$$W' = \left[0.2 + \frac{0.8}{(1 + W_c/W)}\right] W \qquad (4.31)$$

Figure 4.15 is a plot of this equation, with experimental data plotted as points. The data points for steel-cased explosives fit equation (4.31) rather well. But, the remaining data points for other materials can be seen to agree very poorly with the equation.

2.45
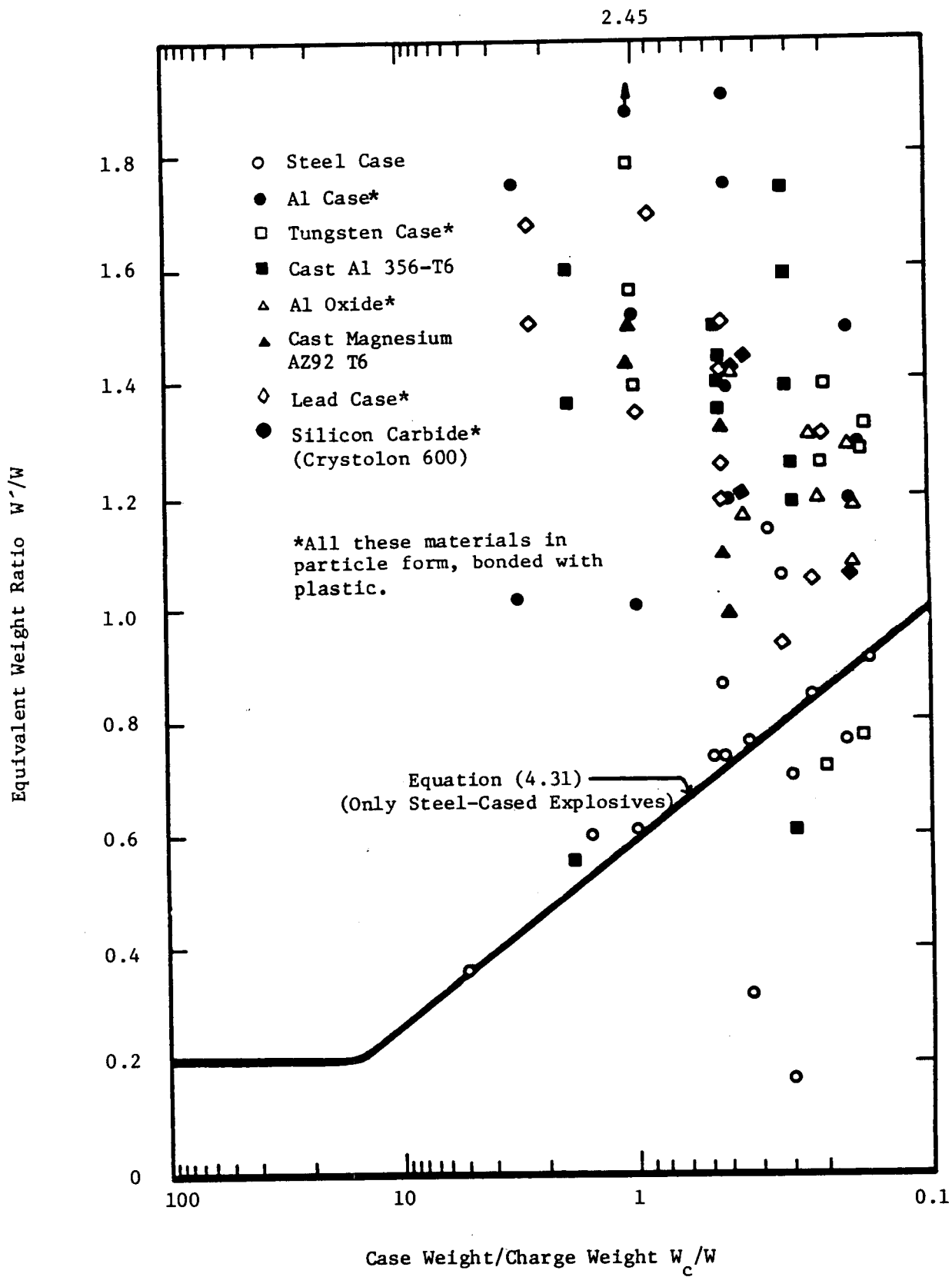
Figure 4.15 Various Methods For Predicting Case Effects

The remaining data were obtained from a test program conducted at BRL [Dewey, et al. (Ref. 4.30)]. The purpose of the test program was to determine a more accurate functional format for determination of blast parameters for cased charges in order to obtain maximum lethality at close scaled stand-off distances $(1 \leq R/W^{1/3} \leq 3 \text{ ft/lb}^{1/3})$. The legend in Figure 4.15 indicates that a variety of materials were used as casings, and W' is generally greater than W, the charge weight. All materials used as casings were highly brittle or were held together with a brittle matrix material. It was also found by Dewey, et al. (Ref. 4.30) that W' itself is dependent on R for a given charge weight W and that Sachs' scaling did not apply to charges cased with light, frangible materials. Dewey, et al. suggested an alternative functional format which seemed to fit the data particularly well for reflected specific impulse. A modified scaled distance is defined:

$$Z' = \frac{R}{(W + W_c)^{1/3}} \tag{4.32}$$

The blast parameters are then calculated as previously stated per Figures 4.5 through 4.7. Equation (4.32) effectively adds the casing mass as additional HE. Specific impulse retains the same energy scaling factor $(W')^{1/3}$ as do duration and arrival time. The data from BRL (Dewey, et al.) and also from a test program conducted by NOL [Filler (Reference 4.31)] are used as the basis for Figures 4.16 through 4.18. The data extend to a maximum scaled distance of 15 $\text{ft/lb}^{1/3}$ Pentolite. The individual data points are not plotted (except for steel casing); rather, a data range is plotted together with a solid curve for bare HE. Pentolite 60/40 was used in both test programs, and hence, W is in pounds of Pentolite 60/40. Note that the steel-cased charges (circles in Figure 4.18) produce the greatest discrepancy in accord with the results of Figure 4.15.

Various explanations have been proposed for the increase in the effective explosive weight W' over bare charge weight W. One proposed explanation is that the casing prevents spallation of HE from the surface of a charge during detonation, effectively increasing the effective charge weight W' over bare charge weight W. Another theory is that a mechanical efficiency is involved, or "impedance matching" between the explosion gases and the casing material. There is an obvious need for more experimental investigation in this subject area.

In addition to a specific impulse from air blast, the shell casing, from the momentum in its fragments, imparts an additional structural specific impulse. The total specific impulse which must be resisted by a structure is the sum of the specific impulses from air blast and from fragments. Although these separate specific impulses do not arrive at the
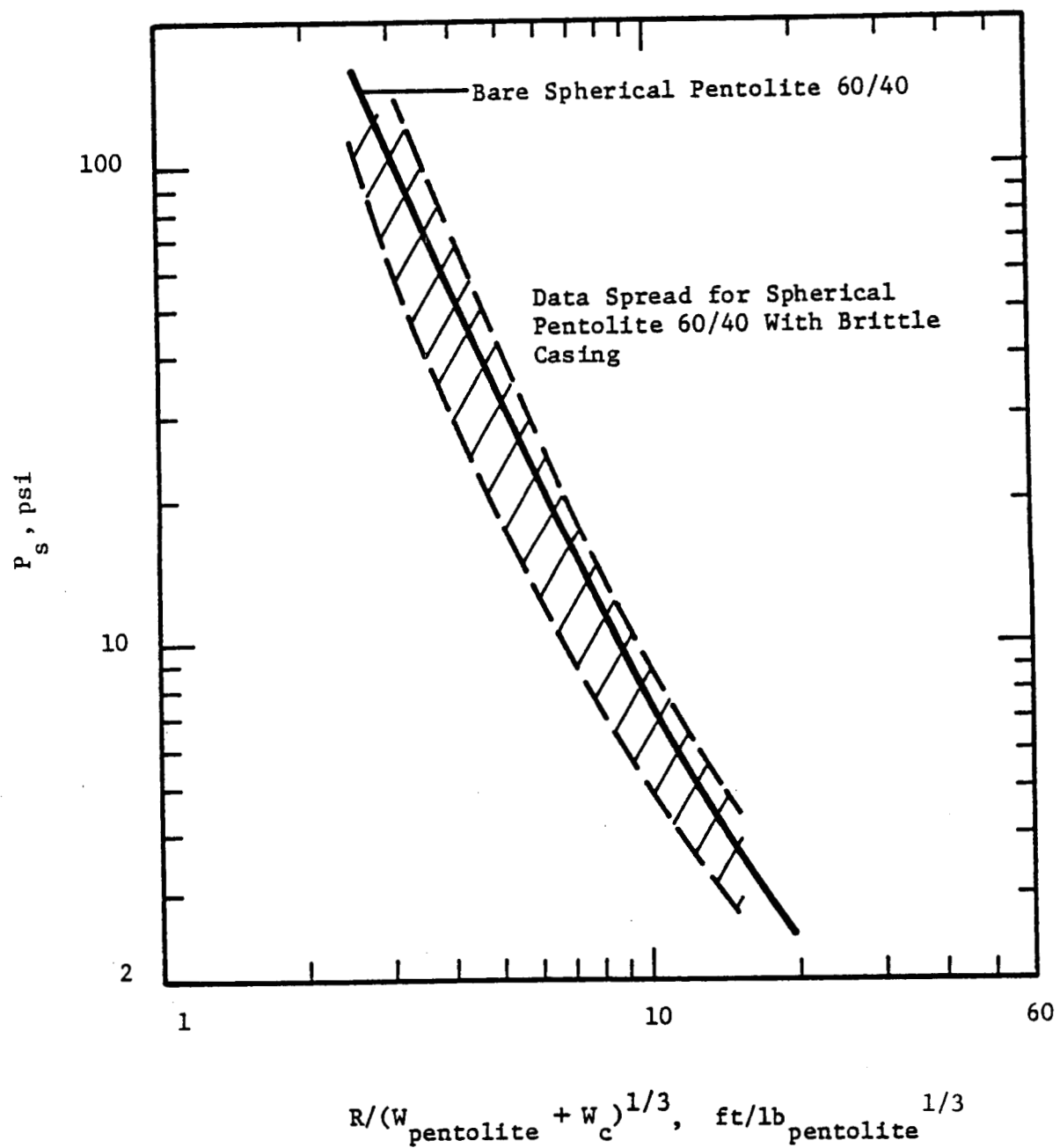
Figure 4.16   Peak Side-On Overpressure for Spherical Pentolite
60/40 with Light, Brittle Case
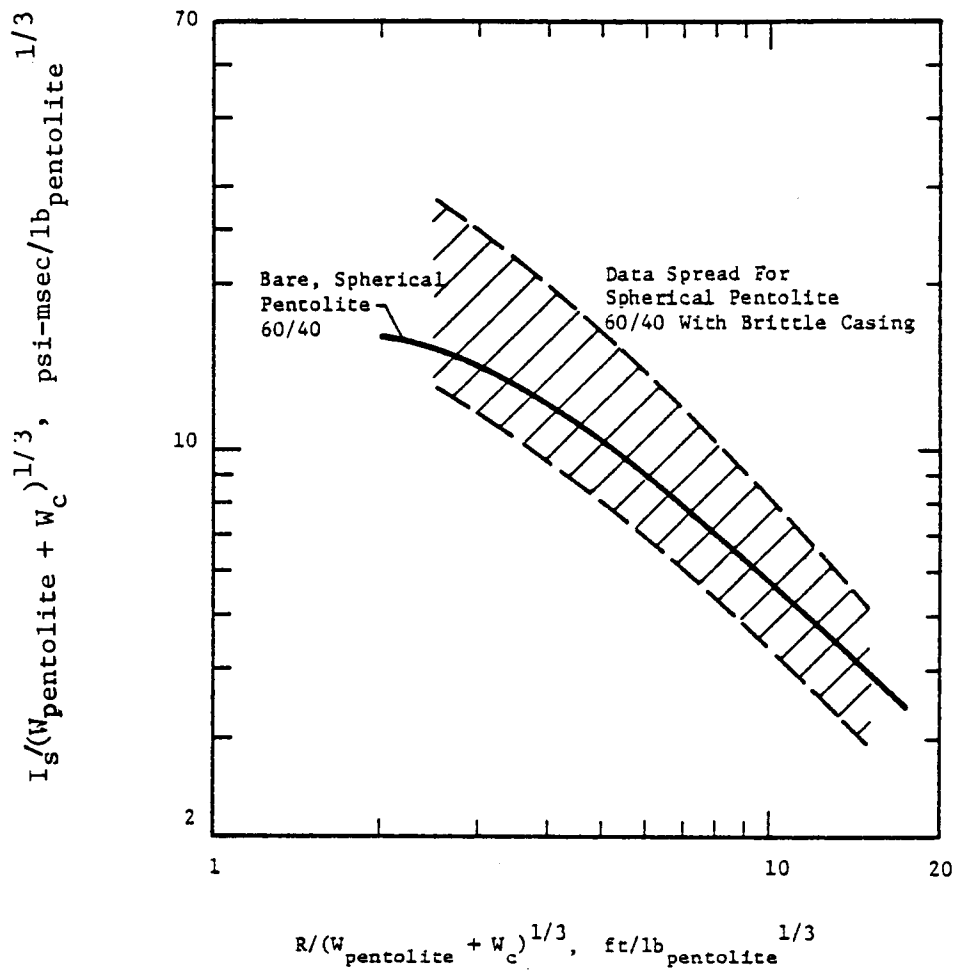
Figure 4.17   Scaled Side-On Impulse for Spherical Pentolite
60/40 with Light, Brittle Case
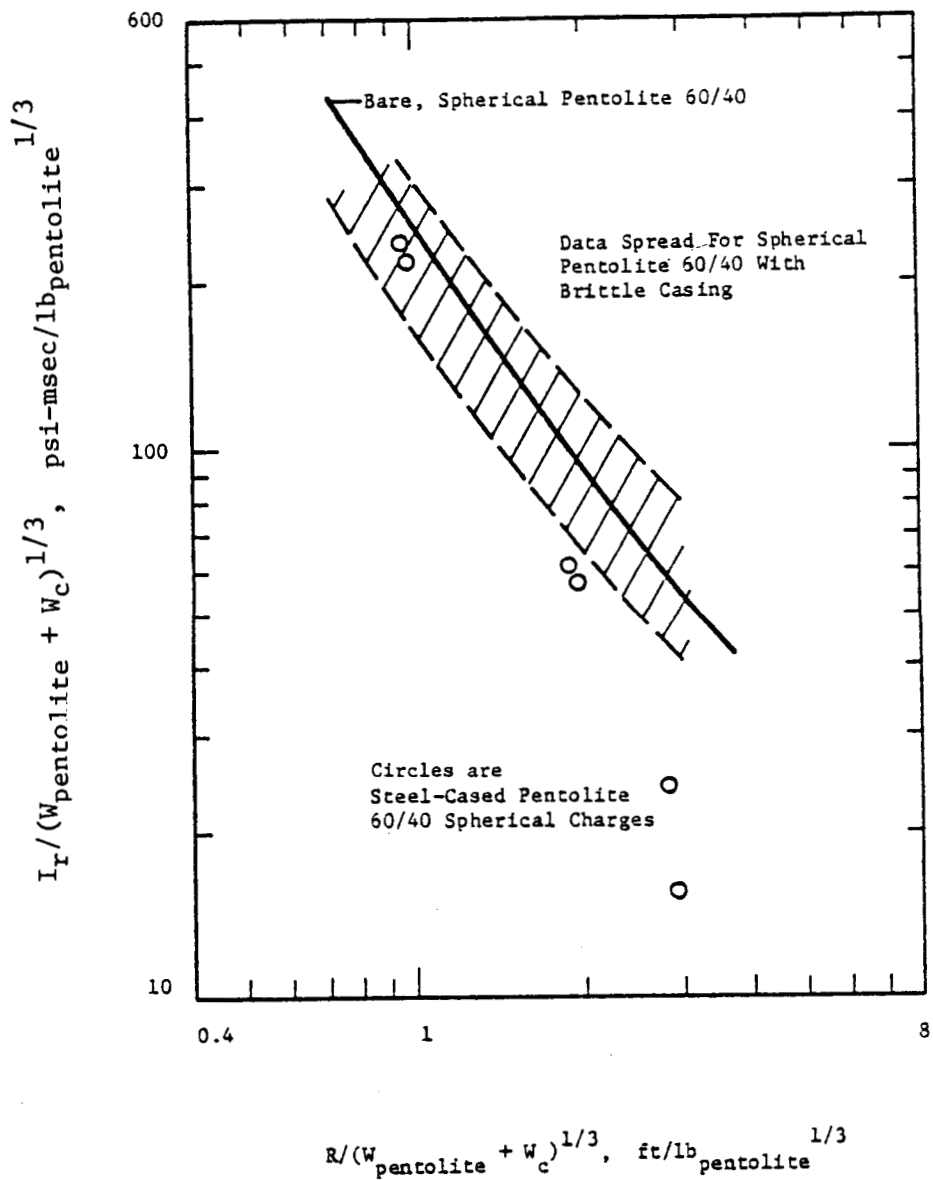
Figure 4.18 Scaled Reflected Impulse for Spherical Pentolite
60/40 with Light, Brittle Case

same time, structural calculations are conservative if this assumption is made. Should one wish to make a more detailed analysis, the times of arrival can be determined separately by using Figure 4.5 to compute the air blast arrival time and by dividing the standoff distance by fragment velocity to estimate the arrival time for fragments.

Chapter 6, Fragmentation, describes approximate relationships for estimating fragment velocities or distributions. These relationships are used to determine the average specific impulse from the many fragment casing particles which strike a structure (plate). Particularly critical in this estimation process is determination of fragment distribution and the Gurney equation (See Table 6.1) in Chapter 6 for fragment velocity. The average reflected specific impulse i_r imparted to the plate from fragment impacts is estimated using Equation (4.33).

$$i_r = \int^{\text{Area}} \frac{m(A)V_f}{A_{\text{plate}}} \cos\Theta \, da \qquad (4.33)$$

where

i_r is the reflected specific impulse,

$m(A)$ is the areal mass distribution of the fragments,

V_f is the average fragment velocity using Gurney equations,

A_{plate} is the surface area of the plate,

Θ is the angle of impact with 90 degrees defined as normal impact.

An expression must be determined for $m(A)$, the areal mass distribution of fragments. The expression will depend on charge shape and plate location. For example, a centrally detonated spherical-cased charge would produce an isotropic fragment distribution, while a cylinder would produce a narrow beam width fragment spray. The impact obliquity factor, $\cos\Theta$, also will depend on charge geometry, standoff, and plate orientation. The impulse thus computed will be an average value over the entire plate and, fragment impact being a discrete phenomenon, any small section of plate could experience a much higher specific impulse. This would be true in particular for casings that produce large, chunky fragments. Hence, one must also design against spallation and perforation by fragments (See Chapter 6, Fragmentation).

EXAMPLE PROBLEM 4.1

PROBLEM*- Find the maximum angle α_I at which regular reflection would occur for a given shock strength inverse ξ, and reflection angle α_R for this α_I.

GIVEN: P_s = peak side-on overpressure

P_o = ambient atmospheric pressure

FIND: α_I and α_R REFERENCE

SOLUTION: 1. $\xi = \dfrac{P_o}{P_s + P_o}$ Eq. (4.28)

2. Read α Extreme corresponding to the calculated ξ Fig. 4.10

3. Read α_R for given ξ and α_I Fig. 4.10

CALCULATION

GIVEN: P_s = 25 psi

P_o = 14.7 psi

FIND: α_I and α_R

SOLUTION: 1. $\xi = \dfrac{14.7}{25 + 14.7} = 0.37$

2. Entering Figure 4.10, the maximum angle α_I for regular reflection is found to be <u>41°</u>

3. Also, from Figure 4.10, the reflection angle α_R is <u>49°</u>

---

*The primary use of Figure 4.10 for an AE is to determine the value of shock obliquity for which the Mach stem starts to form. The figure also gives angle of reflection for given angle of incidence and shock strength, but this is of much less practical use for an AE interested in surface loading.

EXAMPLE PROBLEM 4.2

PROBLEM - Determine the peak reflected overpressure for an obliquely reflected blast wave of intermediate strength.

GIVEN: α_I = angle of incidence of blast wave (degrees)

P_s = peak side-on overpressure of blast wave

FIND: P_r

SOLUTION: 1.   Determine reflected overpressure ratio
             P_r/P_s Fig. 4.11

            2.   Calculate reflected pressure   Eq. (4.25) &
                 $P_r = (P_r/P_s)(P_s)$ Eq. (4.26)

CALCULATION

   GIVEN: α_I = 60°
            P_s = 50 psi

   FIND: P_r

   SOLUTION: 1.   Entering Figure 4.11 P_r/P_s = 1.8
               2. P_r = (1.8)(50) = <u>90 psi</u>

<u>EXAMPLE PROBLEM 4.3</u>

<u>PROBLEM</u> – Determine the blast parameters using Figure 4.5 for a spherical
            free-air blast; and compare to a ground burst of same explosive
            weight, at sea level atmospheric conditions.

   GIVEN: R = distance from center of explosive source
                (standoff [ft])
            W = weight and type of HE

   FIND: Free-Air Blast   <u>REFERENCE</u>

   SOLUTION: 1.   Equivalent TNT explosive weight   Appendix A
                    W = Explosive weight times TNT-   for TNT
                    equivalency factor   Equivalencies
               2.   Calculate Hopkinson-scaled distance
                    $Z = R/W^{1/3}$ Eq. (4.19)
               3.   Determine the required blast parameters
                    corresponding to Z   Fig. 4.5

   FIND: Ground Burst With Cratering

   SOLUTION: 1.   Find adjusted TNT weight $W' = 1.8\ W_{TNT}$ Eq. (4.16)
               2.   Calculate Hopkinson-scaled distance
                    $Z' = R/W'^{1/3}$ Eq. (4.19)
               3.   Determine the required blast parameters
                    corresponding to Z' Fig. 4.5

CALCULATION
_____

GIVEN: R = 20 ft
         W = 58.6 lb Composition B

FIND: Free-Air Blast

SOLUTION: 1. W = (58.6)(1.092) = 64 lb
           2. $Z = 20/64^{1/3}$ = 5 ft/lb$^{1/3}$
           3. Enter Figure 4.5 for Z = 5 ft/lb$^{1/3}$ and read:
               P_s = <u>24 psi</u>

               $\dfrac{i_s}{W^{1/3}}$ = 1 X 10^{-2} psi-sec/lb$^{1/3}$

               $\dfrac{t_d}{W^{1/3}}$ = 1.38 X 10^{-3} sec/lb$^{1/3}$

               $\dfrac{t_a}{W^{1/3}}$ = 1.5 X 10^{-3} sec/lb$^{1/3}$

               For times and impulse, multiply scaled values
               by W$^{1/3}$

               i_s = (1 X 10^{-2})(64$^{1/3}$) psi-sec = <u>4 X 10^{-2} psi-sec</u>

               t_d = (1.38 X 10^{-3})(64$^{1/3}$) sec = <u>5.52 X 10^{-3} sec</u>

               t_a = (1.5 X 10^{-3})(64$^{1/3}$) sec = <u>6.0 X 10^{-3} sec</u>

               These values can be compared to corresponding values
               obtained in Section 4.8 for effect of altitude

FIND: Ground Burst With Cratering

SOLUTION: 1. W′ = 1.8 W = (1.8)(64) = 115.2 lb
           2. $Z′ = 20/115.2^{1/3}$ = 4.11 ft/lb$^{1/3}$
           3. Enter Figure 4.5 for Z = 4.11 ft/lb$^{1/3}$ and read:
               P_s = <u>37 psi</u>

               $\dfrac{i_s}{W^{1/3}}$ = 1.2 X 10^{-2} psi-sec/lb$^{1/3}$

               $\dfrac{t_d}{W^{1/3}}$ = 1.25 X 10^{-3} sec/lb$^{1/3}$

$$\frac{t_a}{W^{1/3}} = 1.04 \times 10^{-3} \ \text{sec/lb}^{1/3}$$

For times and impulse, multiply scaled values
by $W_{TNT}^{1/3}$

$$i_s = (1.2 \times 10^{-2})(115.2^{1/3}) \ \text{psi-sec} = \underline{5.84 \times 10^{-2}} \ \text{psi-sec}$$

$$t_d = (1.25 \times 10^{-3})(115.2^{1/3}) \ \text{sec} = \underline{6.08 \times 10^{-3}} \ \text{sec}$$

$$t_a = (1.04 \times 10^{-3})(115.2^{1/3}) \ \text{sec} = \underline{5.06 \times 10^{-3}} \ \text{sec}$$

EXAMPLE PROBLEM 4.4

PROBLEM – Determine the peak side-on overpressure, reflected overpressure, side-on impulse, and reflected impulse for steel-cased HE.

GIVEN: R = distance from center of explosive source
      (standoff [ft])
    W = weight and type of HE
    W_c = casing weight

			REFERENCE
FIND:	P_s, P_r, i_s, and i_r		
SOLUTION:	1. Equivalent TNT explosive weight		Table 6 of
	W = (W)(TNT Factor)		Appendix A
	2. Calculate an adjusted explosive weight		
	$W' = [0.20 + \dfrac{0.80}{(1 + W_c/W)}] \, W$		Eq. (4.31)
	3. Calculate modified Hopkinson-scaled distance		
	$Z' = R/W'^{1/3}$		Eq. (4.30)
	4. Determine the required blast parameters corresponding to Z		Fig. 4.5 & Fig. 4.6

CALCULATION

GIVEN: R = 20 ft
    W = 9.16 lb Composition B
    W_c = 5 lb

FIND: P_s, P_r, i_s, and i_r

SOLUTION: 1. W = (1.092)(9.16) = 10 lb

2. $W' = [0.20 + \dfrac{0.8}{(1 + 5/10)}]\ 10\ \text{lb}$

   $W' = 7.3\ \text{lb}$

3. $Z' = 20/7.3^{1/3} = 10.3\ \text{ft/lb}^{1/3}$

4. Enter Figure 4.5 and find P_s and $i_s/W^{1/3}$

   $P_s = \underline{5.6\ \text{psi}}$

   $i_s/W^{1/3} = 5\ \text{X}\ 10^{-3}\ \text{psi-sec/lb}^{1/3}$

   Multiply scaled side-on impulse by $W'^{1/3}$

   $i_s = (5\ \text{X}\ 10^{-3})(7.3^{1/3})\ \text{psi-sec} = \underline{9.7\ \text{X}\ 10^{-3}\ \text{psi-sec}}$

   Enter Figure 4.6 and find P_r and $i_r/W^{1/3}$

   $P_r = \underline{15\ \text{psi}}$

   $i_r/W^{1/3} = 1.4\ \text{X}\ 10^{-2}\ \text{psi-sec/lb}^{1/3}$

   Multiply scaled reflected impulse by $W'^{1/3}$

   $i_r = (1.4\ \text{X}\ 10^{-2})(7.3^{1/3})\ \text{psi-sec} = \underline{2.7\ \text{X}\ 10^{-2}\ \text{psi-sec}}$

EXAMPLE PROBLEM 4.5

PROBLEM – Determine the peak side-on overpressure, side-on impulse, reflected
overpressure, and reflected impulse, for HE cased in brittle or frag-
mented casing material.

GIVEN: R = distance from center of explosive source
           (standoff [ft])
        W = weight and type of HE
        W_c = casing weight of brittle material

FIND: P_s, i_s, P_r, and i_r REFERENCE

SOLUTION: 1. Equivalent TNT explosive weight
              W = Explosive weight times TNT-   Table 6 of
              equivalency factor   Appendix A
           2. Calculate modified Hopkinson-scaled
              distance
              $Z' = R/(W + W_c)^{1/3}$ Eq. (4.32)
           3. Determine the required blast parameters   Fig. 4.5 &
              corresponding to Z' Fig. 4.6

CALCULATION

GIVEN: R = 20 ft
       W = 10 lb of TNT
      W_c = 5 lb

FIND: P_s, i_s, P_r, and i_r

SOLUTION: 1. W_{TNT} = (1)(10) = 10 lb

          2. Z' = $20/(10 + 5)^{1/3}$

              Z' = 8.1 $ft/lb^{1/3}$

          3. Enter Figure 4.5 and find P_s and $i_s/W^{1/3}$

              P_s = <u>8.8 psi</u>

              $i_s/W^{1/3}$ = 6.5 X 10^{-3} $psi\text{-}sec/lb^{1/3}$

              Multiply scaled side-on impulse by $W^{1/3}$

              i_s = (6.5 X 10^{-3})($10^{1/3}$) psi-sec = <u>1.4 X 10^{-2} psi-sec</u>

              Enter Figure 4.6 and find P_r and $i_r/W^{1/3}$

              P_r = <u>25 psi</u>

              $i_r/W^{1/3}$ = 1.8 X 10^{-2} $psi\text{-}sec/lb^{1/3}$

              Multiply scaled reflected impulse by $W^{1/3}$

              i_r = (1.8)($10^{1/3}$) psi-sec = <u>3.9 X 10^{-2} psi-sec</u>

EXAMPLE PROBLEM 4.6

PROBLEM - The reflection factor (P_r/P_s) close to an explosive charge may not
         be calculable from Figure 4.6, but instead one may have to use
         Equation (4.27) for these strong shocks. The problem is to deter-
         mine reflection factor (P_r/P_s) and P_r close in to a charge.

GIVEN: Z = scaled distance ($R/W^{1/3}$)

FIND: P_r REFERENCE

SOLUTION: 1. Determine if scaled distance is below
              that where the P_r curve extends in Figure
              4.6. If not, read value of P_r.   Fig. 4.6

2. If not on Figure 4.6, read value of P_s from the curve in Figure 4.5 (which extends to charge surface)

          Fig. 4.5

3. Use Equation (4.27) to solve for reflection factor

          Eq. (4.27)

4. Use results of Step 3 to obtain P_r

CALCULATION

GIVEN: $Z = R/W^{1/3} = 2.0 \times 10^{-1}$

FIND: P_r

SOLUTION:
1. Examining Figure 4.6 shows that the P_r curve does not extend into
$$Z = R/W^{1/3} = 2.0 \times 10^{-1}$$

2. Using Figure 4.5
$$P_s = 7.0 \times 10^3 \text{ psi}$$

3. Using Equation (4.27)

$$\frac{P_r}{P_s} = \frac{2.655 \times 10^{-3}\ (7.0 \times 10^3)}{1 + 1.728 \times 10^{-4}\ (7.0 \times 10^3) + 1.921 \times 10^{-9}\ (7 \times 10^3)^2} + 2 + $$

$$\frac{4.218 \times 10^{-3} + 4.834 \times 10^{-2}\ (7.0 \times 10^3) + 6.856 \times 10^{-6}\ (7.0 \times 10^3)^2}{1 + 7.997 \times 10^{-3}\ (7.0 \times 10^3) + 3.844 \times 10^{-6}\ (7.0 \times 10^3)^2}$$

$P_r/P_s = 12.82 =$ Reflection Factor

$$P_r = (P_r/P_s) \times P_s = 12.82 \times 7.0 \times 10^3 = \underline{8.97 \times 10^4 \text{ psi}}$$

4.3.1.2 Non-Spherical Geometry

A bare high explosive, when properly initiated in free air, will undergo an extremely rapid chemical decomposition with release of energy, in the form of a "detonation wave." The detonation wave, with origin at the site of initiation, will propagate radially through the explosive at a characteristic "steady state" detonation velocity. If the explosive charge is initiated at its center of mass and is spherical in shape, the detonation wave should reach the entire charge surface at the same instant or within a few microseconds of the same time. A shock wave will travel through the surrounding air, its strength a function of radial standoff from the center of the mass of the explosion. The techniques developed for estimation of blast parameters assumed a spherical charge in free air, or equivalently, a hemispherical charge resting on a surface that is a perfect reflector of blast waves.

Most ordnance devices are non-spherical in shape. For a non-spherical charge, a shock wave will not enter the surrounding air as a spherical wave, nor at the same instant over the entire charge surface. The shape and strength of the shock wave entering the air will depend both upon charge geometry, and upon the relative location at which initiation occurred. The blast parameters will be functions not only of radial standoff, but also of azimuth and possibly elevation. There exists no easily determined "correction factor" as was the case, for example, for high altitude ambient atmospheric conditions.

Experimental programs have been conducted by various individuals at various organizations for determination of the blast field around non-spherical explosives of simple, regular geometries (cylinders, cubes, cones, etc.) (See References 4.34 through 4.38). Several observations were common to the investigators. One was that the largest overpressure always occurred in the direction of the charge face with greatest presented surface area, and another, that multiple pressure "peaks" occurred in the initial positive overpressure phase. Short-duration photographs showed that the multiple pressure peaks correspond to multiple shocks, produced along edges of explosive charges where detonation waves from different faces of the charge interface and form what is termed a "bridge wave" analogous to the Mach stem formed with reflected blast waves (Reference 4.34). The secondary shocks tend to overtake and coalesce with the leading shocks as radial standoff from the charge is increased. Experimentally it has been found that the use of hemispherical end caps on cylindrical charges will eliminate the formation of bridge waves. For a charge of a particular non-spherical geometry, as standoff increases, the blast wave becomes more spherical and only small errors are induced by neglecting charge shape.

A large quantity of data for cylindrical charges has been amassed by experimental investigators. Plooster (Reference 4.33) has curve-fit the data obtained from a test program conducted at Denver Research Institute by Wisotski and Snyer (Reference 4.32). The curve fit is of the functional form $P_s = f$

(Z, L/D, θ) where P_s is peak side-on overpressure, Z is the scaled radial standoff from the cylinder, L/D is the cylinder length to diameter ratio, and θ is the azimuth angle (see Figure 4-22 for definition). The data base for the curve fit consisted of Comp B cylinders with length-to-diameter ratios ranging from 1/4 to 10/1. The average ambient atmospheric pressure was 12.03 psia. Peak side-on overpressure values ranged from 2 to 100 psig. Two equations resulted from the curve fit:

For charges L/D $\geq$ 1

$$
\begin{aligned}
y = &[2.0467 - 0.1146X + (0.1285 - 0.0342X)\cos\theta \\
&+ (0.0621 - 0.3280X)\cos 2\theta + (-0.0029 + 0.0304X)\cos 3\theta \\
&+ (-0.1532 - 0.998X)\cos 4\theta] \\
&+ [-2.1617 + 0.1422X + (-0.2079 + 0.1161X)\cos\theta \\
&+ (-0.4178 + 0.3686X)\cos 2\theta + (-0.1372 + 0.0648X)\cos 3\theta \\
&+ (-0.3484 + 0.1191X)\cos 4\theta]\lambda \\
&+ [0.4366 + 0.0418X + (0.0138 + 0.0983X)\cos\theta \\
&+ (0.1178 + 0.1451X)\cos 2\theta + (0.2556 - 0.043X)\cos 3\theta \\
&+ (0.3123 + 0.1616X)\cos 4\theta]\lambda^2,
\end{aligned}
\tag{4.34}
$$

and for disc-shaped charges (L/D < 1):

$$
\begin{aligned}
y = &[2.0467 - 0.1753X + (0.1285 + 0.0728X)\cos\theta \\
&+ (0.0621 - 0.2503X)\cos 2\theta + (-0.0029 + 0.0079X)\cos 3\theta \\
&- 0.1534\cos 4\theta] \\
&+ [-2.1616 + 0.0464X + (-0.2079 - 0.2174X)\cos\theta \\
&+ (-0.4178 + 0.3426X)\cos 2\theta + (-0.1372 - 0.1171X)\cos 3\theta \\
&+ (-0.3484 - 0.3449X)\cos 4\theta]\lambda \\
&+ [0.4366 + 0.0053X + (0.0138 + 0.0006X)\cos\theta \\
&+ (0.1178 - 0.2656X)\cos 2\theta + (0.2556 + 0.2072X)\cos 3\theta \\
&+ (0.3123 - 0.2140X)\cos 4\theta]\lambda^2
\end{aligned}
\tag{4.35}
$$

where:

$$X = \ln(L/D) \qquad\qquad\qquad (a)$$

$$\lambda = \ln(0.0893\ R/W^{1/3}) \qquad\qquad (b)$$

$$y = \ln P_s - 0.20; \quad P_s = 1.22e^y \qquad (c) \qquad\qquad (4.36)$$

The original equations presented by Plooster have been modified to allow calculations at standard sea level conditions with TNT as the explosive.

Empirical curve fits are generally valid only within the range of the data base of the curve fit, and thus, Equations (4.34) and (4.35) should be utilized with the limitations of the data base listed above. Figures 4.19 through 4.21 are plots comparing the curve fit to the actual data (Ref. 4.32). A frequent convention used in presenting data is "equivalent spherical weight" for a non-spherical charge at a particular location relative to the charge. Figures 4.22 through 4.24 are plots of the ratio of equivalent spherical charge weight to cylinder charge weight, as a function of scaled standoff azimuthal location, and L/D ratio.

Some data exist for explosions of non-spherical charges on the ground surface (see Ref. 4.35). But, these data are not extensive enough to develop prediction curves and equations such as Equations (4.34) and (4.35). The presence of an extensive and massive reflecting surface such as the ground or the floor of an explosive bay complicates blast wave prediction for non-spherical charges in two ways: (1) the complex shape of the blast waves from the non-spherical source are made even more complex by reflection from the reflecting surface, and (2) most reflecting surfaces are not ideal and assumptions must be made on energy absorption by the surface.

For estimation of blast parameters for non-spherical charges on the ground, or on floors on grade, it is recommended that, unless specific data such as in Reference 4.35 are available for the particular charge shape, the charge be assumed to be of hemispherical shape located on the surface. A reflection factor of 1.7 to 2.0 should then be used as multiplier for the charge weight to obtain an equivalent free-air sphere weight, which is then used to enter Figures 4.5 through 4.7 for prediction of blast wave properties.

If non-spherical geometry will significantly affect blast wave parameters in Pantex Plant applications, DOE will provide guidance to the AE. Where necessary, this information will be given in the design criteria.
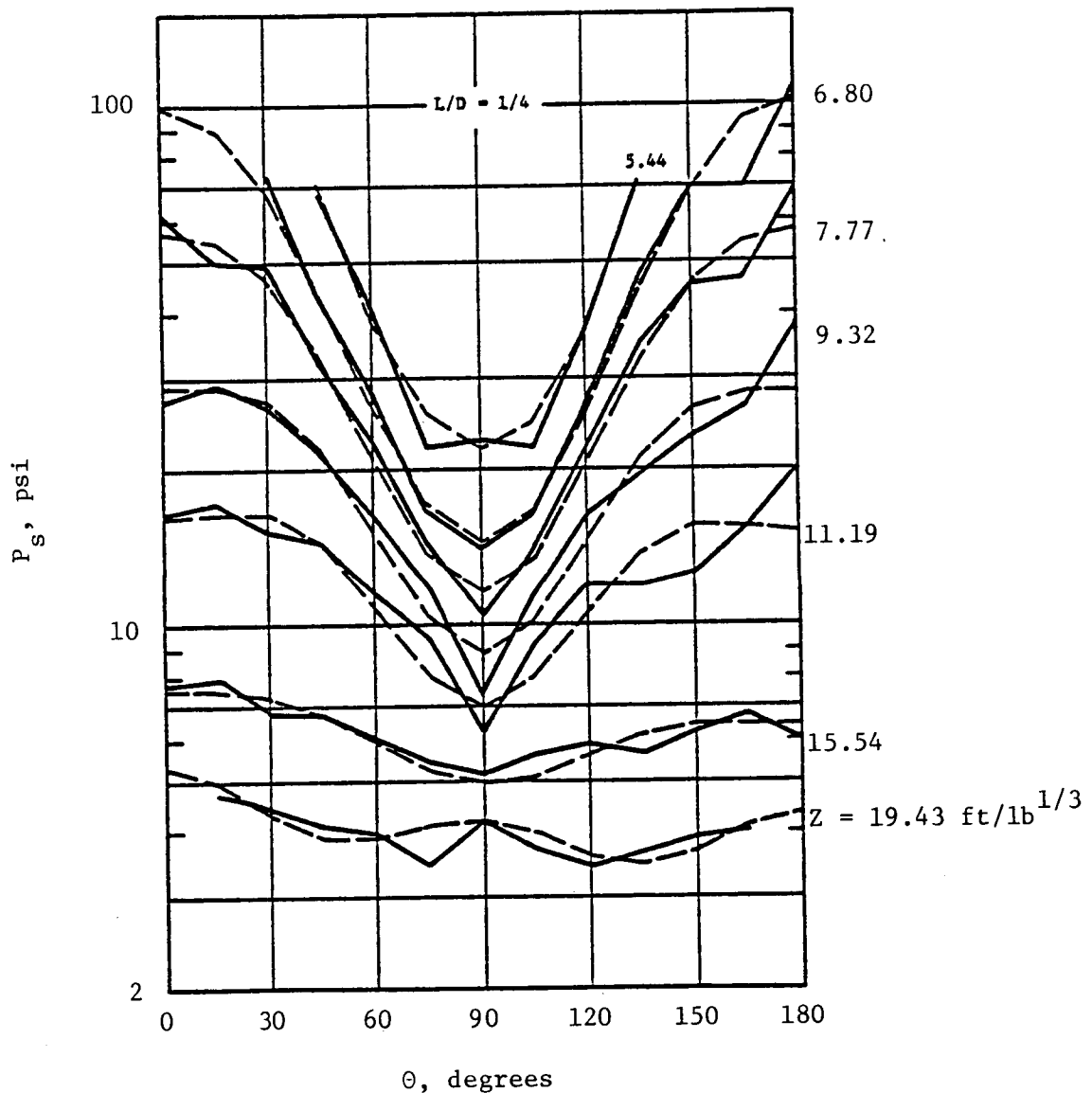
Figure 4.19 Comparison of Experimental Peak Side-on Over-
pressure (solid curves) with Values Calculated from Equation
4.35 (dashed curves) as a Function of Azimuth Angle Θ and
Scaled Distance $(R/W^{1/3})$ from the Charge, for Cylindrical
Charges with L/D Ratio of 1/4. Numbers at Right Indicate
Scaled Distance for Each Pair of Curves
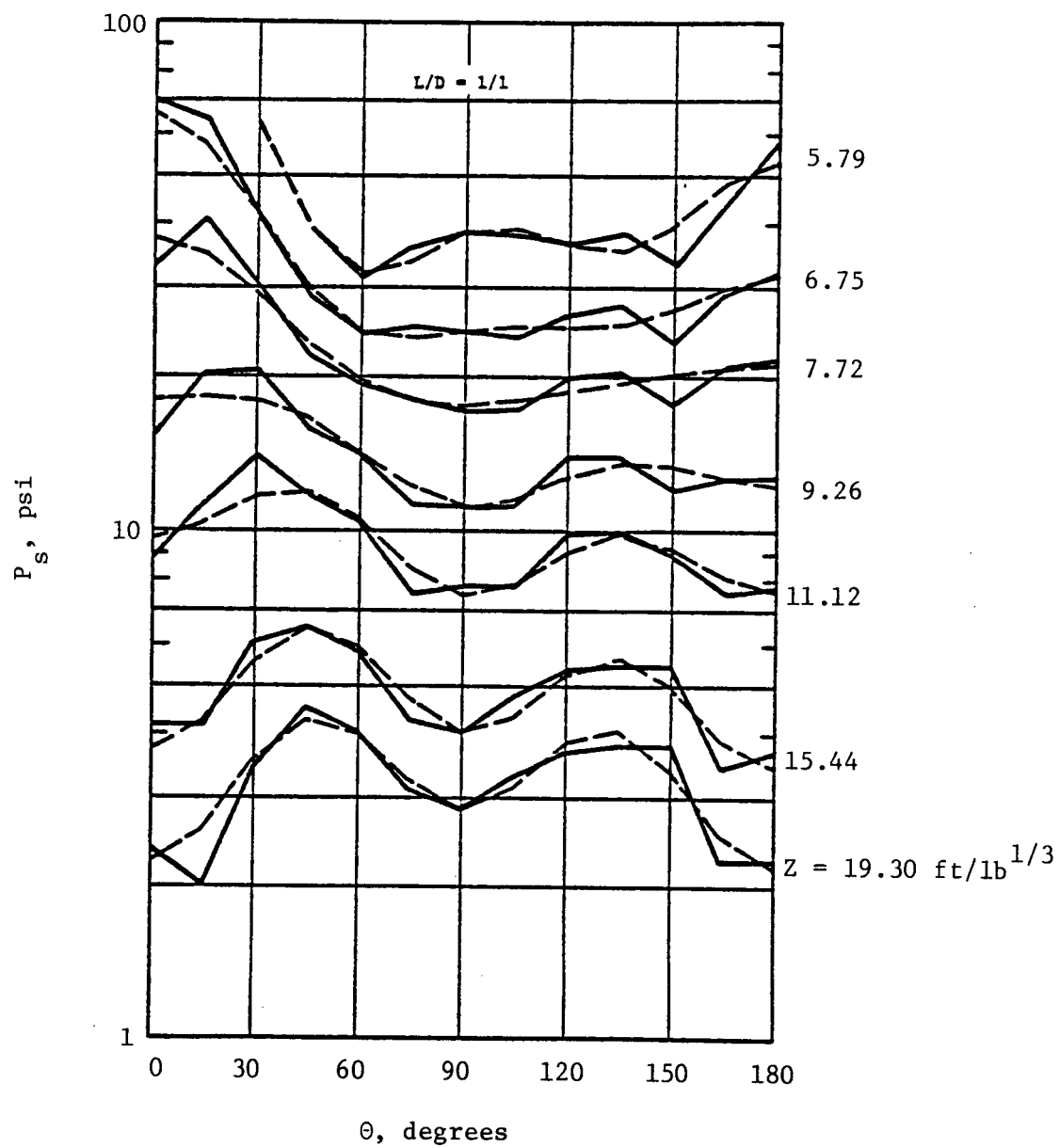
Figure 4.20 As in Figure 4.19, Comparison of Experimental Values to Those Calculated from Equation 4.34, L/D = 1
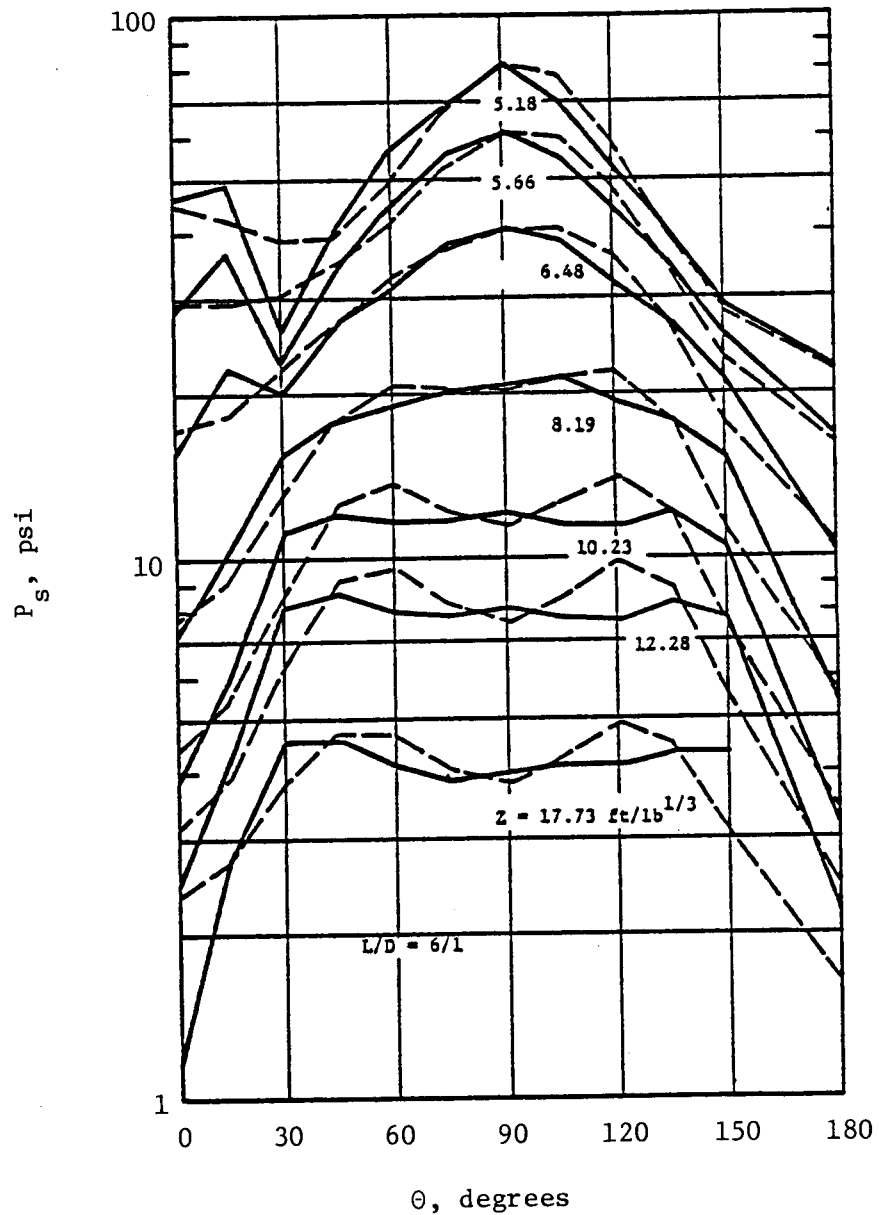
Figure 4.21   As in Figure 4.19, Comparison of Experimental
Values to Those Calculated from Equation 4.34, L/D = 6
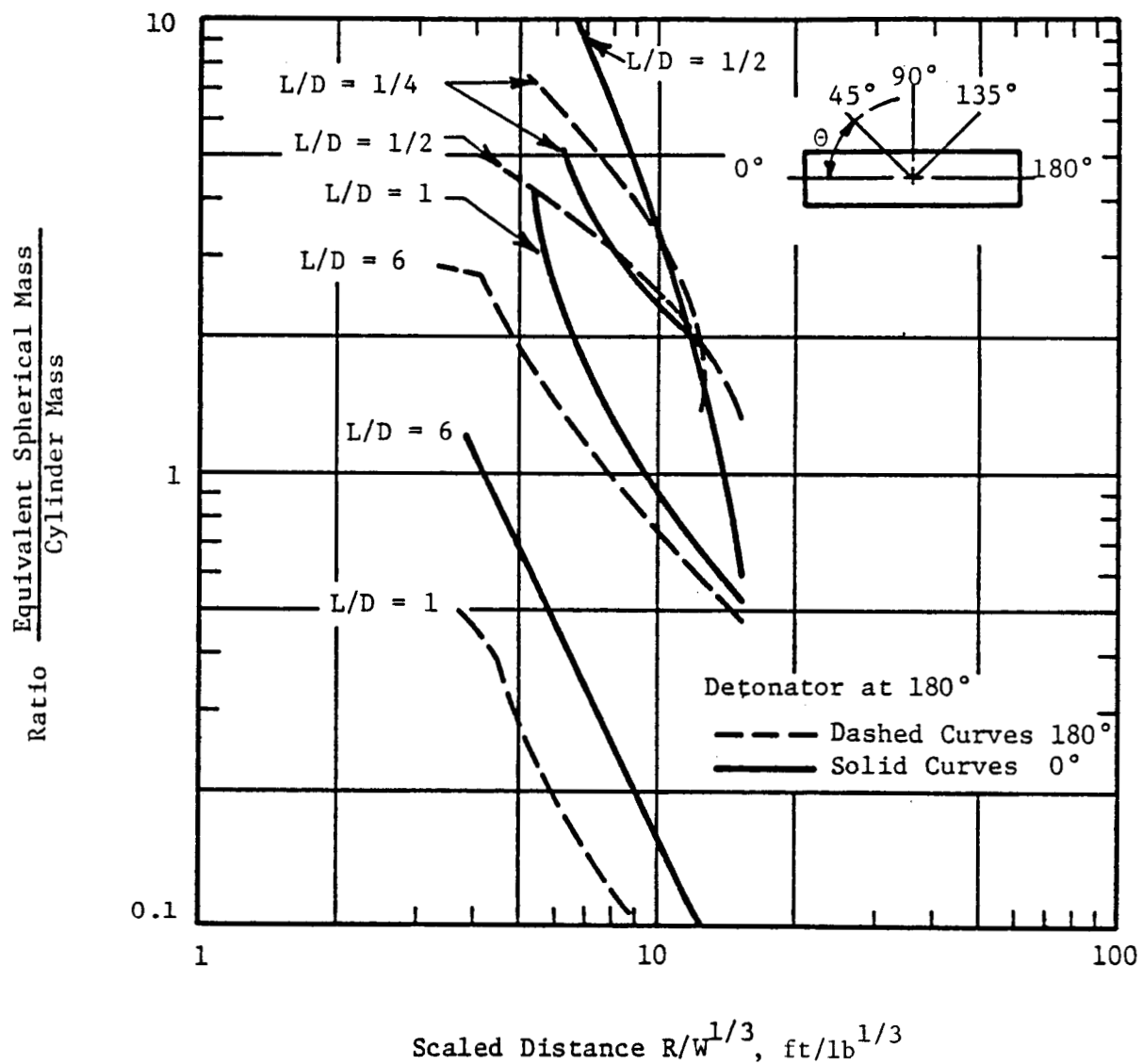
Figure 4.22 Ratio, Equivalent Spherical Mass to Cylinder Mass, (θ = 0°
and 180°) Based on Experimental Peak Side-On Overpressure, at Sea Level
Ambient Atmospheric Conditions

4-61
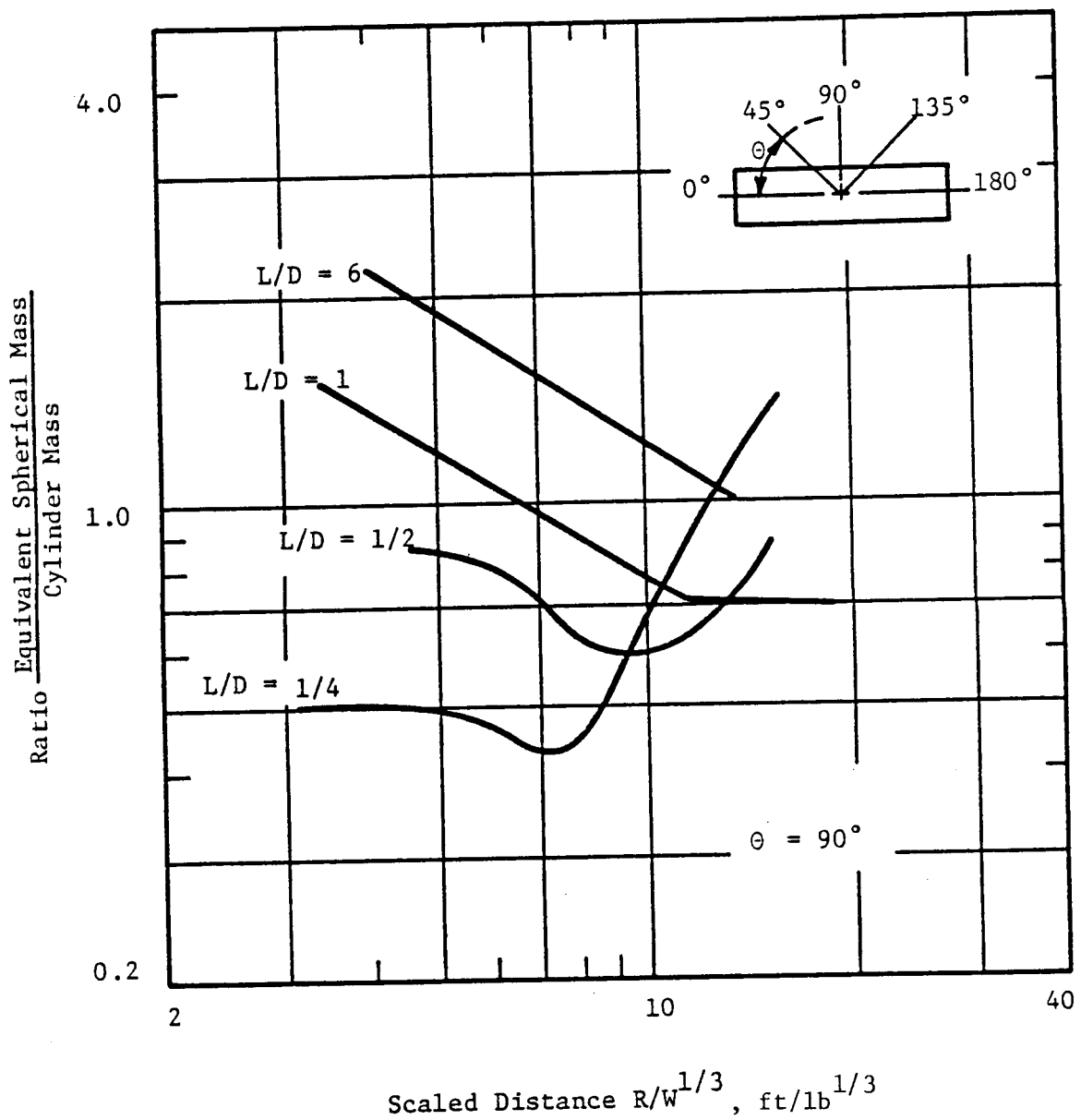
Figure 4.23 Ratio, Equivalent Spherical Mass to Cylinder Mass, (Θ = 90°), Based on Experimental Peak Side-On Overpressure, at Sea Level Ambient Atmospheric Conditions
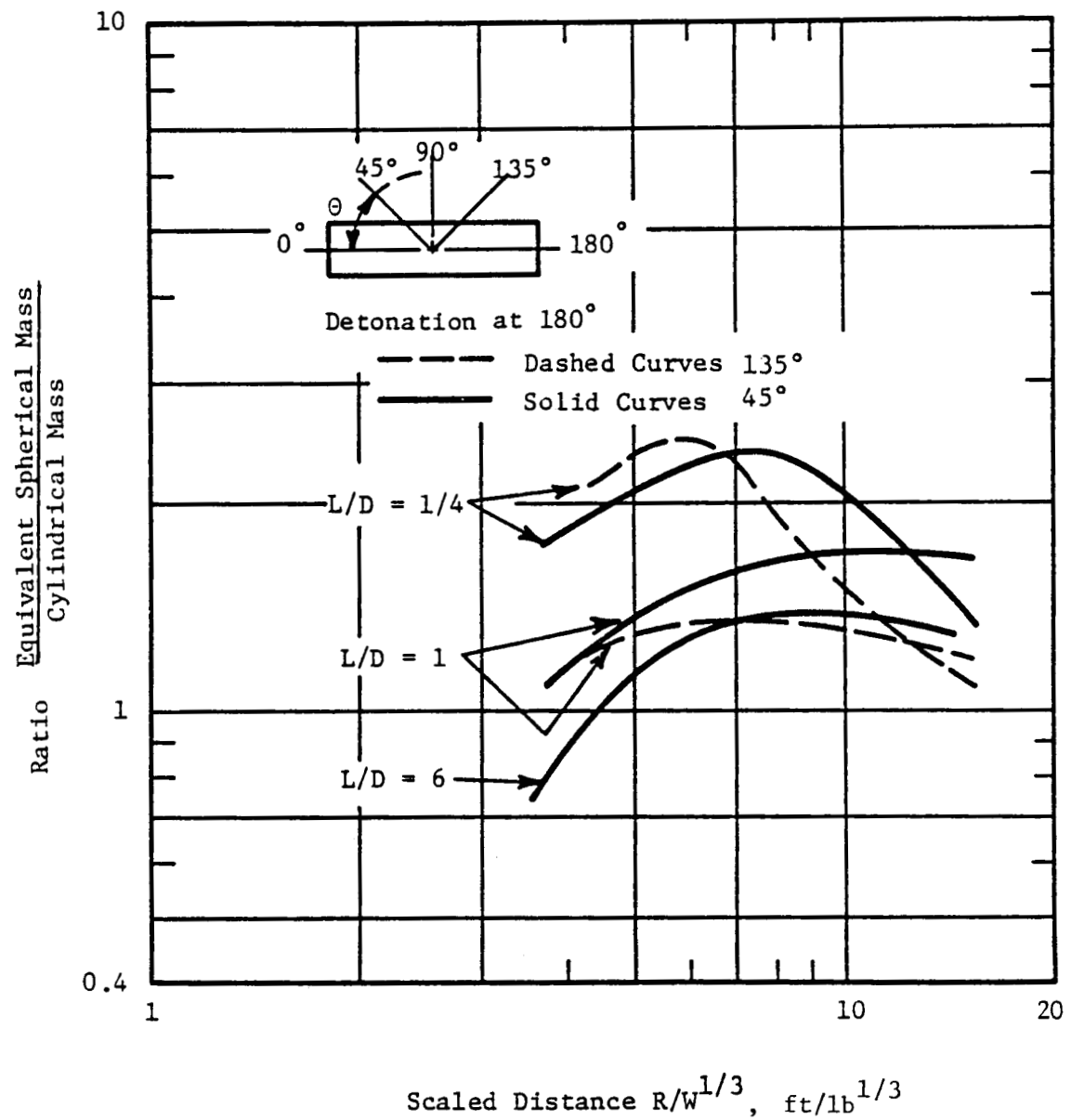
Figure 4.24 Ratio, Equivalent Spherical Mass to Cylinder Mass, (Θ = 45° and 135°) Based on Experimental Peak Side-On Overpressure, at Sea Level Ambient Atmospheric Conditions

EXAMPLE PROBLEM 4.7

PROBLEM – Determine peak side-on overpressure around a bare, cylindrical free-air HE explosion.

GIVEN: R = distance from center of explosive source
        (standoff [ft])

W = weight and type of HE (lb)

Θ = Azimuth angle in degrees (See Figures 4.22 through 4.24)

L/D = length-to-diameter ratio of charge

FIND: P_s

SOLUTION:
1. Equivalent TNT explosive weight
W = Explosive weight times TNT-equivalency factor
2. Calculate Hopkinson-scaled distance
$$Z = R/W^{1/3}$$
3. Calculate modified Hopkinson-scaled distance
$$\lambda = \ln (0.0893 Z)$$
4. Calculate modified L/D ratio
$$X = \ln (L/D)$$
5. Calculate P_s
Obtain y from Equation (4.34), then substitute y into Equation (4.36c)
$$P_s = 1.22 \ e^y$$

REFERENCE

Table 6 of Appendix A for TNT Equivalencies

Eq. (4.19)

Eq. (4.36b)

Eq. (4.36a)

Eq. (4.34) & Eq. (4.36c)

CALCULATION

GIVEN: R = 25 ft
W = 52.6 lb Comp B
Θ = 0, 45, 90 degrees
L/D = 1

FIND: P_s

SOLUTION:
1. Equivalent TNT explosive weight
W = (1.092)(52.6) = 57.4 lb
2. $Z = 25/57.4^{1/3} = 6.48 \ ft/lb^{1/3}$
3. $\lambda = \ln(0.0893 \ X \ 6.48) = -0.547$

4. $X = \ln(1) = 0$
For $\theta = 0°$

$y = [2.0467 + 0.1285 \cos(0) + 0.0621 \cos(0) - 0.0029 \cos(0) - 0.1532 \cos(0)] +$
$[-2.1617 - 0.2079 \cos(0) - 0.4178 \cos(0) - 0.1372 \cos(0) - 0.3484 \cos(0)] X$
$(-0.547) + [0.4366 + 0.0138 \cos(0) + 0.1178 \cos(0) + 0.2556 \cos(0) +$
$0.3123 \cos(0)] X (-0.457)^2 = 4.211$

$P_s = 1.22 \, e^{4.211}$

$P_s = \underline{82.3 \text{ psi}}$

For $\theta = 45°$

$y = [2.0467 + 0.1285 \cos(45) + 0.0621 \cos(90) - 0.0029 \cos(135) - 0.1532 \cos(180)] +$
$[-2.1617 - 0.2079 \cos(45) - 0.4178 \cos(90) - 0.1372 \cos(135) - 0.3484 \cos(180)] X$
$(-0.547) + [0.4366 + 0.0138 \cos(45) + 0.1178 \cos(90) + 0.2556 \cos(135) +$
$0.3123 \cos(180)] X (-0.547)^2 = 3.299$

$P_s = 1.22 \, e^{3.299}$

$P_s = \underline{33.0 \text{ psi}}$

For $\theta = 90°$

$y = [2.0467 + 0.1285 \cos(90) + 0.0621 \cos(180) - 0.0029 \cos(270) - 0.1532 \cos(360)] +$
$[-2.1617 - 0.2079 \cos(90) - 0.4178 \cos(180) - 0.1372 \cos(270) - 0.3484 \cos(360)] X$
$(-0.547) + [0.4366 + 0.0138 \cos(90) + 0.1178 \cos(180) + 0.2536 \cos(270) +$
$0.3123 \cos(360)] X (-0.547)^2 = 3.165$

$P_s = 1.22 \, e^{3.165}$

$P_s = \underline{28.9 \text{ psi}}$

(These values could have been obtained from Figure 4.20, but with one to two digit accuracy.)

EXAMPLE PROBLEM 4.8

PROBLEM – Determine the equivalent spherical weight (TNT) for a cylinder charge.

GIVEN: R = distance from center of explosive source (standoff [ft])
W = weight and type of HE (1b)
θ = azimuth angle in degrees (See Figures 4.22 through 4.24)
L/D = length-to-diameter ratio of charge

FIND: Equivalent Spherical Weight   REFERENCE

SOLUTION: 1. Equivalent TNT explosive weight
W = explosive weight times TNT-   Table 6 of
equivalency factor   Appendix A
2. Calculate Hopkinson-scaled distance   Eq. (4.19)

3. Obtain the ratio, Equivalent Spherical   Fig. 4.22,
   Mass/Cylinder Mass directly from Figures   Fig. 4.23, &
   4.22 through 4.24   Fig. 4.24
4. The equivalent spherical weight of TNT
   is found by multiplying the ratio from
   Step 3 by the cylinder weight W
   Equivalent spherical weight (TNT) = W X ratio

CALCULATION

GIVEN: R = 25 ft
      W = 52.6 lb Comp B
      Θ = 0, 45, 90, 135, 180 degrees
      L/D = 6

FIND: Equivalent Spherical Weight

SOLUTION:
1. Equivalent TNT explosive weight
   W = (1.092)(52.6) = 57.4 lb
2. $Z = 25/57.4^{1/3} = 6.48$ ft/lb$^{1/3}$
3. From Figure 4.22:
   For Θ = 0°
   Ratio = 0.4
   For Θ = 180°
   Ratio = 1.3
   From Figure 4.23:
   For Θ = 90°
   Ratio = 1.6
   From Figure 4.24:
   For Θ = 45°
   Ratio = 1.3
   For Θ = 135°
   Ratio = 1.3
4. The equivalent spherical weight is listed
   below in tabular form, for
   $Z = 6.48$ ft/lb$^{1/3}$, L/D = 6

Θ	Ratio	Equivalent Spherical Weight (lb)
0	0.4	23.0
45	1.3	74.6
90	1.6	91.8
135	1.3	74.6
180	1.3	74.6

These equivalent weights can dictate wall design, for explosions of large L/D cylindrical charges, even at considerable standoffs. The ratio of 1.6 at 90° azimuth angle applies at a rather large scaled distance for accidents in explosive bays.

4.3.2 Multiple Explosion Sources

When a multiple explosion occurs, blast characteristics can be very different from that measured for either a single charge of the total charge weight or any one of the separate charges treated alone. In between two or more charges detonated at the same time or close in time, shock waves will interact through reflection and cause high peak pressures. Outside an area including two or more charges, blast waves can coalesce for some standoff range into a single blast wave with enhanced overpressure. In the following sections methods for predicting blast wave parameters for both sequential and simultaneous detonations are discussed and conservative assumptions in areas where there is a lack of information are given. To date, there appear to be no examples of use of multiple explosion source data in actual facility design. Specific recommendations appear in the following sections.

4.3.2.1 Sequential Detonation

There exist little blast data which can be used to characterize blast waves from sequential detonations. The bulk of the work done was by Zaker (Ref. 4.38) in a two-part study on the subject. His work was directed toward safety studies concerning blast effects near (but not between) both two and three sequentially detonated charges. Zaker notes that an explosion in a single bay of a multiple unit storage facility can cause the initiation of a second explosion in another bay (through fragment impact, for example) with the result that blast characteristics away from the explosion can be similar to blast from an explosive weight of the total of all charges involved instead of any one charge. Although there is a delay in initiation, trailing shock waves can overtake and coalesce with leading shock waves. The lead shock passes through air and compresses the gas, heats it and imparts a momentum to the gas particles. As a second shock travels through this disturbed medium, it will have an increased shock velocity because sound speed increases with temperature, the medium is denser, and there is momentum flow in the direction of shock velocity (Ref. 4.38).

Zaker's work included development of a finite-difference computer model (called BLOWUP) used to determine numerically pressure fields about sequential detonations of spherical charges. Small scale experiments of two and three sequentially detonated equal and unequal charges were conducted for comparison with numerical predictions. This section concentrates on the two-charge experiments. The experiments included 16 two-spherical charge tests with a total charge weight of 2 lb of C-4 explosive separated by a plate at a distance of 10 inches, center to center. This is equivalent to 2.5 lb of TNT.* The test combinations of charges and delay time are shown in Table 4.5. Figure 4.25 shows the test setup which includes pressure measurements along lines both lateral and axial to the charge centers, and a dividing wall between charges (to prevent sympathetic detonation). The data were presented in scaled curves which are reproduced in Figures 4.26 through 4.31. These include time

---

*According to Zaker, which is not the same relationship listed in Appendix A.

Table 4.5 Test Conditions for Sequential Explosions (Reference 4.38)

CHARGE RATIO*	SCALED TIME DELAYS $\bar{t}_{delay}$, ms/lb$^{1/3}$
1:1	0.60, 1.07, 1.58, 2.14, 2.59, 3.17, 3.65, and 4.11
2:1	0.58, 1.16, 1.62, and 2.57
1:2	1.0, 1.64, 2.14, and 3.22

*Ratio of the two charges: 1:1 = 1 lb C-4 each, 2:1 = 4/3 and 2/3 lb C-4,
1:2 = 2/3 and 4/3 lb C-4

→ R

Axial Pressure Gages

6.5 9.0 13.6   20.9   Scaled Distance   37.1   42.0 $\dfrac{ft}{lb^{1/3}}$

Top View

Scaled Distance
From Charge Cen-
ter Of Mass =

$$\frac{R}{W_{TOTAL}{}^{1/3}}$$

Side View

Lateral Pressure Gages

6.5

9.0

13.6

20.9

37.1

42.0

$\dfrac{ft}{lb^{1/3}}$

R

Scaled Distance Between Charges

$$\frac{S}{W_{TOTAL}{}^{1/3}} = 0.614 \ \frac{ft}{lb^{1/3}}$$
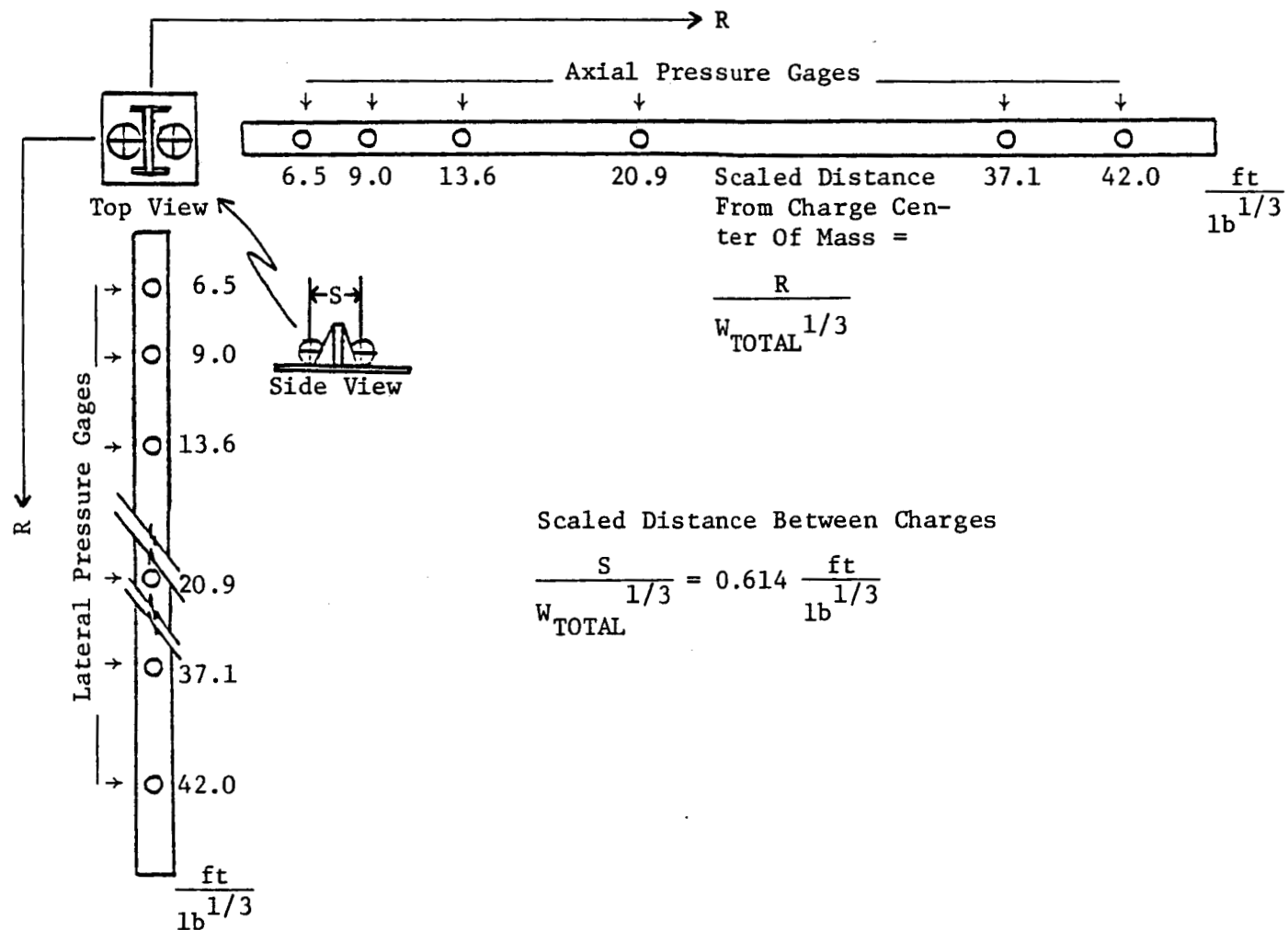
Figure 4.25   Schematic for Sequential Explosion Tests
of Zaker (Reference 4.38)
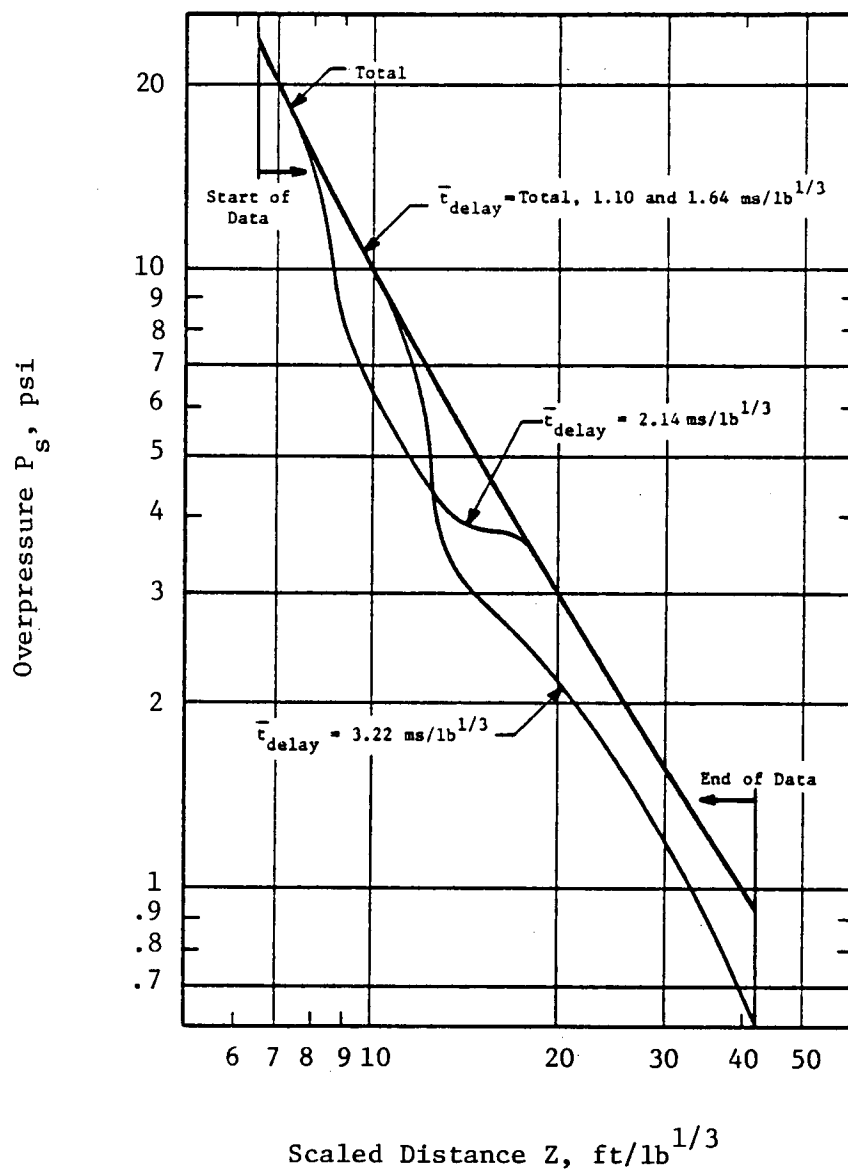
Figure 4.26   Lateral Peak Pressure for a 1:2 Charge Ratio

The graph shows:
- Y-axis: Overpressure P_s, psi (logarithmic scale from 1 to 20+)
- X-axis: Scaled Distance Z, ft/lb$^{1/3}$ (logarithmic scale from 6 to 50)

Start of Data

$\overline{t}_{delay}$ = Total, 1.10, 1.164, and 2.14 ms/lb$^{1/3}$

$\overline{t}_{delay}$ = 3.22 ms/lb$^{1/3}$

End of Data
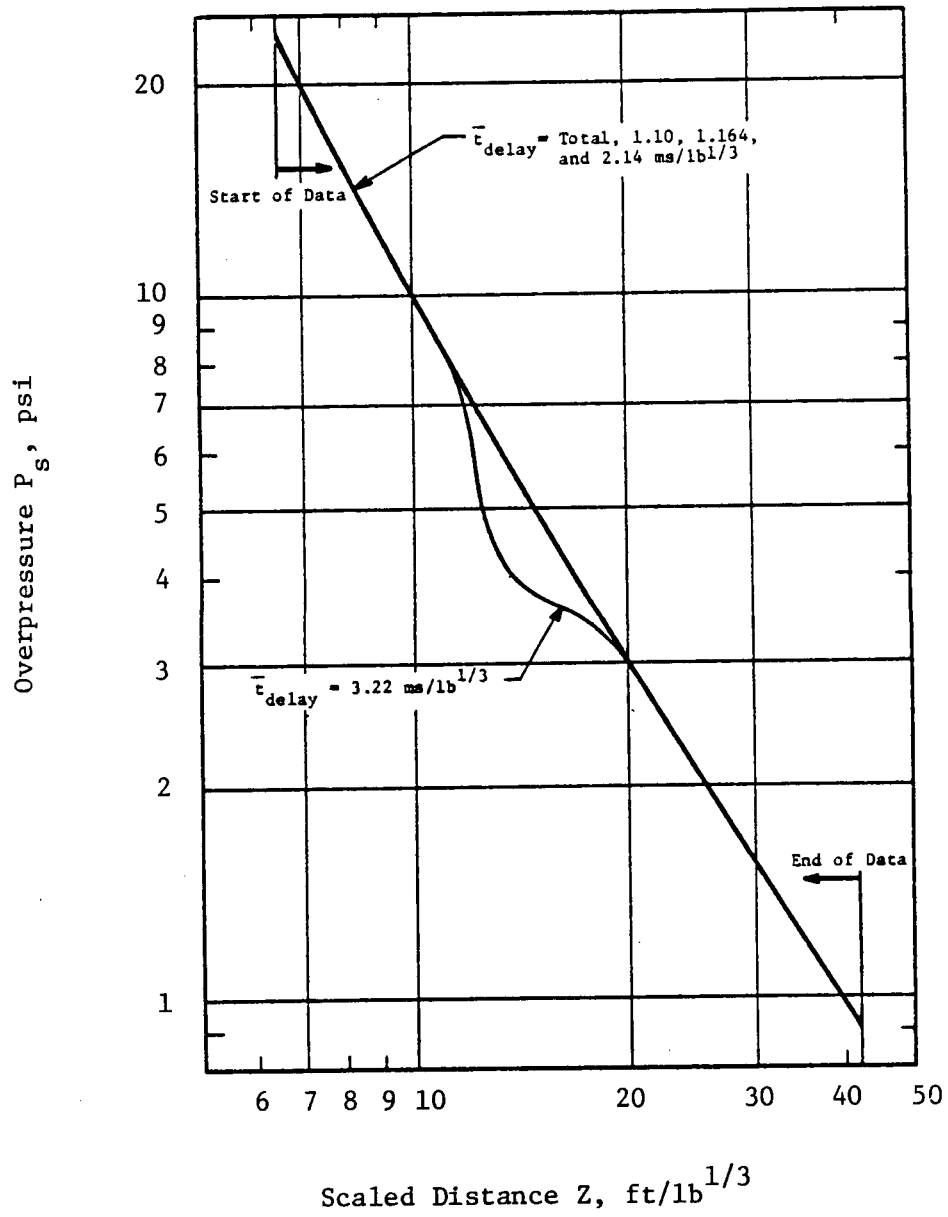
Figure 4.27   Axial Peak Pressure for a 1:2 Charge Ratio
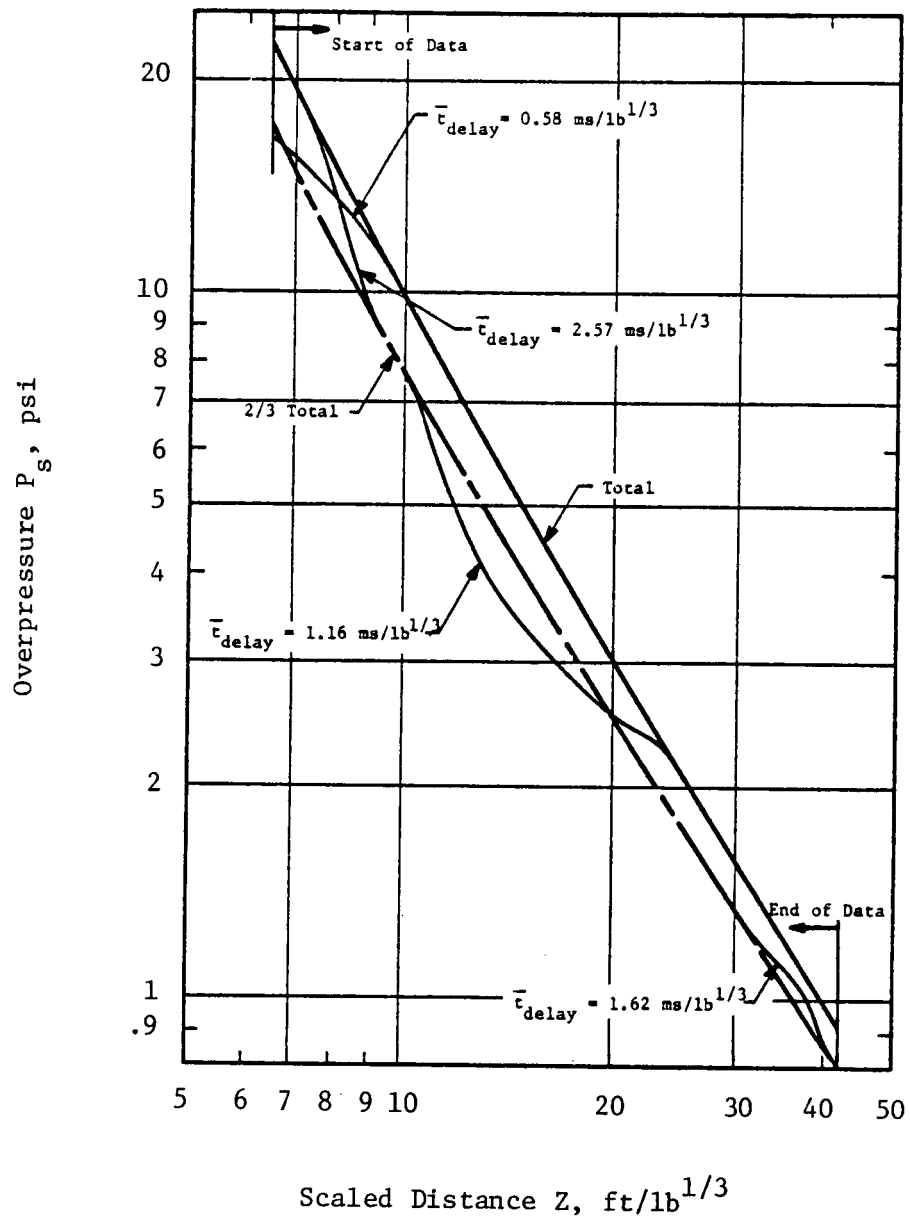
Figure 4.28   Lateral Peak Pressure for a 2:1 Charge Ratio
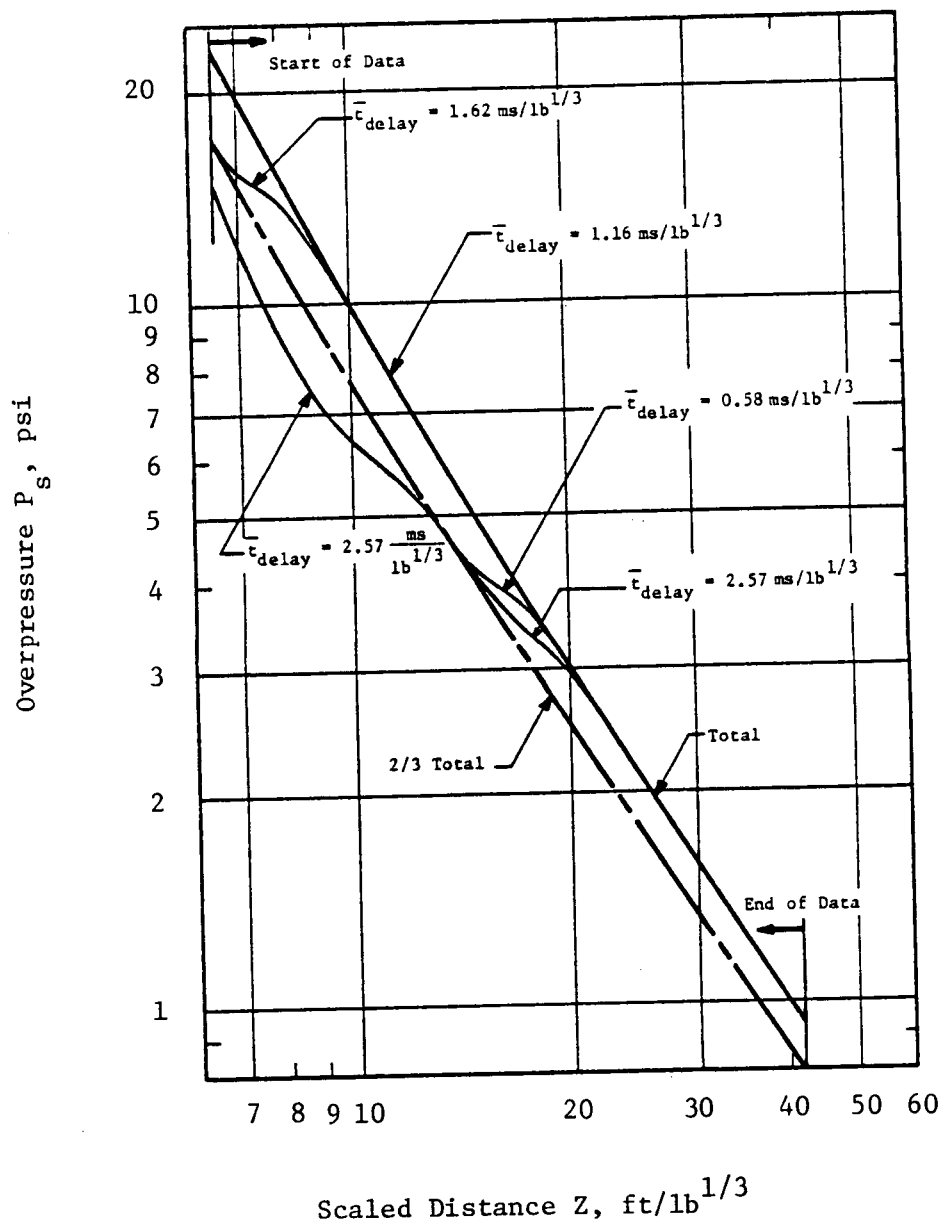
Figure 4.29 Axial Peak Pressure for a 2:1 Charge Ratio

4-74
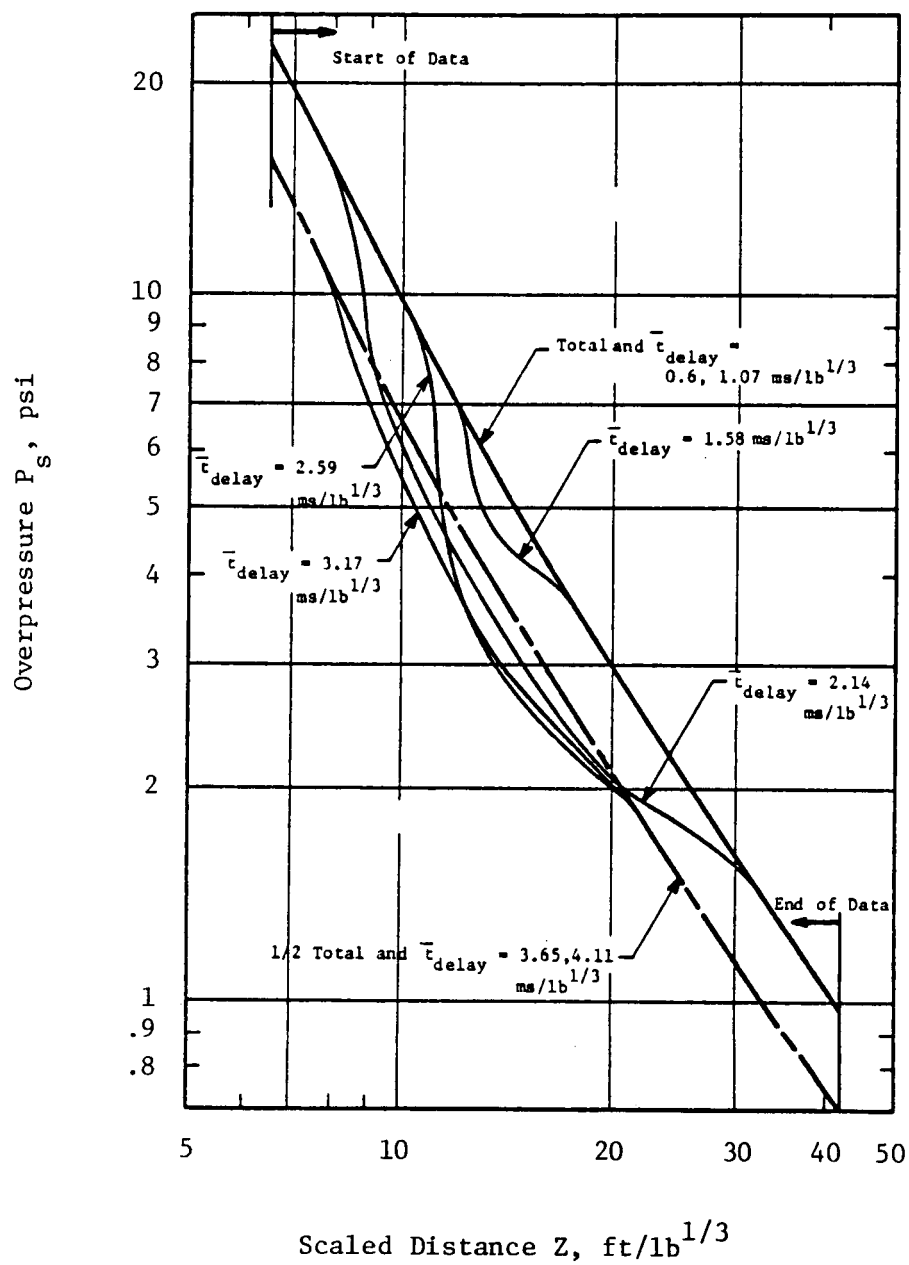
Figure 4.30 Lateral Peak Pressure for a 1:1 Charge Ratio
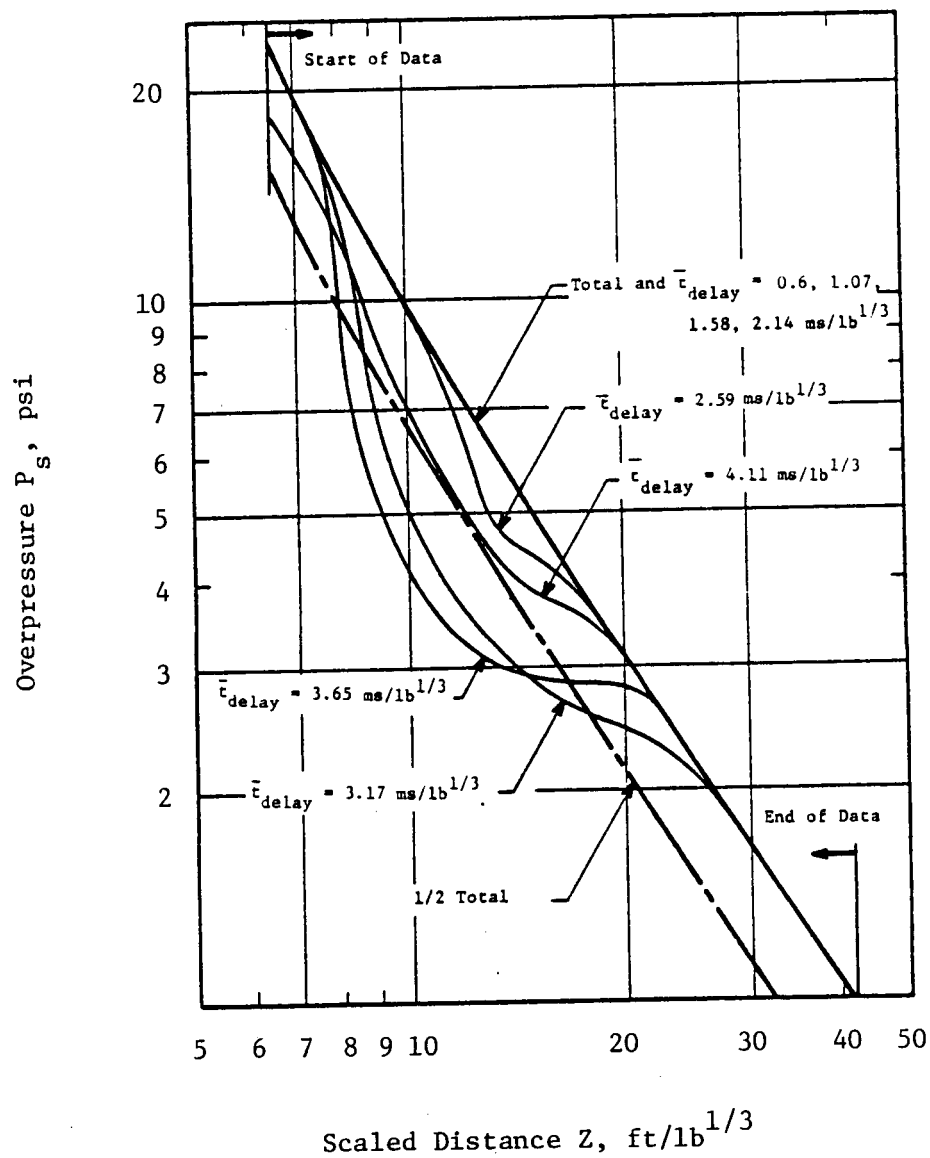
Figure 4.31 Axial Peak Pressure for a 1:1 Charge Ratio

delay isoclines of peak pressure as a function of standoff for a particular direction and charge ratio. This peak pressure is the highest pressure recorded of either shock (but not both peaks) or of the coalesced shock. Zaker's conclusions were:

- The effect of firing the charge farthest from the axial line first and the effect of the dividing wall reduces the time delay in axial direction by about 1.3 $ms/lb^{1/3}$ compared to that in the lateral direction.

- These same two conditions can cause the peak pressure of the first shock, when uncoalesced, to be less than expected for a single charge with no barrier. For long delay times, the second shock may travel within the negative phase of the first, thereby causing lower peak pressure in the second shock. If these two events combine, then neither peak pressure of the two pulses would be as high as the expected peak pressure of the larger of the two charges detonated by itself with no wall.

- The trailing pulse in the uncoalesced wave close in is comparable to that of the reference curve for the total charge weight.

- When coalescence occurs, the peak pressure follows the total reference curve for the total charge weight.

- For 1:1 ratio charges in the lateral direction, there is no tendency for shocks to coalesce within the data limit for time delays larger than 3.2 $ms/lb^{1/3}$. In the axial direction for 1:1, all time delays resulted in coalescence including the longest of 4.11 $ms/lb^{1/3}$. When considering the previously mentioned reduction in time delay of 1.3 $ms/lb^{1/3}$ for axial direction, then adding this to the 3.2 $ms/lb^{1/3}$ (lateral coalescence time), the coalescence is expected to occur up to 4.5 $ms/lb^{1/3}$ in the axial direction.

- Coalescence occurs more readily for 1:2 ratio than for the 2:1 ratio.

- For 2:1 and 1:2 ratios, there is no tendency of coalescence for lateral delays greater than 2.6 $ms/lb^{1/3}$ and 3.7 $ms/lb^{1/3}$, respectively. A reduction of 1.3 $ms/lb^{1/3}$ occurs for both 2:1 and 1:2 threshold coalescence times in the axial direction relative to the lateral direction.

The scaled curves in Figures 4.26 through 4.31 should only be used for scenarios involving similar scaled charge spacing and over the scaled distances shown in the graphs. Although this limits the use of the curves, an alternate approach exists. This approach is to consider the total charge weight in determining peak pressures when sequential detonations are being considered. Specific impulse is not discussed in Zaker's work. A conservative method for predicting impulse would be to calculate the impulse of each charge separately and then sum for a total impulse. This is as opposed to using the total charge weight for determining impulse. The following example shows why:

Consider two 0.5-lb charges of TNT.

$\bar{i}_r$ at a standoff of 10 ft for 1 lb is 1.5 X 10^{-2} psi-sec/lb$^{1/3}$ (See Figure 4.6). This gives an i_r = 1.5 X 10^{-2} psi-sec.

$\bar{i}_r$ at a 10 ft standoff for 0.5-lb TNT is 1.1 X 10^{-2} psi-sec/lb$^{1/3}$.

This relates to an i_r of 8.73 X 10^{-3} psi-sec. Considering twice this amount gives i_r(TOTAL) = 1.75 X 10^{-2} psi-sec which is greater than that from 1 lb of TNT. This occurs because the factor of 2 is not taken to the one-third root in the scaling for the two 0.5-lb charges. This can be important when considering a structure with a slow response time. The two pressure waves could arrive uncoalesced at the structure within a time span which is short compared to the structural response time, and the total impulse should be included. When the spacing between pulses is similar to the response time of the structure, resonance or anti-resonance is possible. (Structural resonance for multiple pulses is discussed in Section 4.4.)

PROBLEM – Determine blast pressure from two equal sequentially detonated charges separated by a short dividing wall. Compare with prediction for a single charge of the total weight.

GIVEN: W = single charge weight = $(1/2)W_{TOTAL}$ = $(1/2)$ Total charge weight

R = standoff
S = separation distance
t_{delay} = time delay in detonation

FIND: P_s REFERENCE

SOLUTION: 1. Determine if scenario matches that of experimental work; i.e., charges on ground, separated by the correct scaled distance, and with similar scaled time delay

2. If scenario is the same, determine scaled distance $(R/W_{TOTAL}^{1/3})$ and use Figures 4.30 and 4.31 for obtaining pressure   Fig. 4.30 & Fig. 4.31

3. Use W_{TOTAL} and ground reflection factor with Figure 4.5 if scenario is not the same or for comparison with Step 2   Fig. 4.5 P_s Curve

CALCULATION

GIVEN: W = 50 lb
W_{TOTAL} = 100 lb
R = 100 ft
S = 2.85 ft
t_{delay} = 9.90 ms

FIND: P_s

SOLUTION: 1. Scaled separation = $S/W_{TOTAL}^{1/3}$ = $2.85/100^{1/3}$ = 0.614 ft/lb$^{1/3}$

Scaled delay time $\bar{t}_{delay}$ = $t_{delay}/W_{TOTAL}^{1/3}$ = 9.90 ms/$100^{1/3}$ = 2.13 ms/lb$^{1/3}$
These scaled values are such that the curve for the time delay of 2.14 ms/lb$^{1/3}$ for the equal double charge curve can be used

2. Scaled standoff Z = $R/W_{TOTAL}^{1/3}$ = $100/100^{1/3}$ = 21.5 ft/lb$^{1/3}$

From Figure 4.30, lateral pressure = <u>2.0 psi</u>

From Figure 4.31, axial pressure = <u>2.7 psi</u>
3. For comparison with a single charge of weight equal to W_{TOTAL}, use a ground reflection factor of 2

$W' = 2 \times W_{TOTAL} = 200$ lb

Calculate scaled distance

$R' = R/W'^{1/3} = 100/200^{1/3} = 17.1$ ft/lb$^{1/3}$

Using P_s curve in Figure 4.5 to obtain

$P' = $ <u>2.55 psi</u>

Note that for this example problem, the blast overpressure obtained using the doubled single charge approximation is essentially the same as the larger of the two pressures for separated charges. For relatively large scaled distances, then, an AE can simply use a single charge with the total weight of the pair of charges. Had the values for $\bar{t}_{delay}$ and Z been different, say 3.17 and 15 respectively, reduction in peak overpressure would have been significant. So, simply summing the charges weight would be very conservative in this other case.

4.3.2.2 Simultaneous Detonation

This section includes a discussion on blast wave interactions and methods for predicting blast field parameters for two or more HE charges detonated simultaneously. There exist little or no data for unequal charges detonated simultaneously. Some equal charge data are available as a result of scaled nuclear blast field enhancement studies. The kill area of a total charge weight has been shown to increase by simultaneously detonating several smaller charges instead of one large charge. There is blast field enhancement between charges where blast waves meet and result in reflective pressures. Outside the line of center of the charges, blast waves coalesce to act as a single total weight charge. Several reports including data on this type of work are reports on the Dipole West test program [Reisler, et al. (Ref. 4.39)] and White Tribe program [Armendt, et al. (Refs. 4.40, 4.41, and 4.42)]. The Dipole West program included two-charge tests of vertically and horizontally separated large-scale charges. The White Tribe experiments concentrated on three-charge tests in a triangular array. Most tests were run with large charges although some small scale tests were made with good comparison. Also, Brode (Ref. 4.27) discusses numerical methods for predicting blast wave enhancement between simultaneously detonated charges. Several of these reports use computer model predictions for comparison in their work.

Work by Hokanson, Esparza, and Wenzel (Ref. 4.43) was done to characterize blast wave parameters on a reflecting surface from simultaneous detonations. In this work, three charges were arranged in three different configurations: grouped, horizontal, and vertical arrays (Figure 4.32) above a near-perfect reflecting surface (the ground). A series of single charge tests of total the three charge weights was conducted to establish a baseline for comparison. The results are given in Reference 4.43 in scaled form using the total charge weight for scaling purposes. Standoff ($R/W_{TOTAL}^{1/3}$) was measured from the reflecting surface to the center of mass of the three charges and charge weight equal to the total weight of the three charges. Scaled charge size was held relatively constant at $0.0425 < r/R < 0.154$ where r = charge radius, R = normal distance from charge to wall, and hence, the use of this work should be limited to situations within this range. The data presented in Reference 4.43 include peak pressure, scaled specific impulse, scaled positive duration, and scaled time of arrival as a function of scaled position. The data curves are drawn from data points which are an average of two measurements. The data, even in scaled form, are too voluminous for inclusion in this manual. But, two useful figures for single-charge data from this and other references are included, Figures 4.12 and 4.13, where X is distance along the reflecting surface measured from charge center of mass projection on wall and $Z = R/W_{TOTAL}^{1/3}$ (See Figures 4.14 and 4.32). These can be used for prediction of strong shock loads on walls supplementing Figure 4.11 for weaker shocks. Figures 4.33 and 4.34 are examples of the many empirical curves from Reference 4.43. These figures give pressures and scaled specific impulses versus scaled distance along the reflecting surface for three equal and evenly spaced charges at a scaled standoff of 1.29 $ft/lb^{1/3}$. The scaled charge spacing S/r is 2.28 (where r is the charge radius).
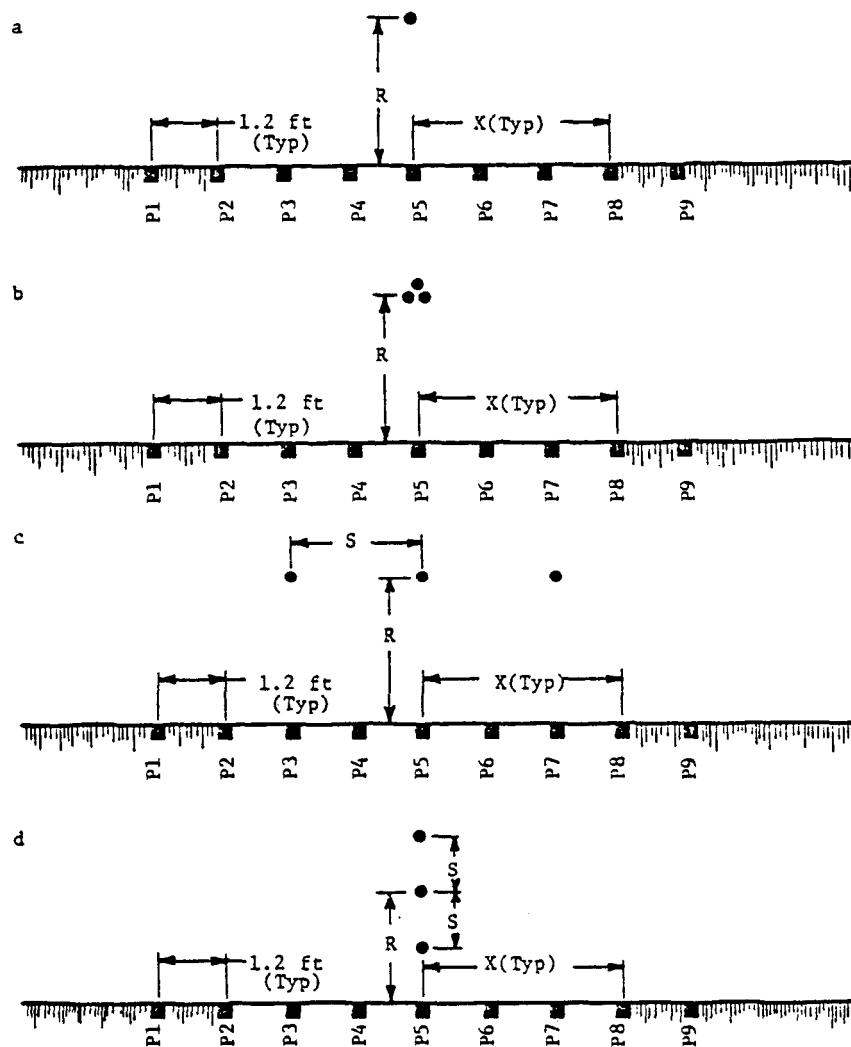
Figure 4.32   Transducer Arrangement and Charge Placement for the
(a) Single Charge, (b) Grouped Array, (c) Horizontal Array and
(d) Vertical Array Tests (Reference 4.43)
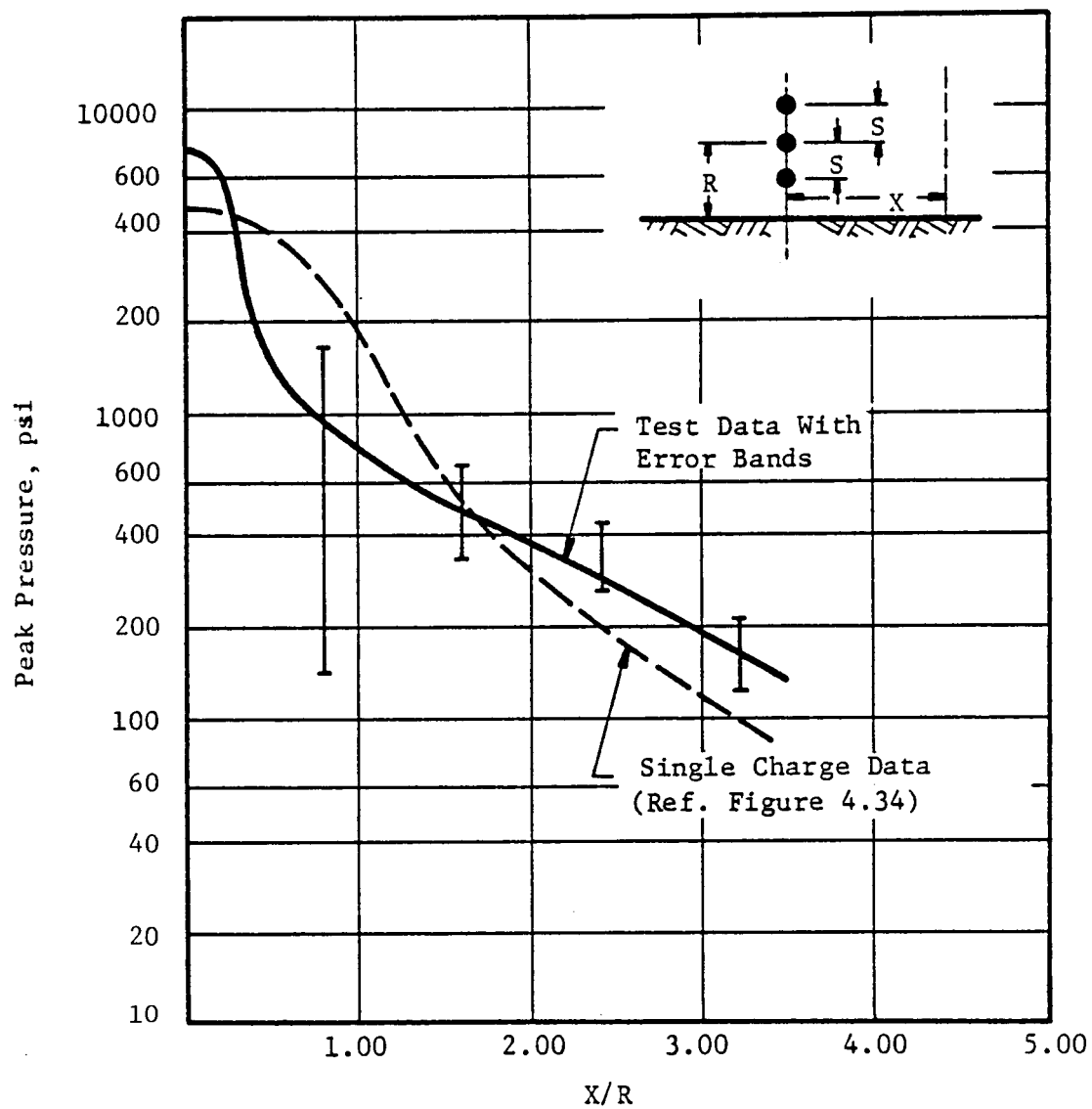
Figure 4.33   Peak Overpressure For Vertical Array Tests
(Reference 4.43)
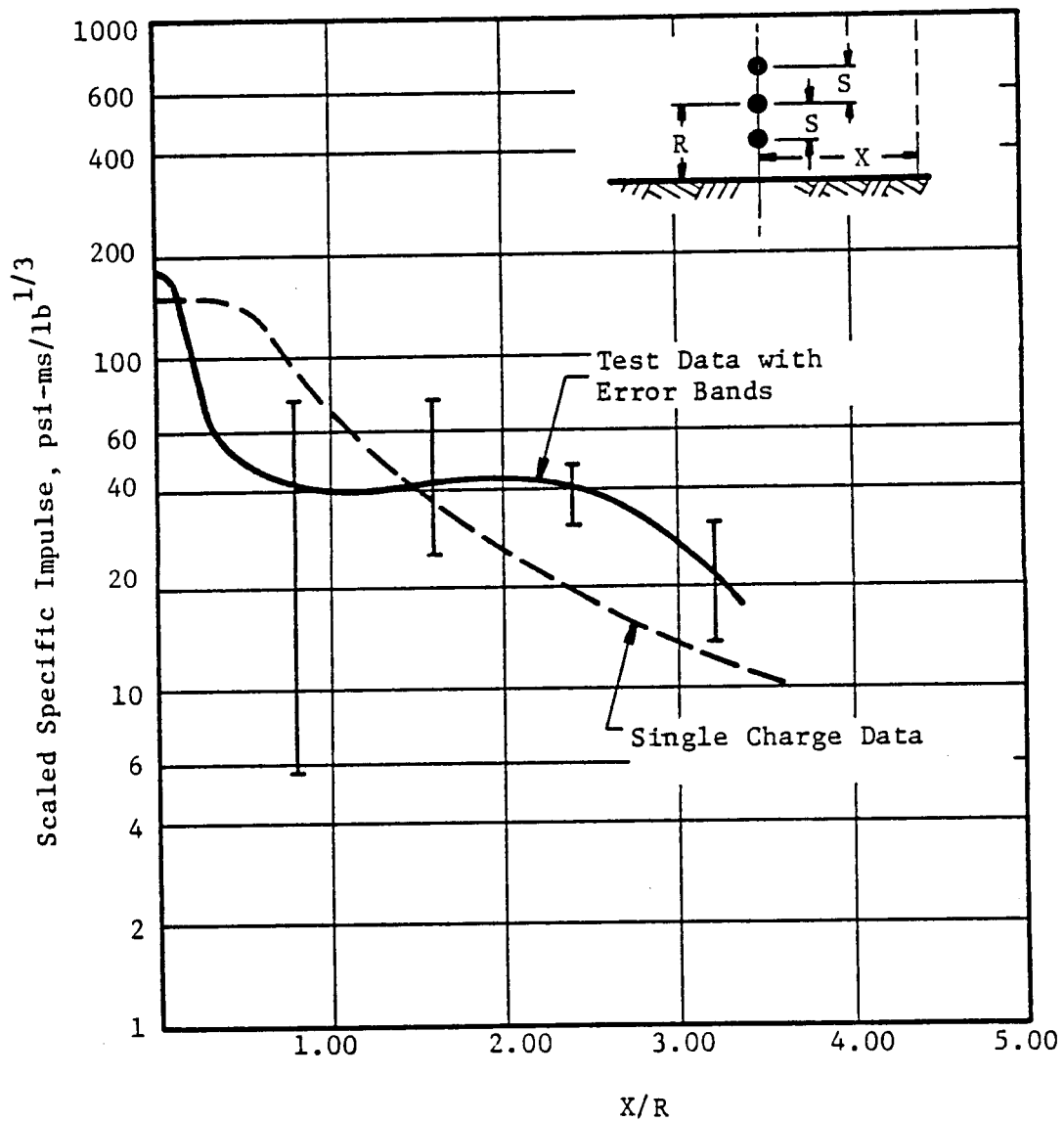
Figure 4.34   Specific Impulse For Vertical Array Tests
(Reference 4.43)

Hokanson, et al. (Ref. 4.43) concluded as follows:

- The pressure and impulse for grouped arrays at small scaled distances are lower than for single charges. The disparity between grouped array and single charge pressures is more pronounced than for impulses.

- For horizontal arrays, regions exist where the pressure and impulse exceed what would be expected from a single charge. The location of maximum response is dependent on the charge spacing and the standoff distance, but generally is found halfway between charges. Other regions of enhanced pressure and impulse exist just beyond the outside charge. For very wide charge spacings, the pressure and impulse are nearly constant over the entire range in X/R. For very narrow charge spacings, the regions of enhanced pressure are less pronounced than for intermediate charge spacings.

- Only one combination of charge spacings and standoff distances was investigated for vertical arrays. The results indicated that two regions of enhanced pressure and impulse exist, one directly under the vertical array and another for X/R > 1.5.

- The tests conducted verified the expectation that at large scaled distances, the blast parameters measured for multiple charges could approach those of a single charge. The distance at which the curves begin to coalesce is apparently the greatest for widely spaced horizontal arrays and the smallest for grouped arrays.

Based on the above observations, the following recommendations are made:

- Where applicable, these measurements can be used to obtain a more rational design for munition processing plants, particularly if the expected accidental explosion configuration falls within the range of scaled data in Ref. 4.43. Caution should be exercised, however, when extrapolation of these results is required beyond scaled distances, positions, or charge sizes tested.

- Only one combination of scaled distance and charge spacing was investigated for vertical arrays. These tests should be repeated to determine whether the trends described in the conclusions will exist for other values of Z and X/R.

- The gage placement for the horizontal array tests resulted in poor resolution of the variation in response as a function of S/r, particularly in the region between charges. Should tests of this nature be repeated in the future, more measurement positions should be provided in this critical region.

- Computer programs which could predict the pressure and impulse acting on a barrier due to multiple charge detonations do not exist at the present time. A three-dimensional program would be required, and even if available, would be very expensive to run. A cheaper and probably as accurate prediction technique can be devised, based on empirical observation. However, the data are probably insufficient to accomplish this goal. Therefore, further multiple detonation tests should be conducted and an attempt should be made to generate empirical prediction techniques.

<u>PROBLEM</u> – Determine blast pressure and specific impulse on a reflecting surface due to three equal spherical charges in a vertical array (see Figure 4.33). Compare with pressure and impulse from one charge of equal weight of the sum of the three on the same surface. Assume charges are located on the ground. The charges are detonated simultaneously.

<u>GIVEN</u>: R = perpendicular distance from surface to center of mass of the three charges
W = charge weight
S = charge spacing
X = distance along surface
ρ = density of HE

<u>FIND</u>: P_r and i_r REFERENCE

<u>SOLUTION</u>: 1. Determine radius of charge and determine if r/R is within acceptable limits

$$0.0425 < \frac{r}{R} < 0.154$$

2. Use ground reflection factor of 2 and total weight of three charges to obtain an effective (W_{eff}). Use W_{eff} to determine scaled standoff (Z)

$$W_{eff} = 2 \times 3 \times W$$
$$Z = R/W_{eff}^{1/3}$$

3. Use charge radius to determine scaled separation distance ($\overline{S}$)

$$\overline{S} = S/r$$

4. Use Figures 4.33 and 4.34 to determine pressure and impulse for various X/R for the separated charges

Fig. 4.33 &
Fig. 4.34

5. Use Figures 4.12 and 4.13 to determine pressure and impulse for various X/R for the single charge

Fig. 4.12 &
Fig. 4.13

<u>CALCULATION</u>

<u>GIVEN</u>: W_{TOTAL} = three charges of 50 lb of TNT each
= 150 lb total

R = 8.7 ft

ρ_{HE} = 0.06 lb/in^3

S = 1.11 ft

X = various

FIND: P_r and i_r

SOLUTION: 1. Determine radius of any one spherical charge of 50 lb:

$$r = \left(\frac{3W}{4\rho\pi}\right)^{1/3} = \left(\frac{3(50.0)}{4(0.06)(3.14)}\right)^{1/3} = 5.84 \text{ in or } 0.487 \text{ ft}$$

$$\frac{r}{R} = \frac{5.84 \text{ in}}{8.7 \text{ ft X 12 in/ft}} = 0.056 \text{ which is within acceptable range of } 0.0425 < r/R < 0.154$$

2. Use a ground reflection factor of 2 and total weight of the three charges to obtain an effective

$$W = W_{eff} = W_{TOTAL} \text{ X 2} = 2 \text{ X 150} = 300 \text{ lb}$$

Use W to solve for Z

$$Z = \frac{R}{W_{eff}^{1/3}} = \frac{8.7 \text{ ft}}{(300)^{1/3}} = 1.3 \text{ ft/lb}^{1/3}$$

3. Calculate $\overline{S}$

$$\overline{S} = \frac{S}{r} = 1.11 \text{ ft}/0.487 = 2.28$$

Figures 4.33 and 4.34 are applicable for this Z value and the $\overline{S}$ value

4. Using Figures 4.33 and 4.34, several values of X/R were evaluated for pressure and impulse from separated charges, on a reflecting surface. The values are listed in Table 4.6

5. Using Figures 4.12 and 4.13, several values of X/R corresponding to Step 4 were evaluated for pressure and impulse from a single charge, on a reflecting surface. The values are listed in Table 4.6

Table 4.6 Pressures and Impulses for Single and Multiple Charges

$\frac{X}{R}$	X ft	From Step 4, Multiple Charges			From Step 5, Single Charge		
		P psi	$\overline{i}$ $\frac{psi\text{-}msec}{lb^{1/3}}$	i psi-sec	P psi	$\overline{i}$ $\frac{psi\text{-}msec}{lb^{1/3}}$	i psi-sec
0	0	$7 \text{ X } 10^3$	200	1.1	$5.5 \text{ X } 10^3$	130	0.69
0.5	4.35	$1.5 \text{ X } 10^3$	55	0.29	$4.2 \text{ X } 10^3$	92	0.49
1.0	8.7	$7.5 \text{ X } 10^2$	42	0.22	$1.7 \text{ X } 10^3$	55	0.29
2.0	17.4	$3.8 \text{ X } 10^2$	42	0.22	$3.0 \text{ X } 10^2$	17	0.090

In this case, pressures and impulses are greater for the multiple charges than for the single charge with the same total weight at X = 0 and X = 17.4 ft, but this pattern reverses at the intermediate distances. One would have to integrate these values over the wall area to compare total impulses applied to the wall.

4.4 EFFECTS OF CONTAINMENT AND VENTING

Explosions which occur within structures normally develop a very complex pressure-time history at any position both inside and outside the structure. Although this complex loading cannot be predicted exactly, approximations and model relationships have been developed which can be used to define blast loads with a great deal of confidence. This section discusses these methods which include determination of blast loads due to initial and reflected shocks, quasi-static pressure, directional and uniform venting effects, and vent closure effects. Also, blast load prediction methods are applied to specific configurations. Example problem 4.11 illustrates the techniques developed in this section.

4.4.1 Effects Within Structures

The loading from a HE detonation within a vented or unvented structure consists of two almost distinct phases. The first phase is the reflected blast loading, which consists of an initial high pressure short duration reflected wave plus perhaps several later reflected pulses. The second phase is a quasi-static pressure pulse. These two phases of loading are discussed in this section.

4.4.1.1 Initial and Reflected Shocks

Initial and reflected shocks consist of the initial high pressure, short duration reflected wave, plus perhaps several later reflected pulses arriving at times closely approximated by twice the average time of arrival at the chamber walls. These later pulses are usually attenuated in amplitude because of an irreversible thermodynamic process, and they are complex in waveform because of the complexity of the reflection process within the structure, whether vented or unvented.

The simplest case of blast wave reflection is that of normal reflection of a plane shock wave from a plane, rigid surface. In this case, the incident wave moves at velocity U through still air at ambient conditions. The conditions immediately behind the shock front are those for the free-air shock wave discussed above. When the incident shock wave strikes the plane rigid surface, it is reflected from it. The reflected wave now moves away from the surface with a velocity U_r into the flow field and compressed region associated with the incident wave. In the reflection process, the incident particle velocity u_s is arrested ($u_s = 0$ at the reflecting surface), and the pressure, density, and temperature of the reflected wave are all increased above the values in the incident wave. The overpressure at the wall surface is termed the normally reflected overpressure and is designated P_r.

Maxima for the initial internal blast loads on a structure can be estimated from scaled blast data or theoretical analyses of normal blast wave reflection from a rigid wall (discussed in Section 4.3).

Following initial shock wave reflection from the walls, the internal blast pressure loading can become quite complex in nature. Figure 4.35 from Gregory (Ref. 4.44) shows a stage in the loading for a cylindrical, vented structure. At the instant shown, portions of the cap, base and cylindrical surface are loaded by the reflected shock and the incident shock is reflecting obliquely from all three internal surfaces. The oblique reflection process can generate Mach waves (Figure 4.9), if the angle of the incidence is great enough, and pressures can be greatly enhanced on entering corners or reflecting near the axis of a cylindrical structure. In box-shaped structures, the reflection process can be even more complex.

Following the initial internal blast loading, the shock waves reflected inward will usually strengthen as they implode toward the center of the structure, and re-reflect to load the structure again. As noted earlier, the second shocks will usually be somewhat attenuated, and after several such reflections, the shock wave phase of the loading will be over.

The shock wave loading can be measured with suitable blast measuring systems, or it can be computed for systems possessing some degree of symmetry. In a spherical containment structure, the loading can be relatively easily predicted for either centrally located or eccentric blast sources [Baker (Ref. 4.45), Baker, et al. (Ref. 4.46)]. In a cylindrical structure, existing (but complex) two-dimensional computer programs can be used to predict actual pressure-time loads for blast sources on the cylinder axis [See Figure 4.36 taken from Gregory (Ref. 4.44)]. For geometries normally encountered in actual facilities, prediction of accurate pressure-time loads is much more difficult, so approximate solutions have been used or measurements made. Kingery, et al. (Ref. 4.47) and Schumacher, et al. (Ref. 4.48) contain most of the internal blast measurements for uniformly vented structures, for cubical and cylindrical geometries, respectively.

As just noted, the initial and reflected air shock loadings on the interior surfaces of structures are quite complex for all real structural geometries. But, simplified loading predictions can often be made rather easily from scaled blast data for reflected waves and several approximate equations. The first approximation we will use is to assume that the incident and reflected blast pulses are triangular with abrupt rises, i.e.,

$$p_s(t) = P_s (1 - t/T_s), \quad 0 \leq t \leq T_s$$

$$p_s(t) = 0, \quad t \geq T_s \tag{4.37}$$

and
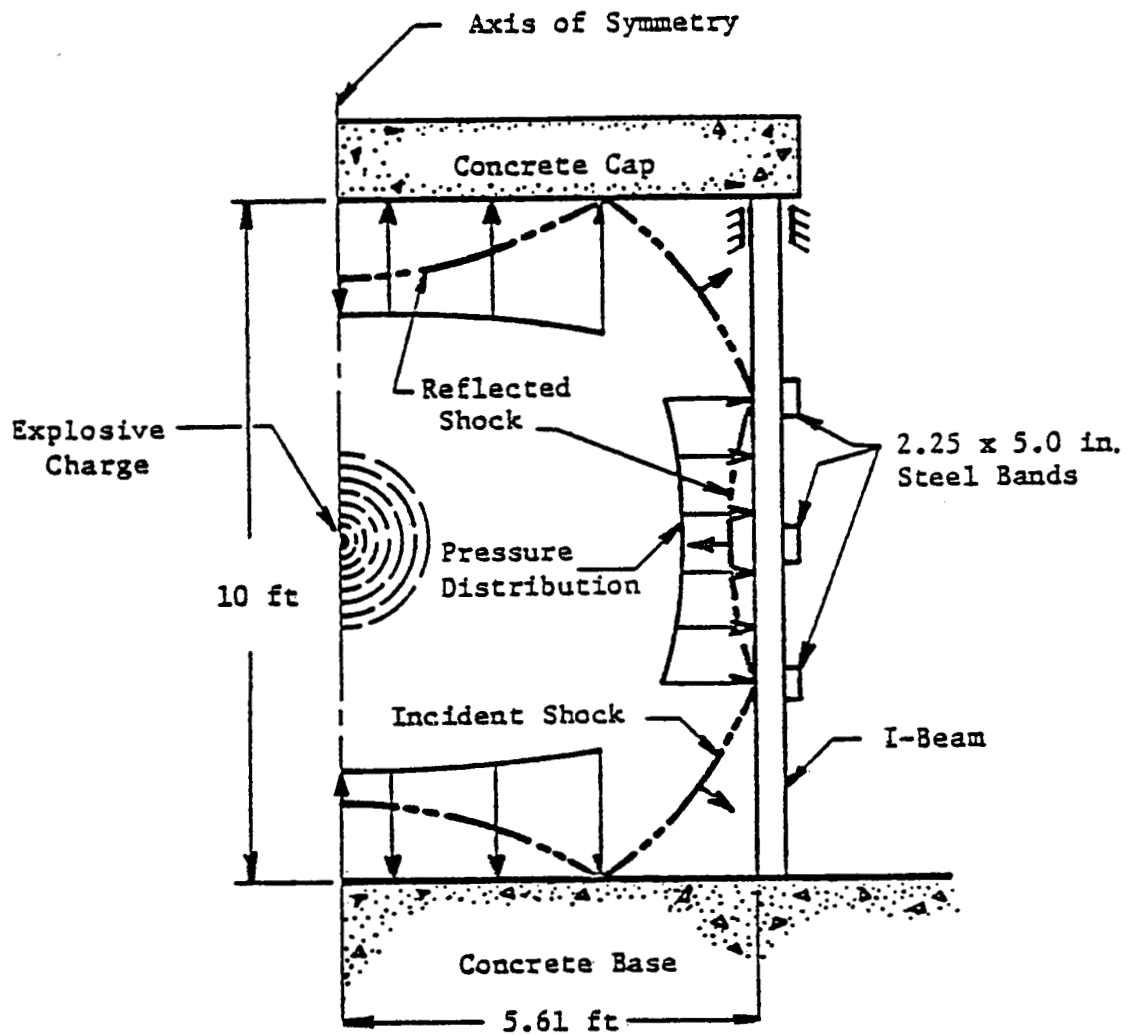
Figure 4.35 Schematic Representation Of Shock Reflections
From Interior Walls Of Cylindrical Containment Structure
(Reference 4.44)
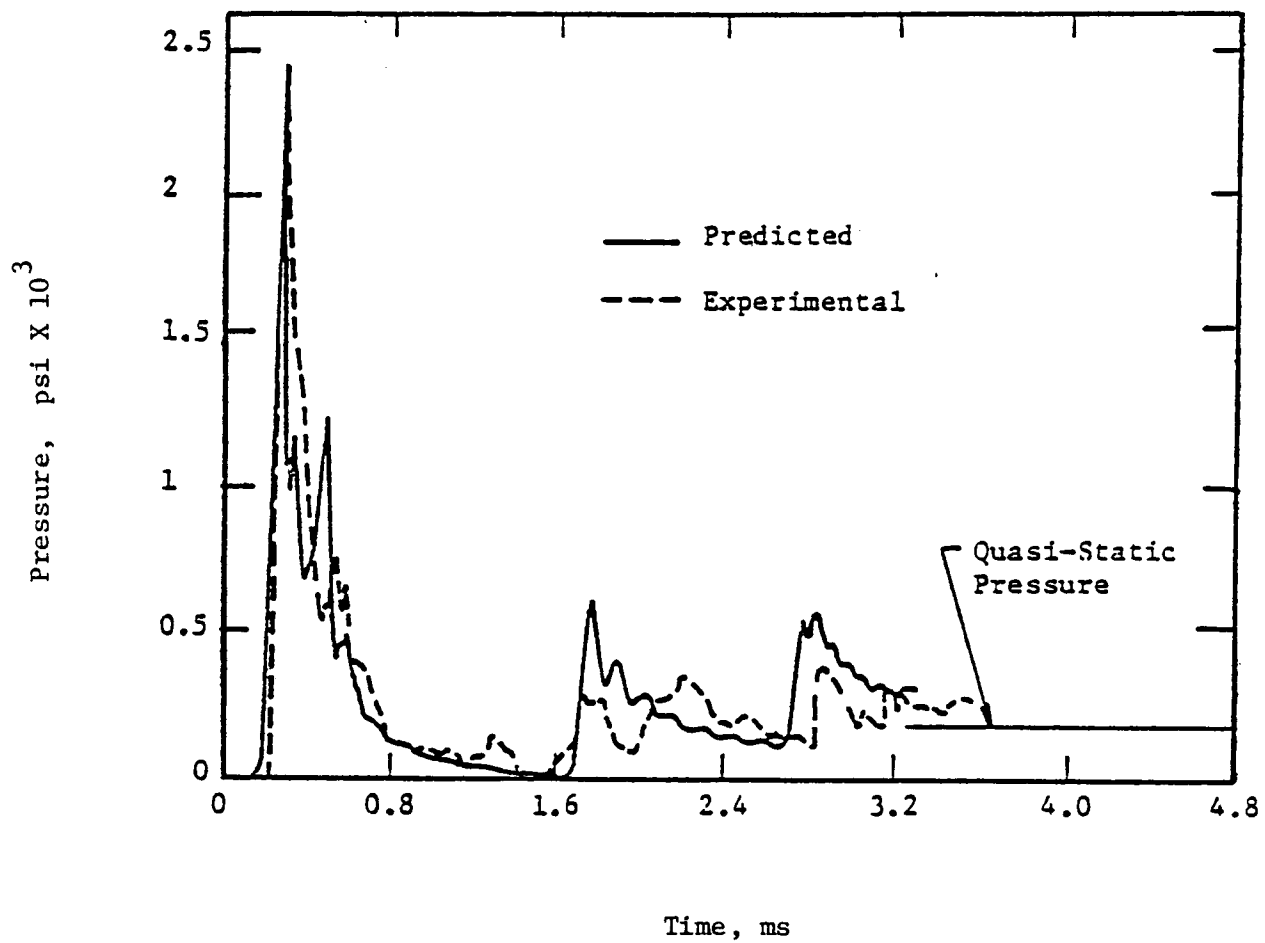
Figure 4.36   Comparison Of Predicted And Measured Pressure
Pulse At Point On Sidewall Of Cylindrical Containment
Structure (Reference 4.44)

$$p_r(t) = P_r (1 - t/T_r), \quad 0 \le t \le T_r$$

$$p_r(t) = 0, \quad t \ge T_r \qquad\qquad (4.38)$$

The durations of these pulses are not the same as the actual blast wave durations T, but instead are adjusted to preserve the proper impulses, i.e.,

$$T_s = \frac{2\, i_s}{P_s} \qquad\qquad (4.39)$$

$$T_r = \frac{2\, i_r}{P_r} \qquad\qquad (4.40)$$

These two equations constitute our second simplifying approximation.

A third simplifying approximation is that the initial internal blast loading parameters are, in most cases, the normally reflected parameters, even for oblique reflections from the structure's walls, provided the slant range is used as the distance R from the charge center to the location on the wall. For strong shock waves, this is almost exactly true up to the angle for limit of regular reflection of slightly greater than 39°, and for weak waves the limit is as great as 70° (See Figure 4.11). For angles beyond the limit of regular reflection, $\overline{P}_s = (P_s/p_o)$ can be calculated as usual for that standoff and P_r determined from Equation (4.27). For structure designs which are box-like with length-to-width ratios near one, shock reflections from the walls will be regular almost everywhere and no Mach waves will be formed.

    a.   <u>Centrally Located Detonation</u>. In enclosed structures, shock waves reflect and re-reflect several times, as discussed earlier. In certain configurations and over limited areas of the inner surface, the reflected waves can reinforce, but generally they are attenuated considerably before again striking the walls, floor or ceiling. For a centrally located detonation, it can be assumed that the second shock was half the amplitude and impulse of the initial reflected shock, the third shock has half the amplitude of the second shock, and that all later reflections are insignificant. The later two reflected pulses are often ignored in estimating the internal blast loading, because the pressures and impulses are much lower than in the initial pulse. Because the combined loads from all three pulses are only 1.75 times those

from the initial pulse, a design simplification can be employed for structures with response times much longer than the longest time in Figure 4.38. This simplification is simply to combine all three pulses, and multiply the amplitude (and equally the impulse) by 1.75. We suggest that an AE use this procedure for centrally located explosive sources. The procedure using the combined triple pulse is documented and recommended for use in Suppressive Shields (Ref. 4.3).

For either vented or unvented structures with response times much shorter than the initial shock wave duration, a simplification can be made by considering only the initial pulse and ignoring the latter two reflected pulses. For structures with response times in the range of the reverberation time ($2 t_a$), structural resonance may occur and no one simple approximation can be employed. The triple pulse problem has been solved for a simple elastic system in order to determine a method for defining the effects of structural resonance. The results of the solution follow.

Consider a simple elastic spring-mass system loaded by repeated triangular blast pressure pulses, Figure 4.37.
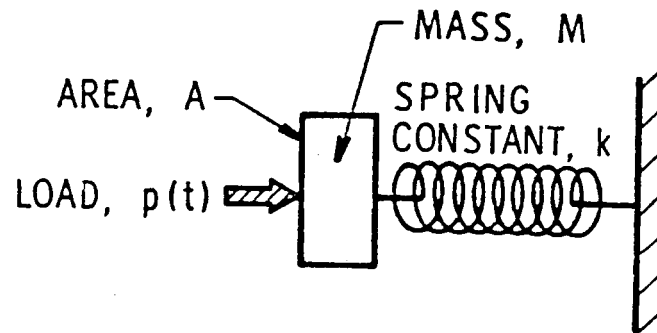
Figure 4.37   Elastic Spring-Mass System

Here, p(t) is shown schematically as Figure 4.38.
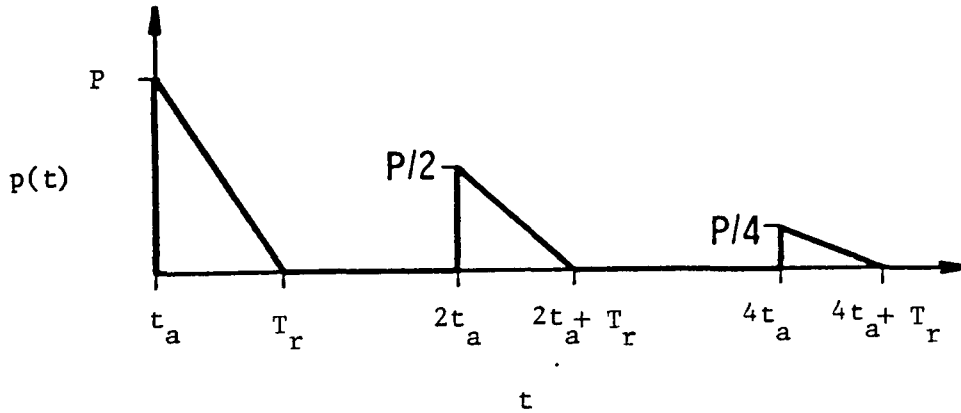
Figure 4.38 Schematic of Repeated Blast Loading

This system can be solved by classical or computer methods for maximum scaled response

$$\overline{X}_{max} = Xk/PA \qquad (4.41)$$

as a function of scaled time

$$\overline{T}_r = \omega T_r = (k/M)^{1/2} T_r \qquad (4.42)$$

The solution is shown graphically in Figure 4.39.

The scaled maximum response, $\overline{X}_{max}$, always lies between the response for the first pulse as a single pulse, and another single pulse consisting of the three repeated pulses combined in amplitude, i.e., having an amplitude of 1.75 P. These envelopes are shown in Figure 4.39. One solution is shown graphically in Figure 4.39. This figure reveals that the true triple pulse can cause maximum deflections in resonance (peaks in the solid curve) as great as the combined triple pulse (upper curve). Hence, this upper limit should be used for a conservative limit. This resonance solution can also be used to
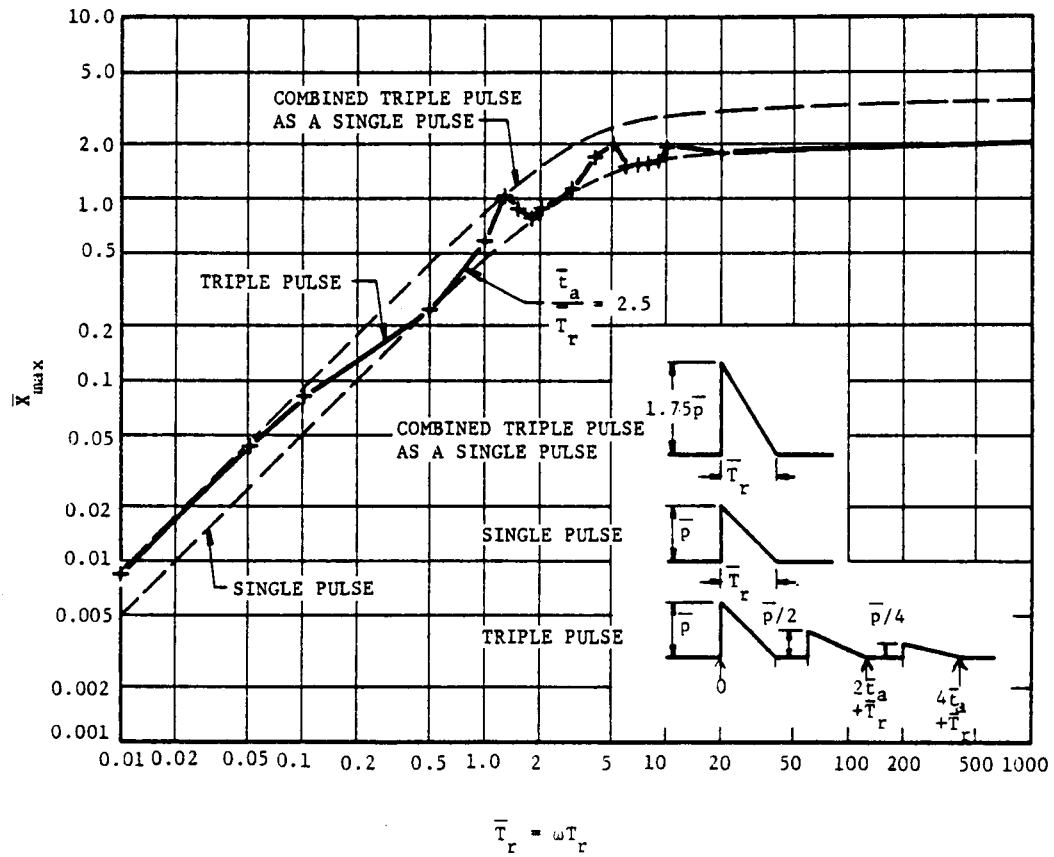
Figure 4.39 Envelope of Solutions for Maximum Displacement for Triple Pulse Blast Loading

determine the transition from resonance to the lower single pulse curve shown in Figure 4.39 (See Example Problem 4.11).

   b. Off-Center Detonation. For explosions near a wall, floor, or roof, the initial reflected blast loads can be predicted for spherical sources using Figures 4.12 and 4.13. But, the reflection processes within a chamber are as complex, or more complex, than the processes described in the previous section on centered detonations. Methods are given in TM 5-1300 for predicting average impulse on walls and roofs for various chamber sizes, ratios of length to height, numbers of enclosing walls and roof, and standoff from the nearest reflecting surface. In TM 5-1300, an impulse is chosen from one of 180 graphs depending on the number of reflecting surfaces (walls, floor, and roof), charge position in structure, room size, and standoff. Each graph has six isoclines of standoff ($R/W^{1/3}$) between which interpolation must be made if the exact standoff is not given. An example of these curves is given in Figure 4.40. The impulse value obtained is used in cases where the ratio of the times of maximum structural response t_m to blast duration t_o is very small. If the pressure duration is long compared to the component response time, the blast pressure time history is assumed triangular and a "fictitious" peak pressure P_f is solved for by:

$$P_f = 2 \text{ X impulse}/t_o$$

where t_o is calculated by methods given in TM5-1300.

   No mention of structural resonance (when t_o and the component response time are similar) is made in TM 5-1300. For initial shock loading of a nearby wall, Figures 4.12 and 4.13 can provide an estimate of both peak pressure distribution and reflected impulse distribution. There are no verified procedures for estimating reflected shock pressures on other surfaces for off-center detonations, but the methods described in TM 5-1300 (Ref. 4.2) do give procedures for predicting average specific impulses, and should be used by an AE. There are also computer programs for calculation of average reflected impulses documented in References 4.73 and 4.74. A comparison of the methods presented in this manual and TM 5-1300 (Ref. 4.2) is given in Example Problem 4.18.

4.4.1.2 Quasi-Static Pressures

   When an explosion from a high explosive source occurs within a structure, the blast wave reflects from the inner surfaces of the structure, implodes toward the center, and re-reflects one or more times. The amplitude of the re-reflected waves usually decays with each reflection, and eventually the pressure settles to a slowly decaying level, which is a function of the
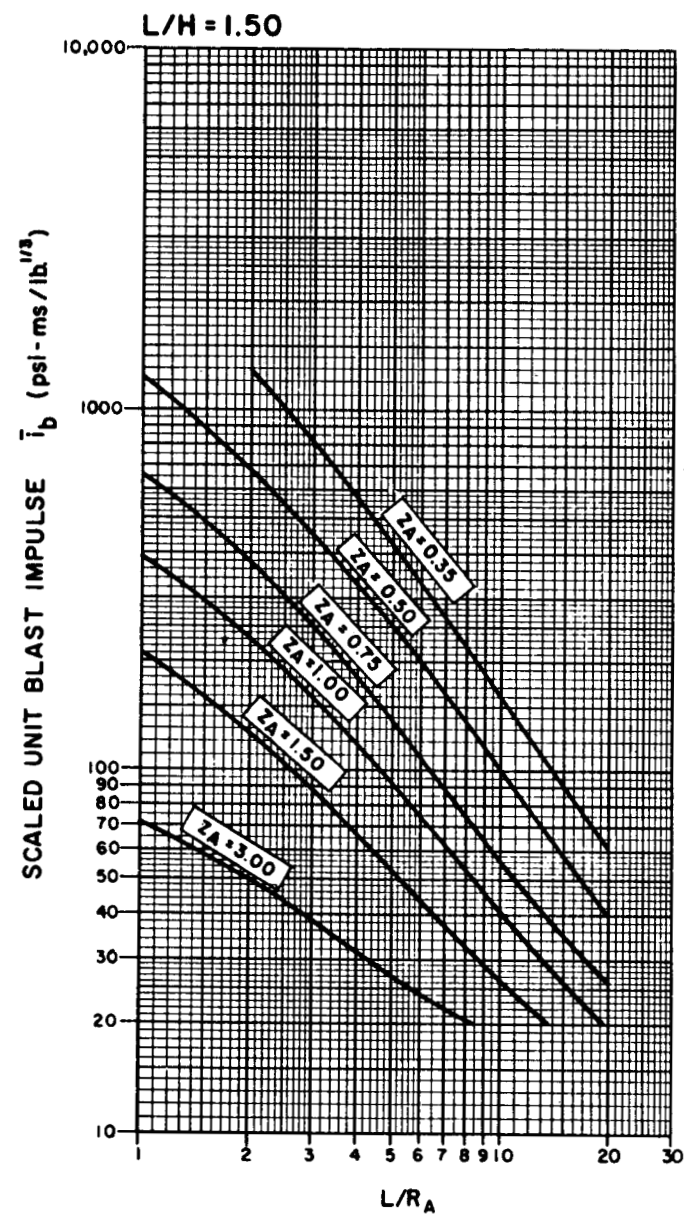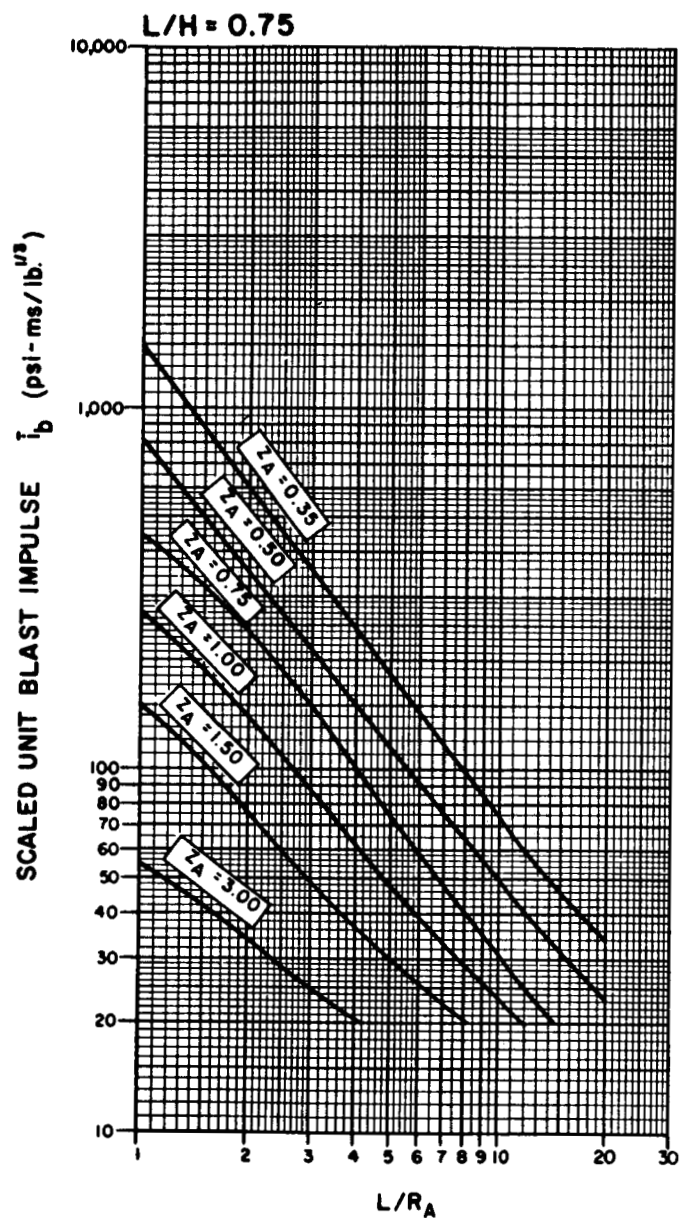
Figure 4.40   Scaled Average Unit Blast Impulse (N = 1, ℓ/L = 0.25 and 0.75, h/H = 0.25)
(Reference 4.2)

L/H = 3.00

L/H = 6.00
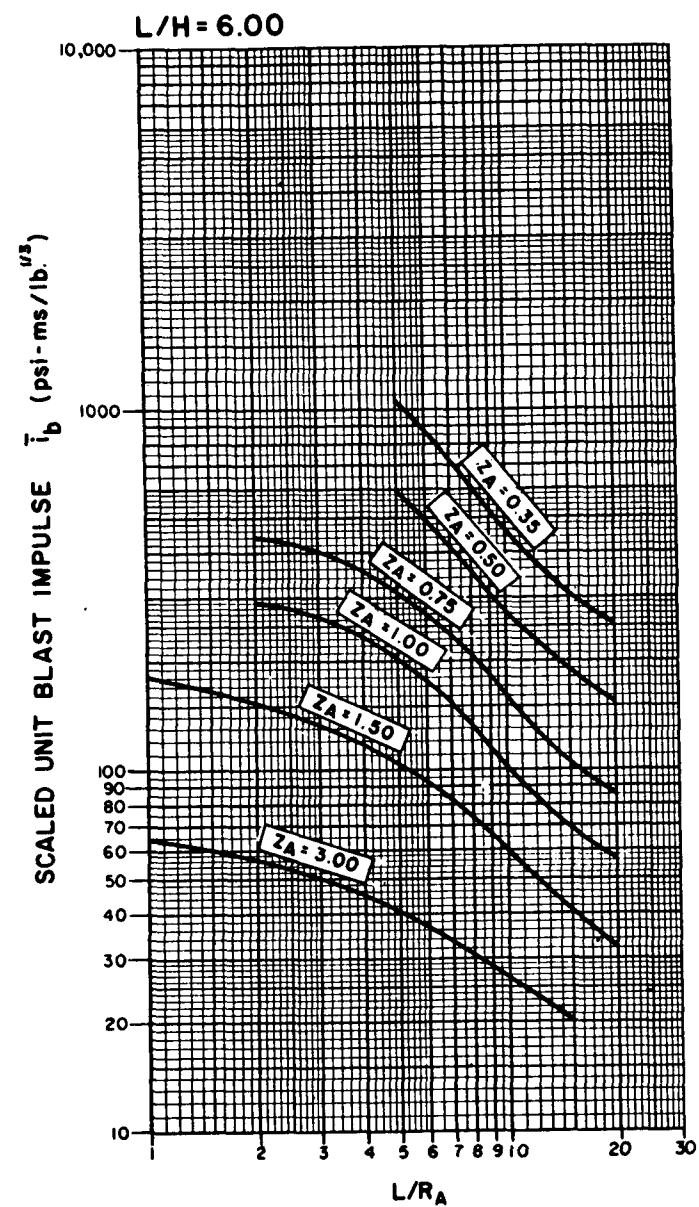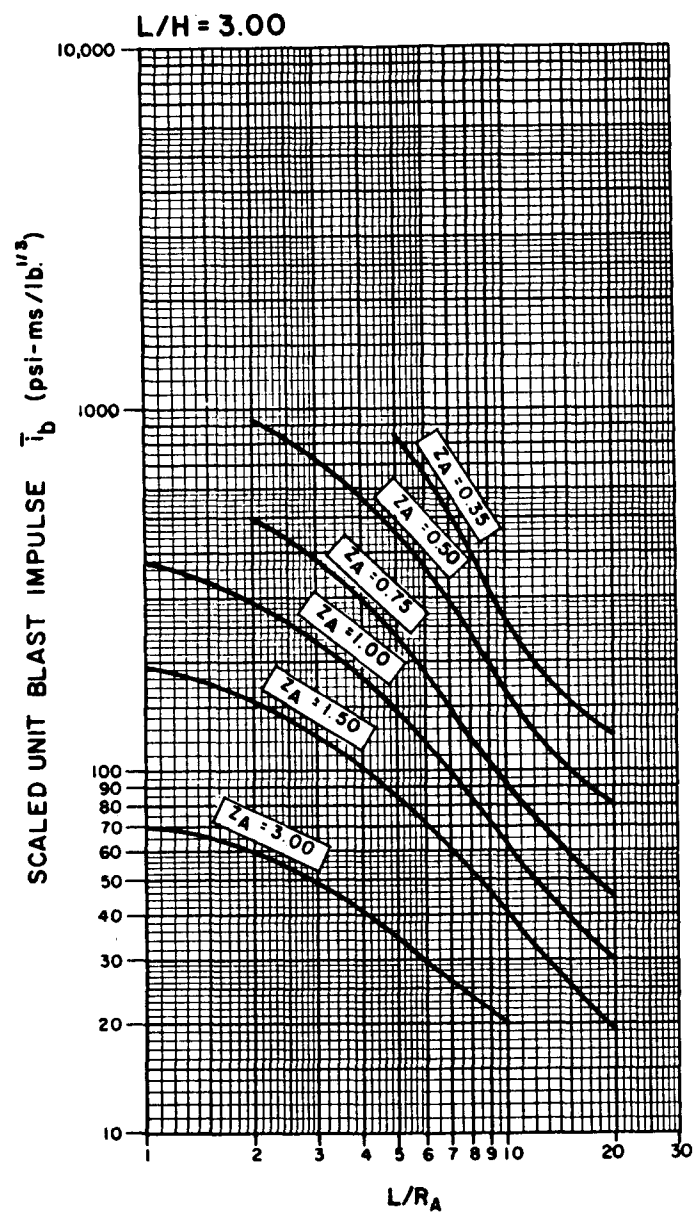
Figure 4.40   (Continued)

volume and vent area of the structure and the nature and energy release of the explosion. A typical time history of pressure at the wall of a vented structure is shown in Figure 4.41. The process of reflection and pressure buildup in either unvented or poorly vented structures has been recognized for some time, dating from World War II research on effects of bombs and explosives detonated within enclosures. More recently, study of these pressures has revived because of interest in design of vented explosion chambers. Esparza, et al. (Ref. 4.49) is the most recent work in this area.

Weibull (Ref. 4.50) reports maximum pressures for vented chambers of various shapes having single vents with a range of vent areas of $(A_v/V^{2/3})$ ≤ 0.0215. He fitted a single straight line to his data, but Proctor and Filler (Ref. 4.51) later showed that fitting a curve to the data, with asymptotes to lines related to heat of combustion for small (W/V) and to heat of detonation with no afterburning for large (W/V), was more appropriate. Additional data on maximum quasi-static pressures and on venting times have been obtained by Keenan and Tancreto (Ref. 4.52) and by Zilliacus, et al. (Ref. 4.53). Concurrent with experimental work which preceded applications to suppressive structures, Proctor and Filler (Ref. 4.51) developed a theory for predicting time histories of quasi-static pressures in vented structures. Kinney and Sewell (Ref. 4.54) did likewise, and also obtained an approximate formula for this time history. Converted to scaled parameters, this equation is:

$$\ln \overline{P} = \ln \overline{P}_1 - 2.130 \, \overline{\tau} \tag{4.43}$$

Here, $\overline{P}$ and $\overline{P}_1$ are scaled absolute pressures given by

$$\overline{P} = P(t)/p_o, \tag{4.44}$$

$$\overline{P}_1 = (P_{QS} + p_o)/p_o \tag{4.45}$$

and P_{QS} is the quasi-static pressure. The quantity $\overline{\tau}$ is a dimensionless time for venting given by

$$\overline{\tau} = \overline{A} \, \overline{t} = \left(\frac{\alpha_e A_s}{V^{2/3}} \right) \left(\frac{t a_o}{V^{1/3}} \right) \tag{4.46}$$

4-101
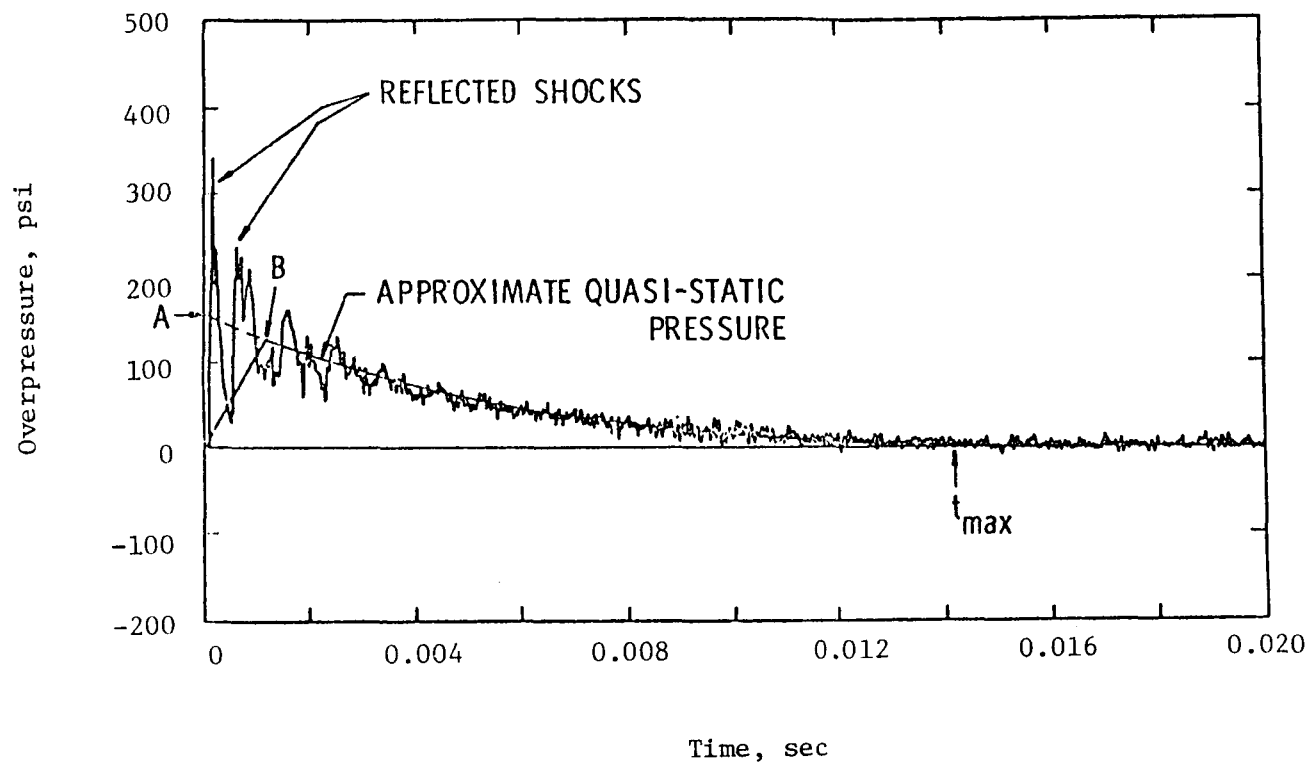
Figure 4.41 Typical Time History of Internal Pressure at Inner Surface of a Suppressive Structure (Reference 4.47)

In this equation, α_e is an effective vent area ratio to be discussed later, A_s is internal surface area of the structure, V is internal volume of the structure, t is time, and a_0 is sound velocity of air in the structure. The rationale for use of these scaled parameters is developed by Baker and Oldham (Ref. 4.55). Equation (4.43) gives a value for scaled venting time $\bar{\tau}$ of

$$\bar{\tau} = 0.4695 \ln \bar{P}_1 \qquad (4.47)$$

The problem of blowdown from a vented chamber is also solved theoretically by Owczarek (Ref. 4.56), given initial conditions in the chamber but assuming isentropic expansion through the vent area.

In the suppressive structures program, sufficient data have been recorded for this class of structure to add significantly to the measurements for other types of vented or unvented chambers [Kingery, et al. (Ref. 4.47), Schumacher, et al. (Ref. 4.48)]. In comparing such data with either previous data or theory, there are several questions raised by the general physics of the process and by the differences in venting through single openings in walls. Referring to Figure 4.41, one can see that the maximum quasi-static pressure is quite difficult to define because it is obscured by the initial shock and first few reflected shocks. Obviously, several reflections must occur before irreversible processes attenuate the shocks and convert their energy to quasi-static pressure. It, therefore, seems inappropriate to call point A in Figure 4.41 the peak quasi-static pressure, although this is the point used by Kingery, et al. (Ref. 4.47) to compare with code predictions from Proctor and Filler (Ref. 4.51) and the Kinney and Sewell equation (Ref. 4.54). A better approach is to allow some time for establishing the maximum pressure, such as point B in Figure 4.41.

Figure 4.41 also illustrates another problem inherent in reduction of vented pressure data, i.e., accurate determination of duration of this pressure. When the pressure traces approach ambient, the shock reflections have largely decayed. But, they approach the baseline nearly asymptotically, so that the duration is quite difficult to determine accurately. A possible duration t_{max} is shown in the figure.

Based on a scaling law by Baker and Oldham (Ref. 4.55) and a theoretical analysis of chamber venting by Owczarek (Ref. 4.56), one can show that $\bar{P} = (P/p_0)$ is a function of ratio of specific heats γ and the scaled time $\bar{\tau}$ (See Equation (4.46)),

$$\bar{P} = f_2 \ (\bar{P}_1, \ \bar{\tau}, \ \gamma) \qquad (4.48)$$

The initial pressure $\bar{P}_1$ for structures with no venting or small venting can be shown to be related to another scaling term,

$$\bar{P}_1 = f_3 \ (E/p_o V) \tag{4.49}$$

where E is a measure of total energy released by the explosion. For tests with explosives of the same type and no change in ambient conditions, a dimensional equivalent of Equation (4.49) is

$$P_1 = f_4 \ (W/V) \tag{4.50}$$

where W is charge weight (lb) and V is chamber volume (ft^3). The scaled pressure-time histories during the gas venting process can be integrated to give scaled gas impulse $\bar{i}_g$. This parameter is defined as

$$\bar{i}_g = i_g \left(\frac{\alpha_e A_s a_o}{p_o V} \right) \tag{4.51}$$

Equations (4.43) and (4.49) can be shown to give

$$\bar{i}_g = \frac{1}{2.130} \left(e^{2.130 \ \bar{\tau}} - 1 \right) - \bar{\tau} \tag{4.51a}$$

For a single layer structure, the vent area ratio α_e is the vent area divided by the total area of the wall, and the product

$$\alpha_e A_s = A_v \tag{4.52}$$

For a multi-layer wall, however, the following relationship is used.

$$\frac{1}{\alpha_e} = \sum_{i=1}^{N} \frac{1}{\alpha_i} \tag{4.53}$$

It reaches the appropriate limits for large and small number of plates, and provides a relative measure of venting for a variety of panel configurations. Definition of the individual values of α_i for each layer in a multi-layered vented panel requires careful study of the panel configuration and experimental verification. Specific formulas and methods for predicting α_e for various suppressive structure panels are presented by Esparza, et al. (Ref. 4.49).

In spite of complexities in the venting process, gas venting pressures and their durations can be predicted with reasonable accuracy, particularly if one differentiates between these relatively long term and low amplitude pressures and the internal blast pressures resulting from blast wave impingement and reflection. Figure 4.42 shows the simplified form for the gas venting pressures which can be assumed.

In this simplified form, the gas venting pressure is assumed to follow the solid curve and rise linearly from zero time until it reaches in time t_1 a curve which is decaying exponentially from an initial maximum value of P_1. The decay then follows the time history

$$P(t) = P_1 e^{-ct} \tag{4.54}$$

until it reaches ambient pressure p_0 at time $t = t_{max}$. The exponential decay is shown to agree well with experiment [Kingery, et al. (Ref. 4.47), Schumacher, et al. (Ref. 4.48)]. The cross-hatched area under the overpressure curve is defined as the gas impulse, i_g, and is given mathematically as

$$i_g = \int_0^{t_{max}} [P(t) - p_0] \, dt$$

$$= \int_0^{t_{max}} (P_1 e^{-ct} - p_0) \, dt$$

$$= \frac{P_1}{c} \left(1 - e^{-ct_{max}} \right) - p_0 t_{max} \tag{4.55}$$
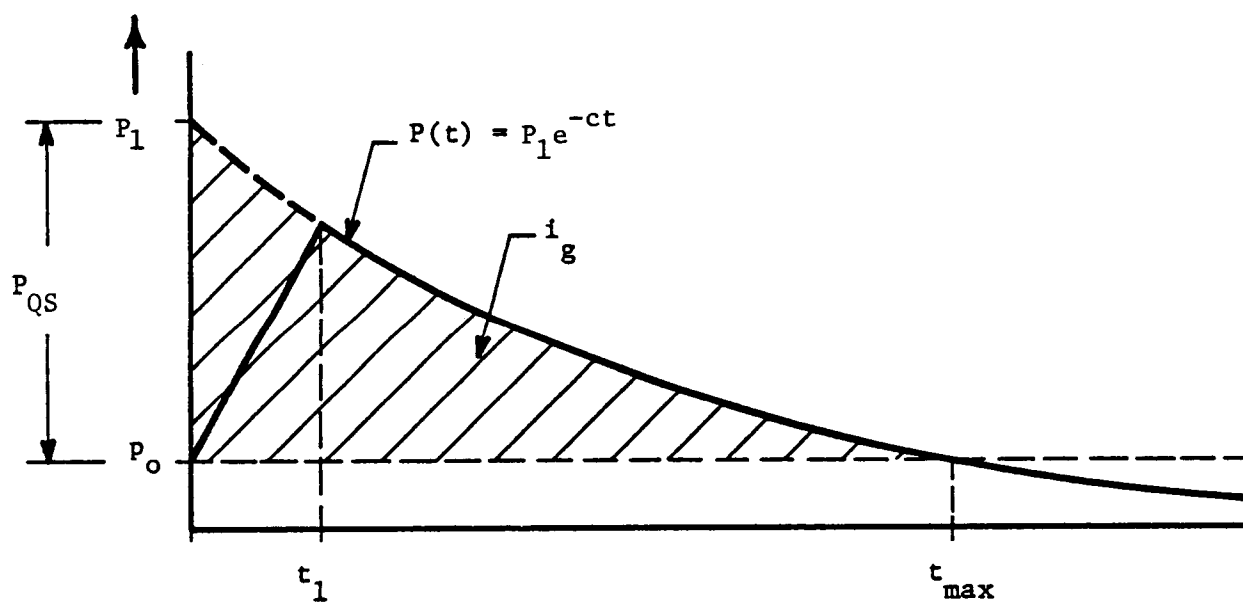
Figure 4.42 Simplified Gas Venting Pressure

The time t_1 we will assume to be the end of the internal blast loading phase.

$$t_1 = 5 \, t_a + T_r \qquad (4.56)$$

where T_r is the duration of a triangular pulse with correct P_r and i_r. This is identical to the end of the triple-pulse loading in Figure 4.38, with time t_a added for first shock arrival.*

The maximum value for the overpressure in the gas venting phase of the loading is the static pressure rise which would occur in an unvented enclosure before heat transfer effects attenuate it, P_{QS}. From data and analyses in several references, the curve of Figure 4.43 has been shown to yield good predictions of P_{QS}, if the quantity of explosive W and the internal volume of the structure V are known.

Other gas venting parameters than P_{QS}, or $P_1 = P_{QS} + p_o$, can be most easily predicted using plots or equations for some of the scaled parameters described earlier. The quantity c in Equation (4.54) is given with reasonable accuracy by

$$c = 2.130 \left(\frac{\alpha_e A_s a_o}{V} \right) \qquad (4.57)$$

For air at standard sea level conditions, $a_o = 1117$ ft/sec, and

$$c = 23 \; \frac{\alpha_e A_s}{V} \; (\text{sec}^{-1}) \qquad (4.58)$$

for A_s in ft^2 and V in ft^3. As indicated, units of c in this last equation are sec^{-1}. Figures 4.44 and 4.45 give scaled durations of gas overpressure $\bar{t}_{max}$ and scaled gas impulse $\bar{i}_g$ as functions of scaled initial pressure $\bar{P}_1 = P_1/p_o$.

---

*This rise-time applies primarily for explosion sources near the chamber center. For off-center charges, it still gives a good estimate, provided the charge is simply assumed to be centered when estimating t_a.
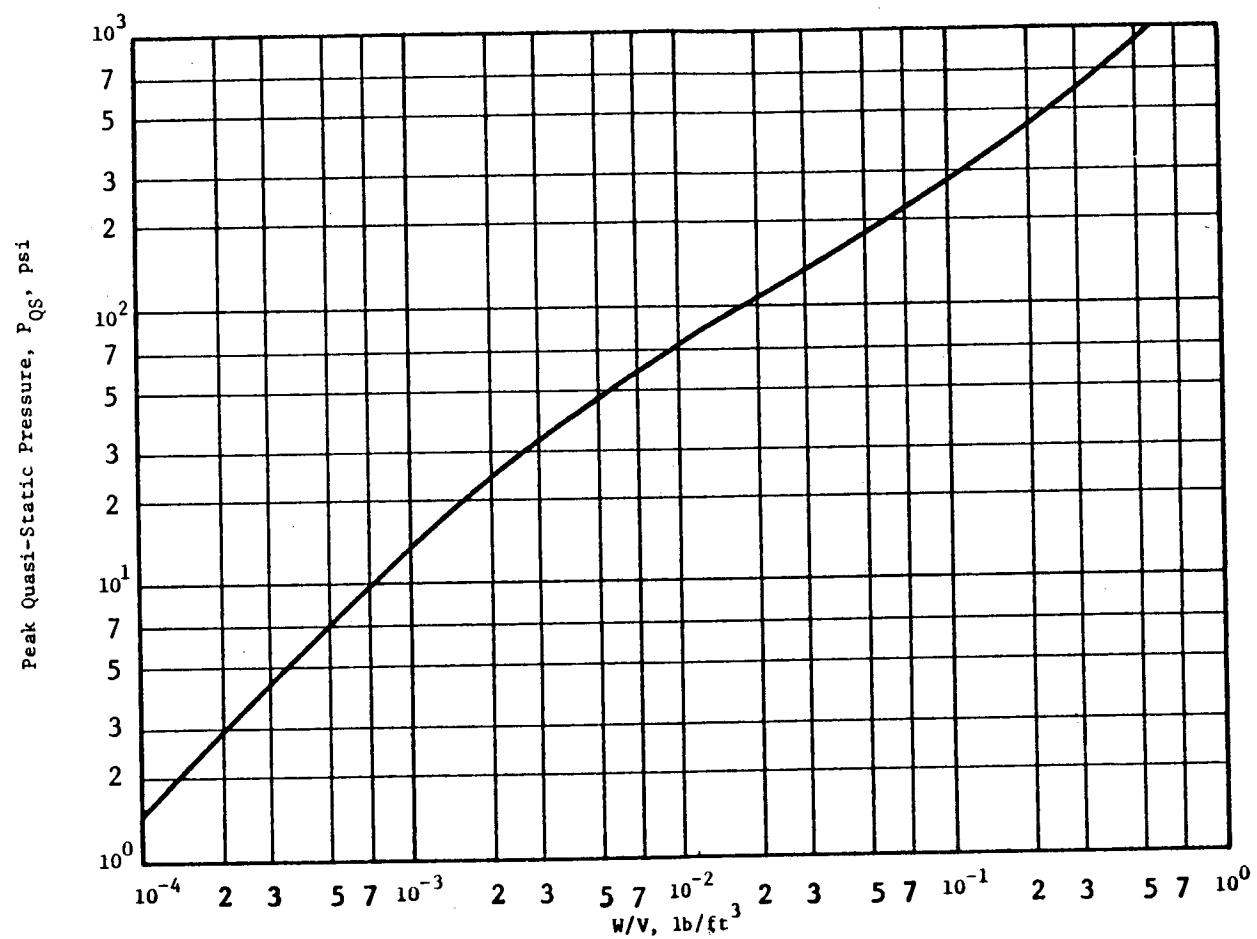
Figure 4.43   Peak Quasi-Static Pressure for TNT Explosion in Chambers

The y-axis is labeled:

$$\bar{P}_1 = \left(\frac{P_1}{P_o}\right) = \frac{P_{QS} + P_o}{P_o}$$

with values 10^0, 2, 4, 6, 10^1, 2, 4, 6, 10^2.

The x-axis is labeled:

$$\bar{\tau} = \left(\frac{t a_o}{V^{1/3}}\right)\left(\frac{\alpha_e A_s}{V^{2/3}}\right)$$

with values 0, 0.5, 1.0, 1.5, 2.0, 2.5.
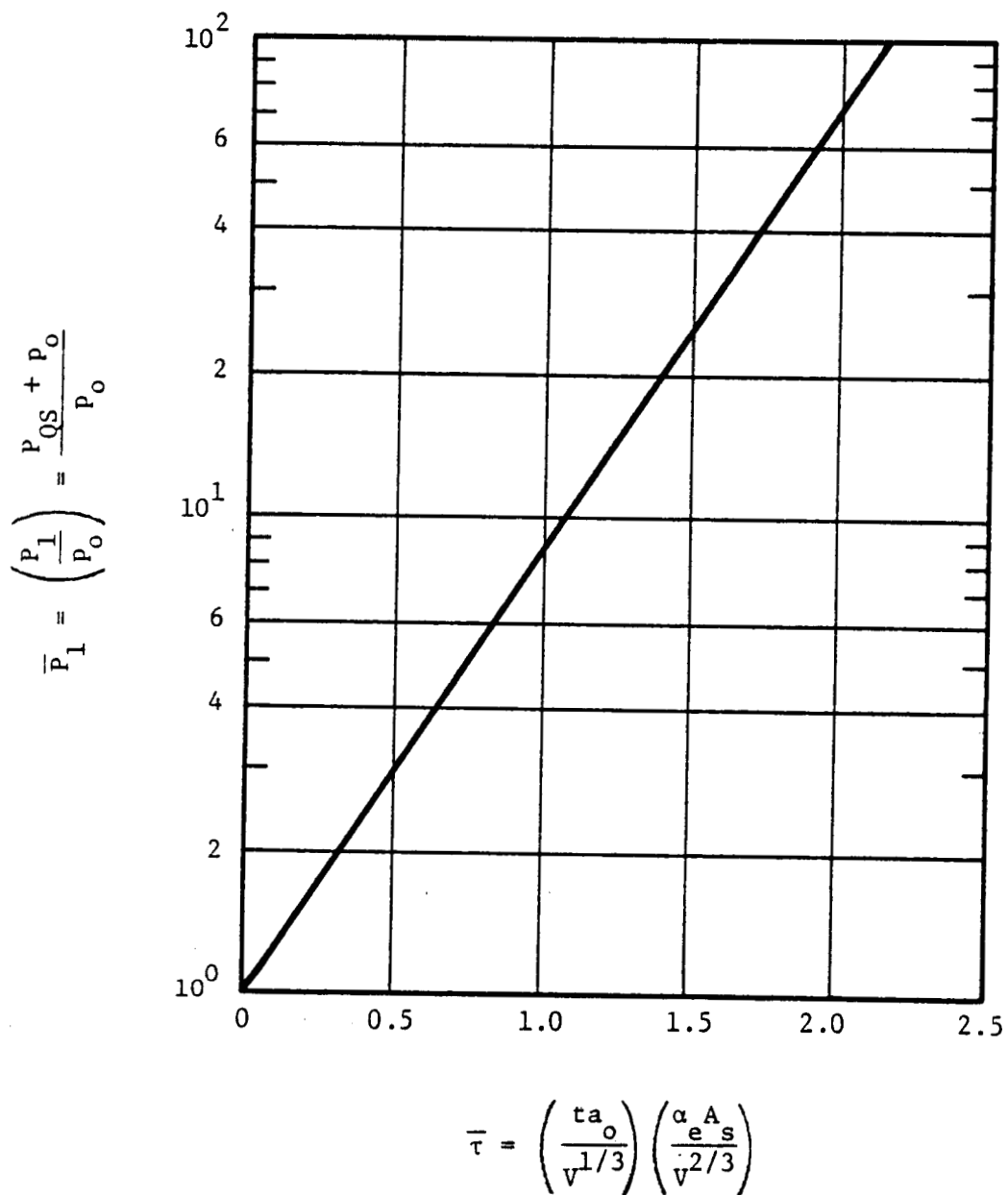
Figure 4.44   Scaled Blowdown Duration versus Scaled Maximum Pressure

4-109

The y-axis is labeled:
$$\bar{i}_g = i_g \left(\frac{\alpha_e A_s a_o}{p_o V} \right)$$

The x-axis is labeled:
$$\bar{P}_1 = (P_1/p_o) = (P_{QS} + p_o)/p_o$$
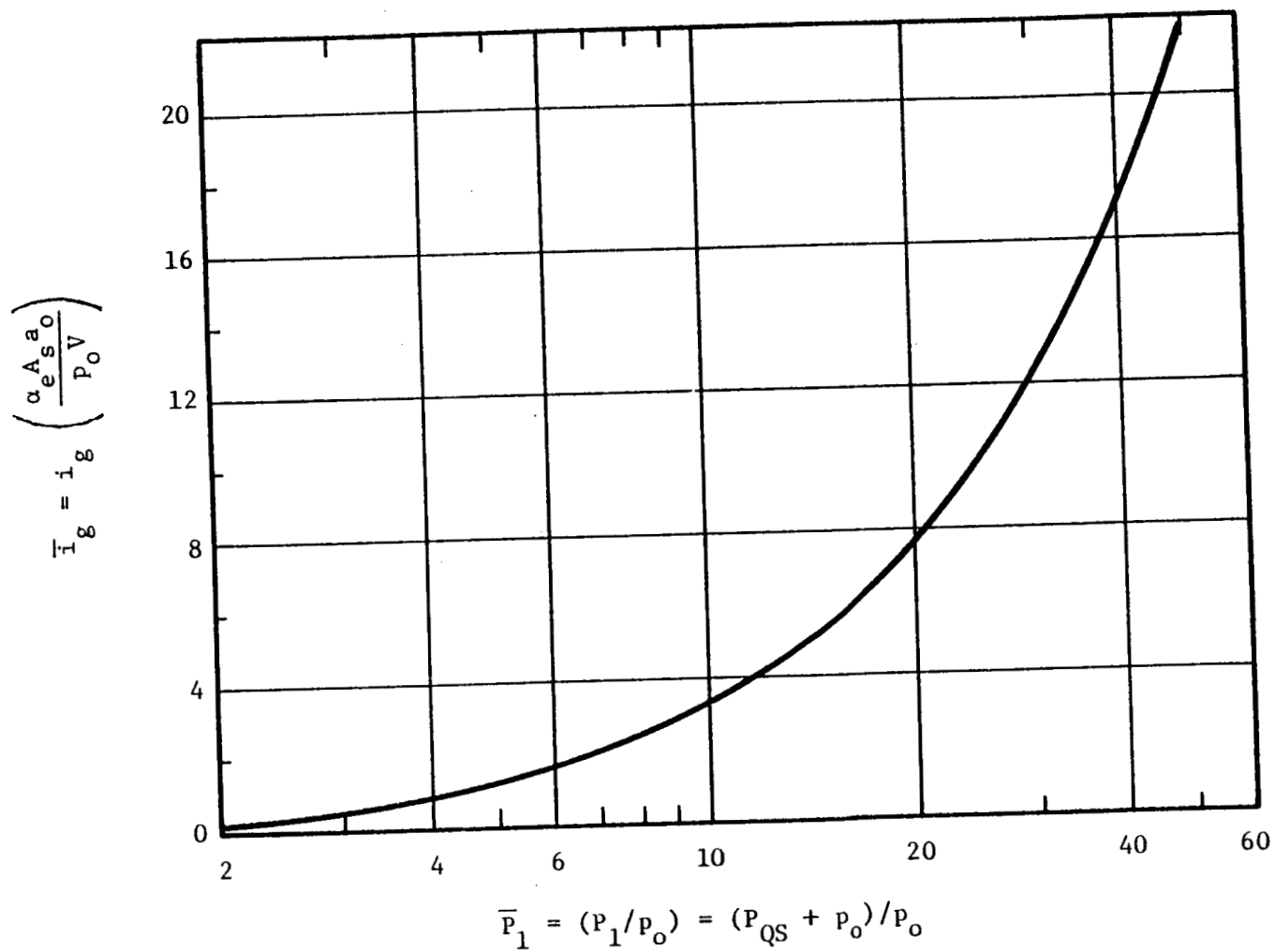
Figure 4.45   Scaled Gas Pressure Impulse versus Scaled Initial Pressure

Equations for the scaled parameters can be inverted to give the corresponding dimensional quantities, as follow:

$$i_g = \bar{i}_g \left(\frac{P_o V}{\alpha_e A_s a_o} \right) \tag{4.59}$$

$$t_{max} = \bar{\tau}_{max} \left(\frac{V}{\alpha_e A_s a_o} \right) \tag{4.60}$$

Self-consistent units must be used when "unscaling" using these equations.

The effective vent area ratio α_e is calculated for the walls and roof of the structure. For single layer panels, the vent area ratio is the vent area divided by the total area of the walls and roof. For multi-layer panels, use Equation (4.53). If the structure consists of panels made of angles, zees, louvres, or interlocked I-beams, α_e is determined by using the information in Figure 4.46. Panels of nested angles which have approximately one opening per projected length are about twice as efficient as a perforated plate in breaking up the side-on peak pressure as it vents (N = 2). For closer nested angles such that there are about two openings per projected length, the angles seem to be four times as efficient as a perforated plate (N = 4). More details on use of this procedure are given in Suppressive Shields (Ref. 4.3). If more conventional open vent areas are used, then the quantity $\alpha_e A_s$ is replaced by vent area A.

In Reference 4.52, the terms "partially vented" and "fully vented" are defined according to values of the scaled vent area ratio $A/V^{2/3}$. If this parameter is greater than 0.60, gas venting times should be less than initial shock loading durations, and the chamber is fully vented, i.e., gas pressure parameters can be ignored. But, if it is less than or equal to 0.60, the chamber is partially vented, and gas pressure parameters must be considered. Figures 4.43 through 4.45 should give conservative (upper limit) predictions compared to data in Reference 4.52.
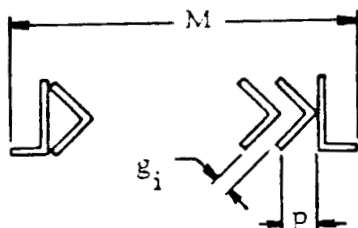
$$A_{vent} = \ell \sum_1^n g_i / N$$

ℓ = length of element

p = projected length of angle

N = 2 or 4 (see text)

A_{wall} = LM

L = length of wall

α = A_{vent}/A_{wall}

(a) Nested Angles
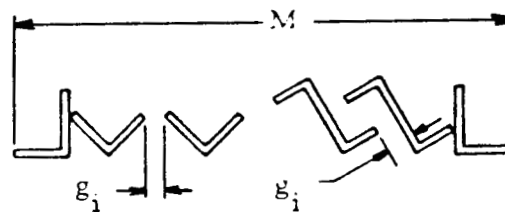
$$A_{vent} = \ell \sum_1^n g_i$$

n = number of openings

A_{wall} = LM

α = A_v/A_w

(b) Side-By-Side Angles Or Zees
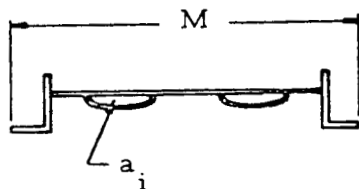
$$A_{vent} = \sum_1^n a_i / 2$$

a_i = open area of louvre

A_{wall} = LM

α = A_v/A_w

(c) Louvres
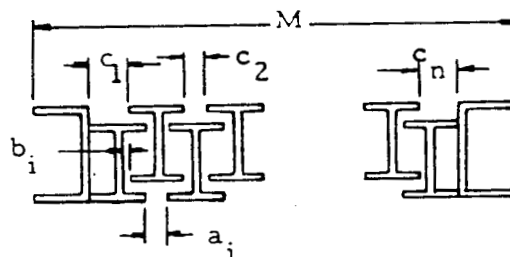
$$A_{v_1} = 2\ell \sum_1^n a_i$$

$$A_{v_2} = A_{v_3} = 2\ell \sum_i^n b_i$$

$$A_{v_4} = 2\ell \sum_1^n c_i$$

$$\alpha_1 = A_{v_1}/A_w, \ldots$$

(d) Interlocked I-Beams

Figure 4.46 Definition Of Effective Area Ratio For
Various Structural Elements (Reference 4.49)

4-112

EXAMPLE PROBLEM 4.11

PROBLEM – Calculate reflected shock and quasi-static pressure along with blow-
down time and gas impulse in a vented, contained bay.

GIVEN: W = charge weight of PBX 9404
        V = room volume
        $A_v = \alpha_e A_s$ = vent area
        R = standoff from nearest wall or surface
        p_o = atmospheric pressure
        a_o = speed of sound in air

FIND: P_r, i_r, P_{QS}, t_{max}, i_g, combined pulse parameters   REFERENCE

SOLUTION: 1. Calculate TNT equivalent weight W   Appendix A
           2. Calculate W/V ratio
           3. Obtain value of P_{QS} Fig. 4.43
           4. Calculate P_{QS}/p_o
           5. Obtain value of scaled blowdown time:

               $$\bar{\tau} = \left(\frac{ta_o}{V^{1/3}}\right)\left(\frac{\alpha_e A_s}{V^{2/3}}\right)$$ Fig. 4.44

           6. Solve for t_{max}:

               $$t_{max} = \frac{\bar{\tau}\, V}{a_o \alpha_e A_s} = \text{blowdown time}$$

           7. Obtain value of scaled gas pressure
               impulse:

               $$\bar{i}_g = i_g \left(\frac{\alpha_e A_s a_o}{p_o V}\right)$$ Fig. 4.45

           8. Solve for gas pressure impulse:

               $$i_g = \bar{i}_g \left(\frac{p_o V}{\alpha_e A_s a_o}\right)$$

           9. Determine scaled distance from surface
               in question (wall, roof, etc.)
               $Z = R/W^{1/3}$ Eq. (4.16)
          10. Determine pressure loading on surface
               (reflected). If Z is large and sur-
               face is small such that pressure is
               fairly constant across surface, use P_r
               from Figure 4.6 for entire surface.
               This would give worst case. If Z is
               small and surface is large, use Figure   Fig. 4.6 &
               4.12   Fig. 4.12

11. Determine specific impulse to surface (reflected). If Z is large and surface is small such that specific impulse is fairly constant across surface, use i_r from Figure 4.13 to obtain i, and calculate $i = \bar{i} \, W^{1/3}$

<div style="text-align:right">Fig. 4.6 & Fig. 4.13
Eq. (4.39) &
Eq. (4.40)</div>

12. Calculate $T = \dfrac{2i}{P}$

CALCULATION – Using the HE treatment room and a wall surface (consider a wall surface within the HE treatment room of the High Explosives Development Machining Facility):

GIVEN: W = charge weight 423 lb of PBX 9404

$V = 12{,}500 \ \text{ft}^3$

$A_v = \alpha_e A_s = 19.8 \ \text{ft}^2$ from 2.83 ft X 7 ft door; no other vents

$R = 3 \ \text{ft}$

$p_o = 14.7 \ \text{psi}$

$a_o = 1116 \ \text{ft/sec}$

FIND: P_r, i_r, P_{QS}, t_{max}, i_g, combined pulse parameters

SOLUTION: 1. W = (charge weight)(TNT equivalent) = (423) (1.107) = 468

2. $W/V = 468 \ \text{lb}/12500 \ \text{ft}^3 = 0.0374 \ \text{lb/ft}^3$

3. From Figure 4.43, $P_{QS} = 150$ psi and $P_1 = P_{QS} + p_o = 164.7$

4. $P_1/p_o = 164.7/14.7 = 11.2$

5. From Figure 4.44

$$\bar{\tau} = \left(\frac{ta_o}{V^{1/3}}\right)\left(\frac{\alpha_e A_s}{V^{2/3}}\right) = 1.13$$

6. Solving for t_{max}:

$$t_{max} = \frac{\bar{\tau} \, V}{a_o \alpha_e A_s} = \frac{(1.13)(12500 \ \text{ft}^3)}{(1116 \ \text{ft/sec})(19.8 \ \text{ft}^2)} = \underline{0.64 \ \text{sec}}$$

7. From Figure 4.45:

$$\bar{i}_g = i_g \left(\frac{\alpha_e A_s a_o}{p_o V}\right) = 3.9$$

8. Solving for i_g:

$$i_g = \bar{i}_g \left(\frac{p_o V}{\alpha_e A_s a_o}\right) = \underline{32 \ \text{psi-sec}}$$

9. $Z = R/W^{1/3} = 3 \ \text{ft}/(468 \ \text{lb})^{1/3} = 0.386 \ \text{ft/lb}^{1/3}$

10. For this case, values of X to cover the wall are much greater than R, and the loading will not be constant over the entire wall. The values of pressure listed in Table 4.7 are obtained from Figure 4.12 for various X/R. The value of Z is not one of the isoclines on Figure 4.12, hence, interpolation is necessary

11. As with pressure, the values of $\bar{i}$ (from Figure 4.13) and i (specific impulse) are listed in Table 4.7

12. $T = 2i/P$ is calculated and is listed in Table 4.7

NOTE: One can use the data in Table 4.7 directly to define nonconstant pressures and impulses over a wall. One can also integrate the impulse values over the surface of the wall to obtain total impulse imparted to the wall. This is done in Example Problem 4.18. Results of this Example Problem will be used in Example Problem 4.13 to predict spall.

Table 4.7 Non-constant Loading over Plate

X/R	X ft	P psi	$\bar{i}$ psi-sec/ lb$^{1/3}$	i psi-sec	T sec
0	0	7.0 X 10^4	1.50	12.0	3.5 X 10^{-4}
0.5	1.5	5.5 X 10^4	0.90	7.0	2.5 X 10^{-4}
1.0	3.0	2.0 X 10^4	0.50	3.9	3.9 X 10^{-4}
1.5	4.5	8.0 X 10^3	0.22	1.7	4.3 X 10^{-4}
2.0	6.0	4.0 X 10^3	0.12	0.93	4.6 X 10^{-4}
2.5	7.5	2.5 X 10^3	0.065	0.51	4.1 X 10^{-4}
3.0	9.0	2.0 X 10^3	0.040	0.31	3.1 X 10^{-4}
3.25	9.75	1.5 X 10^3	0.028	0.22	2.9 X 10^{-4}

*Using methods in TM 5-1300 (Ref. 4.2), average impulse over this wall is calculated to be i_b = 3.392 psi-sec. See Example Problem 4.18 for determination of average wall impulse using methods in this manual.

4.4.2 Effects Outside Structures for Directional Venting

When an explosion occurs in a vented structure, the blast wave outside can be attenuated. The way in which the blast wave is affected depends on the vent characteristics of the structure. This section discusses the effect that directional venting has on blast wave parameters outside of a structure with an internal explosion.

A directionally vented chamber is one with vent openings or panels which are not uniformly provided around all sides of the structure, such as venting on only one or two walls, a roof, a wall and a roof, etc. This type of venting was investigated by Keenan and Trancreto (Ref. 4.52), including model tests and the formation of prediction curves. This section discusses their work. Because their report should be readily available to an AE firm, we include only a few of their curves to show the manner of data presentation.

Six directionally vented chambers were tested with venting on various faces which included roofs alone, walls and roofs, and walls alone. The vents were open areas which could be the entire face or only part of the face. The tests included the detonation of a single HE charge inside a structure and blast measurements made both inside and outside the structure for three different charge weights in each structure. Only external blast parameters shall be discussed in this section.

Keenan and Trancreto (Ref. 4.52) distinguish between a "partially vented" and a "fully vented" chamber. A fully vented chamber has a vent area large enough compared to the chamber volume that the duration of the shock pulse (T) is greater than the duration of the gas pulse (blowdown duration, T_b, see Section 4.4.1.2). A partially vented chamber has a vent area such that $T_b > T$.

It is expected that a fully vented chamber will have larger external peak pressures and specific impulses for the same standoffs than a partially vented chamber. This relationship was shown by Keenan and Trancreto (Ref. 4.52) for roof-vented chambers. Thus, the exterior blast parameter prediction curves for a fully vented chamber are conservative for the design of partially vented chambers.

When an explosion occurs within a chamber with one open side, part of the initial shock wave will escape outside through the vent. Internally, as the remaining shock wave reflects back and forth, secondary shock waves escape through the vent and follow the initial pulse. These trailing shocks can overtake and merge with the lead shock for the same reasons as the coalescing of shocks in simultaneous and sequential detonations (explained in Section 4.3.2). Whether trailing shocks coalesce with leading shocks depends on shock strength and the separation of shocks. Coalescing of shocks was evident for both chambers being considered. For very long rooms with small explosive

weights, coalescing may not occur, due to large separation of shocks and low charge weight, and hence, use of prediction curves would be conservative. For very narrow rooms with large explosive weight, coalescence could occur more quickly than measured for the two chambers and cause higher pressures close in than prediction curves would indicate. Therefore, it is suggested that prediction curves be used only for the ranges of scaled distances shown (Ref. 4.52).

The two test chambers used had open faced vents as opposed to blowout panels or doors. For blowout panel venting, the initial shock wave (and possibly some following shocks depending upon response time) does not escape but is reflected by the blowout panel. Hence, shocks that do escape the chamber are weaker reflections and the peak pressures outside the chamber are not expected to be as high as that from open vented chamber. It is suggested that exterior blast prediction curves can be used as a conservative upper limit for chambers with blowout panel type venting (Ref. 4.52). Figures 4.47 and 4.48 are examples of the many blast parameter prediction curves given in Reference 4.52. They include peak positive pressure and specific positive impulse for front, back, and side directions. Included on the graphs are W/V (charge weight/chamber volume) quantities used for the experiments. These curves should <u>not</u> be used for W/V values outside these limits (large chamber: 0.009 lb/ft^3 ≤ W/V ≤ 0.055 lb/ft^3; small chambers: 0.063 lb/ft^3 ≤ W/V ≤ 0.250 lb/ft^3). The charge type used was Composition B, which has a TNT energy equivalency of 1.092. In terms of TNT energy, the W/V limits will be 0.0093 lb/ft^3 ≤ W/V ≤ 0.060 lb/ft^3 for the large chamber and 0.069 lb/ft^3 ≤ W/V ≤ 0.273 lb/ft^3 for the small chamber. Duration of the positive phase (t_d) of the blast wave can be approximated by considering a triangular-shaped pulse. Keenan and Tancreto (Ref. 4.52) suggest this as follows

$$t_d \approx \frac{2i}{p} \qquad\qquad\qquad (4.61)$$

4.4.3 Effects of Vent Closures

Many vented, explosion-resistant structures must have vents covered by closures to maintain proper internal atmospheric conditions, or for other reasons. These closures are usually intended to be frangible and rapidly displace or fragment under the effects of internal explosions. In this section, we discuss the probable effects of closures on the venting process, and give some prediction curves for the gas venting phase of the internal explosions, based on exercise of a relatively simple gasdynamic computer code.

Typical frangible covers for cells in an explosion-resistant building at Pantex are made of light, commercially available panels mounted on light metal support frames, with weight per unit area of about 6 lb/ft^2. They form the outer walls of bays in the building, with all other walls, roof, and floor
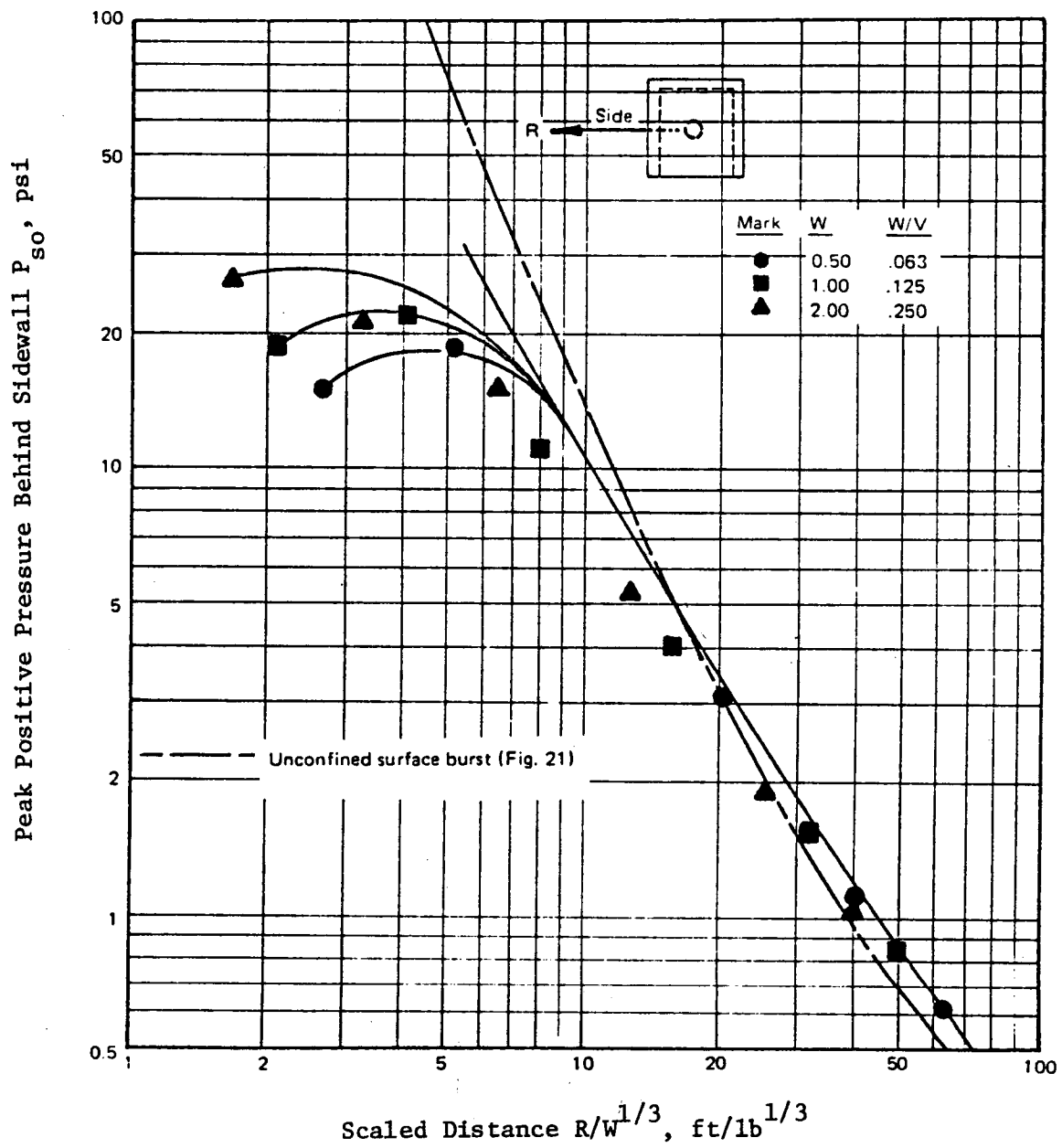
Figure 4.47   Peak Positive Pressure Behind Sidewall Of
Small Three-Wall Cubicle with Roof (Reference 4.52)
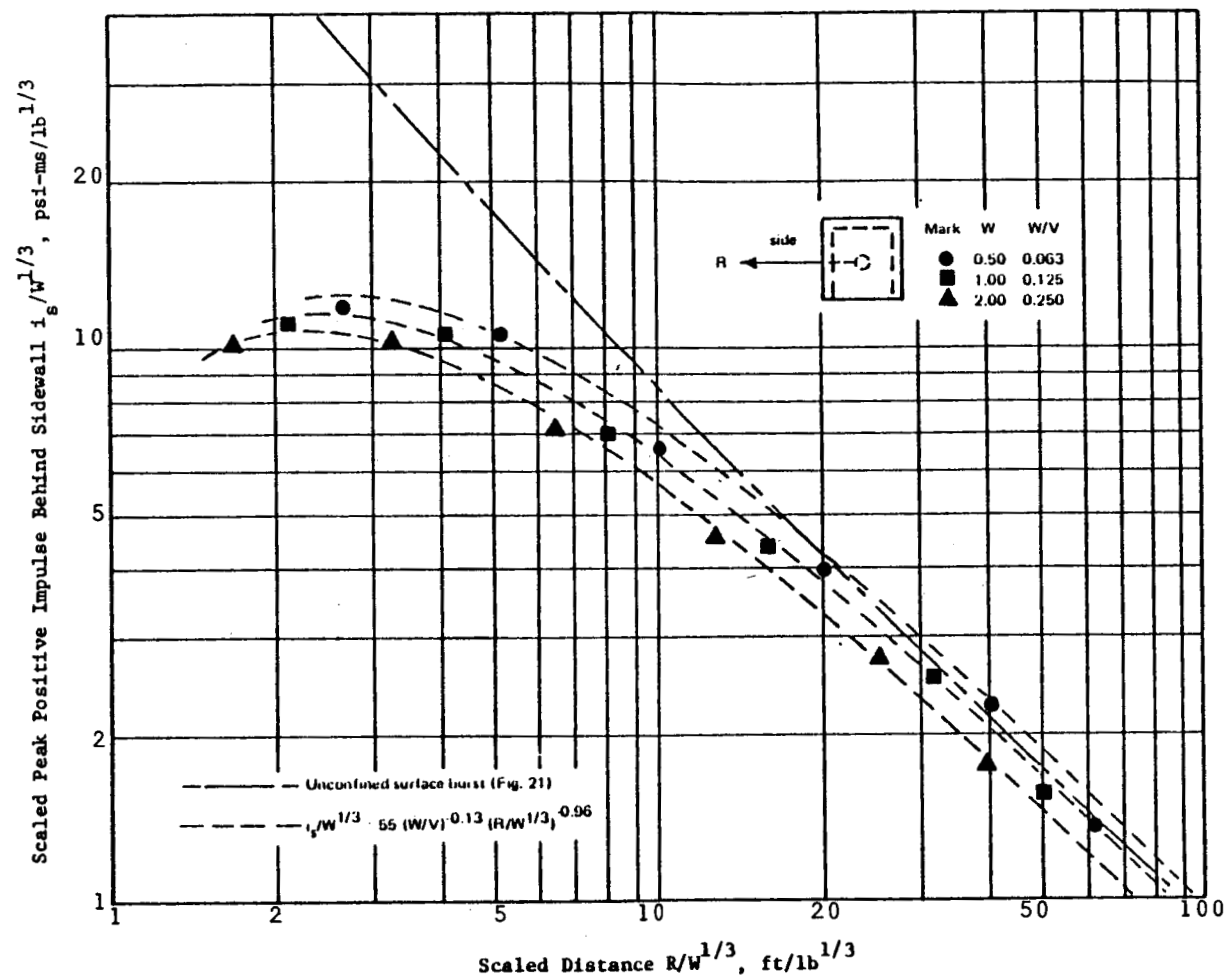
Figure 4.48   Scaled Peak Positive Impulse Behind Sidewall of Small Three-Wall Cubicle with Roof
(Reference 4.52)

being much heavier reinforced concrete construction, with weights per unit area of at least 160 lb/ft^2. When an internal explosion occurs, the first reflected shock loading on both the blast resistant parts of the structure and the frangible vent wall are essentially the same as for an unvented chamber of the same geometry, i.e., the maximum applied pressure is P_r and the maximum applied specific impulse is i_r. But, the frangible vent wall fails within a few milliseconds and moves outward as free body with a velocity u_o approximated by the impulse-momentum theorem,

$$u_o = \frac{i_r A}{M} \tag{4.62}$$

where A is loaded area of the vent wall and M is mass (not weight) of the entire wall.

Even though the vent wall is accelerated and propelled outward by the initial reflected blast wave, no venting can occur initially, and the wave is reflected back into the chamber with very little attenuation in strength, because of the finite inertia of the wall. In some chambers at Pantex, the vent wall must move several feet before it clears the vent opening in the cell, so no true venting can occur until the wall has moved that far. By this time, several shock reflections will have occurred within the cell, and their strengths attenuated by irreversible processes so that the gas venting phase discussed earlier will start. The vent cover will continue to accelerate because of the quasi-static gas pressure, but this pressure can now be vented around the open edges of the cover. Eventually, the quasi-static pressure within the chamber decays to atmospheric pressure, and the gas venting process ends.

Even a very light vent cover such as thin, corrugated fiberglass sheeting used for patio roofing, will not attenuate the initial reflected shock loading. But, the lighter the cover (the lower its M/A), the more rapidly it opens under both initial shock and quasi-static pressures, thus attenuating the gas venting phase of the internal explosion process.

There have been essentially no measurements of internal explosion pressures for vented chambers with covers, and very few past analyses. But, a relatively simple computer code can be used to follow the venting process for covers of various masses per unit area (M/A), various chamber volumes, and various internal explosive charge weights (or energies). We have used such a code to generate predictions of gas venting pressures, and present them here.

The computer code* which we developed is composed of three sections in order to incorporate the three distinct phases of venting for the Pantex facility. The first phase represents the case where a vent cover travels a finite distance, such as through a tunnel or the thickness of a thick wall, before any venting takes place. During this phase of venting, we used the technique demonstrated by Kulesz, et al. (Ref. 4.57) for accidental explosions on board a Navy submarine tender. For this analysis, an equation of motion is developed which describes the effect of the quasi-static pressure on the velocity of the vent panel, and pressure decreases due to simple adiabatic expansion as the volume of the room changes. During the second phase of venting, the vent panel has cleared the tunnel or wall and the room begins to vent into the atmosphere. The energy of the gas is divided among energy expended during gas expansion, the kinetic energy of the vent panel and energy losses due to the gas flowing around the vent panel. To perform this phase of the analysis, our computer program uses a modified version of the technique developed by Taylor and Price (Ref. 4.58), Baker, et al. (Ref. 4.59) and Kulesz, et al. (Ref. 4.57). The third phase of venting occurs after the vent panel is sufficiently far from the vent opening that it no longer interrupts the flow of the exiting gas. During this phase of venting, we use a gas venting computer code which considers gas venting through an orifice based on the ideal gas law and sonic or subsonic gas flow, depending upon the relative pressures between the room and the atmosphere. This portion of the venting process uses the methods described by Owczarek (Ref. 4.56), Baker and Oldham (Ref. 4.55), and Esparza, et al. (Ref. 4.49). The venting computer program developed for this analysis allows one to vary the quasi-static pressure, volume, vent area, vent height, vent width, vent mass, initial vent velocity acquired from blast wave loading, the vent tunnel length, ambient pressure, ambient temperature, discharge coefficients, and time increments during the calculations. The computer code also considers cases where the vent panel is adjacent to the ground or high enough above the ground that gas flow is not affected by the ground surface.

A model analysis was performed to determine the functional format of the parameters involved in the gas venting process. The list of physical parameters is presented in Table 4.8. The dimensionless terms are presented in Table 4.9, with V, p_o and a_o used as "repeating" parameters. Observe that all response terms, $\bar{p}(t)$, $\bar{u}_f$, $\bar{i}_g$, and $\bar{T}$ can be obtained if $\bar{p}(t)$, the scaled pressure history, is known. Some dimensionless terms can be eliminated to simplify the analysis. The ratio of specific heats, γ, can be eliminated, as its value is constant. The scaled quasi-static pressure, $\bar{P}_1$, is a function of scaled charge energy, $\bar{E}$ (See Figure 4.43). Hence, knowledge of the value

---

*The computer code which we developed is a combination of several codes previously published by SwRI. It is described in more detail in Ref. 4.72. The code is only available from SwRI.

Table 4.8 Physical Parameters Affecting Venting

Symbol	Description	Units
E	Energy	FL
V	Volume	L^3
A	Vent area	L^2
P_1	Quasi-Static pressure (absolute)	F/L^2
γ	Ratio of specific heats	-
H	Wall thickness	L
P_o	Ambient pressure	F/L^2
a_o	Speed of sound in air	L/T
M	Mass of vent	FT^2/L
u_o	Initial panel velocity	L/T
t	Time	T
$p(t)$	Pressure history (Pressure as a function of time)	F/L^2
i_g	Gas impulse (Integral of pressure history)	FT/L^2
T_d	Duration of vent stage of internal explosion	T
u_f	Final panel velocity	L/T

Table 4.9   Dimensionless Terms for Vented Chamber

$$\overline{E} = \left(\frac{E}{p_o V} \right)$$

$$\overline{A} = \left(\frac{A}{V^{2/3}} \right)$$

$$\overline{P}_1 = \left(\frac{P_1}{P_o} \right)$$

$$\gamma = (\gamma)$$

$$\overline{H} = \left(\frac{H}{V^{1/3}} \right)$$

$$\overline{M} = \left(\frac{Ma_o^2}{p_o V} \right)$$

$$\overline{u}_o = \left(\frac{u_o}{a_o} \right)$$

$$\overline{t} = \left(\frac{ta_o}{V^{1/3}} \right)$$

$$\overline{p}(t) = \left(\frac{p(t)}{P_o} \right)$$

$$\overline{u}_f = \left(\frac{u_f}{a_o} \right)$$

$$\overline{i}_g = \left(\frac{i_g a_o}{p_o V^{1/3}} \right)$$

$$\overline{T} = \left(\frac{Ta_o}{V^{1/3}} \right)$$

of one of these dimensionless terms implies knowledge of the value of the other, and $\bar{E}$ was eliminated. By a similar process, the term $\bar{u}_o$, initial scaled panel velocity, can be eliminated. The initial panel velocity, for a panel of given mass, will be determined by the initial shock loading (reflected impulse) imparted to the panel (See Figure 4.6). The magnitude of the impulse will be determined by the charge energy (weight) and the geometry (charge shape, orientation, and location inside cubicle). The charge energy is implicitly expressed in $\bar{P}_1$, and the scaled wall panel mass is $\bar{M}$. The same geometry was used in all calculations with the following simplifying assumptions:

1. A bare spherical charge was located in the geometric center of a cubicle.

2. No reflection factor was added for interaction of blast waves with the cubicle floor. (This is conservative because later reflected shocks can further accelerate the vent panel.)

3. The standoff from the charge was assumed to be constant over the entire vent panel (instead of calculating a slant range); hence, producing a specific impulse independent of location on vent panel.

These simplifications were made because the gas venting problem is already complicated without addition of several more dimensionless terms to specify geometry effects. The problem is outlined in Example Problem 4.12 at the end of this section.

The functional format for the pressure history becomes, after the above simplifications,

$$\bar{p}(t) = \frac{p(t)}{P_o} = f\left(\frac{A}{V^{2/3}}, \frac{P_1}{P_o}, \frac{H}{V^{1/3}}, \frac{Ma_o^2}{P_o V}, \frac{ta_o}{V^{1/3}}\right)$$

$$= f(\bar{A}, \bar{P}_1, \bar{H}, \bar{M}, \bar{t}) \qquad (4.63)$$

The gas impulse, $\bar{i}_g$, is the time integral of $\bar{p}(t)$ over the duration, $\bar{T}_d$, of the gas venting:

$$\bar{i}_g = \int_0^{\bar{T}_d} \bar{p}(\bar{t})\,d\bar{t} \qquad (4.64)$$

or

$$\bar{i}_g = \frac{i_g a_o}{p_o V^{1/3}} = f_1(\bar{A}, \bar{P}_1, \bar{H}, \bar{M}) \tag{4.65}$$

Similarly, $\bar{T}_d$, the scaled duration of gas venting is

$$\bar{T}_d = \frac{T_d a_o}{V^{1/3}} = f_2(\bar{A}, \bar{P}_1, \bar{H}, \bar{M}) \tag{4.66}$$

The computer code was run separately for cases where the vent panel was located on the ground and for cases where the panel is off the ground (i.e., where the gas flow is not disturbed by the ground). It was found that for cases where the vent panel is the whole wall, there is no difference in the results. In the limit of small vent panel areas, however, ∿20% of the wall area, the results are unclear at this time due to insufficient numbers of computational runs. The parameter values used in the computations scanned several orders of magnitude, as follows:

Charge energy	1 – 1000 lb TNT
Cubicle volume	1000 – 30,000 ft^3
Vent area	20% – 100% of area of one wall
Wall thickness	0 – 6 ft
Ambient pressure	14.7 psi
Specific weight of vent panel	0 – 300 lb/ft^2
Speed of sound	1116 ft/sec
Discharge coefficient	0.6

Observe that the results can be used at altitudes other than sea level simply by using the proper values for ambient atmospheric pressure and sonic velocity in calculating the scaled values.

The results of the calculations are presented in Figures 4.49 through 4.52. These curves for $\overline{M} = 0$ are similar to those obtained by Esparza, et al. (Ref. 4.49). Figures 4.49 and 4.50 incorporate the effect of a real vent panel with mass, but are for scaled wall thickness of zero. Figures 4.51 and 4.52 incorporate the effect of having a wall thickness or several wall thicknesses for the vent panel to traverse before actual venting can begin. No attempts were made to depict the final vent panel velocities graphically, as the parameter is not essential for structural design, although it may be desirable to know for fragment hazard determinations. Additional work is needed to develop the curves presented in Figures 4.49 through 4.52 fully, to determine final velocities of the vent panel, and to determine errors induced by ignoring or simplifying the geometry of the explosion. When using these figures, one must use a consistent set of units so that the dimensionless terms are truly dimensionless.
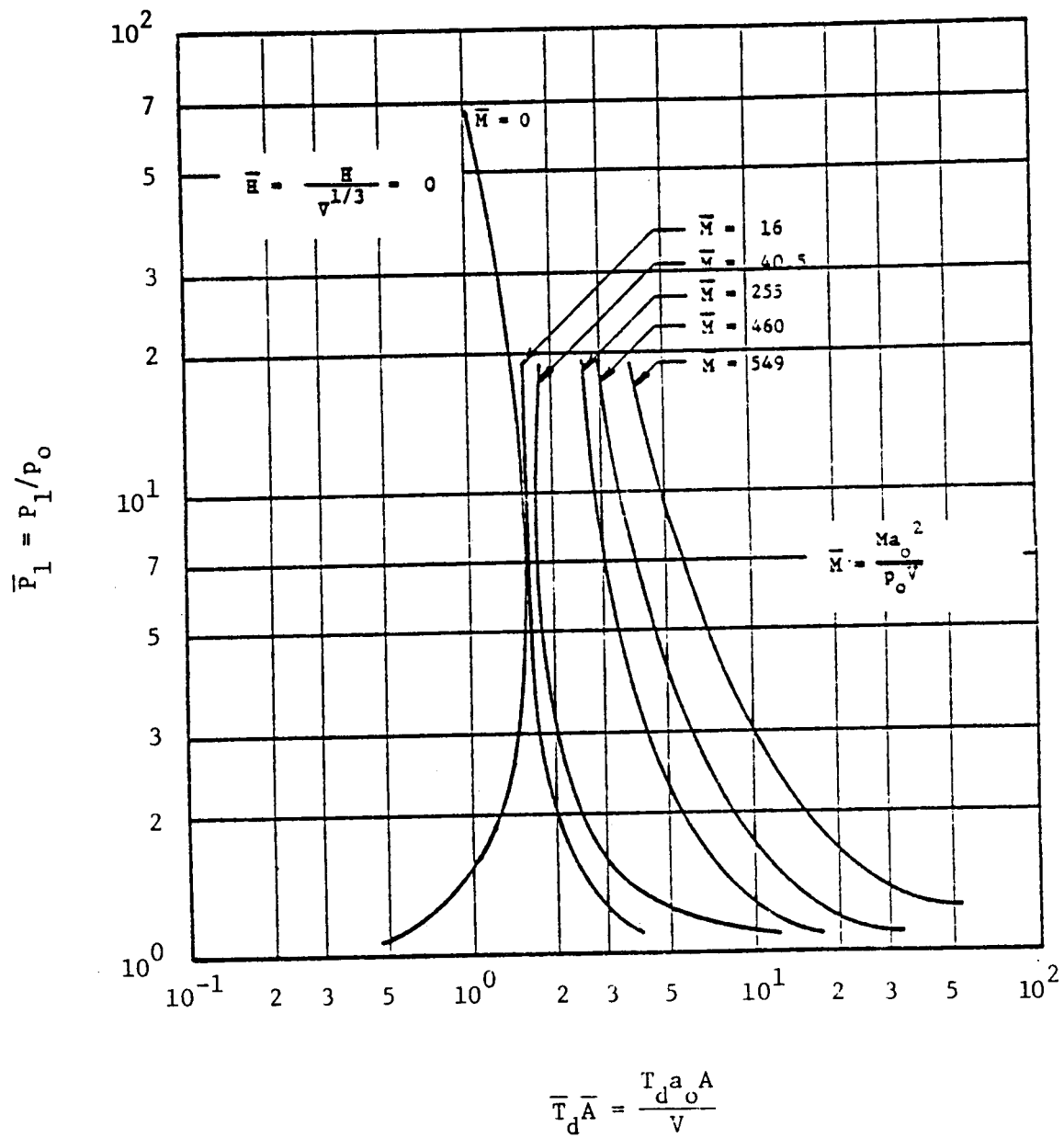
Figure 4.49 Plot of Scaled Pressure versus Scaled Duration,
Various Scaled Masses of Vent Covers $(\overline{M})$, for $\overline{H} = 0$
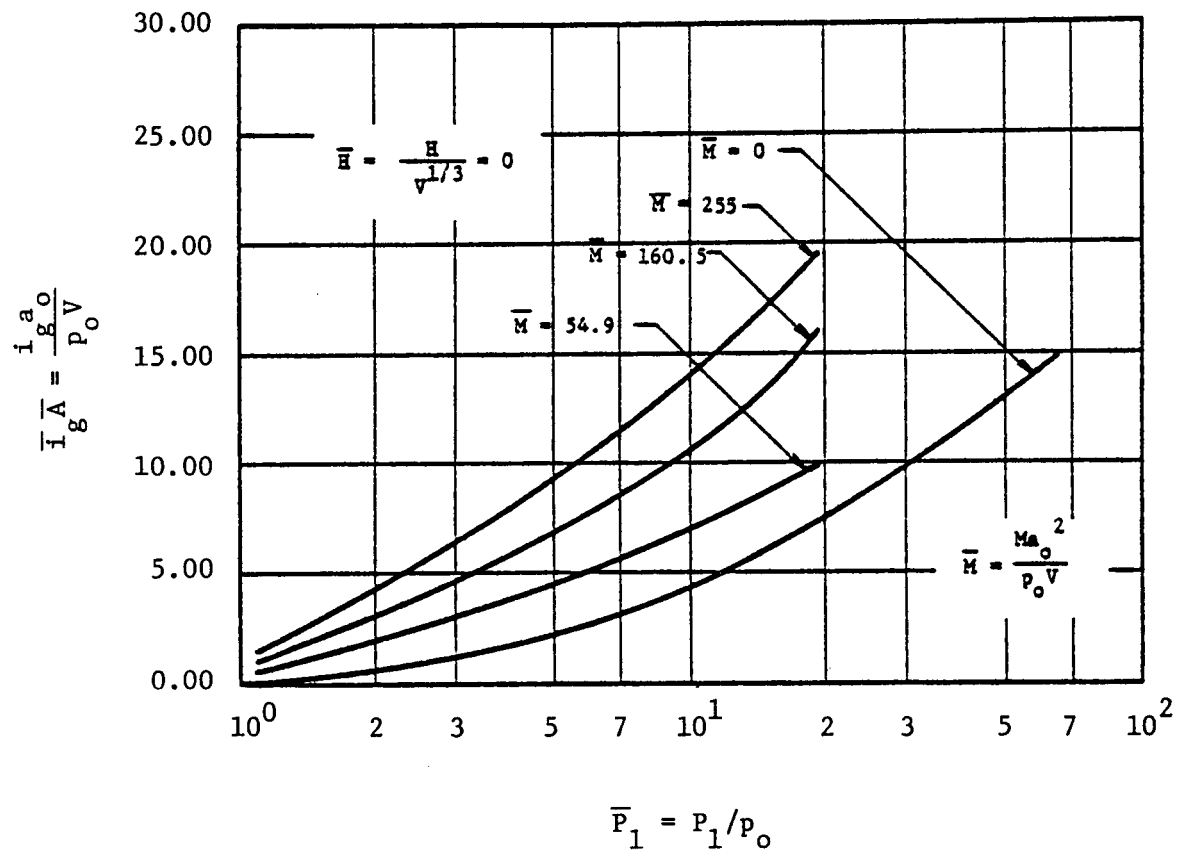
Figure 4.50 Plot of Scaled Gas Impulse versus Scaled Pressure
Various $\overline{M}$, for $\overline{H} = 0$
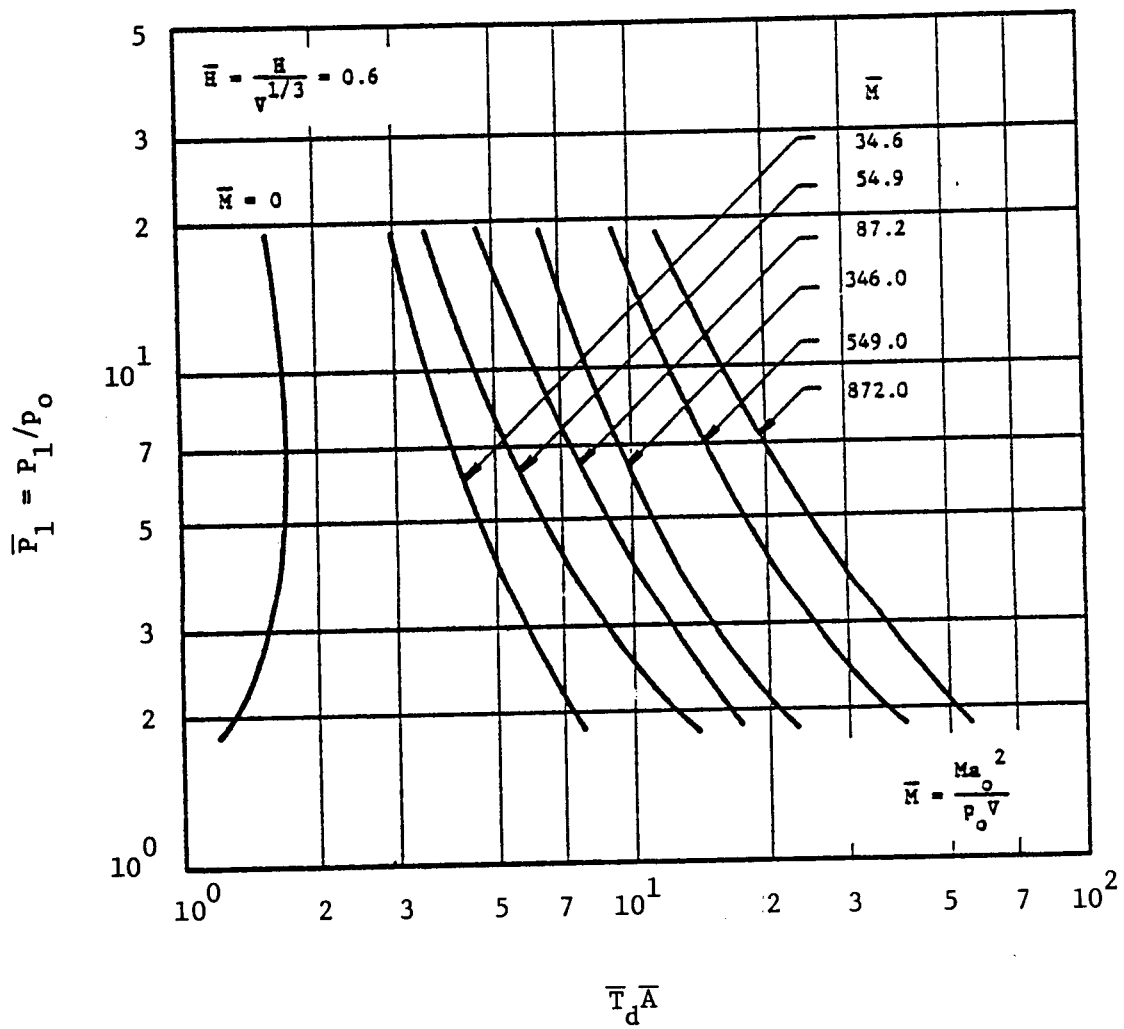
Figure 4.51 Plot of Scaled Pressure versus Scaled Duration,
Various $\overline{M}$, for $\overline{H}$ = 0.6
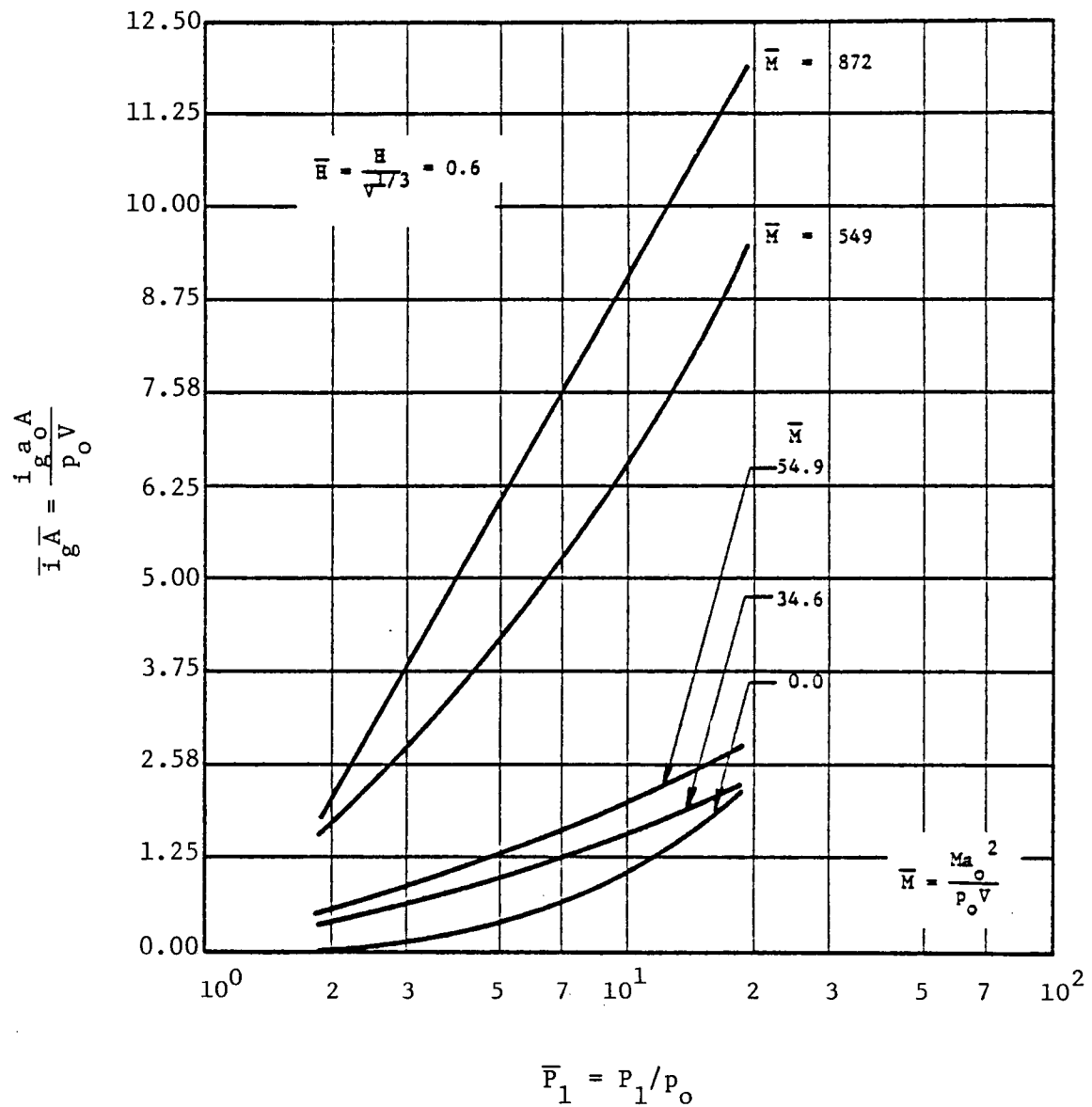
Figure 4.52 Plot of Scaled Gas Impulse versus Scaled Pressure,
Various $\overline{M}$, for $\overline{H} = 0.6$

PROBLEM – Calculate the gas impulse imparted to the walls of a cubicle and the duration of the venting phase, using Figures 4.49 through 4.52.

GIVEN: Charge type and weight
Area of vent panel A
Mass of vent panel M
Volume of cubicle V
Ambient atmospheric pressure p_O
Ambient sonic velocity a_O
Vent panel wall thickness H

FIND: P_{QS}, i_g, and T_d

REFERENCE
See Table 6
of Appendix A
for TNT
Equivalencies

SOLUTION:

1. Equivalent TNT explosive weight
   $W = (W)$ (TNT Factor)

2. Calculate W/V

3. Determine quasi-static overpressures
   P_{QS} (psig)

   Fig. 4.43

4. Calculate scaled quasi-static pressure
   $$\bar{P}_1 = \frac{P_{QS} + p_O}{p_O}$$

5. Calculate scaled vent panel mass
   $$\bar{M} = \frac{Ma_O^2}{p_O V}$$

6. Calculate scaled wall thickness
   $$\bar{H} = H/V^{1/3}$$

7. Calculate scaled vent area
   $$\bar{A} = A/V^{2/3}$$

8. Determine scaled gas impulse
   $$\bar{i}_g \bar{A}$$

   Fig. 4.50 &
   Fig. 4.52

9. Determine scaled vent duration
   $$\bar{T}_d \bar{A}$$

   Fig. 4.49 &
   Fig. 4.51

10. Descale $\bar{i}_g \bar{A}$
    $$i_g = \bar{i}_g \bar{A} \left(\frac{p_O V^{1/3}}{a_O}\right) \frac{1}{\bar{A}}$$

11. Descale $\overline{T}_d$

$$T_d = \overline{T_d A} \left(\frac{V^{1/3}}{a_o} \right) \frac{1}{\overline{A}}$$

CALCULATION

GIVEN: A bare charge of 135 lb of PBX 9404 is handled in a bay having a volume of 38,000 ft^3 and a venting wall with area 861 ft^2. The venting wall is 10 inches of concrete with a weight per unit area of 120 lb/ft^2. Ambient conditions are standard sea level conditions.

$A = 861$ ft^2

$M = (120 \text{ lb/ft}^2)(861 \text{ ft}^2)(\frac{1}{32} \text{ sec}^2/\text{ft})(\frac{1}{12} \text{ ft/in})$

$= 267$ lb sec^2/in.

$V = 38,000$ ft^3

$P_o = 14.7$ psi

$a_o = 13,400$ in/sec

$H = 10$ in

FIND: Vented gas pressure parameters, P_{QS}, i_g, and T_d

SOLUTION:
1. $W = (135)(1.108) = 150$ lb
2. $W/V = 150/38,000 = 3.95$ lb/ft^3
3. From Figure 4.43, $P_{QS} = 40$ psi
4. $\overline{P}_1 = \frac{40 + 14.7}{14.7} = 3.7$
5. $\overline{M} = \frac{267 \times 13,400^2}{14.7 \times 38,000 \times 12^3} = 50$
6. $\overline{H} = 10/[(38,000)^{1/3} \times 12] = 0.025 \approx 0$
7. $\overline{A} = 861/38,000^{2/3} = 0.764$
8. Use Figures 4.49 and 4.50 since $\overline{H} \approx 0$
   From Figure 4.50, $\overline{i_g A} = 3.3$
9. From Figure 4.49, $\overline{T_d A} = 2.0$
10. $i_g = 3.3 \left(\frac{14.7 \times 38,000^{1/3} \times 12}{13,400} \right) \left(\frac{1}{0.764} \right)$
    $i_g = \underline{1.192 \text{ psi-sec}}$

11. $T_d = 2.0 \left(\dfrac{38,000^{1/3} \times 12}{13,400} \right) \left(\dfrac{1}{0.764} \right)$

$T_d = \underline{0.079 \text{ sec}}$

The example presented was also run using the computer code. A special case was selected in which the charge was resting on the floor. In calculating the reflected impulse required to obtain an initial vent panel velocity, the charge weight was doubled to account for reflection off the floor, and slant range was used to determine the average specific impulse imparted to the vent panel. The values obtained for duration differed by about 20 percent and the value obtained for impulse differed by about 3 percent.

The procedure given here has not yet been validated by experiment. It has been used to predict the effect of varying the mass per unit area of the vent panel for one explosives facility at Lawrence Livermore Laboratory. We feel that the predictions give conservative (upper limit) values for the gas pressure parameters, and can be used by an AE in design.

4.4.4 Applications to Specific Configurations

Containment and venting is important in a large number of structures existing or planned at Pantex.

Example problems for prediction of initial shock loads and gas venting loads appear throughout the chapter. Here, we describe one or more buildings and give building sections for each of several categories of structure.

4.4.4.1 Single Cubicles

These are structures sufficiently isolated or strong enough that internal blast loading should be decoupled for each structure. There are no interconnecting passageways strong enough to transmit internal blast from or into these structures from explosions in the cells or in nearby structures.

One such type of structure is an assembly cell in Building 12-44. Figure 4.63 gives a plan view of one such cell, and Figure 4.53 a vertical section. Double equipment blast doors, a revolving personnel door, and gravel pockets shown in Figure 4.63 should isolate or slowly vent any internal blast coming from the donor assembly room so that no nearby structure feels internal blast. The "roof" of an assembly room, shown in Figure 4.53, is a thick layer of gravel on steel cable supports. An internal explosion will throw the gravel roof upward, eventually venting an internal explosion. But, there is no internal blast communicated to an adjacent cell, so again this structure can be treated as a single cubicle for prediction of internal blast loading.

A second type of structure with enough isolation between bays so that each can be considered a single cubicle is Building 12-65. Figures 4.54 and 4.55 show a plan view and an elevation. Here, each bay is an earth-covered, corrugated steel arch structure. The earth cover and separation between individual bays prevent significant direct internal blast communication between bays, and the front walls and doors (if closed) of each bay are strong enough to contain the blast loading down the corridor in the event of an explosion in an adjacent bay.

4.4.4.2 Multiple Bays

Corridors and doors are located in these structures so that internal blast and vented gas pressures can communicate from one bay to another.

An example of this type of structure is Building 11-20, shown in plan view in Figure 4.56. Here, a number of bays open into a common corridor, so that blast waves from an explosion in one bay can reflect and diffract around corners and into adjacent bays. The prediction of internal blast and vented gas pressures is further complicated by frangible walls in each bay.
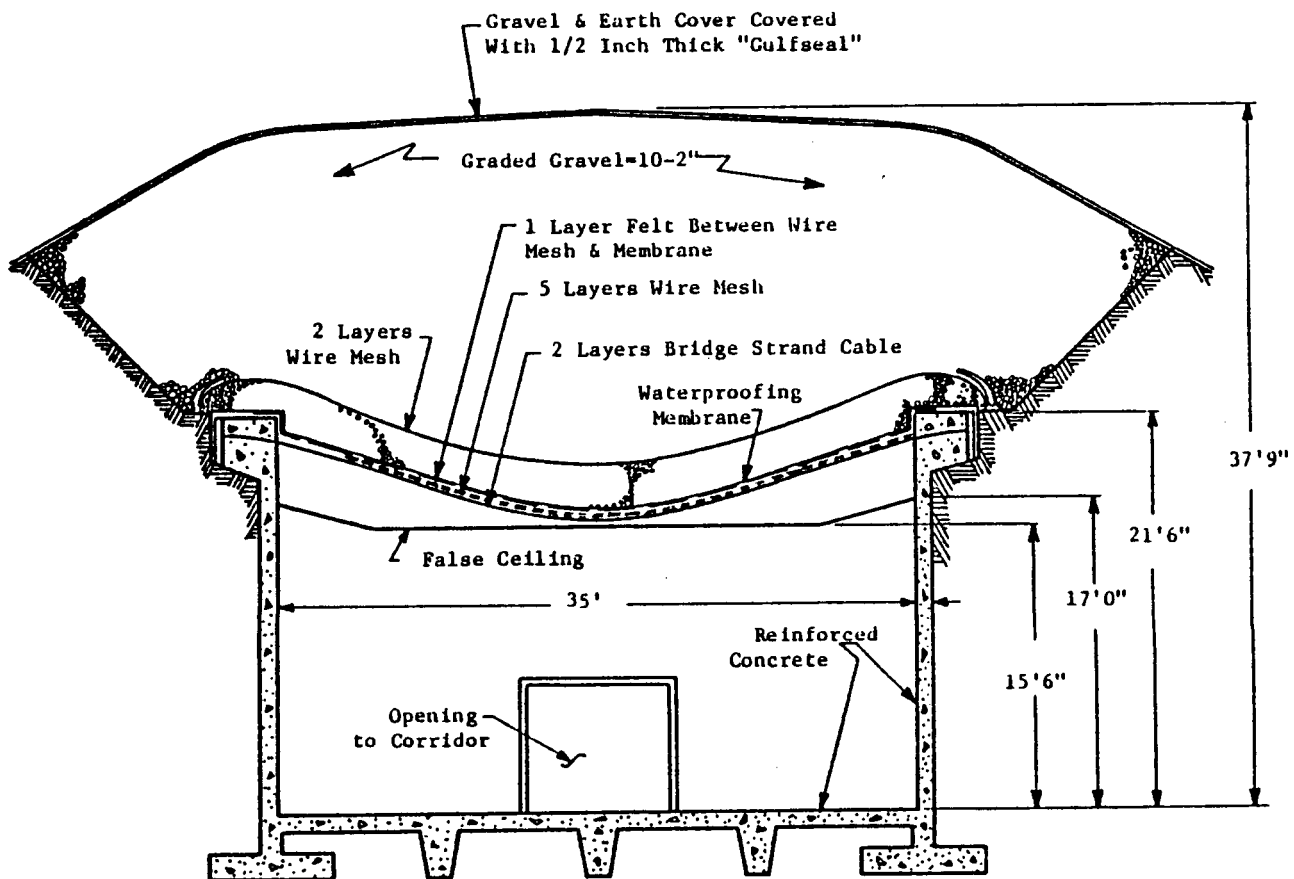
Figure 4.53   Vertical Section of Assembly Cell in Building 12-44

Reinforced Concrete
Retaining Wall

EARTH COVER

Corrugated Steel
Arches

Reinforced Concrete
Head Wall

Bay 6

Bay 7

Mech. Room

Corridor

Ramp
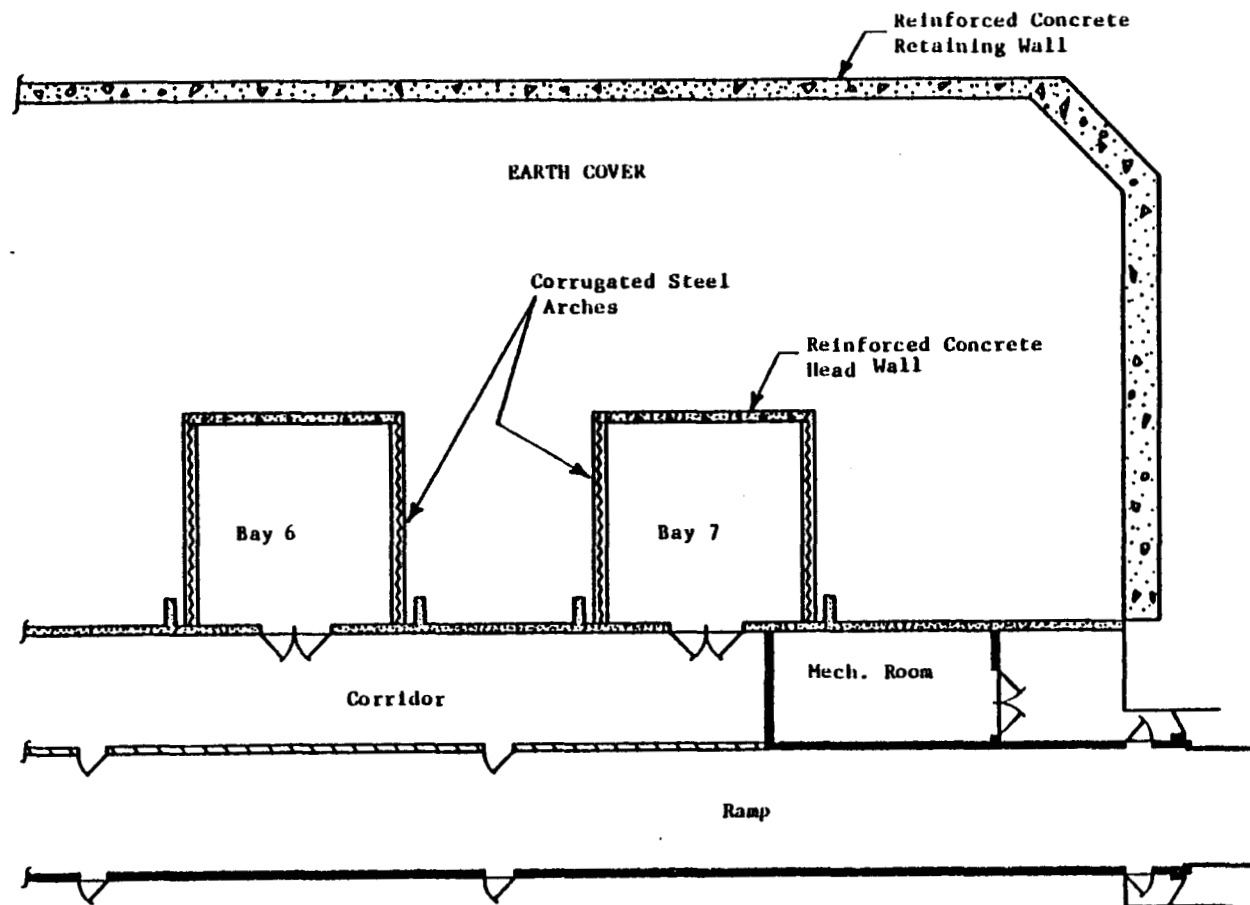
Figure 4.54   Plan View of Bays in Building 12-65

Earth-Covered
Corrugated Steel
Arch

Rubbed Finish
Concrete

Grade

Overburden Covered
on all Faces and Top
With Asphalt Liners
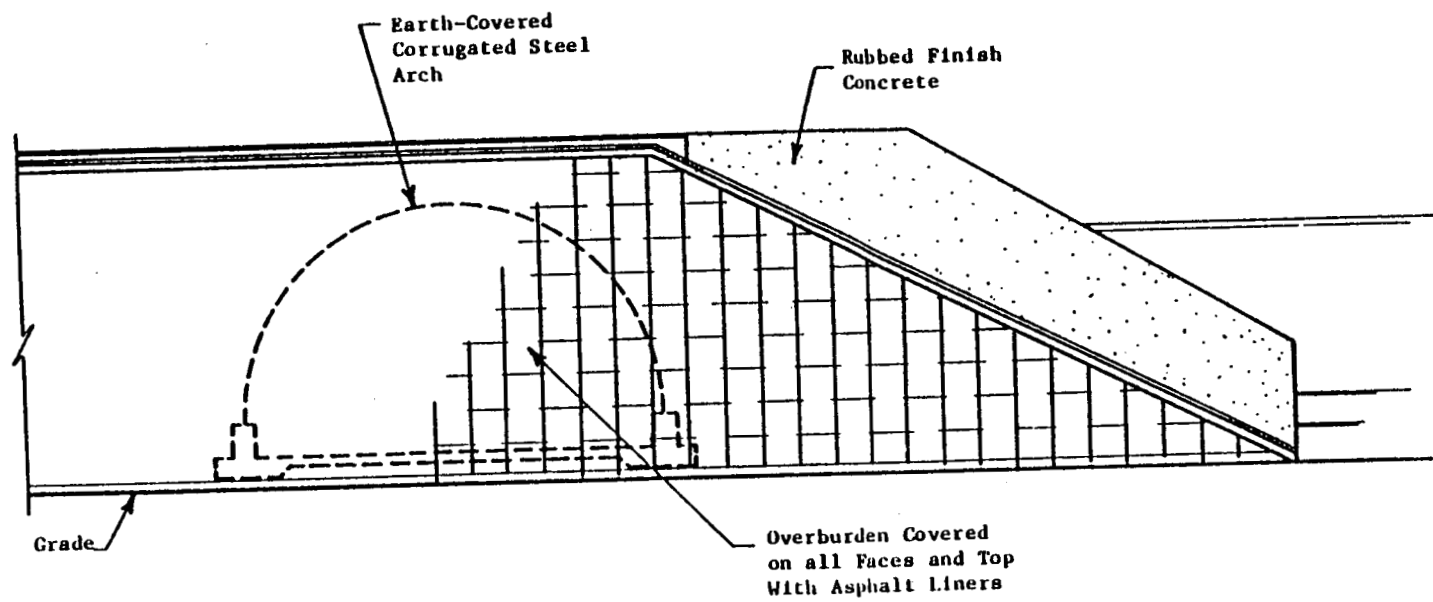
Figure 4.55   Elevation of Earth-Covered Cubicle in Building 12-65
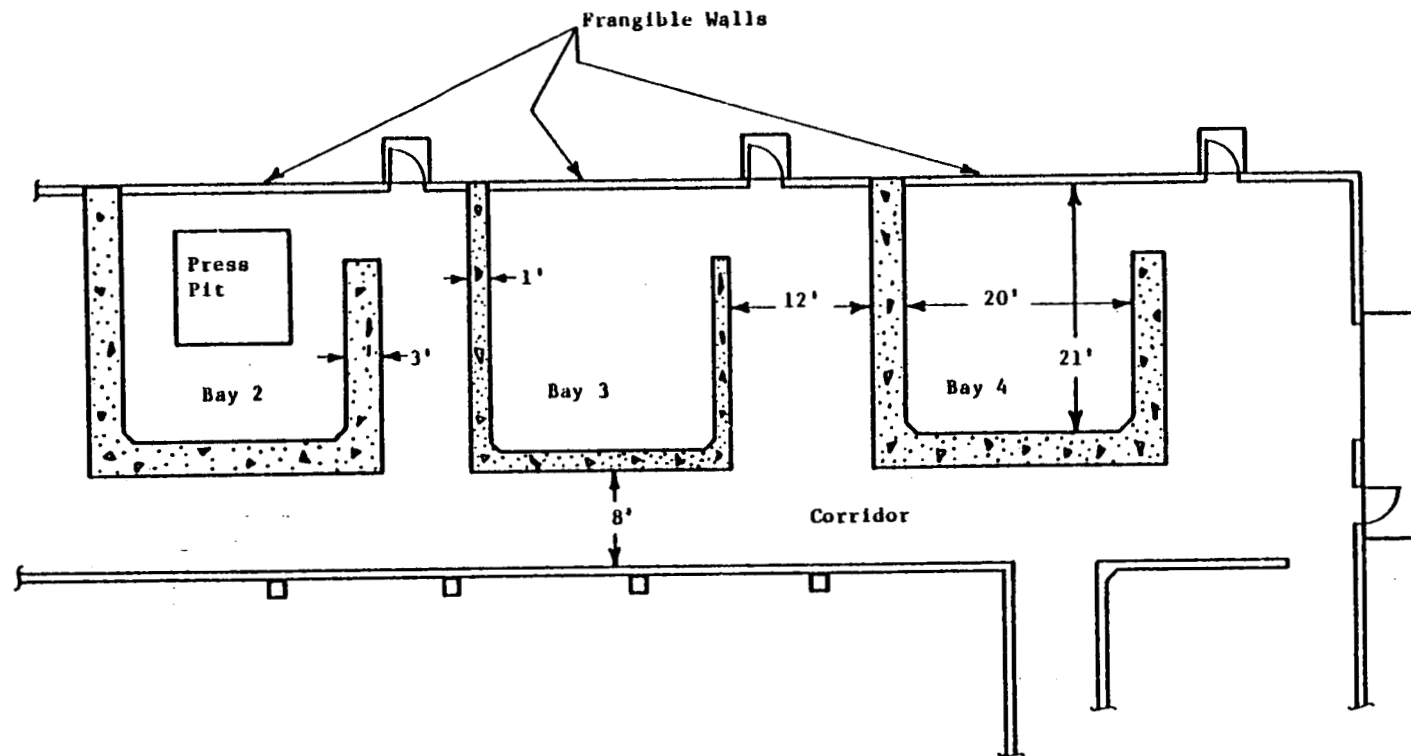
Figure 4.56   Portion of Building 11-20 Showing Multiple Bays Accessed by One Corridor

4.4.4.3 Tunnels Connected to Chambers

Blast waves generated in a tunnel can communicate to one or more chambers, or vice versa, in this type of structure.

Building 12-60 is an example of this type of structure. Figure 4.57 shows a plan view of part of this building. The main access ramp is a tunnel, which provides access via short side tunnels through blast doors to a number of work bays and control booths. The entire building is earth covered. If possible, prediction of initial shock loads is even more complex in this configuration than in the multiple bay structures of Figure 4.56.

4.4.4.4 Blast Doors

These doors can be either personnel or equipment access doors, and can be located in bays or cells or at the ends of tunnels. Blast doors at Pantex have been designed to withstand either internal loads, or external loads, or both.

Two examples are given. Figures 4.58 and 4.59 show inside and outside views of an equipment blast door in a cell in Building 12-44, while Figure 4.58 also shows a revolving, blast-resistant personnel door. The location of these doors in a cell is shown in Figure 4.63.

The second example of a blast door is a flat metal door in a bay in Building 11-20. It is shown in Figure 4.60.

4.4.4.5 Planned New Facilities

Some of these facilities may be designed as complete containment structures, with no or minimal venting, inward opening blast doors, etc. The example we show is the HE Development Machining Facility shown in Figures 2.6 and 2.11. Individual laboratories and bays in this facility are designed with air locks and double, inward-opening blast doors to prevent blast from entering corridors and then into other bays. Light doors which are not blast-resistant close vent openings in outer walls, and open into a maze which allows partial venting, but is designed to arrest fragments. In some cases, steel access equipment panels are set into outer walls. These are designed to be blast-resistant and at least as strong as the walls which support them.

4.5 METHODS OF PREDICTING BLAST LOADING

In this section, we present methods for predicting reflected shock loads and quasi-static pressures, for several structural components of Pantex structures.

Steel Arch

26'

Bay

Bay

Earth Fill

Earth
Fill

Blast Door
(typ)

Tunnel (Main Access Ramp)

Control Booth

Concrete
Head Wall

Reinforced
Concrete

Bay

Earth Fill

Steel Arch
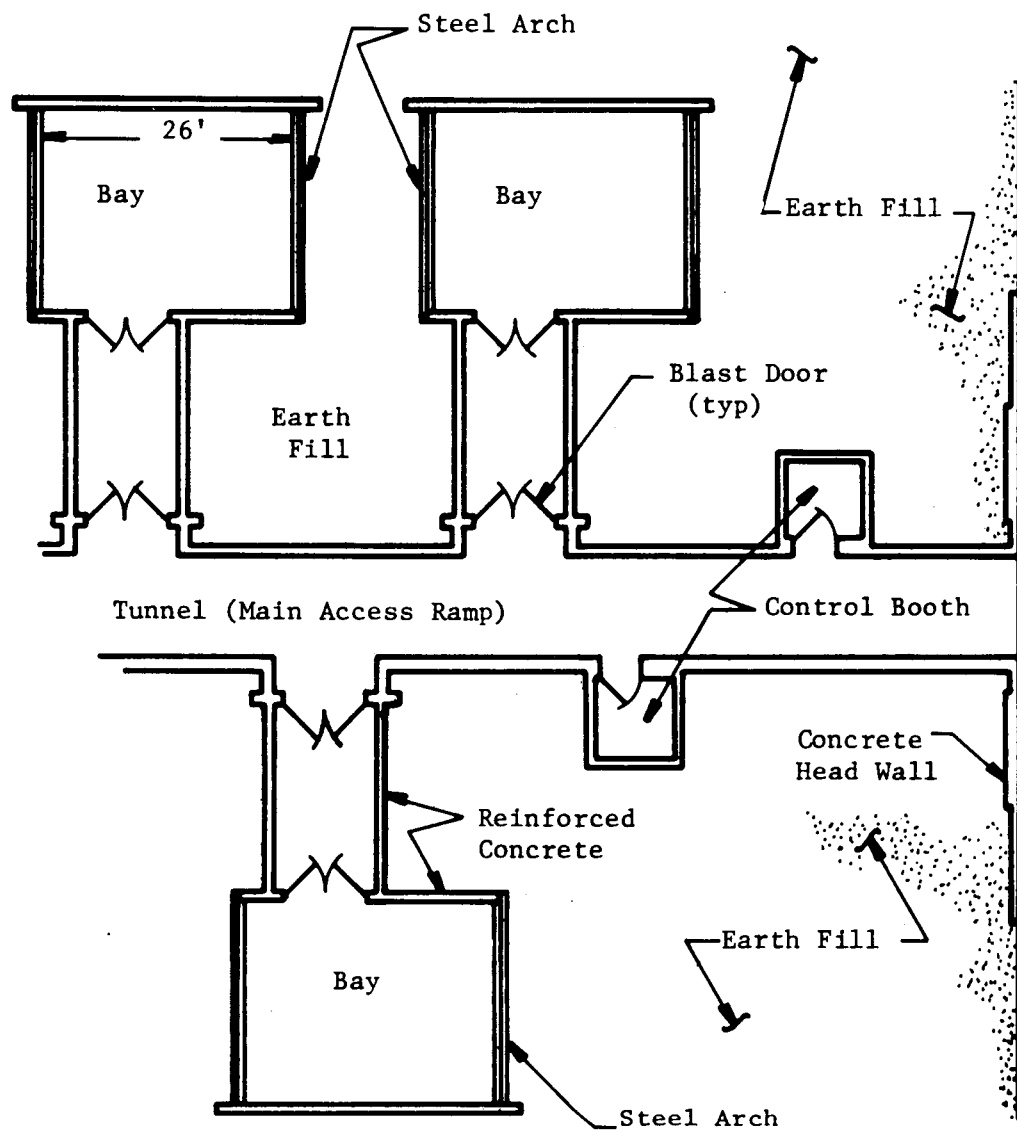
Figure 4.57 Plan View Of Buried Tunnels Connected To
Chambers, Building 12-60
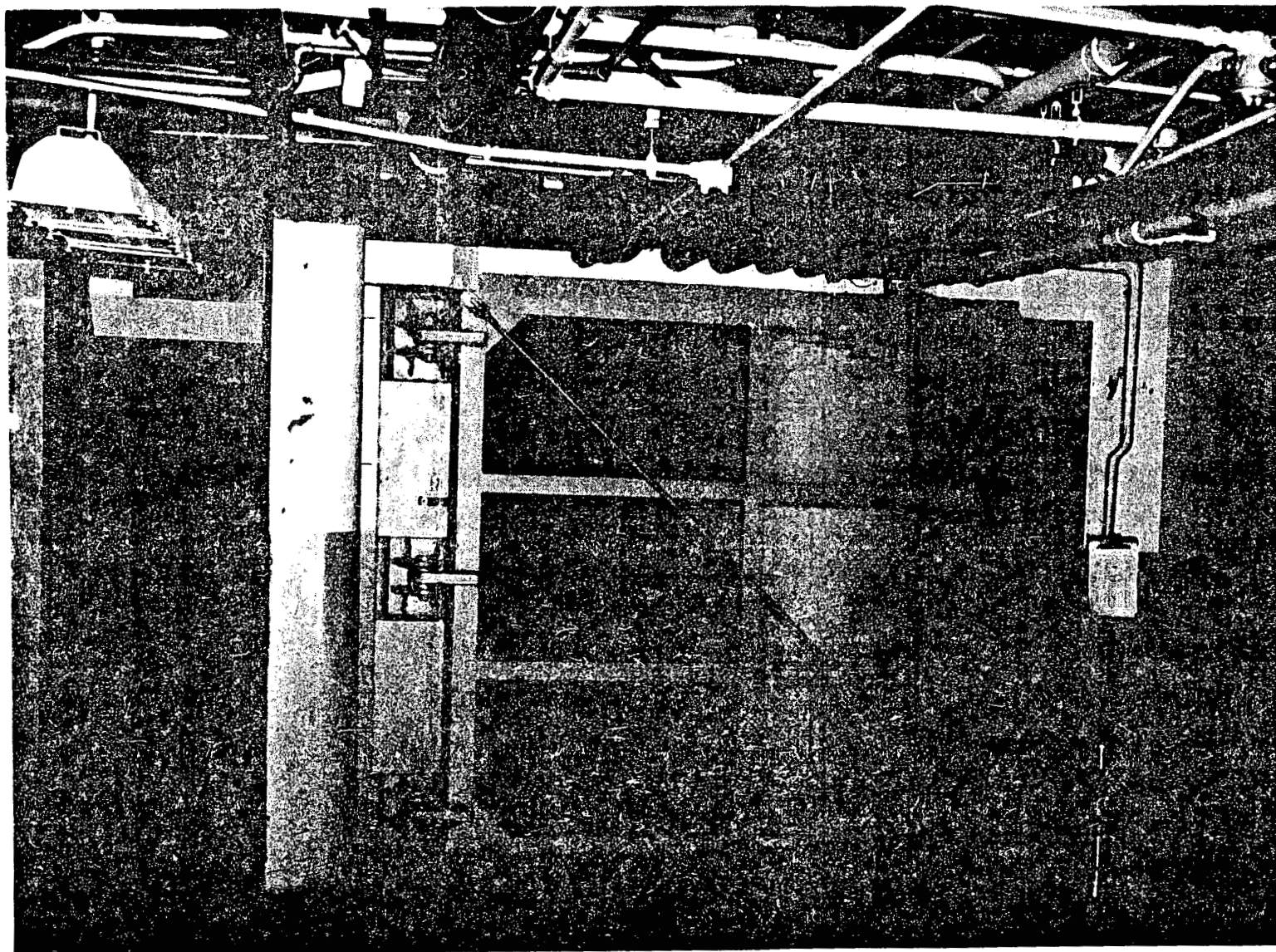
Figure 4.58   Inside View of Equipment and Personnel Blast Doors in Gravel Gertie Cell
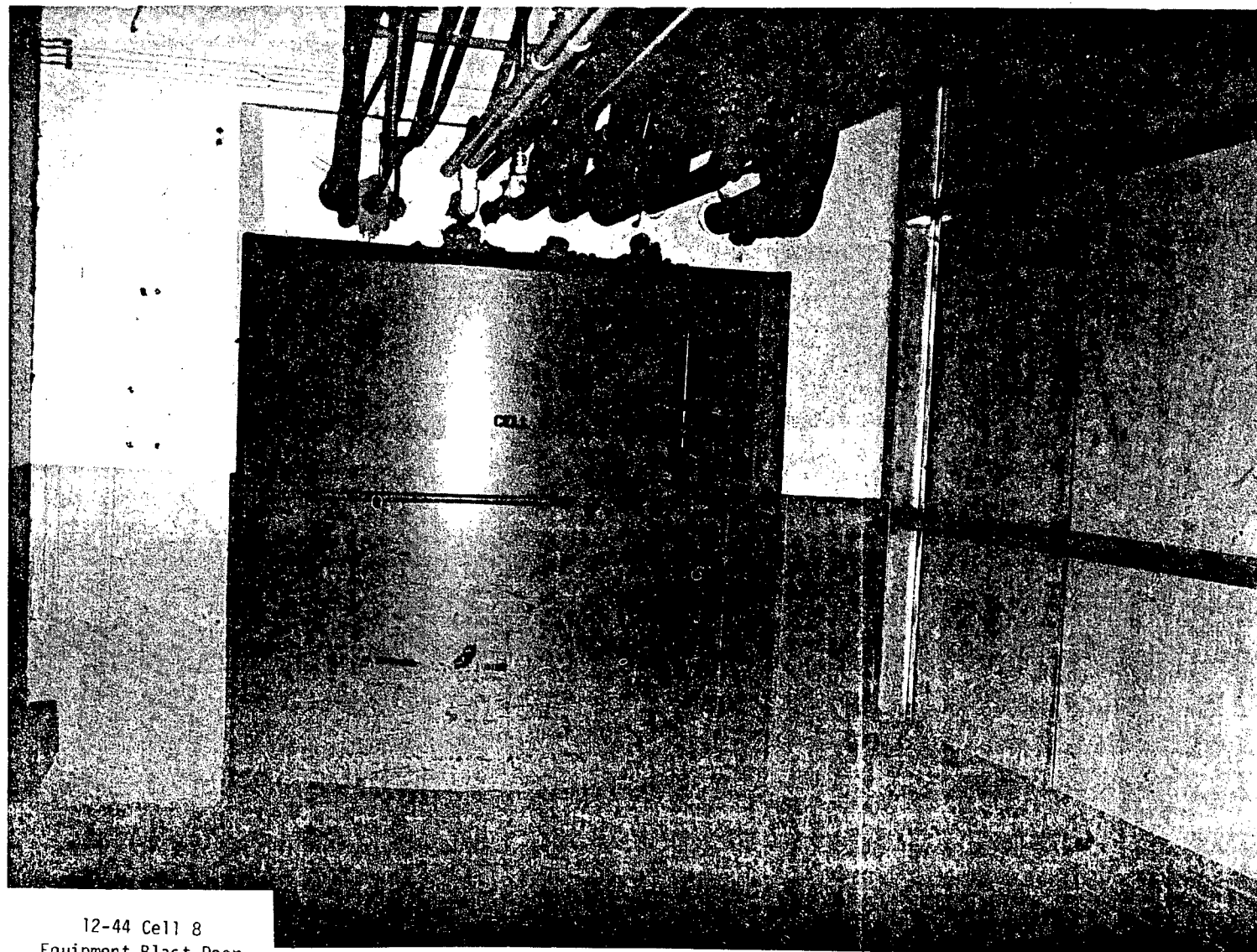
12-44 Cell 8
Equipment Blast Door

Figure 4.59   Outside View Of Equipment Blast Door In Gravel Gertie Cell

11-20
Bay 3; Blast Door
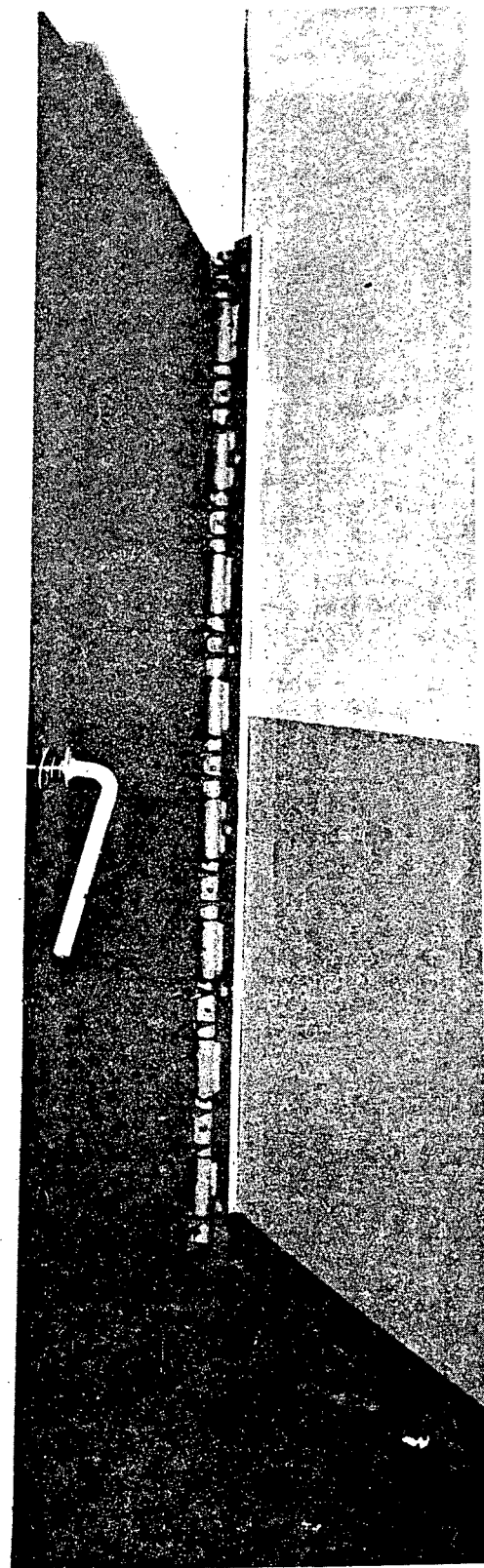
Figure 4.60   Blast Door In Bay 3, Building 11-20

4.5.1 Frangible Panels*

The initial reflected blast pulse loading for frangible panels is essentially identical to the loading on stronger and more massive blast-resistant panels. The methods for predicting the loads on such panels are given in Section 4.4.1.1, and are not repeated here. But, the frangible panel will be fragmented and/or accelerated to significant velocity by the initial reflected impulse [See Equation (4.62)], and may also have moved a significant distance before being struck by repeated reflected shocks within the structure. So, one should only consider the first reflected pressure pulse, and not the repeated reflected pulses shown in Figure 4.36 and idealized in Figure 4.38.

The methods for predicting quasi-static pressures for frangible panels are given in Section 4.4.3. Example Problem 4.12 for prediction of blast loading of a frangible panel is given in that section.

4.5.2 Blast-Resistant Panels

Blast-resistant panels are invariably strong and massive, and can be treated as rigid walls under initial and reflected shock loading. The methods outlined in Section 4.4.1.1 can be used directly for predicting loads on these panels, including the 1.75 multiplier for i_r to account for effects of internal shock reflections, when explosives are centrally located, or nearly so (See Example Problem 4.18).

For blast resistant panels in either vented or unvented chambers, the peak quasi-static pressures, P_{QS}, can be estimated using the methods given in Section 4.4.1.2, and in particular, from Figure 4.43. If the vents in the chamber are open (uncovered), the same section gives prediction methods and curves for time history of vented gas pressure (Equation (4.63)), venting time, t_{max}, (Equation (4.47) and Figure 4.44), and gas impulse, i_g (Equation (4.51a) and Figure 4.45). For vents covered by frangible panels, the prediction curves in Section 4.4.3 should be used for these parameters.

Example Problem 4.11 for shock wave and quasi-static pressure loading on a typical blast-resistant wall panel is given in Section 4.4.1.2.

4.5.3 Corridor Walls

There are a number of facilities at Pantex which have multiple work bays for high explosive operations within the same building complex, with the bays opening into connecting corridors. Two such configurations from a single building complex are shown in Figures 4.61 and 4.62.

---

*These panels are frangible according to the definition in TM 5-1300 (Ref. 4.2)
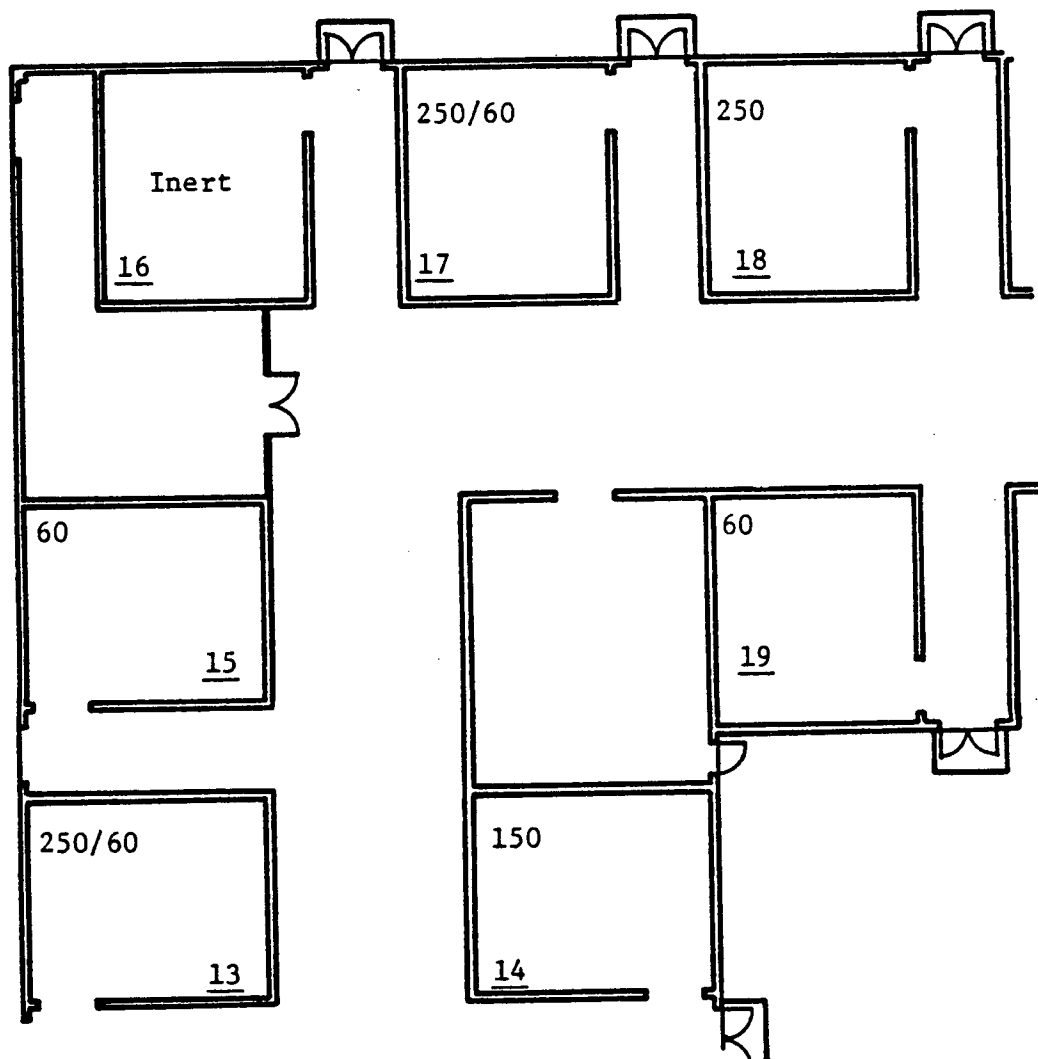
Notes:

1) Underlined numbers are bay numbers

2) Other numbers are HE weight limits.
   For example, 250/60 indicates 250 lb
   staying HE limit and 60 lb operating
   HE limit.

3) If no HE or plutonium are allowed in
   a bay, the word "inert" appears.

Figure 4.61 Portion Of Bay-Corridor Configuration
In Building 12-24, Showing Bays 13 Through 19

240　240　240　5　　250
34

28　　30　　32

29　　31　　33　　37

150　150　120

Inert

35
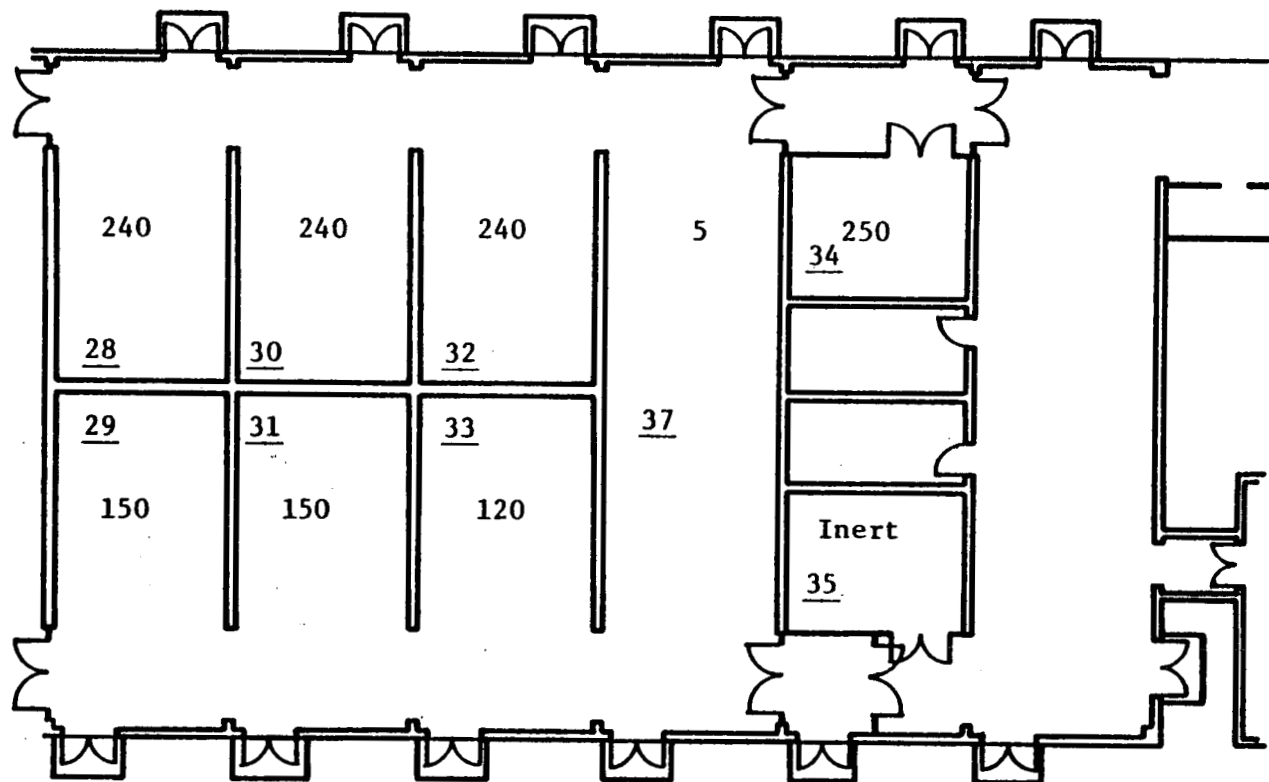
Figure 4.62　Second Type Of Bay-Corridor Configuration In Building 12-24,
Bays 28 Through 34, 37 And 38 (See Notes In Figure 4.61)

Accidental explosions are possible either within individual bays, or cells during operations, or in corridors during transport from one operation to another, or to and from storage. Predictions of loads on floors, walls, and roofs in the immediate vicinity of such an explosion is usually possible using the methods discussed previously in this chapter. But, in general, the current state-of-the-art for prediction of either initial or reflected shock wave loading is quite inadequate for general blast loading predictions in corridors of structures having such complex geometry. The suggested method of approach, if one must accurately predict blast pressures at some distance from the explosion center, is to test on model scale, using strongly built geometric models carefully instrumented with flush-mounted blast pressure transducers. The scale-model test results can be readily scaled to the full-size structures. The testing could be supported by limited computer code predictions, but these predictions are only feasible for the gas phase part of the blast loading.

Because of the complexity of this loading prediction problem, no example problem is given. Referring to Figure 4.62, we can predict the loading on all surfaces in Bay 31, if an explosion were to occur in that bay. We could not, however, make any rational estimates of the blast loads in Bay 37. Multiple shock reflections and diffractions through openings and around corners would occur before the shock front arrived there, and the geometry is too complex to predict these processes.

In the past, model-scale tests have indeed been used to obtain data on transient loads in complex geometry chambers. As an example, a maze entry to cells in the High Explosives Application Facility for Lawrence Livermore Laboratory has been tested in small scale to determine blast loads on surfaces in the maze (Ref. 4.75). For such complex geometries, guidance will be provided an AE by DOE, or included in the design criteria.

4.5.4 Blast Doors

Blast doors used in cells in the Pantex facilities are of three general types, typified by Figures 4.58 through 4.60. These types are:

1. Flat metal doors opening inward or outward into test cells or bays. These doors provide both personnel and equipment access to the cell. (Figure 4.60)

2. Large metal equipment doors to Gravel Gertie cells (Figures 4.58 and 4.59). These doors have main strength members of curved steel, intended to withstand blast by membrane tension when blast-loaded from the inside.

3. Small, revolving, personnel access doors used in Gravel Gertie cells (Figure 4.58). These doors are very strong and massive, and should present significant blast wave venting at all times, even when being used.

For doors of the first type, the closed door is loaded in exactly the same manner as any wall panel in the cell. The methods for predicting loads on these doors is no different from the methods discussed in Section 4.5.2.

Figure 4.63 shows a plan view of a Gravel Gertie cell showing the locations of the second two types of blast doors. As was true for other cell-corridor configurations (Figures 4.56 and 4.61), the internal geometry of this cell and the corridors leading to the blast doors is so complex that rational prediction of initial blast loads for explosions occurring in the cell itself is not possible with the current state-of-the-art. Adequate prediction of gas phase pressures can probably be made using a relatively simple gasdynamic computer code (Refs. 4.49 and 4.51), but the calculations would have to be made for this specific geometry to account for gas flow processes from the cell into the corridor system properly. The motion of the Gravel Gertie roof should be accounted for in the code calculations.

If accurate definition of blast loads on doors in strong containment cell systems such as the Gravel Gerties is needed, the recommended procedure is careful scale model testing, supplemented by limited computer code calculations with a relatively simple gasdynamic code. The scale model testing will define the initial and first several shock wave loads, while the gas dynamic code will predict the longer term quasi-static pressures.

In the past, estimates of shock loading have been made using path lengths from the explosion center through the structure to given walls or other surfaces as a radial distance R, and free-field blast charts such as Figures 4.5 through 4.7 are then used to predict either side-on or reflected overpressures and specific impulses. The accuracy of this procedure is very doubtful, and unfortunately, may not be conservative and predict upper limits to actual loads. So, we reiterate that appropriate model scale testing is probably the best alternative available to an AE for determining shock loads in complex and interconnected chambers.

No example problems are given for loading of blast doors, because the flat doors in box-shaped cells are loaded in exactly the same manner as blast-resistant wall panels, and the corridor configuration in Gravel Gertie cells is too complex for rational prediction of the shock phase of blast loading.

4.5.5 Air Blast Spalling of Concrete Walls

There exists little information concerning air blast spalling of concrete walls. The work which has been done in this area is analytic in nature. The phenomena associated with air blast produced spall and the determination of spall size and velocity are very complex and simplification in analysis is necessary. One simplification used by all investigators to date is that a compressive stress wave travelling through a wall is not attenuated in strength.
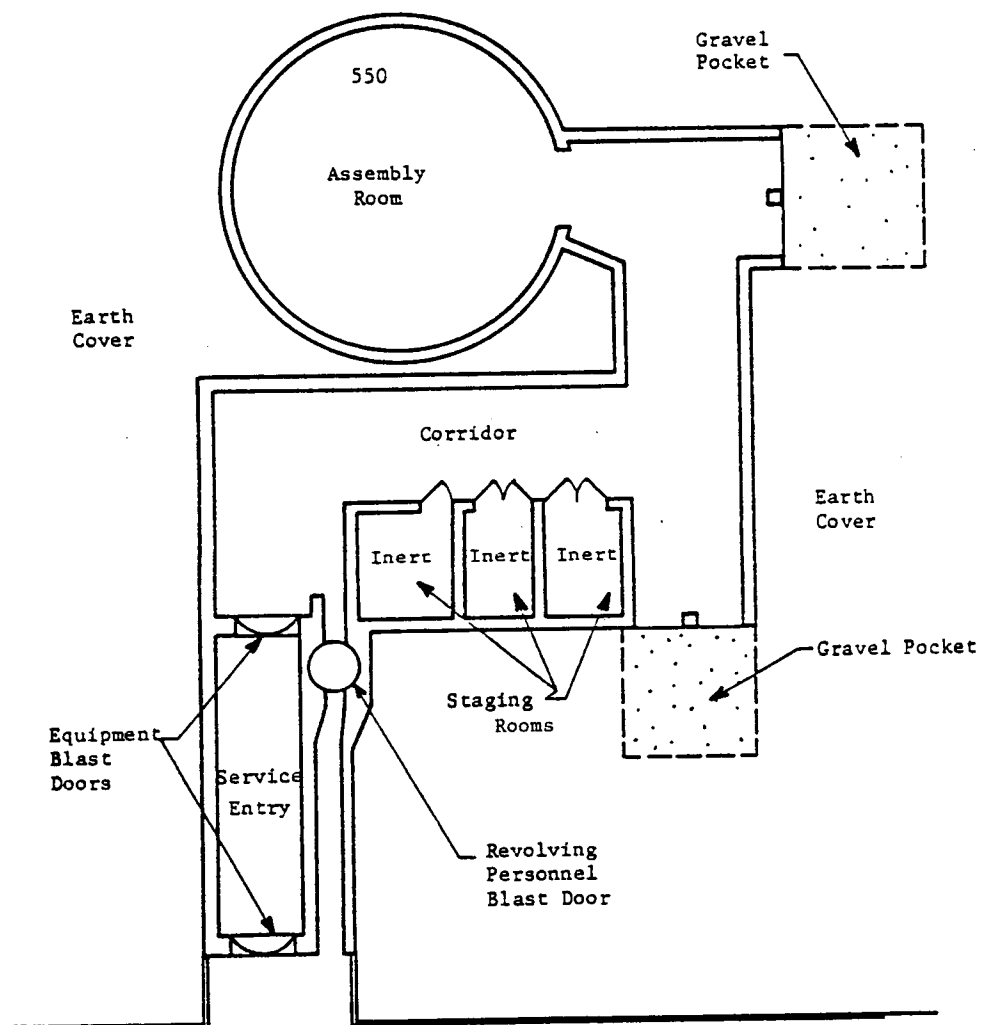
Figure 4.63 Plan View of Building 12-44, Cell 1,
Showing Blast Doors and Corridor

Spalling is the direct consequence of interference near a free surface between the tail of an oncoming incident compressive wave (not yet reflected) and the reflected tensile wave. If a compressive wave strikes a free surface normally, it will be reflected as a tensile wave of equal strength. Oblique reflections are much more complex; however, a tensile wave will be generated that is lesser in magnitude. When portions of the incident compressive wave and other portions of the reflected tensile wave interfere with one another, a stress distribution results which can be conducive to fracture. An example of wave superposition is illustrated in Figure 4.64a, a triangular pressure pulse of intensity P and duration T. In this figure, half of the wave has been reflected. As the wave continues to reflect and move inward, the resulting tension A B increases. The maximum tensile stress that can ever be attained equals P. This stress will be reached in this example at a distance equal to or greater than uT/2 from the free surface. Should the fracture stress of the material (for practical purposes, its ultimate strength σ_u) be less than P, fracture will occur. If P just equals tensile σ_u, fracture will occur at a distance uT/2 from the free surface. For strong stress waves, fracture will occur progressively closer to the free surface. It will occur wherever the stress resultant first exceeds σ_u. Multiple spalls can also occur as new free surfaces are produced by preceeding spalls and as the incident wave continues to dissipate. The maximum stress which can ever be attained by a triangular wave as in Figure 4.64a at each particular point in a material is plotted in Figure 4.64b. Figure 4.64b is a function of position in the material, wave length and stress intensity for points near the free reflecting surface.

A solution for the threshold of spall can be determined by relating blast wave parameters (pressure, impulse and duration) to material properties in the concrete (σ_u). Several assumptions are made which include:

- Uniform loading of the wall with peak reflected overpressure P_r and reflected positive specific impulse i_r.

- The pressure time history of the wave is assumed to be triangular in shape and its duration shall be

$$T = \frac{2 \, i_r}{P_r}$$

- The pressure wave transmits a stress pulse through the concrete which is not attenuated through the wall (i.e., the pressure distribution is assumed the same in magnitude at the back face of the wall as at the front face, only displaced in time).
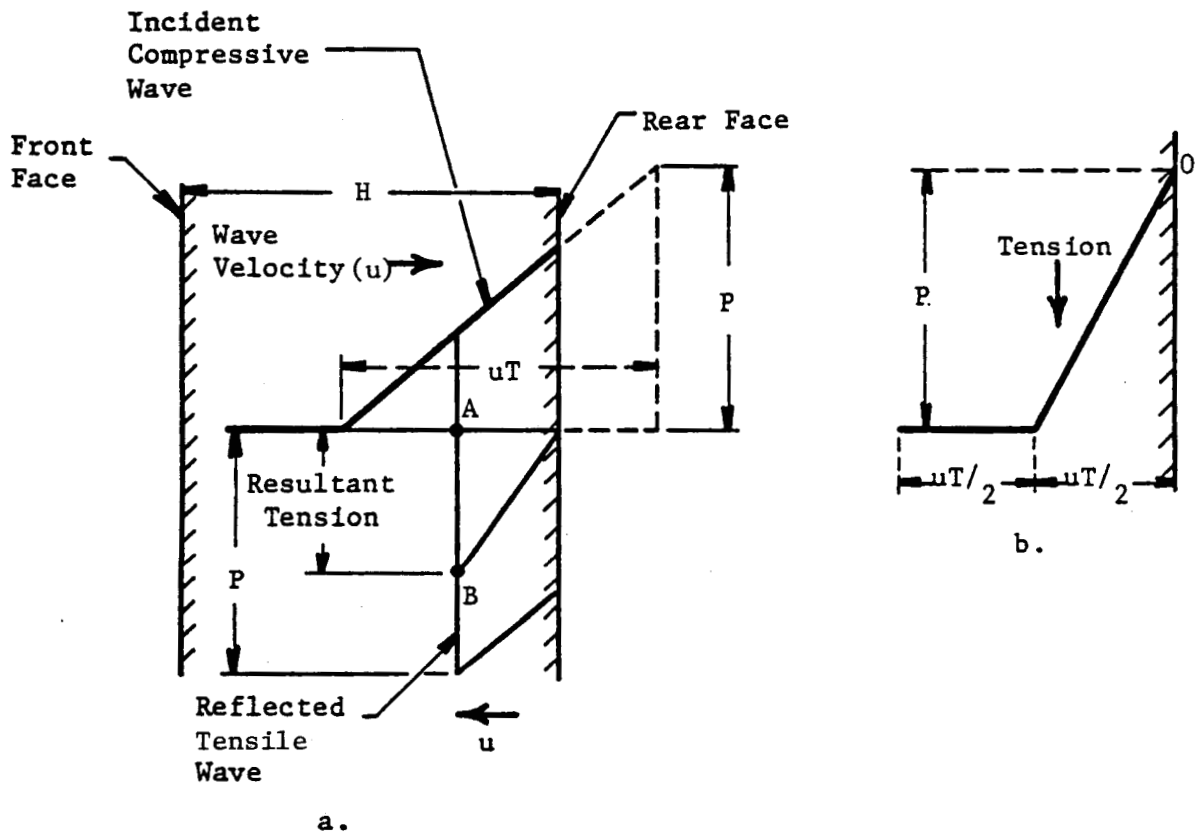
Note: The wave applied to the front face will have
pressure amplitude P and duration T.

Figure 4.64 a.) Superposition of Stresses During
Reflection Process for a Triangular
Pulse Striking a Wall

b.) Maximum Stress versus Position for
a Triangular Wave Form

- The stress wave will travel through the wall at velocity

$$v = \sqrt{\frac{E}{\rho}}$$

(E = Young's modulus, ρ = density). The time for one complete wave transit (from front to back face then return to front face) is

$$\frac{2H}{v} = T_w$$

where H is wall thickness.

Should P_r be greater than σ_u of the concrete, the material will fracture. Thus

$$\frac{T}{T_w} = \frac{vi_r}{HP_r} \leq 1 \text{ for } \frac{P_r}{\sigma} \geq 1.0$$

is a criterion for determining the threshold of spall. On the other hand, compressive pressures will still be applied to the front of a wall when the initial wave front returns if T is greater than P. Under these conditions, if

$$P_r - p(t) \geq \sigma_u \qquad\qquad (4.67)$$

then spall is predicted to occur. Substituting $P_r (1 - t/T)$ for $p(t)$ (triangular pressure pulse) gives:

$$\frac{P_r}{\sigma_u} \frac{t}{T} \geq 1.0 \qquad\qquad (4.68)$$

Finally, substituting $2i_r/P_r$ for the blast wave duration T and $2H/v$ for the wave transit time T_w gives the relationship for spall threshold for long duration air blast waves.

$$\frac{P_r}{\sigma_u} \frac{H P_r}{v \, i_r} \geq 1.0 \text{ for } \frac{v \, i_r}{H \, P_r} \geq 1.0 \qquad\qquad (4.69)$$

The spall thresholds discussed above are presented graphically in Figure 4.65.

The above analysis can be used to determine if concrete spall due to blast loading is predicted to occur; however, it does not give spall size or velocity. In work done by Kot, et al. (Ref. 4.60), spalling of concrete was investigated and analytical solutions were derived for predicting concrete spall size and velocity. This work was done for safety studies concerning air blast effects on power plant structures. In this report, large, thick concrete structures (containment structures) are blast loaded. The size of the structure, compared to charge weights led to the consideration of a non-uniform blast loading, P, I, where P and I are functions of wall position as shown in Figure 4.14. Blast wave parameters were obtained from TM 5-1300 for use in this report. Spalling of concrete at normal and oblique incidence was considered, except for incident angles greater than 45° where no spall was expected to occur. A set of scaled curves is given which includes variations of spall depth and velocity with charge standoff and number of spalls, variation of spall depth and velocity with spall number at various standoff distances, effect of concrete wall thickness on spall depth and velocity, and the effect of angle of incidence on spall depth and velocity. Also considered by Kot, et al. (Ref. 4.60) are wall displacements due to impulsive loads. The comparison between maximum spall and wall displacement velocities is made and it is shown that wall displacement velocities in some cases dominate spall velocities, particularly for heavy spall debris (See Figure 4.66). It is, therefore, suggested that the most severe concrete spallation from blast loads may be due to a coupling of spall formation to gross wall motion. Kot, et al. (Ref. 4.60) suggest a simple method of a "first cut" estimate of spall hazard, which is to limit spall mass to the thickness covering the exterior layer of reinforcing and to the 45° cut-off mentioned earlier. The velocity can be equated to that for wall motion produced by an impulsive load (velocity = total impulse/wall mass). A curve of wall velocity due to impulsive loading versus scaled standoff is provided in the report and is reproduced here (see Figure 4.67). This graph is intended for very large walls and is conservative for small walls. For more details see Reference 4.60.
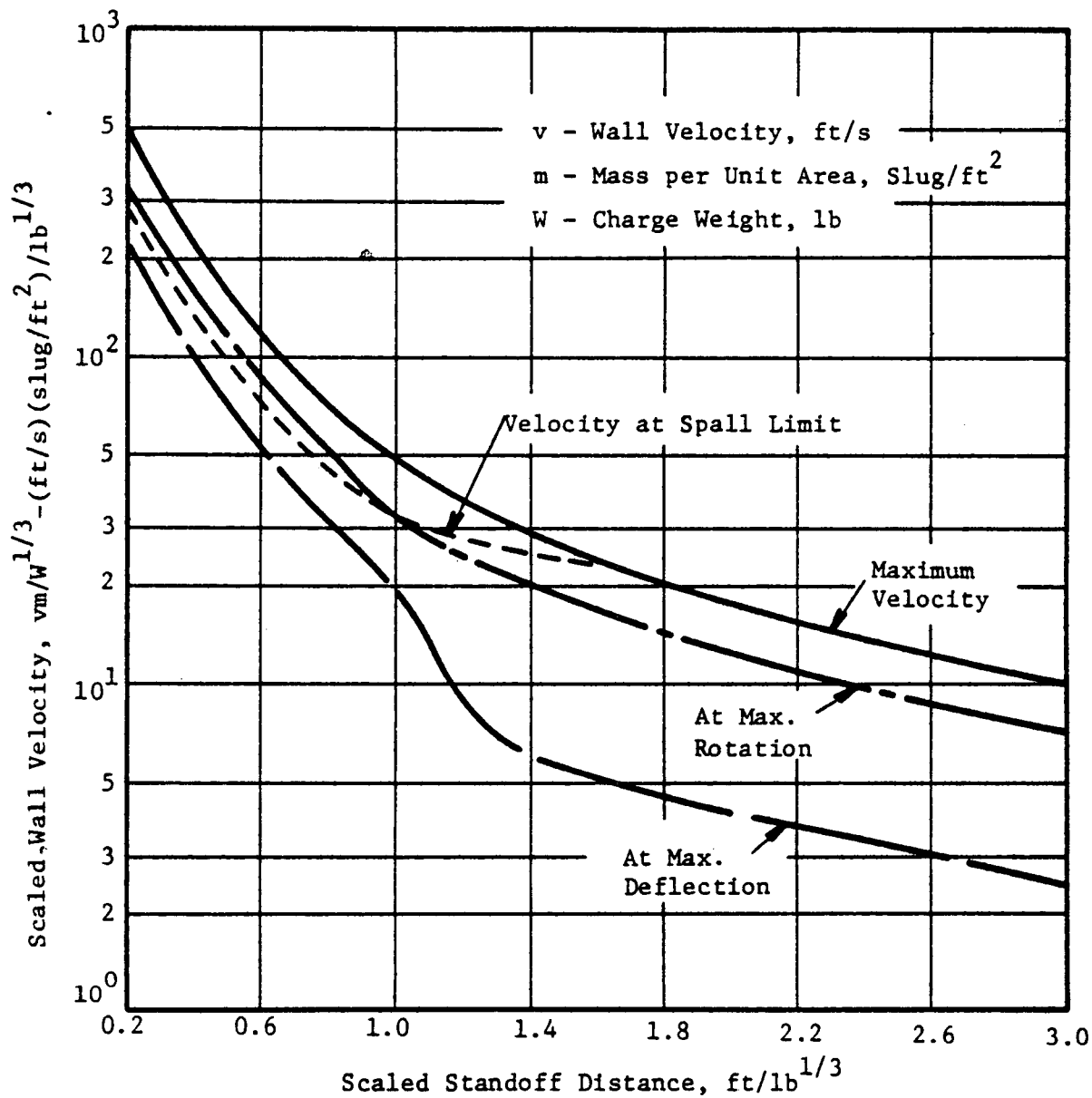
Figure 4.67   Scaled Concrete Wall Velocities Due to Impulsive
Air Blast Loading (Kot, et al., Reference 4.60)

EXAMPLE PROBLEM 4.13

PROBLEM – Calculate concrete spall size and velocity for an explosion near a wall. This calculation should indicate the potential debris hazard in an adjacent bay or corridor.

GIVEN: Blast loading (pressure and impulse) on surface under consideration
Wall dimensions and reinforcing location
σ_u = tensile strength of concrete
E = Young's modulus of concrete
ρ_c = density of concrete

FIND: Concrete spall size and velocity   **REFERENCE**

SOLUTION:
1. Determine if concrete will spall due to blast loading and spall limits   Fig. 4.65
2. If spalling will occur, determine spall velocity by using Figures 4.65 or 4.66 and using the gross wall velocity curves   Fig. 4.65 or which will give an upper velocity   Fig. 4.66
3. Determine spall mass using 45° cutoff and thickness from outside wall to rebar layer or cutoff where end of spall occurs (< 45°)

CALCULATION – Use results of Example Problem 4.11, which gives the blast loading on a wall in the HE treatment room of the High Explosives Development Machining Facility.

GIVEN: Blast loading on wall for a 468 lb charge at a 3-ft standoff as shown in Table 4.10

Table 4.10   Blast Loading on Wall

X ft	P_r psi	i_r psi-sec	T sec
0	7.0×10^4	12	3.5×10^{-4}
1.5	5.5×10^4	7.0	2.5×10^{-4}
3.0	2.0×10^4	3.9	3.9×10^{-4}
4.5	8.0×10^3	1.7	4.3×10^{-4}
6.0	4.0×10^3	0.93	4.6×10^{-4}
7.5	2.5×10^3	0.51	4.1×10^{-4}
9.0	2.0×10^3	0.31	3.1×10^{-4}
9.75	1.5×10^3	0.22	2.9×10^{-4}

Wall dimensions   3'6"

25'

20'

Rebar location

3/4" = 0.0625'

3'6"

3/4" ℄

ρ_c = 2.3 X 10^{-4} lb-sec^2/in^4

σ_u = 300 psi tensile (assumed)*

E = 4 X 10^6 psi (assumed)

FIND: Concrete spall size and velocity

SOLUTION: 1. Spalling will occur due to the first shock of multiple shocks in an enclosed structure. Thus for determining if spall occurs one needs P_r of the first shock only, which is in contrast to summing repeated shocks as one, with 1.75 P_r and 1.75 i_r for structural response or gross wall motion.

Using Figure 4.65, i_r and P_r max (at X = 0)

$$\frac{P_r}{\sigma_u} = \frac{7.0 \times 10^4}{300} = \underline{233}$$

$$v = \sqrt{\frac{E}{\rho_c}} = \sqrt{\frac{4 \times 10^6 \text{ lb/in.}^2}{2.3 \times 10^{-4} \text{ lb-sec}^2/\text{in.}^4}} = \underline{1.32 \times 10^5 \text{ in/sec}}$$

$$\frac{i_r v}{P_r H} = \frac{12 \text{ lb-sec/in.}^2 \ 1.32 \times 10^5 \text{ in./sec}}{7.0 \times 10^4 \text{ lb/in.}^2 \ (42 \text{ in.})} = \underline{0.54}$$

---

*This value was obtained using a typical value for compressive ultimate strength, and dividing by ten. It differs significantly from values assumed by Kot, et al. (Ref. 4.60). See Chapter 7, Dynamic Properties of Materials, for further discussion of this point.

From Figure 4.65 spall will occur at X = 0.
The largest X where spall will occur corresponds
to 45° off normal or X = 3 ft.
Here we determine if spall will occur. If not,
one must go to less than 45° to find extent of
spall here:

$$\frac{P_r}{\sigma_u} = \frac{2 \text{ X } 10^4}{300} = 66.7$$

$$\frac{i_r v}{P_r H} = \frac{3.9 \ (1.32 \text{ X } 10^5)}{2 \text{ X } 10^4 \ (42)} = 0.61$$

From Figure 4.65 spall will occur at X = 3 ft (45°)
Thus, spall limit = 3 ft radius

2. Using Figure 4.66

Scaled wall thickness = $\dfrac{\text{wall thickness}}{W^{1/3}} = \dfrac{3.5}{468^{1/3}} = 0.45 \ \dfrac{\text{ft}}{\text{lb}^{1/3}}$

Scaled distance = $\dfrac{3}{468^{1/3}} = 0.386 \ \dfrac{\text{ft}}{\text{lb}^{1/3}}$

Interpolating from Figure 4.66 gives spall
velocity $\approx$ 150 ft/sec

3. Spall volume involved (to first rebar layer)

$$V = (\pi \ 3^2 \text{ X } .0625) \ \text{ft}^3 = \underline{1.77 \ \text{ft}^3}$$

Spall mass = $1.77 \ \text{ft}^3 \ (4.8 \ \dfrac{\text{lb-sec}^2}{\text{ft}^4}) = \underline{8.5 \ \dfrac{\text{lb-sec}^2}{\text{ft}} \text{ or slugs}}$

Spall weight = $\underline{270 \ \text{lb}}$
Using Figure 4.67
Scaled distance = 0.386 ft/lb$^{1/3}$
From Figure 4.67

Scaled wall velocity = $\dfrac{vm}{W^{1/3}} = 320$

$m = \rho$ concrete times wall thickness = $4.8 \ \dfrac{\text{lb-sec}^2}{\text{ft}^4} \text{ X } 3.5 \ \text{ft} =$

$16.8 \ \dfrac{\text{lb-sec}^2}{\text{ft}^3} \text{ or } \dfrac{\text{slugs}}{\text{ft}^2}$

Hence, wall and spall velocity = $320 \text{ X } \dfrac{W^{1/3}}{m} = 320 \text{ X } 7.76 \ \text{lb}^{1/3}$

$= 16.8 \ \dfrac{\text{lb-sec}}{\text{ft}^3} = \underline{148 \ \text{ft/sec}}$

4.6 HAZARDS TO PERSONNEL FROM AIR BLAST

Literature concerning the harmful effects of blast on humans has been published as early as 1768. However, knowledge of the mechanisms of blast damage to humans was extremely incomplete until World War I, when the physics of explosions were better understood. Since that time, numerous authors have contributed considerable time and effort in the study of blast damage mechanisms and blast pathology. Each accident situation has its own unique environment with trees, buildings, hills, and various other topographical conditions which may dissipate the energy of the blast wave or reflect it and amplify its effect on an individual. Because of these different variational factors involved in an explosion-human body receiver situation, only a simplified and limited set of blast damage criteria will be included here. The human body "receiver" will be assumed to be standing in the free-field on flat and level ground when contacted by the blast wave. Excluding certain reflected wave situations, this is the most hazardous body exposure condition. Air blast effects can be divided into four categories: primary blast effects, tertiary blast effects, ear damage, and blast generated fragments (Ref. 4.61). Secondary effects involving fragment impact by missiles from the exploding device itself or from objects located in the nearby environment which are accelerated after interaction with the blast wave (appurtenances) shall be discussed in Chapter 6.

4.6.1 Primary Blast Damage

Primary blast effects are associated with changes in environment pressure due to the occurrence of the air blast. Mammals are sensitive to the incident, reflected and dynamic overpressures, the rate of rise to peak overpressure after arrival of the blast wave, and the duration of the blast wave (Ref. 4.61). Specific impulse of the blast wave also plays a major role (Refs. 4.62 and 4.63). Other parameters which determine the extent of blast injury are the ambient atmospheric pressure, the size and type of animal, and possibly age. Parts of the body where there are the greatest differences in density of adjacent tissues are the most susceptible to primary blast damage (Refs. 4.61, 4.64, and 4.65). Thus, the air-containing tissues of the lungs are more susceptible to primary blast than any other vital organ (Ref. 4.66).

Pulmonary injuries directly or indirectly cause many of the pathophysiological effects of blast injury (Ref. 4.67). Injuries include pulmonary hemorrhage and edema (Refs. 4.61 and 4.67), rupture of the lungs (Ref. 4.61), air-embolic insult to the heart and central nervous system (Ref. 4.61), loss of respiratory reserve (Ref. 4.61) and multiple fibrotic foci, or fine scars, of the lungs (Ref. 4.64). Other harmful effects are rupture of the eardrums (to be discussed later) and damage to the middle ear, damage to the larynx, trachea, abdominal cavity, spinal meninges, and radicles of the spinal nerves and various other portions of the body (Ref. 4.61).

Bowen, et al. (Ref. 4.65) and White, et al. (Ref. 4.62), have developed pressure versus duration lethality curves for humans which are especially amenable to this document. Some of the major factors which determine the extent of damage from the blast wave are the characteristics of the blast wave, ambient atmospheric pressure, and the type of animal target, including its mass and geometric orientation relative to the blast wave and nearby objects (Ref. 4.62). Although Richmond, et al. (Ref. 4.63) and later White, et al. (Ref. 4.62), both from the Lovelace Foundation, discuss the tendency of the lethality curves to approach isopressure lines for "long" duration blast waves, their lethality curves demonstrate dependence on pressure and duration alone. Since specific impulse is dependent on pressure as well as duration, pressure-impulse lethality or survivability curves appear to be more appropriate. The tendency for pressure-impulse lethality curves to approach asymptotic limits is also very aesthetically appealing from a mathematical point of view. Also, since both pressure and specific impulse at a specified distance from most explosions can be calculated directly using methods described in this document, it is especially appropriate that pressure-impulse lethality (or survivability) curves be developed. This has been done and is described in Reference 4.59. These curves and their use are reproduced here as Figure 4.68.

Simplifying Lovelace's scaling laws in such a manner that only the human species or large animals are considered, one is able to arrive at the following relationships or scaling laws:

1. The affect of incident overpressure is dependent on the ambient atmospheric pressure. That is,

$$\overline{P}_s = \frac{P_s}{P_o} \tag{4.70}$$

where $\overline{P}_s$ is scaled incident peak overpressure, P_s is peak incident overpressure, and P_o is ambient atmospheric pressure.

2. The effect of blast wave positive duration is dependent on ambient atmospheric pressure and the mass of the human target. That is,

$$\overline{T} = \frac{T p_o^{1/2}}{m^{1/3}} \tag{4.71}$$

where $\overline{T}$ is scaled positive duration, T is positive duration, and m is weight of human body.
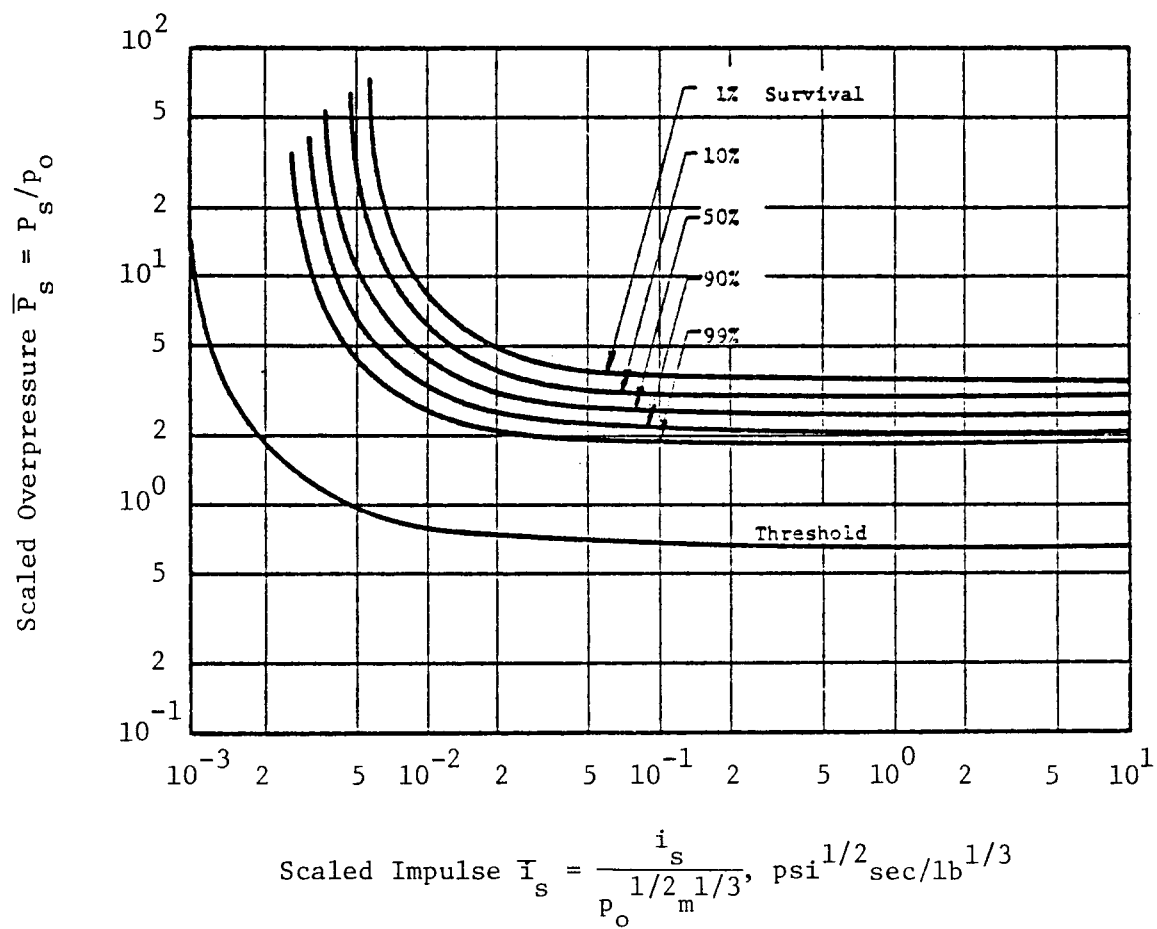
Figure 4.68   Survival Curves for Lung Damage to Man

3. Impulse i_s can be approximated by

$$i_s = \frac{P_s T}{2} \qquad (4.72)$$

Equation (4.72) assumes a triangular wave shape and is conservative, from an injury standpoint, for "long" duration blast waves which approach square wave shapes because it underestimates the specific impulse required for a certain percent lethality. It is also a close approximation for "short" duration blast waves which characteristically have a short rise time to peak overpressure and an exponential decay to ambient pressure, the total wave shape being nearly triangular. Applying the blast scaling developed at the Lovelace Foundation for peak overpressure and positive duration to the conservative estimate for specific impulse determined by Equation (4.72) above, one can arrive at a scaling law for specific impulse:

$$\bar{i}_s = \frac{1}{2}\, \bar{P}_s \bar{T} \qquad (4.73)$$

where $\bar{i}_s$ is scaled specific impulse. From Equations (4.71), (4.72), and (4.73)

$$\bar{i}_s = \frac{1}{2}\, \frac{P_s T}{P_o^{1/2} m^{1/3}} \qquad (4.74)$$

or from Equation (4.72)

$$\bar{i}_s = \frac{i_s}{P_o^{1/2} m^{1/3}} \qquad (4.75)$$

Thus, as indicated by Equation (4.75), scaled specific impulse $\bar{i}_s$ is dependent on ambient atmospheric pressure and the mass of the human target.

Reconstructed curves from Reference 4.59 are shown in Figure 4.68. It should be noted that these curves represent percent survivability, and higher scaled pressure and scaled impulse combinations allow fewer survivors. Presenting the curves in this fashion is advantageous since they apply to all

altitudes with different atmospheric pressures and all masses (or sizes) of human bodies. Once one determines the incident overpressure and specific impulse for an explosion, they can be scaled using Equations (4.70) and (4.75). The proper ambient atmospheric pressure to use for the scaling can be acquired from Figure 4.69, which shows how atmospheric pressure decreases with increasing altitude above sea level (Ref. 4.19). The value for body weight used in the scaling is determined by the demographic composition of the particular area under investigation. It is recommended that 11 lb be used for babies, 55 lb for small children, 121 lb for adult women, and 154 lb for adult males. It should be noticed that the smallest bodies in this case are the most susceptible to injury.
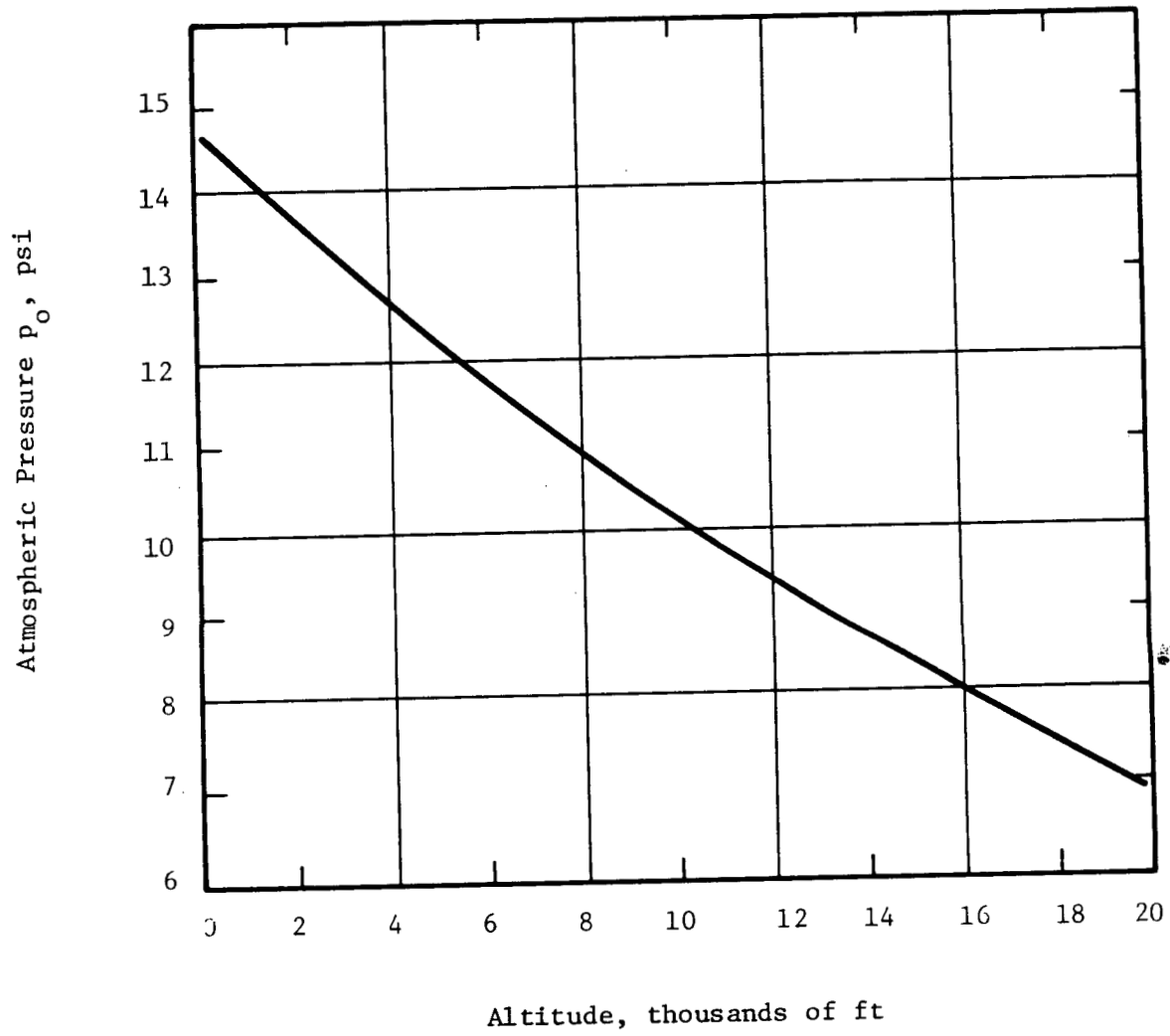
Figure 4.69 Atmospheric Pressure as a Function of
Altitude Above Sea Level

PROBLEM – Assess lung damage to humans at an appropriate distance from a given explosive source.

GIVEN: W = explosive charge weight
R = distance from center of explosive charge
Altitude (no symbol)
m = weight of body of human subject

FIND: Probability of survival

SOLUTION:

		REFERENCE
1.	Determine peak incident overpressure P_s and specific impulse i_s for given charge weight W and distance R	Fig. 4.5
2.	Determine ambient atmospheric pressure from altitude	Fig. 4.69
3.	Calculate scaled incident overpressure $\overline{P}_s$	Eq. (4.70)
4.	Choose weight of the lightest human exposed at distance R	
5.	Calculate scaled specific impulse $\overline{i}_s$	Eq. (4.75)
6.	Plot $\overline{P}_s$ and $\overline{i}_s$ and determine probability of survival	Fig. 4.68

CALCULATION

GIVEN: W = 100 lb
R = 100 ft
Altitude = 4000 ft
m = 130 lb

FIND: Percent survival

SOLUTION:

1. $R/W^{1/3} = 100/100^{1/3} = 21.5$ ft/lb$^{1/3}$
Enter Figure 4.5 and read $P_s = 1.8$ psi

and $i_s/W^{1/3} = 2.55 \times 10^{-3}$ psi-sec/lb$^{1/3}$

"Unscale" to determine i_s

$\dfrac{i_s}{W^{1/3}} \cdot W^{1/3} = 2.55 \times 10^{-3} \times 10^{1/3} = 5.49 \times 10^{-3}$ psi-sec

2. From Figure 4.69 for 4000 ft altitude,
$p_o = 12.6$ psi

3. From Equation (4.70),
   $\overline{P}_s = 1.8/12.5 = 0.144$

4. Given m = 130 lb

5. From Equation (4.75),

$$\overline{i}_s = \frac{i_s}{p_o^{1/2} m^{1/3}} = \frac{5.49 \times 10^{-3}}{12.6^{1/2} \times 130^{1/3}} = 1.08 \times 10^{-3} \frac{\text{psi}^{1/2}\,\text{sec}}{\text{lb}^{1/3}}$$

6. From Figure 4.68, enter with $\overline{P}_s = 0.144$ and $\overline{i}_s = 1.08 \times 10^{-3}$. The point lies well <u>below</u> the threshold for lung damage. So, there is no injury and survival is <u>100%</u>

4.6.2 Tertiary Blast Injury

During whole-body displacement, blast overpressures and impulses interact with the body in such a manner that it is essentially picked up and translated. Tertiary blast damage involves this whole-body displacement and subsequent decelerative impact (Ref. 4.61). Bodily damage can occur during the accelerating phase or during decelerative impact (Ref. 4.68). The extent of injury due to decelerative impact is the more significant (Ref. 4.69), however, and is determined by the velocity change at impact, the time and distance over which deceleration occurs, the type of surface impacted, and the area of the body involved (Ref. 4.61).

Although the head is the most vulnerable portion of the body to mechanical injury during decelerative impact, it is also the best protected (Ref. 4.67). Because of the delicate nature of the head, many may feel that translation damage criteria should be based on skull fracture or concussion. However, since body impact position is likely to be randomly oriented after translation, others may feel that this factor should be taken into account in determining expected amounts of impact damage. In an effort to satisfy proponents of each point of view, both types of impact, essentially head foremost and random body impact orientation, will be considered.

Because of the many parameters involved in decelerative impact, a few assumptions will be made. First of all, translation damage will be assumed to occur during decelerative impact with a hard surface, the most damaging case (Ref. 4.69). Another assumption is that, since impact onto only hard surfaces is being considered, translation damage will depend only on impact velocity. This is, impacting only one type of surface precludes the need for considering change in velocity of the body during impact. This assumption, however, is not entirely valid when one considers that the compressibility of various portions of the body can vary considerably.

White (Refs. 4.61 and 4.62) and Clemedson, et al. (Ref. 4.69), agree that the tentative criteria for tertiary damage (decelerative impact) to the head should be those presented in Table 4.11. White's (Ref. 4.62) recently revised criteria for tertiary damage due to total body impact are summarized in Table 4.12. It is beneficial to note that the mostly "safe" velocity criteria for each type of impact condition are identical.

Baker, et al. (Ref. 4.59) have developed a method for predicting the blast incident overpressure and specific impulse combinations which will translate human bodies and propel them at the critical velocities presented in Tables 4.11 and 4.12. This method and associated prediction curves are reproduced here.

Figure 4.70 contains the pressure-scaled impulse combinations required to produce the velocities for various expected percentages of skull fracture (See Table 4.11) at sea level, while Figure 4.71 contains the pressure-scaled

4-169

Table 4.11 Criteria For Tertiary Damage
(Decelerative Impact) To The Head
(References 4.61, 4.62, and 4.69)

Skull Fracture Tolerance	Related Impact Velocity ft/sec
Mostly "safe"	10
Threshold	13
50 percent	18
Near 100 percent	23

Table 4.12 Criteria For Tertiary Damage
Involving Total Body Impact
(Reference 4.62)

Total Body Impact Tolerance	Related Impact Velocity ft/sec
Mostly "safe"	10
Lethality threshold	21
Lethality 50 percent	54
Lethality near 100 percent	138
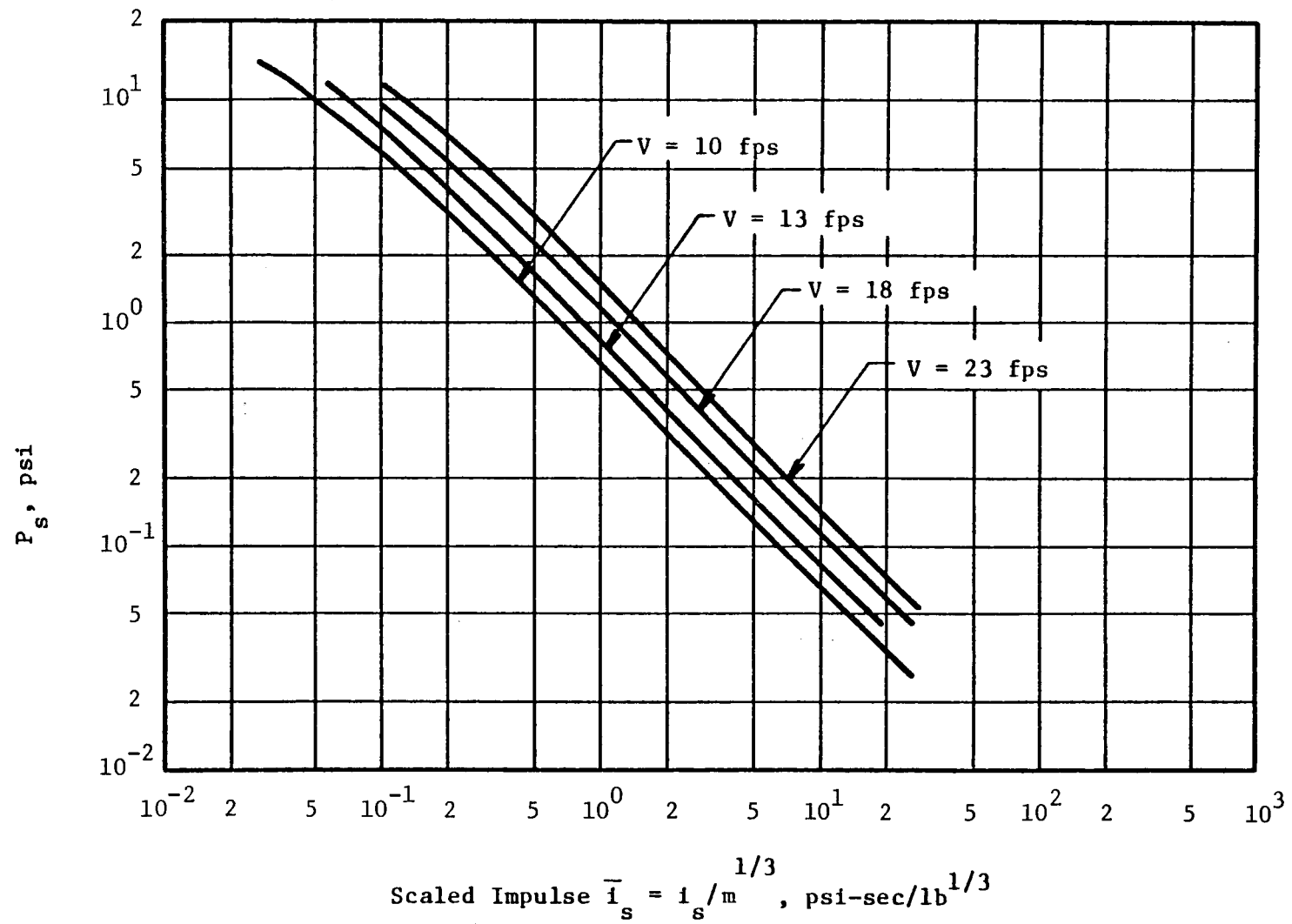
Figure 4.70   Skull Fracture
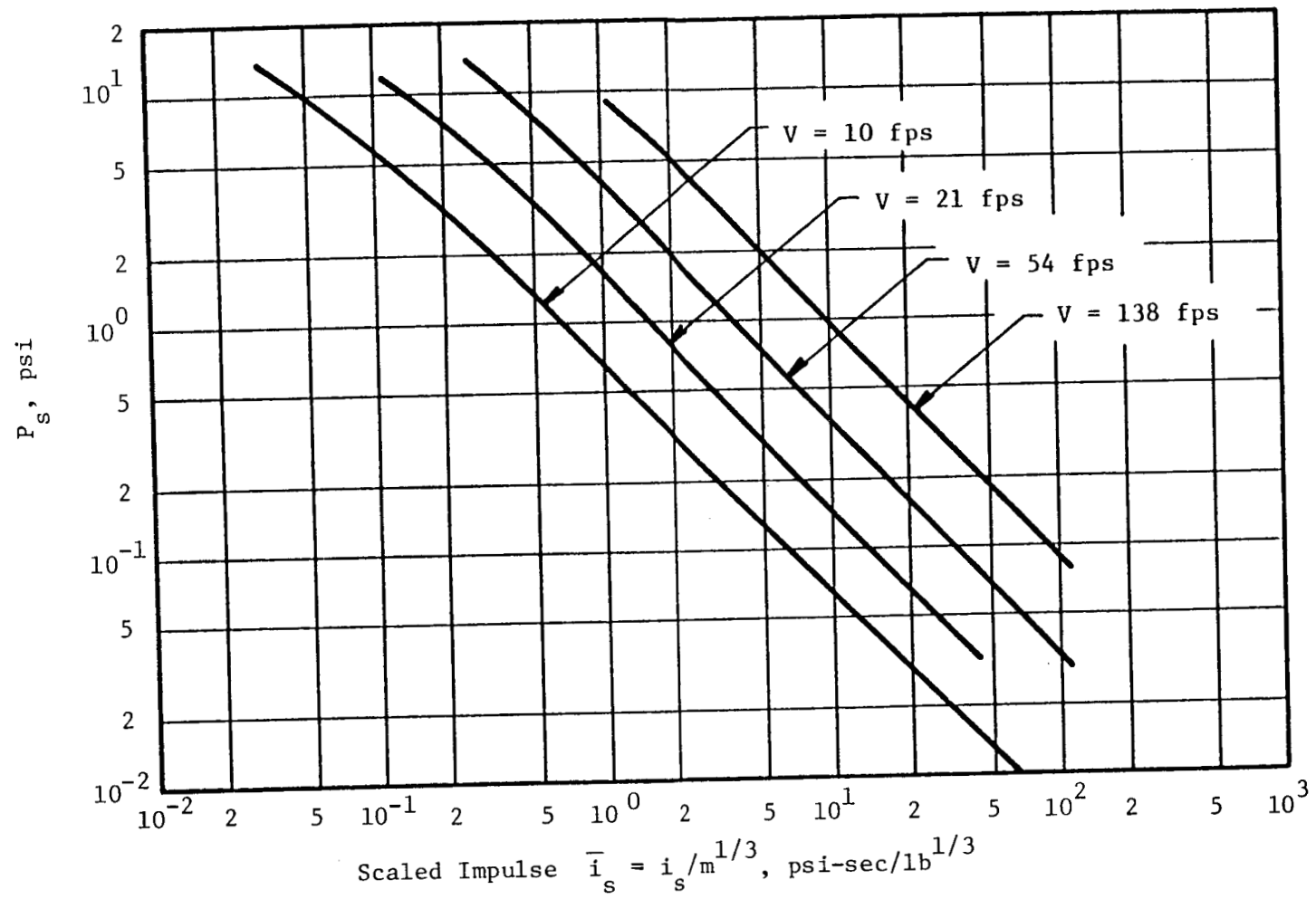
Figure 4.71 Lethality From Whole Body Translation

impulse combinations required to produce the velocities for various expected percentages of <u>lethality</u> from whole body impact (See Table 4.12) at sea level. Curves for other altitudes differ only slightly from the sea level curves.

EXAMPLE PROBLEM 4.15

PROBLEM - Predict possible tertiary blast damage to humans at a specified distance from a given explosive source.

GIVEN: W = explosive weight
        R = distance from center of explosive charge
        m = weight of body of human subject

FIND: Probability of injury   REFERENCE

SOLUTION:
1. Determine peak incident overpressure P_S and specific impulse i_S for given charge weight W and distance R   Fig. 4.5

2. Determine the lightest representative weight of an exposed human, and calculate $i_s/m^{1/3}$

3. Locate P_s and $i_s/m^{1/3}$ on graphs for skull fracture and lethality for whole body translation, and read impact velocities   Fig. 4.70 & Fig. 4.71

4. Determine degree of injury for appropriate impact velocities   Table 4.11

CALCULATION

GIVEN: W = 100 lb
        R = 100 ft
        m = 130 lb

FIND: Tertiary blast injury, based on skull fracture and whole body translation

SOLUTION:
1. $R/W^{1/3} = 100/100^{1/3} = 21.5 \text{ ft/lb}^{1/3}$
Enter Figure 4.9 and read $P_s = 1.8$ psi and
$i_s/W^{1/3} = 2.55 \times 10^{-3} \text{ psi-sec/lb}^{1/3}$

"Unscale" to determine i_s

$\dfrac{i_s}{W^{1/3}} \cdot W^{1/3} = 2.55 \times 10^{-3} \times 100^{1/3} = 1.18 \times 10^{-2} \text{ psi-sec}$

2. Given m = 130 lb. Calculate
$i_s/m^{1/3} = 1.18 \times 10^{-2}/130^{1/3} = 2.33 \times 10^{-3} \text{ psi-sec/lb}^{1/3}$

3. Enter Figure 4.70 with $P_s = 1.8$ and

$i_s/m^{1/3} = 2.33 \times 10^{-3}$. This is off the left side of the Figure, but well below the lowest curves for skull fracture. So, $V \ll 10$ fps. Enter Fig-4.71 with the same numbers. Again, $V \ll 10$ fps

4. Referring to Table 4.11 for correlation of velocities with injury, we find that for either the skull fracture or whole body impact criteria, the impact velocities are well below the mostly "safe" velocities. So, no injury would occur.

NOTE: Had the values for ordinate and abscissa in Figures 4.70 and 4.71 been $P_s = 1$ psi, $i_s/m^{1/3} =$

1 psi-sec/lb$^{1/3}$, the velocities for skull fracture velocity would have been $V = 15$ fps, and for whole body translation $V = 13$ fps. Skull fracture injury probability would lie between threshold and 50%, while lethality due to whole body translation would lie between mostly "safe" and the threshold for lethality. So, the human would have a relatively high probability of skull fracture, but a low probability of death. Whether this level of injury would or would not be acceptable could only be addressed in separate safety criteria.

4.6.3 Ear Damage Due To Air Blast Exposure

The ear, a sensitive organ system which converts sound waves into nerve impulses, responds to a band of frequencies ranging from 20 Hz to 20,000 Hz. This remarkable organ can respond to energy levels which cause the eardrum to deflect less than the diameter of a single hydrogen molecule (Ref. 4.70). Not being able to respond faithfully to pulses having periods less than 0.3 milli-second, it attempts to do so by making a single large excursion (Ref. 4.70). It is this motion which can cause injury to the ear.

The human ear is divided into the external, middle, and inner ear. The external ear amplifies the overpressure of the sound wave by approximately 20 percent and detects the location of the source of sound (Ref. 4.70). Rupture of the eardrum is a good measure of serious ear damage. Unfortunately, the state-of-the-art for predicting eardrum rupture is not as well developed as that for predicting lung damage from blast waves. A direct relationship, however, has been established between the percentage of ruptured eardrums and maximum overpressure. Hirsch (Ref. 4.67) constructed a graph similar to that shown in Figure 4.72 and concluded that 50 percent of exposed eardrums rupture at an overpressure of 15 psi. White (Ref. 4.61) supports this conclusion for "fast" rising overpressures with durations of 0.003 second to 0.4 second occurring at ambient atmospheric pressure of 14.7 psi. Hirsch (Ref. 4.67), also concluded that threshold eardrum rupture for "fast" rising overpressures occurs at 5 psi, which is also supported by White (Ref. 4.61) for the range of duration and at the atmospheric pressure mentioned above.

At lower overpressures than those required to rupture eardrums, a tem-porary loss of hearing can occur. Ross, et al. (Ref. 4.70), have produced a graph of peak overpressure versus duration for temporary threshold shift (TTS). Below the limits of the graphs, a majority (75 percent at least) of those ex-posed are not likely to suffer excessive hearing loss. According to Ross, et al. (Ref. 4.70), their curves should be lowered 10 dB to protect 90 per-cent of those exposed, lowered 5 dB to allow for a normal angle of incidence of the blast wave, and increased 10 dB to allow for occasional impulses. In sum, to assure protection to 90 percent of those exposed and to allow for nor-mal incidence to the ear (the worst exposure case) of an occasional air blast, their curves should be lowered 5 dB.

Limits for eardrum rupture and temporary threshold shift, as presented above, are dependent on peak incident overpressure and duration. Since speci-fic impulse is dependent upon the duration of the blast wave and since both peak incident overpressure and specific impulse at a specified distance from an explosion can be calculated using methods in this document, it is especially appropriate that pressure-impulse ear damage curves be developed from the pres-sure-duration curves. Assuming a triangular shape for the blast wave allows for simple calculations which are conservative from an injury standpoint.
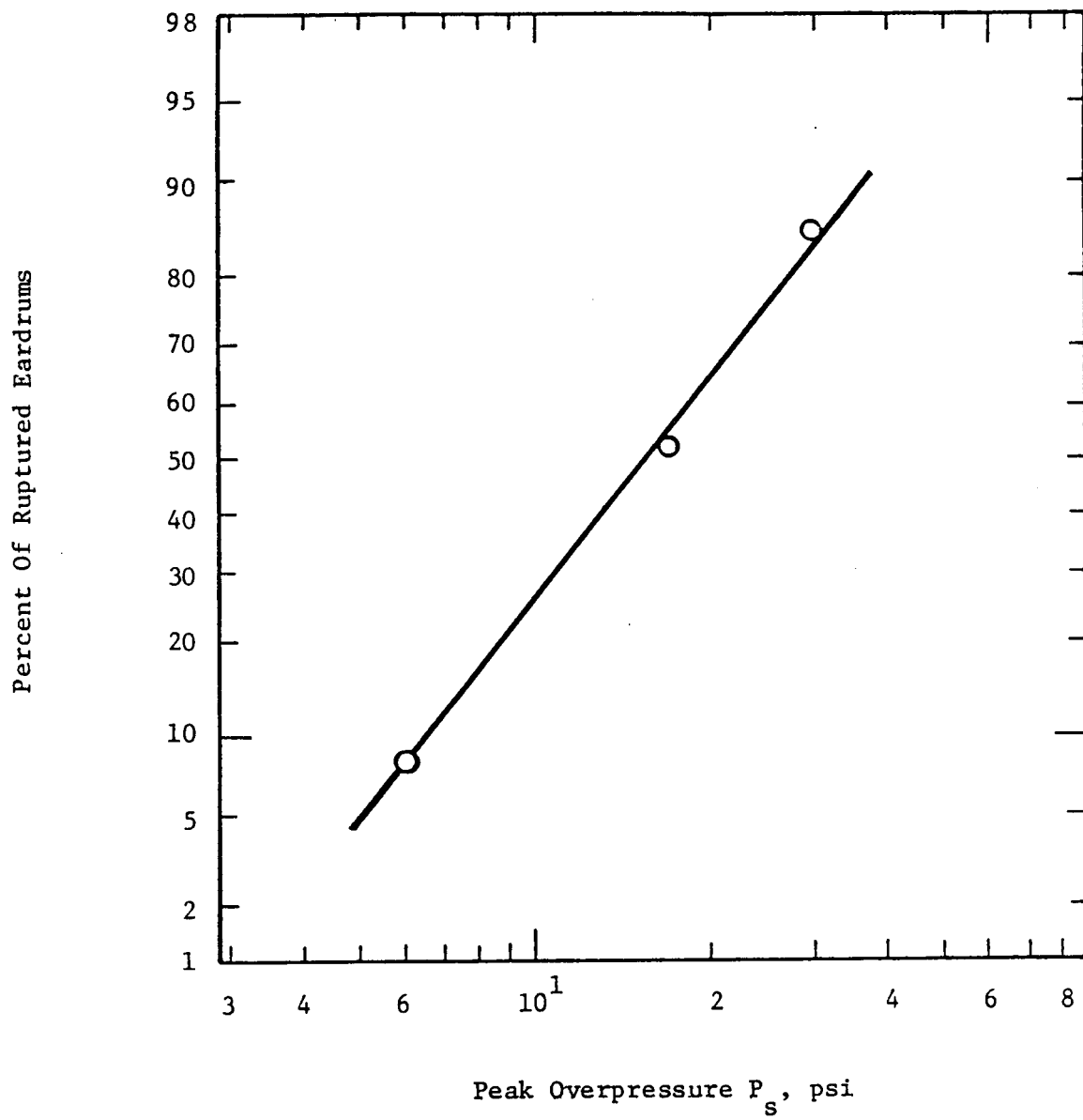
Figure 4.72   Percent Eardrum Rupture as a
Function of Overpressure

The ear damage criteria presented in Figure 4.73 were developed from the criteria for eardrum rupture developed by Hirsch (Ref. 4.68) and White (Ref. 4.61) and from the criteria for temporary threshold shift developed by Ross, et al. (Ref. 4.70). Equation (4.72) was used to calculate specific impulse, and temporary threshold shift represents the case where 90 precent of those exposed to a blast wave advancing at normal angle of incidence to the ear are not likely to suffer an excessive degree of hearing loss. The threshold for eardrum rupture curve is the location below which no ruptured ears are expected to occur and the 50 percent of eardrum rupture curve is the location at which 50 percent of ears exposed are expected to rupture.
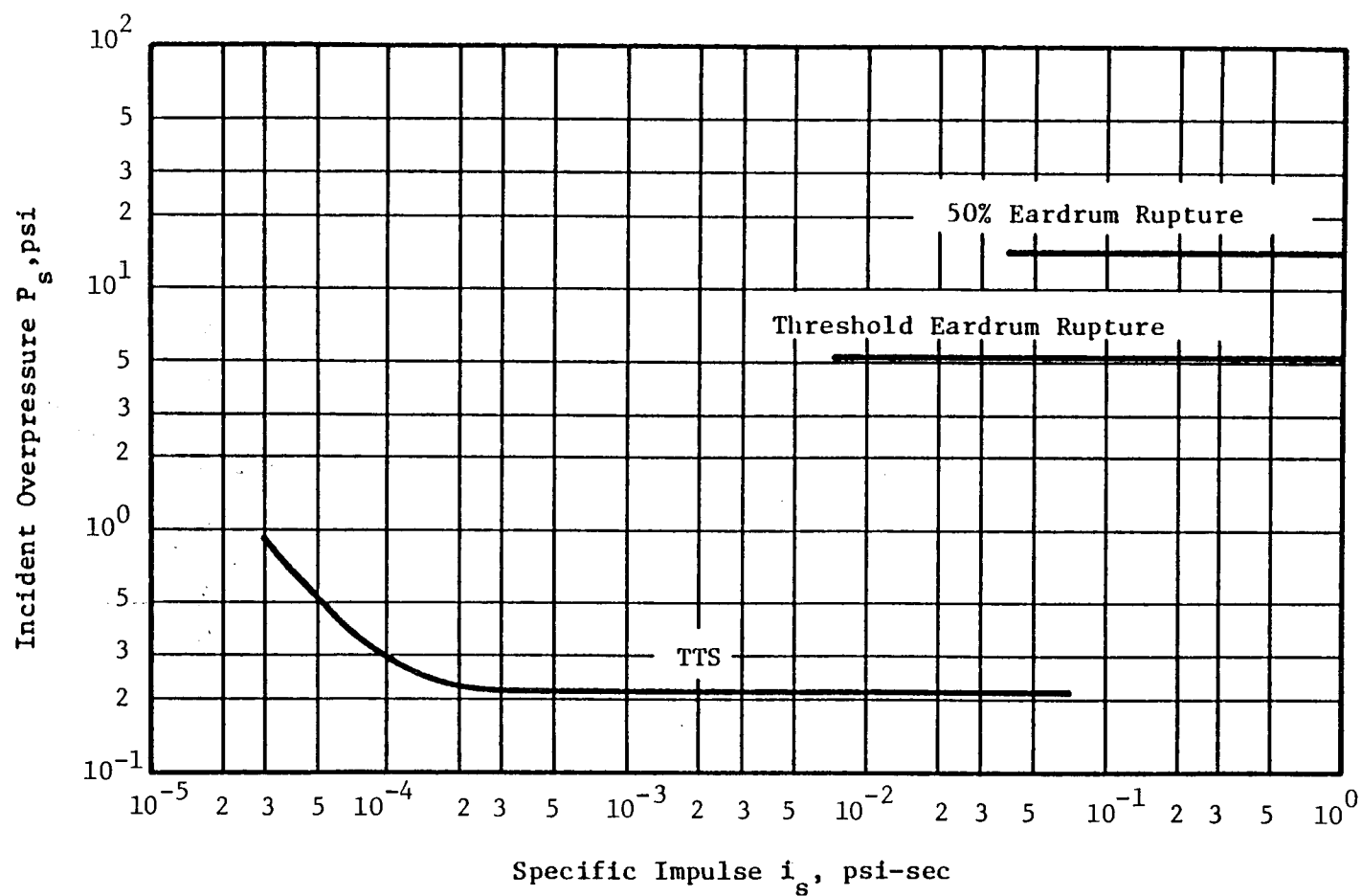
Figure 4.73   Human Ear Damage for Blast Waves Arriving at Normal
Angle of Incidence

EXAMPLE PROBLEM 4.16

PROBLEM – Find the probability of ear injury at a given distance from a speci-
fied explosive source.

GIVEN: W = explosive charge weight
        R = distance from center of explosive charge

FIND: Probability of ear injury   REFERENCE

SOLUTION: 1. Determine peak incident overpressure
               P_S and specific impulse i_S for given
               charge weight W and distance R   Fig. 4.5
           2. Determine degree of injury by plotting
               P_S and i_S on human ear damage curve   Fig. 4.73

CALCULATION

  GIVEN: W = 100 lb (free air)
          R = 100 ft

  FIND: Level of ear injury

  SOLUTION: 1. $R/W^{1/3} = 100/100^{1/3} = 21.5$ ft/lb$^{1/3}$
                 Enter Figure 4.5 and read $P_s = 1.8$ psi

                 and $i_s/W^{1/3} = 2.55 \times 10^{-3}$ psi-sec/lb$^{1/3}$

                 "Unscale" to obtain i_s

                 $\dfrac{i_s}{W^{1/3}} \cdot W^{1/3} = 2.55 \times 10^{-3} \times 100^{1/3} = 1.18 \times 10^{-2}$ psi-sec

             2. Plotting P_s and i_s on Figure 4.73, one
                 finds that the point lies well above the
                 curve for TTS, but below the curve for
                 threshold of eardrum rupture. So, humans
                 would suffer temporary hearing loss, but
                 no serious ear injury.
                 NOTE: When comparing ear injury, primary
                 blast damage, and tertiary blast damage
                 for the same source, as has been done in
                 Example Problems 4.14, 4.15, and 4.16, one
                 invariably finds that ear injury occurs at
                 a greater distance than the other, more
                 serious, types of blast injury. So, if

safety criteria include an ear damage limit, one can be assured that no more serious blast injury will occur at the distances corresponding to the ear damage limit.

4.7 RECOMMENDED TESTS OR ANALYSES

We have found a number of areas in air blast technology which are deficient when applied to definition of loading of structures typical of the Pantex Plant. A listing of the more important such areas follows:

- Definition of air shock loading of interiors of complex geometry cells, corridors, and cell-corridor combinations. A number of typical Pantex configurations should be tested, in small model scale.

- Definition of blast loads from non-spherical sources. In particular, both side-on and reflected specific impulses are poorly defined or completely undefined.

- Air blast from bulk (uncompressed) HE. No data at all exist for such sources.

- Mechanism of failure and venting of light, frangible vent covers. Past studies omitted vent covers altogether. Experimental data are badly needed, for comparison with theoretical curves given in this chapter.

- Determination of blast wave properties for those explosives for which these measurements have not been made. Currently, we assume TNT equivalence based on calculated comparative heats of detonation, rather than on comparison of air blast data.

- Systematic measurements of heats of detonation and combustion of explosives of interest at Pantex. These form the basis for determining TNT equivalence for shock loads and vented gas pressure loads.

- Measurement and code calculation of pressures and impulses for shock waves of intermediate strength from spherical sources located near flat surfaces. These should supplement data in Figures 4.11, 4.12, and 4.13.

- Tests of charges of other geometries than spherical in contact or nearly in contact with reflecting surfaces. Only one set of data exists for cylindrical charges in contact with the ground.

- Tests to determine thresholds of spalling for reinforced concrete walls. Methods in this manual are probably quite conservative, but spalling can cause significant hazards to personnel in bays adjacent to those in which an explosion occurs.

4.8 COMPREHENSIVE ILLUSTRATIVE EXAMPLES

EXAMPLE PROBLEM 4.17

PROBLEM - Determine all side-on and normally reflected blast parameters for a bare spherical HE explosion. This problem illustrates use of the graphs in Figures 4.5 through 4.7 and altitude correction factors.

GIVEN: R = distance from center of explosive source (standoff [ft])
W = weight and type of HE (lb)
H = altitude where explosion occurs (ft)

FIND: All possible blast parameters

REFERENCE

SOLUTION: 1. Equivalent TNT explosive weight
W = (weight of explosive)(TNT Factor)

See Table 6 in Appendix A for TNT Equivalencies

2. Calculate Hopkinson-scaled distance
$$Z = R/W^{1/3}$$

Eq. (4.19)

3. Calculate corrected Z* for altitude H
$$Z* = Z \ (p/p_o)^{1/3}$$

Eq. (4.20)

where p is the ambient pressure at H
$$p = 14.6965 \left[\frac{288.15}{288.15 - 1.9812 \times 10^{-3} H} \right]^{-5.25588} \ psi$$

4. Determine the required blast parameters corresponding to the Z* value

Fig. 4.5 - Fig. 4.7

5. Calculate sound speed at altitude H
$$a = 65.77 \ [\ 288.15 - 1.9812 \times 10^{-3} H]^{1/2} \ ft/sec$$

Eq. (4.18)

6. Correct blast parameters for altitude H

Table 4.3

CALCULATION

GIVEN: R = 20 ft
Charge weight is 58.6 lb of Composition B
H = 3500 ft

FIND: All possible blast parameters

SOLUTION: 1. W = (58.6)(1.092) = 64 lb
2. $Z = R/W^{1/3} = 20/64^{1/3} = 20/4 = 5 \ ft/lb^{1/3}$

3. a). $p = 14.6955 \left[\dfrac{288.15}{288.15 - 1.9812 \text{ X } 10^{-3} \text{ X } 3500} \right]^{-5.25588}$ psi

   $p = 12.93$ psi (rounded to four significant figures)

   b). $Z^* = 5 \left(\dfrac{12.93}{14.70} \right)^{1/3} = 4.791$ ft/lb$^{1/3}$

4. a). Enter Figure 4.5 for $Z^* = R/W^{1/3} = 4.79$ and read:

   $P^*_s = 26.0$ psi

   $i^*_s/W^{1/3} = 1.05 \text{ X } 10^{-2}$ psi-sec/lb$^{1/3}$

   $t^*_d/W^{1/3} = 1.35 \text{ X } 10^{-3}$ sec/lb$^{1/3}$

   $t_a/W^{1/3} = 1.40 \text{ X } 10^{-3}$ sec/lb$^{1/3}$

   For times and impulses, multiply scaled values by $W^{1/3}$

   $i_s = 1.05 \text{ X } 10^{-2} \text{ X } 4 = 4.2 \text{ X } 10^{-2}$ psi-sec

   $t_d = 1.35 \text{ X } 10^{-3} \text{ X } 4 = 5.4 \text{ X } 10^{-3}$ sec

   $t_a = 1.40 \text{ X } 10^{-3} \text{ X } 4 = 5.6 \text{ X } 10^{-3}$ sec

   b). Enter Figure 4.6 for $Z^* = 4.79$ and read:

   $P^*_r = 112$ psi

   $i^*_r/W^{1/3} = 3.30 \text{ X } 10^{-2}$ psi-sec/lb$^{1/3}$

   For impulse, multiply scaled impulse by $W^{1/3}$

   $i^*_r = 3.30 \text{ X } 10^{-2} \text{ X } 4 = 1.32 \text{ X } 10^{-1}$ psi-sec.

   c). Enter Figure 4.7 for $Z^* = 4.79$ and read:

   $Q^* = 13.0$ psi
   $\overline{U}^* = 1.57$ (Mach No.)

   $\overline{U}^*_s = 7.6 \text{ X } 10^{-1}$ (Mach No.)

   $b^* = 1.85$

5. $a = 65.77 \, [288.15 - 1.9812 \text{ X } 10^{-3} \text{ X } 3500]^{1/2}$ ft/sec
   $a = 1102.9$ ft/sec

6. Enter Table 4.3 and determine values of correction factors. The correction factors will be:

   Pressures

   $p/p_o = 12.93/14.70 = 0.880$

   Impulse

   $(a_o/a) \, (p/p_o)^{2/3} = (1116.4/1102.9) \, (12.93/14.70)^{2/3} = 0.93$

Times

$(a_o/a) (p_o/p)^{1/3}$ = (1116.4/1102.9) (14.70/1293)$^{1/3}$ = 1.06

The values of the blast parameters will be:

P_s = P_s^* X 0.88 = 26.0 X 0.88

P_s = <u>22.9 psi</u>

i_s = i_s^* X 0.93 = 1.05 X 10^{-2} X 0.93

i_s = <u>3.91 X 10^{-1} psi-sec</u>

t_d = t_d^* X 1.06 = 5.4 X 10^{-3} X 1.06 sec

t_d = <u>5.7 X 10^{-3} sec</u>

t_a = t_a^* X 1.06 = 5.6 X 10^{-3} X 1.06 sec

t_a = <u>5.9 X 10^{-3} sec</u>

P_r = P_r^* X 0.88 = 112 X 0.88 psi

P_r = <u>98.6 psi</u>

i_r = i_r^* X 0.93 = 1.32 X 10^{-1} X 0.93 psi-sec

i_r = <u>1.23 X 10^{-1} psi-sec</u>

Q = Q* X 0.88 = 13.0 X 0.88 psi

Q = <u>11.4 psi</u>

U = <u>1.57</u>

$\bar{u}_s$ = <u>7.6 X 10^{-1}</u>

b = <u>1.85</u>

This is simply a demonstration problem for use of scaled curves for blast wave parameters. Very seldom will an AE need to determine <u>all</u> of the parameters from all three of the sets of prediction curves in Figures 4.5 through 4.7. The most commonly needed ones are P_s, i_s, t_d, P_r, and i_r.

EXAMPLE PROBLEM 4.18
_____

    The procedures for predicting initial and reflected blast pressures and
impulses and quasi-static pressures on the walls of a conventional rectangular
parallelepiped room or bay, for an internal HE explosion, are different in
this manual and in TM 5-1300 (Ref. 4.2). This example problem provides a
comparison of the methods and predicted loads using the two different sources.
When there are substantial differences in the results, recommendations are
given for choice of the preferred method.

PROBLEM – Determine the blast loading parameters on walls and roof of a rec-
_____   tangular parellopiped structure with an internal explosion of a
            specified explosive source at a specified location within the struc-
            ture. One entire wall is a blowout wall intended to vent the
            explosion. Room dimensions and explosive charge location are shown
            in Figure 4.74.

    GIVEN: W = explosive charge weight
    _____   Room interior dimensions
            Charge location
            w = areal density of blowout wall

    FIND: Blast loads on walls and roof.   REFERENCE
    ____   _____

    SOLUTION: 1. Determine reflected blast wave pressures
    _____   and impulses applied to rear wall, side
                   walls and roof for charge weight W in geo-
                   metry in Figure 4.74.
                   a). Using methods in this manual   Fig. 4.12 &
                                                              Fig. 4.13
                   b). Using methods in TM 5-1300   Sections 4-9 &
                                                              4-10 in Ref.
                                                              4.2

               2. Determine quasi-static pressure loads
                   for given charge weight W, room vol-
                   ume V, and blowout wall with area A
                   and areal density w
                   a). Using methods in this manual   Figs. 4.43,
                                                              4.44 & 4.45
                   b). Using methods in TM 5-1300   Fig. 4-65 in
                                                              Ref. 4.2

CALCULATION
_____

    GIVEN: W = 150 lb
    _____   Room and charge location in Figure 4.74.

            w = 120 lb/ft^2 for blowout wall
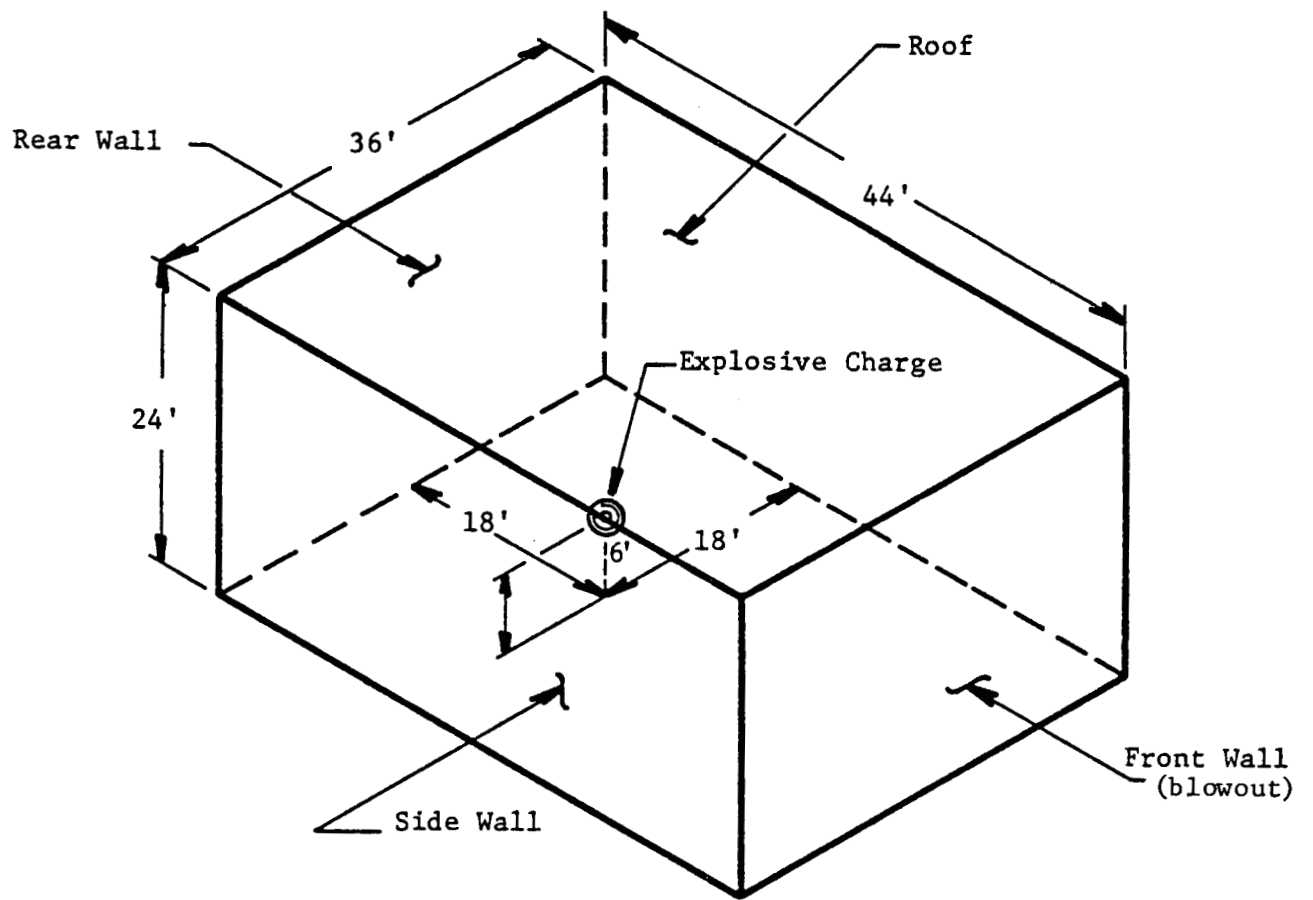
Figure 4.74   Sketch Of Room Loaded By Internal Blast

FIND: Blast loads on walls and roof.

SOLUTION: 1.   a).   Reflected parameters for walls and
                      roof using methods in this manual.
                      Determine effective charge weight
                      relative to each wall and roof
                      $W' = W \times 2.0$
                      $W' = 150 \times 2.0 = 300$ lb TNT for
                      all surfaces
                      Due to proximity of charge to
                      floor, charge weight is doubled.
                      It is important to note that the
                      charge weight is not always
                      doubled, but only occurred in
                      this problem due to charge loca-
                      tion.*   Eq. (4.15)
                      Determine normal (minimum) charge
                      standoff for all surfaces (R).
                      For rear and side walls and roof,
                      minimum charge standoff is 18 ft.
                      For "blowout" panel, the minimum
                      charge standoff is 26 ft.   Fig. 4.74
                      Determine scaled minimum charge
                      standoff

                      $Z' = R/W'^{1/3}$ Eq. (4.9)
                      For 18 ft,
                      $Z' = 2.7$ ft/lb$^{1/3}$
                      For 25 ft,
                      $Z' = 3.88$ ft/lb$^{1/3}$

                      If 0.3 ft/lb$^{1/3}$ $\leq Z' \leq$ 3.0 ft/lb$^{1/3}$
                      use Figure 4.13 to determine
                      specific reflected impulse along
                      the wall, and Figure 4.12 to de-
                      termine peak reflected pressure
                      along wall. Thus Figures 4.13
                      and 4.12 were used for all sur-
                      faces except the "blowout panel,"
                      where

                      $Z' = 3.88$ ft/lb$^{1/3}$
                      Inspection of Figures 4.12 and
                      4.13 indicates that for

---

*The charge is much closer to the floor than other reflecting surfaces,
with the nearest other surface being three times as far away. Mach waves
form very quickly, so most of the walls and the roof "feel" impact of the
coalesced Mach waves. We assume conservatively that the Mach waves load
all of these surfaces.

$Z' = 2.7$ ft/lb$^{1/3}$, interpolation is required. A table and graph were generated for the case of $R = 18$ ft and $W' = 300$ lb. This allowed specific reflected impulse and scaled position to be "descaled."
Because of internal reflections of shocks inside the cubicle, a "reflecting" factor of 1.75 is applied to reflected impulse, and is termed "applied impulse." Peak reflected pressure, reflected impulse, and "applied impulse" are tabulated for various values of wall position X. These quantities are also plotted as a function of wall position X, Figures 4.75 through 4.78.
To obtain an "average" value of specific impulse, various methods can be used; the sophistication depending upon the degree of accuracy required. It was observed that a straight line represented reflected impulse as a function of wall position quite well. An equation representing the line of best "eyeball" fit through the data was determined (See Figure 4.75). It was of the form:
$i(X) = mX + b$
where
$i(X)$ = applied specific impulse
m = slope of line
b = Y intercept
The average specific impulse is then: (See Figure 4.79)

$$i_{av} = \frac{\int\!\!\int^{Area} i(X)\ dA}{A} \tag{4.76}$$

or expressed in polar coordinates
$(X,\ \Theta)$*

_____

*This coordinate system convention is illustrated in Figure 4.14 as $(X,\ \alpha)$.
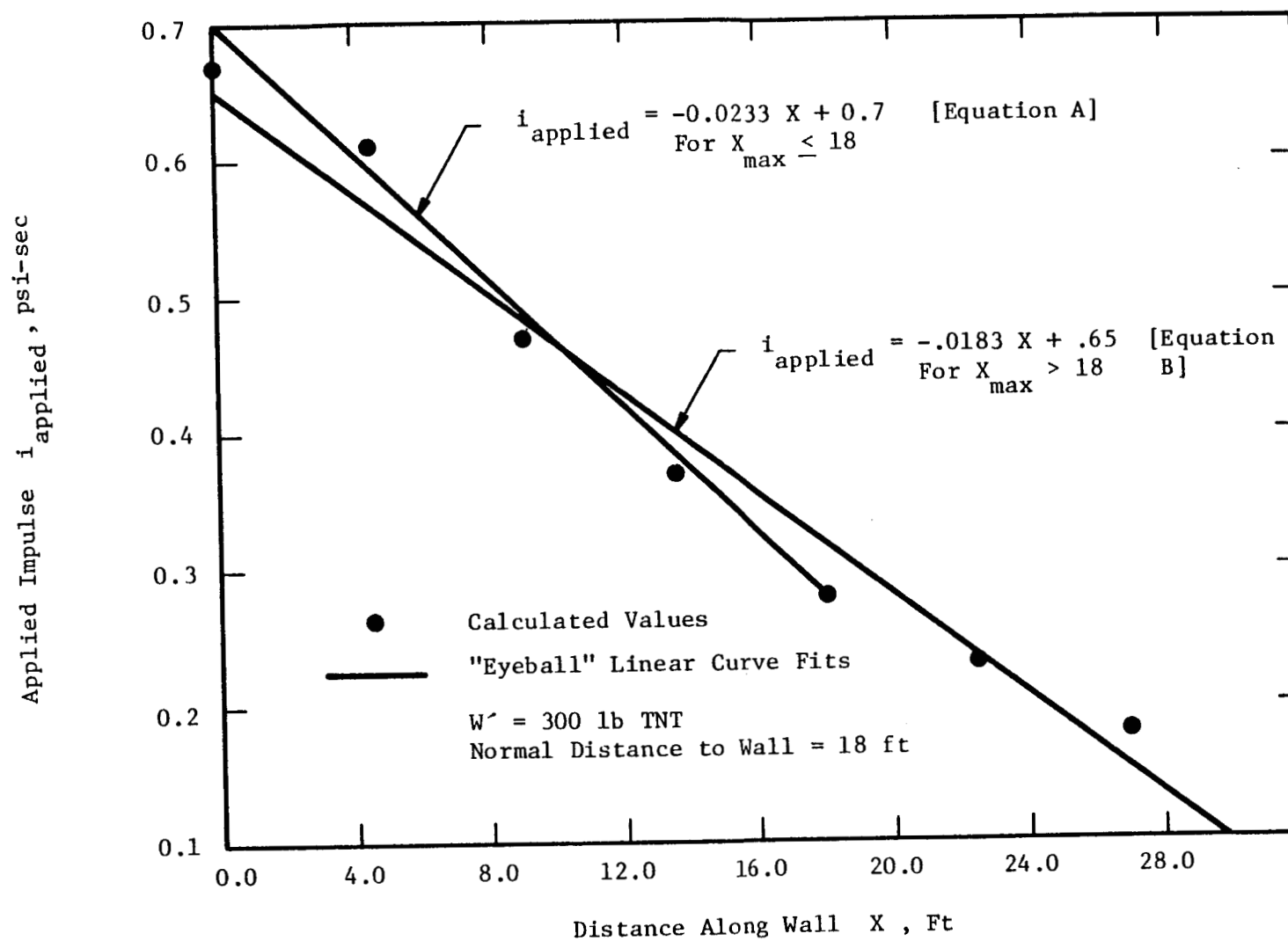
Figure 4.75 Applied Reflected Specific Impulse Along Wall
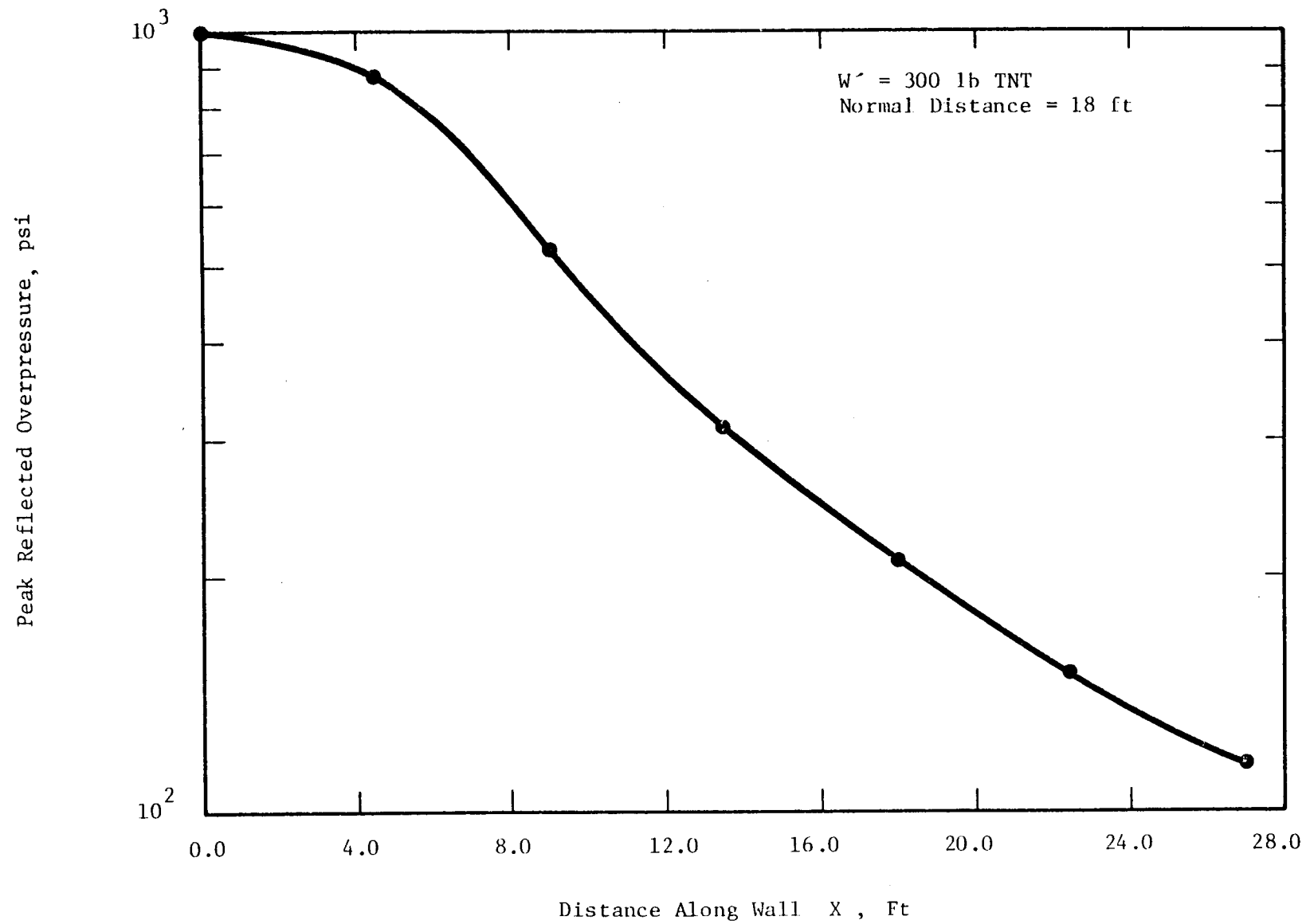
Figure 4.76   Peak Reflected Pressure Along Wall

The graph shows "Applied Specific Reflected Impulse, psi-sec" on the vertical axis (values .1, .2, .3, .4, .5) and "Distance Along Wall X, Ft" on the horizontal axis (values 0, 4, 8, 12, 16, 20, 24, 28).

$$i = .485 - .00604 \, X \quad \text{[Equation C]}$$

W´ = 300 lb TNT
Normal Distance To Wall = 26 ft
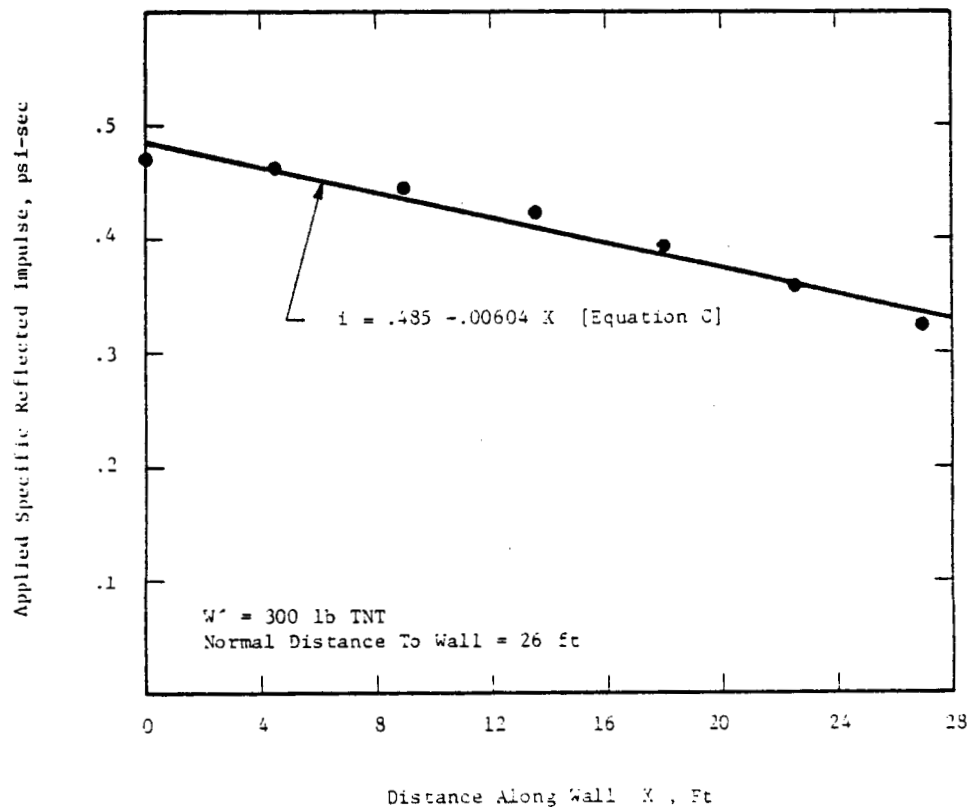
Figure 4.77   Applied Reflected Specific Impulse Along Wall

W´ = 300 lb TNT
Normal Distance = 26 ft
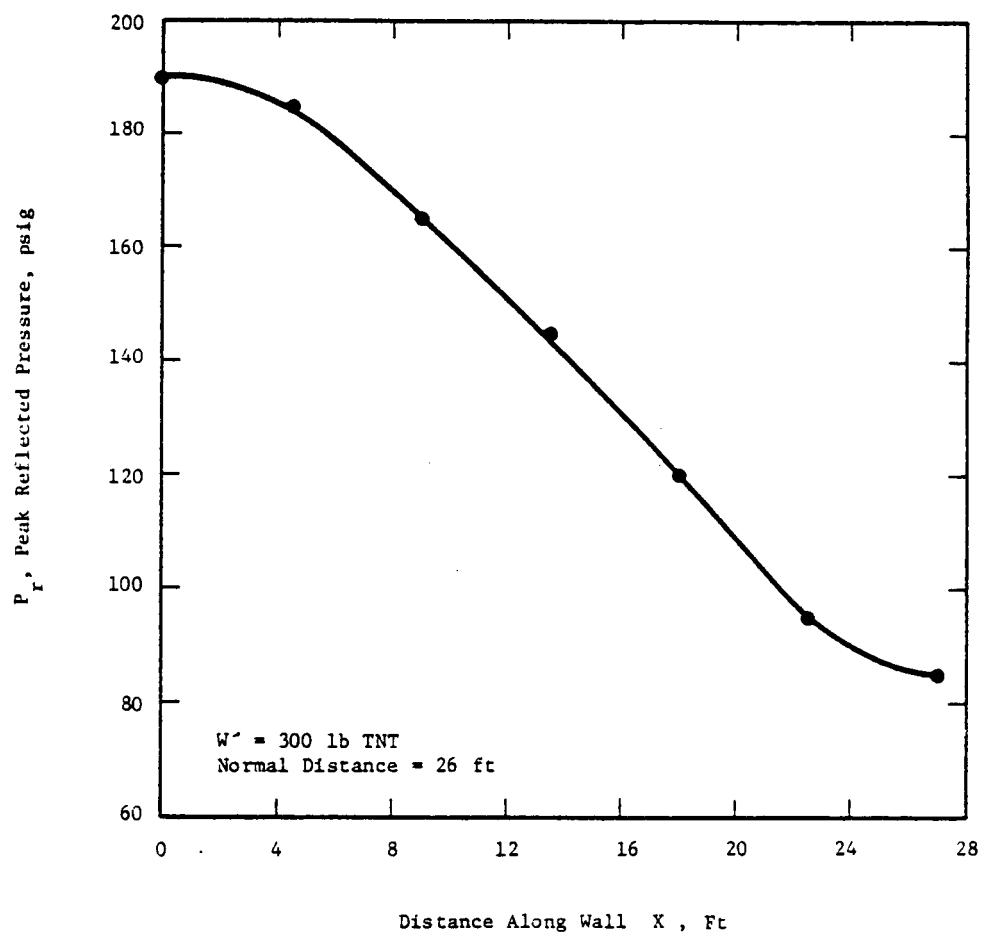
Figure 4.78   Peak Reflected Pressure Along Wall

$$i_{av} = \left(\frac{2}{2YU}\right) \left[\int_{0}^{arc\ tan\ (Y/U)} \int_{0}^{U/cos\Theta} (mX + b)\ XdXd\Theta \right.$$

$$\left. \int_{arc\ tan\ (Y/U)}^{\pi/2} \int_{0}^{Y/sin\Theta} (mX + b)\ XdXd\Theta \right] \qquad (4.77)$$

where
Y and U are defined in Figure 4.79.
The integration of the above expression gives the following equation for the average impulse over a wall or roof surface

$$i_{av} = \left(\frac{1}{2YU}\right) \left[\frac{mU^3}{3} \frac{sin\ \Phi}{cos^2\ \Phi} + \frac{mU^3}{3} log\ tan\ (\pi/4 + \Phi/2) \right.$$

$$\left. - \frac{mY^3}{3} \frac{cos\ \Phi}{sin^2\ \Phi} - \frac{mY^3}{3} (log\ tan\ \Phi/2) + 2bYU \right] \qquad (4.78)$$

where
$$\Phi = arc\ tan\ (Y/U) \qquad (4.79)$$
The average values of reflected specific impulse thus calculated are listed at the bottom of each data table.

If $Z' > 3.0$ ft/lb$^{1/3}$, use slant range and Figure 4.11 to calculate reflected impulse and pressure along the wall or roof (ignore angle of obliquity). This procedure was used to calculate the blast load on the "blowout panel." The slant range is defined in the same manner as in TM 5-1300, i.e.,

$$R' = \sqrt{R^2 + X^2} \qquad (4.80)$$

The scaled slant range for use in Figure 4.11 is
$$Z^* = R'/W^{1/3} \text{ ft/lb}^{1/3}$$
These calculations are tabulated in Tables 4.13 and 4.14 and are also graphed as applied reflected impulse and peak reflected pressure versus wall distance X. Again, a straight line was fitted through the plot of
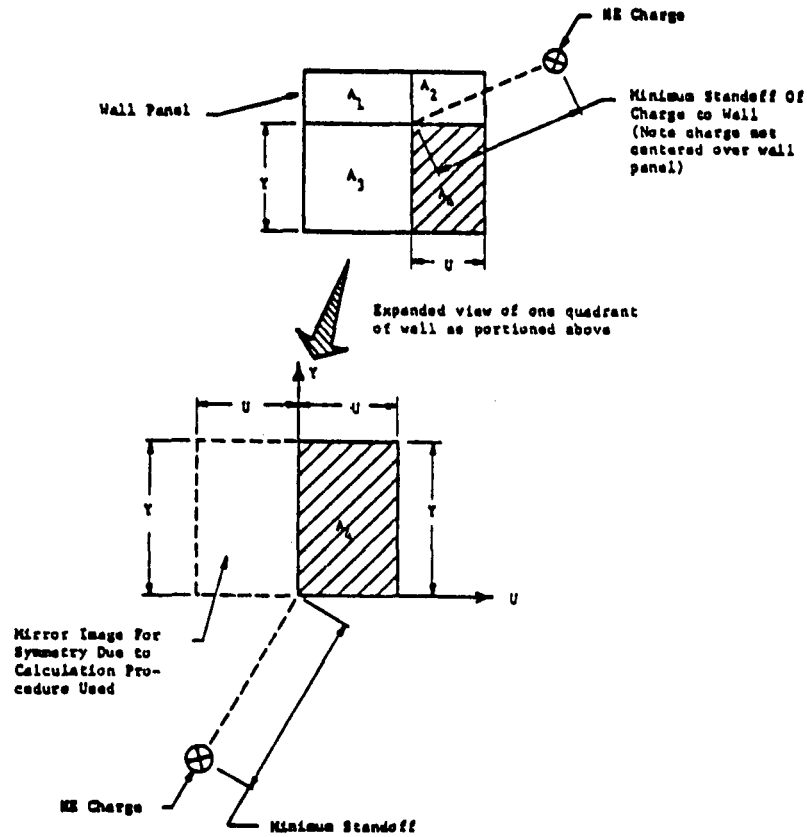
The geometry of Equations (4.76) through (4.79) is illustrated in Figure 4.79.
Fortunately, for the Example Problem, there was some geometric symmetry because
of charge location. The rear and front walls required only one calculation of
average specific impulse, and the roof and sides required two calculations.
For the general case, however, four calculations may be required, one for each
quadrant. The overall average impulse on the wall is then

$$i_{av} = \frac{i_{1av} A_1 + i_{2av} A_2 + i_{3av} A_3 + i_{4av} A_4}{A_1 + A_2 + A_3 + A_4}$$

Figure 4.79   Geometry of Procedure to Calculate Average
Specific Reflected Impulse

Table 4.13 Blast Loads As A Function Of Wall Position X,
For Minimum Standoff = 18 ft, W = 300 lb

X/R	$\dfrac{\bar{i}}{\text{psi-sec}}{\text{lb}^{1/3}}$	X ft	P_r psi	i psi-sec	$i_{applied}$ = 1.75i* psi-sec
0	0.57	0.0	1000.	0.38	0.67
0.25	0.52	4.5	880.	0.35	0.61
0.5	0.41	9.0	530.	0.27	0.47
0.75	0.31	13.5	310.	0.21	0.37
1.0	0.24	18.0	210.	0.16	0.28
1.25	0.19	22.5	150.	0.13	0.23
1.5	0.155	27.0	115.	0.10	0.18

*Average Impulse Over Different Wall Elements

Rear Wall

i_{av} = 0.556 psi-sec [Equation A used. See Figure 4.75]

Side Walls

i_{av} = 0.548 psi-sec [Equation B used. See Figure 4.75]

Roof

i_{av} = 0.540 psi-sec [Equation B used. See Figure 4.75]

Table 4.14 "Blowout Panel" Blast Loads

X ft	Slant Range $\sqrt{R^2 + X^2}$ ft	$Z* = \dfrac{\sqrt{R^2 + X^2}}{W^{1/3}}$ ft/lb$^{1/3}$	i_r psi-sec	P_r psi	i_r applied* psi-sec
0.	26.0	3.88	0.268	190	0.469
4.5	26.4	3.94	0.265	185	0.462
9.	27.5	4.11	0.254	165	0.444
13.5	29.3	4.38	0.241	145	0.422
18.	31.6	4.72	0.224	120	0.392
22.5	34.4	5.14	0.204	95	0.357
27.	37.5	5.60	0.184	85	0.322

*Average Impulse Over Blowout Panel

i_{av} = 0.448 psi-sec [Equation C used. See Figure 4.77]

i versus X, and an average specific
impulse was thus obtained (See Fig-
ures 4.77 and 4.78).
No attempts were made to compute an
average peak reflected pressure over
the wall surface. This was because
the fictitious number developed would
have little meaning in contrast to
average specific impulse. However,
if an "average" peak reflected over-
pressure value is required, it is
suggested that one use the proced-
ure illustrated in TM 5-1300 (also
See 1.b. of this Example Problem).

b). It is assumed that the reader has
access to and has read the TM 5-1300
manual. The details of the proced-
ures used in TM 5-1300 will not be re-
peated in this manual. From the
data given, the following parameters
are determined.*

$N = 4$
$W = 150$ lb
$H = 44$ ft
$L = 36$ ft
$h = 18$ ft
$\ell = 18$ ft
$R_A = 18$ ft
$h/H = 0.409$
$\ell/L = 0.5$
$L/R_A = 2.0$
$L/H = .818$
$W* = W \times 1.20 = 180$ lb
$Z_A = 3.2$ ft/lb$^{1/3}$

It can be seen that to determine $\bar{i}_b$,
the average scaled specific impulse,
interpolation is required in h/H and
L/H, and extrapolation in Z_A using
Figures 4.59 and 4.62 of the TM 5-1300
manual*. The average reflected im-
pulse values thus obtained are:
Rear wall $\bar{i}_b = 0.79$ psi-sec

---

*The nomenclature used here is that of TM 5-1300. Some terms have different
meanings from similar symbols in this manual.

Side walls $\bar{i}_b$ = 0.63 psi-sec

Roof $\bar{i}_b$ = 0.74 psi-sec

The "average" peak reflected pressure on the walls was also calculated (See page 4-12 of TM 5-1300 Manual). The values obtained were:

Rear wall: P_r = <u>145 psig</u>

Side walls: P_r = <u>57 psig</u>

Roof: P_r = <u>67 psig</u>

Observe that TM 5-1300 does not yield the effects of a blast load for a frangible wall.

2. a). Calculate quasi-static pressure load. This problem has already been worked in Example Problem 4.11. The values obtained will be restated below.

P_{QS} = <u>40 psig</u>

i_g = <u>1.192 psi-sec</u>

T_d = <u>0.079 sec</u>

   b). The quasi-static pressure inside the room is calculated in TM 5-1300 to be <u>51 psig</u> (See page 4-60 of TM 5-1300 Manual). No blowdown time T_d (time for pressure to return to ambient) or gas impulse i_g can be obtained from TM 5-1300. The procedure developed above (1.a. and 2.a.) assumes that the only tools available to the user are paper, pencil, and a simple, non-programmable calculator. To a large extent, one must work the above problem in "reverse." First, one must decide what type of structural analysis procedure will be used. Then, depending upon the degree of sophistication of the structural analysis procedure, a "forcing" function or "blast" load of corresponding sophistication is developed. The methods developed in Sections 1.a. and 2.a. allow one to tailor the "blast load" or "forcing function" to his own needs. In contrast, the methods of

TM 5-1300 allow less flexibility and
supply less information, particularly
about quasi-static pressure loads.
Unfortunately, both methods are lim-
ited by lack of data in some regions.
The results obtained by TM 5-1300
were more conservative for this par-
ticular example, although the answers
in general were numerically quite
close.

4.9 LIST OF SYMBOLS

A	loaded area
A_{plate}	surface area of an impulsively loaded plate
A_s	internal surface area of a chamber
A_v	vent area
a	sound velocity
a_o	ambient fluid sound velocity
b	decay constant for air blast wave
c	an exponential decay constant for gas pressure
D	diameter of a cylindrical explosive charge
E	total explosive source energy
E_f	energy flux density in air blast wave
H	wall thickness
i	specific impulse
i_d	dynamic pressure specific impulse
i_g	gas phase positive specific impulse
i_r	positive phase specific impulse in reflected air blast wave
i_s, i_s^+	positive phase specific impulse in side-on blast wave
i_s^-	negative phase specific impulse in side-on blast wave
k	spring constant for simple mechanical system
L	length of a cylindrical explosive charge
M	mass of simple mechanical system

M_A	mass of air engulfed behind a shock front
M_E	mass of explosive
M_T	total mass of explosive and air engulfed behind a strong shock front
m	weight of human subjected to air blast
$\bar{P}, \bar{i}, \bar{R}, \bar{S}$, etc.	barred quantities are nondimensional forms of various physical quantities
P_1	maximum absolute gas pressure
P_{QS}	maximum gage gas pressure
P_r	peak reflected overpressure
P_s, P_s^{+}	side-on peak air blast overpressure
P_s^{-}	side-on peak air blast volume
p	absolute pressure
P_o	ambient atmospheric pressure
P_s	peak absolute pressure in shock wave
Q	peak dynamic pressure in air blast wave
q	dynamic pressure in air blast wave
R	distance from center of explosive source
r	radius of a spherical explosive charge
Ratio	ratio of equivalent spherical charge mass to cylindrical charge mass
S	spacing of double or multiple charges
T_d	duration of gas venting overpressure

T_r	duration of equivalent triangular pulse, reflected blast
T_s	duration of equivalent triangular pulse, side-on blast
t	time
t_a	shock wave arrival time
t_d, t_d^+	duration of positive phase of air blast wave
t_d^-	duration of negative phase of air blast wave
t_{delay}	time delay between sequentially detonated explosives
t_1	end of internal blast loading phase
t_m	time for maximum structural response
t_{max}, t_b	venting time
t_o	blast duration for internal blasts from TM5-1300
U	shock front velocity of air blast wave
U_r	velocity of reflected wave front
u	particle velocity in air blast wave
u_s	peak particle velocity in air blast wave
V	volume of chamber
V_f	average fragment velocity
v	stress wave velocity for spalling
W	total explosive weight
W'	effective charge weight
W_c	weight of charge casing

X	characteristic dimension of uniformly vented chamber; horizontal distance off normal for reflected blast waves
x, y	parameters in cylindrical charge data fits
Z	dimensional scaled distance
Z'	scaled distance modified for casing effect
$Z*$	scaled distance corrected for altitude
α_e	effective vent area ratio
α_I	angle of incidence for oblique shock reflection
α_R	angle of reflection for oblique shock reflection
γ	ratio of specific heats for a gas
ΔH	specific heat of detonation of an explosive
Θ_o	ambient air temperature
Θ_r	peak temperature behind reflected shock wave
Θ_s	peak temperature behind incident shock wave
λ	a general scaling factor; scaling factor for geometry; parameter in cylindrical charge data fit
ξ	inverse of shock strength
ρ	density in air blast wave
ρ_o	ambient fluid density
ρ_r	peak density behind reflected shock wave
ρ_s	peak density in shock front
σ	wave-induced stress

σ_u ultimate tensile strength

τ scaled venting time

ω circular frequency for simple mechanical system

4.10 REFERENCES

4.1 Baker, W. E., _Explosions in Air_, University of Texas Press, Austin, Texas, 1973.

4.2 _Structures to Resist the Effects of Accidental Explosions_, Department of the Army Technical Manual TM 5-1300, Department of the Navy Publication NAVFAC P-397, Department of the Air Force Manual AFM 88-22, Department of the Army, the Navy, and the Air Force, June 1969.

4.3 "Suppressive Shields Structural Design and Analysis Handbook," U. S. Army Corps of Engineers, Huntsville Division, HNDM-1110-1-2, November 1977.

4.4 Swisdak, M. M., Jr., "Explosion Effects and Properties: Part I - Explosion Effects in Air," NSWC/WOL/TR 75-116, Naval Surface Weapons Center, White Oak, Silver Spring, MD, October 1975.

4.5 Goodman, H. J., "Compiled Free Air Blast Data on Bare Spherical Pentolite," BRL Report 1092, Aberdeen Proving Ground, MD, 1960.

4.6 Strehlow, R. A. and Baker, W. E., "The Characterization and Evaluation of Accidental Explosions," _Progress in Energy and Combustion Science_, 2, 1, pp. 27-60, 1976.

4.7 Glasstone, Samuel and Dolan, Philip J., "The Effects of Nuclear Weapons," United States Department of Defense and U. S. Department of Energy, 1977.

4.8 U. S. Energy Research and Development Administration Albuquerque Operations Office, "Report of Investigation of the Explosion with Fatal Injuries in Bldg. 11-14A on March 30, 1977, at the Pantex Plant-Amarillo, Texas," June 1977.

4.9 U. S. Army Material Command, "Engineering Design Handbook, Explosive Series Properties of Explosives of Military Interest," AMCP 706-177, Headquarters, U. S. Army Material Command, January 1971.

4.10 Dobratz, Brigitta M., "Properties of Chemical Explosions and Explosive Simulants," UCRL-51319 Rev. 1, U. S. Atmoic Energy Commission Contract No. W-7405-Eng-48, Lawrence Livermore Laboratory, University of California, Livermore, California, July 1974.

4.11 Johansson, C. H. and Persson, P. A., _Detonics of High Explosives_, Academic Press, London and New York, 1970.

4.12 _Engineering Design Handbook, Principles of Explosive Behavior_, AMCP 706-180, Headquarters, U. S. Army Material Command, Washington, D. C., 1972.

4.13 Hopkinson, B., British Ordnance Board Minutes 13565, 1915.

4.14 Cranz, C., Lehrbuch der Ballistik, Springer-Verlag, Berlin, 1926.

4.15 Sachs, R. G., "The Dependence of Blast on Ambient Pressure and Temperature," BRL Report 466, Aberdeen Proving Ground, MD, 1944.

4.16 Kennedy, W. D., "Explosions and Explosives in Air," in Effects of Impact and Explosion, M. T. White (ed.), Summary Technical Report of Div. 2, NDRC, Vol. I, Washington, D. C., AD 221 586, 1946.

4.17 Potter, R. and Jarvis, C. V., "An Experimental Study of the Shock Wave in Free Air from Spherical Charges of TNT and 60/40 RDX/TNT," United Kingdom Atomic Energy Authority, AWRE Report No. 0 1/73, 1973.

4.18 Goodman, H. J. and Giglio-Tos, L., "Equivalent Weight Factors for Four Plastic Bonded Explosives: PBX-108, PB-109, AFX-103 and AFX-702," Technical Report ARBRL-TR-02057, U. S. Army Ballistic Research Laboratory, Aberdeen Proving Ground, MD, April 1978.

4.19 National Oceanic and Atmospheric Administration, U. S. Standard Atmosphere, 1976, NOAA-S/T 76-1562, U. S. Government Printing Office, October 1976.

4.20 Jack, W. H. Jr. and Armendt, B. F. Jr., "Measurements of Normally Reflected Shock Parameters under Simulated High Altitude Conditions," BRL Report No. 1280, Aberdeen Proving Ground, MD, AD 469014, April 1965.

4.21 Dewey, J. M., Johnson, O. T. and Patterson, J. D., II, "Mechanical Impulse Measurements Close to Explosive Charges," BRL Report No. 1182, Aberdeen Proving Ground, MD, November 1962.

4.22 Johnson, O. T., Patterson, J. D., II, and Olson, W. C., "A Simple Mechanical Method for Measuring the Reflected Impulse of Air Blast Waves," BRL Report No. 1099, Aberdeen Proving Ground, MD, July 1957.

4.23 Jack, W. H., Jr., "Measurements of Normally Reflected Shock Waves from Explosive Charges," BRL Memorandum Report No. 1499, Aberdeen Proving Ground, MD, AD 422886, July 1963.

4.24 Wenzel, A. B. and Esparza, E. D., "Measurements of Pressures and Impulses at Close Distances from Explosive Charges Buried and in Air," Final Report on Contract No. DAAK 02-71-C-0393 with U. S. Army MERDC, Ft. Belvoir, VA, 1972.

4.25 Baker, W. E., "Prediction and Scaling of Reflected Impulse from Strong Blast Waves," Int. Jour. Mech. Sci., 9, pp. 45-51, 1967.

4.26 Doering, W. and Burkhardt, G., "Contributions to the Theory of Detonation," Translation from the German as Tech. Report No. F-TS-1227-IA (GDAM A9-T-4G), Headquarters, Air Material Command, Wright-Patterson AFB, Ohio, May 1949.

4.27 Brode, H. L., "Quick Estimates of Peak Overpressure from Two Simultaneous Blast Waves," Defense Nuclear Agency Report No. DNA4503T, Contract No. DNA001-78-C-0009, R&D Associates, RDA-TR-107006-008, Marina Del Rey, California, December 1977.

4.28 Harlow, F. H. and Amsden, A. A., "Fluid Dynamics---An Introductory Text," LA 4100, Los Alamos Scientific Laboratory, University of California, Los Alamos, New Mexico, February 1970.

4.29 "Internal Blast Damage Mechanisms Computer Program," JTCG/ME-73-3, F08635-71-C-0199, April 1973.

4.30 Dewey, J. M., Johnson, O. T. and Patterson, J. D., II, "Some Effects of Light Surrounds and Casings on the Blast From Explosives," BRL Report No. 1218, (AD 346965), September 1963.

4.31 Filler, W. S., "The Effect of A Case on Air Blast Measurements, Part I, Friable Inert Cases," NOLTR 74-62, Naval Ordnance Laboratory, White Oak, April 9, 1974.

4.32 Wisotski, J. and Snyer, W. H., "Characteristics of Blast Waves Obtained from Cylindrical High Explosive Charges," University of Denver, Denver Research Institute, November 1965.

4.33 Plooster, M. N., "Blast Front Pressure From Cylindrical Charges of High Explosives," Naval Weapons Center Technical Memorandum No. 3631, Navy Contract No. N00123-76-C-0166, Denver Research Institute, September 1978.

4.34 Makino, R. C. and Goodman, H. J., "Air Blast Data on Bare Explosive of Different Shapes and Compositions," BRL Report No. 1015, 1956.

4.35 Reisler, R. C., "Explosive Yield Criteria," Minutes of 14th Explosives Safety Seminar, New Orleans, 8-10 November 1972, Department of Defense Explosives Safety Board, pp. 271-288.

4.36 Adams, Channing L., Sarmousakis, James N. and Sperrazza, Joseph, "Comparison of the Blast from Explosive Charges of Different Shapes," Ballistic Research Laboratories, Aberdeen Proving Ground, MD, Report No. 681, January 1949.

4.37 Trancreto, J. E., "Effects of Charge Composition and Surface Conditions on Blast Environment," Minutes of the 16th Explosives Safety Seminar, Vol. I, Hollywood, FL, pp. 301-334, September 1974.

4.38 Zaker, T. A., "Blast Pressures From Sequential Explosions," IIT Research Institute, Chicago, Illinois, Phase Report II, Project J6166, March 25, 1969.

4.39 Reisler, R. E., Kennedy, L. W. and Keefer, J. H., "High Explosive Multi-burst Air Blast Phenomena (Simultaneous and Non-Simultaneous Detonations), U. S. BRL Technical Report No. ARBRL-TR-02142, February 1979.

4.40 Armendt, B. R., Hippensteel, R. G., Hoffman, A. J., Kingery, C. N., "The Air Blast From Simultaneously Detonated Explosive Spheres," Ballistic Research Laboratories, Aberdeen Proving Ground, Maryland, BRL Report No. 1294, August 1960.

4.41 Armendt, B. F., Hippensteel, R. G., Hoffman, A. J., Keefer, J. H., "Project White Tribe: Air Blast From Simultaneously Detonated Large Scale Explosive Charges," Ballistic Research Laboratories, Aberdeen Proving Ground, Maryland, BRL Report No. 1145, September 1961.

4.42 Armendt, B. F., Hippensteel, R. G., Hoffman, A. J., Schlueter, S. D., "The Air Blast From Simultaneously Detonated Explosive Spheres: Part II - Optimization," Aberdeen Proving Ground, Maryland, Ballistic Research Laboratories, Department of the Army Project No. 503-04-002, BRL Memorandum Report No. 1384, January 1962.

4.43 Hokanson, J. C., Esparza, E. D. and Wenzel, A. B., "Reflected Blast Measurements Around Multiple Detonating Charges," Minutes of the Eighteenth Explosives Safety Seminar, Vol. I, pp. 447-471, September 1978.

4.44 Gregory, F. H., "Analysis of the Loading and Response of a Suppressive Shield When Subjected to an Internal Explosion," Minutes of the 17th Explosive Safety Seminar, Denver, Colorado, September 1976.

4.45 Baker, W. E., "The Elastic-Plastic Response of Thin Spherical Shells to Internal Blast Loading," Jour. of Appl. Mech., 27, Series E, 1, pp. 139-144, March 1960.

4.46 Baker, W. E., Hu, W. C. L. and Jackson, T. R., "Elastic Response of Thin Spherical Shells to Axisymmetric Blast Loading," Jour. of Appl. Mech., 33, Series E, 4, pp. 800-806, December 1966.

4.47 Kingery, C. N., Schumacher, R. N. and Ewing, W. O., Jr., "Internal Pressures from Explosions in Suppressive Structures," BRL Interim Memorandum Report No. 403, Aberdeen Proving Ground, MD, June 1975.

4.48 Schumacher, R. N., Kingery, C. N., Ewing, W. O., Jr., "Air Blast and Structural Response Testing of a 1/4 Scale Category I Suppressive Shield," BRL Memorandum Report No. 2623, May 1976.

4.49 Esparza, E. D., Baker, W. E. and Oldham, G. A., "Blast Pressures Inside and Outside Suppressive Structures," Edgewood Arsenal Contractor Report EM-CR-76042, Report No. 8, December 1975.

4.50 Weibull, H. R. W., "Pressures Recorded in Partially Closed Chambers at Explosion of TNT Charges," Annals of the New York Academy of Sciences, 152, Art. 1, pp. 256-361, October 1968.

4.51 Proctor, J. F. and Filler, W. S., "A Computerized Technique for Blast Loads from Confined Explosions," Minutes of the 14th Annual Explosives Safety Seminar, New Orleans, Louisiana, pp. 99-124, 8-10 November 1972.

4.52 Keenan, W. A. and Trancreto, J. E., Tech. Report TR-828, Army MIPR 51-027, "Blast Environment from Fully and Partially Vented Explosions in Cubicles," Civil Engineering Laboratory, Naval Construction Battalion Center, Port Hueneme, CA, November 1975.

4.53 Zilliacus, S., Phyillaier, W. E. and Shorrow, P. I., Naval Ship R&D Center Report 3987, "The Response of Clamped Circular Plates to Confined Explosive Loadings," NSRDC, Bethesda, MD, February 1974.

4.54 Kinney, G. F. and Sewell, R. G. S., NWC Technical Memorandum 2448, "Venting of Explosions," Naval Weapons Center, China Lake, CA, July 1974.

4.55 Baker, W. E. and Oldham, G. A., "Estimates of Blowdown of Quasi-static Pressures in Vented Chambers," Edgewood Arsenal Contractor Report EM-CR-76029, Report No. 2, November 1975.

4.56 Owczarek, J. A., Fundamentals of Gas Dynamics, Int. Textbook Co., Scranton, PA, 1964.

4.57 Kulesz, J. J., Moseley, P. K. and Baker, W. E., "Fragment and Blast Hazards From Explosions in a Tender Torpedo Workshop," Vol. 1, Final Report Prepared for the David Taylor Ship Research and Development Center, Contract No. N00014-77-C-0658, November 1978.

4.58 Taylor, D. B. and Price, C. F., "Velocities of Fragments from Bursting Gas Reservoirs," ASME Transactions, Journal of Engineering for Industry, November 1971.

4.59 Baker, W. E., Kulesz, J. J., Ricker, R. E., Bessey, R. L., Westine, P. S., Parr, V. B. and Oldham, G. A., "Workbook for Predicting Pressure Wave and Fragment Effects of Exploding Propellant Tanks and Gas Storage Vessels," NASA CR-134906, November 1975.

4.60 Kot, C. A., Valentin, R. A., McLennan, D. A., Turula, P., "Effects of Air Blast on Power Plant Structures and Components," Argonne National Laboratory Report No. ANL-CT-78-41, Argonne National Laboratory, 9700 South Cass Avenue, Argonne, Illinois, 60439, Prepared for Division of Engineering Standards, Office of Standards Development, U. S. Nuclear Regulatory Commission, October 1978.

4.61 White, C. S., "The Scope of Blast and Shock Biology and Problem Areas in Relating Physical and Biological Parameters," Annals of the New York Academy of Sciences, Vol. 152, Art. 1, pp. 89-102, October 1968.

4.62 White, C. W., Jones, R. K., Damon, E. G., Fletcher, E. R. and Richmond, D. R., "The Biodynamics of Air Blast," Technical Report to Defense Nuclear Agency, DNA 2738T, Lovelace Foundation for Medical Education and Research, AD 734-208, July 1971.

4.63 Richmond, D. R., Damon, E. G., Fletcher, E. R., Bowen, I. G. and White, C. S., "The Relationship Between Selected Blast Wave Parameters and the Response of Mammals Exposed to Air Blast," Annals of the New York Academy of Sciences, Vol. 152, Art. 1, pp. 103-121, October 1968.

4.64 Damon, E. G., Yelverton, J. T., Luft, U. C. and Jones, R. K., "Recovery of the Respiratory System Following Blast Injury," Technical Progress Report to Defense Atomic Support Agency, DASA 2580, Lovelace Foundation for Medical Education and Research, AD 618369, October 1970.

4.65 Bowen, I. G., Fletcher, E. R., Richmond, D. R., "Estimate of Man's Tolerance to the Direct Effects of Air Blast," Technical Report to Defense Atomic Support Agency, DASA 2113, Lovelace Foundation for Medical Education and Research, AD 693105, October 1968.

4.66 Damon, E. G., Richmond, D. R., Fletcher, E. R. and Jones, R. K., "The Tolerance of Birds to Air Blast," Final Report to Defense Nuclear Agency, DNA 3314F, Lovelace Foundation for Medical Education and Research, AD 785259, July 1974.

4.67 von Gierke, H. E., "Biodynamic Models and Their Applications," Aerospace Medical Research Laboratory, Wright-Patterson AFB, Ohio, AD 736-985, 1971.

4.68 Hirsch, A. E., "The Tolerance of Man to Impact," Annals of the New York Academy of Sciences, Vol. 152, Art. 1, pp. 168-171, October 1968.

4.69 Clemedson, C. J., Hellstrom, G. and Lingren, S., "The Relative Tolerance of the Head, Thorax, and Abdomen to Blunt Trauma," Annals of the New York Academy of Sciences, Vol. 152, Art. 1, pp. 187+, October 1968.

4.70 Ross, R., et al., "Criteria for Assessing Hearing Damage Risk from Impulse-Noise Exposure," Human Engineering Laboratory, Aberdeen Proving Ground, MD, AD 666-206, August 1967.

4.71 Reed, J. W., Pape, B. J., Minor, J. C. and DeHart, R. C., "Evaluation of Window Pane Damage Intensity in San Antonio Resulting from Medina Facility Explosion on November 13, 1963," Annals of the New York Academy of Sciences, Vol. 152, Art. 1, pp. 565-584, October 1968.

4.72 Kulesz, J. J. and Friesenhahn, G. J., "Explosion Venting in Buildings," Minutes of the 19th Explosives Safety Seminar, (to be published).

4.73 Levy, S., "An Improved Computer Program to Calculate the Average Blast Impulse Loads Acting on a Wall of a Cubicle," PA-TR-4070, May 1970.

4.74 Ferritto, J. M., "Optimum Dynamic Design of Reinforced Concrete Slabs Under Blast Loading," CEL TN No. N-1494, Naval Facilities Engineering Center, Port Hueneme, CA, July 1977.

4.75 Bacigalupi, C. M., "Design of a Maze Structure to Attenuate Blast Waves," UCRL-52921, Lawrence Livermore Laboratory, Livermore, CA, March 1980.

CHAPTER 5

CRATERING AND GROUND SHOCK

5.1 INTRODUCTION

If an accidental explosion occurs, many different types of ground
shock problems can arise. The ground shock is capable of causing soil
craters to be formed; walls, floors, and roofs of adjacent structures to
fail; explosives, equipment, and personnel inside adjacent structures to
be vibrated; and off-site neighbors to be disturbed because of cracked
walls and physically felt tremors. All of these problems are caused by
ground shock and any subsequent cratering. At interline standoff
distances, buildings are usually safe from ground shock related
damage, but this should be checked. At the Pantex Plant, at least three
different ground shock related accident scenarios can be envisioned. The
first problem can be described as an explosion in an earth-covered storage
igloo. If explosives fill most of the igloo, this problem can be idealized
as a buried detonation without a gap between the explosive and the soil.
A crater will be formed as ejecta are flung into the air and a strong ground
shock will be propagated away from the scene of the accident as the coupling
between the explosive and the soil will be extremely strong.

The second type of accident can be described as an explosion caused
by impact when a charge accidentally falls on a floor or walkway, thus
causing a contact explosion on the surface of the ground. Only minor
cratering will occur near the point of contact from a contact explosion,
but a shock wave will be propagated through the soil. Deep in the ground
directly beneath the explosion, the ground shock will be small, but near
the surface, Rayleigh-type shock waves can result in ground motion of
significant amplitude.

The third accident scenario can be envisioned as an accidental explo-
sion in a building such as Building 12-44, a Gravel-Gertie type bay.
Such an accident is a buried detonation; however, a large air gap or void
now exists between the explosive charge and the soil behind the walls of
the bay. The ground shock transmitted into the soil will be greatly
reduced because a large air gap results in decoupling the explosive charge
from the ground, thereby having an effective energy release which is
much smaller than the actual energy release. Another subproblem which
exists in this third accident scenario is breeching of the roof.

All of these possible accidents involve direct-induced ground shock
which subsequently result in structural damage or injured personnel. The
major difference in these solutions involves the coupling of the blast source
with the soil. In addition to the directly induced ground shock, air-

induced ground motions are possible; especially for extremely large detonations such as those associated with nuclear weapons or the equivalent energy releases. For the design of Pantex-type buildings, an A-E firm does not have to consider air-induced ground shock because the possible energy releases are too small to be significant for conventional chemical explosives.

This report was written to aid A-E firms in the design of ammunition plants. If an accidental explosion occurs, total destruction often occurs in the near field. Therefore, emphasis is placed on ground shock effects in the far field rather than close to the donor.

In Section 5.2, a general discussion of what makes soil different from other continua is presented. This discussion includes how sands differ from clays, what is effective stress, and why continuum solutions are used even though pore air and pore water pressures influence results. We discuss how soil particle velocity is related to shock front pressure P_s and how maximum soil displacement X is related to the impulse in a shock wave i_s. In addition, this section discusses what soils should be expected at the Pantex plant site, and references a report for obtaining additional on-site soil details.

Section 5.3 is a general discussion of ground shock. Subjects discussed in this section include: 1) wave propagation through a homogeneous, isotropic, semi-infinite elastic medium, 2) a sketch of typical ground motion-time history, 3) the distinction between P-waves, S-waves, and R-waves, 4) insight into the effects of layering on wave propagation, 5) insight into how waves are damped, and 6) references on trenches and other screening devices. Finally, an approximate graphical solution is given for predicting the radial soil displacement X and the maximum soil particle velocity U from tamped buried explosive charge detonations.

Section 5.4 presents a coupling solution for modifying the buried detonation ground motion analysis so detonations in the middle of a cavity can be analyzed. This coupling solution yields an effective energy release Weff which can then be substituted into ground motion solutions to obtain soil particle velocity and radial displacement.

Section 5.5 gives explosive cratering results for determining: 1) if a camouflet or crater is formed, 2) the size and volume of apparent craters, true craters, camouflets, and 3) the maximum range of ejecta from a buried detonation. All of these solutions are empirical curve fits to test data.

In Section 5.6, the effects of ground motion on buildings, equipment, and people are discussed. This is accomplished by deriving shock spectra criteria with a qualitative model and then presenting various criteria which historically have been used to limit the amplitude of ground motions. Other approximate solutions are presented for estimating stresses due to buried explosions for: 1) buried pipe, 2) beam-like strips out of buried bunkers, and 3) buried cylinders or spheres.

Section 5.7 identifies some special problems which need further development. Among the problems in need of additional data and the development of better analysis procedures are screening of ground shock, P-wave prediction, maximum ejecta radius, and shock propagation through walls and soil into adjacent bays.

In order to make this manual more useful to design personnel, different example problems are presented throughout the text. A flow diagram for guiding designers to the appropriate sections and illustrative examples on ground shock and cratering is presented in Section 5.8. A list of symbols in Section 5.9 and a list of references in Section 5.10 complete this section of the design guide.

5.2 SOIL MECHANICS OVERVIEW

5.2.1 General Discussion

To study the state of stress in the various constituents of soil, consider a cross section through two soil grains as in Figure 5.1. The total cross-sectional area subject to load P is the total area A. The two grains are only in actual physical contact over a very small area of solid contact A_s. In addition to the soil grains, the voids or pores in the medium can be filled with a combination of water and air. If the soil is not saturated so that water does not fill all of the void, the water generally forms a meniscus in the narrow cracks near the grain boundaries. This means that one can speak of the area of fluid-solid contact A_w and the area of gas-solid contact A_g.

Stresses or pressures in the three phases are p_s in solid, p_w in the water, and p_g in the gas. All of these are overpressures which are above atmospheric pressure. Requiring that the sum of forces be in equilibrium gives:

$$P = \sigma A = p_s A_s + p_w A_w + p_g A_g \qquad (5.1)$$

In equation (5.1), σ is the total stress averaged over the total area. If we define the ratio $\dfrac{A_s}{A}$ to be a and the ratio $\dfrac{A_w}{A}$ to be x, then the total stress σ can be written as:

$$\sigma = a p_s + x p_w + (1 - a - x) p_g \qquad (5.2)$$

The quantity a is very small as the granular contacts generally occur at a point. This observation means that a is much less than both 1 and x. The quantity ap_s is not insignificant, however, because p_s can be very large. The quantity ap_s is the effective stress $\bar{\sigma}$ in soil mechanics. As can be seen in equation (5.2), effective stress is related to intergranular pressure, but it is not equal to intergranular pressure because
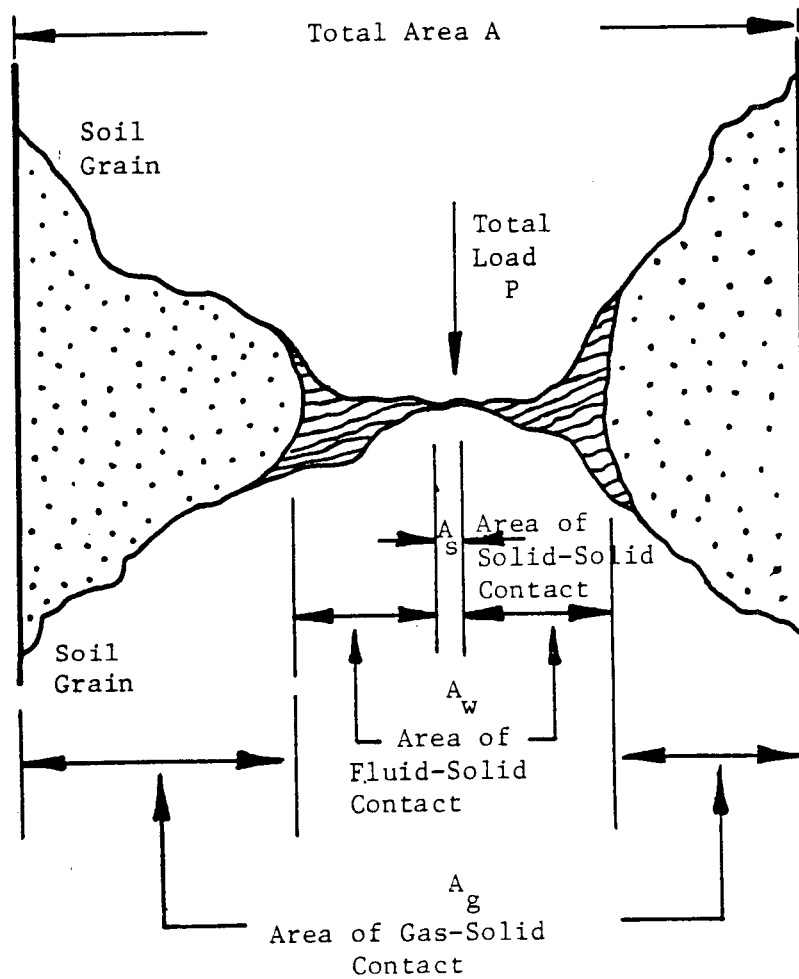
Figure 5.1 Intergranular Stress on Area

of the contact area ratio a. As far as soil failure is concerned, effective stress $\bar{\sigma}$ (or ap_s) is important and not the total stress σ, because movement will occur when the grains move or displace relative to one another. Instead of using a total stress versus strain constitutive relationship, soil mechanics classically requires an effective stress versus strain constitutive relationship.

If we make the approximations which have just been described, equation (5.2) can be written as:

$$\sigma = \bar{\sigma} + xp_w + (1 - x)\, p_g \qquad (5.3)$$

When a soil is 100 percent saturated, x equals 1 and equation (5.3) becomes

$$\sigma = \bar{\sigma} + p_w \quad (100\% \text{ saturated}) \qquad (5.3a)$$

Equation (5.3a) is the classical relationship which is generally taught in all introductory soil mechanics courses. As should be emphasized, equation (5.3a) is based on 100 percent saturation. The other extreme is 0.0 percent saturation, which would give:

$$\sigma = \bar{\sigma} + p_g \quad (0.0\% \text{ saturation}) \qquad (5.3b)$$

Both extremes show that the effective stress is the total stress minus the pore pressures. The conclusion drawn is that the pores can be filled with a relatively incompressible fluid such as water, or with a very compressible fluid such as air. In either case, the instantaneous state of effective stress depends upon the pore pressures which will also be increased when a soil sample is loaded.

Statically, equations (5.3) and these interrelationships cause no problems; however, dynamically, experimenters have not been very successful in separating out pore pressure and effective stress. Whereas, static pitot tubes can be used to measure pore pressures, dynamic instrumentation which might be inserted into these extremely small pores, either fail to have proper response time or give a poor impedance match. The point of this discussion is that pore pressures are important, but dynamically we do not understand them. Unfortunately, this is only the first problem in any attempt to understand soil behavior.

The second major problem in understanding soils is that even in the absence of pore pressures, soils include many types of medium. At one extreme are the coarse, large-grained materials which include sands and gravels. These materials are composed of particles so large that no significant interparticle forces exist. In the absence of interparticle forces, these granular materials develop their strength from gravitational effects, or from the overburden. To penetrate a granular material or shear it, the other particles have to be shoved aside. A penetrometer pushed into a dry sand has a linearly increasing total stress versus depth

relationship because more and more overburden is being mustered as greater depths are obtained. Another illustration of this same behavior is walking on a sandy beach. Up in the dunes one sinks in above the ankles until enough overburden is obtained to resist penetration. Down at sea level where the sand is saturated, a walker sinks only a few millimeters because the pore water pressures are carrying the person's weight. If the walker stands still at the water's edge, the pore pressures flow away from the loaded area and the person begins to sink as the effective stresses must carry more and more of the load with time. Eventually the standing person will sink to a finite depth when the overburden of sand and water are adequate to support him. This behavior illustrates both the behavior of a gravitational medium and the role pore pressures play, especially if a soil is saturated.

The other extreme in soil behavior is with clays. These materials are effectively colloids (often with a characteristic size of microns). In these materials, interparticle forces dominate and gravitational effects are insignificant. A penetrometer pushed into a heavily overconsolidated clay will show no change in strength with depth. Such a material has inherent constitutive strength in the classical sense, provided one speaks of an effective stress versus strain relationship.

Of course, few soils are a pure clay or a pure sand. Silts are an in-between medium exhibiting both behaviors, and sandy clays, clayey silts, and all types of mixtures can exist. In addition, a soil site can be layered from the contributions of different geological eras.

In this section of the design guide, the reader will find soils treated as continua and as single phase media. This treatment is not necessarily correct; it is what everyone does out of ignorance concerning better ways of treatment. So although soil is not a continuum, total stress solutions are used. The results are often subject to judgments based on insight provided by this background information.

5.2.2 Soils at Pantex Facility

As part of a seismic hazard evaluation, URS and John Blume and Associates (Ref. 5.1) made a geological evaluation of the area around the Pantex facility. While most of this evaluation involves strata far deeper than the strata of interest in accident evaluations, the following information can be used for approximate initial evaluations. Any careful in-depth study should use bore log information or more on-site evaluations of local conditions.

The uppermost layer at Pantex varies from 7 to 12 ft in thickness and has a compressive P-wave velocity c of from 950 to 1300 ft/sec. Generally, this medium is topsoil. The next layer down is a moist clay with lenses of caliche from 10 to 20 ft in thickness. The P-wave velocity

in this layer ranges from 1500 to 1900 ft/sec with lenses as fast as 2100 to 2700 ft/sec. The third zone begins at a depth of about 30 ft and exhibits velocities of from 3400 to 5000 ft/sec. This third zone can be some 20 ft thick and is a very stiff to hard clay with some caliche content. In all cases, the ground water table is not a factor as 300 ft depths and greater are typically experienced. If average values are used for P-wave velocities, these should be towards the slower limits, perhaps, 950 ft/sec in the top soil, 1550 ft/sec in the second zone, and 3800 ft/sec in the third zone.

All of the following computations will use wave velocity and soil density as input parameters defining soil properties. Although the URS/ John Blume report does not report soil densities, 114 lb/ft^3 is an assumed representative weight density for all three layers, probably accurate to within $\pm$ 15 percent.

5.2.3 Relationship Between Ground Motion and Loads

Often it is desirable to go from ground motion such as soil displacement X and particle velocity U to the maximum pressure P_s and impulse i_s in a ground shock. This conversion can be done using the Rankine-Hugoniot relationships for conservation of mass and momentum. For a stationary coordinate system with a shock front moving at velocity V, the Rankine-Hugoniot equations are:

$$-\rho_s V = \rho_a (U - V) \qquad (5.4a)$$

$$\rho_s V^2 = P_s + \rho_a (U - V)^2 \qquad (5.4b)$$

where ρ_a is the density behind the shock front, ρ_s is the mass density of undisturbed soil, and P_s is the peak side-on overpressure. Multiplying both sides of equation (5.4a) by (U-V) and then subtracting the two equations gives:

$$P_s = \rho_s VU \qquad (5.5)$$

Equation (5.5) states that peak overpressure is the product of soil density, shock front velocity, and peak particle velocity. In a fairly incompressible medium such as soil with its massive particles, the shock front propagation velocity V very rapidly decays to the compressive P-wave seismic velocity c_p. This final substitution of c_p for V gives a relationship which will be used many times to approximately relate P_s and U.

$$P_s = \rho_s c_p U \qquad (5.6)$$

To relate side-on impulse i_s and the maximum radial soil displacement X, one can treat ρ_s and c_p as constants and integrate equation (5.6). Because the time integral of pressure is impulse and the time integral of

5-7

velocity is displacement, integrating equation (5.6) gives:

$$i_s = \rho_s c_p X \qquad (5.7)$$

Equations (5.6) and (5.7) will be used repeatedly to relate ground motions to loads from ground shock. In developing any solution for loads on any adjacent structure, the ground motions U and X will be predicted first (see Section 5.3.2) and then related to the loads P_s and i_s by using these relationships.

PROBLEM – Assume that other calculations given in Section 5.3.2 give the maximum radial soil velocity and maximum radial soil displacement. What will be the side-on pressure P_s and side-on impulse i_s imparted to a slab on grade in the Pantex top soil where the P-wave velocity c_p and the soil's mass density are given in Section 5.2.2?

GIVEN: c_p = P-wave velocity (in./sec)
ρ_s = Mass density (lb-sec^2/in.^{4})
U = Soil particle velocity (in./sec)
X = Soil displacement (in.)

FIND: Side-on pressure and impulse   REFERENCE

SOLUTION: 1. Side-on pressure (psi)
$$P_s = \rho_s c_p U$$ Eq. (5.6)

2. Side-on impulse (psi-sec)
$$i_s = \rho_s c_p X$$ Eq. (5.7)

CALCULATION

GIVEN: c_p = 11,400 in./sec
ρ_s = 1.71 x 10^{-4} lb-sec^2/in.^{4}
U = 2.0 in./sec
X = 0.1 in.

FIND: Side-on pressure and impulse

SOLUTION: 1. $P_s = \rho_s c_p U$
$P_s = (1.71 \times 10^{-4})(11,400)(2.0)$
$P_s = \underline{3.90\ psi}$

2. $i_s = \rho_s c_p X$
$i_s = (1.71 \times 10^{-4})(11,400)(0.1)$
$i_s = \underline{0.195\ psi\text{-}sec}$

5.2.4 Determination of Wave Length

Another calculation which will be required when the depth of Rayleigh-type R-waves (see page 5-12) and the effects of layering are discussed, is the determination of wave length L. If one knows the maximum displacement X and the peak particle velocity U (see Section 5.3.2), as well as the seismic compression P-wave propagation velocity c_p, an approximate wave length is known for the P-wave. Similarly, if the propagation velocity, particle velocities and displacements are associated with either a shear or Rayleigh wave, then the wave length is known for the wave being described. By assuming undamped harmonic motion, the maximum velocity U is related to the period T and the displacement X through the equation:

$$U = \frac{2\pi}{T} X \tag{5.8}$$

The wave length L then relates to the period T and propagation velocity c through the equation

$$L = cT \tag{5.9}$$

Eliminating T from equations (5.8) and (5.9) and solving for L gives:

$$L = 2\pi \frac{c}{U} X \tag{5.10}$$

No subscripts are placed on c, U, X and L because these apply for any of three types of waves (P-wave, S-wave and R-wave) which will be described in Section 5.3.1. Equation (5.10) gives the wave length as a function of c, X and U. For most accidents, this wave length is fairly long, typically on the order of hundreds of feet. The importance of this long wave length will become apparent in subsequent discussions.

To relate frequency to period, one uses equation (5.11) as would be given by many texts on simple harmonic motion.

$$f = \frac{1}{T} \tag{5.11}$$

EXAMPLE PROBLEM 5.2

PROBLEM – Assume that other calculations given in Section 5.3.2 give the maximum radial soil velocity and maximum radial soil displacement. What will be the wave length, period, and frequency of Rayleigh waves for a Rayleigh wave velocity determined in Section 5.3.1 for the Pantex top soil given in Section 5.2.2?

GIVEN:　U　= Peak particle velocity (in./sec) (assume this is caused by R-wave)

X　= Maximum soil displacement (in.) (assume this is caused by R-wave)

c_R = R-wave propagation velocity (in./sec)

FIND:　Wave length, period and frequency　　　　　　　　　REFERENCE

SOLUTION:　1.　Determine the wave length (in.)

$$L = 2\pi \frac{c_R}{U} X$$　　　　　　　　　Eq. (5.10)

2.　Determine the period (sec) and frequency $f(sec^{-1})$

$T = L/c_R$　　　　　　　　　Eq. (5.9)

$f = 1/T$　　　　　　　　　Eq. (5.11)

CALCULATION

GIVEN:　U　= 2.0 in./sec
X　= 0.1 in.
c_R = 7,600 in./sec

FIND:　Wave length, period and frequency

SOLUTION:　1.　$L = 2\pi \dfrac{c_R}{U} X$

L = 2π (7,600) (0.1)/2.0
L = 2,388 in.

2.　$T = L/c_R$

T = 2,388/7,600
T = 0.3142 sec
f = 1/T
f = 3.183 Hz

5.3 EFFECTS OF GROUND SHOCK

5.3.1 Theoretical Wave Propagation Through Soil

To solve wave propagation problems in soils, one uses models which are but approximations of reality. Usually, the simplest case is applied with the soil treated as a homogeneous, isotropic semi-infinite elastic solid. In reality, soils are multi-phased, nonisotropic, and layered media. Elastic constants depend upon the state of stress in the ground, and deformations may in turn affect the initial internal stresses which always exist. Fortunately, for the purposes of design, a precise theory of wave propagation is not required.

A disturbance near the surface of the ground will emit compression P-waves, shear S-waves, and Rayleigh surface R-waves in a semi-infinite elastic medium. Deeply buried disturbances will emit only P-waves and S-waves, but in the far field, interface effects will result in R-waves being produced. For all of these wave types, the time interval between wave front arrivals becomes greater and the amplitude of the oscillations becomes smaller with increasing standoff distance from the source. Figure 5.2 (Ref. 5.2) presents (a) radial displacement and (b) vertical displacement time histories at a surface location in an elastic half space.

Figure 5.2 shows that the first wave to arrive is the P-wave, the second the S-wave, and the third the R-wave. Lamb (Ref. 5.3) refers to the P-wave and S-wave as minor tremors, as these waves are followed by **a much larger oscillation when the R-wave arrives.** The R-wave is the **major** tremor because: 1) two-thirds of the total energy at the source goes into the R-wave, and 2) the R-wave dissipates much less rapidly with distance than either the less energetic P-wave or S-wave. P-waves and S-waves dissipate with distance r to a power of r^{-1} to r^{-2}. At the surface, P-waves and S-waves dissipate with distance as r^{-2}, while R-waves dissipate with distance as $r^{-0.5}$. The greater energies being transmitted by R-waves and the slower geometric dissipation of this energy causes R-waves to be the major tremor, the disturbance of primary importance for all disturbances on the surface. Figure 5.3 is a schematic drawing of the wave motions propagated from a buried detonation. The Love wave motion shown in Figure 5.3 does not occur in unlayered media, but it will be discussed later in this section.

The locus of surface particle motion for an R-wave describes a retrograde ellipse in the plane of the radial from the source as shown in Figure 5.3. The motion begins by raising the surface slightly and moving towards the source. Eventually, the surface moves away and down. In the absence of layering, there is no transverse motion in the horizontal plane; hence, no third axis is shown in Figure 5.2. All R-waves travel extensively near the surface as they dissipate rapidly with depth. Figure 5.4 (Ref. 5.2) presents scaled plots of the radial and vertical R-wave amplitudes as functions of scaled depth. As can be observed, the vertical

(a) radial displacement history (+ away)

(b) vertical displacement history (+ down)
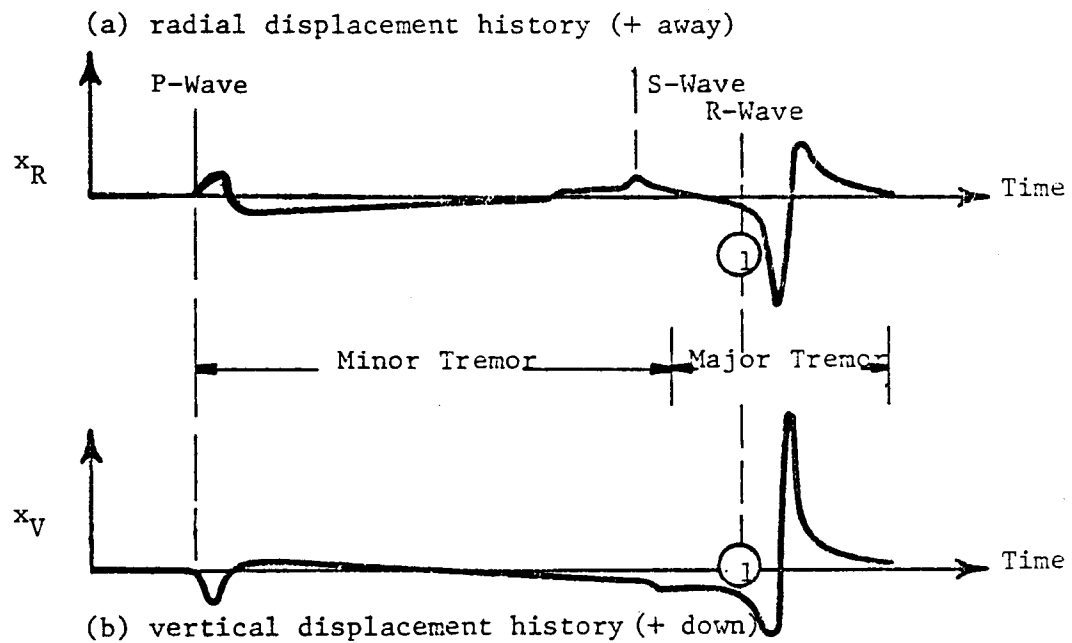
Figure 5.2   Radial Displacement History (a) and Vertical Displacement History
(b) from Point Source at Surface of Elastic Medium (Reference 5.2)
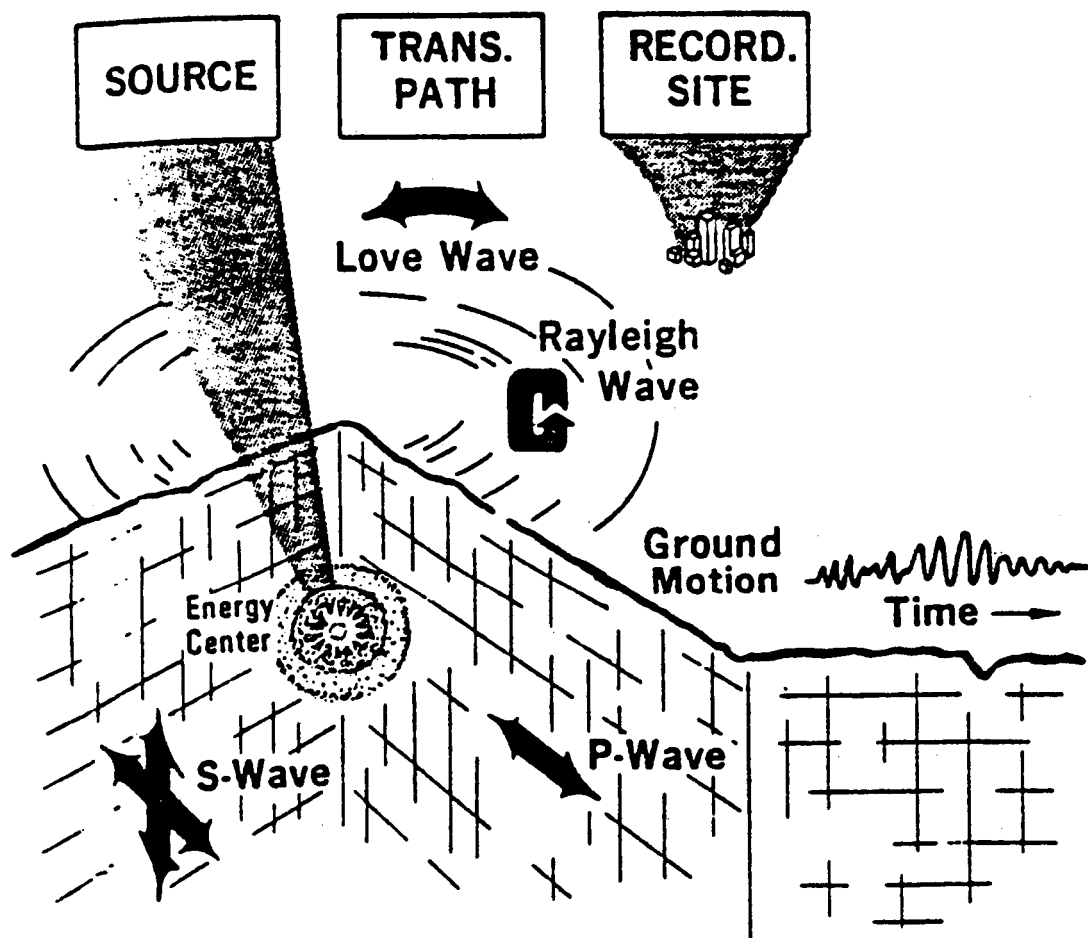
Figure 5.3. Schematic Illustration of the Waves
Propagated from an Energy Source

displacement component is a maximum at a depth of approximately 0.16 wave-
lengths. At depths up to approximately 0.4 wavelengths, the vertical compo-
nent of the R-wave changes relatively little. At depths greater than 0.5
wavelengths, the vertical displacement decays rapidly (almost exponentially)
with added depth. The radial R-wave displacement component begins to decay
immediately with increased depth from the surface. At depths greater than
0.2 wavelengths, the particle motion associated with the R-waves changes
from describing a retrograde ellipse to describing prograde motion, motion
which begins by raising the particle and moving away from the source and
finally moves towards the source and down. The negative signs in Figure 5.4
mean that motion has changed from retrograde to prograde motion.

Figure 5.5 presents the relationship between P-wave, S-wave, and
R-wave velocities of propagation in a plot of wave velocity divided by the
S-wave velocity as a function of Poisson's ratio. All of these wave
velocities are functions of $\sqrt{G/\rho}$ (where G is shear modulus and ρ is density)
and are a function of Poisson's ratio ν. As is also apparent in Figure
5.2, the P-wave travels much faster than other waves, the R-wave travels
the slowest, but it travels at just under the S-wave velocity of propaga-
tion. The shear wave velocity of propagation c_s is related to the shear
modulus of elasticity G and the mass density ρ_s by equation (5.12).

$$c_s = \sqrt{G/\rho_s} \qquad (5.12)$$

Vibration measurements around sources show that the disturbance
is not confined to the vertical plane through the radial line from the
source. Waves transverse to the vertical plane generally arise from layer-
ing or various strata in a soil. The appearance of another soil layer
causes at least two different phenomena. The first phenomenon is the
appearance of another type of surface wave called the Love wave or L-wave.
The L-wave causes transverse horizontal oscillations to occur as seen in
Figure 5.3, and is sustained by repeated multiple reflections between the
surface and underlying layer. For an L-wave to arise, the shear modulus
of underlying layer must be greater than the shear modulus of the overlaying
layer. The L-wave will not occur if the covering layer is stiffer. The
velocity of an L-wave is between the shear wave velocities of the covering
and the underlying layers. Barkan (Ref. 5.4) has an excellent discussion
of the L-wave phenomenon.

The second phenomenon that occurs in a layered system is a distortion
in R-wave propagation velocity and in the elliptical trajectories associated
with particle motion. Figure 5.6 from Reference 5.4 is a plot of the
scaled increase in propagation velocity c_a/c as a function of the shear
modulus $G = E/2(1+\nu)$ (G_1 in the top layer and G in the bottom layer) and
the scaled layer thickness in wavelengths H/L. If H/L is larger than
0.5, the influence of a second underlying layer is minimal in Figure 5.6.
On the other hand, when H/L is less than 0.5, an intense increase occurs
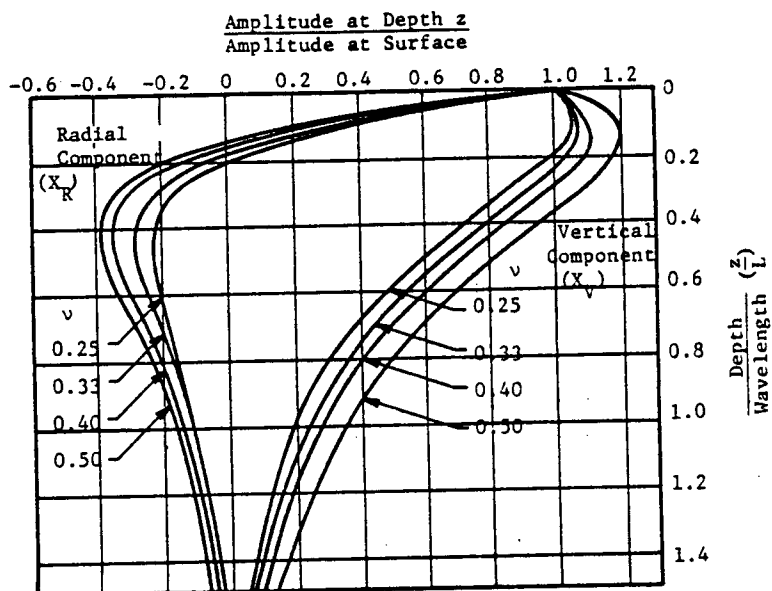
Figure 5.4   Dimensionless Displacement versus Depth
Ratios for R-Wave (Ref. 5.2)
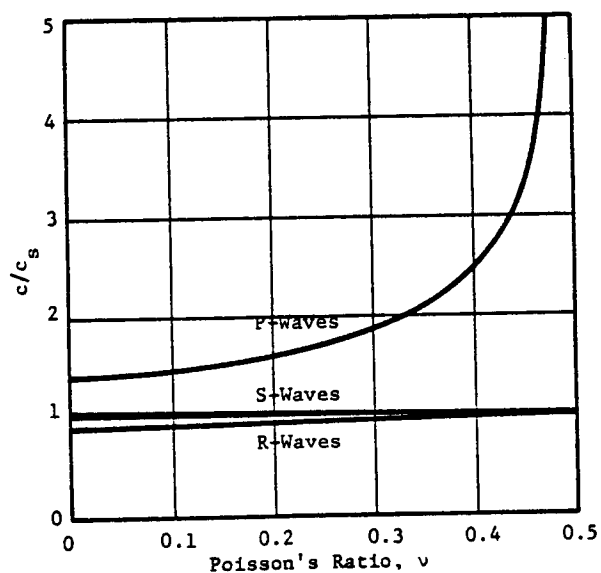
Figure 5.5   Velocity of Wave Front
Propagation (Ref. 5.2)

in wave propagation velocity with this change almost proportional to the wavelength. The coefficient of proportionality depends upon the shear modulus ratio; it increases as the underlying layer grows stiffer than the overlying layer.
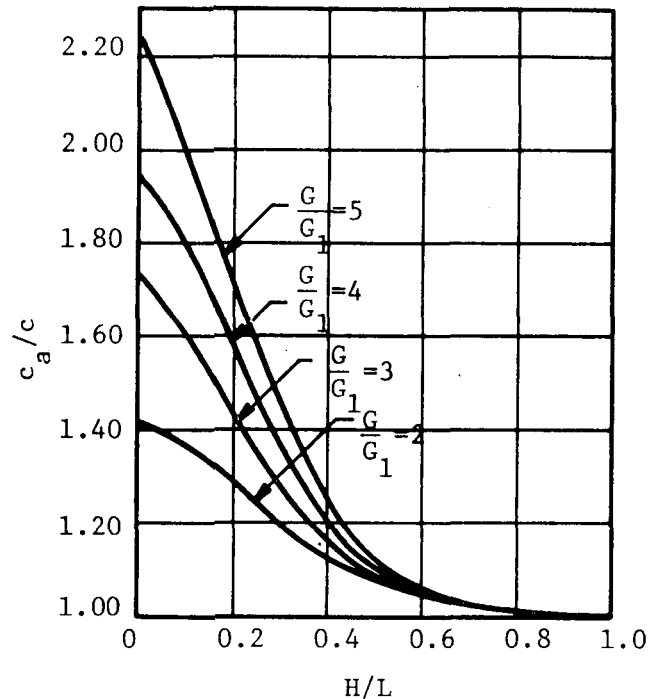
Figure 5.6   Effect of Layering on Increasing Wave
Propagation Velocity (Ref. 5.4)

Figure 5.7 shows the change in the ratio of radial to vertical displacements on the surface of an upper layer when a stiff underlying layer is present. For short waves with L/H < 2.0, the ratio of radial and vertical displacement components change very little. For wavelengths in layer thicknesses between around 2.0 and 4.0, the ellipse of particle motions becomes elongated in the vertical direction, and when the wavelengths grow larger than 4.0, these ellipses are elongated in the radial direction. Larger differences in the shear moduli G cause enhanced changes in the ratio of radial to vertical displacement.

5-17
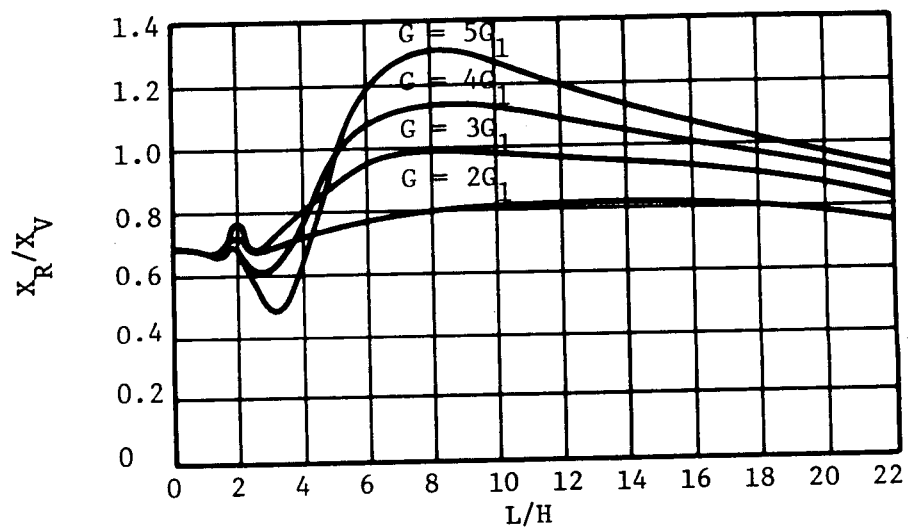
Figure 5.7 Effect of Layering on Particle Motions
(Ref. 5.4)

PROBLEM – Borings show that a soil 14 ft deep overlies a very deep sub-
layer. Measured P-wave propagation velocity in the top layer
is 950 ft/sec and in the bottom layer is 1645 ft/sec. What will
be: 1) the R-wave velocities in each medium, 2) the effective
R-wave propagation velocity in the top layer, and 3) the maximum
vertical particle displacement, if calculations in Section 5.3.2
show that the radial maximum soil displacement equals 0.001 ft?
Assume that the wavelength of the disturbance is 199 ft, and
Poisson's ratio equals 0.3.

GIVEN: H = depth of top layer of soil (ft)
L = wavelength (ft)
X_R = radial soil displacement (ft)

c_{P_1} = P-wave velocity in top layer (fps)

c_{P_2} = P-wave velocity in underlying layer (fps)

ν = Poisson's ratio

FIND: R-wave velocities in each layer, effective R-wave velocity
in top layer because of layering, and vertical soil particle
displacement.

REFERENCE

SOLUTION: 1. Obtain the ratios

$$\frac{c_R}{c_S} \text{ and } \frac{c_P}{c_S}$$

Fig. 5.5

2. Obtain c_R for both layers

$$c_R = \left(\frac{c_R}{c_S}\right)(c_P)/\left(\frac{c_P}{c_S}\right)$$

3. Determine the ratio of the thickness of the
top layer to the wavelength
H/L

4. Calculate c_{S_1} and c_{S_2}

$$c_S = \left(c_P\right)/\left(\frac{c_P}{c_S}\right)$$

5. Calculate the shear moduli ratio

$$\frac{G}{G_1} = \left(\frac{c_{S_2}}{c_{S_1}}\right)^2$$

Eq. (5.12)

6. Determine the effective wave propagation velocity relative to actual propagation velocity

$$\frac{c_a}{c}$$

Fig. 5.6

7. Calculate $c_{a_{R\text{-wave}}}$

$$c_{a_{R\text{-wave}}} = \left(\frac{c_a}{c}\right) c_{R_1}$$

8. Determine the ratio of the wavelength to the thickness of the top layer

L/H

9. Determine the ratio of radial to vertical maximum particle displacements

$$\frac{X_R}{X_V}$$

Fig. 5.7

10. Calculate X_V

$$X_V = X_R / \left(\frac{X_R}{X_V}\right)$$

CALCULATION

GIVEN: H = 14 ft
L = 199 ft
X_R = 0.001 ft
ν = 0.3
c_{P_1} = 950 fps
c_{P_2} = 1645 fps

FIND: R-wave velocities if unlayered, R-wave velocity in top layer because of layering, and maximum vertical particle displacement.

SOLUTION: 1. $\dfrac{c_R}{c_S}$ = 0.94

$\dfrac{c_P}{c_S}$ = 1.86

2. c_{R_1} = (0.94)(950)/(1.86) = <u>480 fps</u>

c_{R_2} = (0.94)(1645)/(1.86) = <u>831 fps</u>

3. H/L = 14/199 = 0.070

4. $c_{S_1} = (950)/(1.86) = \underline{511 \text{ fps}}$

5. $\dfrac{G}{G_1} = \left(\dfrac{884}{511}\right)^2 = 3.0$

6. $\dfrac{c_a}{c} = 1.65$

7. $c_{a_{R-wave}} = (1.65)(480) = \underline{792 \text{ fps}}$

8. $L/H = 199/14 = 14.2$

9. $\dfrac{X_R}{X_V} = 0.93$

10. $X_V = 0.001/0.93 = \underline{0.001075 \text{ ft}}$

5.3.2 Approximate Buried Explosive Ground Motion Relationships

To predict the extent of damage from underground detonations, one needs to determine the radial ground motions - radial maximum soil displacement X and radial maximum particle velocity U. The basis for prediction of the displacement X and velocity U are empirical relationships for buried HE charges in contact with the soil. These empirical equations predict the ground motion maximums created by contributions from all of the wave forms. As has been discussed, the R-wave is probably the major source of excitation; nevertheless, in using these and other empirical relationships, investigators do not consider which wave might be most important. The wave speed used to characterize the strength of the soil is the P-wave propagation velocity. Although R-wave propagation velocities would more logically be used with R-wave ground motions, the P-wave velocity can be used because the two velocities only differ by a constant if Poisson's ratio ν is constant (see Figure 5.5).

At locations very deep in the ground or directly under the explosive source where R-waves cannot form, this empirical solution and others are not valid. This restriction is not that serious for most Pantex-type operations because the wavelengths associated with most of these waves are long. For example, a 600-lb explosive charge might result in a wave which is from 200 to 600 ft long. If one refers back to Figure 5.4, he will see that very significant R-waves exist at depths of 0.8 of a wavelength. Thus, for depth of interest in the area of 160 to 480 ft or less, the R-wave is the major disturbance. Most Pantex-type operations are at shallow depths relative to these. Even a 60-lb charge can have a corresponding large wavelength of from 100 to 300 ft. The R-wave and its propagation are the major ground shock interest in any potential Pantex accidents. This R-wave solution is subsequently extended to account for coupling when a charge and the soil have an air gap between them.

The relationships which we will use for R-waves from buried detonations (Ref. 5.5) are given by equation (5.13), radial displacement, and equation (5.14), radial particle velocity.

$$\frac{X}{R}\left(\frac{P_o}{\rho_s c_p^2}\right)^{1/2} = \frac{0.04143\left(\dfrac{W}{\rho_s c_p^2 R^3}\right)^{1.105}}{\tanh^{1.5}\left[18.24\left(\dfrac{W}{\rho_s c_p^2 R^3}\right)^{0.2367}\right]} \tag{5.13}$$

$$\frac{U}{c_p}\left(\frac{P_o}{\rho_s c_p^2}\right)^{1/2} = \frac{6.169 \times 10^{-3}\left(\dfrac{W}{\rho_s c_p^2 R^3}\right)^{0.8521}}{\tanh\left[26.03\left(\dfrac{W}{\rho_s c_p^2 R^3}\right)^{0.30}\right]} \tag{5.14}$$

where X = maximum radial soil displacement
U = peak radial soil particle velocity
R = standoff distance
W = explosive energy release
ρ_s = mass density of the soil or rock
c_p = seismic P-wave velocity in the soil or rock
p_o = atmospheric pressure.

Any self-consistent set of units may be used in applying these relationships for all terms; $X/R \, (p_o/\rho_s c_p^2)^{1/2}$, $U/c_p \, (p_o/\rho_s c_p^2)^{1/2}$, and $W/\rho_s c_p^2 R^3$ are nondimensional. Test data on explosive sources ranging from 0.03 lb to 19.2 kilotons (nuclear blast equivalency) will be used in subsequent discussion to demonstrate the validity of these relationships. The data used to substantiate these results cover nine orders of magnitude from $W/\rho_s c_p^2 R^3$ of 4.4×10^{-11} to 4.4×10^{-2} in scaled explosive energy release.

Figures 5.8 and 5.9 respectively, are plots of nondimensionalized displacement and nondimensionalized velocity as given by equations (5.13) and (5.14). Because the data appear to collapse into a unique function, these results give a graphical solution. Scatter exists; however, no experiments or test site appears to yield systematic errors.

The continuous lines placed through the data in Figures 5.8 and 5.9 were presented as equations (5.13) and (5.14). Both are the result of an approximate rather than least-squares curve fit to test data. For the data in Figures 5.8 and 5.9, the observed values of scaled displacement and particle velocity were divided by their respective predictive values to obtain a large sample of data around a mean value of 1.0. In both figures, one standard deviation computed from this enlarged data base is ± 0.50. Although straight lines can be fitted to segments of the results in Figures 5.8 and 5.9, the rate of change for either X or U with respect to either W or R varies, depending upon the scaled charge weight $W/\rho_s c_p^2 R^3$. These variations are reasonably close to those given by others and will be discussed. This discussion is not presented because we advocate the use of any of these procedures; it is presented so that those with backgrounds in this field will understand that the procedure which has been advocated is an inclusive analysis procedure.

At first glance, equations (5.13) and (5.14) may appear to be different from some of the other empirical relationships in the literature; however, these two equations are more general and can be shown to encompass most other results. Equations (5.13) and (5.14) are not log linear as are many other relationships, the test data base covers many orders of magnitude, and a coupling term $(p_o/\rho_s c_p^2)^{1/2}$ is multiplied by the scaled displacement and velocity. The presence of atmospheric pressure in the prediction relationships does not mean atmospheric pressure is a physical phenomenon influencing the results. The quantity $\rho_s c_p^2$ is a measure of the compressibility of the shock propagation media. Hence, the quantity p_o
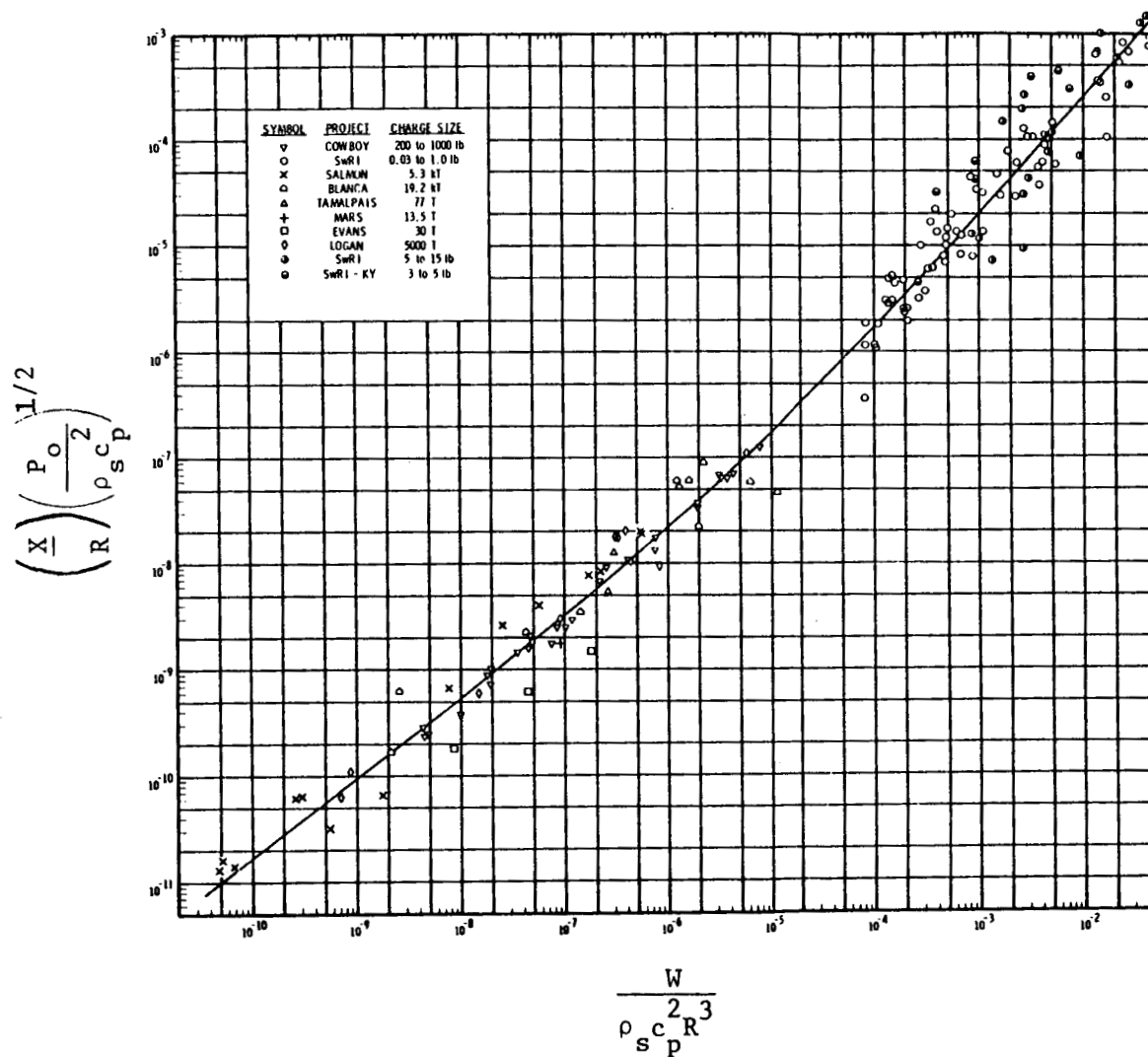
Figure 5.8   Radial Maximum Displacement versus Scaled
Energy Release in Rock and Soil (Reference 5.5)

SYMBOL	PROJECT	CHARGE SIZE
▽	COWBOY	200 to 1000 lb
○	SwRI	0.03 to 1.0 lb
×	SALMON	5.3 kT
◇	BUREAU of MINES	VARIOUS
◑	SwRI	5 to 15 lb
◒	SwRI - KY	3 to 5 lb

Vertical axis: $U \dfrac{\rho_o}{c_p} \left(\dfrac{P_o}{\rho_s c_p^2} \right)^{1/2}$

Horizontal axis: $\dfrac{W}{\rho_s c_p^2 R^3}$
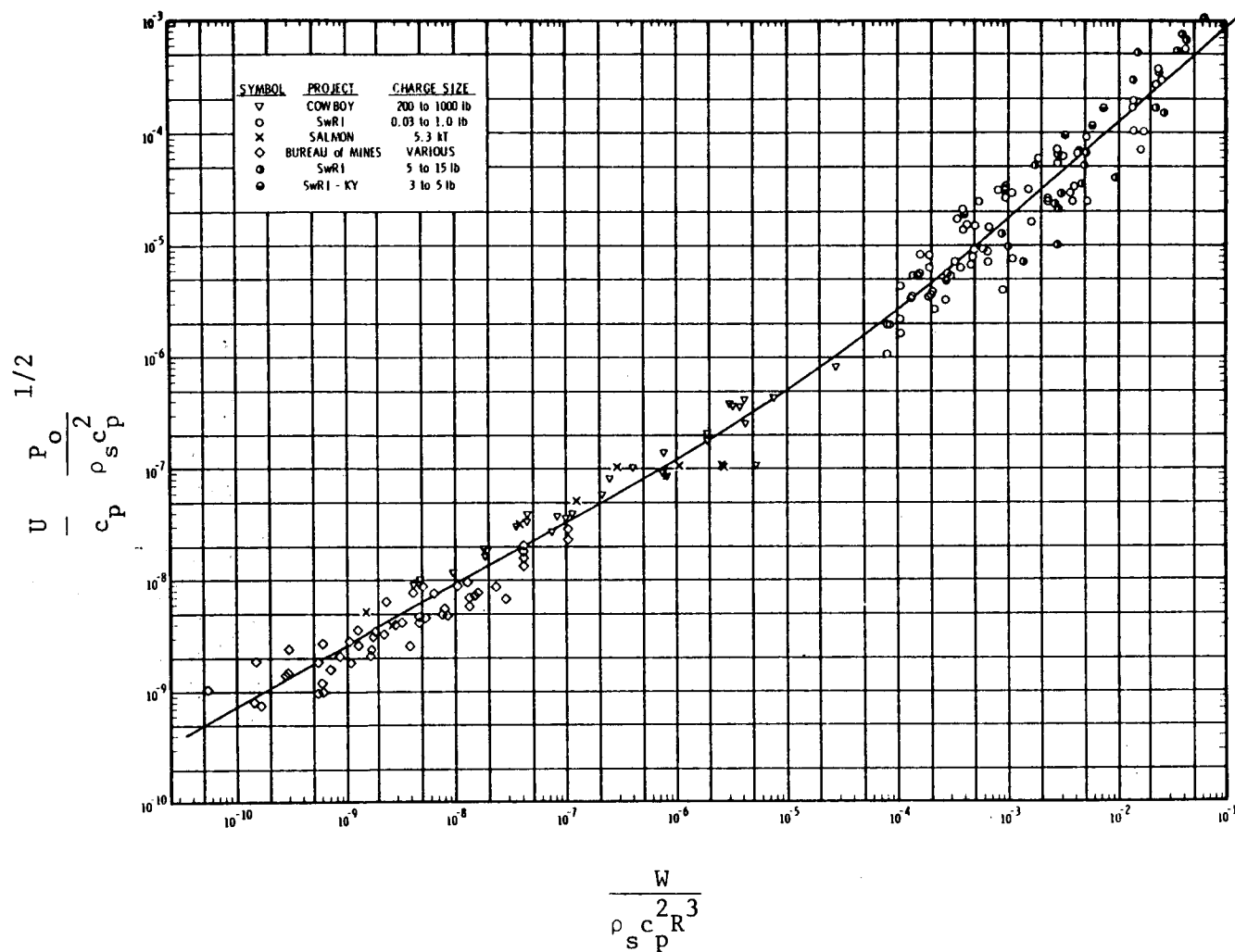
Figure 5.9   Radial Particle Velocity versus Scaled Energy
Release in Rock and Soil (Reference 5.5)

is a standard (compressibility of air) and introduces empirically relative
compressibilities for different media such as soil and rock.

Two different groups of ground shock propagation procedures have
been used in the past and are in the literature for empirical relationships
interrelating charge weight, standoff distance, and ground motion. A
statistical approach generally used is a propagation law of the form

$$A = KW^{N_W}R^{N_R} \tag{5.15}$$

where A = the peak amplitude for either velocity or displacement
N's = constant exponents
K = a constant.

This format is popular because the logarithm can be taken of both sides
to obtain:

$$[\ln A] = [\ln K] + N_W[\ln W] + N_R[\ln R] \tag{5.16}$$

Because this equation is linear, a least squares curve fit could be made
to obtain the three coefficients $\ln K$, N_W, and N_R. The weakness of this
approach is that this format is assumed regardless of what happens
physically. The resulting equations are dimensionally illogical. A
serious problem is the use of an incomplete expression. Other parameters
enter the ground shock propagation problem, especially soil properties,
which are ignored. Because these properties are ignored, the definition
of the problem is incomplete, and the results do not represent a general
solution.

By using equation (5.16), various investigators obtain different
results depending upon the amount and range of their data. Typical
values found in the literature (Refs. 5.6 through 5.15) have a range for
N_W from 0.4 to 1.0 and for N_R from -1 to -2 with A as particle displace-
ment or velocity. This situation arises because investigators use data
from different segments of the curve as given by equations (5.13) and
(5.14).

The second group of investigators, usually those associated with
the old Atomic Energy Commission (AEC) or newly named Department of
Energy (DOE), present their results in the format:

$$U \propto \left(\frac{W^{1/3}}{R}\right)^{N_W} \tag{5.17}$$

$$\frac{X}{W^{1/3}} \propto \left(\frac{W^{1/3}}{R}\right)^{N_X} \tag{5.18}$$

This approach is an extension of the Hopkinson-Cranz scaling law for air blast waves, and is a dimensional version of a model analysis. If soil properties such as ρ and c_p are treated as constants and atmospheric pressure does not vary significantly, then equations (5.13) and (5.14) in functional format can be written as equations (5.15) and (5.16). An example (Ref. 5.16) of curve fits for displacement and velocity to equations (5.17) and (5.18) is:

$$\frac{UR^{1.65}}{W^{0.55}} = \text{constant} \qquad (5.19)$$

$$\frac{XR^{1.5}}{W^{0.833}} = \text{constant} \qquad (5.20)$$

All of the data in equations (5.19) and (5.20) were taken for chemical explosive detonations in Halite (salt domes), and cover scaled charge weight $W/\rho_s c_p^2 R^3$ over three orders of magnitude. The general format given by equations (5.17) and (5.18) does not have to be directly proportional over all regions as shown.

By using equations (5.13) and (5.14) we are encompassing domains for most of the previous empirical equations. Those interested in understanding the coupling term $(p_o/\rho_s c_p^2)$ better, should read Westine (Ref. 5.5). This solution should <u>not</u> be used for predicting ground motions from P-waves or S-waves. No need exists to predict these waves except when a point of interest is either directly over or directly under the explosive source. This situation is not a critical Pantex one so it will not be pursued further. After radial ground motion has been determined, vertical ground motion, the effects of trenching, and the influences of layering can all be approximated by using some of the other qualitative discussion in this section of this manual.

PROBLEM – Assume that the soil's density and P-wave propagation velocity have been measured. For a known buried energy release, determine the maximum radial soil displacement and maximum radial particle velocity.

GIVEN: ρ = soil mass density ($lb\text{-}sec^2/ft^4$)

c_p = P-wave propagation velocity (ft/sec)

R = standoff from charge (ft)

P_o = atmospheric pressure (lb/ft^2)

W = explosive yield (ft-lb) [for TNT equals $1.7 \times 10^{+6}$ ft-lb/lb times weight of the charge]*

FIND: The maximum radial soil displacement and maximum radial particle velocity   REFERENCE

SOLUTION: 1. Calculate the following nondimensional quantities

$$\bar{P}_o = \frac{P_o}{\rho_s c_p^2} \;,\; \bar{W} = \frac{W}{\rho_s c_p^2 R^3}$$

2. Calculate the scaled displacement.

$$\frac{X}{R}(\bar{P}_o)^{1/2} = \frac{0.04143\,(\bar{W})^{1.105}}{\tanh^{1.5}[18.24(\bar{W})^{0.2367}]}$$
     Eq. (5.13) or Fig. 5.8

3. Calculate the scaled velocity.

$$\frac{U}{c_p}(\bar{P}_o)^{1/2} = \frac{6.169 \times 10^{-3}\,(\bar{W})^{0.8521}}{\tanh[26.03(\bar{W})^{0.30}]}$$
     Eq. (5.14) or Fig. 5.9

CALCULATION

GIVEN: ρ_s = 3.54 $lb\text{-}sec^2/ft^4$

c_p = 950 ft/sec

R = 40 ft

W = 20 lb ·(1.7 x 10^6 ft-lb/lb) = 3.4 x 10^7 ft-lb

P_o = 14.7 psi = 2,117 lb/ft^2

---

*In Table 2, Appendix A, the value of heat of detonation for TNT is 1.97 x 10^6 ft-lb/lb. This is a calculated value. The experimental value is as given in this problem.

FIND: Maximum radial soil displacement and velocity

SOLUTION: 1. $\bar{P}_o = \dfrac{P_o}{\rho_s c_p^2}$

$\bar{P}_o = \dfrac{2,117}{3.54(950)^2} = 6.63 \times 10^{-4}$

$\bar{W} = \dfrac{W}{\rho_s c_p^2 R^3}$

$\bar{W} = \dfrac{3.4 \times 10^7}{3.54(950)^2 \, 40^3} = 1.66 \times 10^{-4}$

2. $\dfrac{X}{R}\left(\dfrac{P_o}{\rho_s c_p^2}\right)^{1/2} = \dfrac{0.04143(\bar{W})^{1.105}}{\tanh^{1.5}[18.24(\bar{W})^{0.2367}]}$

$\dfrac{X}{R}(6.63 \times 10^{-4})^{1/2} = \dfrac{0.04143\,(1.66 \times 10^{-4})^{1.105}}{\tanh^{1.5}[18.24(1.66 \times 10^{-4})^{0.2367}]}$

$\dfrac{X}{R} = 1.10 \times 10^{-4}$

$X = 4.4 \times 10^{-3}\,\text{ft} = \underline{0.0528 \text{ in.}}$

Figure 5.8 can also be used to solve this equation graphically.

3. $\dfrac{U}{c_p}(\bar{P}_o)^{1/2} = \dfrac{6.169 \times 10^{-3}\,(\bar{W})^{0.8521}}{\tanh[26.03(\bar{W})^{0.3}]}$

$\dfrac{U}{c_p}(6.63 \times 10^{-4})^{1/2} = \dfrac{6.169 \times 10^{-3}(1.66 \times 10^{-4})^{0.8521}}{\tanh[26.03(1.66 \times 10^{-4})^{0.30}]}$

$\dfrac{U}{c_p} = 1.51 \times 10^{-4}$

$U = 0.143 \text{ ft/sec} = \underline{1.72 \text{ in./sec}}$

Figure 5.9 can also be used to solve this equation graphically.

5.3.3 Screening of Propagated Surface Waves

In order to decrease vibrations in structures from ground shocks or vibrations which are moderately too intense, one can erect either trenches or barricades. Some success and in other cases a total lack of success, has been encountered when either sheet piling or trench barriers has been placed between the vibration source and the receiver. Two types of barriers have been used, active barriers which are placed close to the source, and passive barriers which are placed close to the receiver. Off hand, for either type of barrier, one would expect a void to be more effective than a solid or fluid barrier. This may or may not be the case because a trench cannot always be constructed without threat of collapse or filling with rain water. Ground motion reduction factors (soil displacement divided by soil displacement without a barrier) have been observed to be a factor of 1/8; however, generally the reduction is less.

Two major problems exist besides expense in using barriers to shield ground shocks from explosive detonations. Both of these reasons are associated with the reflection and diffraction process of wave fronts striking barriers. Although the intensity may be reduced in some regions, in other regions wave fronts can be focused and shock levels increased. In the case of accidents, one cannot always be sure of where the detonation will occur. This factor means that the designer must try to shield a region (some structure) from shock waves that can travel from anywhere in another region (anywhere the accident can occur). To accomplish this objective without having increases in shock strength at an undesirable location is very difficult under some sets of circumstances.

The second problem with barriers is that they must be very deep; at least 0.5 wavelengths in width and depth, if not larger. The length of waves associated with accidental buried detonations typically are hundreds of feet in length. This means that very large barriers are needed.

Most of the work that has been done to date on barriers is empirical. No good generalized solution exists yet. Because the use of barriers is probably unattractive for Pantex operations, we will not pursue this subject to any greater extent. Those interested in studying this subject further should read Barkan (Ref. 5.4), who has done more than anyone else in evaluating the effectiveness of all types of barriers. R. D. Woods (Ref. 5.17) in the USA, has generated some experimental test results on the effectiveness of trenches.

5.4 COUPLING BETWEEN EXPLOSIVE AND SOIL

If an explosive charge is placed in a cavity, so that an air gap exists between the charge and the walls of the cavity, the radial soil

particle velocity and displacement may be much less than for a buried tamped charge. This large reduction is caused by inefficient coupling between the explosive and the soil when a cavity is present. To account for the reduced coupling whenever charges are detonated in a buried cavity, an effective energy release W_{eff} can be determined which then can be used to calculate radial maximum soil particle velocity and radial maximum displacement using the tamped buried explosive ground motion solutions, Figures 5.8 and 5.9. Figure 5.10 is a graphical solution for determining this effective energy release W_{eff}.

The lower insert to Figure 5.10 illustrates the actual problem. An explosive charge with energy W is centered in the middle of an underground cavity of radius R_o and at atmospheric pressure p_o. The ground surrounding this cavity is a homogeneous isotropic medium of mass density ρ_s and seismic P-wave velocity c_p. First, the scaled abscissa $W/p_o R_o^3$ is calculated using any self-consistent set of units, resulting in a non-dimensional quantity. By entering Figure 5.10 for any given abscissa, the scaled ordinate $[(W_{eff}/W) (\rho_s c_p^2/P_o)^{0.76}]$ is read. The extra term $\rho_s c_p^2/p_o$ represents a coupling term between the compressibility of soil and the compressibility of air in the cavity. Finally, the ratio (W_{eff}/W) is obtained by multiplying the scaled ordinate by $[(p_o/\rho_s c_p^2)^{0.76}]$. This effective energy release can be used to calculate either soil particle velocity or displacement or the associated soil shock front pressures and impulses associated with these corresponding ground motions.

Figure 5.10 comes from a curve fit to only one segment of the peak reflected pressure versus energy release curve. For this reason it is only valid for values of $W/p_o R_o^3$ between 1 and 1000 as given in Figure 5.10. The ratio W_{eff}/W is often near unity in soft soils, but this ratio can be a small number like 1/100 in hard rock. If a number slightly larger than 1.0 is calculated for W_{eff}/W, this is a mathematical quirk associated with the approximations being used. A maximum value of 1.00 should be used for W_{eff}/W. Figure 5.10 has only been developed for a detonation in a cavity; it should not be used to estimate shock transmission from soil into air. We have no data on shock transmission from soil into air, and Figure 5.10 is not intended for such use.

To demonstrate the validity of this solution, test data (Ref. 5.16) obtained by detonating various size explosive charges in cavities of 6 ft or 15 ft radius, are plotted in Figures 5.11 and 5.12. Figure 5.11 is a plot of observed divided by predicted particle velocity versus $R/W_{eff}^{1/3}$, and Figure 5.12 is a plot of observed divided by predicted maximum soil displacement versus $R/W_{eff}^{1/3}$. Ideally, both solutions would collapse into single horizontal lines at a value of 1.0. Because the shape of symbol denotes amount of energy release, and the shaded or unshaded symbols denote size of cavity, variations in the energy release, cavity size, and standoff distance have all been included in these figures. The conclusion to be drawn from Figures 5.11 and 5.12 is that Figure 5.10 works, but the accuracy is only plus and minus a factor of about 2.0.
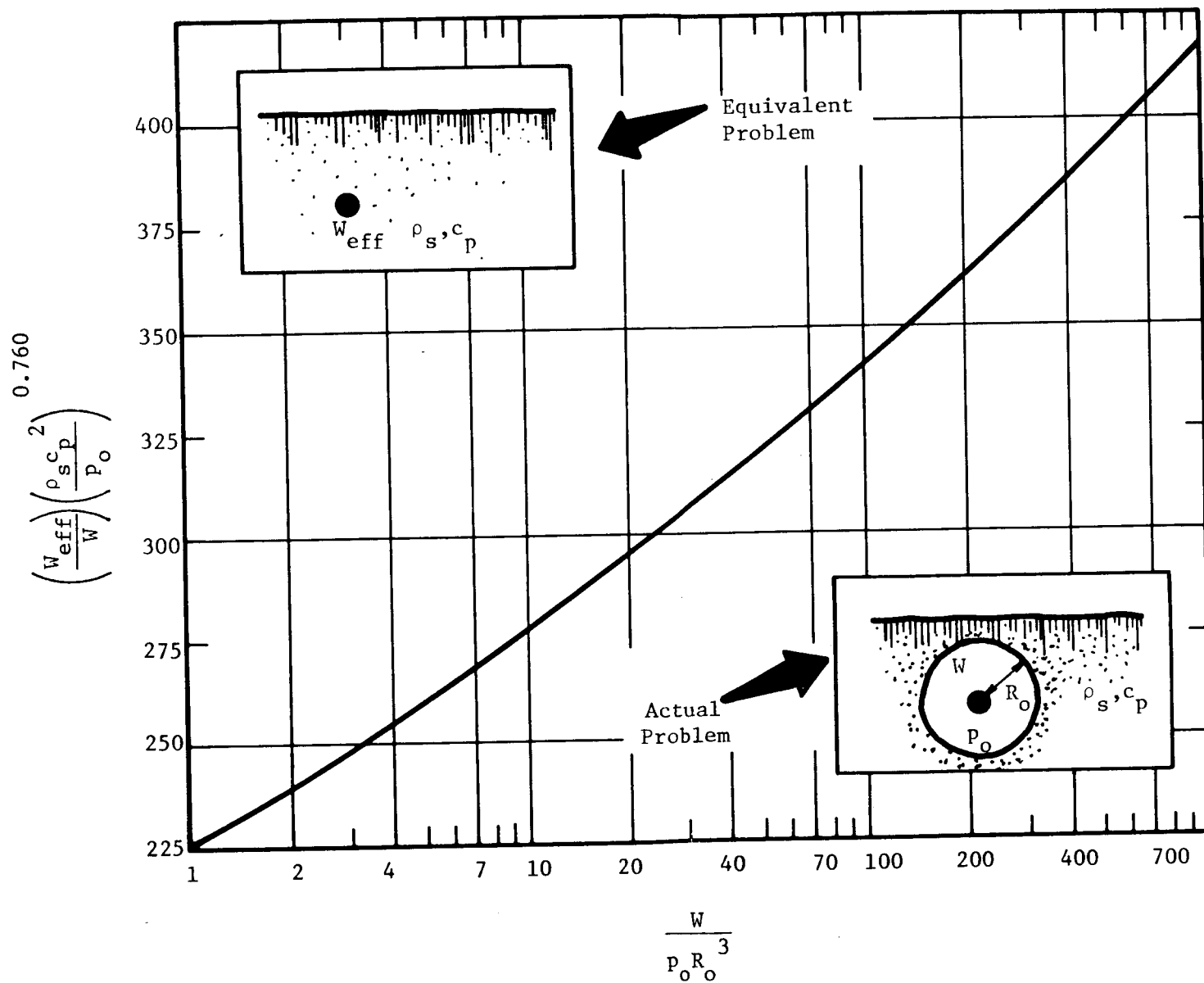
Figure 5.10 Equivalent Effective Release for Buried Detonations Inside a Cavity

Actually, this much scatter is to be expected because the solutions for a continuous medium given by Figures 5.8 and 5.9 have essentially the same degree of accuracy as these coupled ground motions. These observations concerning scatter mean that an appropriate factor of safety should be used whenever these results are applied.

The curve in Figure 5.10 is a calculated one. We should discuss the principles behind the calculations so the procedure could be used if off-center charges were to be detonated in a cavity. Basically, off-center charges could be evaluated by making R_o the distance between the charge and the wall. Figure 5.10 is based upon coupling a shock wave in the air to the wave which would be transmitted into the ground. First, the quantity $R_o/W^{1/3}$ was determined for the distance from the center of the charge to the interface between the cavity and the soil. Then Figure 4.6 in Chapter 4 was used to determine the peak reflected pressure P_r. This reflected pressure would be the one transmitted to an infinitely rigid shell of inner radius R_o. In practice, the soil is not an infinitely rigid shell because the soil particles are unrestrained and the cavity grows. This means that the shock wave transmitted into the soil will have a shock front pressure P which is less than P_r. Based upon the empirical results shown in Figures 5.11 and 5.12, we have assumed that the shock front pressure transmitted into the soil equals $P_r/2$. Another method of stating this assumption is that a gauge in a shell which cannot move will have twice the pressure of a gauge at the surface of the cavity which is free to move with the soil particles. Next, by using the formula $P_s = \rho_s c_p U$, the maximum radial soil particle velocity U can be calculated. Then Figure 5.9 is used by forming the scaled quantity $(U/c)(p_o/\rho_s c_p^2)^{1/2}$. Reading $W/\rho_s c_p^2 R_o^3$ from the graph in Figure 5.9 or computing it from equation (5.14) allows W_{eff} to be calculated after multiplying by $\rho_s c_p^2 R_o^3$. The quantity W_{eff} represents an equivalent charge size detonated in a continuous medium. Had reflected impulse and radial and soil displacement as in Figure 5.8 been used rather than reflected pressure and soil particle velocity to determine the effective equivalent energy release ratio W_{eff}/W, essentially the same numerical values would have been obtained. Figure 5.12 substantiates this conclusion.

A word of caution is in order in using other procedures from the literature for soil coupling procedures. One approach determines the energy in a quasi-static pressure buildup with a cavity of volume $(4/3) \pi R_o^3$. We do not recommend using this procedure, because the ground motions are caused by shock waves and not the quasi-static pressure buildup. Another procedure uses the acoustic transmission factors for different density media such as:

$$\frac{P_T}{P_I} = \frac{2}{1 + \dfrac{\rho_I c_I}{\rho_T c_T}}$$

(5.21a)
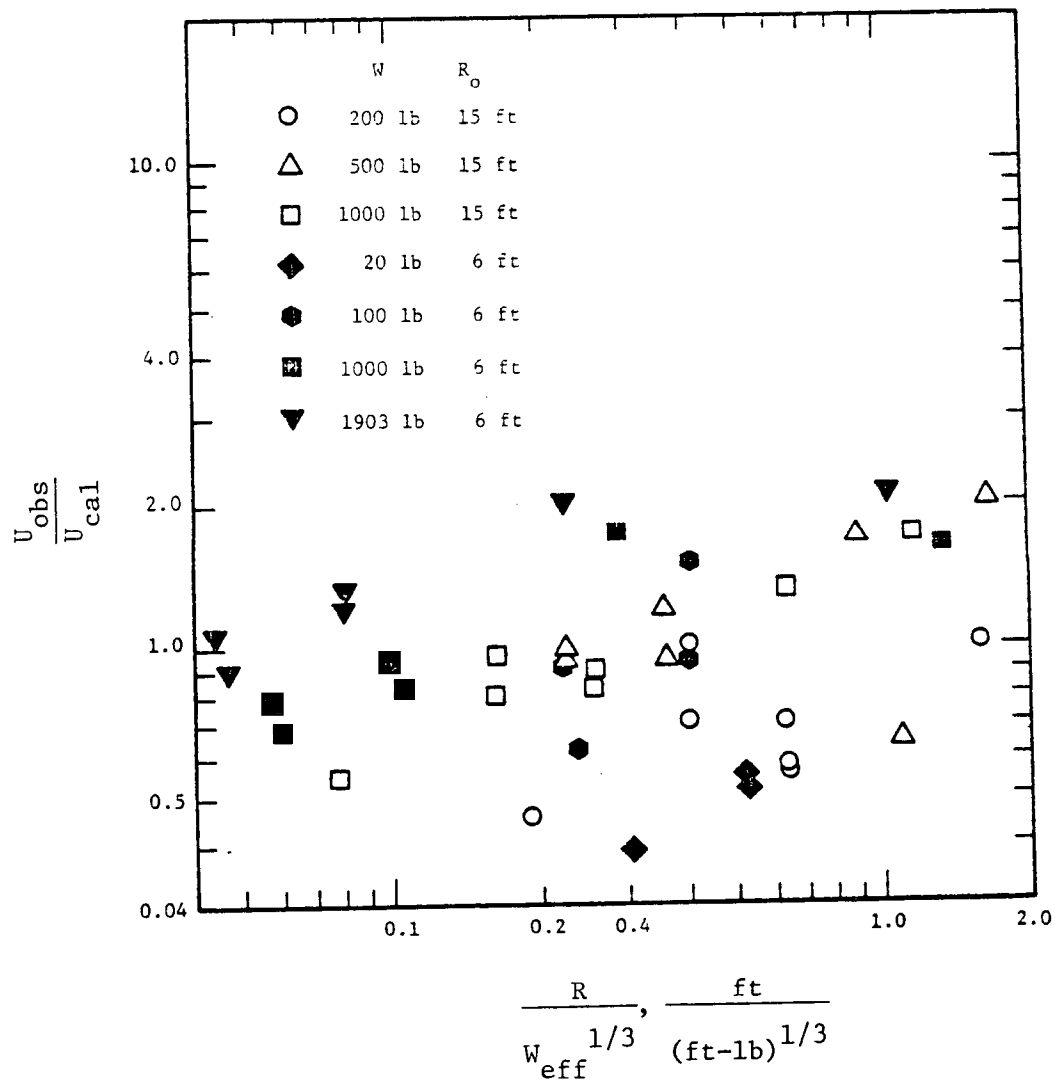
Figure 5.11   Observed versus Predicted Particle Velocity
for Coupled Buried Detonations
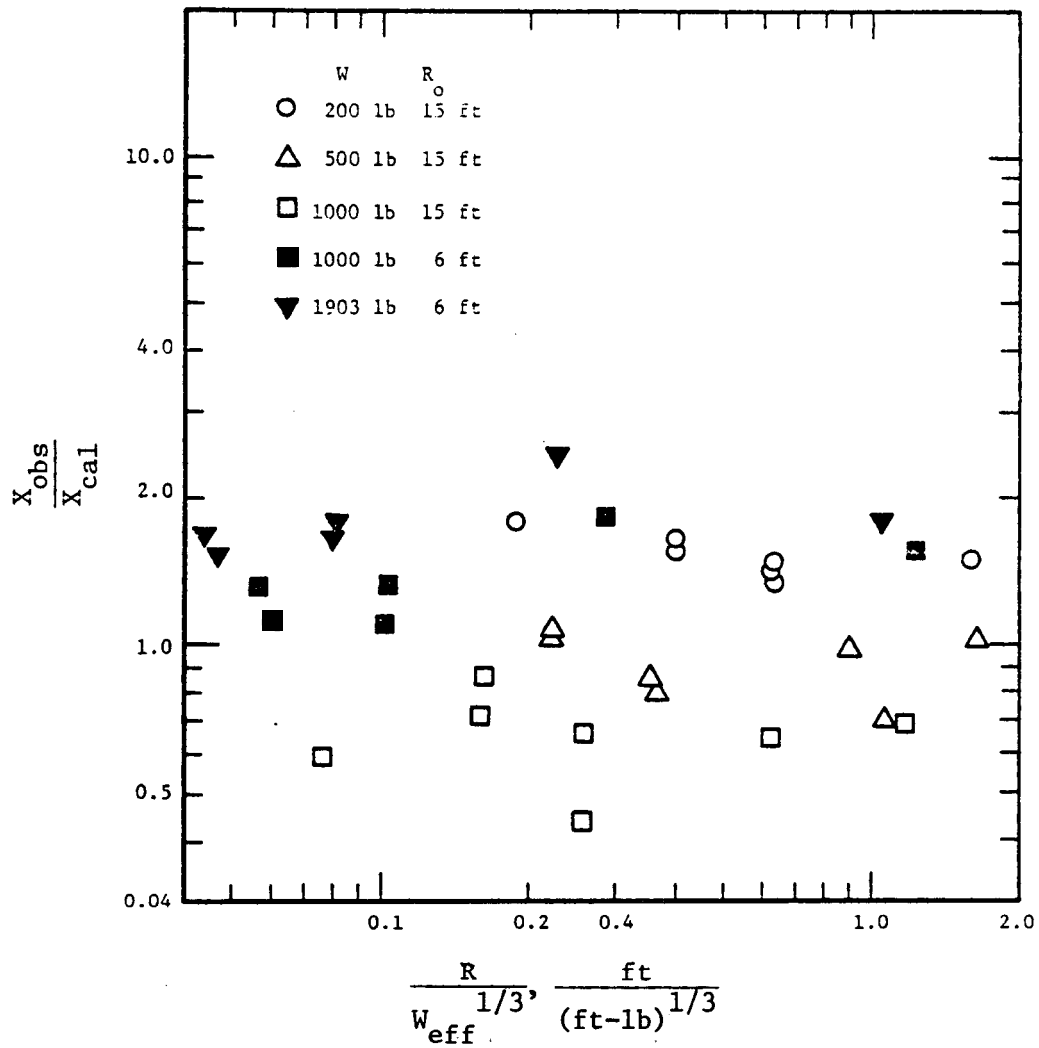
Figure 5.12   Observed versus Predicted Radial Soil Displacement
for Coupled Buried Detonations

For impedance matches where air is the incident medium and soils or rock is the transmitting medium, the ratio $\rho_I c_I / \rho_T c_T \ll 1.0$, and equation (5.21a) becomes

$$\frac{P_T}{P_I} = 2 \qquad\qquad (5.21b)$$

The impedance match predicts that the shock pressure in the soil transmitting medium will be only twice the shock pressure in the incident air medium. The approach used in this handbook does not give this same conclusion.

Another coupling factor which needed to be developed, but for which much less data exist, is for calculating U and X for a charge lying on the surface of the ground. Experimental test results from Project Essex (Ref. 5.18) and from the Navy Civil Engineering Laboratory (Ref. 5.19) were plotted and compared to the radial R-wave velocity and displacement results in Figures 5.8 and 5.9. This comparison established that within the scatter in Figures 5.8 and 5.9, no distinction can be made in R-wave velocity and displacement between buried and surface detonations. This observation means that A-E's can assume that the coupling factor for R-wave propagation from a surface detonation equals 1.0, and can use Figures 5.8 and 5.9 directly for surface as well as buried detonations.

None of this discussion has considered P-wave propagation. For problems such as bomb detonations on the roof of a buried shelter, where no R-wave propagation occurs, the results given in Figures 5.8 and 5.9 should not be used. For Pantex-type facility accidents, P-waves should not be a serious consideration. If for some unforeseen reason, a surface detonation occurs directly over the roof of a buried structure, P-waves will dominate, and use of these R-waves results is incorrect.

If a P-wave should happen to be inovolved in a completely buried circumstance, we would use the entire energy in the explosive, and the results in Figures 5.8 and 5.9 only for values of $W/\rho c^2 R^3$ greater than 10^{-4}. The change in slope in Figures 5.8 and 5.9 is probably caused by changing from a region where P-waves dominate in close to where R-waves dominate at large standoffs. Should a charge happen to be tangent to the surface and P-waves dominate, we would use $W/11$ for the energy release, and the approximate P-wave results, provided $W/\rho c^2 R^3$ was greater than 10^{-4}, as has already been stated. For larger standoffs where $W/\rho c^2 R^3$ might be less than 10^{-4}, we have provided no results, but in this region the shock loadings are not very severe.

EXAMPLE PROBLEM 5.5
================

PROBLEM – Assume that one wishes to determine the maximum radial soil
displacement X and the peak particle velocity U at some
standoff distance R resulting from detonation of a buried
charge within a spherical cavity. The cavity is of radius R_o
and the soil has a mass density of ρ_s and a P-wave propagation
velocity of c_p. In this calculation the soil can be assumed to
be unlayered.

GIVEN: R = standoff (ft)
       W = explosive yield (ft-lb)

P_o = atmospheric pressure (lb/ft^2)

ρ_s = mass density $(lb\text{-}sec^2/ft^4)$
c_p = propagation velocity (ft/sec)
R_o = radius of cavity (ft)

FIND: Equivalent energy releases and maximum radial soil   REFERENCE
displacement and velocity

SOLUTION: 1. Calculate the following nondimensional quantities

$$\bar{P} = \frac{P_o}{\rho_s c_p^2} \qquad \bar{W} = \frac{W}{P_o R_o^3}$$

2. Obtain the quantity from Figure 5.10

$$\left(\frac{W_{eff}}{W}\right)\left(\frac{\rho_s c_p^2}{P_o}\right)^{0.76}$$
                                               Fig. 5.10

3. Multiply result step 2 by $(\bar{P})^{0.76}$ to obtain
W_{eff}/W

4. Multiply result of step 3 by W to obtain W_{eff}

5. Continue at step 2 of Example Problem 5.4
in Section 5.3.2 to find X and U

ALTERNATE
SOLUTION: 1a. Compute $R_o/W^{1/3}$ $(ft/lb^{1/3})$

2a. Read P_r off of graph   Fig. 4.6

3a. Half P_r to obtain P_s

4a. Compute U from P_s by rearranging Equation (5.6)   Eq. (5.6)

5a. Make up the quantity

$$\frac{U}{c_p}\left(\frac{P_o}{\rho_s c_p^2}\right)^{1/2}$$

6a. Compute $W_{eff}/\rho_s c_p^2 R_o^3$ from figure 5.9

7a. Multiply by $\rho_s c_p^2 R_o^3$ to obtain W_{eff}

8a. Divide by energy equivalency to obtain W'_{eff}

9a. Continue at step 2 of Example Problem 5.4 in Section 5.3.2 to find X and U

CALCULATION

GIVEN: $R = 40$ ft
$W = 3.4 \times 10^{+7}$ ft-lb (this is equivalent to 20 lb of TNT)
$P_o = 2117$ lb/ft^2
$\rho_s = 3.54$ lb-sec^2/ft^4
$c_p = 950$ ft/sec
$R_o = 20$ ft

FIND: Equivalent energy release and maximum radial soil displacement and velocity

SOLUTION: 1. $\bar{P} = \dfrac{P_o}{\rho_s c_p^2} = \dfrac{2117}{(3.54)(950)^2} = 6.63 \times 10^{-4}$

$\bar{W} = \dfrac{W}{P_o R_o^3} = \dfrac{3.4 \times 10^{+7}}{(2117)(20)^3} = 2.01$

2. $\left(\dfrac{W_{eff}}{W}\right)\left(\dfrac{\rho_s c_p^2}{P_o}\right)^{0.76} = 239$

3. $\dfrac{W_{eff}}{W} = (239)(6.63 \times 10^{-4})^{0.76} = 0.918$

4. $W_{eff} = (0.918)(20) = \underline{18.4 \text{ lb TNT}}$

ALTERNATE
SOLUTION: 1a. $\dfrac{R_o}{W^{1/3}} = \dfrac{20}{(20)^{1/3}} = 7.37$

2a. $P_r = 34.5$ psi

3a. $P_s = \dfrac{P_r}{2} = 17.25$ psi $= 2484$ lb/ft^2

4a. $U = \dfrac{P_s}{\rho_s c_p} = \dfrac{2484}{(3.54)(950)} = 0.739$ ft/sec

5a. $\dfrac{U}{c_p} \left(\dfrac{P_o}{\rho_s c_p^2} \right)^{1/2} \dfrac{0.739}{950} (6.63 \times 10^{-4})^{1/2} = 2.00 \times 10^{-5}$

6a. $\dfrac{W_{eff}}{\rho_s c_p^2 R_o^3} = 1.20 \times 10^{-3}$

7a. $W_{eff} = (1.20 \times 10^{-3})(3.54)(950^2)(20^3) = 3.06 \times 10^{+7}$ ft-lb

8a. $W_{eff} = \dfrac{3.06 \times 10^{+7}}{1.7 \times 10^{+6}} = \underline{18.0 \text{ lb TNT}}$

5
or
9a.

Calculate U and X by using Figures 5.8 and 5.9

$U = 0.132$ ft/sec = $\underline{1.58 \text{ in./sec}}$ at $R = 40$ ft

$X = 3.96 \times 10^{-3}$ ft = $\underline{0.0475 \text{ in.}}$ at $R = 40$ ft

5.5 EXPLOSIVE CRATERING

Whenever a buried explosive charge is detonated, a cavity or void is formed within the soil. If the energy release is relatively close to the surface, the cavity or void vents to the atmosphere and a crater is formed. Large amounts of ejecta are flung upwards and outwards if the cavity vents to the atmosphere. Some of this ejecta falls back into the cavity, whereas other amounts of it settle on the lip of the crater. Because large quantities of ejecta settle into the cavity, two different craters can be discussed: the apparent crater formed by the surface of the ejecta and the true crater formed by the crater boundaries without regard to the ejecta. Illustrations, shown graphically in Figure 5.13, depict the differences in true and apparent craters. Although Figure 5.13 and some investigators (Ref. 5.21) treat craters venting to the atmosphere as two separate and distinct modes of response dependent upon whether the craters are somewhat hemispherical or cylindrical in shape, we will make no such distinction. Any void venting to the atmosphere will be treated as responding in the cratering mode.

If, on the other hand, the energy release is deep within the ground, the cavity or void is created without any appreciable venting to the atmosphere. This mode of response, as shown in Figure 5.13, is termed the camouflet mode. A large spherical void (or camouflet) is formed beneath the surface of the soil. Because different physical phenomena can be important dependent upon whether: 1) craters or camouflets, or 2) true or apparent crater contours are of interest, any empirical relationship must be applied only to the appropriate mode of response.

For engineering analysis, soil properties such as the density of soil ρ_s and seismic P-wave propagation velocity c are of secondary importance in determining either true or apparent crater size. All of the approximate empirical relationships which we will present are for sand, clays, or rock both wet and dry. None of these curves fits based on experimental test results will have soil properties, but those with an interest should read Reference 5.22.

Essentially, all cratering prediction formuli can be written in the format

$$\text{Response is a function of } \frac{W^{1/3}}{d} \text{ and } \frac{W^{1/4}}{d} \qquad (5.22)$$

where W is the explosive weight in pounds and d is the charge burial in feet. The response in Equation (5.22) can be the scaled radius R/d, the scaled depth D/d, the scaled volume $V^{1/3}/d$ in apparent craters or true craters in the camouflet or cratering mode. In fact, the term response can also mean mode of response, camouflet or crater. Naturally, the functional format will vary dependent upon response to be predicted. An equation such as Equation (5.22) is a three-parameter space which inter-relates the response to the ratio of: 1) energy release relative to the
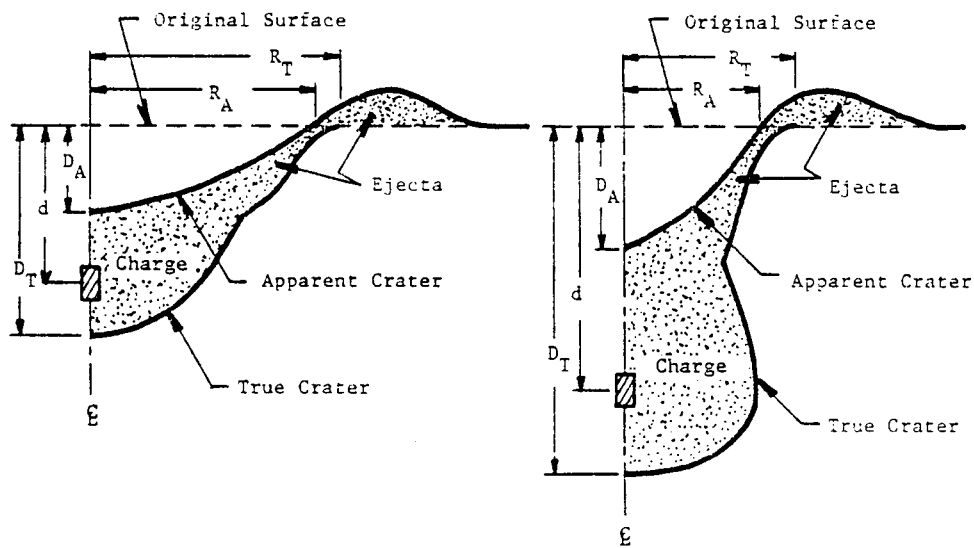
CRATERING MODES
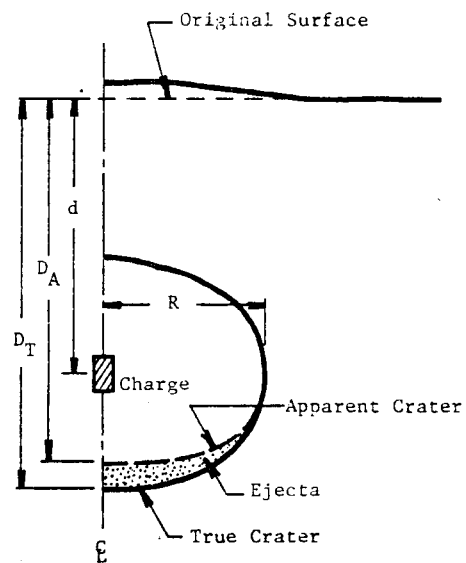
CAMOUFLET MODE

Figure 5.13 Modes of Response and Nomenclature

soil's compressibility effects $W^{1/3}/d$, and 2) the energy release relative to gravitational effects $W^{1/4}/d$. Remember that the soil properties ρ_s and c_p are considered to be constants as in the acceleration of gravity g. If $W^{1/3}/d$ was cubed and transformed into the nondimensional ratio $W/\rho_s c_p^2 d^3$, the statement that the energy release is related to soil compressibility effects becomes apparent. Similarly, the term $W^{1/4}/d$ can be transformed into the ratio $W/\rho_s g d^4$ which emphasizes that the energy release is being related to gravitational effects.

Various formuli and graphs state that a response is related to only $W^{1/3}/d$ or only to $W^{1/4}/d$. Whenever the observation is made that only $W^{1/3}/d$ matters, the results infer that gravitational effects are of secondary importance. Similarly, if only $W^{1/4}/d$ matters, the soil's compressibility effects are of secondary importance. Finally, some relationships state that $W^{7/24}/d$ is important, which is equivalent to saying all effects matter and that $W^{1/3}/d$ and $W^{1/4}/d$ empirically combine as multiples to give $W^{7/12}/d^2$ (this quantity equals $W^{7/24}/d$ when the square root is taken). Now that this background discussion has been presented, we are ready to discuss various empirical relationships.

The first thing is to determine whether a given charge and soil overburden combination results in a crater or camouflet being formed. This calculation comes first because the mode must be known before the damage can be described by using the appropriate cratering or camouflet formuli.

The curve fit for mode of response comes from a compilation of test data (Ref. 5.23) with explosive charge weights ranging from 5.0 grams of C-4 to 750-lb bombs. Two quantities X and Y must be calculated:

$$X = 4.605 + \ln \frac{W^{1/4}}{d} \tag{5.23}$$

$$Y = \left[6.438 + 1.398 \ln \frac{W^{1/3}}{d} \right] \tanh^5 \left[2.00 + 0.4343 \ln \frac{W^{1/3}}{d} \right] \tag{5.24}$$

where W is the explosive weight in pounds and
        d is the depth of burial in feet.

If the quantity X is <u>greater than</u> Y, a camouflet will be formed. If the quantity X is <u>less than</u> Y, the response will be in the cratering mode. In mathematical format this statement means

$$\begin{array}{lll} X > Y & \text{camouflet mode} & \text{(5.25a)} \\ X < Y & \text{cratering mode} & \text{(5.25b)} \end{array}$$

The result X equal to Y means that the response is at the threshold of shifting from one mode to the other mode. The energy release W is actually supposed to be in equivalent pounds of C-4; however, relative to the scatter, differences in yields for chemical explosives do not vary

enough to matter, especially when such weak exponents as 1/3 and 1/4 are taken. For Pantex safety studies, the energy release does not have to be converted to a standard explosive.

The same experimental data base used for determining mode of response (Ref. 5.23) was employed in curve fits of <u>true</u> crater dimensions. The formuli are given by:

$$\frac{R_T}{d} = 2.155 \left(\frac{W^{1/3}}{d}\right)^{0.865} \qquad \left\{\begin{matrix} \text{True Crater} \\ \text{Radius} \end{matrix}\right\} \qquad (5.26a)$$

$$\frac{D_T}{d} = 2.312 \left(\frac{W^{1/3}}{d}\right)^{0.683} \qquad \left\{\begin{matrix} \text{True Crater} \\ \text{Depth} \end{matrix}\right\} \qquad (5.26b)$$

$$\frac{V_T^{1/3}}{d} = 2.046 \left(\frac{W^{1/3}}{d}\right)^{0.785} \qquad \left\{\begin{matrix} \text{True Crater} \\ \text{Volume} \end{matrix}\right\} \qquad (5.26c)$$

One standard deviation calculated from experiments equals essentially 12 percent for all normalized dependent variables in Equation 5.26 with the exception of R_T/d which has a standard deviation of approximately 20 percent. This scatter is very reasonable especially when secondary effects such as soil conditions are not included. Observe also that a true crater follows a $W^{1/3}/d$ law which infers that gravitational effects are insignificant as was discussed previously. This observation is not true for apparent craters.

In the camouflet mode, Equations (5.26) for true crater must be replaced with Equations (5.27) for true camouflet size.

$$\frac{R_T}{d} = 1.053 \left(\frac{W^{7/24}}{d}\right)^{0.865} \qquad \left\{\begin{matrix} \text{True Camouflet} \\ \text{Radius} \end{matrix}\right\} \qquad (5.27a)$$

$$\frac{D_T}{d} = 2.244 \left(\frac{W^{7/24}}{d}\right)^{0.432} \qquad \left\{\begin{matrix} \text{True Camouflet} \\ \text{Depth} \end{matrix}\right\} \qquad (5.27b)$$

$$\frac{V_T^{1/3}}{d} = 1.718 \left(\frac{W^{7/24}}{d}\right)^{0.865} \qquad \left\{\begin{matrix} \text{True Camouflet} \\ \text{Volume} \end{matrix}\right\} \qquad (5.27c)$$

One standard deviation for all of these scaled true camouflet dimensions also equals essentially 12 percent. Notice now that gravitational effects and compressibility effects both matter, so a $W^{7/24}/d$ law is followed.

Apparent crater dimensions also follow a $W^{7/24}/d$ law. Because apparent craters can be either cylindrically shaped or hemispherically shaped, the prediction equations are not log-linear relationships. Figures 5.14, 5.15, and 5.16 show graphically obtained relationships for R_A/d, $V_A^{1/3}/d$, and D_A/d as functions of $W^{7/24}/d$. The test data compilation used in these figures came from Reference 5.24. The greater depth of burial craters with $W^{7/24}/d$ less than 0.4 in these figures represent cylindrical as opposed to hemispherical craters. Although it is not shown in this compilation with different quantities of explosive in one soil (a desert alluvium), other soils including sand, clays, and rock also scatter randomly about the prediction lines given in Figures 5.14 through 5.16.

We present no prediction procedure for determining apparent camouflet size. The differences in true and apparent craters are much more difficult to determine in a camouflet as essentially all the soil in a camouflet is compressed rather than flung into the air as ejecta. True crater dimensions are a reasonable accurate measure of the extent of ground damage in a camouflet.

Historically the early work in the 1940's and 1950's advocated both $W^{1/4}/d$ and $W^{1/3}/d$ scaling laws for apparent crater. Another early investigator, Albert Chabai (Ref. 5.24), suggested a $W^{1/3.4}/d$ scaling law, but for practical purposes, $W^{7/24}/d$ equals $W^{1/3.4}/d$. If only small variations in charge weight were involved, using either the 1/3 or 1/4 exponent was sufficiently close to 1/3.4 for no apparent error to arise. Only in the mid-1960's after some nuclear cratering data became available to extend the range over which W had been varied, did the 1/3.4 or 7/24 exponent on energy release become universally accepted.

A final crater ejecta problem of interest is the determination of the maximum distance that ejecta will be flung. This information is obtained by scaling test results from References 5.18 and 5.25. Only a limited amount of data exist, but Figure 5.17 is for the maximum ejecta radius so that less than one missile per square foot exists beyond the radius given in Figure 5.17. For purposes of definition, a missile is defined as a soil chunk greater than approximately 2.0 in. in diameter. Notice that Figure 5.17 follows a $W^{7/24}/d$ rule as both gravitational and constitutive effects are important. Although some ejecta are flung beyond the distance given by Figure 5.17, we are forced to use these results as an approximation to the end of the ejecta field. Any absolute determination of the end of any ejecta field is impossible and would be a subjective opinion with different investigators.
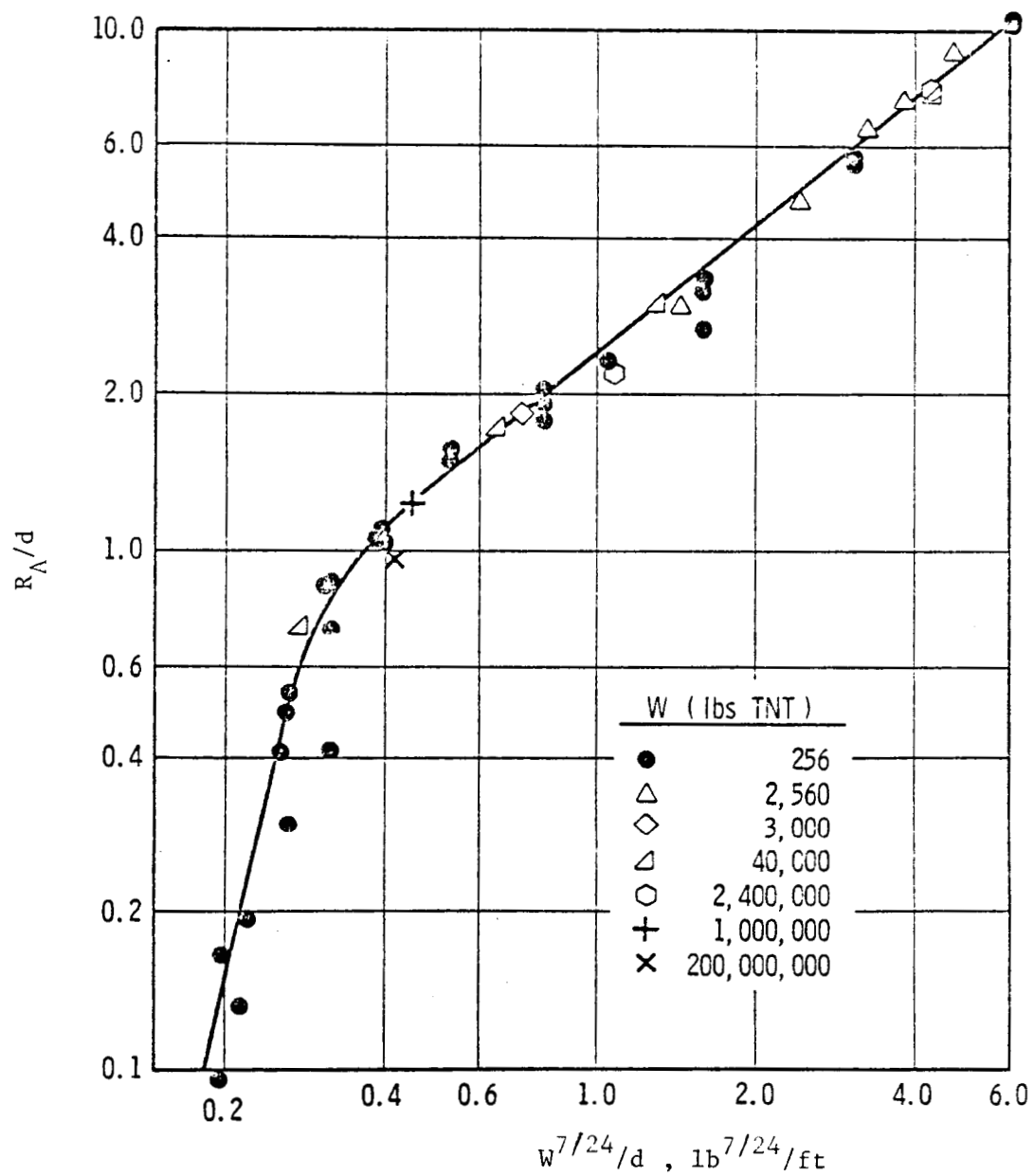
Figure 5.14   Apparent Crater Radius R_A/d versus $W^{7/24}/d$ in Alluvium
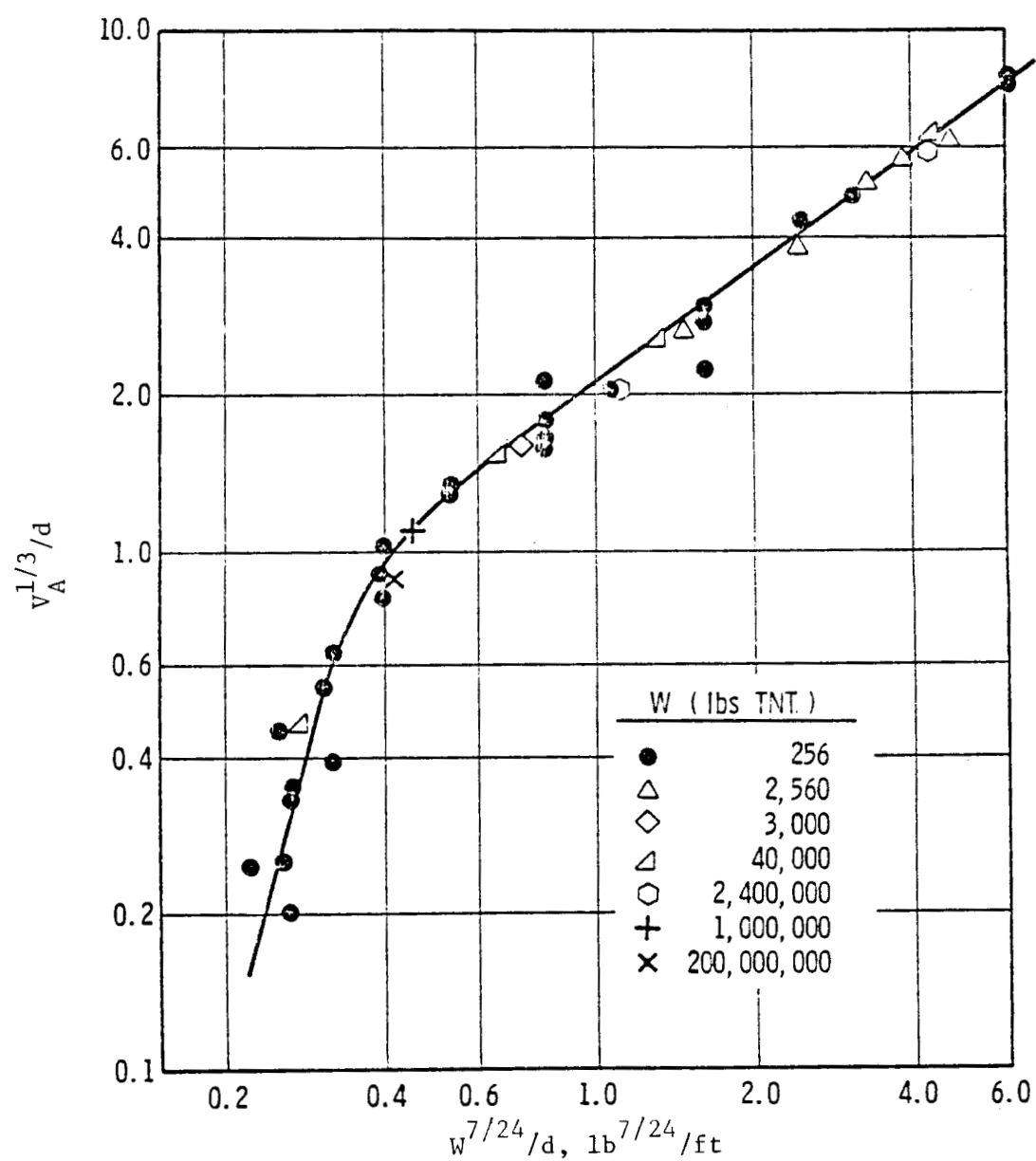
Figure 5.15 Apparent Crater Volume $V_A^{1/3}/d$ versus $W^{7/24}/d$ in Alluvium
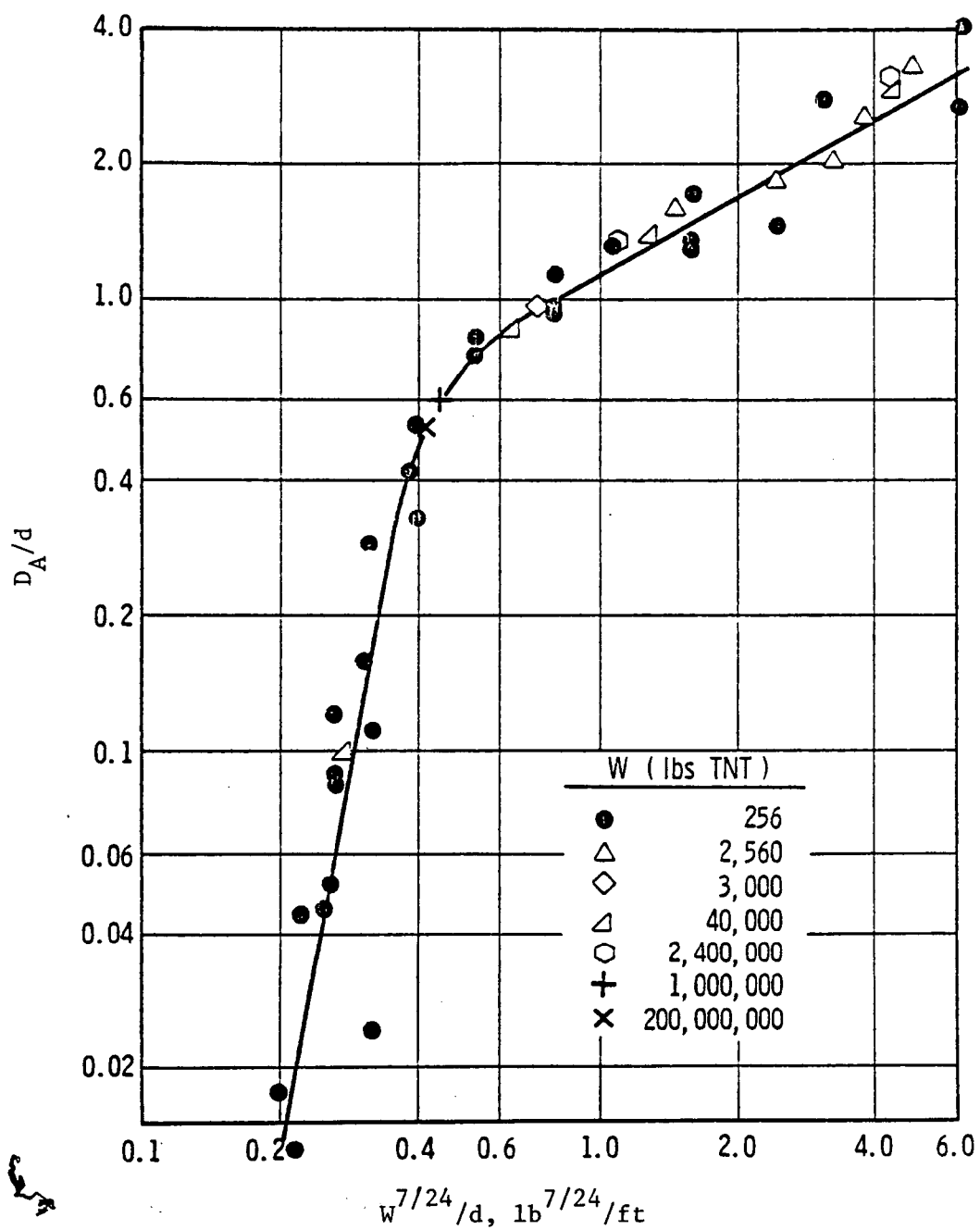
Figure 5.16 Apparent Crater Depth D_A/d versus $W^{7/24}/d$ in Alluvium
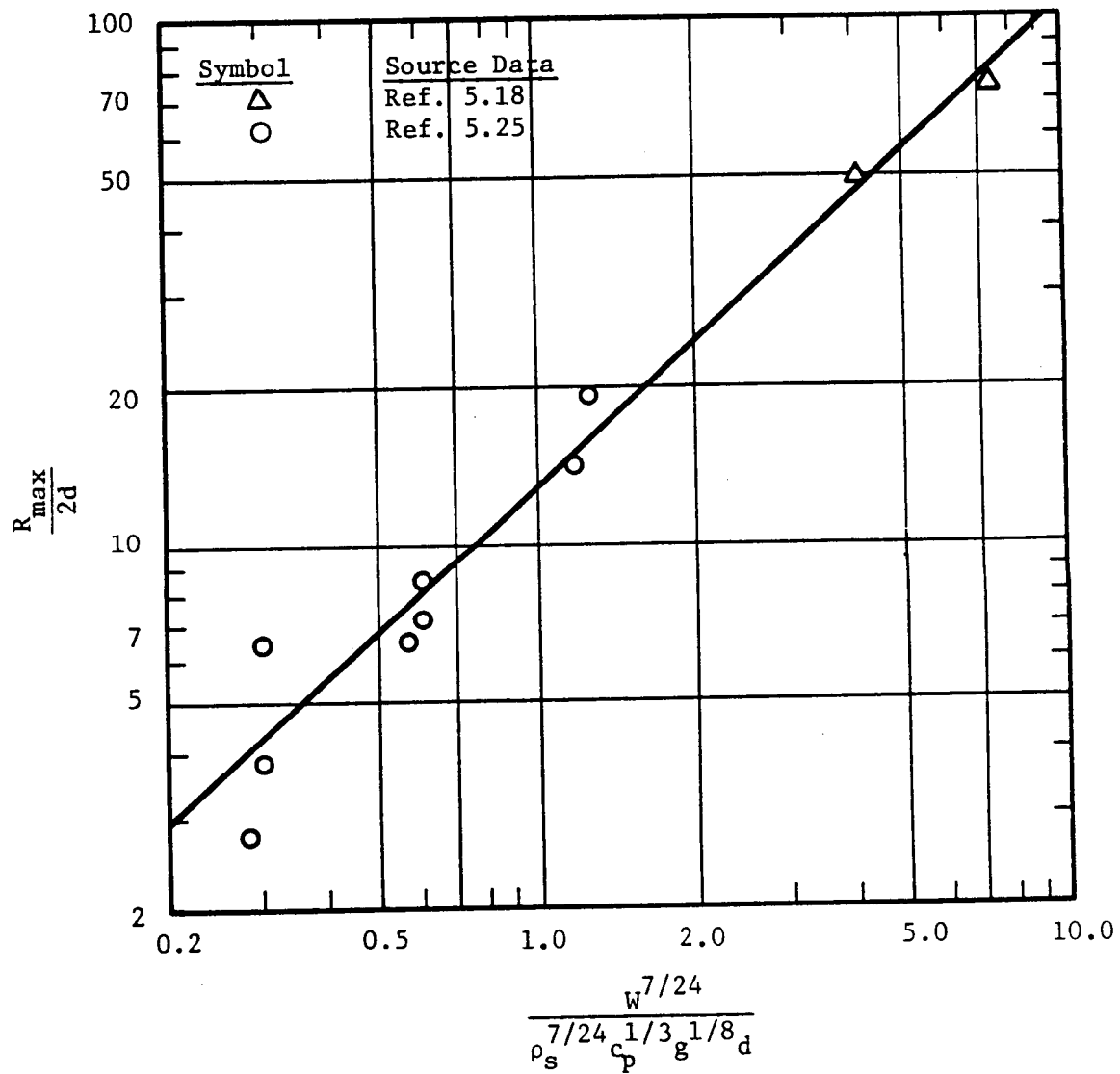
Figure 5.17   Maximum Ejecta Radii for Large Soil Chunks

Although we have not discussed the subject of cratering from surface bursts or cratering from air bursts, some empirical results can be found in Reference 5.26. For small conventional high explosive charges detonated above ground, cratering is insignificant. Generally, nuclear energy releases are needed for above-ground cratering to become significant.

To the best of our knowledge, no data or prediction procedure exists for estimating crater size or ejecta patterns when charges are detonated inside cavities within the earth. Further work is required in this area if a prediction procedure is to be developed.

EXAMPLE PROBLEM 5.6

PROBLEM – Assume that one wishes to determine whether a crater or a camouflet is formed when a buried charge is detonated. In addition, the true crater/camouflet and apparent crater/camouflet dimensions should be calculated.

GIVEN: W = charge weight (lb)
d = depth of burial (ft)

FIND: Crater/camouflet modes and dimensions   REFERENCE

SOLUTION:
1. Calculate X
   $$X = 4.605 + \ln \frac{W^{1/4}}{d}$$ Eq. (5.23)

2. Calculate Y
   $$Y = \left[6.438 + 1.398 \ln\left(\frac{W^{1/3}}{d}\right) \right] \tanh^5 \left[2.00 + 0.4343 \ln\left(\frac{W^{1/3}}{d}\right) \right]$$ Eq. (5.24)

3. Determine if a crater or camouflet is formed.
   a. If X is less than Y a crater is formed. Continue at Step 4.   Eq. (5.25b)
   b. If X is greater than Y a camouflet is formed. Continue at Step 5.   Eq. (5.25a)

4. Calculate the true crater dimensions.
   a. $\dfrac{R_T}{d} = 2.155 \left(\dfrac{W^{1/3}}{d}\right)^{0.865}$ (scaled radius)   Eq. (5.26a)

   b. $\dfrac{D_T}{d} = 2.312 \left(\dfrac{W^{1/3}}{d}\right)^{0.683}$ (scaled depth)   Eq. (5.25b)

   c. $\dfrac{V_T^{1/3}}{d} = 2.046 \left(\dfrac{W^{1/3}}{d}\right)^{0.785}$ (scaled volume)   Eq. (5.26c)

5. Calculate the true camouflet dimensions.
   a. $\dfrac{R_T}{d} = 1.053 \left(\dfrac{W^{7/24}}{d}\right)^{0.865}$ (scaled radius)   Eq. (5.27a)

   b. $\dfrac{D_T}{d} = 2.244 \left(\dfrac{W^{7/24}}{d}\right)^{0.432}$ (scaled depth)   Eq. (5.27b)

   c. $\dfrac{V_T^{1/3}}{d} = 1.718 \left(\dfrac{W^{7/24}}{d}\right)^{0.865}$ (scaled volume)   Eq. (5.27c)

6. Obtain apparent crater dimensions.   Figs. 5.14, 5.15, 5.16

5-50

CALCULATION

GIVEN: W = 500 lb
       d = 15 ft

FIND: Crater/camouflet mode and dimensions

SOLUTION:
1. $X = 4.605 + \ln\left(\dfrac{500^{1/4}}{15}\right) = 3.45$

2. $Y = \left[6.438 + 1.398 \ln\left(\dfrac{500^{1/3}}{15}\right)\right] \tanh^5\left[2.0 + 0.4343 \ln\left(\dfrac{500^{1/3}}{15}\right)\right]$

   $Y = 4.03$

3. $X < Y$, <u>therefore crater is formed.</u>

4. $\dfrac{R_T}{15} = 2.155 \left(\dfrac{500^{1/3}}{15}\right)^{0.865}$

   $R_T = \underline{18.6\ ft}$

   $\dfrac{D_T}{15} = 2.312 \left(\dfrac{500^{1/3}}{15}\right)^{0.683}$

   $D_T = 22.45\ ft$

   $\dfrac{V_T^{1/3}}{15} = 2.046 \left(\dfrac{500^{1/3}}{15}\right)^{0.785}$

   $V_T = \underline{6,456\ ft}^3$

6. Apparent crater dimensions:

   $R_A = 17.25\ ft$

   $D_A = 7.8\ ft$

   $V_A = \underline{3,375\ ft}^3$

EXAMPLE PROBLEM 5.7

PROBLEM – Assume that one also wishes to determine the maximum radius where significant amounts of ejecta will fall. The same charge and depth of burial can be used as in Example Problem 5.6.

GIVEN: W = charge yield (ft-lb)
       c_p = propagation velocity (ft/sec)
       ρ_s = mass density (lb-sec^2/ft^4)
       g = gravity (ft/sec^2)
       d = depth of burial (ft)

FIND: Maximum radius for crater ejecta

SOLUTION: 1. Calculate the abscissa for Figure 5.17.

$$\frac{W^{7/24}}{\rho_s^{7/24} \, c_p^{1/3} \, g^{1/8} \, d}$$

2. Find the value of the ordinate and determine the maximum range.   Fig. 5.17

CALCULATION

GIVEN: $W = 8.5 \times 10^8$ ft-lb (500 lb of explosive)
$c_p = 950$ ft/sec
$\rho_s = 3.54$ lb-sec^2/ft^4
$g = 32.2$ ft/sec^2
$d = 15$ ft

FIND: Maximum radius for crater ejecta

SOLUTION: 1. $\dfrac{W^{7/24}}{\rho_s^{7/24} \, c_p^{1/3} \, g^{1/8} \, d} = 1.22$

2. $\dfrac{R}{2d} = 15.5$; R = <u>465 ft</u>

5.6 EFFECTS OF GROUND MOTION ON BUILDINGS, EQUIPMENT AND PERSONNEL

5.6.1 Shock Spectra

Much work has been done on deciding when ground shocks are annoying to individuals and damage structures. Unfortunately, no overall concise criteria have arisen. Each investigator in the past has been concerned within narrow bounds that pertain to his particular problem. On occasion, the results from various investigators conflict with one another. In addition, there has been a tendency to mix sinusoidal or cyclic oscillations from machinery, traffic and railways with impulsive single-pulse sources such as explosions. In spite of these problems, some insight into the various criteria can be obtained by studying a single-degree-of-freedom, linearly elastic oscillator. The oscillator system seen in Figure 5.18 can be used to represent the effects of surface waves on a structure or person.
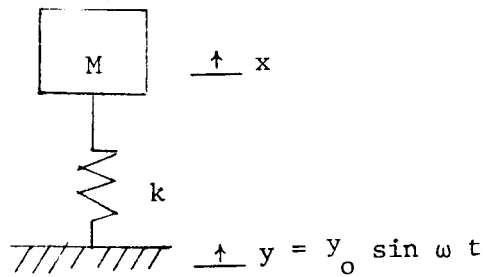
Figure 5.18 Qualitative Ground Oscillation Model

Usually one wishes to limit the maximum force imparted to the mass in this oscillator to values less than some specific threshold force, if buildings are not to be damaged and people are not to be annoyed. Because the maximum force in this oscillation equals $k(x-y)_{max}$, a maximum difference in displacement criterion can also be used as being equivalent to a limiting force, provided that limiting value is specified for each type of accident. Hence, we will proceed by limiting $(x-y)_{max}$ to certain magnitudes so explosives will not be jarred off of tables, plaster in buildings will not crack, or people will not be annoyed. The equation of motion for this oscillator is:

$$m \frac{d^2 x}{dt^2} + k x = k y_o \sin\omega t \tag{5.28}$$

If at time $t = 0$, x and $dx/dt = 0$, the difference in displacements will be given by:

$$(x-y) = \frac{y_o \omega^2}{\left(\frac{k}{m} - \omega^2\right)} \sin\omega t - \frac{y_o \omega \sqrt{\frac{k}{m}}}{\left(\frac{k}{m} - \omega^2\right)} \sin\sqrt{\frac{k}{m}}\, t \tag{5.29}$$

Equation (5.29) has two parts to the solution: the particular solution in which the natural frequency $\sqrt{k/m}$ of the oscillator predominates and the complementary solution where the frequency of the excitation ω predominates. Which sine term is most important depends upon two things: 1) damping, which we have not included in this solution, and 2) the nature of the excitation, whether it is a pulse or harmonic oscillation. If the system were to include damping and be heavily damped so that the particular solution is unimportant, or excited harmonically with insignificant start-up transients, the complementaty solution dominates and Equation (5.29) becomes:

$$(x-y) = \frac{y_o \omega^2}{\left(\frac{k}{m} - \omega^2\right)} \sin \omega t \qquad \binom{\text{complementary}}{\text{solution only}} \qquad (5.30)$$

For low frequency excitations with $\omega/\sqrt{k/m} \ll 1.0$, the maximum value for $(x-y)$ becomes:

$$\frac{\left(\frac{k}{m}\right)(x-y)_{max}}{(y_o \omega^2)} = 1.0 \qquad \text{for} \qquad \frac{\omega}{\sqrt{\frac{k}{m}}} \ll 1.0 \qquad \binom{\text{complementary}}{\text{solution only}} \qquad (5.31)$$

On the other hand, if the amount of damping is insignificant or the excitation is a short pulse so that start-up transients are important, then the particular solution dominates and Equation (5.29) becomes:

$$(x-y) = \frac{-y_o \omega \sqrt{\frac{k}{m}}}{\left(\frac{k}{m} - \omega^2\right)} \sin \sqrt{\frac{k}{m}} t \qquad \binom{\text{particular}}{\text{solution only}} \qquad (5.32)$$

Which when $\omega/\sqrt{k/m} \ll 1.0$ has a maximum absolute value for $(x-y)$ of:

$$\frac{\left(\sqrt{\frac{k}{m}}\right)(x-y)_{max}}{\left(y_o \omega\right)} = -1.0 \qquad \text{for} \qquad \frac{\omega}{\sqrt{\frac{k}{m}}} \ll 1.0 \qquad \binom{\text{particular}}{\text{solution only}} \qquad (5.33)$$

Equation (5.33), when the particular solution dominates, is a maximum particle velocity criterion, whereas Equation (5.31), when the complementary solution dominates, is a maximum acceleration criterion. Because both criteria relate to the maximum force imparted to the mass, one can see that, dependent upon the character of the excitation and amount of damping, either velocity or acceleration of the ground can be the proper criterion for deciding when ground shock damages structures or disturbs people.

If $\omega/\sqrt{k/m} \gg 1.0$, the complementary solution given by Equation (5.30) dominates and the maximum value of (x-y) is given by:

$$\frac{(x-y)_{max}}{y_o} = 1.0 \qquad \text{for} \qquad \frac{\omega}{\sqrt{\frac{k}{m}}} \gg 1.0 \qquad (5.34)$$

Equation (5.34) shows that for high frequencies the criterion can become a displacement criteria. For oscillations, this situation is seldom encountered as engineers usually design structures with $\omega/\sqrt{k/m} < 1.0$ so no resonance will be experienced should higher harmonics be excited. Naturally, when accidents occur, $\omega/\sqrt{k/m}$ can be unintentionally greater than 1.0, and a displacement criterion might arise. Those interested in learning more about shock spectra and their derivation should read Reference 5.27.

These computations for the response of a linear-elastic oscillator can be shown graphically using shock spectra as criteria for damaging structures or annoying people because of ground shock. All of these shock spectra present a limiting velocity, acceleration, or displacement for some band of excitation frequencies. Some of the earliest of these were criteria for annoying people.

Various investigators have inferred that people begin to perceive vibration, clearly perceive vibrations, or are annoyed based on a ground velocity of vibration criteria. Plotted in Figure 5.19 are vibration data summarized by Steffens (Ref. 5.28) for vibrations from traffic, railways, pile driving, and machinery. As can be seen, Steffens would conclude that ground velocities between 0.01 to 0.03 in./sec are just perceptible, 0.03 in./sec and 0.10 in./sec are clearly perceptible, and over 0.10 in./sec are annoying. The frequencies are fairly low in Figure 5.19 (less than 80 Hz) and would indicate that our qualitatively derived velocity criterion for constant differences in displacement of the ground and c.g. of the responding system are correct. Because our system is a linear-elastic oscillator, the criterion of a constant difference in displacements is also a statement that the peak force imparted to the mass is a constant, and that the peak acceleration experienced by the mass is also constant.

Reiher and Meister (Ref. 5.29) would concur with the results given in Figure 5.19. Actually, Steffens followed Reiher and Meister and decided that their conclusions covered reasonably well all values given by others. Reiher and Meister indicate that a peak ground velocity of 0.01 in./sec is the threshold of being barely noticeable; whereas, 0.10 in./sec is the threshold of being troublesome.
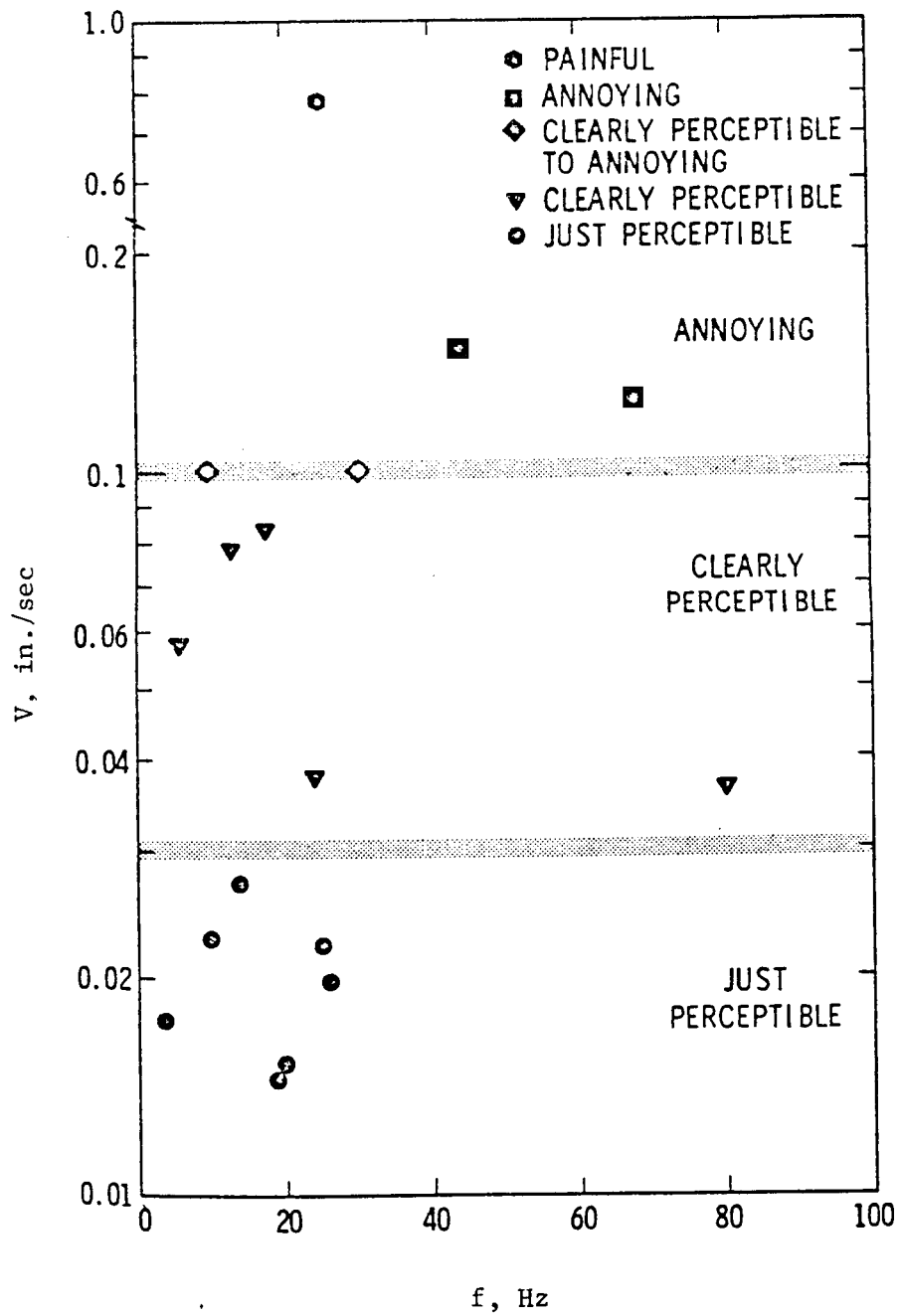
Figure 5.19   Human Thresholds for Ground Vibrations (Reference 5.28)

In 1943 Rausch (Ref. 5.30) presented steady-state vibration criteria for safe operation of machinery. At very low frequencies below 33 Hz Rausch's criterion is a peak velocity one of 1.0 in./sec (Equation 5.33, particular solution); however, at slightly higher frequencies over 33 Hz, he uses a peak soil acceleration criterion of 0.5 g (Equation 5.31, complementary solution). Because machinery involves steady-state vibrations in which the complementary solution definitely becomes important, an acceleration criterion makes sense.

A convenient method of presenting various investigators' vibration data on annoying people is a shock spectra diagram as seen in Figure 5.20. This diagram simultaneously shows limiting displacement, velocity, and acceleration values and the associated frequencies. Points falling above limiting values violate "failure" criterion, while points falling below represent satisfactory conditions. Figure 5.20 gives the limiting conditions of: 1) Reiher and Meister for shocks being barely noticeable to people and for being troublesome to people, 2) Rausch for vibrating machines and machinery foundations, and 3) the U. S. Bureau of Mines for blasting, even though their limits were generated using vibrators. The existence of very low frequency velocity response criteria and higher frequency acceleration criteria are apparent in Figure 5.20.

Besides annoying people, the damaging of buildings can be an important, and for some scenarios more important, accidental explosion consideration. Numerous investigators have conducted experiments and proposed criteria for protecting structures. This work will be reviewed so that these efforts can be brought into perspective.

The Bureau of Mines (Ref. 5.14) conducted experiments in 1942 because of damage and litigation arising from the detonation of buried explosive charges. Because the Bureau had difficulty locating structures which could be blast loaded to damage, 13 tests were conducted using a mechanical vibrator with an unbalanced rotor. Force and frequency were adjusted with upper limits of 1000 pounds and 40 Hz, respectively. The Bureau report based upon these results recommended an acceleration criterion with no damage at less than 0.1 g's, minor damage between 0.1 and 1.0 g's, and major damage at greater than 1.0 g's. These Bureau of Mines results were later to become a subject of controversy as Duvall and Fogelson (Ref. 5.31) used these same data to show statistically that major damage correlated with acceleration.

In the Boston Society of Civil Engineers (Ref. 5.32), Crandell proposed a constant velocity criterion for protecting structures from blasting. His lower limit for caution to structures corresponds to a peak ground velocity of approximately 3.0 in./sec. Crandell used test
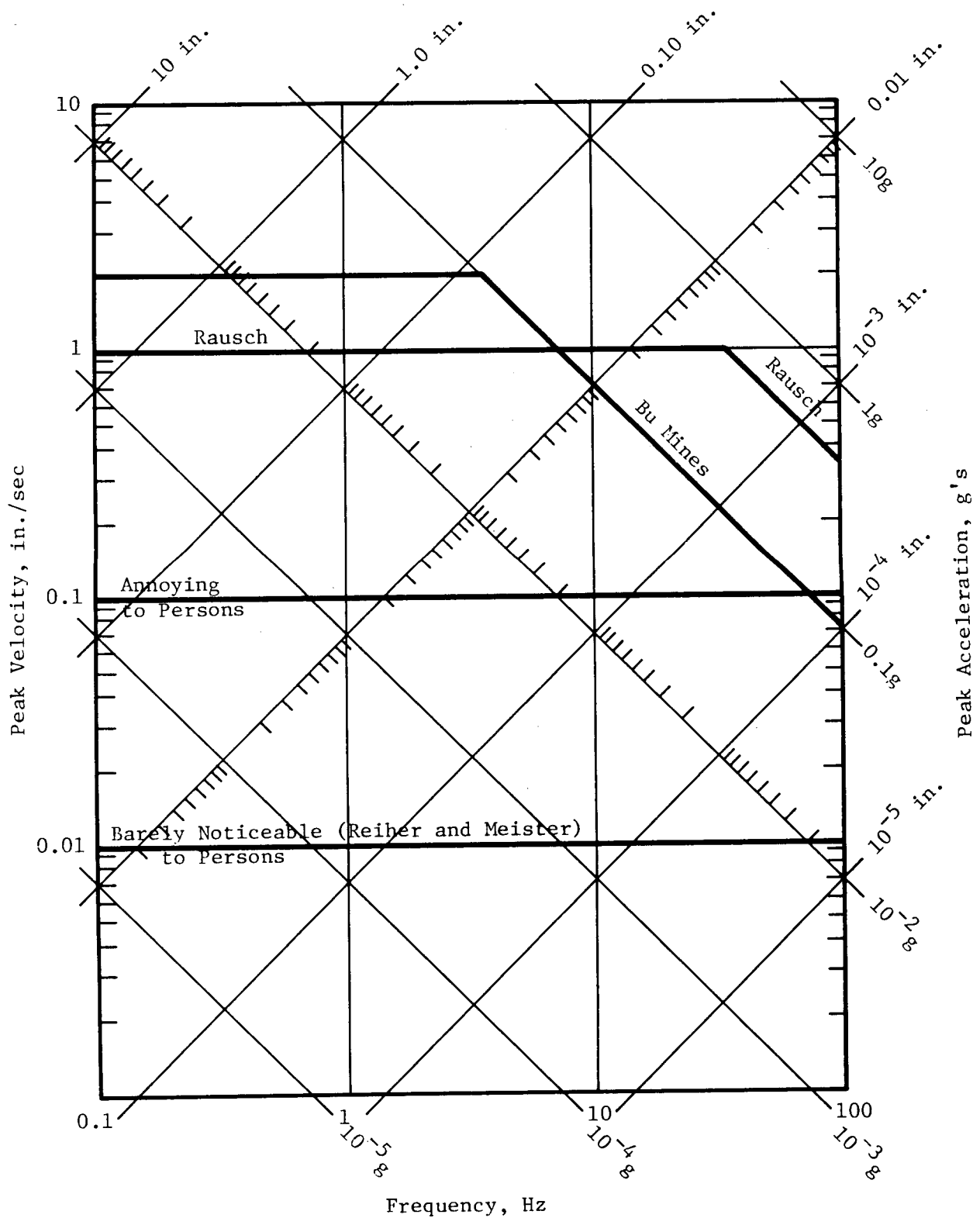
Figure 5.20 Shock Spectra Diagram

results to relate this velocity (he calls it an energy ratio) to standoff distance, charge weight, and a ground transmission constant. Many state codes are based upon this work.

In the State of Texas, interim blasting standards promulgated by the U. S. Department of the Interior and published in the Federal Register on December 13, 1977, were tentatively adopted by the Texas Railroad Commission in February of 1978. The U. S. Department of the Interior made the interim blasting standard final in the Federal Register of March 13, 1979. Final adoption by the Texas Railroad Commission was made in November 1979 in Coal Mining Regulations for the Surface Mining Division. Both the interim and final blasting standards limit maximum peak particle velocity of the ground motion in any direction to one in./sec at the location of any usable building. Arguments at the pre-adoption hearing for a two in./sec "limiting" velocity were presented, but were rejected. Both the interim and the final permanent regulations use a form of Morris' equation (Ref. 5.11) to relate the charge weight (W in pounds of explosive) and the standoff distance (D in feet).

$$W = \left(\frac{D}{60}\right)^2 \qquad (5.35)$$

This equation need not be used where a seismograph has been installed to monitor particle velocity, which still should not exceed one in./sec. Inside the grounds owned or leased by the party doing the blasting, that person does not have to adhere to the maximum peak particle velocity limitation. This regulation is to protect neighboring parties and not the blaster himself from the consequences of ground shock.

In Sweden (Ref. 5.33) a large data base was accumulated during a reconstruction project requiring blasting near buildings. Because large blasts were desired for economy of operation, a policy was adopted whereby minor damage, which could be replaced at moderate cost, was acceptable. Thus, these investigators were able to record and analyze a large amount of data on actual damage to buildings from more than 100 blasting tests.

By and large, these Swedish frequencies were higher than those recorded elsewhere, 50 to 500 Hz. Once again, particle velocity became the best damage criterion for failure of plaster. Velocities of 2.8 in./sec resulted in no noticeable damage, 4.3 in./sec in fine cracking and fall of plaster, 6.3 in./sec in cracking, and 9.1 in./sec in serious cracking.

Edwards and Northwood (Ref. 5.34) conducted controlled blasting tests on six residences slated for removal for the St. Lawrence River Power Project. Acceleration, particle velocity, and displacement were all measured for charges ranging from 47 to 750 lb buried at depths of 15 to 30 ft at various distances from their buildings. Frequencies ranged

from 3 to 30 Hz. They concluded that damage was more closely related to velocity than displacement or acceleration, and that 4 to 5 in./sec was likely to cause damage. A safe vibration limit of 2.0 in./sec was recommended based on this study.

In Czechoslovakia (Ref. 5.35), Dvorak published results for buried explosive charges of 2 to 40 lb placed 16 to 100 ft from one to two-story brick buildings. His frequencies were in the range of 1.5 to 15 Hz. Dovak concluded that threshold damage occurred at particle velocities between 0.4 to 1.2 in./sec, minor damage at 1.2 to 2.4 in./sec and major damage above 2.4 in./sec.

Now that all these building damage threshold criteria have been discussed, the question arises as to which are best. For ground shock from blasts or impacts, a velocity criterion is most appropriate in the low frequency domain. Of the criteria discussed, only Rausch (Ref. 5.30) and Bureau of Mines (Ref. 5.14) have an acceleration domain. Both of these groups of experiments were largely based upon vibrations, either from machinery or from vibrators. The point which we would make is that steady-state vibrations can result in the complementary solution being dominant. We have shown that the complementary solution in Equation (5.29) can lead to an acceleration criterion. On the other hand, single pulses should have a significant particular solution. A particular solution leads to a velocity criterion in the low frequency domain. All of the other data bases with explosions as a source for test results have velocity criteria. This result seems correct, and one should not be disturbed by different velocity criteria having been obtained by different investigators. Equation (5.33) shows that $(x-y)_{max}$ is not a function of only velocity $(y_o \omega)$, but rather it is a function of $(y_o \omega)/\sqrt{k/m}$. Naturally, different locations and structural configurations can have a variety of natural structural frequencies $\sqrt{k/m}$.

One of the best summaries of low frequency blasting criteria was put together by Nicholls et al. (Ref. 5.36). Basically, Nicholls took the three best data sources--Thoenen and Windes (Ref. 5.14), Langefors et al. (Ref. 5.33), and Edwards and Northwood (Ref. 5.34)--to show a composite plot of displacement amplitude versus frequency data. Three degrees of structural damage severity were considered: no damage, minor damage such as new crack formation or opening of old cracks, and major damage such as serious cracking and fall of plaster. These data cover a wide range in frequencies from a low of 2.5 to 28 Hz for the Edwards and Northwood St. Lawrence Project to a high of 46 to 450 Hz for the Langefors et al. Swedish data. The Thoenen and Windes Bureau of Mines data fall in between at 7 to 40 Hz. Figure 5.21 shows this displacement versus frequency plot of Nicholls. Notice that after conducting a regression analysis, the slope of the lines for the different degrees of damage are all constant velocity curves. The magnitude of the particle
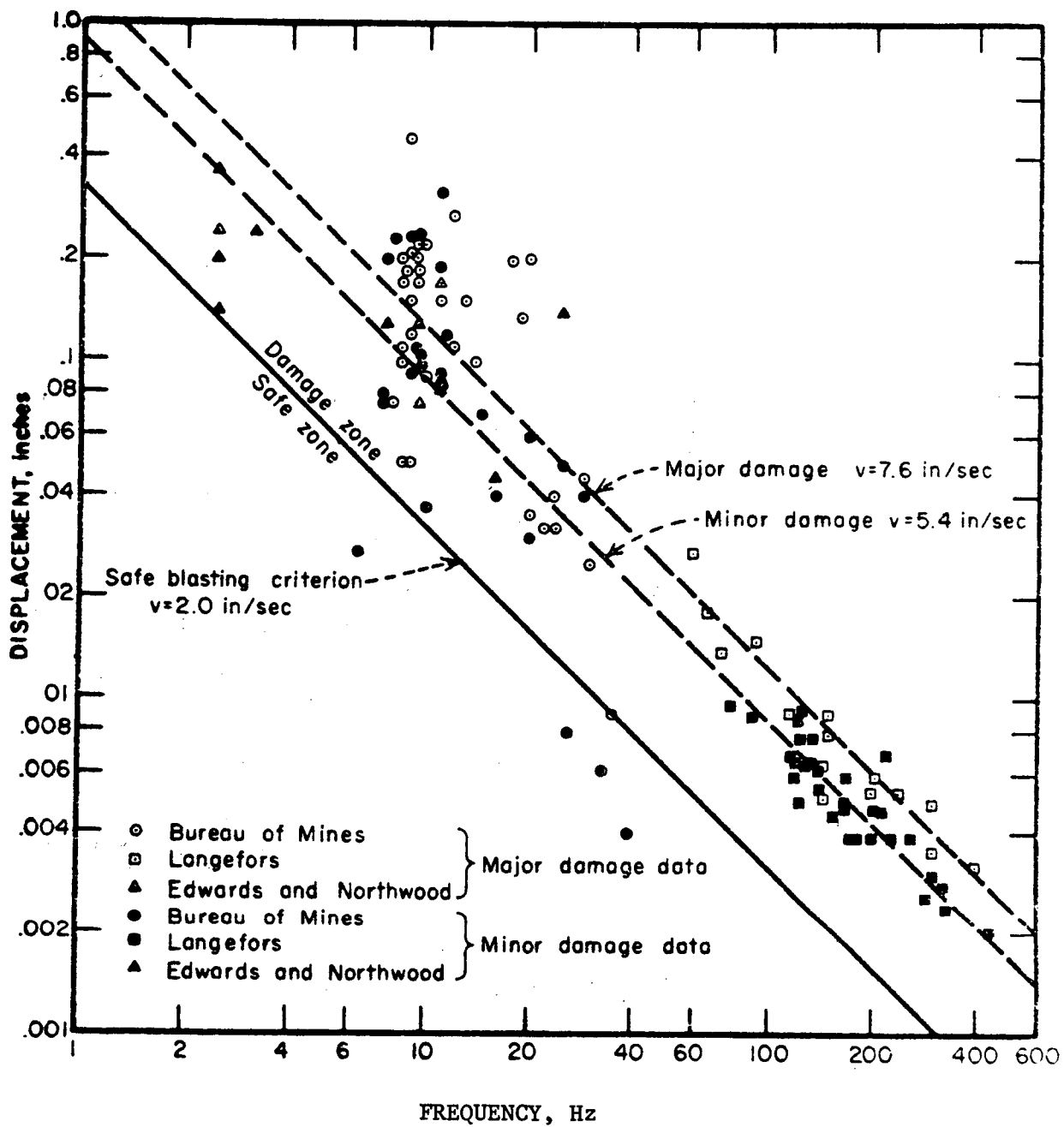
Figure 5.21   Displacement versus Frequency, Combined Data
with Recommended Safe Blasting Criterion
(Ref. 5.35)

velocity for major damage is 7.6 in./sec. The minor structural damage
threshold velocity of 5.4 in./sec is based almost exclusively on the
Swedish data (Ref. 5.33) as the results of others were found to be statis-
tically inconclusive. Both major and minor damage results in Figure 5.21
would reject a displacement slope of 0 or acceleration slope of -2.
In Figure 5.21, the outer limit for safe blasting could not be obtained
statistically, but the safe zone particle velocity of 2.0 in./sec
recommended by Duvall and Fogelson (Ref. 5.31) is shown and seems
reasonable.

The results shown in Figure 5.21 are recommended for use in
Pantex safety studies as they are based upon an evaluation of the largest
data base and the results reach the correct theoretical limit for low
frequency ground shock from blasting. In using the results in Figure
5.21 remember that the criterion actually involves both the velocity
($y_o\omega$) and the natural frequency of the structure ($\sqrt{k/m}$). In Figure
5.21, the upper frequency bound is 450 Hz; however, this bound is based
upon buildings in Sweden as tested by Langefors (Ref. 5.33). If the
buildings of interest have other natural frequencies, the upper frequency
could be either greater or less than 450 Hz in other buildings.

In addition to the structural thresholds presented in Figure 5.21,
we would add the thresholds for annoying people or for being perceptible
given in Figure 5.19. The thresholds given in Figure 5.19 are not dangerous
ones; however, circumstances can arise where, in the interest of public
relations, the threat of bothering neighbors should be avoided.

For personnel exposed to air blast, ground shock is not a critical
injury-producing mechanism. Even for those within shelters, ground shock
should not be critical as both minor and major damage will be imparted
to structures before direct injury is imparted to individuals. Even though
the average human being is a very strong structure for resisting blast,
both the indirect and the direct injury scenarios must be the concern of
designers.

One shock spectrum mechanism which has not been discussed is the
effect of ground shock on mechanical or electrical equipment within struc-
tures. Equipment within a structure fails because of its own properties
and the loads which are transmitted through the structure to the casing
of the equipment itself. This problem is further complicated by the fact
that the equipment can be shock mounted or isolated through the proper
design of mounts. We will not solve this complicated problem in this
manual. One very approximate procedure does exist whereby free-field
shock spectrum are used rather than the shock spectra for individual
equipment items. This approach has the advantage of being simple,
but accuracy will suffer accordingly.

Odello and Price (Ref. 5.37) present an elementary free-field response spectrum diagram for damaging internal equipment when shocks are transmitted through a foundation. Figure 5.22 presents this shock spectrum which describes the capability of the base excitation to excite systems of various natural frequencies. All three domains (acceleration, velocity, and displacement) can be found in Figure 5.22. Odello and Price call the excitations pseudo-velocity, pseudo-displacement and pseudo-acceleration to emphasize that these bounds are approximate spectral bounds rather than true motions. To evaluate the response spectrum bounds for equipment vulnerability in blast-hardened structures, the authors recommend that: 1) the displacement boundary be increased by a factor of 1.6, 2) the velocity boundary be increased by a factor of 1.8, and 3) the acceleration boundary be increased by a factor of 2.0 whenever Figure 5.22 is used. Both the soft structure and hardened structure boundaries are shown in Figure 5.22.

Whenever data are available on the response spectra of specific equipment of concern, this information should be used rather than Figure 5.22 as these data should be more accurate. The information contained in Figure 5.22 is for equipment with specific natural frequencies. Equipment can be designed with springs that change the frequency or energy absorbing materials to dampen the response. Another simplifying assumption associated with Figure 5.22 is that structures tend to move with and experience the same shock levels as the ground. The nature of a building's foundation could significantly alter the soil-structure interaction and make this assumption invalid. Figure 5.22 should only be used as an approximate guide or indicator that equipment damage might be possible. The shock wave forms are too complex and the structure with internal equipment is too complicated to solve this problem in this manual by using other techniques.

Very little information is available on shock spectra for high frequency excitation. Generally, structures found on the surface of the earth are in a low frequency domain; however, buried bunkers, buried arches, and buried pipe can respond to displacement (a high frequency criterion) because a large mass of earth combines with the mass of the structure to give a large value for $(\sqrt{m/k}\ \omega)$. Although not cast in the format of shock spectra, some results for these buried structures will be presented in subsequent sections.

Those interested in further discussion of shock spectra should read Eubanks and Juskie (Ref. 5.38). In addition to a generalized discussion, this reference contains shock test information for various equipment items such as fasteners, compressors, fans, heat exchangers, motors, pumps, valves, batteries, circuit breakers, fuseboxes, relays, rectifiers, switchboards, oscilloscopes, etc. It also contains a discussion on two-degree-of-freedom systems as would exist when an isolator
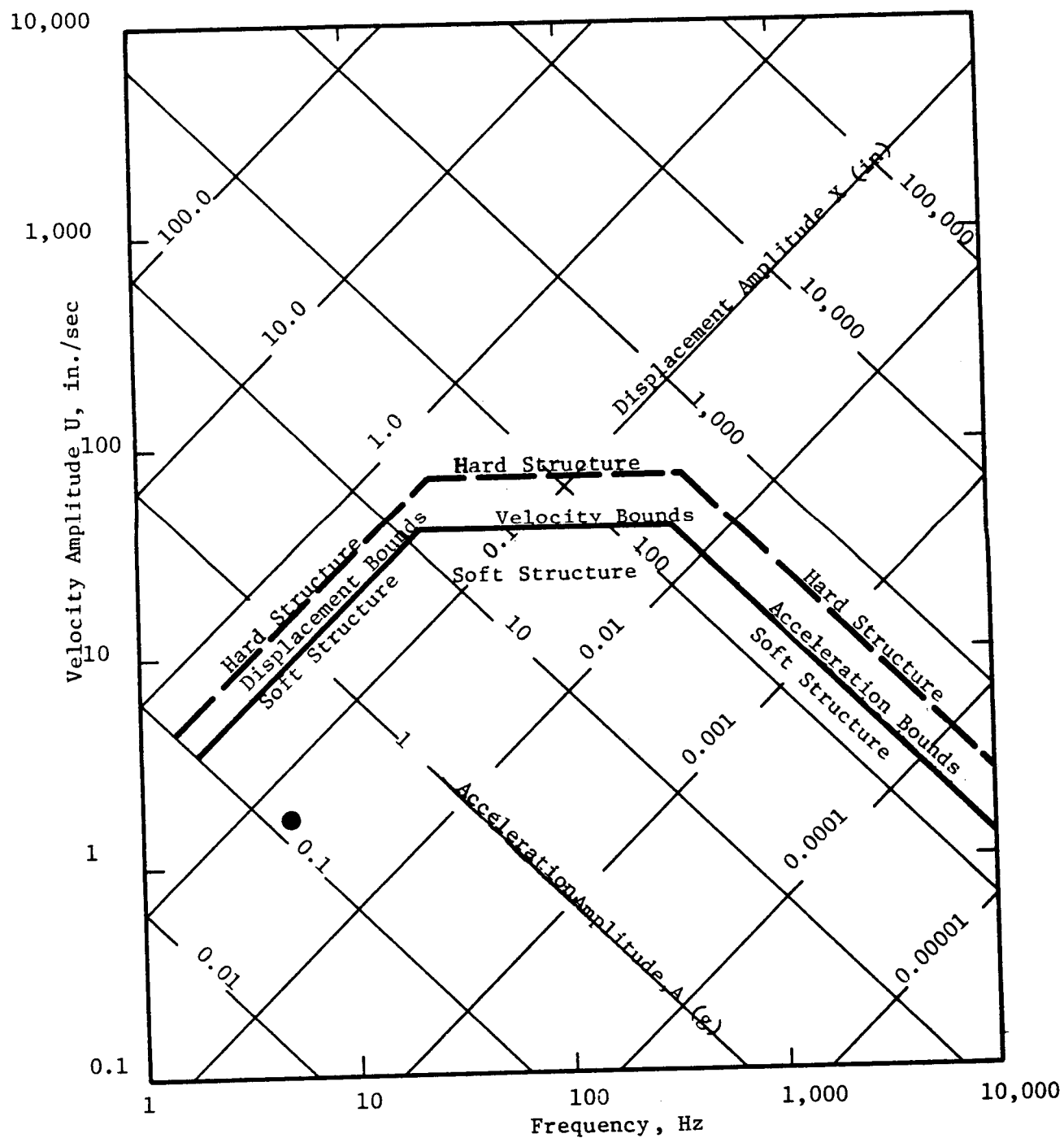
Figure 5.22. Shock Spectra for Damage Within a Structure (Ref. 5.37)

is inserted in series with the equipment and the source. A number of
Corps of Engineers studies (Refs. 5.39, 5.40, 5.41 and 5.42) have also
been conducted to determine the effects of ground shock on equipment inside
missile silos for the Safeguard Program. The reports from these studies
may be valuable if the possibility exists that internal equipment can be
damaged. Further details on shock isolation design are not presented as
they are beyond the scope of this manual.

PROBLEM – Assume that one wishes to determine whether: 1) structural damage, 2) disturbance of personnel, and 3) equipment damage inside hardened structures can occur due to a buried explosive detonation.

GIVEN: U_v = peak vertical particle velocity (in./sec)

X_v = maximum vertical displacement (in.)

NOTE: These values may be determined as described in Sections 5.3.1 and 5.3.2.

FIND: Effects of ground shock   REFERENCE

SOLUTION: 1. Calculate the period by rearranging
              Equation (5.8).

$$T = \frac{2\pi}{U_v} X_v$$ Eq. (5.8)

           2. Calculate the frequency.
              $f = 1/T$ Eq. (5.11)
           3. Determine whether structural damage will occur.   Fig. 5.21
           4. Determine whether personnel will be disturbed   Fig. 5.19
              by the shock.
           5. Determine whether damage will occur within the   Fig. 5.22
              structure.

CALCULATION

GIVEN: U_v = 1.978 in./sec

X_v = 0.0607 in.

FIND: Effects of ground shock

SOLUTION: 1. $T = \frac{2\pi}{U_v} X_v = 0.193$ sec

           2. $f = 1/T = 5.19$ Hz
           3. No damage will occur, but Figure 5.21 indicates that we
              are extremely close to the threshold for blasting safety.
           4. Figure 5.19 shows that the shock exceeds the threshold for
              annoying people.
           5. This case is marked on Figure 5.22 as a circled point at
              $U = 1.98$ in./sec and $f = 5.2$ Hz, which falls below the

threshold for both weak unhardened structures and hardened
structures. This means that no damage would be expected
for equipment in either unhardened or hardened structures.

This solution is a very approximate one; therefore, actual
accidents might yield other results.

5.6.2 Structural Loading from Ground Shock

Before stresses in a buried wall, pipe or shelter can be estimated by using structural response procedures as discussed in Chapter 8, the loads imparted to a buried structure have to be estimated. Although the loads and the resulting structural response are not decoupled problems, in this section we will treat them as decoupled by assuming that the buried object being loaded is rigid.

In Section 5.6.3, some approximate stress calculation procedures will be presented which bypass this procedure of estimating loads. Only approximate "order of magnitude" answers will be obtained using the results in Section 5.6.3. These procedures for estimating loads are needed as an intermediate step when more sophisticated procedures are used to determine stresses in buried structures.

5.6.2.1 Load on Buried Wall

Earlier discussions showed how to estimate soil particle velocity U and soil displacement X in the free field. Once the ground motion U and X are known, the free-field pressure P_s and i_s are also known using Equations (5.6) and (5.7), respectively. A structure buried in the ground does not "feel" the free-field pressures and impulses; it "feels" the reflected pressures and impulses. This process is directly analogous to a structure in air feeling reflected pressures and impulses rather than side-on or free-field ones. The major difference is that over a much larger range, the normally reflected pressures and impulses imparted to a buried object in soil will be much closer to the lower acoustic limit of 2.0 times free-field ones. This effect is caused by soil particles being much denser than air. For all practical buried structure applications, a factor of 2.0 will be used automatically so no nonlinear approximations need to be developed.

The other major difference in studying structural response in buried structures is that a large mass of earth will move along with the walls of a shock-loaded buried structure. Generally, this mass of earth far exceeds any mass in the structure itself. As a rule of thumb, the mass of earth moving with the structure can be approximated as that mass of earth between the charge and the structure itself. This rule of thumb applies for detonations both overhead and off to the side.

Probably the best way of illustrating the load imparted to a buried structure is to use an example. This will be done by estimating the load imparted to a beam-like strip out of a wall loaded with a buried detonation as in Figure 5.23. The load imparted to the strip will not be uniform as the standoff distances differ and only at mid-span is the loading normal to the beam. Assuming that the soil's particle motion is arrested by the beam, the peak reflected pressure for a target normal to a radial line from the charge is given by:

$$P_r = 2\rho_s c_p U$$
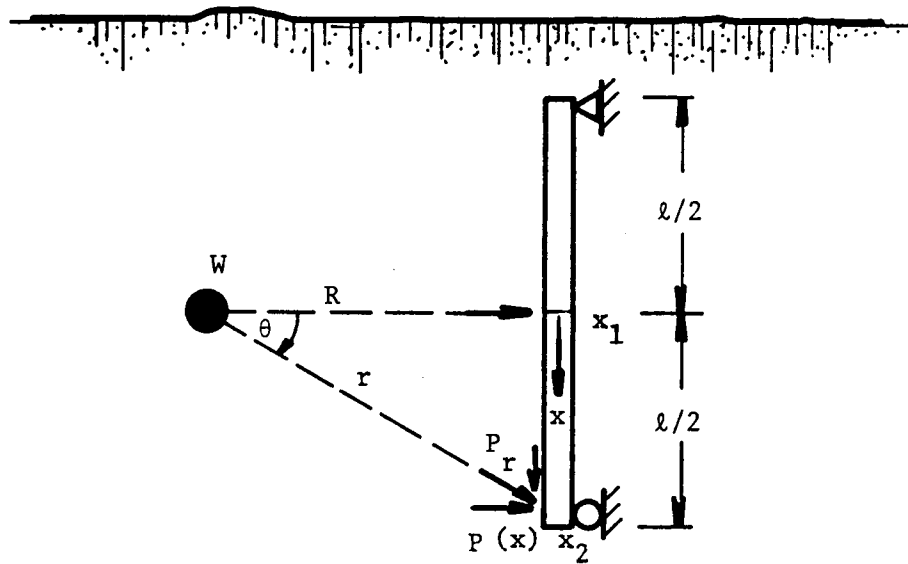
Figure 5.23   Example of a Load Imparted to a
Strip from a Buried Wall

and because U is given by:

$$\frac{U}{c_p}\left(\frac{P_o}{\rho_s c_p^2}\right)^{1/2} = \frac{6.169 \times 10^{-3}\left(\dfrac{W}{\rho_s c_p^2 r^3}\right)^{0.852}}{\tanh\left[26.03\left(\dfrac{W}{\rho_s c_p^2 r^3}\right)^{0.30}\right]} \tag{5.37}$$

The reflected pressure for a normally oriented target is:

$$\frac{P_r}{\rho_s c_p^2} = \frac{1.234 \times 10^{-2}\left(\dfrac{\rho_s c_p^2}{P_o}\right)^{1/2}\left(\dfrac{W}{\rho_s c_p^2 r^3}\right)^{0.852}}{\tanh\left[26.03\left(\dfrac{W}{\rho_s c_p^2 r^3}\right)^{0.30}\right]} \tag{5.38}$$

But targets are typically not normally oriented. At any point x, the normal component of the load to the beam is approximated by using the direction cosine. This assumption is not strictly valid especially when the angle equals 90 degrees; however, in any practical problem this condition will not occur. After substituting $\sqrt{R^2+x^2}$ for r, the peak pressure P(x) imparted to the beam at any point x is given by:

$$\frac{P(x)}{\rho_s c_p^2} = \frac{1.234 \times 10^{-2}\left(\dfrac{\rho_s c_p^2}{P_o}\right)^{1/2}\left(\dfrac{R}{\sqrt{R^2+x^2}}\right)\left(\dfrac{W}{\rho_s c_p^2 (R^2+x^2)^{3/2}}\right)^{0.852}}{\tanh\left[26.03\left(\dfrac{W}{\rho_s c_p^2 (R^2+x^2)^{3/2}}\right)^{0.30}\right]} \tag{5.39}$$

In a similar manner, the impulse distribution can also be determined. The major difference would be that

$$i_r = 2\rho_s c_p X \tag{5.40}$$

and

$$\frac{X}{r}\left(\frac{P_o}{\rho_s c_p^2}\right)^{1/2} = \frac{0.04143\left(\dfrac{W}{\rho_s c_p^2 r^3}\right)^{1.105}}{\tanh^{1.5}\left[18.24\left(\dfrac{W}{\rho_s c_p^2 r^3}\right)^{0.237}\right]} \tag{5.41}$$

At any point x the impulse i(x) imparted to the beam is given by:

$$\frac{i(x)}{\rho_s c_p R} = \frac{0.08286 \left(\dfrac{\rho_s c_p^2}{P_o}\right)^{1/2} \left(\dfrac{W}{\rho_s c_p^2 (R^2+x^2)^{3/2}}\right)^{1.105}}{\tanh^{1.5} \left[18.24 \left(\dfrac{W}{\rho_s c_p^2 (R^2+x^2)^{3/2}}\right)^{0.237}\right]} \qquad (5.42)$$

The only other consideration in any structural response compu-
tation is the addition of an added mass for soil. In this example, this
extra mass per unit length of strip would equal:

$$\begin{bmatrix} \text{Added mass} \\ \text{soil per} \\ \text{unit length} \end{bmatrix} = \rho_s bR \qquad (5.43)$$

where b is the loaded width of strip. Because $\rho_s bR$ is often much larger
than $\rho_{beam} A$, the added mass of earth is the important mass to the response
of a buried structure. Both frequency and amplitude of response will be
estimated much more accurately when this large effective mass is used.

Should the load sweep over the roof of the buried structure,
side-on or incident pressures and impulses should be used just as one
would consider orientation for air blast loadings. The most difficult
problems involve shielding of a portion or segment of a buried shelter.
When shielded so complex wave patterns are formed, we do not know the
actual loading and should the circumstances arise, tests have to be per-
formed. Full-scale expensive tests do not have to be performed; small
subscale replica model tests should work excellently and can give ground
shock loads with adequate accuracy for design purposes.

<u>EXAMPLE PROBLEM 5.9</u>

<u>PROBLEM</u> – Assume that one wishes to determine the peak reflected pressures and impulses at mid-span where a buried strip is normally loaded and at an arbitrary point on a beam strip. The geometry of where a buried charge is located relative to a strip from an outer wall of a buried bunker is illustrated in Figure 5.23.

<u>GIVEN</u>: W = explosive yield (ft-lb)
R = standoff (ft)
x = distance from point of normal loading to point of interest (ft)
c_p = propagation velocity (ft/sec)
ρ_s = mass density of soil (lb-sec^2/ft^4)
P_o = atmospheric pressure (lb/ft^2)

<u>FIND</u>: Loading on a buried beam   <u>REFERENCE</u>

<u>SOLUTION</u>:   1.   Calculate the following quantities.

$$\bar{P} = \frac{\rho_s c_p^2}{P_o} \ , \quad \bar{W} = \frac{W}{\rho_s c_p^2 R^3} \ , \quad \bar{W}_1 = \frac{W}{\rho_s c_p^2 (R^2+x^2)^{3/2}}$$

2.   Calculate the peak reflected pressure at the center of the strip.

$$\frac{P_r}{\rho_s c_p^2} = \frac{1.234 \times 10^{-2} \ (\bar{P})^{1/2} (\bar{W})^{0.852}}{\tanh [26.03(\bar{W})^{0.30}]}$$ Eq. (5.38)

3.   Calculate the peak reflected impulse at the center of the strip.

$$\frac{i_r}{\rho_s c_p R} = \frac{0.08286(\bar{P})^{1/2}(\bar{W})^{1.105}}{\tanh^{1.5}[18.24(\bar{W})^{0.237}]}$$ Eq. (5.42)

4.   Calculate the peak pressure at an arbitrary point (x).

$$\frac{P(x)}{\rho_s c_p^2} = \frac{1.234 \times 10^{-2}(\bar{P})^{1/2}\left(\dfrac{R}{\sqrt{R^2+x^2}}\right)(\bar{W}_1)^{0.852}}{\tanh [26.03(\bar{W}_1)^{0.30}]}$$ Eq. (5.39)

5.   Calculate the peak impulse at an arbitrary point (x).

$$\frac{i(x)}{\rho_s c_p R} = \frac{0.08286 \ (\bar{P})^{1/2} \ (\bar{W}_1)^{1.105}}{\tanh^{1.5}[18.24(\bar{W}_1)^{0.237}]}$$ Eq. (5.42)

CALCULATION

GIVEN:
$W = 6.84 \times 10^7$ ft-1b
$R = 50$ ft
$x = 10$ ft
$\rho_s = 3.54$ lb-sec^2/ft^4
$c_p = 950$ ft/sec
$P_o = 2,117$ lb/ft^2

FIND: Loading on buried beam

SOLUTION:

1. $\bar{P} = \rho_s c_p^2/P_o = 1,509$

   $\bar{W} = W/\rho_s c_p^2 R^3 = 1.71 \times 10^{-4}$

   $\bar{W}_1 = W/\rho_s c_p^2 (R^2+x^2)^{3/2} = 1.61 \times 10^{-4}$

2. $\dfrac{P_r}{3.54(950)^2} = \dfrac{1.234 \times 10^{-2} (1509)^{1/2} (1.71 \times 10^{-4})^{0.852}}{\tanh [26.03 (1.71 \times 10^{-4})^{0.30}]}$

   $P_r = 986$ lb/ft^2 = 6.85 psi

3. $\dfrac{i_r}{(3.54)(950)(50)} = \dfrac{0.8286(1509)^{1/2} (1.71 \times 10^{-4})^{1.105}}{\tanh^{1.5} [18.24(1.71 \times 10^{-4})^{0.237}]}$

   $i_r = 38.3$ lb-sec/ft^2 = 0.266 psi-sec

4. $P(x = 10$ ft$) = 921$ lb/ft^2 = 6.40 psi

5. $i(x = 10$ ft$) = 35.9$ lb-sec/ft^2 = 0.249 psi-sec

Change 1 - 15 August 1981

5.6.2.2 Load on Buried Pipe

Many pipes are buried in ground and can be deformed or fractured from buried accidental detonations. Actually, pipes are generally very tough structures; nevertheless, to analyze them, a load distribution is needed. Figure 5.24 from Reference 5.43 shows an assumed impulse distribution imparted to buried pipe. At the front of the pipe, the impulse and pressure will be normally reflected ones equal to 2 i_s or 2 P_s. At the top and bottom of the pipe, these loads will be incident or side-on ones. Although the exact distribution is not known between the front and top of the pipe, a convenient mathematical expression which can approximate this distribution and which goes to the correct limits is given by:

$$i = i_s \left(1 + \frac{2\theta}{\pi}\right) \qquad \text{for } 0 < \theta < \pi/2 \qquad (5.44)$$

$$P = P_s \left(1 + \frac{2\theta}{\pi}\right) \qquad \text{for } 0 < \theta < \pi/2 \qquad (5.45)$$

The back side of the pipe will also be loaded by the shock wave diffracting around the pipe. At $\theta = -\pi/2$ on the very rear surface of the pipe, the impulse exceeds i_s, but is probably less than 2 i_s. In Reference 5.43, this was solved by assuming the applied impulse equaled $(1 + m)$ i_s where m was some number between 0 and 1 which was to be obtained later from experimental test results. The test data in this reference indicate that the best value for $(1 + m)$ is 1.78. This same reflection factor can be used for pressures as well as for impulse. If a similar assumed distribution is used over the back of the pipe, the impulse and pressure relationships can be estimated by:

$$i = i_s \left(1 - \frac{1.56\theta}{\pi}\right) \qquad \text{for } 0 > \theta > -\pi/2 \qquad (5.46)$$

$$P = P_s \left(1 - \frac{1.56\theta}{\pi}\right) \qquad \text{for } 0 > \theta > -\pi/2 \qquad (5.47)$$

The negative sign appears in Equation (5.46) and (5.47) because the angle θ is measured in a negative direction. Although this solution was developed for pipes, it can also be used to determine the load distribution on buried arches.

$$i = i_s \left(1 + \frac{2\theta}{\pi}\right) \quad \text{for} \quad 0 < \theta < \frac{\pi}{2}$$

$$i = i_s \left(1 - \frac{1.56\theta}{\pi}\right) \quad \text{for} \quad 0 > \theta > -\frac{\pi}{2}$$
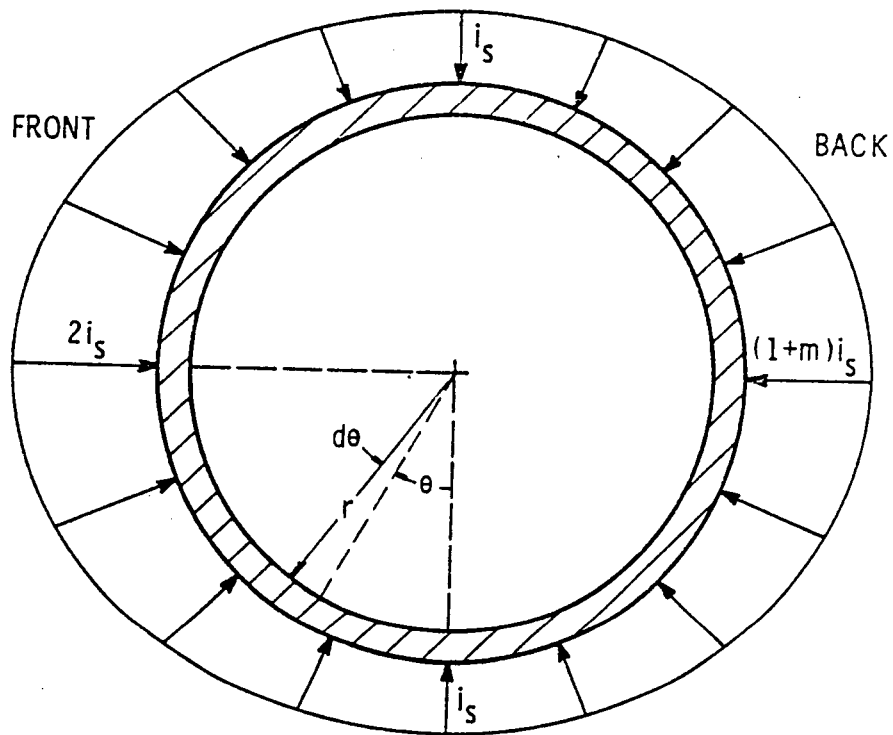
Figure 5.24 Assumed Distribution of Impulse Imparted to a Pipe

EXAMPLE PROBLEM 5.10

PROBLEM – Assume that one wishes to determine the maximum pressure at various points around a buried pipe subjected to ground shock.

GIVEN: U = peak radial particle velocity (ft/sec)
ρ_s = mass density (lb-sec^2/ft^4)

c_p = propagation velocity (ft/sec)
θ = angle to point of interest as defined in Figure 5.24

FIND: Ground shock pressure on buried pipe   REFERENCE

SOLUTION: 1. Calculate side-on pressure.
$$P_s = \rho_s c_p U$$ Eq. (5.6)
2. Calculate the pressure at various points around the pipe.
a. $P = P_s(1 + \frac{2\theta}{\pi})$ for $0 \leq \theta \leq \pi/2$ Eq. (5.46)

b. $P = P_s(1 - \frac{1.56\theta}{\pi})$ for $0 \geq \theta \geq -\pi/2$ Eq. (5.47)

CALCULATION

GIVEN: U = 0.125 ft/sec
ρ_s = 3.54 lb-sec^2/ft^4

c_p = 950 ft/sec
θ = +90°, +45°, 0°, -45°, -90°

FIND: Ground shock pressure on buried pipe

SOLUTION: 1. P_s = (3.54)(950)(0.125) = 420 lb/ft^2 = <u>2.92 psi</u>
2. P($\theta=\pi/2$) = <u>5.84 psi</u>
P($\pi/4$) = <u>4.38 psi</u>
P(0) = <u>2.29 psi</u>
P($-\pi/4$) = <u>4.06 psi</u>
P($-\pi/2$) = <u>5.20 psi</u>

5.6.3 Approximate Buried Structural Solutions

Now that the loading can be approximated, structural calculations can be made on any buried structural configuration. The type of structural engineering analysis which is required can depend upon what accuracy is needed and how well the source is defined. The most sophisticated and expensive analysis would be a finite element or finite difference multi-degree-of-freedom computer program. The least sophisticated solutions, but yet sufficiently accurate for some applications, involve either one-degree-of-freedom equivalent oscillators (called Bigg's Method) or energy solutions. We will not describe any of these techniques in detail as this information is found in Chapter 8; however, some approximate graphical solutions will be given which can provide first-order engineering estimates.

The first of these solutions is shown in Figure 5.25 for detonating a buried charge at some standoff near a buried beam-like member. First the ℓ/R ratio is computed so that the value of Y can be graphically determined. Then this value of Y is set equal to one of scaled-stress or strain quantities given in the insert to Figure 5.25. The proper Y quantity depends upon whether: 1) an elastic-bending solution, 2) a rigid plastic bending solution, or 3) an elastic extensional solution is being evaluated. Provided a self-consistent set of units is used, any system is acceptable because the scaled-stress and strain quantity Y is non-dimensional. To use this solution, be sure to convert the energy release over to energy units. If a cavity exists around the charge, be sure to convert the energy release to W_{eff} before substituting into this solution. The insert to Figure 5.25 graphically shows the problem being solved if uncertainty exists from this description. This solution has not been derived in any publications; however, the details of a similar solution for a surface burst are presented in the appendix to Baker, Garza, and Westine (Ref. 5.20).

The American Gas Association is interested in the stresses in buried pipes from underground blasting. Some curve fits to experimental test data given in Reference 5.43 can be used to estimate maximum elastic longitudinal and circumferential stresses caused by buried detonations. The solutions are conducted by first computing a quantity called $\bar{\sigma}$.

$$\bar{\sigma} = \frac{46.53 \sqrt{E} \ (W)}{\sqrt{h} \ R^{2.5}} \tag{5.48}$$

where R is standoff (ft)
      W is charge weight (lb)
      E is elastic modulus of pipe (psi)
      h is pipe thickness (in.)
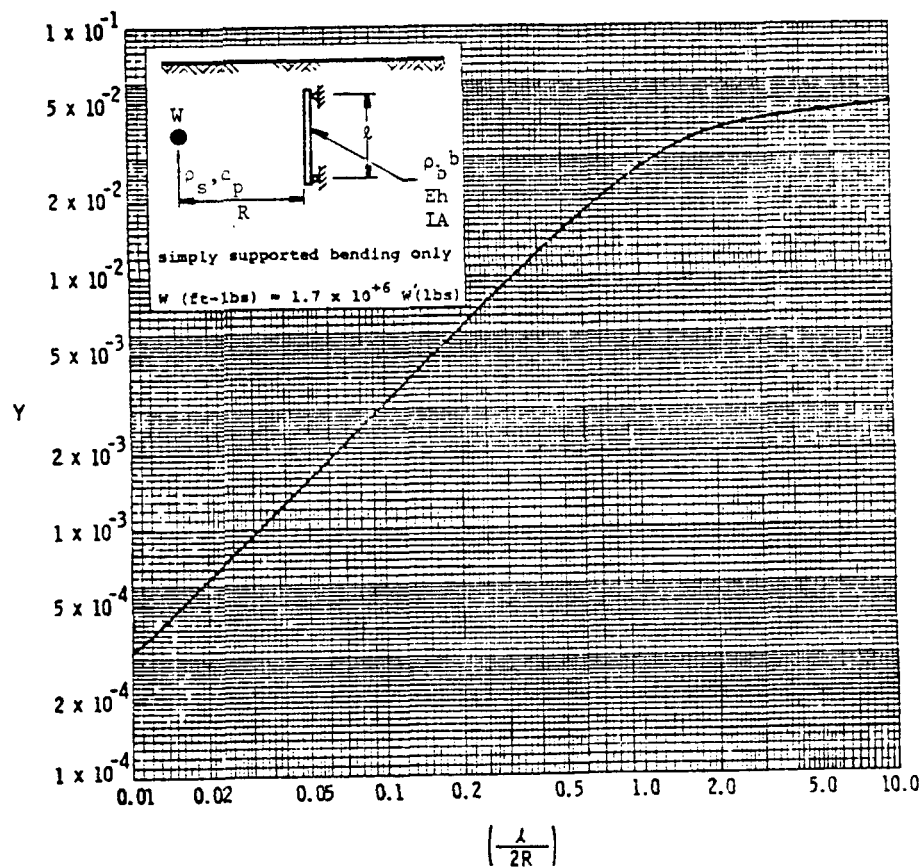
TABLE FOR Y

Type Response	Quantity
Elastic Bending	$\dfrac{759\ \sigma_{max}^2\ I\ \ell\ c_\rho^{1.52}\ R^{2.28}\ (\rho_s\ Kb + \rho_b\ A)}{E\ \rho_s^{0.24}\ w^{1.76}\ h^2\ b^2}$
Plastic Bending	$\dfrac{596\ \sigma_{max}\ \sigma_y\ Z\ \ell\ c_\rho^{1.52}\ R^{2.28}\ (\rho_s\ Rb + \rho_b\ A)}{\rho_s^{0.24}\ w^{1.76}\ b^2\ h}$
Elastic Extension	$\dfrac{4050\ \sigma_{max}^2\ A\ \ell\ c_\rho^{1.52}\ R^{2.28}\ (\rho_s\ Rb + \rho_b\ A)}{E\ \rho_s^{0.24}\ w^{1.76}\ b^2}$

Figure 5.25 Normal Stresses in Beam-Like Members

Then for $\bar{\sigma} < 2675$, the circumferential and longitudinal stresses in psi are given by:

$$\sigma_{cir} = 1.0 \, \bar{\sigma} \qquad \qquad \text{(5.49a)}$$
$$\text{for } \bar{\sigma} \leq 2675$$
$$\sigma_{long} = 0.253 \, \bar{\sigma}^{1.304} - \bar{\sigma} \qquad \qquad \text{(5.49b)}$$

For $\bar{\sigma} \geq 2675$, the circumferential and longitudinal stresses in psi are given by:

$$\sigma_{cir} = 21.7 \, \bar{\sigma}^{-0.740} - 47.55 \, \bar{\sigma}^{-0.584} \qquad \qquad \text{(5.50a)}$$
$$\text{for } \bar{\sigma} \geq 2675$$
$$\sigma_{long} = 47.55 \, \bar{\sigma}^{-0.584} \qquad \qquad \text{(5.50b)}$$

This solution gives only the elastic stress contribution from a buried detonation. If the pipe is pressurized or loaded through other mechanisms, these stresses would have to be superimposed on the blasting ones before the total state of maximum stresses could be determined in a pipe. These curve fits could also be used for detonations in a buried cavity or for a surface detonation; however, the appropriate coupling factors would have to be determined so that the equivalent buried charge could be determined.

The approximate solutions for determining stresses and strains in buried structures are only for simple rudimentary configurations such as beams and pipes. This is naturally so as other more complicated configurations associated with doors, connections, irregular structural configurations, and internal equipment do not lend themselves to idealized generalizations. The loading principles discussed in this section can still be used to understand the loading of these more complicated shapes, but more complex computational methods using multi-degree-of-freedom computer programs will be needed to determine stresses and strains adequate under these conditions.

PROBLEM – Assume that one wishes to compute the elastic bending stress in a beam-like strip taken from a buried wall which results when a buried charge is detonated.

GIVEN: R = standoff (in.)
        W = explosive yield (ft-lb)
        I = moment of inertia of area
        b = beam width (in.)
        h = beam thickness (in.)
        c_p = soil propagation velocity (in./sec)
        ρ_s = soil mass density (lb-sec^2/in.^{4})
        ℓ = length of beam (in.)
        E = modulus of elasticity (psi)
        ρ_b = mass density of beam (lb-sec^2/in.^{4})
        A = cross-sectional area of beam (in.^{2})

FIND: Elastic bending stress in beam from ground shock   REFERENCE

SOLUTION: 1. Calculate the abscissa for Figure 5.25.

$$\frac{\ell}{2R}$$

2. Find Y.   Fig. 5.25
3. Solve for σ_{max}.

$$Y = \frac{\sigma^2_{max}\ I\ \ell\ c_p^{1.52}\ R^{2.28}\ (\rho_s Rb + \rho_b A)}{759\ E\ \rho_s^{0.24}\ W^{1.76}\ h^2\ b^2}$$ Fig. 5.25

CALCULATION

GIVEN: W = 40 lb (1.7 x 10^6 ft-lb/lb) x 12 in./ft = 8.16 x 10^8 in.·lb
        R = 840 in.
        I = 5832 in.^{4}
        b = 12 in.
        h = 18 in.
        c_p= 11,400 in./sec
        ρ_s = 1.707 x 10^{-4} lb-sec^2/in.^{4}
        ℓ = 300 in.
        E = 5 x 10^6 psi
        ρ_b = 7.33 x 10^{-4} lb-sec^2/in.^{4}
        A = 216 in.^{2}

FIND: Elastic bending stress in beam from ground shock

SOLUTION: 1. $\ell/2R = 0.178$

2. $Y = 5.6 \times 10^{-3}$

3. $5.6 \times 10^{-3} = \dfrac{\sigma^2_{max} \, (5832)(300)(11{,}400)^{1.52}(840)^{2.28}[1.707 \times 10^{-4}(840)(12) + (216)(7.33 \times 10^{-4})]}{759 \, (5 \times 10^6) \, (1.707 \times 10^{-4})^{0.24} \, (8.16 \times 10^8)^{1.76} \, (1.8)^2 \, (12)^2}$

$\sigma_{max} = \underline{5396 \text{ psi}}$

EXAMPLE PROBLEM 5.12

PROBLEM – Assume that one wishes to estimate the circumferential and longitudinal stresses in a buried pipe subjected to blast loading from a buried explosive charge.

GIVEN: R = standoff (ft)
W = charge weight (lb)
E = elastic modulus of pipe (psi)
h = pipe thickness (in.)

FIND: Stresses in buried pipe from ground shock   REFERENCE

SOLUTION: 1.   Calculate $\bar{\sigma}$.   Eq. 5.48

$\bar{\sigma} = \dfrac{46.53 \sqrt{E} \, (W)}{\sqrt{h} \, R^{2.5}}$

2.   If $\bar{\sigma} \leq 2675$, continue at Step 3.   Eq. 5.49a
If $\bar{\sigma} \geq 2675$, continue at Step 4.   Eq. 5.49b

3. $\sigma_{cir} = 1.0 \, \bar{\sigma}$ Eq. 5.50a
$\sigma_{long} = 0.253 \, \bar{\sigma}^{1.304} - \bar{\sigma}$

4. $\sigma_{cir} = 21.7 \, \bar{\sigma}^{0.740} - 47.55 \, \bar{\sigma}^{0.584}$ Eq. 5.50b
$\sigma_{long} = 47.55 \, \bar{\sigma}^{0.584}$

CALCULATION

GIVEN: R = 70 ft
W = 40 lb
E = 30 x 10^6 psi
h = 0.344 in.

FIND: Stresses in buried pipe from ground shock

SOLUTION: 1. $\bar{\sigma} = \dfrac{46.53 \ (30 \times 10^6)^{1/2} \ (40)}{(0.344)^{1/2} \ (70)^{2.5}}$

$\bar{\sigma} = 424$

2. $424 < 2675$, continue at Step 3.

3. $\sigma_{cir} = 1.0 \ \bar{\sigma}$

$\sigma_{cir} = \underline{424 \ psi}$

$\sigma_{long} = 0.253 \ \bar{\sigma} \ 1.304 - \bar{\sigma}$

$\sigma_{long} = \underline{251 \ psi}$

5.7 FUTURE NEEDS

From the material contained in this section of the manual, we can see six problem areas which could be improved. The importance of each area differs dependent upon the application; hence, the order in which these recommendations are presented is insignificant.

1) Screening of Shock Waves

This problem can be calculated using large computer programs; however, the AE may not have such a computer program. The information presented in this text is limited in scope. Testing was for a specific condition without the corresponding effort to generalize test results so they could be more universally applied. A need exists for further work in this area if screening is to be used, but it is not considered to be effective at this time.

2) P-Wave Propagation

The solution which has been presented for R-waves is very inclusive and easy to use. A corresponding solution for P-waves should be possible and capable of development along similar lines. For Pantex, the development of such a solution is of less importance than it would be for soil mechanics in general. However, if detonations ever occur directly over a roof or directly under a structure, this P-wave solution would be essential.

3) Ejecta Radius

The data in Figure 5.17 are very limited in scope. The variation in explosive charge weight is not even one order of magnitude. Some extremely small scale tests (using gram charges) were performed at the University of Dayton, but the method of establishing the maximum crater radius was not the same. On an extremely small scale, ejecta can also become confused with dust on the floor. A thorough study might establish that 25 percent, 50 percent, 75 percent, 95 percent, etc. of the ejecta was within a scaled radius of some specific number. To the best of our knowledge, this detailed mapping has not been performed. The 7/24 scaling rule used on the current maximum ejecta radius in Figure 5.17 is based upon what the writer theoretically believes to be correct rather than a careful testing over a wide range in charge weight.

4) Cratering in a Cavity

A problem area which occurs at Pantex is cratering when the charge is within a cavity. The reader should notice that all cratering solutions were for charges in contact with the surrounding earth. Model tests might be possible to obtain the required data less

expensively, but the development of an analysis procedure should
accompany any test program.

5) Explosive Coupling

The solution which was presented for coupling appears to work
well; however, other viewpoints have been in existence. Un-
fortunately, this manual could not become a research project to
evaluate all approaches and decide which is best. We have
advocated one approach that looks reasonable. The solution
which was presented as Figure 5.10 could also be made more
accurate. A log linear approximation to the air blast reflected
pressure versus scaled standoff $R/W^{1/3}$ curve was made in the
region for the data in Figures 5.11 and 5.12 This approach
leads to a simple solution which is valid in the correct domain,
but the user can misuse the solution by applying it outside
the domain in which it is valid. The use of a more complicated
functional relationship for relating P_R to $R/W^{1/3}$ would lead to
a plot similar to that in Figure 5.10, but the function could be
made more accurate.

6) Shock Passage into Adjacent Bays

The actual problem of an accidental explosion in an underground
bay is a complex one. An air blast will load a concrete wall
which in turn will transmit a shock on into soil that eventually
will load another concrete wall, and finally will transmit a shock
into the adjacent air-filled room. The resulting effects of this
shock on equipment, parts, explosive, and personnel are the final
answer to a complex series of phenomena. Although this scenario
can represent an actual accident, it is not explicitly answered
using computations. At best, we crudely ignore the presence
of concrete walls and use shock spectra as an estimation of
internal adjacent bay conditions. If engineering calculations
are to be made more accurately, model testing and associated
work on analytical calculations will be required to study shock
transmission into adjacent bays.

5.8 FLOW DIAGRAM

Many different ground shock and cratering subproblems have been
presented and illustrative examples solved throughout this chapter. To
aid the analyst in gathering this information into a logical sequence,
Figure 5.26 is presented. Figure 5.26 is a flow diagram which begins
at the top with the definition of a Pantex ground shock problem and
leads throughout a series of yes-no questions and analysis blocks. Each
analysis block refers to some subsection in this section of the manual
where an analysis procedure and an example problem can be found. If
the arrows are followed into and out of each box in Figure 5.26, the
subsequent analysis should lead to an acceptable engineering design.
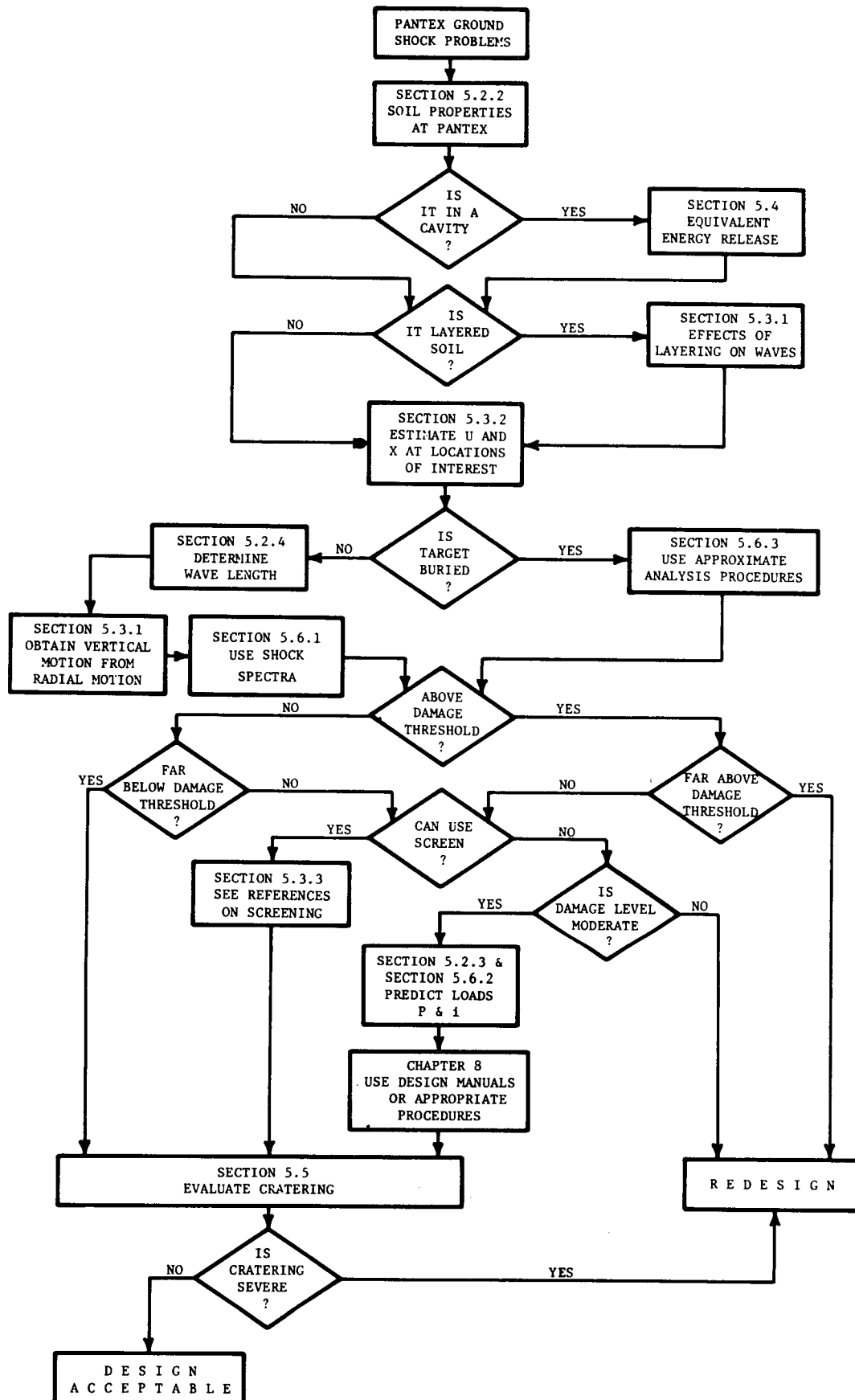
Figure 5.26   Flow Diagram of Pantex Ground Shock Problem

5.9 LIST OF SYMBOLS

A peak amplitude for velocity or displacement; total area

A_g area of gas-solid contact

A_s small area solid contact

A_w area of fluid-solid contact

a contact area; ratio of A_s/A

b loaded beam width

c propagation velocity

c_P P-wave propagation velocity

c_R R-wave propagation velocity; Rayleigh wave

c_s S-wave propagation velocity; Shear wave

c_a/c effective wave velocity divided by simple layer wave velocity because of a layered media

D_A/d scaled apparent crater depth

D_T/d scaled true crater depth

d depth of burial in soil

E modulus of elasticity

f frequency (Hz)

G shear modulus

g gravity

H/L thickness of top soil divided by wavelength

h thickness

I second moment of area

i_s	impulse in a shock wave
K	constant
k	spring constant
k/m	natural frequency
L	wavelength
L/H	wavelength divided by thickness of top soil
ℓ	length of beam
M	mass
N	constant exponent
P	load
P_r	peak reflected pressure
P_s	shock front pressure, peak side-on overpressure
P_g	stress or pressure in gas
P_o	atmospheric pressure
P_w	stress or pressure in water
R	standoff distance
R_A/d	scaled apparent crater
R_T/d	scaled true crater radius
R_o	radius of cavity
r	distance
T	time period
t	time

t_g thickness of gravel

U maximum radial soil particle velocity

U_v peak vertical particle velocity

V shock front velocity

$V_A^{1/3}/d$ scaled apparent crater volume

$V_T^{1/3}/d$ scaled true crater volume

W explosive energy release; charge yield; explosive weight

W_{eff} effective energy release; effective explosive weight

w ratio A_w/A

X maximum radial soil displacement

X_R maximum radial soil displacement, used when radial motion must be separated from vertical motion

X_V maximum vertical displacement

x position on beam in Figure 5.23

y_o maximum displacement

Y nondimensional stress as defined in the table associated with Figure 5.25

Greek Symbols

α constant

θ angle

ν Poisson's ratio

ρ mass density

ρ_a mass density behind the shock front

ρ_s mass density of the soil

$\bar{\sigma}$ effective stress

ω circular frequency (rad/sec)

5.10 REFERENCES

5.1 URS/John A. Blume & Associates, "Seismic Hazard and Building Structure Behavior at the Pantex Facility," April 1976.

5.2 Richart, F. E. Jr., Hall, J. R. Jr., and Woods, R. D., Vibration of Soils and Foundations, Prentice-Hall, Inc., Englewood Cliffs, New Jersey, 1970.

5.3 Lamb, H., "On the Propagation of Tremors Over the Surface of an Elastic Solid," Philosophical Transactions of Royal Society London, Series A, Volume 203, September 1904.

5.4 Barkan, D. D., Dynamics of Bases and Foundations, McGraw Hill Book Co., New York, NY, 1962.

5.5 Westine, P. S., "Ground Shock from the Detonation of Buried Explosives," Journal of Terramechanics, Vol. 15, No. 2, pp. 69-79, 1978.

5.6 Carder, D. S., and Cloud, W. K., "Surface Motion from Large Underground Explosions," J. Geophys. Res., 64, 1471-1487, 1959.

5.7 Crandell, F. J., "Transmission Coefficient for Ground Vibrations Due to Explosions," J. Boston Soc. Civil Engineering, 47, 152-168, 1960.

5.8 Habberjam, G. M. and Whetton, J. T., "On the Relationship Between Seismic and Amplitude and Charge of Explosive Fired in Routine Blasting Operations," Geophysics, 17, 116-128, Jan., 1952.

5.9 Hudson, D. E., Alford, J. L., and Iwan, W. D., "Ground Accelerations Caused by Large Quarry Blasts," Bull. Seismic Soc., A, 51, 191-202, 1961.

5.10 Ichiro, I., "On the Relationship Between Seismic Ground Amplitude and the Quantity of Explosives in Blasting," Reprint from Memoirs of the Faculty of Engineering, Kyoto University, 15, 579-587, 1953.

5.11 Morris, G., "The Reduction of Ground Vibrations from Blasting Operations," Engineering, pp. 460-465, April 1957.

5.12 Ricker, N., "The Form and Nature of Seismic Waves and the Structure of Seismograms," Geophysics 5, 348-366, 1940.

5.13 Teichmann, G. A., and Westwater, R., "Blasting and Associated Vibrations," Engineering, pp. 460-465, April 1957.

5.14 Thoenen, J. R., and Windes, S. L., "Seismic Effects of Quarry Blasting," _Bureau of Mines Bulletin_, 442, 83, 1942.

5.15 Willis, D. E. and Wilson, J. T., "Maximum Vertical Ground Displacement of Seismic Waves Generated by Explosive Blasts," _Bulletin Seismic Safety of America_, 50, 455-459, 1960.

5.16 Murphey, B. F., "Particle Motions Near Explosions in Halite," _Journal of Geophysical Research_, Vol. 66, No. 3, March 1961, pp. 947-958.

5.17 Woods, R. D., "Screening of Surface Waves in Soils," _Journal of Soil Mechanics and Foundations Division_, American Society of Civil Engineers, Vol. 94, No. SMS, pp. 951-979, July 1968.

5.18 Harvey, William, Dishan, John III, and Thomas, Tami, "Near-Surface Cratering Experiments, Fort Polk, Louisiana," U. S. Army Waterways Experiment Station, Livermore, CA, AFWL-TR-351, November 1975.

5.19 Ferritto, J. J. and Forrest, J. B., "Ground Motion from Pacific Cratering Experiments 1,000-Pound Explosive Shots: Data Supplement," U. S. Navy Civil Engineering Laboratory Technical Report R 8085, January 1975.

5.20 Baker, E. J., Garza, L. R. and Westine, P. S., "Development of a Design of a Relocatable Command and Control Bunker," Waterways Experiment Station Contractor Report N-77-1, March 1977.

5.21 Kvammen, Asbjorn Jr., Pichumani, Raman and Dick, James L. Jr., "Pavement Cratering Studies," Univ. of New Mexico, Eric H. Wang Research Facility Report for Air Force Weapons Laboratory, 1973.

5.22 Westine, Peter S., "Explosive Cratering," _Journal of Terramechanics_, VII, 2, pp. 9-19, 1970.

5.23 Westine, Peter S., "Bomb Crater Damage to Runways," Southwest Research Institute Contract F29601-72-C-0053 for Air Force Weapons Laboratory, February 1973.

5.24 Chabai, Albert J., "Crater Scaling Laws for Desert Alluvium," SC-4391, Sandia Corporation, Albuquerque, New Mexico, December 1965.

5.25 Rooke, Allen D. Jr., "Essex-Diamond Ore Research Program, Apparent Crater Measurements for Simulated, Low Yield Nuclear Explosions Project Essex I, Phases 1 and 2," Waterways Experiment Station, WES MP N-78-3, March 1978.

5.26 Anon, "Effects of Air Blast, Cratering, Ground Shock, and Radiation on Hardened Structures," Air Force Systems Command Manual, AFSCM 500-8, January 1976.

5.27 Thomson, W. T., _Mechanical Vibrations_, Prentice-Hall, New York, NY, 1948.

5.28 Steffens, R. J., "The Assessment of Vibration Intensity and Its Application to the Study of Building Vibrations," _National Building Studies Special Report No. 19_, Department of Scientific and Industrial Research, Building Research Station, London, England, 1952.

5.29 Reiher, H. and Meister, F. J., "Die Empfindlichkeit der Menschen gegen Erschutterungen," _Forsch. Gebiete Ingenieur wesen_, Vol. 2, No. 11, pp. 381-386, 1931.

5.30 Rausch, E., _Maschinenfundamente Und Andere Dynamische Bauaufgaben_, Vertrieb VDE Verlag G.M.B.H. (Berlin), 1943.

5.31 Duvall, Wilbur I. and Fogelson, D. E., "Review of Criteria for Estimating Damage to Residences from Blasting Vibrations," Bureau of Mines Report of Investigation 5968, 1962.

5.32 Crandell, F. J., "Ground Vibrations Due to Blasting and Its Effect Upon Structures," _Journal Boston Soc., Civil Engineers_, Vol. 36, p. 245, 1949.

5.33 Langefors, Ulf, Kihlstron, B. and Westerberg, H., "Ground Vibrations in Blasting," _Water Power_, pp. 335-338, 390-395, 421-424, Feb. 1958.

5.34 Edwards, A. T. and Northwood, T. D., "Experimental Studies of the Effects of Blasting on Structures," _The Engineer_, V. 210, pp. 538-546, September 30, 1960.

5.35 Dvorak, A., "Seismic Effects of Blasting on Brick Houses," _Proce Geofyrikeniha Ustance Ceskoslavenski Akademie_, Vol. No. 169, Geofysikalni Sbornik, pp. 189-202, 1962.

5.36 Nicholls, R. W., Johnson, C. F. and Duvall, W. I., "Blast Vibrations and their Effects on Structures," Bureau of Mines Bulletin 656, p. 105, 1971.

5.37 Odello, R. and Price, P., "Ground Shock Effects from Accidental Explosions," Picatinny Arsenal Technical Report 4995, November 1976.

5.38 Eubanks, R. A. and Juskie, B. R., "Shock Hardening of Equipment," _Shock and Vibrations Bulletin_, No. 32, Part III, December 1963.

5.39 Batchelder, F. E., et al., "Hardness Program - Non-EMP, Hardness Program Plan for Safeguard Ground Facilities," Vol. 1, Management and Technical Plan, U. S. Army Corps of Engineers, Huntsville Division, HNDDSP-73-153-ED-R, 16 August 1974.

5.40 Meireis, E. C. and Wright, A. R., "Hardness Program - Non-EMP, Hardness Program Plan for Safeguard Ground Facilities," Vol. 2, Safeguard Structures and TSE Description, U. S. Army Corps of Engineers, Huntsville Division, HNDDSP-73-153-ED-R, November 1973.

5.41 Anon., "Hardness Program Non-EMP, Subsystem Hardness Assurance Report for Safeguard Ground Facilities," Vol. 1, Executive Summary, U. S. Army Corps of Engineers, Huntsville Division, HNDDSP-72-156-ED-R, 30 June 1975.

5.42 Anon., "Hardness Program Non-EMP, Subsystem Hardness Assurance Report for Safeguard Ground Facilities," Vol. 2, Final Report, U. S. Army Corps of Engineers, Huntsville Division, HNDDSP-72-156-ED-R, 30 June 1975.

5.43 Westine, P. S., Esparza, E. D., and Wenzel, A. B., "Analysis and Testing of Pipe Response to Buried Explosive Detonations," SwRI Final Report for American Gas Association, July 1978.

CHAPTER 6

FRAGMENTATION

6.1 INTRODUCTION

Most discussions, testing, accident investigations, and explosive accident predictions involve studies of blast waves and their effects. But often, significant damage in accidental explosions is caused by the impact of fragments or objects which were generated during the explosions and hurled against targets (or"receivers") at high speed.

Fragments from equipment or machinery in contact with or very near a detonating explosive charge can be accelerated to very high velocities and pose a threat to nearby personnel and equipment. Fragments can impact a nearby high explosive charge with sufficient velocity to cause it to detonate and cause further damage and destruction. If the detonating explosive charge is of sufficient size to dismember the surrounding bay area or building, large numbers of fragments of various sizes can be hurled into nearby work areas and buildings and cause considerable destruction and possible personnel fatalities.

In this chapter, we first define some of the terms used in studying missile generation and impact effects. We discuss the generation of fragments from objects in contact with the detonating high explosive, their velocities, mass distributions, and size and shape distributions. We then discuss the development of fragments from objects which are not in direct contact with the detonating explosive charge such as nearby machinery, both unconstrained and constrained, or portions of the surrounding building. We then include methods for calculating fragment trajectories and impact conditions. Next appear techniques for assessing fragment impact damage, including explosive initiation by fragments. This is followed by an assessment of the confidence in the prediction methods. Finally, we recommend tests and analyses to validate the assumptions or reduce uncertainties. Example calculations appear throughout the chapter to clarify the use of the text.

6.2 GENERAL PHENOMENA

Let us first define some basic terminology. Definitions of some basic terms involved with fragmentation and impact effects follow.

● Primary Fragments

The term "primary fragment" denotes a fragment from a casing or container for an explosive source or a fragment from an object in contact with an explosive. If the source is a true high explosive, the container

or casing usually ruptures into a very large number of small primary fragments which can be projected at velocities up to several thousand feet per second by the explosion (Ref. 6.1). For bomb and shell casings, typical masses of damaging fragments recovered in field tests are about 0.002 lb (Ref. 6.1). These primary fragments, although irregular, are usually of "chunky" geometry, i.e., all linear dimensions are of the same order of magnitude.

- Secondary Fragments

Containers or casings which fragment or burst during accidental explosions are not the only sources of fragments and missiles. The blast waves from severe explosions can interact with objects located near the explosion source, tear them loose from their moorings if they are attached, and accelerate them to velocities which can cause impact damage. The objects could be pieces of machinery, small tools, materials such as pipes and lumber, parts of buildings and other structures disrupted by the explosion, large pieces of equipment such as autos or portable generators, etc. The usual terms for these potentially damaging objects are "secondary missiles" or "secondary fragments."

- Drag-type and Lift-type Fragments

Once fragments or missiles have been formed and accelerated by the explosion, they will move along a specific trajectory until they impact a target (receiver), or the ground. The forces acting on the fragments and affecting their trajectories are inertia, gravitation, and fluid dynamic forces. The fluid dynamic forces are determined by the instantaneous velocity of the fragment at each instant in time. Generally, fragments are quite irregular in shape and may be tumbling, so a completely accurate description of the fluid dynamic forces during flight is difficult, if not impossible. In the trajectory analysis for fragment flight, one usually resorts to some simplified description of the fluid dynamic forces, and uses the concepts from aerodynamics of division of these forces into components called drag (along the trajectory or normal to the gravity vector) and lift (normal to the trajectory or opposing gravity). Then, the force components are given at any instant by

$$F_L = C_L \, A_L \, (1/2) \, \rho V^2 \tag{6.1}$$

and

$$F_D = C_D \, A_D \, (1/2) \, \rho V^2 \tag{6.2}$$

where C_L and C_D are lift and drag coefficients determined empirically as a function of shape and orientation with respect to the velocity vector, and the magnitude of the velocity V (see Figure 6.1). In the equations, ρ is air density and $q = (1/2) \, \rho V^2$ is termed the dynamic pressure. If a fragment is of chunky shape, so that $C_D \gg C_L$ for any flight orientation, it is called a <u>drag-type fragment</u>. If, on the other hand, $C_L \geq C_D$ for
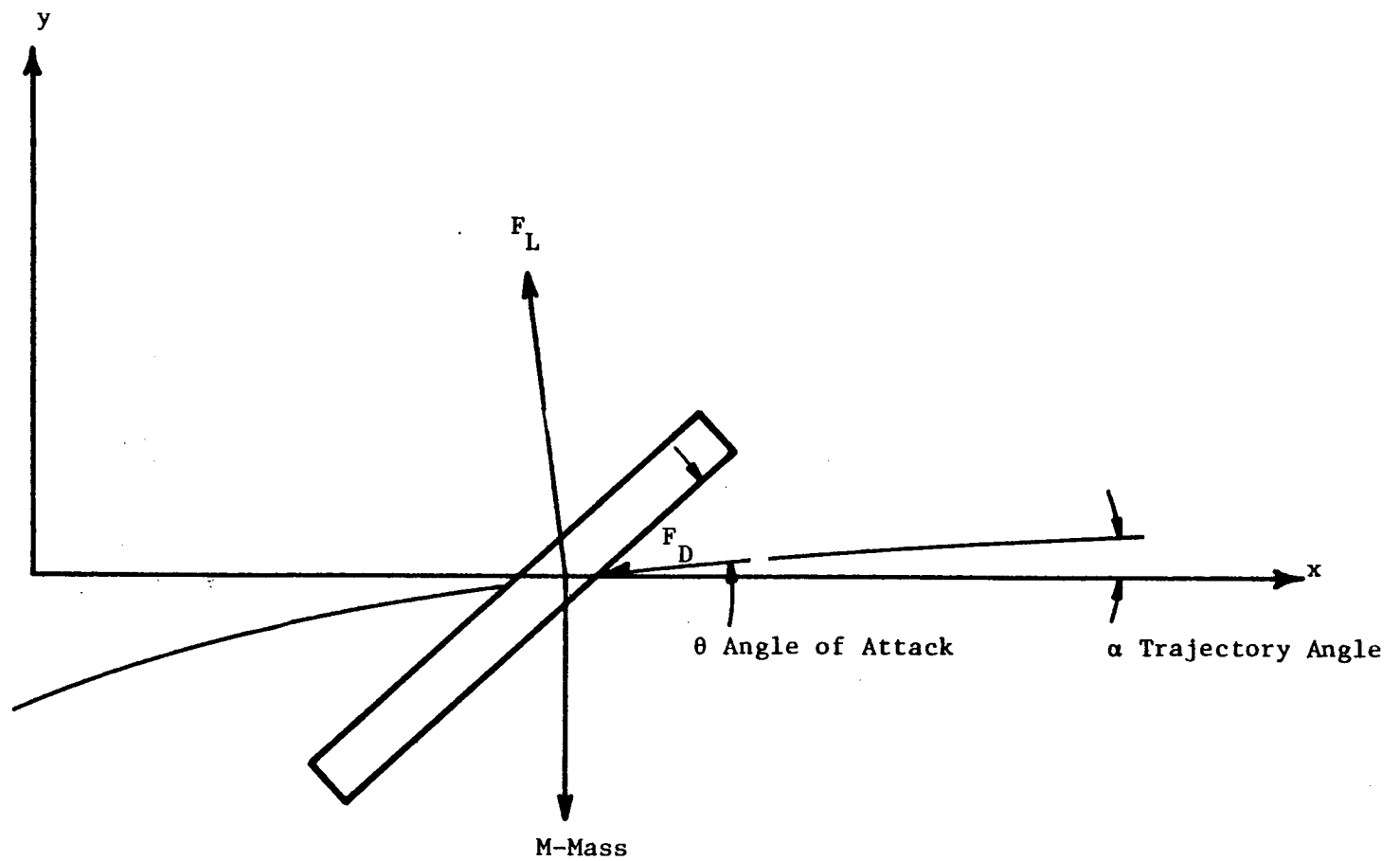
Figure 6.1. Nomenclature for Fragment Trajectory Analysis

some flight orientation, the fragment is called a lifting-type fragment. We will discuss in Section 6.2.4 the methods of trajectory predictions for drag-type fragments.

- Terms Relating to Fragment and Missile Impact Effects

Trajectory analyses and test results can give predictions of fragment ranges, masses, impact velocities, and even the probability of striking a given target (see Refs. 6.1 - 6.3). Impact effects determine the degree of missile hazards. We will define here a number of terms related to missile impact effects.

An impacting fragment can cause damage to a multitude of types of receivers by striking and either penetrating or rebounding without penetrating. The term penetration usually means that the fragment or missile disrupts or displaces some of the target material during impact, but does not pass through the target. The missile may or may not remain lodged in the target. On the other hand, if the missile passes entirely through, the target is said to have been perforated.

Impacting missiles may damage a target by simple momentum transfer, and various wave transmission effects. The term "spalling" will be used to indicate the process by which impact-induced compression waves in solids cause failures in tension after wave reflection from a free surface. The process is quite well described by Rinehart (Ref. 6.4). In brittle materials such as concrete or plaster, spalling can occur for missile impacts at relatively low velocities, less than 300 feet per second (Ref. 6.5).

There is much confusion in the literature concerning definitions for "spalling" and "scabbing." Often, the two terms are used interchangeably, or one author will use a definition for one of the terms which another author would use for the other term. TM5-1300 (Ref. 6.6), which is a document widely used by design engineers, defines "direct spalling" as the dynamic disengagement of the concrete surface of an element, resulting from a tension failure in the concrete normal to its free surface, caused by shock pressures of an impinging blast wave being transmitted through the element. The same document defines "scabbing" as the dynamic disengagement of the concrete surface of an element, resulting from a tension failure in the concrete normal to its free surface, caused by large strains in the flexural reinforcement.

6.2.1 Primary Fragments

A large number of primary fragments are generated when a high explosive source detonates within and in contact with a metal casing which cannot contain the explosion. The fragments which result from bomb and

shell casings containing high explosives are usually small, less than 0.002 lb, "chunky" in shape, and have initial velocities of nearly ten thousand feet per second (Ref. 6.1). The size and shape of the fragments will depend greatly on the metallographic history of the casing, its physical condition (such as dents, grooves, bends, or internal cracks or flaws), and the condition of joints, most notably weld joints. The pages which follow discuss methods for determining velocities, mass distributions and size and shape distributions for primary fragments.

6.2.1.1 Velocities

The fragment velocity of major concern is the velocity with which the "design fragment(s)" (the worst fragment which the structure must be designed to withstand) strikes the protective structure (Ref. 6.7). This striking velocity is expressed as

$$V_s = V_o \, e^{-12k_v R} \tag{6.3}$$

where V_s = fragment velocity at a distance R from the center of the detonation (ft/sec)

V_o = initial (maximum) fragment velocity (ft/sec)

R = distance from the center of detonation (ft)

k_v = velocity decay coefficient

The velocity decay coefficient is $k_v = (A/W_f) \, \gamma_o C_D$

where A/W_f = fragment form factor, the ratio of the presented area of the fragment (in.^{2}) to the fragment weight (see Section 6.2.1.3) in lb.

γ_o = specific weight of air (4.438 x 10^{-5} lb/in.^{3})

C_D = drag coefficient (dimensionless) (0.6 for V > 1100 ft/s for spinning, chunky fragments, Ref. 6.8)

Figure 6.2 shows the variation of primary fragment velocity with distance. The term initial velocity refers to the maximum fragment velocity as the fragment is ejected from the charge. Due to the extremely high rates of fragment acceleration, this velocity is considered to be attained by the fragment prior to moving appreciably from its initial position.

The most common technique for calculating the initial velocity of fragments in contact with an explosive charge is the Gurney Method (Ref. 6.9). This work was originally done for cylindrical and spherical geometries. Henry (Ref. 6.10) later derived additional formulas for other geometries. Gurney's original work consisted primarily of a theoretical analysis for predicting mean velocities of fragments from various types of military ordnance. He demonstrated that his analysis (Ref. 6.9) could successfully predict mean fragment velocities from a grenade containing 1.5 oz of HE to a bomb containing 3000 lb of HE. However, the literature does not address limitations in terms of the ratio W/W_c for the use of the Gurney formulas. Hence, it has been customary to use the Gurney formulas for all values of W/W_c.

Figure 6.2. Variation of Primary Fragment Velocity
with Distance (Ref. 6.7)
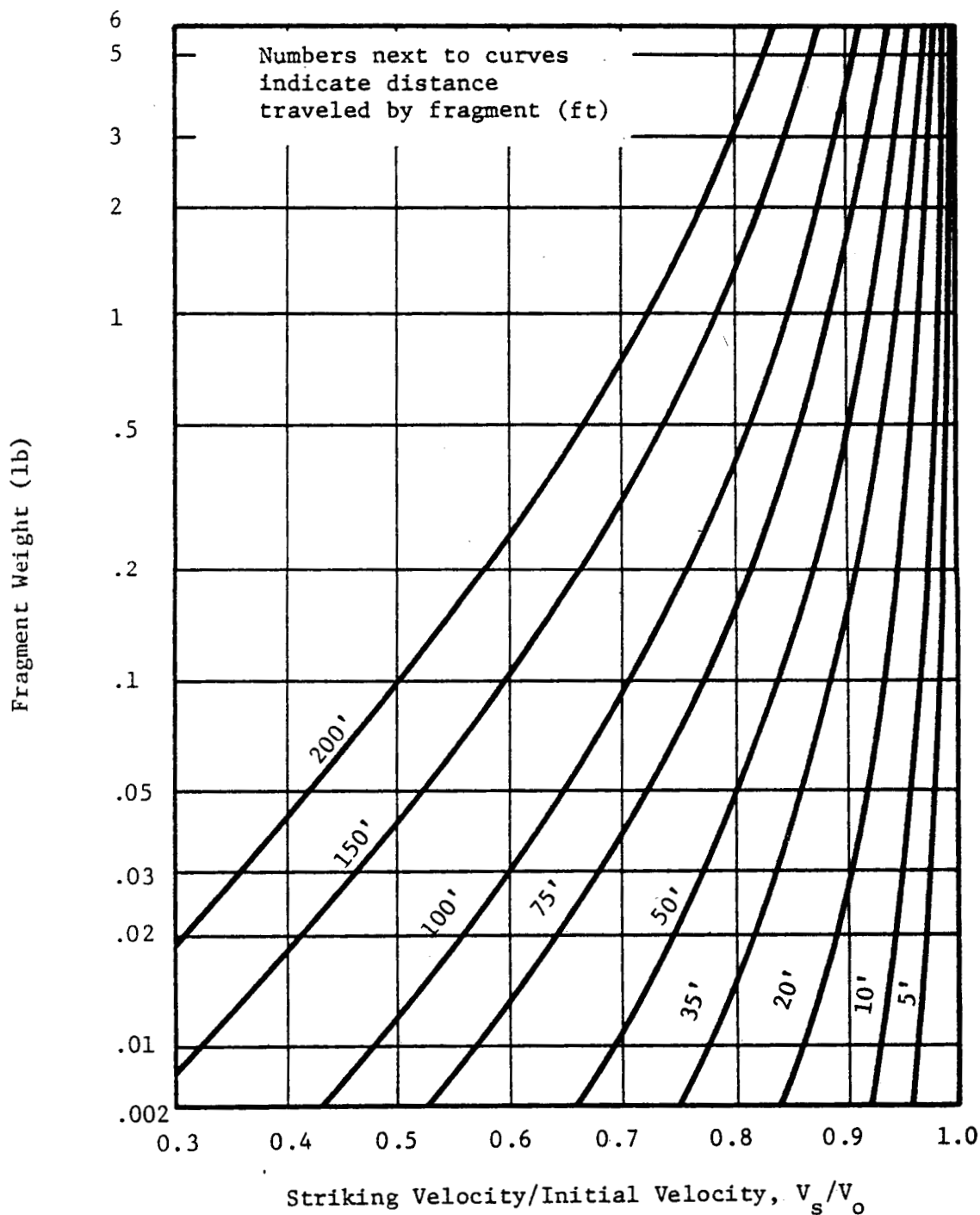
NOTE: Standard Fragment Shape Assumed, See Section 6.2.1.3.

Gurney found that the initial velocity of primary fragments resulting from the detonation of a cased explosive was a function of the explosive output of the explosive and the ratio of the explosive charge weight to the casing weight (Ref. 6.7). Figure 6.3 contains Gurney formulas for some simple geometries (Ref. 6.7).

These equations assume that the conversion from chemical energy to "Gurney" energy is accomplished with no losses (Ref. 6.11). However, the Gurney energy E' is a specific kinetic energy, determined experimentally by measuring the maximum velocity of primary fragments, and as such, the energy conversion efficiency appears limited. The time required to transfer energy across an expanding gas cloud to a moving metal plate (fragment) increases rapidly as the gas density decreases. The energy transfer process is eventually terminated by losses in any real system before the transfer is completed (Ref. 6.11).

It is useful to recognize that the chemical energy is simply the heat of detonation, ΔH, and that by expressing E' and ΔH in the same units an energy conversion efficiency can be defined. The ratio of Gurney energy to chemical energy, $E'/\Delta H$, represents the conversion efficiency (Ref. 6.11). Note then, that if E' is unknown for a particular explosive, and ΔH is known, $E'/\Delta H$ may be determined for a similar explosive (i.e., similar density ΔH), and the value used to estimate the Gurney energy (Ref. 6.11).

Figure 6.4 contains a plot of velocity versus charge to casing weight ratio for various geometries. The term $\sqrt{2E'}$ which appears in each formula is known as the "Gurney Constant," or Gurney characteristic velocity, and is a constant for a given explosive as shown in Table 6.1 (Ref. 6.11). As shown in the formulas, the ratio of final metal velocity V to the characteristic velocity $\sqrt{2E'}$ is an explicit function of the charge to metal mass ratio, W/W_c.

The Gurney characteristic velocities in Table 6.1 were calculated using maximum velocity data from carefully conducted experiments in which end losses and gas leakage through fractures in the metal were minimized. The effective value of $\sqrt{2E'}$ may decrease by as much as 20 percent if end losses or fracturing of the driven metal occur early in the acceleration period (Ref. 6.2).

6.2.1.2 Mass Distribution

Upon detonation of an encased explosive, the casing breaks up into a large number of high velocity fragments with varying weights and velocities. The destructive potential of these fragments is a function of their kinetic energy distribution. Therefore, through testing or analysis the velocity and weight of the "worst case" fragment must be determined and utilized as a design criterion for fragment shields.
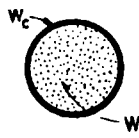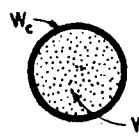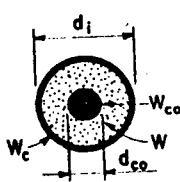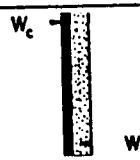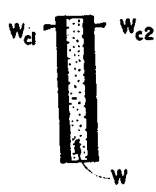
Type	Cross-Sectional Shape	Initial Fragment Velocity v_o	Maximum v_o
Cylinder		$\sqrt{2E'}\left[\dfrac{\dfrac{W}{W_c}}{1+\dfrac{W}{2W_c}}\right]^{1/2}$	$\sqrt{2E'}\,\sqrt{2}$
Sphere		$\sqrt{2E'}\left[\dfrac{\dfrac{W}{W_c}}{1+\dfrac{3W}{5W_c}}\right]^{1/2}$	$\sqrt{2E'}\,\sqrt{\tfrac{5}{3}}$
Steel cored cylinder	d_i $-W_{co}$ W_c W d_{co}	$\sqrt{2E'}\left[\dfrac{\dfrac{W}{W_c}}{1+\dfrac{(3+a)W}{6(1+a)W_c}}\right]^{1/2}$ where $a=\dfrac{d_{co}}{1.6d_i}$	$\sqrt{2E'}\sqrt{\dfrac{6(1+a)}{(3+a)}}$
Plate		$\sqrt{2E'}\left[\dfrac{\dfrac{3W}{5W_c}}{1+\dfrac{W}{5W_c}+\dfrac{4W_c}{5W}}\right]^{1/2}$	$\sqrt{2E'}\,\sqrt{3}$
Sandwich plates	W_{c1} W_{c2} W	If $W_{c1}\neq W_{c2}$ $\sqrt{2E'}\left[\dfrac{W}{W_{c1}+W_{c2}g+\dfrac{W}{3}(1-g+g^2)}\right]^{1/2}$ where $g=\dfrac{W_{c1}+\dfrac{W}{2}}{W_{c2}+\dfrac{W}{2}}$ if $W_{c1}=W_{c2}=W_c$ $\sqrt{2E'}\left[\dfrac{\dfrac{W}{2W_c}}{1+\dfrac{W}{6W_c}}\right]^{1/2}$	$\sqrt{2E'}\,\sqrt{3}$

Figure 6.3 Velocity of Primary Fragments*

---

*See Table 4-3, TM5-1300, for remarks on use of these formulas.
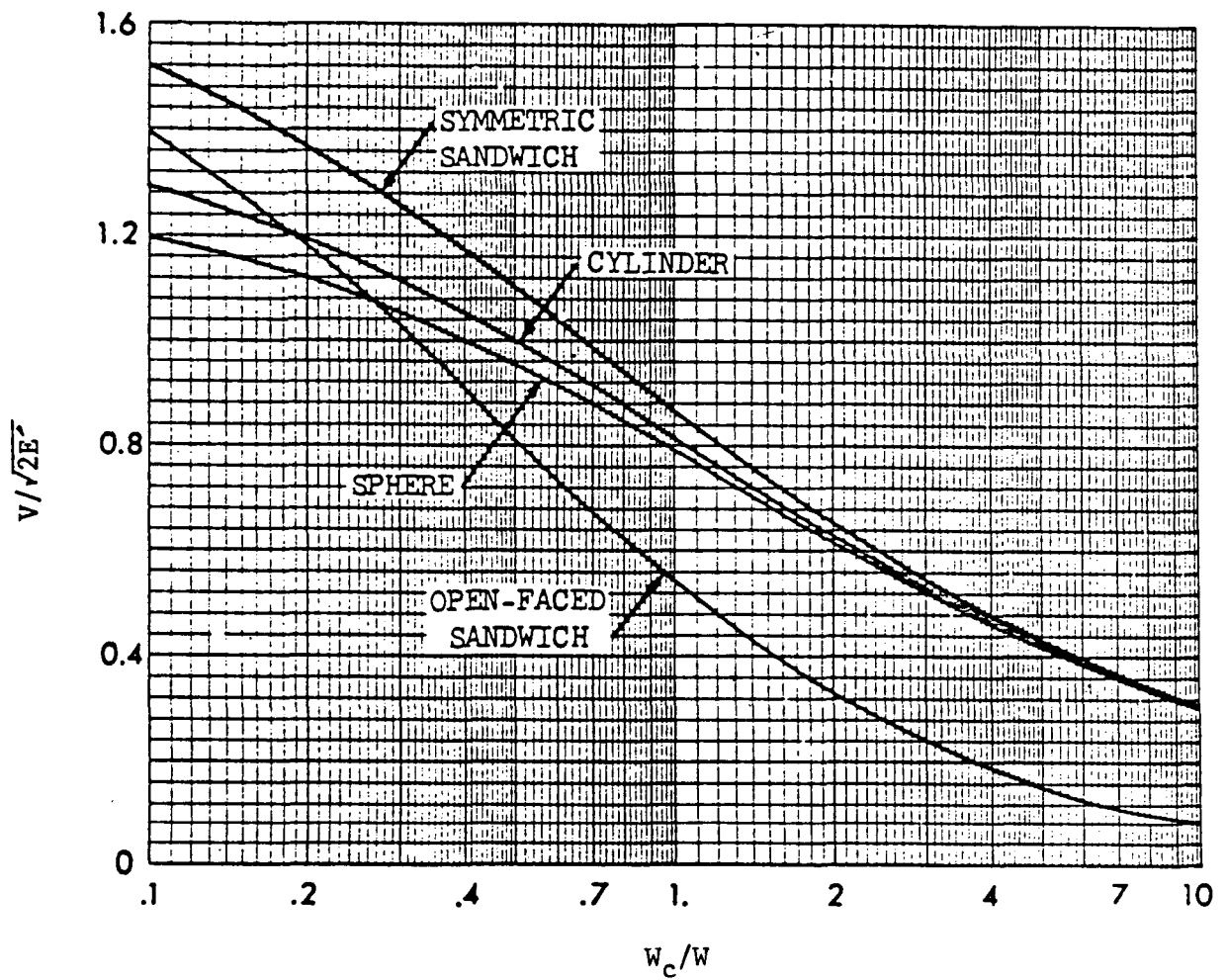
Figure 6.4. Dimensionless Velocity of Metal as a Function of
Loading Factor W_c/W (Ref. 6.10)

Table 6.1 Gurney Energies for Various Explosives (Ref. 6.9)

Specific Weight lb/in^3	Explosive	$\sqrt{2E}$ ft/s
0.0639	RDX	9600
0.0578	Composition C-3	8800
0.0588	TNT	8000
0.0621	Tritonal* (TNT/Al = 80/20)	7600
0.0621	Composition B (RDX/TNT)	9100
0.0682	HMX	9750
0.0664	PBX-9404	9500
0.0585	Tetryl	8200
0.0581	TACOT	7000
0.0411	Nitromethane	7900
0.0635	PETN	9600
	duPont Sheet:	
0.0527	EL506D	8200
0.0563	EL506L	7200
0.0397	Trimonite No. 1*	3400

*Denotes nonideal.

NOTE: Corrections were applied to the data on Refs. 6.10 and 6.12 as discussed in Ref. 6.13 to estimate true speed of metal before calculating Gurney energy, E.

The Mott equation (Ref. 6.7) yields estimates of the fragment mass distribution resulting from the high-order detonation of evenly distributed explosive within a uniform thickness cylindrical casing for naturally fragmenting casings and the Gurney equation (Section 6.2.1.1) predicts velocities. Mott's equations do not hold for casings designed to fragment in a specific manner. The Mott equation is:

$$\ln N_x = \ln (C'M_A) - M/M_A \qquad (6.4)$$

where N_x = the number of fragments with weight greater than W_f

C' = fragment distribution constant

     $= W_c/(2M_A{}^3)$

W_c = total casing weight (lb)

M = $(W_f)^{1/2}$

W_f = fragment weight (lb)

M_A = fragment distribution parameter

     $= B \, t_c{}^{5/6} d_i{}^{1/3} \, (1 + t_c/d_i)$

t_c = average casing thickness (in.)

d_i = average inside diameter of casing (in.)

B = explosive constant (Table 6.2) (see Section 6.7.2)

The Mott equation assumes that the fragments result from the high-order detonation of a uniform thickness cylindrical casing filled with evenly distributed explosive. Since actual weapons do not conform to these ideal conditions, the resulting fragment sizes and velocities vary in angular orientation with respect to the projectile nose (Refs. 6.14 and 6.15). There is no exact procedure for predicting the fragment mass distribution from a non-cylindrical container. Consequently, such cases are approximately treated by considering the casing as a series of equivalent cylindrical containers (Ref. 6.9).

A number of relationships and design equations can be obtained by expressing the Mott equation (Eq. 6.4) in the following form:

$$N_x = C'M_A e^{-M/M_A} \qquad (6.5a)$$

or by substituting for $C' = W_c/(2M_A{}^3)$ and $M = (W_f)^{1/2}$,

$$N_x = \frac{W_c e^{-\sqrt{W_f}/M_A}}{2M_A^2} \qquad (6.5b)$$

Setting the fragment weight W_f to zero, the following expression for the total number of fragments N_T is obtained:

Table 6.2 Mott Scaling Constants for Mild Steel Casings
and Various Explosives (Ref. 6.16)

Explosive	B ($lb^{1/2}$ $inches^{-7/6}$)	Heat of Detonation* ft-lb/lb
Baratol	0.128	1,036,000
Comp B	0.0554	2,150,000
Cyclotol (75/25)	0.0493	2,198,000
H-6	0.0690	1,292,000
HBX-1	0.0639	1,286,000
HBX-3	0.0808	1,228,000
Pentolite (50/50)	0.0620	1,722,000
PTX-1	0.0554	
PTX-2	0.0568	
TNT	0.0779	1,526,000
Comp A-3	0.0549	
RDX/WAX (95/5)	0.0531	2,114,000
Tetryl	0.0681	1,595,000

*These are empirical values used by Mott.

$$N_T = W_c/2M_A^2 \qquad (6.6)$$

Hence, the average particle weight $\bar{W}_f$ can be found:

$$\bar{W}_f = W_c/N_T = 2M_A^2 \qquad (6.7)$$

Equation (6.5b) can then be expressed as:

$$N_x = N_T \, e^{-\sqrt{W_f}/M_A} \qquad (6.8a)$$

or

$$\frac{N_x}{N_T} = e^{-\sqrt{W_f}/M_A} \qquad (6.8b)$$

The ratio N_x/N_T represents that fraction of the total number of fragments which have a weight greater than W_f. The Mott equation predicts a continuous distribution of fragments ranging in size from a large number of lightweight particles to a small number of very heavy casing fragments. This is indicated by the observation that the average fragment weight ($2M_A^2$) corresponds to an N_x/N_T value of 0.243, implying that 75.7 percent of all primary fragments generated by the detonation have weight less than the overall average.

For design purposes, a confidence level CL, where $(0 < CL < 1)$, can be defined as the probability that the weight, W_f, is the largest weight fragment released. The expression for the design fragment weight corresponding to a prescribed design confidence level (CL) is given as (Ref. 6.9):

$$CL = 1 - N_x/N_T = 1 - e^{-\sqrt{W_f}\,/M_A} \qquad (6.9a)$$

or

$$e^{-\sqrt{W_f}\,/M_A} = 1 - CL \qquad (6.9b)$$

Then, taking the logarithm and squaring both sides of the equation,

$$W_f/M_A^2 = \ln^2(1 - CL) \qquad (6.9c)$$

or

$$W_f = M_A^2 \, \ln^2(1 - CL) \qquad (6.9d)$$

Equation (6.9d) can then be used to calculate the design fragment weight for a prescribed design confidence level. Note that Equation (6.9d) uses an infinite distribution to describe a physical phenomenon which has a finite upper limit. Equation (6.9d) may be used for CL $\leq$ 0.9999. If CL > 0.9999, use:

$$W_f = M_A^2 \, \ell n^2 \left[1 - CL\left(1 - e^{-\sqrt{W_c}/M_A}\right)\right] \tag{6.10}$$

Fragment masses for primary fragments from several explosions reported in the files at DDESB could be estimated using Mott scaling. However, this formula can only be employed to calculate masses of primary fragments which evolve from accidents involving an explosive detonation within a container of some sort, like a casing, storage tank, or a confining piece of machinery such as a centrifuge or press. Masses of fragments created as a result of a given quantity of explosive detonating while being machined or in unconfined space within a building must be estimated using other methods. Some of these methods are discussed in Sections 6.2.2, 6.2.2.1, 6.2.2.2, 6.2.3 and 6.2.4.2.

6.2.1.3 Size and Shape Distributions

In order to determine the damage potential of primary fragments, it is necessary to evaluate the caliber density and shape of the fragments, as well as the previously described weight and striking velocity (Ref. 6.7). When a container fragments, a random distribution of fragment shape results. Section 6.2.1.2 contained a method for determining the mass distribution of primary fragments. From the mass of the fragment and shape of the containment vessel, one can estimate the size of individual fragments. This section discusses a method for performing an engineering estimate of a standard design fragment(s) for use in fragment impact damage.

The influence of the fragment weight to fragment diameter ratio is expressed in terms of the caliber density D of the fragment which is defined as:

$$D = W_f/d^3 \tag{6.11}$$

where W_f = total fragment weight (lb)

   d = fragment diameter (in.)

The nose shape factor N is defined as follows:

$$N = 0.72 + 0.25 \sqrt{n - 0.25} \tag{6.12}$$

where n = caliber radius of the tangent ogive of the assumed fragment nose

Two possible fragment shapes with their corresponding caliber densities and nose factors are shown in Figure 6.5. The blunt fragment

shape in Figure 6.5 is considered as the standard fragment in the design
charts presented in the following section. While the standard fragment
has a milder nose shape than the alternate fragment, the standard fragment
is generally considered appropriate for use in design since: (a) only a
small number of fragments will strike the structure nose-on; and (b) only
a small fraction of these fragments will have a more severe nose shape
than the standard fragment. In addition, the length-to-diameter ratio of
these fragments is felt to be more representative of an average fragment
configuration. For convenience, a plot of fragment weight in pounds
versus fragment diameter for these two fragment shapes is given in
Figure 6.6 (Ref. 6.9).
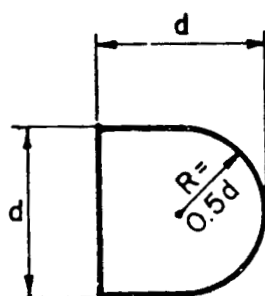
$n = 0.5$

$N = 0.845$

$\text{Volume} = 0.654d^3$

$W_f = 0.186d^3$

$D = 0.186 \text{ lb/in.}^3$

$A = \pi d^2/4$

(a)   Standard Fragment Shape
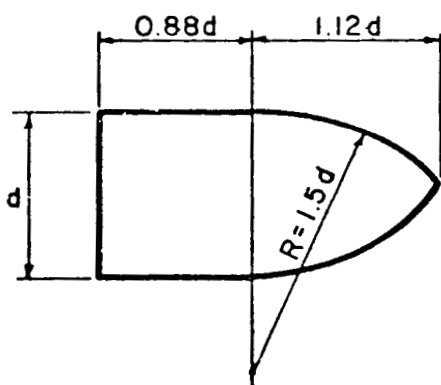
$n = 1.5$

$N = 1.00$

$\text{Volume} = 1.2d^3$

$W_f = 0.34d^3$

$D = 0.34 \text{ lb/in.}^3$

$A = \pi d^2/4$

(b)   Alternate Fragment Shape

NOTE: N = Nose shape factor = $0.72 + 0.25 \sqrt{n-0.25}$

n = Caliber radius of tangent ogive of fragment nose = R/d

D = Caliber density = W_f/d^3

A = Presented area for use in striking velocity determinations

(Calculations are for steel fragments with a specific weight of 0.283 lb/in.^{3})

Figure 6.5. Primary Fragment Shapes
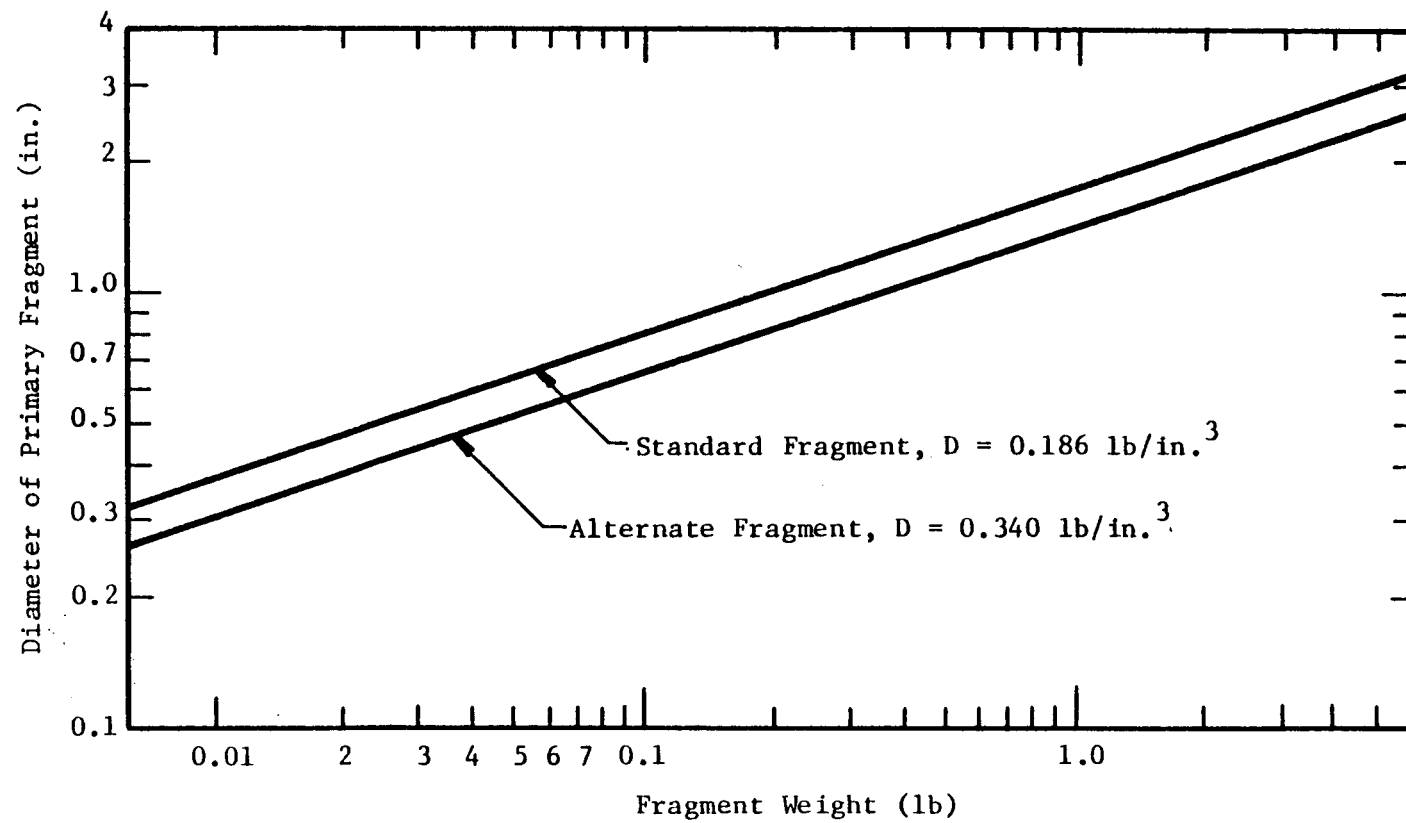
Figure 6.6. Relationship Between Fragment Weight
and Fragment Diameter

PROBLEM – Determine the initial (maximum velocity) V_O and striking velocity V_s of a primary fragment ejected from a spherical casing containing TNT.

GIVEN: W = weight of explosive (lb)

W_c = weight of casing (lb)

$\sqrt{2E'}$ = Gurney energy (ft/sec)

γ_o = Specific weight of air (lb/in.^{3})

C_D = drag coefficient (dimensionless)

R = distance from center of charge to target impact location (ft)

W_f = weight of fragment (lb)

FIND: V_o, V_s REFERENCE

SOLUTION: 1. Calculate the initial fragment velocity.

$$V_o = \sqrt{2E'}\left[\frac{\dfrac{W}{W_c}}{1 + \dfrac{3W}{5W_c}}\right]^{1/2}$$

<div style="text-align:right">Fig. 6.3
for equation,
Table 6.1
for Gurney
energy</div>

2. Determine the presented area of the fragment. (Assume a standard fragment shape as defined in Figure 6.5 unless information on the actual shape is available.)

$$A = \frac{\pi d^2}{4}; \quad d^2 = \frac{W_f^{2/3}}{0.186^{2/3}}$$

<div style="text-align:right">Fig. 6.5</div>

$$A = \frac{\pi W_f^{2/3}}{(4)(0.186)^{2/3}} = 2.41\, W_f^{2/3}$$

3. Calculate the velocity decay coefficient k_v.

$$k_v = (A/W_f)\,\gamma_o C_D$$

<div style="text-align:right">Eq. (6.3)</div>

4. Calculate the striking velocity at some distance R.

$$V_s = V_o\, e^{-12k_v R}$$

<div style="text-align:right">Eq. (6.3)</div>

CALCULATION

GIVEN: W = 100 lb of TNT
        W_c = 10 lb of steel
        $\sqrt{2E'}$ = 8000 ft/sec
        γ_o = 4.438 x 10^{-5} lb/in.^{3}
        C_D = 0.6
        R = 30 ft
        W_f = 0.01 lb

        Standard design shape fragment

FIND: V_o, V_s

SOLUTION: 1. $V_o = \sqrt{2E'} \left[\dfrac{\dfrac{W}{W_c}}{1 + \dfrac{3W}{5W_c}} \right]^{1/2}$

        $V_o = 8000 \text{ ft/sec} \left[\dfrac{\dfrac{100}{10}}{1 + \dfrac{(3)(100)}{(5)(10)}} \right]^{1/2}$

        $V_o = 9560 \text{ ft/sec}$

        2. $A = 2.41 \, W_f^{2/3}$
            $A = 0.112 \text{ in.}^2$

        3. $k_v = (A/W_f) \, \gamma_o C_D$
            $k_v = (0.112 \text{ in.}^2/0.01 \text{ lb}) \, (4.438 \times 10^{-5} \text{ lb/in.}^3) \, (0.6)$
            $k_v = 2.98 \times 10^{-4} \text{ in.}^{-1}$

        4. $V_s = V_o \, e^{-12k_v R}$
            $V_s = (9560 \text{ ft/sec}) \, e^{-12(2.98 \times 10^{-4} \text{ in.}^{-1})(30 \text{ ft})}$
            $V_s = (9560 \text{ ft/sec}) \, e^{-0.1073}$
            $V_s = \underline{8590 \text{ ft/sec}}$

EXAMPLE PROBLEM 6.2

PROBLEM – Determine the average fragment weight $\bar{W}_f$ for a primary fragment
ejected from a uniform cylindrical steel casing containing
Composition B; the total number of fragments N_T ejected; and the
design fragment weight W_f; the number N_x of fragments weighing
more than the design fragment.

Comp B explosive

t_c = average casing thickness (in.)

d_i = average inside diameter of casing (in.)

W_c = total casing weight (lb)

CL = confidence level (see Equation 6.9)

FIND:	$\bar{W}_f$, N_T, W_f, N_x	REFERENCE

SOLUTION: 1. Determine the explosive constant B for   Table 6.2
             Composition B.

2. Determine fragment distribution parameter M_A.

$$M_A = B \, t_c^{5/6} \, d_i^{1/3} \, (1 + t_c/d_i)$$ Eq. (6.4)

3. Determine the average weight of the fragments
    $\bar{W}_f$.

$$\bar{W}_f = 2M_A^2$$ Eq. (6.7)

4. Determine the total number of fragments N_T.

$$N_T = W_c/2M_A^2$$ Eq. (6.6)

5. Determine the design fragment weight W_f.

$$W_f = M_A^2 \, \ln^2 (1 - CL)$$ Eq. (6.9d)
                                        or (6.10)

6. Determine the number of fragments N_x which
    weigh more than the design fragment.

$$\frac{N_x}{N_T} = e^{-\sqrt{W_f}/M_A}$$ Eq. (6.8b)

$$N_x = \frac{N_x}{N_T} \cdot N_T$$

CALCULATION

GIVEN: Comp B explosive

t_c = 0.25 in.

d_i = 6.0 in.

W_c = 16.34 lb

CL = 0.995

FIND: $\bar{W}_f$, N_T, W_f, N_x

SOLUTION: 1. Using Table 6.2, $B = 0.0554 \text{ lb}^{1/2}/\text{in.}^{7/6}$ for Comp B explosive

2. $M_A = B \, t_c^{5/6} \, d_i^{1/3} \, (1 + t_c/d_i)$

$M_A = (0.0554)(0.25)^{5/6} \, (6)^{1/3} \, [1 + (0.25/6)]$

$M_A = 3.303 \times 10^{-2} \text{ lb}^{1/2}$

3. $\bar{W}_f = 2M_A^2$

$\bar{W}_f = 2.182 \times 10^{-3} \text{ lb}$

4. $N_T = W_c/2M_A^2$

$N_T = 16.34/2.182 \times 10^{-3}$

$N_T = \underline{7490 \text{ fragments (total)}}$

5. $W_f = M_A^2 \, \ln^2 (1 - CL)$

$W_f = (3.303 \times 10^{-2})^2 \, \ln^2 (1 - 0.995)$

$W_f = \underline{3.063 \times 10^{-2} \text{ lb}}$

6. $\dfrac{N_x}{N_T} = e^{-\sqrt{W_f}/M_A}$

$\dfrac{N_x}{N_T} = e^{-0.175/3.303 \times 10^{-2}} \, e^{-\sqrt{3.063 \times 10^{-2}}/3.303 \times 10^{-2}}$

$\dfrac{N_x}{N_T} = 5 \times 10^{-3}$ $(100 \times 5 \times 10^{-3} = 0.5\%$ of the fragments are heavier than the design fragment)

$N_x = (0.005)(7490)$

$= 37 \text{ to } 38$ fragments heavier than the design fragment

NOTE: An alternate (and simpler) method for determining the number of fragments which are heavier than the design fragment would be to use Equation (6.9a). That is

$CL = 1 - N_x/N_T$

$N_x = (1 - CL) \, (N_T)$

$N_x = (1 - 0.995)(7490) = \underline{37 \text{ to } 38 \text{ fragments}}$

EXAMPLE PROBLEM 6.3

PROBLEM – Determine the area presented by a design fragment striking a target.

GIVEN: W_f = weight of the fragment (lb)

Shape of the fragment (i.e., standard or alternate)

FIND: A

SOLUTION: 1.   Choose design shape (alternate shaped assumed)   Fig. 6.5
          2.   Determine the diameter of the fragment

$$d = W_f^{1/3}/0.34^{1/3}$$ Fig. 6.5
$$d = 1.433\ W_f^{1/3}$$

          3.   Find the presented area

$$A = \frac{\pi d^2}{4};\quad d^2 = W_f^{2/3}/0.34^{2/3}$$ Fig. 6.5
$$A = 1.61\ W_f^{2/3}$$

CALCULATION

GIVEN: W_f = 0.03 lb

FIND: A

SOLUTION: 1.   Assume alternate shape.
          2. $d = 1.433\ W_f^{1/3}$
$$d = 1.433\ (0.03)^{1/3}$$
$$d = 0.445\ \text{in.}$$
          3. $A = 1.61\ W_f^{2/3}$
$$A = (1.61)(0.03)^{2/3}$$
$$A = \underline{0.155\ \text{in.}^2}$$

6.2.2 Secondary Fragments

The explosion of HE during some manufacturing or forming process (i.e., nitration, centrifuging, pressing, machining on lathe, etc.) can result in a large number of secondary fragments which vary greatly in size, shape, initial velocity, and range. Each of these parameters affects the damage potential of an accidental explosion and, therefore, should be considered in the design of protective structures.

The current state-of-the-art for assessing damage potential requires that the design engineer estimate the conditions which are likely to exist at the time of the accident, and perform a structural assessment of any equipment which will be involved. Some of the initial factors to consider are:

- Type and amount of HE
- Configuration (i.e., sphere, cylinder, cased, uncased, etc.)
- Location of HE (i.e., attached to lathe, resting on support table, contained in centrifuge, proximity to walls and other equipment, etc.)
- Type of propagation after initiation (i.e., high order, burning, partial detonation, etc.)

As an example of predicting the fragmentation of a machine, the explosion which occurred at the Pantex Plant in Building 11-14A on March 30, 1977 is considered. In this incident, two billets of HE were involved: ∿75 lb of LX-09-0 and ∿75 lb of LX-14, both plastic-bonded explosives with a TNT equivalence of 1.3. A consequent investigation concluded that the following conditions may have existed at the time of the accident. The LX-09-0 was attached via a vacuum holding fixture to a Monarch lathe and was in the process of being rough cut or centered. The lathe was adjacent to a 3-ft concrete wall analyzed to withstand an impulse of 2100 psi-ms. The billet of LX-14 was approximately 15 ft from the LX-09-0, and was resting on a granite table adjacent to a masonry block wall. Both billets were 3 to 4 ft above the floor. The investigation suggested that the billet on the lathe may have detonated first and that missiles generated at the lathe subsequently led to the detonation of the LX-14 (Ref. 6.17). Both explosions were high-order detonations.

When the initial explosion occurred at the lathe, secondary fragments were ejected in all directions. In general, the elements of the lathe were interlocked with each other (i.e., bolted, welded, etc.) allowing us to consider individual fragments as having been constrained. Therefore, a finite amount of energy released by the explosion was utilized in "tearing apart" the lathe. Fairly massive and heavily constrained parts such as the cam lock spindle adapter and the cam lock spindle nose, which were among the closest parts to the charge, sustained substantial plastic deformation or melting before being torn free from the lathe. The missile

maps which were constructed of the accident scene indicate the areal
fragment distribution which resulted (Ref. 6.17).

In general, the smallest fragments originated closest to the charge.
This may be explained, in part, by considering those parts of the lathe
adjacent to the charge to be primary fragments. The difficulties that
arise from assuming that these elements are primary fragments stems
from a lack of total encasement (i.e., very few parts of the lathe are
in actual contact with the HE); variations in the amount of constrainment
of the machine parts; and a varying mass distribution (i.e., the charge
may be contacted by a virtually unconstrained cutter on one side and the
heavily constrained spindle assembly on another side). The situation is
further complicated in that a relatively small force acting on a part from
one direction may cause it to fragment while a much larger force acting
along some other line of action may not result in fragmentation.

If the fragmentation pattern varies with the initial conditions,
the Architectural Engineer must examine several likely scenarios to
evaluate the damage potential.

To estimate the weight, shape, and velocity of fragments which
result from detonation of an HE during a manufacturing or forming process,
one would perform the following steps:

1) Determine distance (R_i) from the center of the explosive to
   the ith point of interest on the machine (refer to structural
   details of the machine).
2) Determine the size and shape of the expected fragment (refer
   to structural details of the machine).
3) Determine the fragment velocity (refer to Sections 6.2.2.1 and
   6.2.2.2).

6.2.2.1 <u>Unconstrained Secondary Fragments</u>

To predict velocities to which objects are accelerated by ex-
plosions, one must consider the interaction of blast waves with solid
objects. Figure 6.7a (Ref. 6.3) shows schematically in three stages the
interaction of a blast wave with an irregular object. As the wave strikes
the object, a portion is reflected from the front face, and the remainder
diffracts around the object. In the diffraction process, the incident
wave front closes in behind the object, greatly weakened locally, and a
pair of trailing vortices is formed. Rarefaction waves sweep across the
front face, attenuating the initial reflected blast pressure. After
passage of the front, the body is immersed in time-varying flow field.
Maximum pressure on the front face during this "drag" phase of loading is the
stagnation pressure.
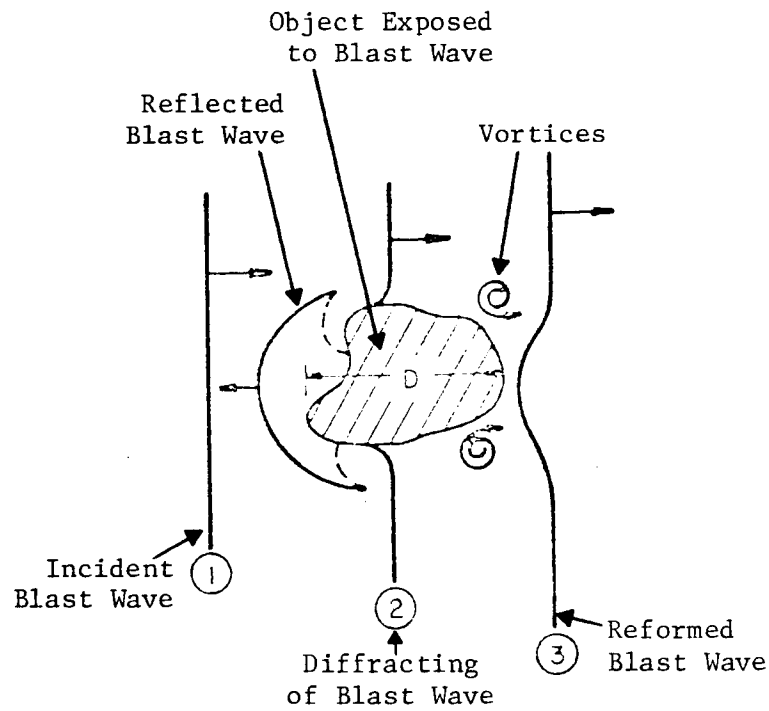
Figure 6.7a   Interaction of Blast Wave with Irregular Object

$$f(t) = C_D \, q(t) = C_D \cdot \frac{1}{2} \rho \, u^2$$
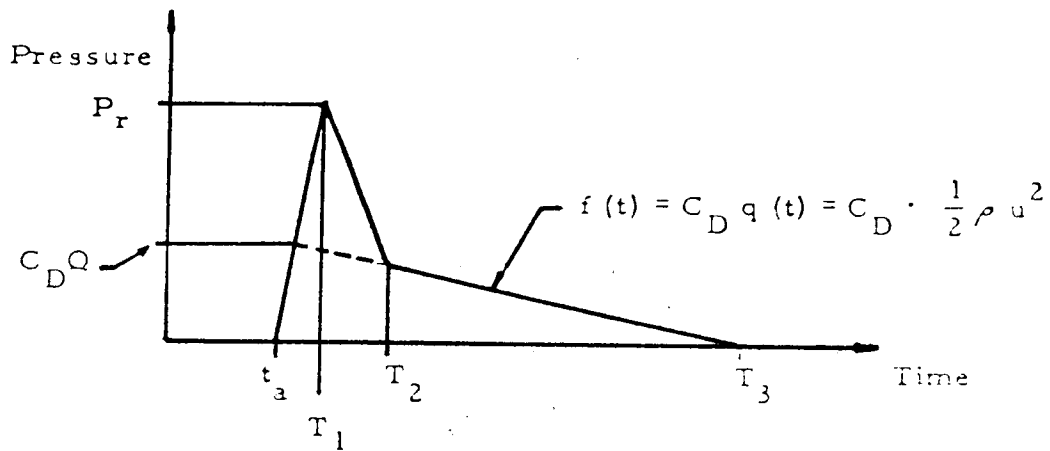
Figure 6.7b   Time History of Net Transverse Pressure on
Object During Passage of a Blast Wave

(See Section 4.3.1.1 For Definitions of Parameters)

To predict the effect of a blast wave on the object, it is necessary to examine the net transverse pressure on the object as a function of time. This loading, somewhat idealized, is shown in Figure 6.7b. After time of arrival t_a, the net transverse pressure rises linearly from zero to a maximum peak reflected pressure P_r in time $(T_1 - t_a)$. For an object with a flat face nearest the approaching blast wave, this time interval is zero. Pressure then falls linearly to drag pressure in time $(T_2 - T_1)$ and decays more slowly to zero in time $(T_3 - T_2)$.

Once the time history of net transverse pressure loading is known, the prediction of the object's velocity can be made. The basic assumptions for unconstrained secondary fragments are that the object behaves as a rigid body, that none of the energy in the blast wave is absorbed in breaking the object loose from its moorings or deforming it elastically or plastically, and that gravity effects can be ignored during this acceleration phase of the motion. The equation of motion of the object is then

$$A \, p(t) = M\ddot{x} \qquad (6.13)$$

where A = area of the object presented to the blast front
  p(t) = net transverse pressure according to Figure 6.7b
  x = displacement of the object
  $\ddot{x}$ = acceleration of the object
  M = mass of the object

The object is assumed to be at rest initially, so that

$$x(0) = 0, \; \dot{x}(0) = 0$$

Equation (6.13) can be integrated directly. With use of the initial conditions and Figure 6.7b, this operation yields, for appurtenance velocity,

$$\dot{x}(T_3) = \frac{A}{M} \int_{t_a}^{T_3} p(t)dt = \frac{A}{M} i_d \qquad (6.14)$$

where i_d = total drag and diffraction impulse
  $\dot{x}$ = velocity of the object

The integration in Equation (6.14) can be performed explicitly if the pressure time history is described by suitable mathematical functions, or performed graphically or numerically if p(t) cannot be easily written in function form. In either case, Equation (6.14) yields the desired result—a predicted velocity for an object. The integral in Equation (6.14) is merely the area under the curve in Figure 6.7.

For shocks of intermediate strength, $P_s/p_o \leq 3.5$ where P_s is side-on overpressure and p_o is atmospheric pressure, the solution of Equation (6.14) can be found in Reference 6.3. A rather long equation develops in which

$$\left(\frac{M V a_o}{p_o A (KH + X)} \right) \text{ is a function of } \left(\frac{P_s}{P_o} \right) \text{ and } \left(\frac{C_D i_s a_o}{P_s (KH + X)} \right), \qquad (6.15)$$

or, in abbreviated form,

$$\overline{V} \text{ is a function of } \overline{P} \text{ and } \overline{i}$$

where M = mass of object

     V = velocity of object

    a_o = velocity of sound in air

    p_o = atmospheric pressure

    A = mean presented area of object

    K = constant (4 if object is on the gound or reflecting surface and 2 if object is in air)

    H = minimum transverse dimension of the mean presented area of object

    X = distance from the front of object to location of its largest cross-sectional area

    P_s = peak incident overpressure

    C_D = drag coefficient

    i_s = incident specific impulse

A pictorial explanation of the appurtenance parameters A, H, and X is shown in Figure 6.8. Values for drag C_D can be found in Hoerner (Ref. 6.18) for various shaped objects. In addition, a value of drag coefficients for objects of various shapes is given in Figure 6.9. Since this analysis is appropriate for objects "far" from the charge, the object is not in a high-velocity flow field (i.e., subsonic) and C_D is essentially a constant. For example, for a standoff distance (distance from the center of the explosive charge to the nearest surface of the object) of 33 charge radii, the peak particle velocity equals the speed of sound in air and decreases rapidly with increasing standoff distance. For computational purposes, Equation (6.15) is presented in Figure 6.10 where $\overline{P} = P_s/p_o$, $\overline{i}$ is the nondimensional term containing i_s, and $\overline{V}$ is the nondimensional term containing V. The figure contains several curves for different values of $\overline{V}$ and is quite useful for the range of $\overline{P}$ and $\overline{i}$ presented. When using the figure, the values of $\overline{P}$, $\overline{i}$ and $\overline{V}$ must have no dimensional units. This figure can be used in most cases where the distance in charge radii from the object and center of a spherical charge is greater than 20, which is normally considered to be "far" from the charge. For objects at closer scaled standoff distances, one can calculate the specific impulse imparted to the target.

Object Exposed
to Blast Wave

Incident
Blast Wave

Distance from
Front of Object
to the Largest
Sectional Area
Normal to the
Plane of the
Shock Front

X
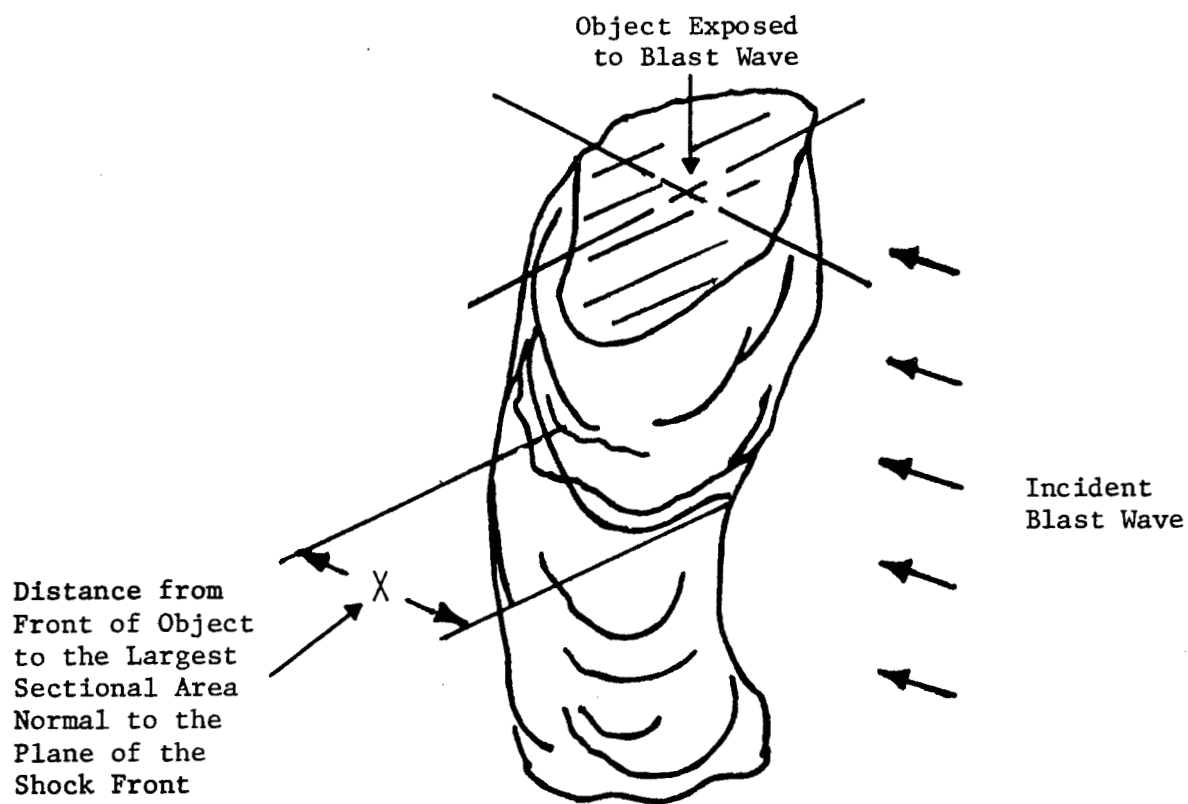
Isometric View of Object

Mean Presented
Area = A

H

Minimum Transverse Dimension
of Mean Presented Area
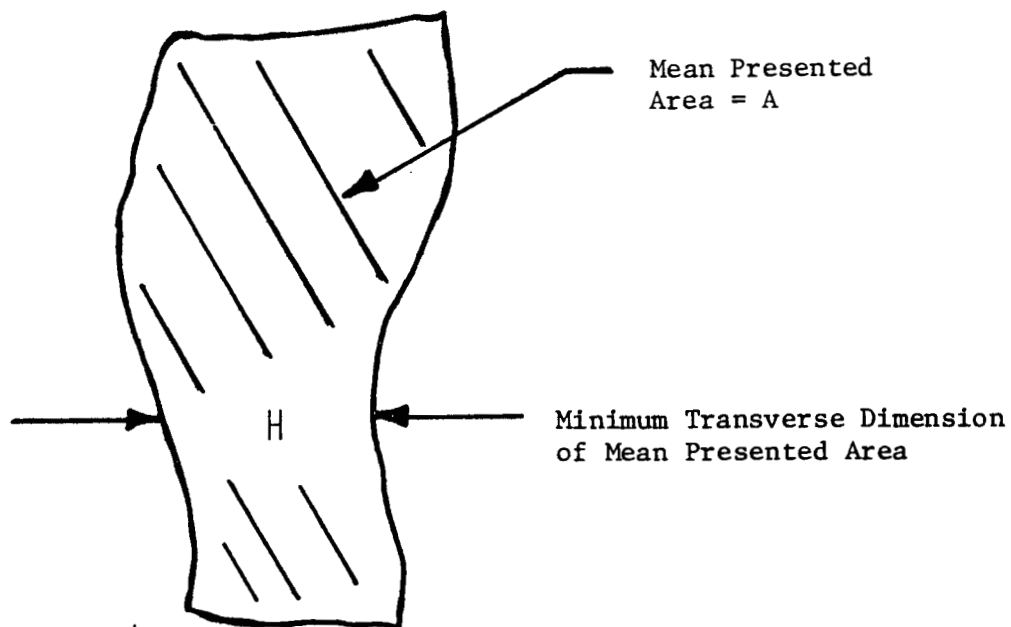
Front View of Object

Figure 6.8 Pictorial Explanation of Appurtenance Variables
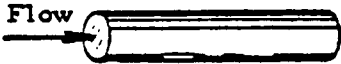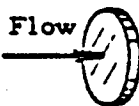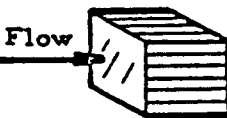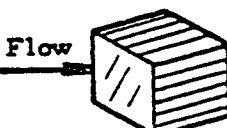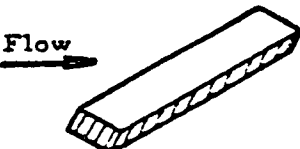
SHAPE	SKETCH	C_D
Right Circular Cylinder (long rod), side-on	Flow	1.20
Sphere		0.47
Rod, end-on	Flow	0.82
Disc, face-on	Flow or	1.17
Cube, face-on	Flow	1.05
Cube, edge-on	Flow	0.80
Long Rectangular Member, face-on	Flow	2.05
Long Rectangular Member, edge-on	Flow	1.55
Narrow Strip, face-on	Flow	1.98

Figure 6.9 Drag Coefficient, C_D, for Various Shapes
(Baker, Kulesz, et al., Ref. 6.3)
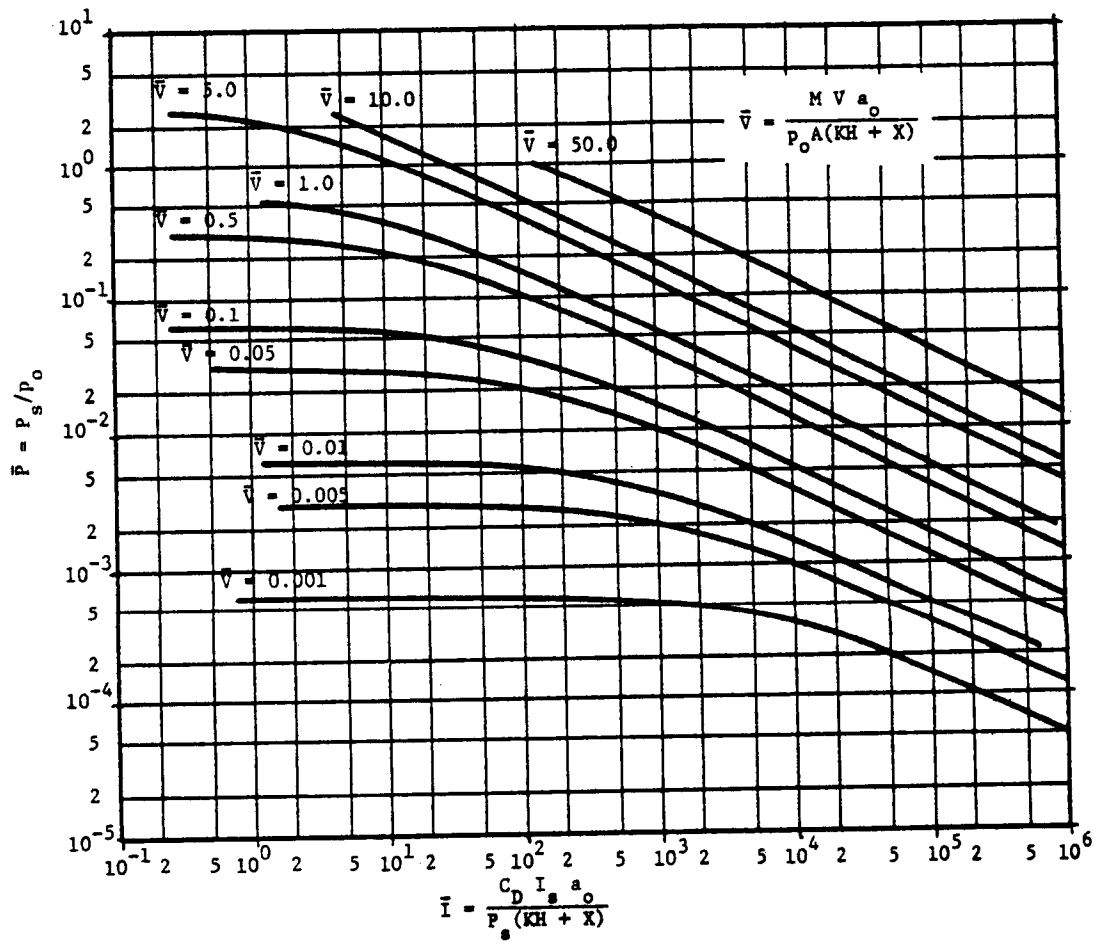
Figure 6.10 Nondimensional Object Velocity $\bar{V}$ as a Function of Nondimensional Pressure $\bar{P}$ and Nondimensional Impulse $\bar{I}$

6-30

To calculate the specific impulse imparted to the target, Westine (Ref. 6.19) conducted a model analysis for a target aligned parallel to a line charge which is larger than the target as shown in Figure 6.11. After eliminating terms which are invariant under similar atmospheric conditions such as the density of air, atmospheric pressure and the speed of sound and assuming that the effect of length of the target relative to the radius of the explosive is relatively insignificant, one has

$$\frac{i}{\beta R_e} \text{ is a function of } \left(\frac{R}{R_e}\right), \left(\frac{R_t}{R_e}\right) \text{ and } \left(\frac{\ell_e}{R_e}\right) \qquad (6.16)$$

where i = specific acquired impulse ($lb_f - s/ft^2$)

β = nondimensional shape factor of the target

R_e = radius of the explosive (ft)

R = standoff distance (ft)

R_t = target radius (ft)

ℓ_e = length of explosive line (ft)

An experimental program was conducted at the Ballistic Research Laboratories to determine empirically the functional format for Equation (6.16). In order to determine the specific impulse applied to a target when a blast from a line charge occurs, tests were conducted in which small spheres and cylinders were placed at various standoff distances from the center line of various size cylindrical explosive Comp B charges as shown in Figure 6.11. The test procedure was to detonate an explosive line charge and measure the resulting velocity imparted to unconstrained targets. The specific impulse imparted to the target could then be determined from

$$i = \frac{MV}{A\beta} \qquad (6.17)$$

where M = mass of object

V = velocity of object

A = projected area of object

The results of the curve fit to the experimental data are shown by the top curve in Figure 6.12. The ordinate in this figure has a quantity called R_{eff} in it instead of $R_e(\ell_e/R_e)^{0.333}$. This quantity R_{eff} stands for the effective radius of the equivalent sphere of explosive which could be formed from a cylinder of Radius R_e and length ℓ_e. The term R_{eff} is related to R_e and ℓ_e through

Cylindrical charge: $R_{eff} = 0.9086 \left(\frac{\ell_e}{R_e}\right)^{0.333} R_e \qquad (6.18a)$

Spherical charge: $R_{eff} = R_e \qquad (6.18b)$

The existence of two straight line regions for values of R/R_e less than and greater than 5.25 (cylindrical charges) is apparent in Figure 6.12. In the near field where R/R_e is less than 5.25, the slope of the line
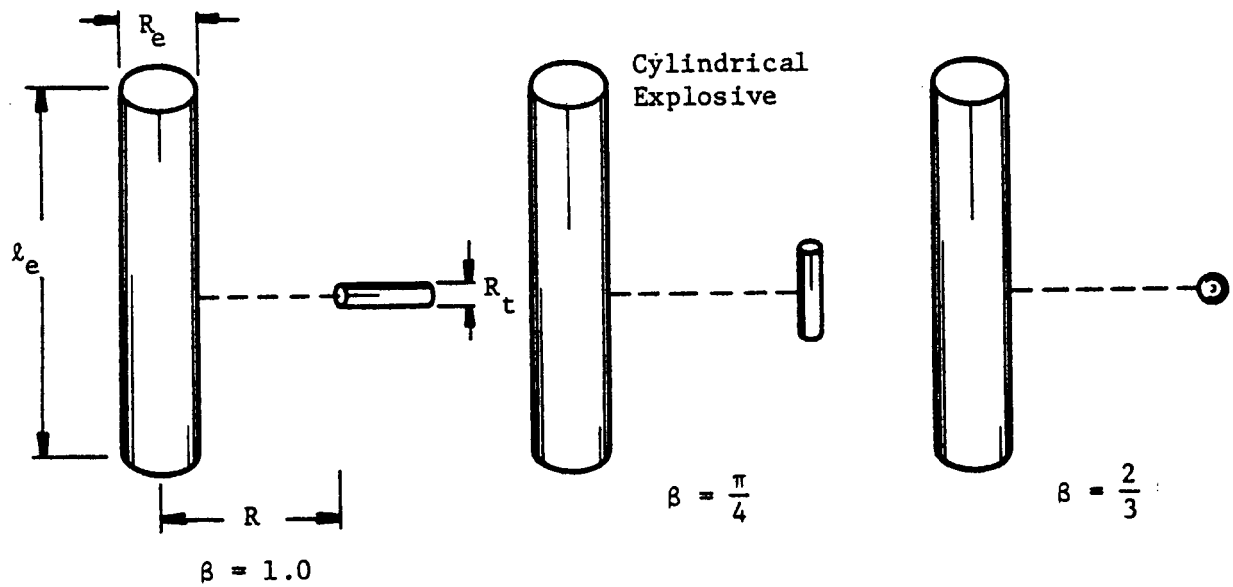
(a) Exposed Flat Face

(b) Exposed Cylindrical Surface

(c) Exposed Spherical Surface
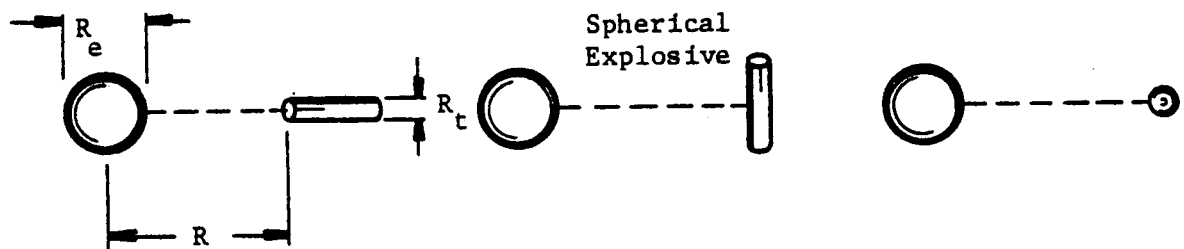
Figure 6.11 Target Orientation for Unconstrained Tests
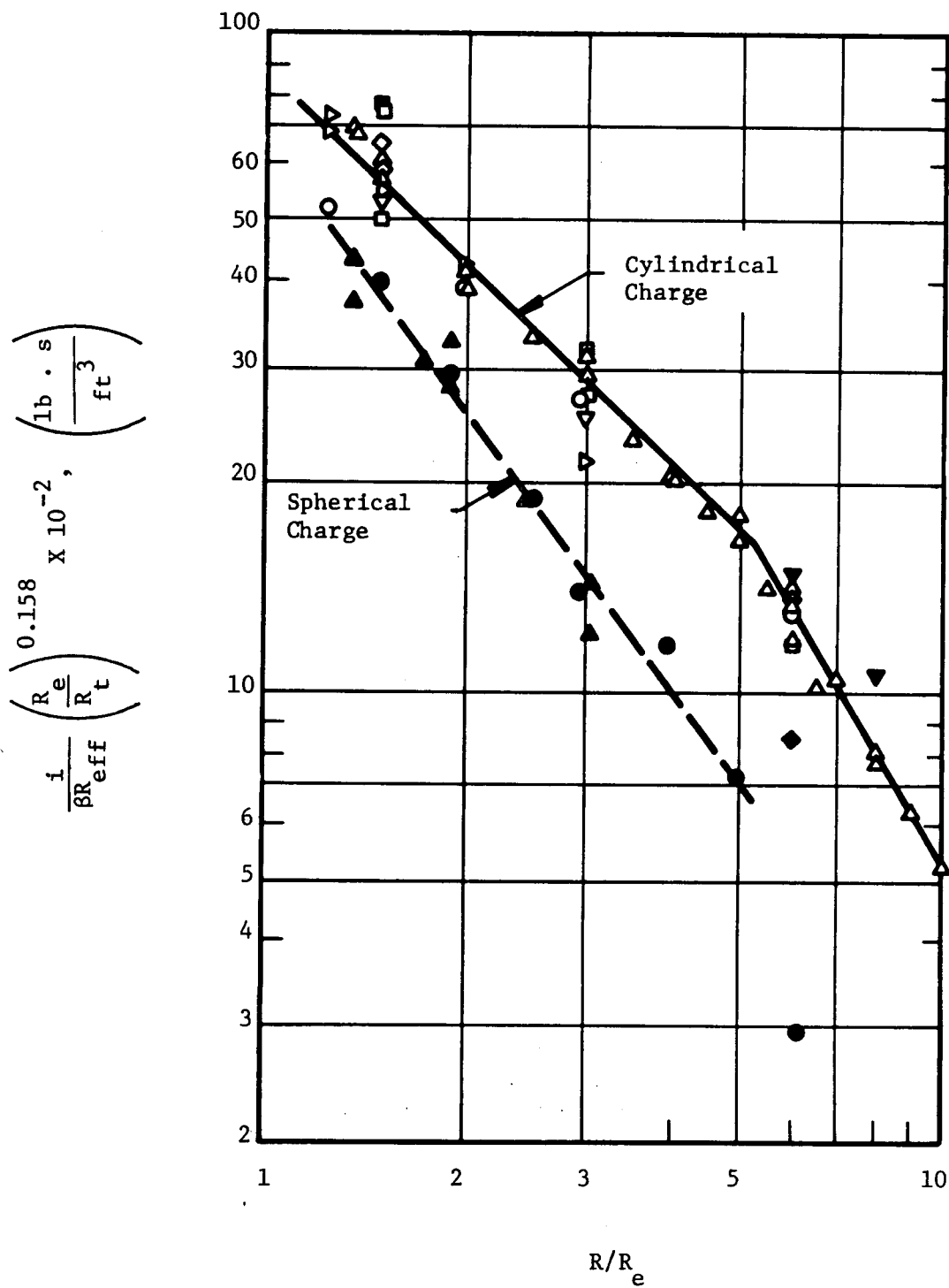
Figure 6.12. Specific Acquired Impulse
(Explanation of Symbols
Appear on Following Page)

for cylindrical charges in Figure 6.12 is minus 1.0 which means that $(i/\beta R_{eff}$ times (R/R_e) equals a constant for invariant R_e/R_t. The normally reflected specific impulse close to the line charge is thus caused primarily by momentum of the explosive products. In other words, the impulse close to the charge is caused by adding up the mass times the velocity products of all the particles from the explosive, casing, and engulfed air. Because the specific impulse i is caused by momentum in explosive products, it decays with standoff distance inversely as the surface area of a cylinder enclosing the line source, which equals $2\pi R\ell_e$. Only as standoff distances grow larger do the effects of momentum loss through air drag and gravitational effects reduce this phenomenon sufficiently for shock wave phenomena to become more important and the slope of the line to change, as shown by the top curve in Figure 6.12.

A similar relationship holds for objects exposed to nearby spherical charges of Comp B as shown by the bottom curve in Figure 6.12 which was determined by directly applying Westine's relationship to the data developed by Kineke (Ref. 6.20) for cylinders exposed end-on to spherical charges. Because the specific impulse i imparted to a target close to the charge is caused by momentum in explosive products, it decays with standoff distance inversely as the surface area of a sphere enclosing the spherical source, which equals $4\pi R^2$. (Standoff distance is the distance of the center of the charge to the nearest face of object.) The area of this sphere of engulfed air is larger than the area of the cylinder of engulfed air described above whenever $R > \ell_e$. Therefore, the specific impulse i imparted to objects exposed to spherical charges should decrease more rapidly with distance (for $R > \ell_e$) for objects exposed to cylindrical charges oriented as in Figure 6.11. This relationship is demonstrated by the steeper slope of the bottom curve (spherical charge) in Figure 6.11. When R equals R_e, the target is in contact with the charge and specific impulse imparted to the target should approach the same value for spherical and cylindrical charges. If one extends the curves in Figure 6.11 to R/R_e equal to one, one can observe that this relationship holds within the scatter of the data.

Baker (Ref. 6.21) performed a similar analysis in order to predict normally reflected impulses close to spherical explosive charges He experimentally determined that the scaling law applies for distances corresponding to a mass of engulfed air which is considerably less than (approximately one-tenth) the mass of the explosive. For a spherical Comp B explosive source, this would correspond to

$$\frac{R}{R_e} = \left[\frac{(0.1)\ \rho_{expl}}{\rho} \right]^{1/3} = 5.07$$

Examining the bottom curve in Figure 6.12, one will notice a transition in the curve near R/R_e equal to 5.07. However, lack of sufficient data hinders the determination of an accurate experimental transition point.

Thus, the curves in Figure 6.12 should not be used at distances beyond those shown by the lines in the figure. For longer distances from the explosive charge, Figure 6.10 can be used.

The straight lines plotted in Figure 6.12 can easily be put in equation form. These predictive equations are:

Cylindrical charges:

$$\frac{i}{\beta R_{eff}} \left(\frac{R_e}{R_t}\right)^{0.158} = 8.40 \times 10^3 \left(\frac{R_e}{R}\right) \text{ for } \frac{R}{R_e} \leq 5.25 \tag{6.19}$$

$$\frac{i}{\beta R_{eff}} \left(\frac{R_e}{R_t}\right)^{0.158} = 2.92 \times 10^4 \left(\frac{R_e}{R}\right)^{1.75} \text{ for } \frac{R}{R_e} \geq 5.25 \tag{6.20}$$

Spherical charges:

$$\frac{i}{\beta R_{eff}} \left(\frac{R_e}{R_t}\right)^{0.158} = 6.86 \times 10^3 \left(\frac{R_e}{R}\right)^{1.4} \text{ for } \frac{R}{R_e} \leq 5.07 \tag{6.21}$$

The units for the expression on the left-hand side in Equations (6.19), (6.20) and (6.21) are $lb \cdot sec/ft^3$.

If an explosive other than Composition B is used, the value for impulse i obtained from Figure 6.12 and the previous three equations need to be adjusted as follows:

$$i_{Comp\ B} = \frac{\left[\left(\Delta H_{Comp\ B}\right)^{1/2} \rho_{Comp\ B}\right]}{\left[\left(\Delta H_{expl}\right)^{1/2} \rho_{expl}\right]} \left(i_{expl}\right) \tag{6.22}$$

where ΔH is energy (heat of detonation) per unit mass,
ρ is density,
subscript "Comp B" represents Composition B explosive,
subscript "expl" represents explosive being used, and
$i_{Comp\ B}$ is the value of i obtained from Figure 6.12 or the previous three equations.
(NOTE: This equation was derived by Mr. Peter S. Westine of Southwest Research Institute using a model analysis.)

EXAMPLE PROBLEM 6.4

PROBLEM — Determine the velocity V of an unconstrained object close to an
exploding HE charge (See Figure 6.11). For illustrative purposes,
assume that a spherical charge of RDX explodes while being held
in a lathe. A cylindrical tool holder made of steel is resting
(unconstrained) on the lathe bed such that its longitudinal axis
is perpendicular to the radial line from the charge to the target.

GIVEN: W   = weight and type of HE (lb)
         R   = distance from center of explosive source to the sur-
                   face of object (standoff distance) (ft)
         R_e = radius of explosive (ft)
         R_t = radius of target (ft)
         β = shape factor for target
         M   = mass of target (lb-sec^2/ft)
         A   = mean presented area of target (ft^2)
         ΔH_{expl} = energy factor for explosive (same units as $\Delta H_{Comp\ B}$)
         $\Delta H_{Comp\ B}$ = energy factor for Comp B explosive (same units as ΔH_{expl})
         ρ_{expl} = density of explosive (same units as $\rho_{Comp\ B}$)
         $\rho_{Comp\ B}$ = density of Comp B explosive (same units as ρ_{expl})

FIND: V   REFERENCE

SOLUTION: 1. Calculate the ratio of standoff distance R
               and radius of explosive R_e
               R/R_e Fig. 6.11
           2. If R/R_e is less than 10 for cylindrical charges Fig. 6.12
               or less than 5 for spherical charges, determine
               the imparted impulse.
           3. If the explosive is not Comp B adjust impulse   Table 6 of
               by multiplying the impulse imparted to the   Appendix A
               target by the energy/density ratio.   (Physical
                                                               Properties
                                                               of Explosives)

$$i_{Comp\ B} = \frac{\left[\left(\Delta H_{Comp\ B}\right)^{1/2} \rho_{Comp\ B}\right]}{\left[\left(\Delta H_{expl}\right)^{1/2} \rho_{expl}\right]} \left(i_{expl}\right)$$ Eq. (6.22)

           4. Calculate the velocity of the unconstrained
               object.
               $$V = \frac{A\ \beta\ i_{expl}}{M}$$ Eq. (6.17)

6-36

CALCULATION

GIVEN: a spherical charge of RDX
W = 10 lb
R = 1.0 ft

$$R_e = \left(\frac{3W}{4\pi\rho}\right)^{1/3} = \left[\left(\frac{3}{4\pi}\right)\frac{(10 \text{ lb})}{(1.806 \text{ g/cm}^3)(1 \text{ lb}/454 \text{ g})(2.54 \text{ cm/in.})^3(12 \text{ in./ft})^3}\right]^{1/3} = 0.28 \text{ ft}$$

R_t = (1.0 in.) (1.0 ft/12 in.) = 0.083 ft

β = $\pi/4$

M = $(\pi r^2 \ell)\rho$ = $\pi(1.0 \text{ in.})^2(8.0 \text{ in.})(7.36 \times 10^{-4} \text{ lb-sec}^2/\text{in.}^4)$
= 5.89×10^{-3} lb-sec^2/in.

A = (2.0 in.)(8.0 in.)(1.0 ft^2/144 in.^{2}) = 0.11 ft^2

ΔH_{RDX} = 0.909 (TNT equivalent weight)

$\Delta H_{Comp\ B}$ = 0.881 (TNT equivalent weight)

ρ_{RDX} = 1.806 g/cm^3

$\rho_{Comp\ B}$ = 1.74 g/cm^3

FIND: V

SOLUTION: 1. R/R_e = 1.0 ft/0.28 ft = 3.6

2. R/R_e is less than 5 (spherical charge). Vertical axis of Figure 6.12 has a value of ∿12 lb-s/ft^2. Therefore, i = 12 $\beta R'(R_t/R_e)^{0.158} \times 10^2$ where $R' = R_e$ for spherical charges.

$$i = \left(12\frac{\text{lb}-\text{s}}{\text{ft}^3}\right)\left(\frac{2}{3}\right)\left(0.28 \text{ ft}\right)\left(\frac{0.083 \text{ ft}}{0.28 \text{ ft}}\right)^{0.158} \times 10^2 \text{ lb}-\text{s/ft}^3 = 185 \text{ lb}-\text{s/ft}^2$$

Note that one could have substituted the appropriate values into Equation (6.22) to determine the value for i.

3. $$i_{RDX} = \frac{\left[\left(\Delta H_{RDX}\right)^{1/2} \rho_{RDX}\right]}{\left[\left(\Delta H_{Comp\ B}\right)^{1/2} \rho_{Comp\ B}\right]}\left(i_{Comp\ B}\right)$$

$$i_{RDX} = \frac{(0.909)^{1/2} (1.806 \text{ g/cm}^3)}{(0.881)^{1/2} (1.74 \text{ g/cm}^3)} \ 185 \text{ lb}-\text{s/ft}^2 = $$
195 lb - s/ft^2

4. $$V = \frac{A\ \beta\ i_{RDX}}{M} = \frac{(0.11 \text{ ft}^2)\ (2/3)\ (195 \text{ lb}-\text{s/ft}^2)}{(12 \text{ in./ft})(5.89 \times 10^{-3} \text{ lb-sec}^2/\text{in.})} = \underline{202 \text{ ft/s}}$$

EXAMPLE PROBLEM 6.5

PROBLEM - Determine the velocity V of an unconstrained object far from
an exploding HE charge $(R/R_e >> 10)$ (see Figure 6.8). For
illustrative purposes, assume that a spherical charge of RDX
explodes while being held in a lathe. A cylindrical tool holder
made of steel is resting (unconstrained) on a nearby table next
to the lathe such that its longitudinal axis is perpendicular
to the radial line from the charge to the target.

GIVEN: M = mass of object (lb-sec^2/ft)
        A = mean presented area of object (ft^2)
        K = constant (4 if object is on the ground or reflecting
            surface and 2 if object is in air)
        H = minimum transverse distance of the mean presented area of
            object (ft)
        X = distance from the front of object to location of its
            largest cross-sectional area (ft)
        C_D = drag coefficient
        a_o = velocity of sound in air (ft/sec)
        p_o = atmospheric pressure (psi)
        P_s = peak incident overpressure (psi)
        i_s = incident specific impulse (psi-sec)

FIND: V   REFERENCE

SOLUTION: 1. Calculate nondimensional pressure. P_s from
               $\bar{P} = P_s / p_o$ Chapter 4
                                                            (as function
                                                            of standoff
                                                            distance R
                                                            and charge
                                                            weight W)

           2. Calculate nondimensional impulse.

               $\bar{i} = \dfrac{C_D i_s a_o}{P_s (KH+X)}$ C_D from Fig.
                                                            6.9, i_s from
                                                            Chapter 4
                                                            (as function
                                                            of standoff
                                                            distance R
                                                            and charge
                                                            weight W)

3. Locate the point $(\bar{I}, \bar{P})$ on Figure 6.10 and
   determine nondimensional velocity $\bar{V}$.   Fig. 6.10

4. Calculate the velocity of object.

$$V = \frac{\bar{V} p_o A(KH+X)}{M a_o}$$ Fig. 6.10

CALCULATION

GIVEN: In example problem 6.4, $R_e = 0.28$ ft. For this problem, let
         $R = 10$ ft and $W = 10.28$ lb of RDX. Thus $R/R_e = 10/0.28 = 36$.

   $M = 7.07 \times 10^{-2}$ lb-sec^2/ft (see example problem 6.4)

   $A = 0.11$ ft^2 (see example problem 6.4)

   $K = 4$ (object on ground or reflecting surface)

   $H = 0.17$ ft (diameter of object in this case – see example
       problem 6.4)

   $X = 0.083$ ft (radius of object in this case – see example
       problem 6.4)

   $C_D = 1.20$ (figure 6.9 for cylinder loaded perpendicular to axis)

   $a_o = 1100$ ft/sec

   $p_o = 14.7$ psi

   $P_s = 33$ psi $\left.\begin{array}{l} \\ \\ \end{array}\right\}$ Chapter 4 (scaled distance $R/W^{1/3} =$

   $i_s = 0.025$ psi-sec $\quad$ 10 ft/(10.28 lb × 1.149)$^{1/3}$ = 4.39 ft/lb$^{1/3}$

FIND: V

SOLUTION: 1. $\bar{P} = P_s/p_o = 33$ psi/14.7 psi = 2.24

   2. $\bar{i} = \dfrac{C_D\, i_s\, a_o}{P_s\,(KH+X)} = \dfrac{(1.20)(0.025\ \text{psi-sec})(1100\ \text{ft/sec})}{(33\ \text{psi})\,[(4)(0.17\ \text{ft})+(0.083\ \text{ft})]} = 1.31$

   3. $\bar{V} = 5.0$

   4. $V = \dfrac{\bar{V}\, p_o\, A(KH+X)}{M\, a_o}$

$$= \frac{(5.0)(14.7\ \text{lb/in.}^2)(144\ \text{in.}^2/\text{ft}^2)(0.11\ \text{ft}^2)[(4)(0.17\ \text{ft}) + (0.083\ \text{ft})]}{(7.07 \times 10^{-2}\ \text{lb-sec}^2/\text{ft})\ (1100\ \text{ft/sec})}$$

= <u>11.4 ft/sec</u>

EXAMPLE PROBLEM 6.6

PROBLEM – Same as the example problem 6.5 in this section except R/R_e
          is slightly greater than 10.

CALCULATION

GIVEN: In example problems 6.4 and 6.5, R_e = 0.28 ft. For illustrative
purposes, assume that the standoff distance R is 3.0 ft.
Thus, R/R_e = 3.0/0.28 = 11.

W = 10.28 lb of RDX

M = 7.07 x 10^{-2} lb-sec^2/ft (see example problem 6.4)

A = 0.11 ft^2 (see example problem 6.4)

K = 4 (object on ground or surface)

H = 0.17 ft (diameter of object in this case)

X = 0.083 ft (radius of object in this case)

C_D = 1.20 (figure 6.9 for cylinder loaded perpendicular to axis)

a_o = 1100 ft/sec

p_o = 14.7 psi

P_s = 560 psi $\left.\begin{array}{l} \\ \\ \end{array}\right\}$ Chapter 4 (scaled distance $R/W^{1/3}$) =

i_s = 0.0342 psi-sec $\quad$ 3.0 ft/(10.28 lb x 1.149)$^{1/3}$ = 1.32 ft/lb$^{1/3}$

FIND: V

SOLUTION: 1. $\bar{P} = P_s/p_o$ = 560 psi/14.7 psi = 38.1

2. $\bar{i} = \dfrac{C_D\, i_s\, a_o}{P_s\,(KH+X)} = \dfrac{(1.20)(0.0342 \text{ psi-sec})(1100 \text{ ft/sec})}{(560 \text{ psi})\,[(4)(0.17 \text{ ft})+(0.083 \text{ ft})]} = 0.106$

3. Since the point ($\bar{i}$, $\bar{P}$) is outside the range of Figure 6.10,
one is unable to calculate the velocity accurately. One
can overestimate the velocity by assuming that the object
is closer to the charge and using Figure 6.12 for R/R_e = 5.0
(see example problem 6.4).

6.2.2.2 Constrained Secondary Fragments

Westine (Ref. 6.19) has developed an engineering procedure for estimating secondary fragment velocities when objects are exposed to explosive detonations. This objective was accomplished by dividing the problem into two parts. The first part concerned estimating the specific impulse imparted to unconstrained flat, cylindrical, and spherical secondary fragments in the vicinity of cylindrical explosive charges. The second part concerned estimating the velocity of constrained beams of any material and cross-sectional area which could become secondary fragments because of this impulsive load.

The first half of Westine's analysis, consisting of predicting the specific impulse imparted to objects in the vicinity of cylindrical explosive charges, was described in the previous section. A method for predicting the specific impulse imparted to objects in the vicinity of spherical explosive charges is also given in the previous section. For unconstrained objects, values of imparted specific impulse can be used directly to determine velocity.

The second half of Westine's analysis consisted of the development of a method to determine the amount of energy consumed in freeing the constrained object from its moorings. The strain energy U consumed in fracturing a cantilever beam was estimated by assuming a deformed shape and substituting the appropriate mechanics relationships for different modes of response in both ductile and brittle beams. A number of different solutions resulted which had sufficient similarities to permit generalization after the strain energies were developed.

To develop the analysis, Westine determined the strain energy at fracture by assuming a deformed shape with appropriate boundary conditions. Westine performed the analysis using ductile bending, brittle bending, ductile shear, and brittle shear failure modes and various shapes of beam cross sections. The results of the analysis appear in Table 6.3. In this table, U is strain energy, T is toughness (the area under the stress-strain curve), A is the cross-sectional area of the beam, and ℓ is the length of the beam. Also, Z is the plastic section modulus, h is the depth of the beam, S is the elastic section modulus, and ν is Poisson's ratio.

The major point which should be made from these solutions for strain energy for the four different modes of failure is that, no matter what mode of failure is hypothesized, the strain energy at failure equals (TAℓ) times a constant. For some modes of failure, the constant may be a weak function of the cross-sectional shape of the fragment (a function of S/Ah or Z/Ah), but this constant varies little. Table 6.3 demonstrates the limited variation in these constants.

Table 6.3 Variations in Strain Energy Coefficients $\frac{U}{TA\ell}$

Shape Of Beam Cross Section \ Type of Failure	Ductile Bending	Brittle Bending	Ductile Shear	Brittle Shear
General Solution	$\frac{4}{\pi}\frac{Z}{Ah}$	$\frac{S}{Ah}$	$\frac{1}{2}$	$\frac{1}{2(1+\nu)}$
Circular Solid	0.270	0.125	0.500	0.385
Rectangular Solid	0.318	0.167	0.500	0.385
I-Beam	$\sim$0.637	$\sim$0.500	0.500	0.385

The second major conclusion is that toughness T appears to be the only mechanical property of importance. All four solutions give the result that this area under the stress-strain curve times the volume of the specimen times a constant equals the strain energy U expended in fracturing the specimen.

For analysis purposes these conclusions indicate that the mode of failure does not have to be determined. The solution can proceed by assuming that strain energy is given by Equation (6.19) and that the constant C can be obtained from experimental test results.

$$U = C(TA\ell) \tag{6.23}$$

The use of a different deformed shape will not change the conclusions that U is directly proportional to $(TA\ell)$; however, a different shape will result in a slightly different numerical proportionality constant C. Because C is determined experimentally, the qualitative conclusions still can be applied in the development of a solution.

All four modes of failure were developed for failure in a cantilever beam. Other boundary conditions such as clamped-clamped, simply supported, etc., will give similar qualitative results; however, the proportionality coefficient C is a function of support conditions (Ref. 6.19).

Using the conservation of momentum and allowing the structural constraint to reduce the imparted impulse by an amount I_{st}, one has

$$I - I_{st} = mV \tag{6.24}$$

where I is the total impulse acquired by the target. Substituting $\sqrt{2m\Delta H}$ for I_{st} and rearranging terms yields the conservation of momentum relationship

$$\frac{I}{\sqrt{m\Delta H}} = \sqrt{2} + \frac{\sqrt{mV}}{\sqrt{\Delta H}} \tag{6.25}$$

Total impulse I equals $ib\ell$ where b is the loaded width, ℓ is the loaded length, and total mass m of the fragment equals $\rho_s A\ell$ where ρ_s is the density of the constrained object and A is its cross-sectional area in the plane perpendicular to the long axis of the target. Substituting these relationships and the strain energy U as given by Equation (6.23) into Equation (6.25) one has

$$\frac{i \, b \, \ell}{\sqrt{(\rho_s A\ell)(CTA\ell)}} = \sqrt{2} + \frac{\sqrt{\rho_s A\ell} \, V}{\sqrt{CTA\ell}} \tag{6.26}$$

or after reduction

$$\frac{i \, b}{\sqrt{\rho_s T} \, A} = \sqrt{2C} + \frac{\sqrt{\rho_s} \, V}{\sqrt{T}} \tag{6.27}$$

Equation (6.27) is a two-parameter space for nondimensional energy ratios. If the term $\sqrt{\rho_s} \, V/\sqrt{T}$ is squared, this group is the ratio of fragment kinetic energy per unit volume to strain energy expended per unit volume. The square of the term $i \, b/A \sqrt{\rho_s T}$ represents the energy put into the fragment per unit length divided by the strain energy expended per unit length of fragment. This solution infers that the constrained secondary fragment velocity is independent of beam length ℓ. Test results show that this conclusion is not quite accurate.

After curve fitting to experimental data, Westine (Ref. 6.19) concluded that the velocity of the constrained fragment could be described by

$$\frac{\sqrt{\rho_s} \, V}{\sqrt{T}} = -0.2369 + 0.3931 \left(\frac{i \, b}{\sqrt{\rho_s T} \, A}\right)\left(\frac{\ell}{b/2}\right)^{0.3}$$

$$\text{for} \quad \left(\frac{i \, b}{\sqrt{\rho_s T} \, A}\right)\left(\frac{\ell}{b/2}\right)^{0.3} \geq 0.602 \tag{6.28}$$

$$V = 0 \quad \text{for} \quad \left(\frac{i \, b}{\sqrt{\rho_s T} \, A}\right)\left(\frac{\ell}{b/2}\right)^{0.3} \leq 0.602$$

where V = fragment velocity
      ρ_s = fragment mass density
      T = toughness of fragment material
      b = loaded width of beam
      ℓ = length of target
      A = cross-sectional area
      i = specific impulse

This pair of equations works for <u>cantilever beams</u> of any materials and any cross-sectional area. To estimate the velocity, the specific impulse i imparted to the beam is an estimate from the standoff distance and line charge geometry using the technique described in the previous section. Substituting this impulse, beam properties and beam geometry into Equation (6.28) gives the fragment velocity (see Figure 6.13). If the quantity $(i\, b/\sqrt{\rho_s T}\, A)(\ell/b/2)^{0.3}$ is less than 0.602, the fragment will not break free; hence, its velocity is zero.

An equation similar in format to Equation (6.28) but with different coefficients for slope and intercept can also be used for beams with other boundary or support conditions. Although Westine did not have a large quantity of data available to demonstrate this observation, enough data existed on <u>clamped-clamped beams</u> to show that the coefficients -0.6498 instead of -0.2369 and 0.4358 instead of 0.3931 work better for this boundary condition.

The chart plots $V\sqrt{\rho_s/T}$ (vertical axis) versus $\left(\dfrac{ib}{(\sqrt{\rho_s T})A}\right)\left(\dfrac{\ell}{b/2}\right)^{0.3}$ (horizontal axis).

SYM	MATERIAL	λ/B/2	λ
◇	1020 STEEL	6	π/4
◆	1020	12	π/4
	1020	18	π/4
◆	1095	6	π/4
△	1095	12	π/4
▲	1095	18	π/4
▲			π
▲			π
▷	1095	13.5	1.0
✕	2024-T3AL	12	π/4
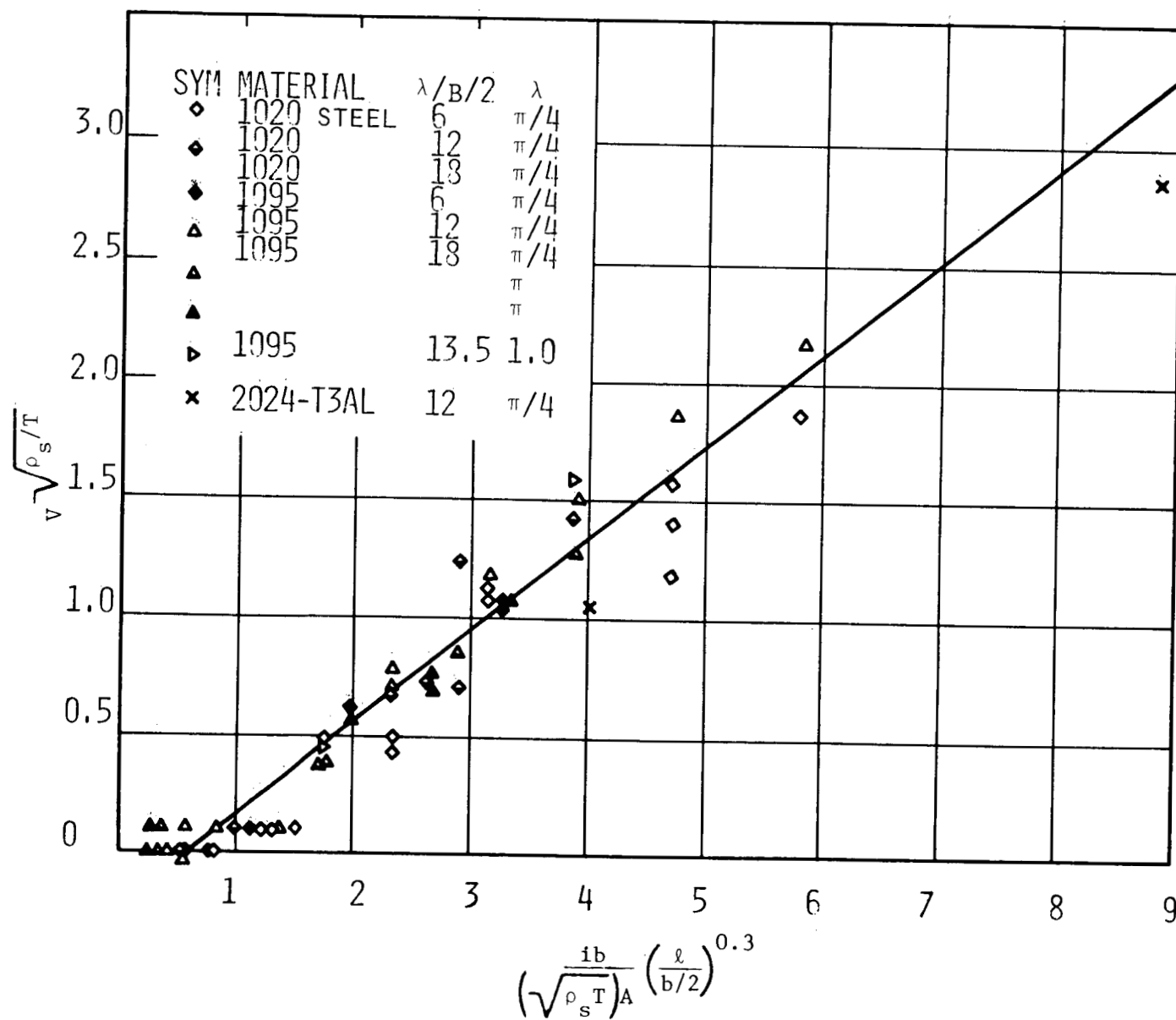
Figure 6.13   Scaled Fragment Velocities for Constrained Cantilever Beams

PROBLEM – Determine the velocity V of a constrained object close to an
exploding HE charge. For illustrative purposes, assume a
spherical charge of RDX explodes while being held in a lathe.
A cylindrical tool holder made of steel is clamped (constrained
cantilever) to the lathe bed such that its longitudinal axis
is perpendicular to the radial line from the charge to the
target. (See example problem 6.4 of section 6.2.2.1 for
numerical values to be used in this problem.)

GIVEN: ρ = fragment mass density (lb-sec/in^4)
         T = toughness of fragment material (in.-lb/in.^{3})(toughness is
             the area under the true-stress vs true-strain curve)
         ℓ = length of object (in.)
         b = loaded width of object (in.)
         A = cross-sectional area of the member (in.^{2})
         i = specific impulse imparted to object (psi-sec)
         boundary condition = cantilever or clamped-clamped

Find: V

SOLUTION: 1. $\left(\dfrac{i\,b}{\sqrt{\rho T}\;A}\right)\left(\dfrac{\ell}{b/2}\right)^{0.3}$ REFERENCE
                                                                  Eq. 6.28
            2.   V

CALCULATION

GIVEN: ρ = 7.324 x 10^{-4} lb·s^2/in^4
         T = 17,000 in.-lb/in.^{3}
         b = 2.0 in.
         ℓ = 8.0 in.
         A = (2.0 in.)(8.0 in.) = 16 in.^{2}
         i = (195 lb sec/ft^2)(1.0 ft^2/144 in.^{2}) = 1.35 lb-sec/in.^{2}
             (see example problem 6.4 in section 6.2.2.1)

FIND: V

SOLUTION: 1. $\left(\dfrac{i\,b}{\sqrt{\rho T}\;A}\right)\left(\dfrac{\ell}{b/2}\right)^{0.3} = \dfrac{(1.35\text{ lb-sec/in.}^2)(2.0\text{ in.})}{\sqrt{(7.324\times10^{-4}\text{ lb-sec}^2/\text{in.}^4)17{,}000\left(\dfrac{\text{in.-lb}}{\text{in.}^3}\right)}\,(16\text{ in.}^2)}$

            $\times \left[\dfrac{(8.0\text{ in.})}{(2.0\text{ in.}/2)}\right]^{0.3}$

            = 0.0892

2. V = 0 (object does not break loose)

NOTE: An implicit assumption is that the lathe will remain
       intact. This may or may not be true. The AE should
       consider all reasonable failure modes.

6.2.3 Building Fragmentation

Estimating, for design considerations, the manner(s) in which a structure will fragment when subjected to an internal blast, involves several considerations.

The AE should take into account:

- type and configuration of explosive;
- location and size of charge; and
- structural strength.

The type of explosive is considered in order to estimate the probability of a high-order detonation. Note that if a deflagration is expected instead of a detonation, it may be possible to achieve blast attenuation through the proper use of vent panels (see Chapter 4). The configuration of the charge (i.e., cased, uncased, shaped charge, etc.) is considered as a means of predicting the occurrence and possibly the direction of primary fragments. Note that the location and size (weight) of the charge is important to estimate overpressure and impulses at various points on the structure. This information is also helpful in estimating any blast enhancement which may occur as the shock wave reflects within the structure.

The structural strength of the building is the primary consideration for predicting fragment distributions. The AE should evaluate the most likely failure mode(s) (i.e., spalling, shear, bending, etc.) for various points of the structure. His evaluation should be based on the expected blast and fragment parameters as determined in the first two considerations and the strength of the structure in the various modes of failure. For illustrative purposes, general observations of the response of specific structures involved in accidental explosions, safe-separation studies, and a protective design experiment follow. The cases considered include the free-standing building involved in an accidental detonation at the Pantex plant on March 30, 1977 (Ref. 6.17), full-scale igloo tests (Ref. 6.22), and the Swedish protective structure tests (Ref. 6.23). These illustrative examples were included to give the AE an idea of some of the things to look for when predicting building fragmentation.

- Pantex Plant

The information contained in this section of the manual is a summary of an HE accident which occurred at the Pantex Plant. If the AE needs additional information, he should read Reference 6.17.

The area of the building involved in the accidental explosion on March 30, 1977, may be viewed as a free-standing cubicle with three blast-resistant walls. These walls were 3-ft, 1-ft, and 1-ft thick concrete.

They were analyzed after the accident and determined capable of sustaining impulsive loads of 2100, 415 and 350 psi-ms before failure (values differ due to reinforcement variations). The fourth wall was constructed of concrete blocks with no dowels extending into the foundation, allowing it "... to act as a blow-out wall" (Ref. 6.17). The 1-ft thick concrete walls experienced shear failure at the floor and wall intersections, as would be predicted using TM5-1300 (Ref. 6.6). The 1-ft wall closest to the charge was discovered to have a 4-ft diameter hole in an area essentially perpendicular to the charge. The block wall "exploded" outward perpendicular to its original position. The poured lightweight roof was ejected as fragments in a rough hemisphere in response to the orientation of the charge within the structure (Ref. 6.17).

The explosion at the Pantex Plant caused several modes of structural failure resulting in a disparate distribution of fragments. The apparent shearing and subsequent motion of the 1-ft concrete walls resulted in large short range fragments which inflicted extensive damage on the walls of neighboring bays. Overpressure also caused extensive damage throughout the building.

● Igloo Tests

The Eskimo igloo test series was conducted to determine the minimum permissible spacing between earth-covered, steel-arch magazines (Ref. 6.22). As a result, very little data were collected with regard to the manner in which a donor structure fragmented, although in one case a limited survey was made of the fragment dispersion.

This test involved a steel-arch igloo constructed of one-gage corrugated steel, in accordance with the Office of the Chief of Engineers Specification 33-15-64-62, and covered with a compacted earth mound, 2-ft thick at the top with side slopes of one in two. The igloo was 14-ft, 4-in. high inside, 25-ft wide at the curbs, and 59-ft long. An earth barricade was constructed in front of the igloo, with a distance of 25 ft between the igloo and the toe of the barricade. The barricade was 3-ft thick at the top, about 14-ft high, had side slopes of one in two, and was long enough to subtend a full 60° angle to the door of the igloo. The only compaction of the soil was that incidental to the passage of earth-moving equipment during construction (Ref. 6.22).

Similar igloos, without a barricade in front, were constructed on either side of the donor igloo. These igloos were separated from the donor igloo by 58 ft and 70 ft, corresponding to $1.25 \times W^{1/3}$ and $1.5 \times W^{1/3}$, respectively. The three igloos were connected via a concrete headwall designed to shear between the igloos as shown in Figure 6.14. The donor charge consisted of 100,000 lb ($W^{1/3} = 46.4$) of Composition B, packed in 2,106 sealed, 9.5-in. cubical cans, with 47.5 lb of explosive in each container (Ref. 6.22).
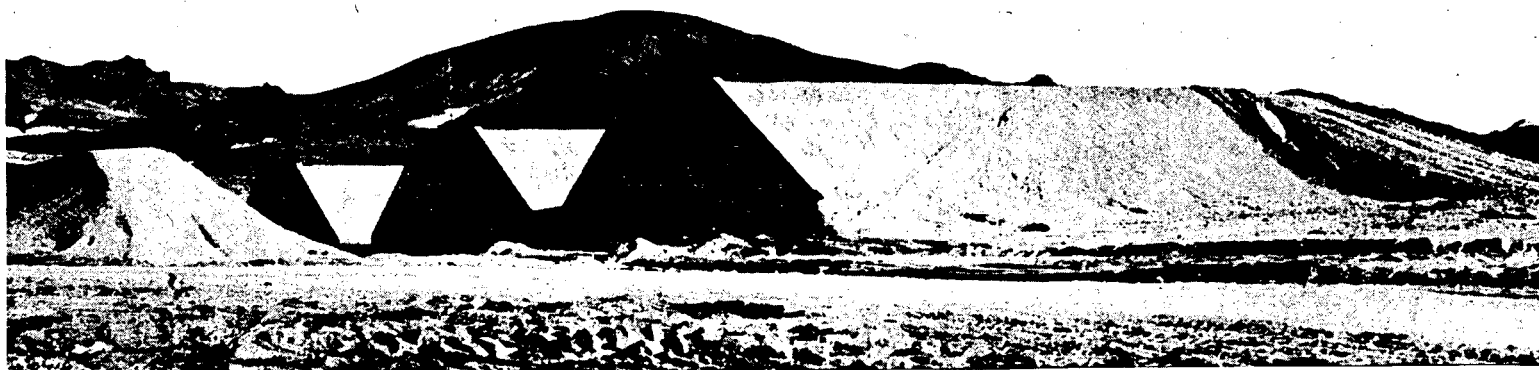
Figure 6.14 Magazines and Barricades (Ref. 6.22)

Detonation of the 100,000 lb charge resulted in complete destruction of the donor magazine. A limited survey revealed that four main types of fragments were thrown long ranges. These included fragments of steel reinforcing bars, steel arch, concrete, and clods of earth. The maximum range of soil fragments was 3300 ft. The clod which travelled this distance weighed approximately 15 lb before impact and broke into smaller pieces at impact. This size was typical of many other clods. The larger pieces of steel arch, 50 percent to 80 percent of a complete panel, were limited to a radius of 1600 ft, with one 24-in. x 24-in. fragment being found 2900 ft in front of the igloos. Most of the larger concrete fragments were scattered to 800 ft in front of the igloos, with the main concentration in zones of 25° to 50° from the igloo center line. The earth barricade effectively intercepted most of the steel door fragments and limited their travel to approximately 200 ft beyond the barricade. However, a few small door to door-frame fragments were found 2000 to 2450 ft in front of the magazines.

● Protective Structures

Swedish protective structures are designed for use in three ranges of explosive quantity (Ref. 6.23):

Class A - 1 to 20 lb of TNT
Class B - 21 to 200 lb of TNT
Class C - 201 to 2000 lb of TNT

Structures containing less than 20 lb of TNT are designed to remain intact in the event of an explosion. Structures containing explosive quantities in the Class B or C range are expected to fail, but are designed to fail in a specific manner, allowing safety zones to be well defined.

In the range from approximately 20 lb to 200 lb of TNT, a "kinematic chain design" has been used to some extent in Sweden. This design is based on varying the strength of the joints between adjoining plate elements. The weak connections have short pins through construction joints, supplying enough strength to place the failure threshold due to ripping forces just beyond the wind and snow load. The strong connections have continuous reinforcing bars, some of which are specially fashioned to provide an unimpeded hinge effect. In the general design, all the walls are connected to the foundation by strong hinges. The roof is similarly hinged to one of the walls and all other connections are weak. These hinged joints allow the building to unfold, limiting the building debris to the immediate vicinity. Also, since the response of the heavy plate elements is slow with respect to the velocity of most "primary" fragments emanating from around the charge, many will be stopped by the structures (Ref. 6.23).

For structures involving approximately 200 to 2000 lb of TNT a similar design procedure is followed. The major difference in this design is that hinges are no longer used to try to restrain the walls and roof. Instead, connection between plates are built to fail at different strengths so that fragments may be directed in predetermined zones (Ref. 6.23).

6.2.4 Trajectories and Impact Conditions

6.2.4.1 Trajectories

After a fragment has acquired an initial velocity, that is, the fragment is no longer accelerated by an explosion or pressure rupture, two forces act on the fragment during its flight. These are gravitational forces and fluid dynamic forces. Fluid dynamic forces are usually sub-divided into drag and lift components (see Figure 6.1). The effect of drag and lift will depend both on the shape of the fragment and its direction of motion with respect to the relative wind. The fluid dynamic force components of drag and lift at any instant can be expressed as:

$$F_D = C_D \, A_D \, (1/2) \, \rho \, V^2 \tag{6.29}$$

and

$$F_L = C_L \, A_L \, (1/2) \, \rho \, V^2 \tag{6.30}$$

where C_D and C_L are drag and lift coefficients determined empirically as a function of shape and orientation with respect to the velocity vector and A_D and A_L are drag and lift areas, respectively. V is the velocity of the fragment and ρ is the density of the medium. Most of the fragments generated during explosives accidents described in this manual will be "chunky" drag fragments.

In a simplified trajectory problem (Ref. 6.16), where the fragment is considered to move in one plane, equations of motion can be written for acceleration in the X and Y direction.

The acceleration in the Y direction (drag only) is:

$$\ddot{Y} = -g - \frac{A \, C_D \, \rho \, (\dot{X}^2 + \dot{Y}^2)}{2M} \sin \alpha \tag{6.31}$$

and for the X direction (drag only):

$$\ddot{X} = - \frac{A \, C_D \, \rho \, (\dot{X}^2 + \dot{Y}^2)}{2M} \cos \alpha \tag{6.32}$$

where A = area of fragment

C_D = drag coefficient

at t = 0

$$\dot{X} = V_i \cos \alpha_i \tag{6.33}$$

$$\dot{Y} = V_i \sin \alpha_i \tag{6.34}$$

where V_i = initial velocity

α_i = initial trajectory angle

The equations shown above can be solved simultaneously using the Runge-Kutta method and can be used for fragment velocities up to Mach 1 for standard conditions. Baker, Kulesz, et al. (Ref. 6.3) have exercised the FRISB program to determine fragment range for a number of conditions. Some of this work was duplicated by Baker, Kulesz, et al. (Ref. 6.16) and put in a more convenient form. Figure 6.15 summarizes the results for fragments affected only by drag forces.

The curve in Figure 6.15 was developed by first performing a model analysis to generate dimensionless parameters which describe the general problem. There the computer code FRISB was used to determine ranges for selected cases, and to plot results. It should be noted that, in generating this curve, several initial trajectory angles were used in the analysis to obtain the <u>maximum range</u> for the respective fragments. Thus, one does not need to know the initial trajectory angle of the fragment in order to use Figure 6.15.

When using Figure 6.15, units should be chosen for each of the parameters such that the terms on the axes have dimensionless units. Figure 6.6 contains drag coefficients C_D for various simple geometries. If needed, maximum ranges for lifting fragments can be acquired from range curves in Reference 6.20.

$$\frac{\rho_o C_D A_D R}{M}$$

$$\frac{\rho_o C_D A_D V_o^2}{Mg}$$
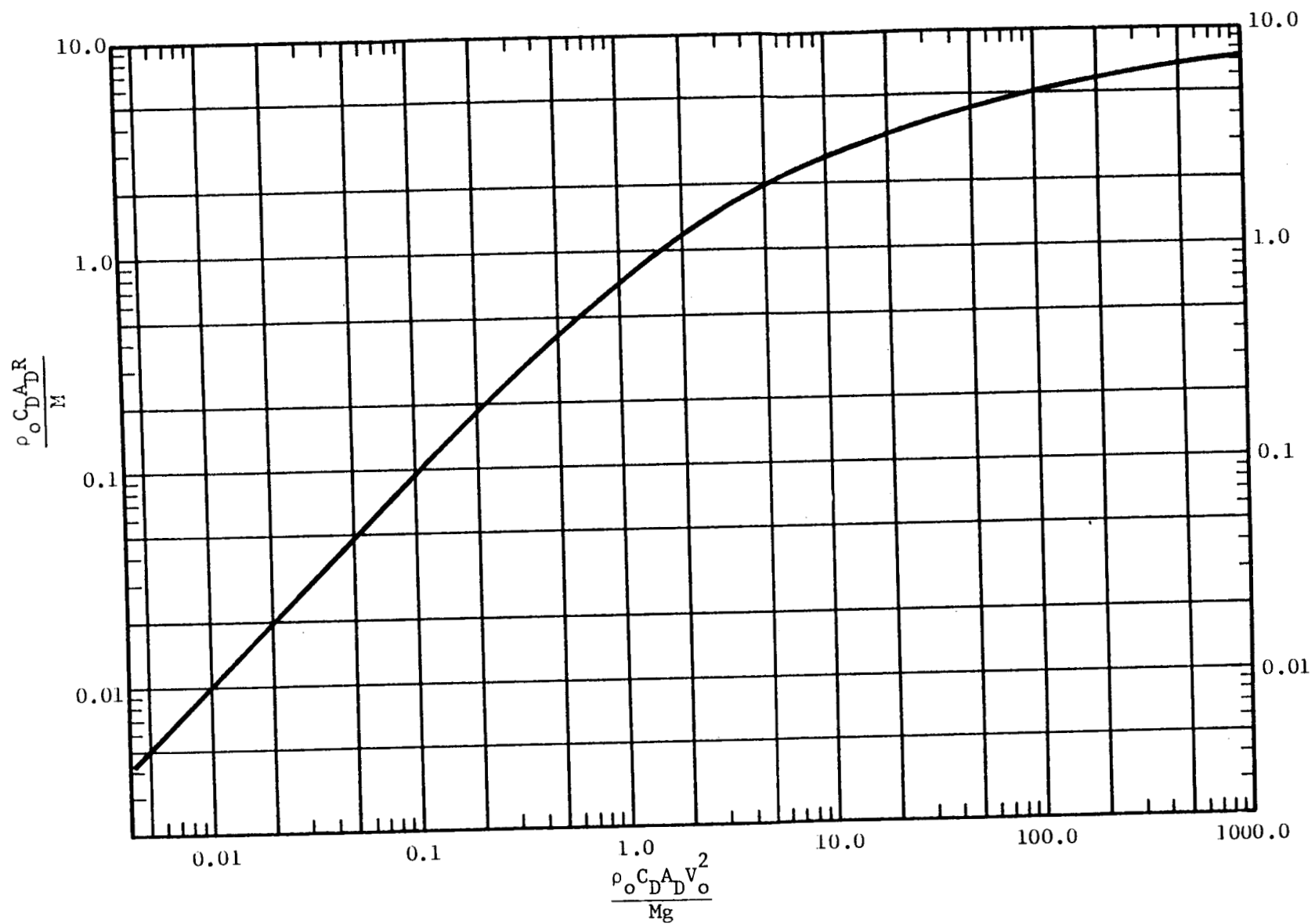
Figure 6.15. Scaled Curves for Fragment Range Prediction (Drag Fragments)

EXAMPLE PROBLEM 6.8

PROBLEM – Determine the maximum range R of a fragment. For illustrative purposes, assume a cube of concrete is hurled face-on.

GIVEN: ρ_o = mass density of air (2.378 x 10^{-3} lb-sec^2/ft^4)

C_D = drag coefficient (Figure 6.9)

A_D = drag area (ft^2)

M = mass

V_o = initial velocity (ft/sec)

g = gravity constant (32.2 ft/sec^2)

FIND: R

REFERENCE

SOLUTION: 1. Calculate nondimensional velocity.

$$\bar{V} = \frac{\rho_o \; C_D \; A_D \; V_o^2}{Mg}$$

Fig. 6.15

2. Read the value of nondimensional range $\bar{R}$ from Figure 6.15.

$$\bar{R} = \frac{\rho_o \; C_D \; A_D \; R}{M}$$

Fig. 6.15

3. Calculate maximum range.

$$R = \frac{M}{\rho_o \; C_D \; A_D} \; \bar{R}$$

CALCULATION

GIVEN: The cube of concrete has an edge dimension of 6.0 in.

ρ_o = 2.378 x 10^{-3} lb-s^2/ft^4

C_D = 1.05

A_D = 6.0 in. x 6.0 in. (1.0 ft^2/144 in.^{2}) = 0.25 ft^2

M = (0.084 lb/in.^{3})(6.0 in.)^3 [(1/32.2)(lb-sec^2/lb ft)]

   = 0.56 lb – sec^2/ft

V_o = 100 ft/sec

g = 32.2 ft/sec^2

FIND: R

SOLUTION: 1. Nondimensional velocity.

$$\frac{\rho_o \, C_D \, A_D \, V_o^2}{Mg} = \frac{(2.378 \times 10^{-3} \, \text{lb} - \text{sec}^2/\text{ft}^4)(1.05)(0.25 \, \text{ft}^2)(100 \, \text{ft/sec})^2}{(0.56 \, \text{lb} - \text{sec}^2/\text{ft})(32.2 \, \text{ft/sec}^2)}$$

$$= 0.35$$

2. Enter Figure 6.14 and read nondimensional range $\bar{R} = 0.30$.
3. Calculate maximum range.

$$R = \frac{M}{\rho_o \, C_D \, A_D} \, \bar{R}$$

$$= \frac{(0.30)(0.56 \, \text{lb} - \text{sec}^2/\text{ft})}{(2.378 \times 10^{-3} \, \text{lb} - \text{sec}^2/\text{ft}^4)(1.05)(0.25 \, \text{ft}^2)}$$

$$= \underline{270 \, \text{ft}}$$

6.2.4.2 Impact Mass Distributions and Impact Range Distributions

A thorough fragment data base was created from a literature search through the available files at the Department of Defense Explosive Safety Board for accident reports containing fragmentation data from accidental explosions in structures such as those at the Pantex plant. Extracted data include characteristics of the explosion source, building descriptions and characteristics of fragments, such as weight, size and range. Those references which had the most useful information were selected as a data base and were separated into three groups by estimated energy of the explosion or explosive yield. Table 6.4 summarizes the explosion source and building characteristics for seven references in the data base. The one reference in Group A consisted of an explosion with estimated energy of approximately 1.6×10^7 ft-lb. Group B explosions had explosive energies on the order of 5×10^8 ft-lb. Group C consisted of three sources with explosion energies near 1×10^{10} ft-lb. Fragment characteristics for each group were extracted from associate missile maps or calculated from descriptions given in the references.

Statistical analyses have been performed on fragment weight, range, nondimensionalized range (by area) and nondimensionalized energy. These useful relationships between the parameters allow one to predict fragment scatter in weight and range following an accidental explosion of a given energy in a building similar to those buildings described in this data base.

A discussion of the statistical analyses performed to determine impact weight, range and size distributions is given below. This is followed by a procedure for using the graphs presented to estimate fragment weight and range for similar explosions.

The fragment weight and range data for each of the energy levels were sorted in ascending order. The total number of fragments for all of the accidental explosions in each energy level were counted. The ordered data (by weight and range) for explosions from each energy level were then divided into groups containing 5 percent of the total number of fragments. Thus, the data were subdivided into groups from the 5th through the 95th percentile by number of fragments as shown in Table 6.5. For example (see Table 6.5), for those explosions having an energy of 1.6×10^7 ft-lb, 5 percent of the fragments had a weight below 0.22 lb, 10 percent below 0.58 lb, 15 percent below 0.87 lb, etc. Also, 5 percent of the fragments were in the 0.22 - 0.58 lb range, 5 percent in the 0.58 - 0.87 lb range, etc.

Figures 6.16 and 6.17 are plots of the percentile points along with an "eyeball" line fit to the points. The mean was estimated as the logarithm (to the base e) of the 50th percentile. The standard deviation was estimated (Ref. 6.24) as two-fifths of the difference between the logarithms of the 90th and 10th percentiles.

Table 6.4   Data Base for Building Fragmentation
(Group A)

| Reference | EXPLOSION SOURCE | | | | | BUILDING CHARACTERISTICS | | | |
	Material	Quantity (lb)	Shape	Orientation To Bldg	Estimated Energy (ft.lb)	Shape	Dimensions	Volume (ft^3)	Construction/Material
Explosion in Nitration Bldg 3045 Radford Army Ammunition Plant, VA 11-02-78	Nitrocellulose (Nc)	$\geq$ 10 lb for resultant damages to have occurred analysis concluded 10.81 lb	Slurry	On second floor of Bldg 3045 in feeder to centrifuge	1.6×10^7	Four story rectangular	36 ft x 72 ft x 33 ft high (11 ft between floors)	$\approx 28,512$ ft^3 per floor; however, an opening was provided in third floor above centrifuges up to fourth so volume of third floor is increased to include fourth; volume of system involved = 995 ft^3.	Steel frame with reinforced concrete slab floors, separated by steel I-section columns; brick masonry endwalls; arcylic plastic glazed side walls (unbarricaded); dimensions of bricks in end walls: Inner course- 2-1/2 in. x 3-7/16 in. x 7-3/4 in. Outer - 2-1/2 in. x 3-5/8 in. x 8 in.

Table 6.4 (Continued)
(Group B)

6-59

	EXPLOSION SOURCE					BUILDING CHARACTERISTICS			
Reference	Material	Quantity (lb)	Shape	Orientation To Bldg	Estimated Energy (ft.lb)	Shape	Dimensions	Volume (ft^3)	Construction/Material
Bacchus Plant Accident Report WA No. 112, Contract AF 04(647) -243, Hercules Powder Company Magna, Utah 10-05-61	Rocket propel- land slurry mix (VCA)	350.0	Slurry		5.2×10^8	Retangular			Three sides - 12 in. rein- forced concrete One side - wood frame; wood floors; asbestos shingle roof; no fire walls or doors; three concrete sides backed up with earth mound. Front protected by a 12 in. sand filled, wood constructed bullet shield.
Hercules Powder Company, VA. Explosion in Bldg 3560, Block Breaker C-line Area.	Nitrocellulose for M-5 Formulation	130.0 in equip- ment; 440.0 in buggy	Blocks of nitrocel- lulose to be mech- anically broken down	Inside, (fairly centered)	8.4×10^8	Box-like	15.6 ft x 15.6 ft; height not given; long porch on front		Wood frame on concrete founda- tion; asbestos shingle roof
Explosion at Pantex Plant, Amarillo, TX 03-30-77 (Two deton- ations of two different H.E. explosives.	LX-09 LX-14	76.0 75.0 ――― 151.0 Total	Rough billets to be machined	Within Bay 8, along south wall of Bldg 11-14A	3.4×10^8	One-story rectangular	151 ft x 63 ft x 18 ft high	171,234	Concrete cavity-wall type block; interior steel frame consisted of 4 H.E. machining bays, an H.E. remote operation bay, a remote control room, a metrology lab work area, a staging and material storage area and an office.

Table 6.4 (Continued)
(Group C)

6-60

	EXPLOSIVE SOURCE					BUILDING CHARACTERISTICS			
Reference	Material	Quantity (lb)	Shape	Orientation To Bldg	Estimated Energy (ft-lb)	Shape	Dimensions	Volume (ft³)	Construction/ Material
Incident at Alleghany Ballistics Lab 04-27-63 (Hercules Powder Company)	①-Four Polaris A3 Second Stage Fiberglass cased Motors; ②-90% Nitroglycerin Casting Solvent; ③-High Energy Casting Powder; ④-Scrap Casting Solvent (above); ⑤-Residual Casting Solvent	①-33,500 lb (propellant) ②- 4,800 lb ③- 865 lb ④- 250 lb ⑤- 30 lb	①-Four Motors were in various stages of processing; ②-In two stainless steel desiccators suspended from overhead Monorail beam; ③-In metal powder boxes	①-Throughout casting bay area in Bldg (one awaiting transfer to pit); ②-In a room adjacent to casting bay and nearest to pit containing one motor; ③-In room adjoining solvent mentioned in aspirator catch tank.	②- 1.0 x 10¹⁰	Rectangular high bay with smaller rectangular building attached.	High bay: 71 ft x 42 ft x 48 ft high. Smaller building: 32 ft x 42 ft x 20.67 ft high.	170,912	Concrete block and wood frame.
Explosion in NG Area No. 2 Radford Army Ammunition Plant, Virginia 01-06-78 (Mainly Bldg 9463) Nitration House	Nitroglycerin	4,200 lb		Within Bldg 9463	9.3 x 10⁹	Rectangular	62.5 ft x 37.5 ft approximated from drawing;height is approximately 15 ft from first floor to ceiling; basement in bldg.		Reinforced concrete walls backed by earth in Nitration House; steel houses are light wood frame, ballast board (Collapsible).
Motor Detonated High Order During Static Testing; Redstone Arsenal, Alabama. 08-19-59 Bldg 7857	One Nike Zebls sustainer motor	6891 lb of Petrin Arylate in Battleship Hardware (loaded weight of motor and nozzle = 10,654 lb)		Within North Bay in test stand	1.2 x 10¹⁰	Rectangular			18 in. Reinforced concrete walls, barricaded on North and South walls by 12 in. reinforced concrete further reinforced by earth covered with minimum width of 23 ft and minimum depth of 3 ft; roof was 18 in. reinforced concrete slab over test bays

Table 6.5   Cumulative Percentiles for Plotting Fragment
Weights and Ranges

Percentile	$E = 1.6 \times 10^7$ ft-lb		$E = 5.0 \times 10^8$ ft-lb		$E = 1.0 \times 10^{10}$ ft-lb	
	Weight (lb)	Range (ft)	Weight (lb)	Range (ft)	Weight (lb)	Range (ft)
5	0.22	6	0.20	44	0.054	218
10	0.58	7	0.40	58	0.082	270
15	0.87	9	0.65	70	0.120	325
20	1.02	11	0.88	89	0.160	375
25	2.18	11	1.20	103	0.220	410
30	2.61	11	1.68	113	0.300	460
35	3.92	11	2.26	118	0.410	496
40	4.35	11	2.72	125	0.490	532
45	5.22	12	3.65	132	0.650	566
50	7.61	14	4.90	141	0.870	616
55	8.70	16	6.72	147	1.260	672
60	10.44	19	9.08	159	1.520	710
65	11.55	24	10.50	170	2.000	780
70	15.37	28	13.08	180	2.670	832
75	24.36	32	21.90	193	4.200	920
80	31.32	46	29.58	207	5.440	1000
85	50.20	52	45.48	233	10.000	1080
90	104.40	77	84.00	266	16.320	1218
95	187.90	146	172.10	324	50.000	1485
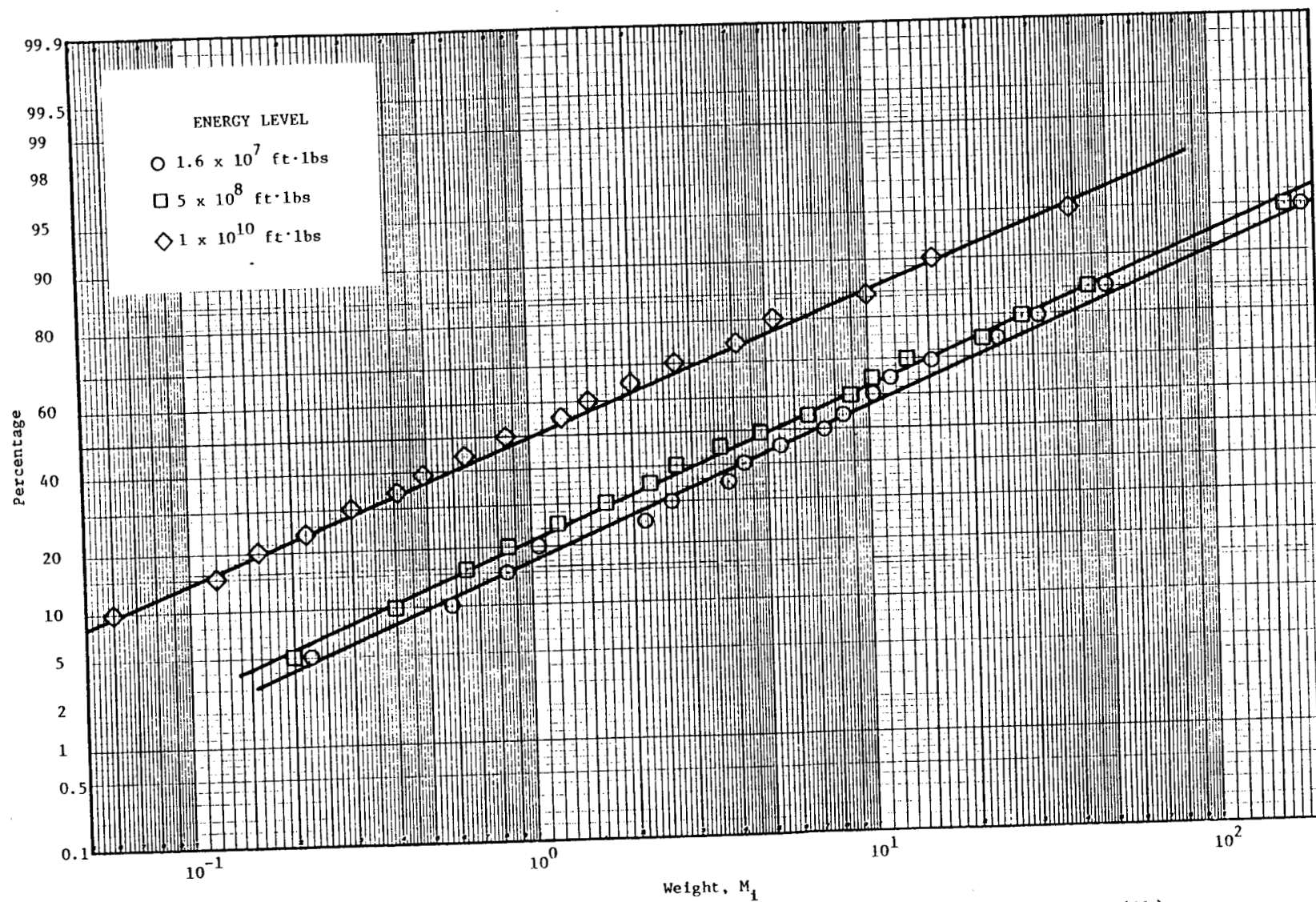
Figure 6.16 Cumulative Probability Distribution, Fragment Weight (lb)
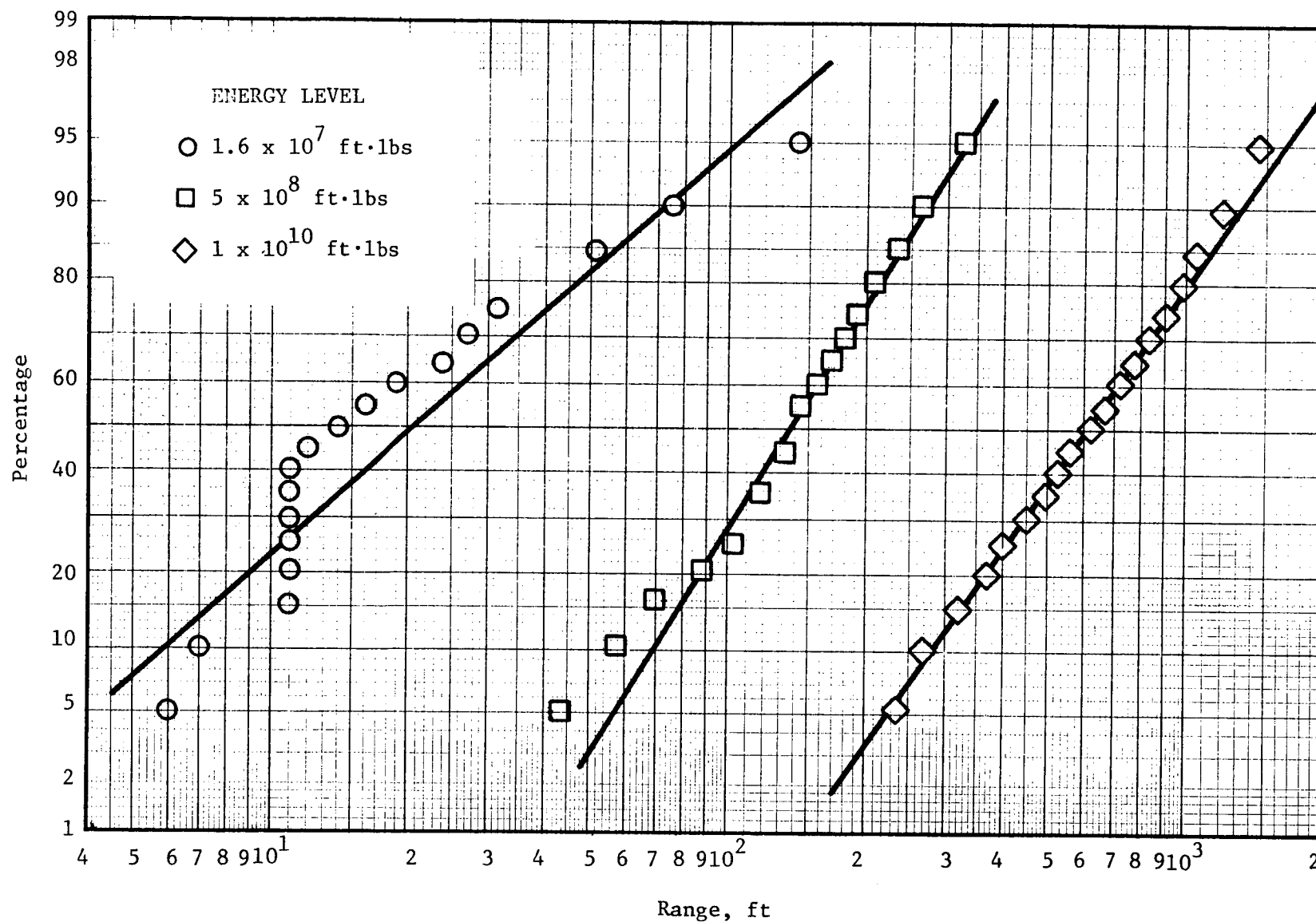
Figure 6.17 Cumulative Probability Distribution, Fragment Range (ft)

Table 6.6 is a listing of the estimated means and standard deviations for the log normal (to the base e) distributions. A "WP"statistic (Ref. 6.24) for goodness of fit was calculated for each of the distributions. The approximate probability of obtaining the calculated test statistic, given that the chosen distribution is correct, was then determined. These results are also shown in Table 6.6. Figure 6.18 is a graph of the probability percentage points of the "W" statistic. As it is customary to consider values of probability for the "W" statistic exceeding 2 to 10 percent as adequate grounds for not rejecting the hypothesis that the data belong to the chosen distribution, the fits for all data except the range data for an energy of 1.6×10^7 ft-lb are much more than adequate. The "W" statistic for ranges in that energy level is slightly less than 10 percent and, thus, is still adequate.

Figure 6.16 can be used to estimate the percentage of fragments (for a given energy level) which will have a weight, W, equal to or less than a particular W. For example, if we wished to estimate the percentage of fragments which would have a weight equal to or less than 10 lb for an energy level of 1.0×10^{10} ft-lb, we would refer to Figure 6.16 and on the weight axis (abcissa) at 10 lb go upward to the intersection of the line for 1.0×10^{10} ft-lb. Then, at the intersection point read the value from the ordinate, which is 86 percent. Conversely, if we wanted to estimate what weight 90 percent of the fragments would not exceed, we would enter the chart on the 90 percent line, go over to the intersection with the curve and read downward to the weight axis the value 16 lb. Estimates for percentage of fragments between two weights can be made by determining the difference between corresponding percentage points. Figure 6.17 can be used in the same manner for the range.

Statistical analyses were also performed for nondimensionalized range $\bar{R}$ $(R/\sqrt{A})$ a. a nondimensionalized energy $\bar{E}$ (RMg/E). However, they were not included in this manual since they do not add any additional useful information for building fragmentation at the present time. Before these nondimensionalized terms can be fully used, more data need to be accumulated. Cumulative frequency distributions and statistical analyses for goodness of fit for nondimensionalized range and energy can be found in Reference 6.25.

It is interesting to note that the lines on Figure 6.16 are almost parallel. That is, the standard deviations are almost equal for all the log normal distributions. This leads to the speculation that if more experimental data are acquired in the future at various energy levels, it may be possible to derive a scale factor from the energy ratios and magnitude which is related to the mean of the weight distribution. Figure 6.17, the plot for the range percentiles, is an exception to this

Table 6.6   Listing of Estimated Means, Standard Deviations,
and "W" Statistics for Log-Normal Distributions
for Weights and Ranges of Fragments

Weight

Energy Level (ft-lb)	Estimated Mean	Estimated Standard Deviation	"W" Statistic [*]	Probability
1.6×10^7	1.94	2.11	0.992	0.999
5.0×10^8	1.64	2.12	0.990	0.996
1.0×10^{10}	0	2.22	0.981	0.935

Range

Energy Level (ft-lb)	Estimated Mean	Estimated Standard Deviation	"W" Statistic [*]	Probability
1.6×10^7	3.0204	0.9611	0.915	0.095
5.0×10^8	4.9900	0.5487	0.980	0.922
1.0×10^{10}	6.4052	0.6305	0.989	0.994

[*] See Figure 6.18
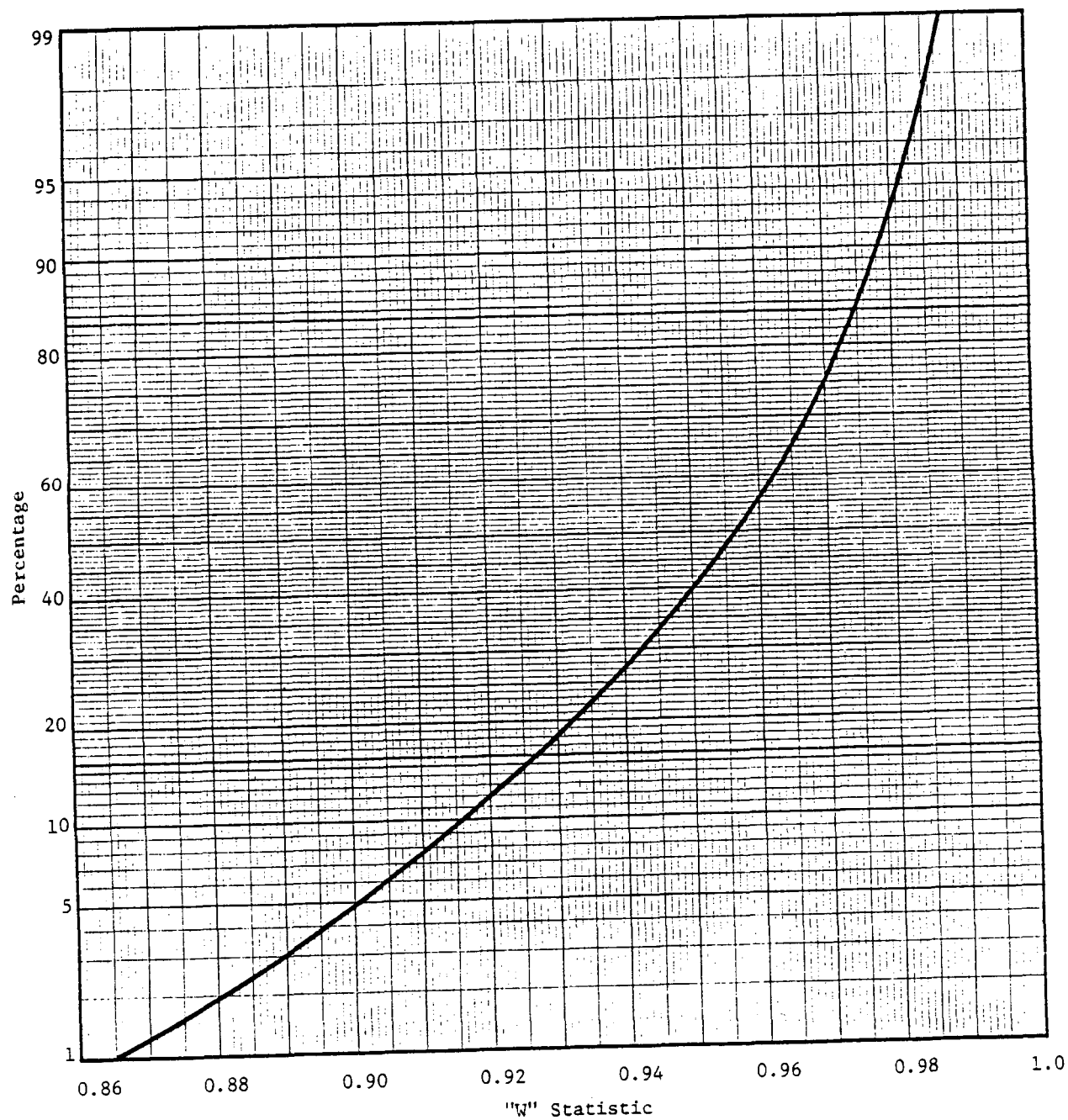
Figure 6.18 Approximate Probability Percentage Points
(n-19)

speculation due to the large number of fragments collected at one close-in distance (11 ft) from the explosion with an energy of 1.6×10^7 ft-lb (see Table 6.5). It should be noted that data from only one accident were included at this energy level. A larger data base may have caused the distribution to shift to a position more nearly parallel with the distributions of range for the other two energy levels.

A procedure for estimating the number of fragments of a given mass interval which will fall within a given distance from an explosion source in a building is as follows:

1) Estimate M_B = total destroyed weight of the building (portion of the building which has fragmented). This estimate will depend mainly upon the amount of explosive stored or machined in the building at any given time and the building structure and shape. (This document does not discuss methods for determining the total mass of the building destroyed. This calculation will have to be performed using other sources.)

2) Using the weight distribution in Figure 6.16, obtain the average weight of a fragment from the explosion, M_a, by reading it off the appropriate curve at the 50th percentile.

The total number of fragments from the explosion is then

$$N_f = \frac{M_B}{M_a} \tag{6.35}$$

3) Using the range distribution in Figure 6.17, take equal percentage increments (0-10%, 10-20%, etc.) or equal range increments (0-10 ft, 10-20 ft, etc.) and find the number of fragments, N_{f_i}, in each increment. (If equal percentage increments were taken, the number of fragments in each increment is, of course, the same.)

4) Again using the weight distribution in Figure 6.16, determine the percentage of fragments in a particular weight interval. The total numbers of fragments in each range interval have already been calculated (Step 3). Thus, the number of fragments of a particular mass in a particular range interval (distance out from the source) can be determined.*

---

*The major assumption made in this procedure is that all weights are distributed log normally in a given interval of range. Since we could find no correlation between weight and range, for a given energy level and since weight is log normally distributed over each energy level (which covers the 'entire range), there is no reason to assume that weight is not log normally distributed within a given range increment.

PROBLEM – Determine the estimated number of fragments N_{R_k} of a given weight which will fall within a given distance from an explosion source of a given yield in a building. Using this number, determine an average fragment density ρ_k over the area covered within that distance.

GIVEN: M_B = total destroyed weight of the building (lb) (total weight of the debris)

E = energy of the explosion source (ft-lb)

R_i = range of fragments under consideration (ft)

M_i = weight of fragments under consideration (lb)

FIND: N_{R_k}, ρ_k

		REFERENCE
SOLUTION:	1. Determine average weight M_a of a fragment from the explosion. This number is read off the curve for the desired energy, E, at 50%.	Fig. 6.16 (Weight Distribution)
	2. Calculate the total number of fragments from the explosion.	
	$$N_f = \frac{M_B}{M_a}$$	Eq. (6.35)
	3. Taking equal percentage increments (0-10%, 10-20%, etc.) or equal range increments (0-10 ft, 10-20 ft, etc.), find the number of fragments in each range increment, N_{f_i}.	Fig. 6.17 (Range Distribution)
	$$N_{f_i} = (\%)(N_f)$$	
	4. Determine the percentage of fragments in the particular weight interval of concern.	Fig. 6.16 (Weight Distribution)
	5. Determine the number of fragments of the particular weight in a particular range interval, R_k.	
	$$N_{R_k} = (\% \text{ in weight interval})(N_{f_k})$$	
	6. Calculate the area of the ring defined by the range interval, R_k.	
	$$A_k = \pi(R_{k_2}^2 - R_{k_1}^2)$$	

where the interval R_k is bounded by radii R_{k_1} and R_{k_2}.

7. Determine average fragment density over the entire range interval (ring).

$$\rho_k = \frac{N_{f_k}}{A_k}$$

CALCULATION

GIVEN: M_B = 10,000 lb

E = 5 x 10^8 ft-lb

R_1 = 90-100 ft ⎫ Due to structures and personnel in
R_2 = 150-170 ft ⎭ these areas, the number of fragments which will land here is of concern.

M_1 = 5-10 lb

FIND: $N_{R_{(90-100 \text{ ft})}}$, $N_{R_{(150-170 \text{ ft})}}$, $\rho_{(90-100 \text{ ft})}$, $\rho_{(150-170 \text{ ft})}$

SOLUTION: 1. M_a at the 50th percentile for E = 5 x 10^8 ft-lb equals 5.1 lb.

2. Total number of fragments.

$$N_f = \frac{M_B}{M_a} = \frac{10,000 \text{ lb}}{5.1 \text{ lb}} = 1,961$$

3. Number of fragments in each of the two range increments.
N_{f_1} = (29% - 22%)(1,961) = 137 fragments

N_{f_2} = (66% - 58%)(1,961) = 157 fragments

4. Percentage of fragments weighing 5-10 lb.
64% - 50% = 14%

5. Number of 5-10 lb fragments in each of the two range intervals.
N_{R_1} = (14%)(137) = 19 fragments

N_{R_2} = (14%)(157) = 22 fragments

6. Area of each circular interval.
$A_1 = \pi(100^2 - 90^2) = 5970 \text{ ft}^2$

$A_2 = \pi(170^2 - 150^2) = 20100 \text{ ft}^2$

7. Average fragment densities (if fragments distributed evenly over the area of the ring).

$$\rho_1 = 137/5970 \ ft^2 = \underline{0.023 \ fragments/ft^2}$$

$$\rho_2 = 157/20100 \ ft^2 = \underline{0.0078 \ fragments/ft^2}$$

NOTE: The above solution could be repeated for different weight and range intervals to generate a complete missile map.

6.2.4.3 Impact Kinetic Energies

Recall that kinetic energy is one-half the product of mass and velocity squared ($MV^2/2$). From the accident reports mentioned previously, we have been able to describe statistically the weight and range distributions from which the mass can be determined. However, none of the accident reports contained any information on impact velocities or impact kinetic energies. In order to acquire such information, it would be necessary to simulate an accident, probably in model scale for cost effectiveness, and measure fragment impact masses and velocities either photographically or by damage indicators. Information of this type has been acquired in the vicinity of various ordnance explosions in order to define kill probabilities but this information is not appropriate for the purposes of this handbook. Impact velocities of primary and secondary fragments can be determined using the initial trajectory parameters of the fragments and trajectory computer codes such as FRISB (Ref. 6.3) which give fragment impact conditions.

An impact damage criterion for humans which is widely used by the military is the 58 ft-lb criterion; that is, it is assumed that the onset of serious injury occurs when a fragment striking an individual has an impact kinetic energy equal to or greater than 58 ft-lb.* Figure 6.16 shows that 50 percent or more of the fragments have masses of 1 lb or greater. A 1-lb fragment would only have to fall 58 ft or a 58 lb fragment fall 1 ft in order to equal the 58 ft-lb impact damage criterion. Therefore, it is not difficult to conclude that many of the fragments from buildings subjected to internal accidental explosions which strike individuals will cause serious injuries.

6.3 MISSILE DISPERSION

6.3.1 Experimentally Based Methods

Accurate, complete missile maps which indicate missile dispersion as well as range are limited in the data base for accidental explosions. Different research teams pick up and map different fragments; thus, a complete map, which is necessary to make accurate predictions of dispersion, is rare. The missile maps which make up the data base described

---

*Much more accurate measures of impact injury are possible, but they are also quite complex. We do not recommend the 58 ft-lb criterion, but refer the reader instead to the literature on impact trauma and effects of penetrating fragments on humans. (See Sections 6.5.1 and 6.5.2).

in Section 6.2.1 were used to extract fragment positions in relation to the position of the charge in the building. The area surrounding an explosion was divided into eight coarse sectors of 45° each. The sectors were numbered consecutively clockwise with angular sector number 1 being centered directly in front of the explosive charge where the fragments are most dense (see Figure 6.19 for an example of a sectored missile map pattern). Angles are measured from the zero-line indicated in Figure 6.19. These angular sectors were then further divided by range increments of 40 ft. Fragments were counted and a density of fragments per square foot was calculated for each sector.

In order to formulate a model for predicting where a fragment will land after an accidental explosion occurs, a multiple linear regression analysis was performed on fragment density data from energies of 5×10^8 ft-lb and 1×10^{10} ft-lb. In both cases, the fitted model is of the form

$$\ln z = a_0 + a_1 x + a_2 y \tag{6.36}$$

where z = density (fragments/square foot)
    x = angle (radians)
    y = distance (feet)

The coefficients a_i and partial correlation coefficients ν_{xz} and ν_{yz} for each case are listed in Table 6.7. High correlation was found between fragment density and distance as indicated by the ν_{yz} values; however, the correlation between density and angle (dispersion), while acceptable as a statistical value in the analysis, was quite low. More data would allow better prediction of dispersion patterns for explosions of the type described in this manual.

Fragment densities in sectors 1 through 4 ($0 < x \le 3.14$) were used in the regression analysis since the densities increased as the angle increased. A different pattern was observed for sectors 5 through 8 ($3.14 < x < 6.28$); thus, a different equation would result using those data in a regression analysis. It should be stressed that the equations and correlation coefficients derived from this analysis are based on the limited dispersion data available at this time. Thus, this dispersion analysis can provide an estimate of how fragment density can vary with angular position around a building such as those located at the Pantex facility. Further data would be beneficial in order to refine the analysis.

Some recent model scale tests performed in Switzerland and Sweden (Ref. 6.23) indicate distinct dispersion patterns for explosions occurring in buildings. The model buildings were of reinforced concrete structure with different-sized charges centered inside. Upon detonation
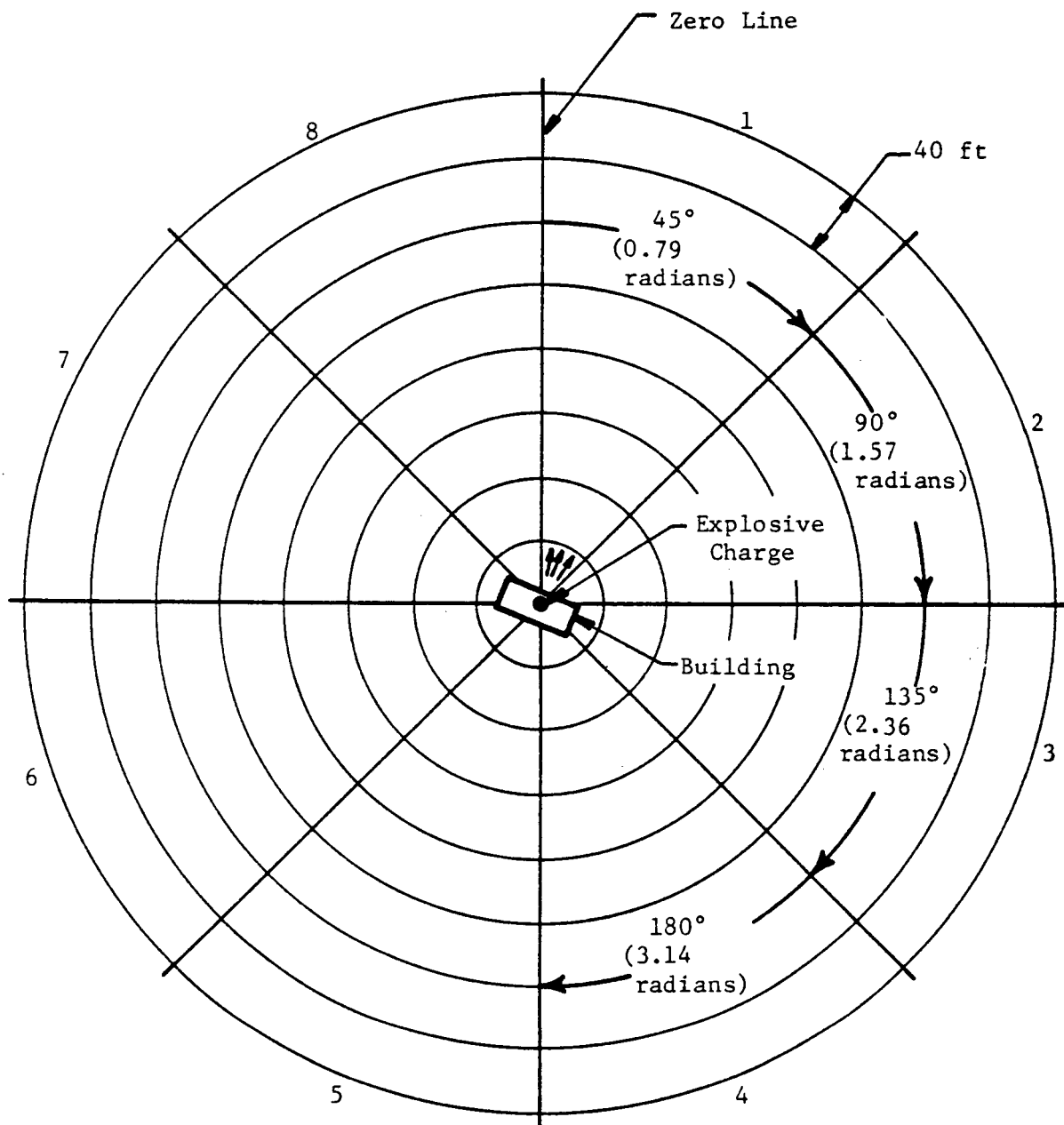
Figure 6.19.   Example Sectored Missile Map Pattern for
Measurement of Fragment Density

Table 6.7 Resultant Coefficients from Multiple Linear
Regression Analysis on Missile Dispersion

$E = 5.0 \times 10^8$ ft-lb

$a_0 = -2.23$ $\nu_{xz} = -0.268$

$a_1 = -0.363$

$a_2 = -0.0348$ $\nu_{yz} = -0.924$

$E = 1.0 \times 10^{10}$ ft-lb

$a_0 = -4.79$ $\nu_{xz} = -0.276$

$a_1 = -0.417$

$a_2 = -0.00729$ $\nu_{yz} = -0.792$

of the charge, resultant debris was concentrated in highly directional
paths perpendicular to each of the four walls. In comparison, very little
debris was scattered in the diagonal direction out from the corners of
the building. This was not the case in the accident data. However,
dispersion was a major concern in the performance of these model tests;
therefore, great care was taken to collect, weigh, and record all possible
debris. If more accurate missile maps were available from accidental
explosions, a more in-depth study of disperson could be performed to
compare results with the results of these model scale tests. However,
a direct comparison between these model scale tests and the accidental
explosions described earlier cannot be made because the building types
for the scale models are vastly different from the building type in
the accidental explosions.

PROBLEM – Estimate the density z_k of fragments located in a given angular sector outward from an explosion source. (Due to the limited data on dispersion, the calculations presented here will only be applicable with explosive energies of 5.0×10^8 ft-lb and 1.0×10^{10} ft-lb. Also, the prediction model used here is only applicable for densities in sectors 1 through 4. See Figure 6.19 for sector identification.)

GIVEN: E = energy of explosion source

x = angular position of the sector in relation to the explosion source (radians)(see Figure 6.19)

y = distance outward from the explosion source, i.e., the midpoint of a range interval R_i (ft) (see example problem 6.9 in section 6.2.4.2)

N_{f_k} = total number of fragments within range interval (see example problem 6.9 in section 6.2.4.2)

θ = subtended angle of the sector under consideration (radians)

$\left.\begin{array}{c} a_0 \\ a_1 \\ a_2 \end{array}\right\}$ regression parameters for particular energy level (Table 6.7)

FIND: z_k REFERENCE

SOLUTION: 1. With parameters a_0, a_1, a_2 defined for the desired energy level, calculate estimated fragment density, z_i.

$$\ln z_i = a_0 + a_1 x + a_2 y \qquad\qquad \text{Eq. (6.36)}$$

in each of the four sectors 1 through 4.

2. Sum the densities z_i, $i = 1,4$. Determine a percentage p_i of the total density z_T for each sector.

$$p_i = z_i / z_T$$

3. Determine density of fragments in the sector defined by angle and distance from the explosion source.

$$z_k = p_k \frac{(1/2)N_{f_k}}{(\theta/2\pi)\,\pi\,(R_{k_2}^2 - R_{k_1}^2)}$$

$$= p_k \frac{N_{f_k}}{\theta(R_{k_2}^2 - R_{k_1}^2)}$$

CALCULATION

GIVEN: E = 5 x 10^8 ft-lb
        x = 1.5708 radians (90° - sector 2 on Figure 6.19)
        y = 160 ft [midpoint of interval R_2 in example problem
             6.9 in section 6.2.4.2 (150-170 ft)]
        N_{f_2} = 157 fragments (from example problem 6.9 in section
             6.2.4.2)
        θ = 0.7854 radians
        a_0 = -2.23
        a_1 = -0.363
        a_2 = -0.0348

FIND: z_k

SOLUTION: 1. $\ln z_1$ = -2.23 + (-0.363)(0.785) + (-0.0348)(160)

               $\ln z_1$ = -8.08

                 z_1 = 0.000310 fragments/ft^2

               $\ln z_2$ = -2.23 + (-0.363)(1.57) + (-0.0348)(160)

               $\ln z_2$ = -8.37

                 z_2 = 0.000233 fragments/ft^2

               $\ln z_3$ = -2.23 + (-0.363)(2.32) + (-0.0348)(160)

               $\ln z_3$ = -8.64

                 z_3 = 0.000178 fragments/ft^2

               $\ln z_4$ = -2.23 + (-0.363)(3.14) + (-0.0348)(160)

               $\ln z_4$ = -8.94

                 z_4 = 0.000132 fragments/ft^2

           2. $\sum_{i=1}^{4} z_i$ = 0.000853 fragments/ft^2

               Percentages of fragments located in each sector are,
               thus,

               P_1 = 0.000310/0.000853 = 0.363

               P_2 = 0.000233/0.000853 = 0.273

               P_3 = 0.000178/0.000853 = 0.209

               P_4 = 0.000132/0.000853 = 0.155

           3. Density of fragments in the second sector between 150
               and 170 ft from the explosion described in example

problem 6.9 in section 6.2.4.2 would be

$$z_2 = (0.273)(157/0.785)(170^2 - 150^2) =$$
$$= \underline{0.0085} \text{ fragments/ft}^2$$

NOTE: If one compares this density for the second
sector between 150 and 170 ft (0.0085 fragments/
ft^2) with the average density over the same
range interval obtained in example problem 6.9
in section 6.2.4.2 (0.0078 fragments/ft^2),
one finds that there is a higher than average
concentration of fragments in the area described
in this problem. Due to the limited amount of
fragment dispersion data, we recommend that
section 6.2.4.2 be used to determine fragment
density for most situations. This method is
more accurate for "frontal" fragments (Sector 1).

6.3.2 Analytically Based Methods

At the present time, there are no suitable analytically based solutions for predicting missile dispersion. We presented a solution based on our accident data base in the previous section which could be used to estimate dispersion from an explosion in a building similar to the ones in the data base. Thus, that solution is extremely limited in its application. Both experimental and analytical work needs to be performed to predict missile dispersion more accurately. We recommend that model tests in conjunction with a nondimensional analysis be performed in the future in order to better define missile dispersion characteristics.

6.4 METHODS FOR ASSESSING FRAGMENT IMPACT DAMAGE

Structures which can be damaged by fragments include light to heavy industrial buildings, office buildings, frame or masonry structures, cars, and many others. Damage can be superficial, such as denting of metal panels or breakage of panes of glass. But, massive fragments can cause more extensive damage such as perforation of wooden roofs, severe crushing of small buildings and cars, etc. Most of the fragments will be nonpenetrating and will cause damage by imparting impulsive loads during impact. The impacts will almost certainly be of short enough duration to be purely impulsive for almost any "target" structure or structural component. Impact conditions with large fragments which can be certain to cause significant structural damage can probably also be established by equating kinetic energy in the fragment to energy absorption capability for typical roof panels, roof supporting beams, etc.

Most experimental data and prediction methods for fragment penetration or perforation are limited to the worst-case normal impact obliquity. Impacts of other obliquities present a greater thickness of material to be penetrated, and at great enough obliquity, will cause richochet. For bullets and other military projectiles, richochet has been studied extensively. But, fragment richochet has been studied in only a cursory way, and insufficient data are available for inclusion in this manual.

6.4.1 Impacts on Metal Structures

The structures that are considered here are metal plates and sheets. There does not appear to be any effect of the curvature of the target; therefore, it is reasonable to use data for flat targets and apply them to any general shape that may be of interest.

6.4.1.1 General Solution for Penetration of Metal Targets by Fragments

The methods which follow (Ref. 6.3) are based upon an examination of data of fragment and hailstone impact upon metal sheets and plates (Refs. 6.6, 6.22 and 6.23). In these studies, synthetic hail-

stones (ice spheres) were fired at target sheets of aluminum alloys, and various shapes of fragments were fired at steel targets. A model analysis using the methods described by Baker, Westine and Dodge (Ref. 6.26), gives the parameters of interest listed in Table 6.8.

This analysis is concerned with plastic deformation, which makes the yield strength σ_t more important than the modulus of elasticity of the target material. Also, the fragment is assumed to be either a rigid body, or a very weak, crushable body, which makes the strength of the fragment an unnecessary parameter. The model analysis and a study of the data result in the nondimensional terms in Table 6.9. When $(\delta h/a^2)$ is plotted versus $(\rho_p V/\sqrt{\sigma_t \rho_t})$, the data follow a straight line with some scatter in the points (see Figure 6.20) as shown by the shaded area of the figure. The line intersects the horizontal axis at a positive value of velocity. This is expected because there is a finite fragment velocity below which no permanent target deflection occurs.

For given fragment properties, a given target, and a given normal component of fragment velocity, δ can be obtained. Of course, for very low fragment velocities, there is no permanent deflection.

This method was developed for impacts not very close to the edge of a sheet or plate. For fragment impact near the unsupported edge of a sheet or plate, the deflection may be twice the deflection that would be otherwise expected from use of the figure.

The V_{50} limit velocity is defined as the velocity at which a projectile will have a 50 percent chance of perforating a given target. Given the properties of the projectile (fragment) and the target, V_{50} can be obtained from Figure 6.21.

The solid line in Figure 6.21 gives the relationship between limit velocity and target thickness. As the graph shows, there is uncertainty in this relation. For hard fragments which are less likely to deform, a lower nondimensional limit velocity (more conservative) should be chosen. For softer fragments, a higher limit velocity can be used.

At this time, it is not known whether this relationship holds for values of h/a greater than about 2.2.

This method is good for the impact of a fragment with its velocity normal to the target surface. According to one report (McNaughtan and Chisman, Ref. 6.29) for oblique impacts the penetration velocity is minimum at an angle of 30° from the normal direction. The difference between the penetration velocities at 0° and at 30° may be as great as 20 percent. Therefore, if oblique impact is expected, the penetration velocity obtained by use of Figure 6.21 should be multiplied by 0.8.

Table 6.8 List of Parameters for Penetration
of Metal Sheets and Plates

a   radius of fragment (assuming spherical shape)

h   thickness of target

V   velocity of fragment

δ permanent deflection of target at point of impact

ρ_p density of fragment (projectile)

ρ_t density of target

σ_t yield stress of target material

Table 6.9   Nondimensional Terms for Penetration of
Metal Sheets and Plates

$$\overline{V} = \left(\frac{\rho_p V}{\sqrt{\sigma_t \rho_t}} \right)$$ dimensionless projectile velocity

$$\overline{\delta} = \left(\frac{\delta h}{a^2} \right)$$ dimensionless target deflection

$$\overline{h} = \left(\frac{h}{a} \right)$$ dimensionless target thickness
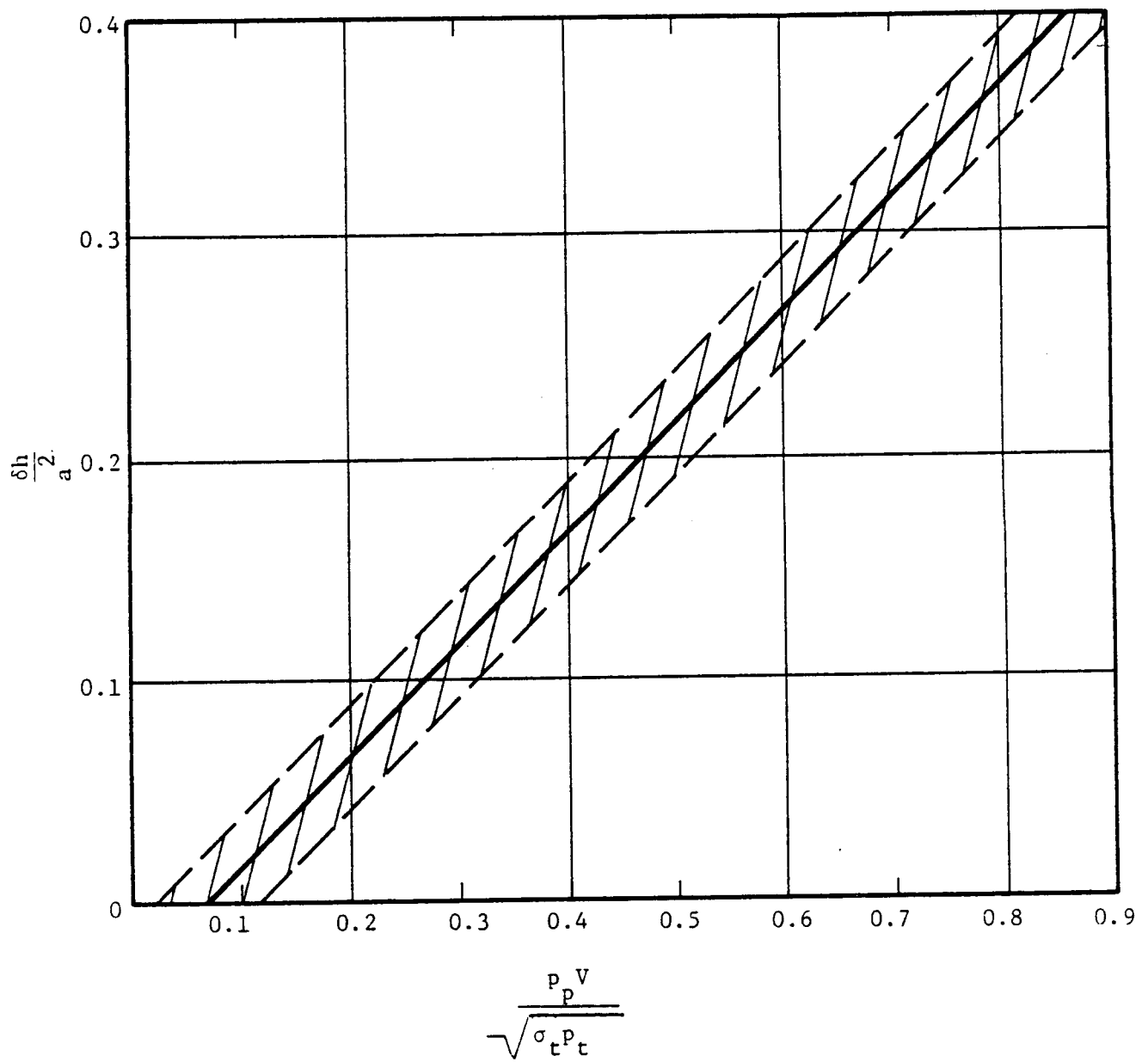
Figure 6.20   Nondimensional Deflection versus Nondimensional Velocity for "Chunky" Crushable Fragments
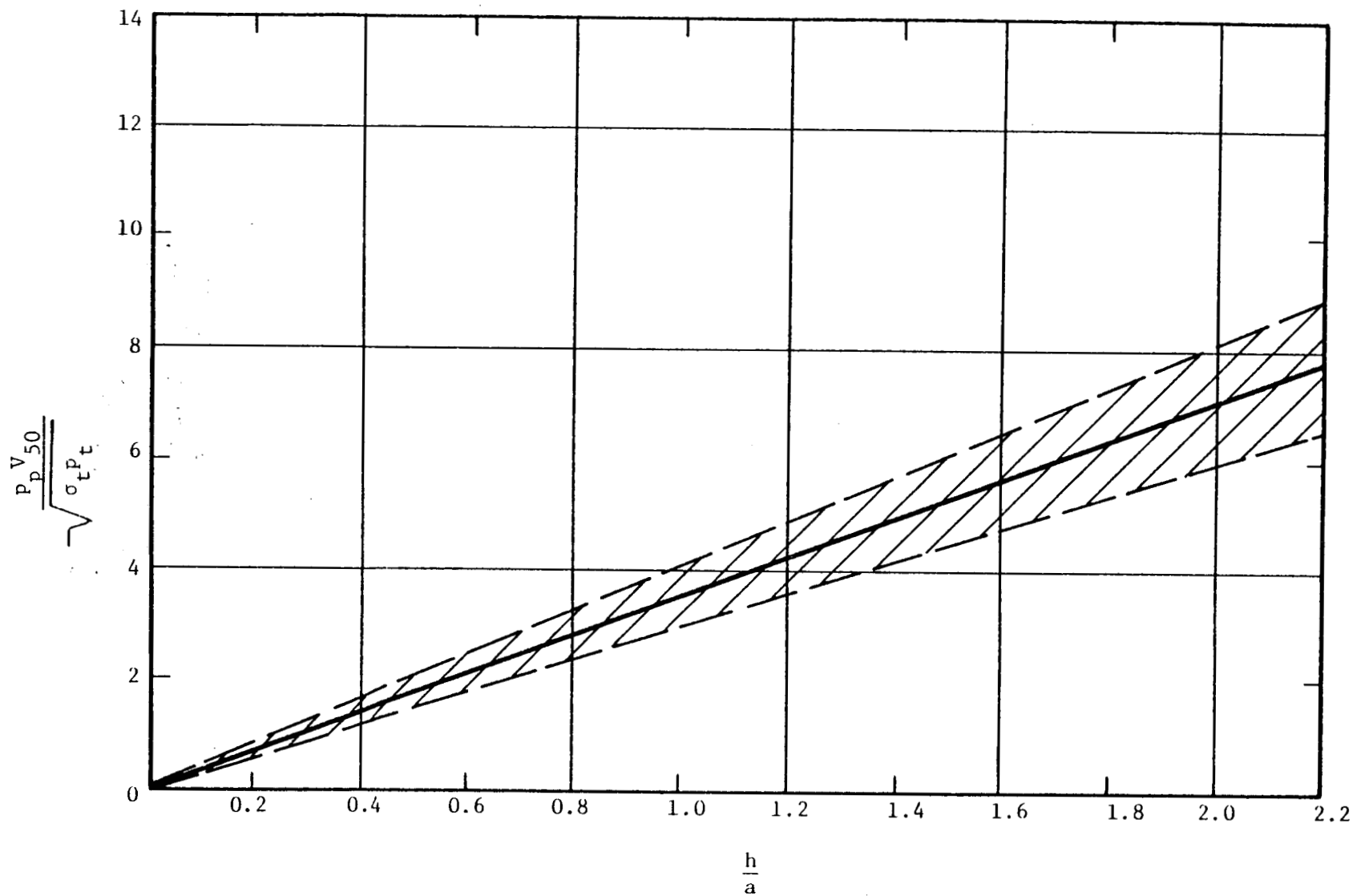
Figure 6.21 Nondimensional Limit Velocity versus Nondimensional Thickness for "Chunky," Non-Deforming Fragments

This analysis has been formulated for spherical fragments To apply this to fragments of other shapes, let a = [m/ρ_p (4π/3)]$^{1/3}$, where m is the mass of the fragment. More research must be done to determine other effects of fragment shape. Table 6.10 is a list of the important properties (density and yield stress) of a few selected fragment and target materials.

6.4.1.2 Penetration of Steel Targets by Wooden Rods

Baker, Hokanson and Cervantes (Ref. 6.5) have conducted a number of experiments in which solid wooden cylinders with length-to-diameter ratios of 31:1 were impacted end on into thin mild steel targets. Fitting a curve to the data, they came up with the following penetration equation:

$$\frac{\rho_p V_s^2}{\sigma_t} = 1.751 \left(\frac{h}{d}\right)\left(\frac{\ell}{d}\right)^{-1} + 144.2 \left(\frac{h}{d}\right)^2 \left(\frac{\ell}{d}\right)^{-1} \tag{6.37}$$

where V_s = striking velocity for 50% perforation (V_{50})

ρ_p = density of the projectile

σ_t = yield strength of the target

h = thickness of the target
ℓ = length of the projectile
d = diameter of the projectile

6.4.1.3 Penetration of Steel Plates by Compact Steel Fragments

Another recommended method for predicting compact steel fragment penetration of steel plate(s) is based on the procedures of References 6.28 and 6.29, and is shown in outline form in Figure 6.22. The prediction method and quantities required for its utilization are discussed further below:

Input Parameters: Quantities needed to begin the procedure are:

- plate thickness, t inches;
- angle of obliquity = angle between line of flight of fragment and the normal to the plate surface, θ degrees;
- orientation angle = least angle between any flat fragment surface and the plate surface, ϕ degrees;
- fragment length-to-diameter ratio, L/D;
- fragment area presented to plate, A_p in.^{2};
- fragment striking weight, W_s lb;
- fragment striking velocity, V_s fps.

These quantities will either be known or can be estimated for the problem of interest. Otherwise, they must be assumed.

6-84

Table 6.10   Material Properties[*]

Material	Specific Weight γ (lb /ft^3)	Yield Stress σ (psi)
Steel	489	
1015		50,000–65,000
1018		53,000
1020 (large grained)		64,000
1020 (sheet)		45,000
A36		36,000
Aluminum Alloys (sheet)	173	
2024-0		12,800
2024-T3		53,000
2024-T4		53,000
6061-T6		35,000
Titanium Alloy	282	
6Aℓ4V		160,000

* Refer to Chapter 7, Section 7.4, for properties of other materials (structural steels and others).

† To obtain a nondimensional term for use in plots or equations involving nondimensional parameters, it may be necessary to convert lb /ft^3 to lb − sec^2/ft^4 by multiplying density by 1 lb − sec^2/32.2 lb /ft.
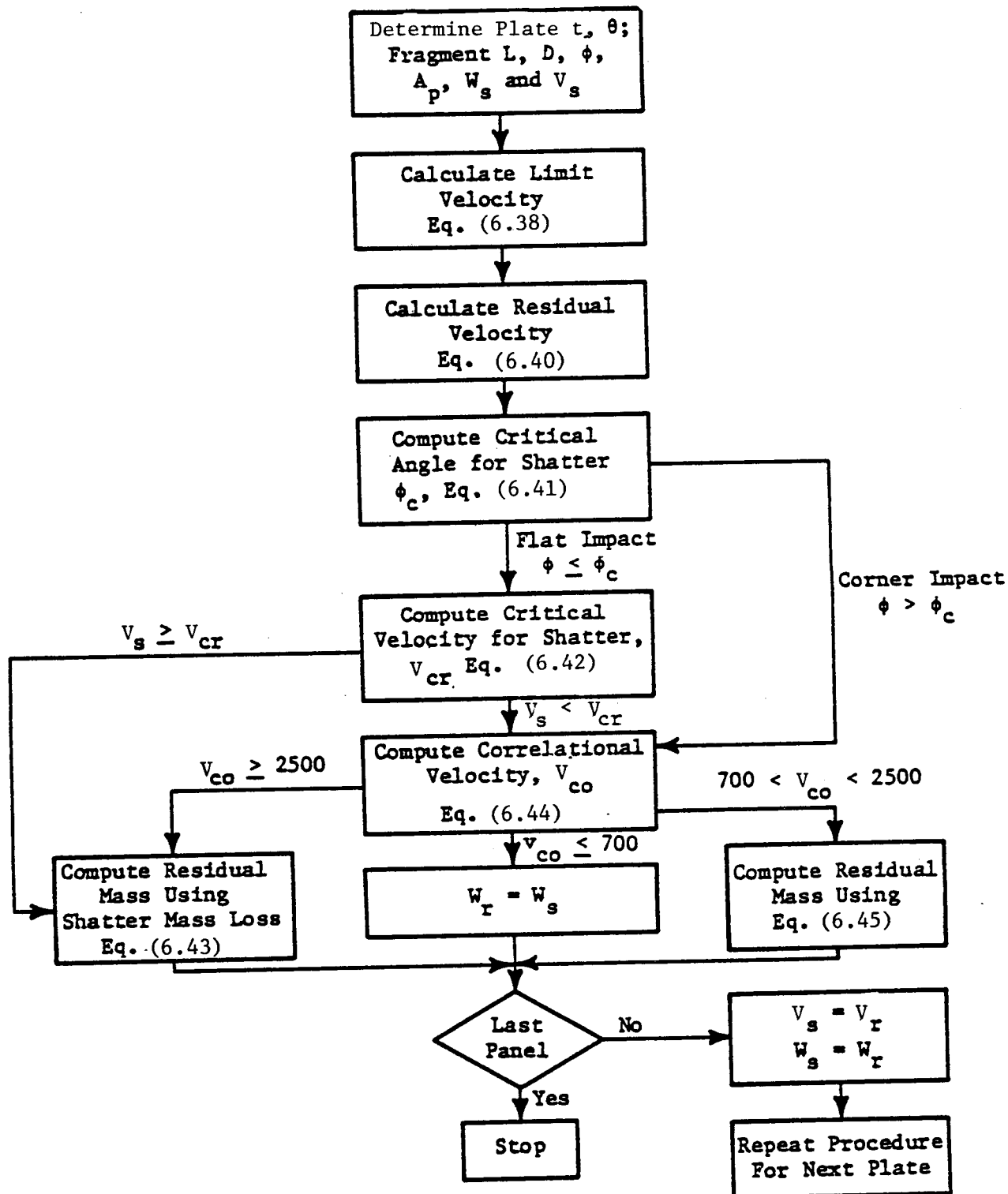
Figure 6.22 Prediction of Penetration of Steel Plate

Ballistic Limit Velocity: The ballistic limit velocity is defined as the lowest striking velocity that results in perforation of the target with zero residual velocity. The ballistic limit velocity for compact fragments striking mild steel targets can be estimated as:

$$V_\ell = \frac{A_o}{\sqrt{W_s}} A_p^m \, (t \sec \theta)^n \qquad (6.38)$$

where V_ℓ is the ballistic limit velocity in fps; A_o, m and n are constants defined in Table 6.11; and the other terms are as previously defined.

Equation (6.38) is also applicable to perforated plates with the substitution of $R^2 A$ for A_p, where R is the perforation factor. The perforation factor is defined as

$$R = 1 - d_p/h_p \qquad (6.39)$$

where d_p is the diameter of the perforations and h_p is the average center-to-center distance between perforations. Values of the perforation factor as a function of vent area ratio, α_e, for hexagonal and square hole patterns are shown in Figure 6.23.

Residual Velocity: In order to predict the residual velocity of a fragment that has perforated a mild steel plate, a quantity

$$x = \frac{V_s}{V_\ell} - 1$$

is computed first where V_s is the striking velocity and V_ℓ is the ballistic limit velocity. Then

$$V_r = V_\ell \beta \left[\frac{ax^2 + bx + c\sqrt{x}}{x + 1} \right] \qquad (6.40)$$

but $V_r \leq V_s$

where $\beta = \dfrac{1}{\left[1 + \gamma A_p t/W_s \right]^{1/2}}$ for $L/D \leq 2$

$\beta = 1$ for $L/D > 2$

γ = density of the target plate, $lb/in.^3$ (should take account of holes for perforated plates)

a,b,c = constants from Table 6.12

Critical Angle for Shatter: A fragment which has perforated a mild steel plate may or may not lose mass depending upon the orientation angle ϕ between any flat fragment face and the target. If ϕ is small enough, the impact is essentially flat, or $\phi \leq \phi_c$, where ϕ_c is the critical orientation angle in degrees for shatter.

Table 6.11

Empirical Constants for Predicting Compact Fragment
Limit Velocity for Mild Steel Targets

L/D	$\dfrac{t}{R\sqrt{A_p}}$ *	A_o	m	n
$\le$ 5	$0 \le 0.46$	1414	0.295	0.910
$\le$ 5	$0.46 \le 1.06$	1936	0.096	1.310
$\le$ 5	≥ 1.06	2039	0.064	0.430
> 5		1261	0.427	0.647

* R is the perforation factor for perforated plates;
  see Equation (6.39).

Table 6.12

Empirical Constants for Predicting Compact Fragment
Residual Velocity for Mild Steel Targets

Constant	L/D < 5	L/D $\ge$ 5
a	1.12	1.10
b	0.52	0.80
c	1.29	1.45
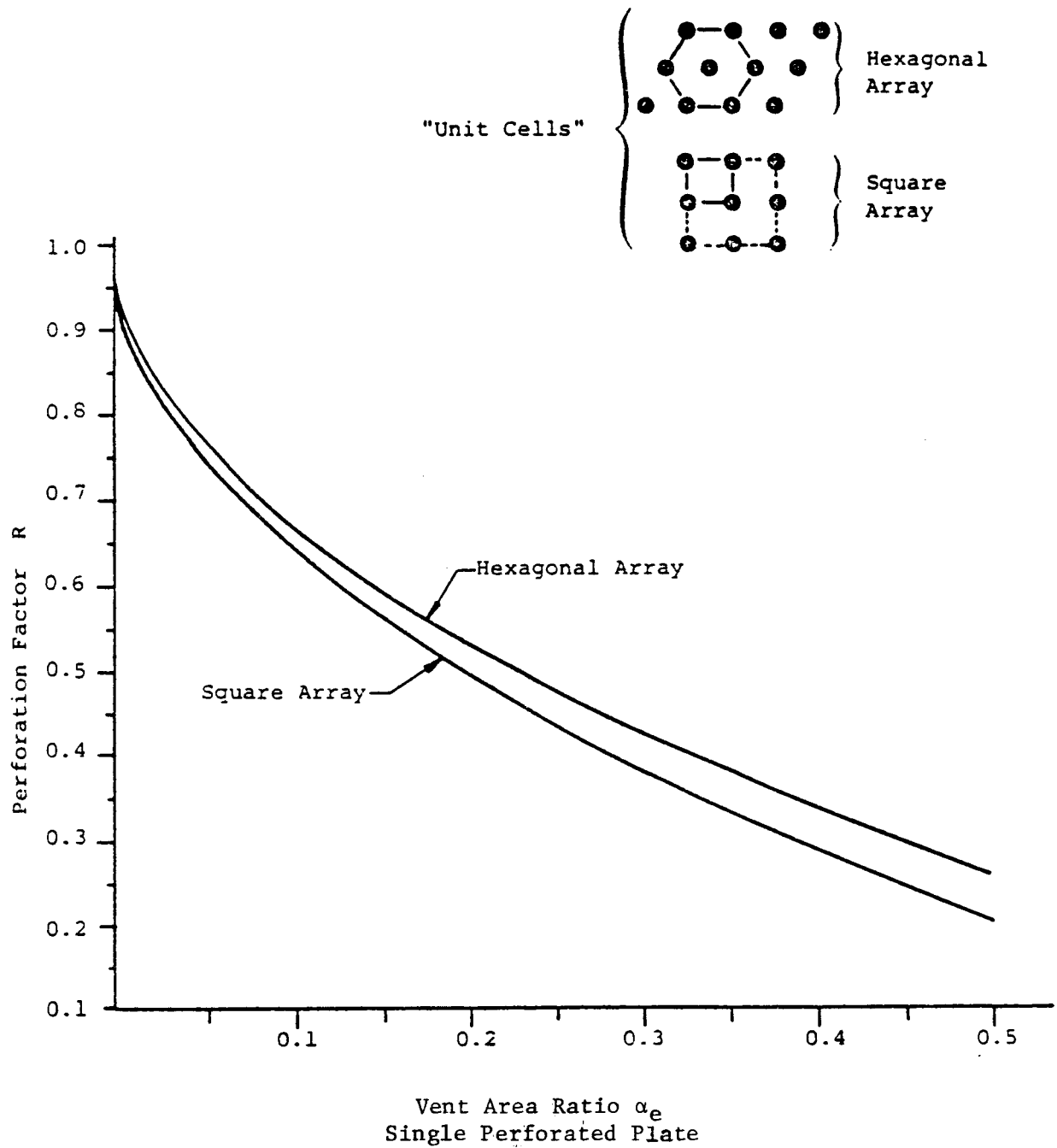
Figure 6.23   Perforation Factor versus Vent Area Ratio for Drilled Hole Patterns

$$\phi_c = \arcsin \left(V_s \cos\theta/c_p\right) \qquad (6.41)$$

where c_p = sonic velocity of the plate = 18,010 fps for steel. If $\phi > \phi_c$, the impact is considered to be a corner or edge impact. Define a critical velocity as

$$V_{cr} = 2000 \text{ fps}/\cos\theta \qquad (6.42)$$

Then, for a flat impact with a striking velocity equal to or greater than the critical velocity, i.e.,

$$\phi \leq \phi_c$$

$$V_s \geq V_{cr}$$

the fragment will be in the shatter mass loss mode. The residual weight of the fragment for this case is determined by

$$W_r = W_s \left[1 - 0.002063 t^{0.138} W_s^{0.074} (\sec\theta)^{0.143} V_s^{0.761}\right] \qquad (6.43)$$

where all terms are as previously defined.

For flat impacts with a striking velocity less than the critical velocity, i.e.,

$$\phi \leq \phi_c$$

$$V_s < V_{cr}$$

and for all corner or edge impacts, i.e.,

$$\phi > \phi_c$$

the fragment is in the deformation mass loss mode. To determine the fragment residual mass for this mode, a correlation velocity is computed first. The correlation velocity in fps is defined as

$$V_{co} = \frac{V_s}{\left[1 + \frac{\cos\theta}{\left(\frac{0.6 t \gamma A_p}{W_s} + 0.15\right)}\right]} \qquad (6.44)$$

where all terms are as previously defined. Then,

For $V_{co} \leq 700$ fps: $W_r = W_s$

$V_{co} \geq 2500$ fps: $W_r = W_s \left[1 - 0.002063 t^{0.138} W_s^{0.074} (\sec\theta)^{0.143} V_s^{0.761}\right]$

700 fps $< V_{co} < 2500$ fps: $W_r = W_s \left[1 - 0.0000151 (V_{co} - 700)^{1.42}\right]$ $\qquad (6.45)$

The penetration prediction method outlined above can be expected to give conservative results, particularly for fragment residual mass estimates. Two further assumptions can be made when investigating multi-layer panels that will increase the conservatism of the method and reduce the number of calculations required. These are: 1) to set $\beta = 1$ in Equation (6.40), and 2) to neglect any fragment loss of mass. If the panel defeats the fragment with the resulting known higher residual velocity and larger mass, it is clearly safe. If the fragment defeats the panel with these two assumptions, the calculations should be repeated using more accurate fragment residual velocity and mass.

EXAMPLE PROBLEM 6.11

PROBLEM – Determine the deflection δ which results when a metal sheet
is struck by a "chunky" crushable fragment. For illustrative
purposes, assume that a piece of concrete strikes an aluminum
panel.

GIVEN: M = mass of the fragment

ρ_p = density of fragment

ρ_t = density of target

σ_t = yield stress (nominal) of target

h = thickness of target

V = striking velocity

(use any self-consistent units)

FIND: δ REFERENCE

SOLUTION: 1. Radius of fragment (a) (assume spherical shape)

ρ_p = M/vol; vol = $(4/3)\pi a^3$

$a^3 = 3M/4\pi\rho_p$

$a = \sqrt[3]{3M/4\pi\rho_p}$

2. Calculate nondimensional velocity.

$\bar{V} = \rho_p V\sqrt{\sigma_t \rho_t}$ Table 6.9

3. Determine dimensionless deflection $\bar{\delta}$.   Fig. 6.20

4. Calculate actual deflection.

$\bar{\delta} = \delta h/a^2$ Table 6.9

$\delta = \bar{\delta}a^2/h$

CALCULATION

GIVEN: M = 3.1 x 10^{-3} lb-sec^2/ft

ρ_p = 3.7 lb-sec^2/ft^4

ρ_t = 5.4 lb-sec^2/ft^4

σ_t = 7.63 x 10^6 lb/ft

h = 2.5 x 10^{-3} ft

V = 200 ft/s

FIND: δ

SOLUTION: 1. $a = \left(\dfrac{3}{4}\dfrac{m}{\pi\rho_p}\right)^{1/3}$

$$a = \left(\frac{3}{4} \frac{3.1 \times 10^{-3}}{\pi \quad 3.7} \right)^{1/3}$$

$$a = 0.058 \text{ ft}$$

2. $\bar{V} = \rho_p \, v / \sqrt{\sigma_t \, \rho_t}$

$$\bar{V} = (3.7)(200) / \sqrt{7.63 \times 10^6 (5.4)} = 0.12$$

3. Entering Figure 6.20, determine nondimensional deflection, $\bar{\delta}$, and calculate actual deflection δ.

$$\bar{\delta} = 0.026$$

$$\delta = \bar{\delta} a^2 / h$$

$$\delta = (0.026)(0.058)^2 / (2.5 \times 10^{-3})$$

$$\delta = 3.5 \times 10^{-2} \text{ ft} = \underline{0.42 \text{ in.}}$$

EXAMPLE PROBLEM 6.12

PROBLEM – Determine the limit velocity V_{50} for a "chunky" nondeforming fragment striking a metal plate. This is an example to show whether existing metal plate siding on a building will or will not be perforated by a steel fragment.

GIVEN: h = target thickness
a = radius of fragment (assume spherical)
ρ_p = density of fragment
σ_t = yield stress of target
ρ_t = density of target

(use any self-consistent set of units)

FIND: V_{50} REFERENCE

SOLUTION: 1. Calculate dimensionless target thickness.
$\bar{h} = h/a$ Table 6.9

2. Find dimensionless limit velocity.
$\bar{V}_{50}$ Fig. 6.21

3. Calculate limit velocity
$V_{50} = \bar{V}_{50} \sqrt{\sigma_t \, \rho_t} / \rho_p$ Table 6.9

CALCULATION

GIVEN: h = 0.03 in.
a = 0.031 in.
ρ_p = 7.33 × 10^{-4} lb-sec^2/in.^{4}
ρ_t = 2.6 × 10^{-4} lb-sec^2/in.^{4}
σ_t = 53,000 lb/in.^{2}

<u>FIND:</u> V_{50}

<u>SOLUTION:</u>   1. $\bar{h} = h/a$
                    $\bar{h} = 0.03/0.03$
                    $\bar{h} = 1$

          2.   Entering Figure 6.21, determine nondimensional limit
               velocity, $\bar{V}_{50}$.

                $\bar{V}_{50} = 3.5$

          3.   Calculate actual limit velocity V_{50}.

                $V_{50} = \bar{V}_{50}(\sqrt{\sigma_t \rho_t}/\rho_p)$

                $V_{50} = (3.5)\sqrt{(53{,}000)(2.6 \times 10^{-4})}/(7.33 \times 10^{-4})$

                $V_{50} = 1.77 \times 10^4$ in./sec

                     $= \underline{1477 \text{ ft/s}}$

EXAMPLE PROBLEM 6.13

<u>PROBLEM</u> – Determine the thickness, h, of a mild steel plate required to
            make the striking velocity of a wooden rod equal to the
            limit velocity.

  <u>GIVEN:</u> V_s = striking velocity

          ρ_p = density of fragment

          σ_t = yield strength of target

          ℓ = length of projectile
          d = diameter of projectile

          (use any self-consistent set of units)

<u>FIND:</u>   h   <u>REFERENCE</u>

<u>SOLUTION:</u>   1.   Rearrange Equation (6.37) to solve for h.

$$h = \frac{\dfrac{1.751}{\ell} \pm \sqrt{\left(\dfrac{1.751}{\ell}\right)^2 - (4)\left(\dfrac{144.2}{\ell d}\right)\left(\dfrac{-\rho_p V_s^{\,2}}{\sigma_t}\right)}}{(2)\left(\dfrac{144.2}{\ell d}\right)} \qquad \text{Eq. (6.37)}$$

          NOTE: This is the solution to a quadratic equation.
          Only the positive solution for h is valid.

CALCULATION

<u>GIVEN</u>: $V_s = 1000$ ft/s

$\rho_p = 1.55$ lb-sec^2/ft^4

$\sigma_t = 7.2 \times 10^6$ lb/ft^2

$\ell = 2$ ft

$d = 0.1$ ft

<u>FIND</u>: h

<u>SOLUTION</u>:

1. $h = \dfrac{\dfrac{1.751}{\ell} \pm \sqrt{\left(\dfrac{1.751}{\ell}\right)^2 - (4)\left(\dfrac{144.2}{\ell d}\right)\left(\dfrac{-\rho_p V_s^2}{\sigma_t}\right)}}{(2)\left(\dfrac{144.2}{\ell d}\right)}$

$h = \dfrac{\dfrac{-1.751}{2} \pm \sqrt{\left(\dfrac{1.751}{2}\right)^2 - (4)\left[\dfrac{(144.2)}{(2)(0.1)}\right]\left[\dfrac{-(1.55)(1000)^2}{(7.2 \times 10^6)}\right]}}{(2)\left[\dfrac{(144.2)}{(2)(0.1)}\right]}$

$h = 1.67 \times 10^{-2}$ ft

$h = \underline{0.20 \text{ in.}}$

<u>EXAMPLE PROBLEM 6.14</u>

<u>PROBLEM</u> – Determine the ballistic limit velocity (V_ℓ) for a compact fragment striking a mild steel target.

<u>GIVEN</u>: W_s = fragment striking weight (lb)

t = plate thickness (in.)

θ = angle of obliquity (degrees)

A_p = presented area (in.^{2})

L/D = length-to-diameter ratio of fragment

<u>FIND</u>: V_ℓ <u>REFERENCE</u>

<u>SOLUTION</u>: 1. Find empirical constants.

A_o, m, n, $t/R\sqrt{A_p}$ Table 6.11

2. Calculate the ballistic limit velocity (ft/s).

$V_\ell = (A_o/\sqrt{W_s}) \, A_p^m \, (t \sec \theta)^n$ Eq. (6.38)

CALCULATION

GIVEN: W_s = 0.1 lb

t = 0.25 in.

θ = 0°

A_p = 0.5 in.^{2}

L/D = 0.886

FIND: V_ℓ

SOLUTION: 1. $\dfrac{t}{R\sqrt{A_p}} = \dfrac{(0.25)}{(1)\sqrt{(0.5)}} = 0.35$

Using Table 6.11 and the value for $(t)/[(R)\sqrt{A_p}]$ and L/D, find A_o, m and n.

A_o = 1414

m = 0.295

n = 0.910

2. $V_\ell = (A_o/\sqrt{W_s}\, A_p^m)\,(t \sec \theta)^n$

$V_\ell = (1414/\sqrt{0.1})(0.5)^{0.295}\,(0.25 \sec 0°)^{0.910}$

V_ℓ = <u>1032 ft/sec</u>

<u>EXAMPLE PROBLEM 6.15</u>

PROBLEM – Calculate the residual velocity, $\bar{V}_r$, for a compact fragment striking a mild steel target.

GIVEN: W_s = fragment striking weight (lb)

t = plate thickness (in.)

θ = angle of obliquity (degrees)

A_p = presented area (in.^{2})

L/D = length-to-diameter ratio

V_s = striking velocity (ft/s)

γ = target specific weight (lb/in.^{3})

FIND: V_r REFERENCE

SOLUTION: 1. Calculate the ballistic limit velocity V_ℓ.   Example
                                                              Problem
                                                              6.14

2. Find empirical constants.
   a, b, c   Table 6.12

3. Calculate the following quantities.

$$x = \frac{V_s}{V_\ell} - 1 \qquad \text{Eq. (6.40)}$$

$$\beta = \frac{1}{[1 + \gamma A_p t/W_s]^{1/2}}; \quad L/D \leq 2$$

$$\beta = 1; \quad L/D > 2$$

4. Calculate the residual velocity.

$$V_r = V_\ell \, \beta \left[\frac{ax^2 + bx + c\sqrt{x}}{x + 1} \right] \qquad \text{Eq. (6.40)}$$

CALCULATION

GIVEN: W_s = 0.1 lb

t = 0.25 in.

θ = 0°

A_p = 0.5 in.^{2}

L/D = 0.886

V_s = 1500 ft/s

γ = 0.283 lb/in.^{3}

FIND: V_r

SOLUTION: 1. From example problem 6.14

V_ℓ = 1032 ft/sec

2. a = 1.12

b = 0.52

c = 1.29

3. $x = \dfrac{V_s}{V_\ell} - 1 = \dfrac{1500}{1032} - 1 = 0.453$

$\beta = \dfrac{1}{[1 + \gamma A_p t/W_s]^{1/2}} = \dfrac{1}{[1 + (0.283)(0.5)(0.25)/(0.1)]^{1/2}}$

$= 0.859$

4. $V_r = V_\ell \, \beta \left[\dfrac{ax^2 + bx + c\sqrt{x}}{x + 1} \right]$

$V_r = (1032) \times (0.859) \left[\dfrac{(1.12)(0.453)^2 + (0.52)(0.453) + (1.29)\sqrt{0.453}}{(0.453 + 1)} \right]$

$V_r = \underline{814 \text{ ft/s}}$

EXAMPLE PROBLEM 6.16

PROBLEM – Determine the residual weight, W_r, of a fragment which has penetrated a mild steel plate.

GIVEN:
θ = angle of obliquity (degrees)(see beginning of section 6.4.1.3)
ϕ = orientation angle (degrees)
V_s = striking velocity (ft/sec)
c_p = sonic velocity of plate (ft/sec)
W_s = fragment weight (lb)
t = plate thickness (in.)
γ = specific weight of plate (lb/in.^{3})
A_p = presented area (in.^{2})

FIND: W_r REFERENCE

SOLUTION:
1. Calculate critical shatter angle.

$$\phi_c = \sin^{-1}(V_s \cos\theta/c_p)$$ Eq. (6.41)

2. Calculate critical velocity.
$$V_{cr} = 2000 \ (ft/s)/\cos\theta$$ Eq. (6.42)

3. Determine mass loss mode.
- If $(\phi \leq \phi_c)$ and $(V_s \geq V_{cr})$ then shatter mode. Continue at Step 4.
- If $(\phi \leq \phi_c)$ and $(V_s < V_{cr})$ or $\phi > \phi_c$, then deformation mode. Continue at Step 5.

4. Calculate residual weight.
$$W_r = W_s\left[1 - 0.002063t^{0.138}W_s^{0.074}(\sec\theta)^{0.143}V_s^{0.761}\right]$$ Eq. (6.43)

5. Calculate the correlation velocity.

$$V_{co} = \frac{V_s}{\left[1 + \Big/\left(\dfrac{0.6t\gamma A_p}{W_s} + 0.15\right)\right]}$$ Eq. (6.44)

6. Determine the proper equation to use for calculating the residual weight.
- If $V_{co} \leq 700$ ft/s, then $W_r = W_s$
- If $V_{co} \geq 2500$ ft/s, then
$$W_r = W_s[1 - 0.002063t^{0.138}W_s^{0.074}(\sec\theta)^{0.143}V_s^{0.761}]$$

Eq. (6.43)

- If $700 \text{ ft/s} < V_{co} < 2500 \text{ ft/s}$, then

$$W_r = W_s [1 - 1.51 \times 10^{-5}(V_{co} - 700)^{1.42}] \qquad \text{Eq. (6.45)}$$

CALCULATION

GIVEN: $\theta = 0°$

$\phi = 20°$

$V_s = 1500 \text{ ft/sec}$

$c_p = 18000 \text{ ft/sec}$

$W_s = 0.116 \text{ lb}$

$t = 0.25 \text{ in.}$

$\gamma = 0.283 \text{ lb/in.}^3$

$A_p = 0.5 \text{ in.}^2$

FIND: W_r

SOLUTION: 1. $\phi_c = \sin^{-1}(V_s \cos\theta/c_p)$

$= \sin^{-1} [(1500)\cos(0°)/(18000)] = 4.8°$

2. $V_{cr} = 2000/\cos\theta = 2000/\cos(0°) = 2000 \text{ ft/s}$

3. $\phi > \phi_c$; therefore, use deformation mode equation and continue at Step 5.

4. Omit.

5. $V_{co} = \dfrac{V_s}{\left[1 + \dfrac{\cos\theta}{\left(\dfrac{0.6t\gamma A_p}{W_s} + 0.15\right)}\right]}$

$V_{co} = \dfrac{1500}{\left\{1 + \dfrac{\cos(0°)}{\left[\dfrac{(0.6)(0.25)(0.283)(0.5)}{(0.116)} + 0.15\right]}\right\}}$

$V_{co} = 375 \text{ ft/s}$

6. $V_{co} \leq 700 \text{ ft/sec}$, therefore, $W_r = W_s$. That is, the residual weight of the fragment is the same as the striking weight of the fragment.

6.4.2 Impact on Concrete and Masonry Structures

Several tests by various researchers have been conducted to examine the problem of penetration of concrete targets by low-velocity projectiles. Most of these tests were conducted to examine the possibility of tornado-borne missiles damaging concrete nuclear reactor containment walls.

Baker, Hokanson and Cervantes (Ref. 6.5) performed several experimental tests in which model wooden utility poles or model schedule 40 pipe were impacted normal to the center of concrete test panels. As was the case for their tests with sheet steel impacts, the targets were sufficiently large to confine residual deformation to the central portions of the target. Deformation profiles were somewhat irregular, with discontinuities near fracture planes, but were quite similar in nature to profiles reported by Vassalo (Ref. 6.30). Although the limited number of tests conducted precluded repeat shots, the formation of spall craters and fragments appeared to be consistent from test to test. Baker, Hokanson and Cervantes (Ref. 6.5) later reviewed available test data obtained both in the United States and abroad, and summarized the available data. Their summary is included here.

6.4.2.1 Steel Pipe Missiles

Prediction curves are based on a total of 66 tests in which steel pipe missiles were impacted against concrete panels. Nine tests for short pipes ($6.06 < \ell/d < 9.74$) were reported by Vassalo (Ref. 6.30). Stephenson (Ref. 6.31) and Stephenson et al. (Ref. 6.32) present the results of 14 full-scale tests in which long pipes ($13.8 < \ell/d < 36.3$) were propelled by a rocket sled into concrete panels. The most complete series of tests is reported by Jankov et al. (Ref. 6.33), where the results of 36 quarter-scale ($4.5 < \ell/d < 24.3$) missile penetration tests are presented. Unfortunately, about half of these tests were conducted against panels which had been impacted previously. The remaining seven tests were reported by Baker, Hokanson and Cervantes (Ref. 6.5). This series of tests is unique in that the panels are thought to be more representative of actual concrete containment structures than the panels in any of the previously cited reports. This is because the rebars were spaced very close together. The model pipe missile not only could not pass between the rebars, but impacted against at least four of them. Three of the tests were for pipe missiles with a 30° nose angle. The results of these three tests indicate that a considerable amount of the projectile kinetic energy is expended in deforming the nose of the missile, leaving less energy to deform the target. Apparently, blunt-end pipe missiles represent the most severe threat to concrete panels.

Figure 6.24 presents the scabbing threshold for blunt-end steel pipe missiles penetrating reinforced concrete panels. The format of the

figure is the same as originally presented by Jankov et al. (Ref. 6.33); scaled kinetic energy versus scaled target thickness. Note that the vertical axis is dimensional. The data are grouped into three sets depending on the wall thickness to diameter ratio ($2t_w/d$) of the missile. The lines of the figure are prediction curves, with scabbing predicted above the curves and not below. Because of the limited amount of data, prediction of the scabbing threshold of pipe missiles impacting concrete panels is limited to the regions shown in the figure. Futher efforts in this area of research should include systematic investigations of the significance of the influence of different amounts of rebar. At the present time, calculations should be limited to conditions specified in Figure 6.24.

Rotz (Ref. 6.34) has presented a simple empirical equation for predicting the thickness of threshold of spalling, t_w, for steel pipe missiles. We do not include this formula here, because it is dimensional, and can be shown to give inaccurate predictions for tests conducted at scales other than the small series on which Rotz based the equation. In later unpublished work, however, Rotz has modified his equation to make it dimensionally homogeneous.

6.4.2.2 Utility Pole Missiles

There is a total of 15 tests in which model utility poles were fired against concrete panels. Nine tests are reported by Vassalo (Ref. 6.30), Stephenson (Ref. 6.31), Stephenson et al. (Ref. 6.32) and Jankov et al. (Ref. 6.33); while four tests are given by Baker, Hokanson and Cervantes (Ref. 6.5). The remaining tests are for composite concrete and steel panels reported by Ting (Ref. 6.35). Spall damage of any level was observed in only three tests. Two of these tests [Jankov et al. (Ref. 6.33)] were conducted at velocities well above the postulated velocity of a tornado-accelerated utility pole. The other test in which spallation occurred [Baker, Hokanson and Cervantes (Ref. 6.5)] was the only one in which the projectile did not fail on impact. Apparently, the utility pole missile is not a threat to heavily reinforced concrete walls.

6.4.2.3 Rod Missiles

We have located 66 tests in which solid steel rod projectiles with long ℓ/d ratios were fired at concrete targets. Twenty-six of these tests were conducted in the United States by Barber (Ref. 6.36), Vassalo (Ref. 6.30), Ting (Ref. 6.35), Stephenson (Ref. 6.31) and Jankov (Ref. 6.33). Barber, Ting and Stephenson's data are for long ℓ/d ($15 < \ell/d < 40$) rods, Fiquet (Ref. 6.38) presents 22 and Goldstein (Ref. 6.39) presents 18 short ℓ/d rod tests. The panels from these three references had much heavier reinforcing than did the panels of other researchers. In many cases, five layers of rebar were used, each layer more closely spaced than the layers found in the American panels. The influence of the heavier rebar
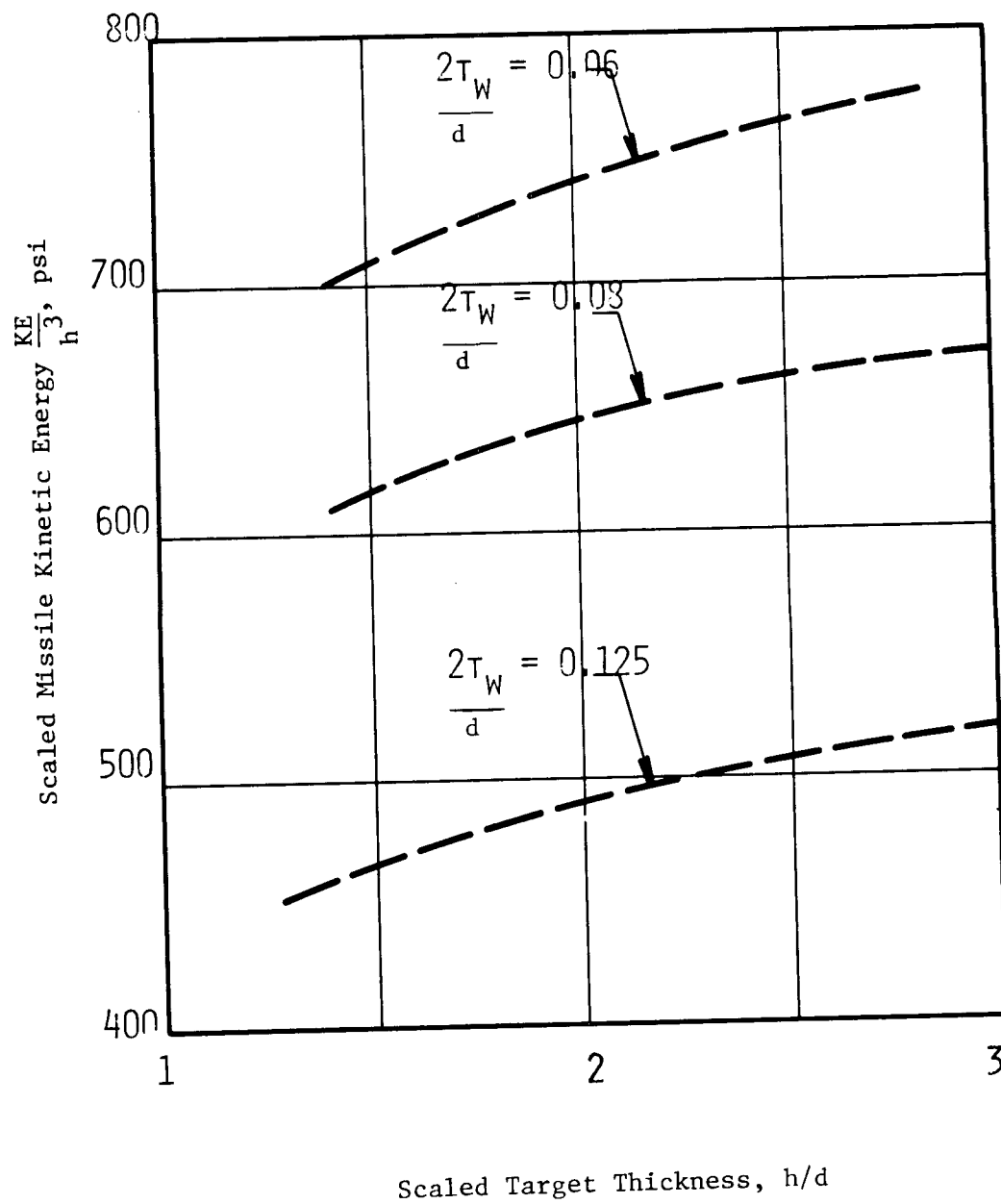
Figure 6.24   Scabbing Threshold for Steel Pipes
On Reinforced Concrete Panels

is to raise the scabbing threshold. The more densely reinforced panels require considerably more kinetic energy to induce scabbing than do panels which are lightly reinforced. The lines on Figure 6.25 are prediction lines for heavily and lightly reinforced panels.

Westine and Vargas (Ref. 6.40) have developed a model to predict incipient spallation from targets which are struck by fragments whose cross-sectional width at impact is much less than the lateral dimensions of the target. In their analysis, they consider as a worst case a cylindrical fragment strikes a plate normally (at a zero angle of obliquity) as shown in Figure 6.26. The high pressures associated with this impact process send a stress wave into the material in a fashion similar to that described for the air blast wave. The major differences in this impact are that the time histories of the stress waves are not necessarily triangular. Waves now propagate through the fragment as well as into the target, and some wave dissipation occurs because the loading is applied locally, rather than uniformly, to a surface. Mathematically the solution to this problem is not an easy one; however, dimensional analysis, physical reasoning and test data can be applied to develop an empirical solution which designers can use to determine the threshold of spall.

Using dimensional analysis, the threshold of spall can be determined from

$$\frac{P}{\sigma} \text{ is a function of } \left(\frac{ia}{Ph_2}\right) \text{ and } \left(\frac{d_1}{h_2}\right) \tag{6.46}$$

where P = peak contact pressure
  σ = ultimate strength of the target material
  i = specific impulse imparted to the target
  a = speed of sound in the target material
  h_2 = target thickness
  d_1 = impact diameter of the fragment

This relationship states essentially that the peak stress wave relative to the ultimate strength of the target material is some function of the duration of loading (i/P) relative to the transit time (h/a) for a wave through the material; and, for nonuniform loadings as in Figure 6.26, a function of the relative dimensions of the fragment and the target (d_1/h_2). The ratio (ia/Ph) is the number of transits of the wave through the target material before the fragment comes to rest.

Using dimensional analysis, experimental test data were cast into ordered pairs of nondimensional impulse $\bar{i}$ and nondimensional pressure $\bar{P}$ where

$$\bar{i} = \frac{ia_2}{2Ph_2} = \frac{\rho_1 \ell_1}{2\rho_2 h_2}\left(1 + \frac{\rho_2 a_2}{\rho_1 a_1}\right) \tag{6.47}$$
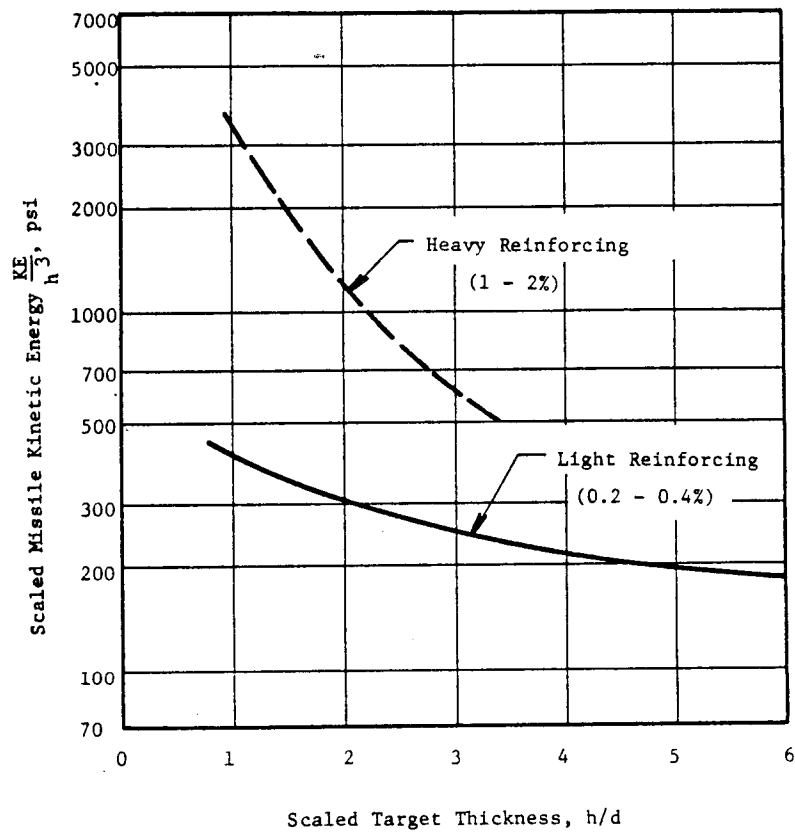
Figure 6.25   Scabbing Threshold for Solid Rod Missiles
Impacting Reinforced Concrete Panels
(Reference 6.39)
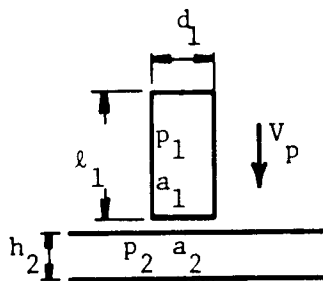
Figure 6.26   Sketch of a Fragment Impact

and

$$\bar{P} = \frac{P}{\sigma}\left(\frac{d_1}{h_2}\right)^{0.4} = \frac{\left(\frac{d_1}{h_2}\right)^{0.4} \rho_2 a_2 V_p}{\sigma\left(1 + \frac{\rho_2 a_2}{\rho_1 a_1}\right)}$$ (6.48)

where ρ_2 = density of target

ρ_1 = density of rod

a_1 = speed of sound in the rod

a_2 = speed of sound in the target

V_p = impact velocity

ℓ_1 = length of rod

Figure 6.27 contains a plot of $\bar{P}$ versus $\bar{i}$ as obtained from Baker et al. (Ref. 6.41) which shows the threshold of spall for rod missiles impacting plate targets. Missiles and targets were made of various materials. For values of $\bar{i}$ greater than 40, the value for $\bar{P}$ for threshold of spall is approximately 5.25.

6.4.2.4 Steel Plate Approximation for Concrete Target

For a very quick and crude rule-of-thumb estimate of the effectiveness of reinforced concrete panels in resisting penetration by steel fragments, it can be assumed that 1 in. of mild steel is equivalent to 9 in. of concrete, i.e., if it is known that a 1-in. thickness of mild steel will defeat a particular fragment threat, it can be estimated that 9 in. of reasonable quality reinforced concrete will also defeat the fragment. When more realistic estimates of concrete penetration are desired, the methods from Reference 6.6 summarized below can be utilized.

6.4.2.5 Armor-Piercing Fragments

A certain amount of experimental data analogous to primary fragment penetration has been accumulated in connection with projects to determine the effects of bomb and projectile impact on concrete structures. These data were analyzed and relationships developed where the amount of fragment penetration into concrete elements could be expressed in terms of the physical properties of both the metal fragment and the concrete (Ref. 6.28). The general expression for the maximum penetration X_f in inches of a compact armor-piercing fragment was derived in terms of the fragment weight W_f in pounds and striking velocity V_s in fps, i.e.,

$$X_f = 4.91 \times 10^{-6} W_f^{0.4} V_s^{1.8}$$ (6.49)
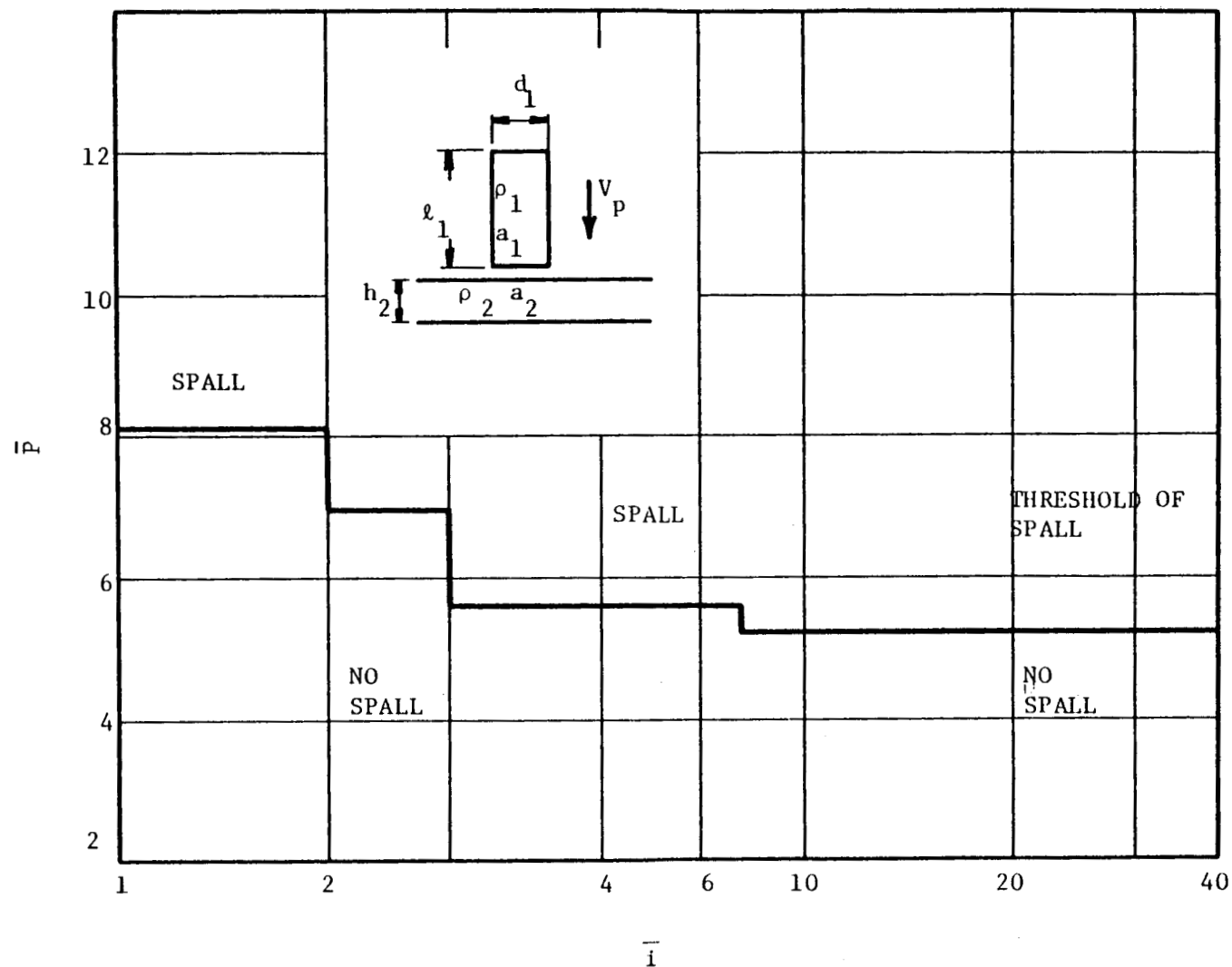
Figure 6.27 Spall Threshold for Fragment Impacts
(Various Projectile and Target Materials)

Equation (6.49) is based on a concrete compression strength f'_c equal to 5,000 psi and its limits in terms of fragment weight and velocity and target penetration thickness is unknown. Maximum penetrations of fragments in concrete of other strengths may be obtained by multiplying the value of X_f of Equation (5.45) by the square root of the ratio of 5,000 psi to the compressive strength of the concrete in question.

The limiting thickness of concrete at which perforation will occur can be obtained from Figure 6.28 and is a function of the fragment weight, striking velocity, and maximum penetration and the dilatational velocity C_s of the elastic wave through concrete where

$$C_s = 5.16 \ E_c^{1/2} \ \text{(ft/sec)} \tag{6.50}$$

and the modulus of elasticity E_c is defined to be

$$E_c = 33 \ \gamma_c^{1.5} \ \sqrt{f'_c} \ \text{(psi)} \tag{6.51}$$

where γ_c = specific weight of concrete, lb/ft^3

f'_c = static unconfined compressive strength of concrete, psi

The equation for the upper line in Figure 6.28 is

$$C_1 = 2.00 \ \left[(2.52) \left(\frac{W_f}{X_f} \right)^{1/3} \right]^{1.37} \tag{6.52}$$

and the equation for the lower line is

$$C_1 = 0.100 \ \left[(2.52) \left(\frac{W_f}{X_f} \right)^{1/3} \right]^{1.25} \tag{6.53}$$

Fragments which perforate a concrete element will have a residual velocity V_r which may endanger the receiver system. The magnitude of this velocity may be approximated from the expression which defines the velocity of the fragment at any time as it penetrates the concrete, i.e.,

$$(V_r/V_s)^{1.8} = 1 - (T_c/X_f) \tag{6.54}$$

where T_c = thickness of concrete element, in.

V_r = residual velocity of fragment as it leaves concrete element, fps

Equation (6.54) applies when the depth of penetration is greater than two fragment diameters. If the depth of penetration X_f is less than two fragment diameters d, Healey et al. (Ref. 6.7) recommend

$$(V_r/V_s)^{1.8} = 1 - (T_c/X_f)^2 \tag{6.55}$$

Plots of the ratio V_r/V_s against T_c/X_f are given in Figure 6.29.
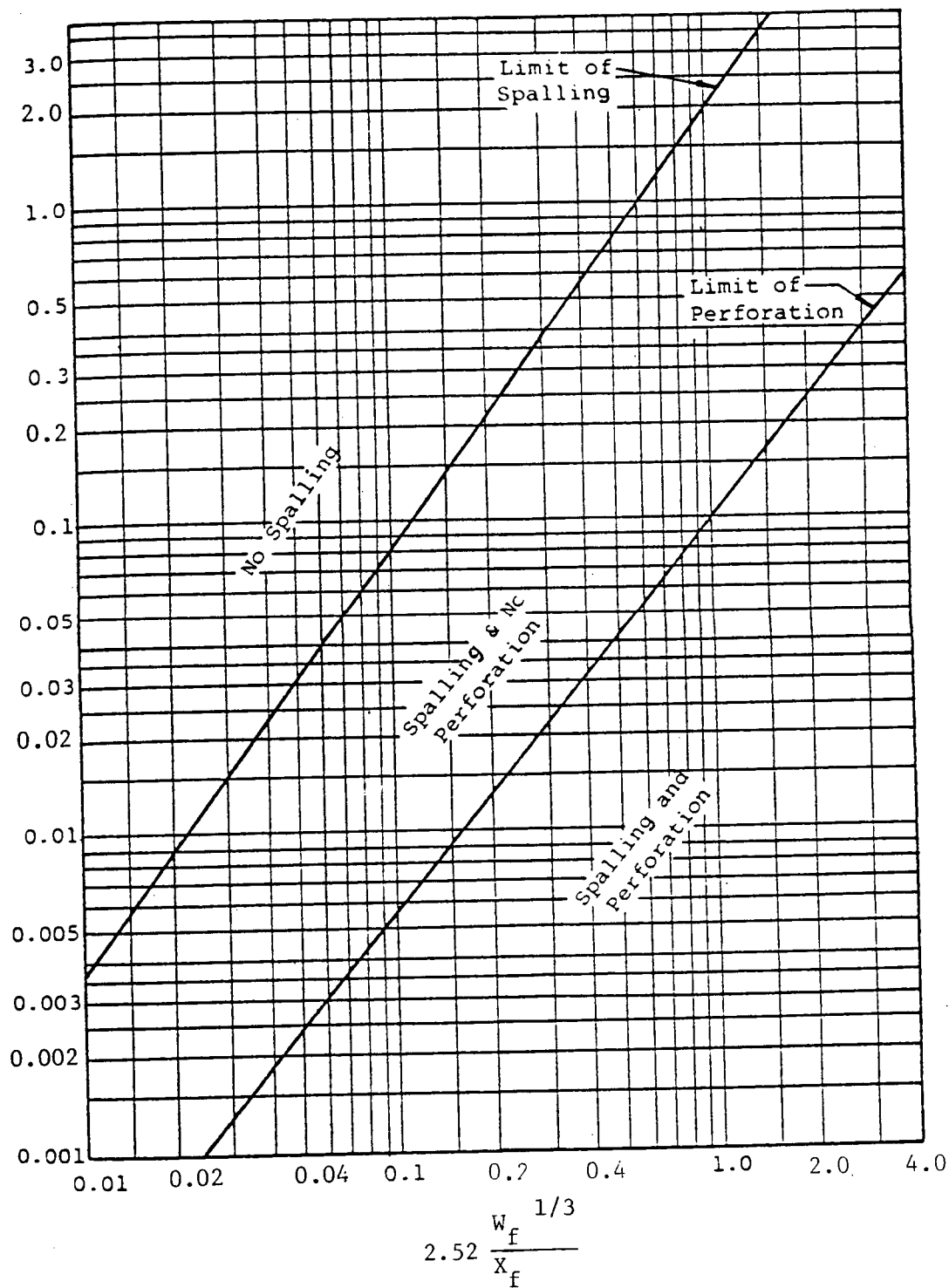
Figure 6.28 Limits of Concrete Spalling and Perforation
(Reference 6.6)

6-108

The above analysis applies to compact armor-piercing fragments. For irregular shapes, one can calculate an equivalent fragment diameter from

$$d = \left(\frac{M}{\frac{4}{3} \pi \rho_p} \right)^{1/3} \tag{6.56}$$

where M = mass of the fragment, $lb-sec^2/in.$
ρ_p = its mass density $lb-sec^2/in.^4$

6.4.2.6 Other Fragments

To estimate the concrete penetration of metal fragments other than armor piercing, a procedure has been developed to relate the concrete penetrating capabilities of such fragments to those of armor-piercing fragments. This relationship is expressed in terms of relative metal hardness (the ability of the metal to resist deformation) and density, and is represented by constant C_2 in Equation (6.57)(Ref. 6.6)

$$X_f' = C_2 X_f \tag{6.57}$$

where X_f' = maximum penetration in concrete of metal fragments other than armor-piercing
The numerical values of C_2 for several of the more common casing metals are listed in Table 6.13.

Table 6.13 Penetration Factors

Type of Material	C_2
Armor-piercing steel	1.00
Mild steel	0.70
Lead	0.50
Aluminum	0.25
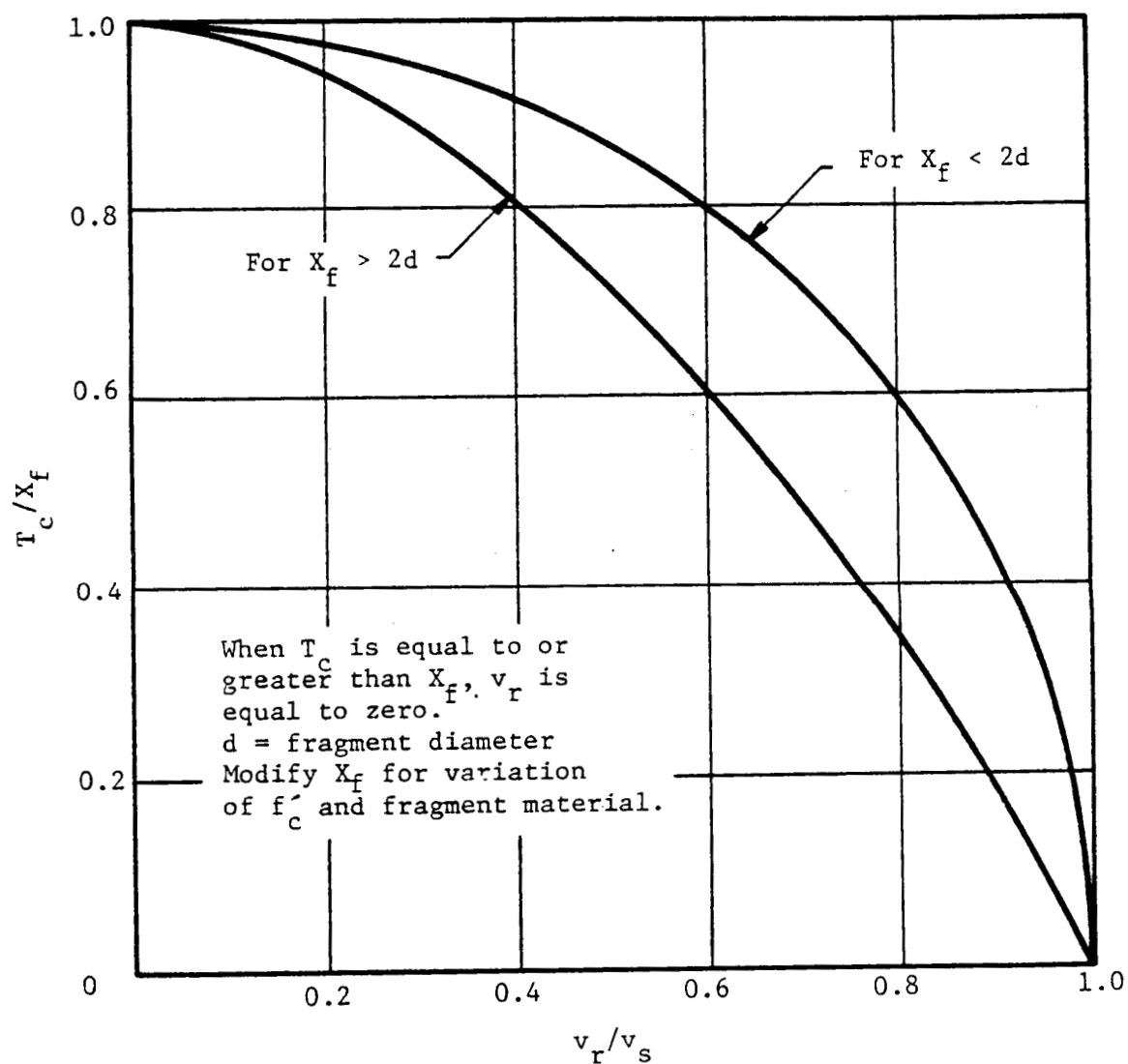
Figure 6.29   Residual Velocity of Primary Fragment
after Perforation (Ref. 6.23 and 6.26)
($f_c' = 5000$ psi)

EXAMPLE PROBLEM 6.17

PROBLEM – Determine if scabbing will occur when a steel pipe missile
          impacts a reinforced concrete panel.

GIVEN: h = target thickness (in.)
        d = missile diameter (in.)
        W_s = missile weight (lb)
        V_s = striking velocity (in./sec)
        t_w = wall thickness of missile (in.)

FIND: Probability of scabbing   REFERENCE

SOLUTION: 1. Calculate the scaled target thickness.
               $\bar{h} = h/d$ Fig. 6.24
           2. Calculate scaled kinetic energy.

               $$\frac{KE}{h^3} = \frac{W_s V_s^2}{(2)(386)h^3}$$ Fig. 6.24

               (NOTE: Units of scaled kinetic energy are psi.)
           3. Calculate the quantity $(2t_w/d)$ and determine
               the appropriate curve on Figure 6.24.
           4. Plot the point $(\bar{h}, KE/h^3)$ on Figure 6.24 and
               determine if scabbing will occur. Note that
               points above the appropriate $(2t_w/d)$ curve
               are above the scabbing threshold.

CALCULATION

GIVEN: h = 10 in.
        d = 4 in.
        W_s = 5 lb
        V_s = 10000 in./sec
        t_w = 0.2 in.

FIND: Probability of scabbing

SOLUTION: 1. $\bar{h} = h/d = 10/4 = 2.5$
           2. $KE/h^3 = W_s V_s^2/[(2)(386)h^3] = (5)(10000)^2/[(2)(386)(10)^3]$
                        = 648 psi
           3. $2t_w/d = (2)(0.2)/(4) = 0.1$
           4. Scabbing will occur.

PROBLEM – Determine if scabbing will occur when a solid, rod-type missile impacts a reinforced concrete panel.

GIVEN: h = target thickness (in.)
        d = missile diameter (in.)
        W_s = missile weight (lb)
        V_s = striking velocity (in./s)

FIND: Probability of scabbing   REFERENCE

SOLUTION: 1. Calculate the scaled target thickness.
             $\bar{h} = h/d$

       2. Calculate scaled kinetic energy.

$$\frac{KE}{h^3} = \frac{W_s V_s^2}{(2)(386)h^3}$$

       (NOTE: Units of scaled kinetic energy are psi.)

       3. Plot the point $(\bar{h}, KE/h^3)$ on Figure 6.25.

       4. Determine if scabbing will occur. Note that   Fig. 6.25
          points above the appropriate curve are above
          the scabbing threshold.

CALCULATION

GIVEN: (light reinforcing)
        h = 18 in.
        d = 6 in.
        W_s = 20 lb
        V_s = 6000 in./sec

FIND: Probability of scabbing

SOLUTION: 1. $\bar{h} = h/d$
           $\bar{h} = 18/6 = 3$

       2. $$\frac{KE}{h^3} = \frac{W_s V_s^2}{(2)(386)h^3}$$

$$= \frac{(20)(6000)^2}{(2)(386)(18)^3}$$

$$= 160 \text{ psi}$$

       3. Find point on Figure 6.25.

       4. No scabbing should occur.

EXAMPLE PROBLEM 6.19

PROBLEM – Determine if spalling will occur when a wood projectile strikes a concrete panel.

GIVEN: d_1 = impact diameter of fragment

h_2 = target thickness

ρ_2 = density of target

ρ_1 = density of fragment

σ_2 = ultimate strength of target materials

a_2 = speed of sound in target material

V_p = striking velocity

a_1 = speed of sound in fragment

ℓ_1 = length of fragment

(or use any self-consistent set of units)

FIND: Probability of spalling

REFERENCE

SOLUTION: 1. Calculate scaled impulse.

$$\bar{i} = \frac{\rho_1 \ell_1}{2\rho_2 h_2}\left(1 + \frac{\rho_2 a_2}{\rho_1 a_1}\right)$$

Eq. (6.47)

2. Calculate scaled pressure.

$$\bar{P}_1 = \frac{(d_1/h_2)^{0.4}\, \rho_2 a_2 V_p}{\sigma_2\left(1 + \frac{\rho_2 a_2}{\rho_1 a_1}\right)}$$

Eq. (6.48)

3. Plotting the point $(\bar{i}, \bar{P}_1)$ on Figure 6.27 and comparing it with the threshold of spall curve, determine if spalling occurs.

CALCULATION

GIVEN: d_1 = 0.5 ft

h_2 = 1.5 ft

ρ_2 = 4.67 lb-sec^2/ft^4

ρ_1 = 2.17 lb-sec^2/ft^4

σ_2 = 7.2 x 10^5 lb/ft^2

a_2 = 4000 ft/s

V_p = 200 ft/s

$$a_1 = 1000 \text{ ft/s}$$

$$\ell_1 = 9 \text{ ft}$$

<u>FIND</u>: Probability of spalling

<u>SOLUTION</u>: 1. $\bar{i} = \dfrac{\rho_1 \ell_1}{2\rho_2 h_2}\left(1 + \dfrac{\rho_2 a_2}{\rho_1 a_1}\right)$

$$= \frac{(2.17)(9)}{(2)(4.67)(1.5)}\left[1 + \frac{(4.67)(4000)}{(2.17)(1000)}\right]$$

$$= 13.4$$

2. $\bar{P}_1 = \dfrac{(d_1/h_2)^{0.4}\, \rho_2 a_2 V_p}{\sigma_2\left(1 + \dfrac{\rho_2 a_2}{\rho_1 a_1}\right)}$

$$= \frac{(0.644)(4.67)(4000)(200)}{(7.2 \times 10^5)\left[1 + \dfrac{(4.67)(4000)}{(2.17)(1000)}\right]}$$

$$= \frac{(0.5/1.5)^{0.4}(4.67)(4000)(200)}{(7.2 \times 10^5)\left[1 + \dfrac{(4.67)(4000)}{(2.17)(1000)}\right]}$$

$$= 0.348$$

3. No spalling occurs. Plotting the point $(\bar{i},\bar{P})$ = 13.4, 0.348) on Figure 6.27, one can see that it falls well below the spall threshold line. Therefore, no spalling will occur. Note that the curve in Figure 6.27 asymptotically approaches a limit as the value of $\bar{i}$ increases. Thus, if $\bar{P}$ remains constant, increasing just $\bar{i}$ will never cause the panel to spall.

<u>EXAMPLE PROBLEM 6.20</u>

<u>PROBLEM</u> – For a metal fragment striking concrete, determine penetration, perforation, spalling, and residual velocity.

<u>GIVEN</u>: f'_c = compressive strength of concrete (psi)

W_f = fragment weight (lb)

V_s = striking velocity (ft/sec)

γ_c = specific weight of concrete (lb/ft^3)

T_c = thickness of concrete (in.)

d = fragment diameter (in.)

FIND: X_f, probability of perforation and spalling, V_r

SOLUTION:
1. Calculate maximum penetration (in.) for armor-piercing steel fragment.

    $$X_f = 4.91 \times 10^{-6} \, W_f^{0.4} \, V_s^{1.8}$$ Eq. (6.49)

    Note that for concrete targets with a compressive strength different from 5000 psi, X_f must be multiplied by

    $$\sqrt{5000 \text{ psi/strength of concrete (psi)}}$$

2. Determine C_2. Table 6.13

3. Calculate the maximum penetration of a metal fragment.

    $$X_f' = C_2 \, X_f$$ Eq. (6.57)

4. Calculate the dilatation velocity of the elastic wave (ft/sec).

    $$C_s = 5.16 \, E_C^{1/2}$$ Eq. (6.50)

    where

    $$E_C = 33 \, \gamma_c^{1.5} \, \sqrt{f_c'} \text{ (psi)}$$ Eq. (6.51)

5. Determine if perforation and/or spalling occurs. Fig. 6.28

    $$\text{Abscissa} = 2.52 \frac{W_f^{1/3}}{X_f'}$$

    $$\text{Ordinate} = \left[\frac{T_c + 0.877 \, W_f^{1/3} - 1}{X_f'} \right] \left[\frac{C_s}{V_s} \right]^{1/3}$$

6. Calculate residual velocity.

    a) if $X_f'/d > 2$

    $$\left(\frac{V_r}{V_s} \right)^{1.8} = 1 - \frac{T_c}{X_f'}$$ Eq. (6.54)

    b) if $X_f'/d < 2$

    $$\left(\frac{V_r}{V_s} \right)^{1.8} = 1 - \frac{T_c}{X_f'}^2$$ Eq. (6.55)

CALCULATION

GIVEN: Steel fragment
$$f_c' = 6000 \text{ psi}$$

W_f = 0.5 lb

V_s = 1500 ft/sec

γ_c = 150 lb/ft^3

T_c = 18 in.

d = 1 in.

FIND: X_f, probability of perforation and spalling, V_r

SOLUTION:

1. $X_f = 4.91 \times 10^{-6} \, W_f^{0.4} \, V_s^{1.8}$ (for $f_c' = 5000$)

   $X_f = 4.91 \times 10^{-6} \, W_f^{0.4} \, V_s^{1.8} \, \sqrt{5000/6000}$ (for $f_c' = 6000$)

     = 1.77 in.

2. $C_2 = 0.70$

3. $X_f' = C_2 \, X_f = (0.7)(1.77) = 1.24$ in.

4. $C_s = 5.16 \, E_C^{1/2}$

   $E_C = 33 \, \gamma_c^{1.5} \, \sqrt{f_c'} = (33)(150)^{1.5} \sqrt{6000} = 4.70 \times 10^6$

   $C_s = (5.16)(4.70 \times 10^6)^{1/2}$

   $C_s = 1.12 \times 10^4 \cdot \text{ft/sec}$

5. Abscissa $= 2.52 \, (W_f^{1/3}/X_f')$

          $= 2.52 \, (0.5^{1/3}/1.24) = 1.61$

  Ordinate $= \left(\dfrac{T_c + 0.877 \, W_f^{1/3}}{X_f'} - 1 \right) \left(\dfrac{C_s}{V_s} \right)^{1/3}$

        $= \left[\dfrac{(18) + (0.877)(0.5)^{1/3}}{1.24} - 1 \right] \left[\dfrac{1.12 \times 10^4}{1500} \right]^{1/3}$

        $= 27.5$

  Figure 6.28 predicts that no perforation or spalling
  will occur.

6. $\dfrac{X_f'}{d} = \dfrac{1.24}{1} = 1.24$

  $\left(\dfrac{V_r}{V_s} \right)^{1.8} = 1 - \left(\dfrac{T_c}{X_f'} \right)^2$

  There is no residual velocity in this case because
  $X_f' < T_c$.

6.4.3 Impacts on Interior Walls

To date, penetration studies involving target materials which might be used in interior wall construction have been extremely limited. As a result, this section will only deal with two materials, strawboard and fiberboard. Strawboard is a material with a specific weight of about 45 lb/ft^3, similar to that of white oak. Fiberboard is a similar material with specific weights ranging from 16 to 28 lb/ft^3 (Ref. 6.42). Some common trade-names for fiberboard are Celotex, Plastergon, Insulite, Flintkote and Smoothlite.

For both target materials and impact by steel fragments, the following functional form was empirically fit to the available data (Ref. 6.42):

$$V = c(h\bar{A})^{\alpha} W_f^{\beta} \qquad (6.58)$$

where V = ballistic limit (ft/s)
    h = thickness of target (in.)
    $\bar{A}$ = estimated average impact area of fragment (in.^{2})
    W_f= weight of the fragment (lb)
    c, α, β are empirically determined constants for each material

Note that by inputting the fragment striking velocity for the ballistic limit, the equation may be rearranged to solve for the target thickness, h. This value defines the target thickness for which there is a 50 percent probability that the fragment will perforate the material (Ref. 6.42). Equating this predicted target thickness to the depth of penetration yields conservative penetration values if the target is thicker than the thickness associated with the ballistic limit (Ref. 6.43).

The empirically fitted equation for strawboard is:

$$V = 59,010 \ (h\bar{A})^{0.606} \ (7000W_f)^{-0.674} \qquad (6.59)$$

and the equation for fiberboard is:

$$V = 44,740 \ (h\bar{A})^{0.75} \ (7000W_f)^{-0.75} \qquad (6.60)$$

where the terms are defined previously for Equation (6.58). Table 6.14 gives the experimentally validated ranges for Equations (6.59) and (6.60).

Table 6.14 Ranges of Velocity for Equations (6.59) and (6.60)
(Reference 6.42)

Target Material	Fragment Weight W_f (lb)	Specific Weight γ (lb/ft^3)	Target Thickness h (in.)	EA ($E = 3/12 \cdot \gamma$) A = Fragment Impact Area	Striking Velocity V (ft/s)	Angle of Obliquity
Strawboard	0.0023 – 0.03	43 → 46	0.21 → 4.3	0.8 – 21	500–2800	0°
Fiberboard	0.00036 – 0.034	16 → 28	0.013 → 8	0.01 – 16	400–4900	0°

EXAMPLE PROBLEM 6.21

PROBLEM – Determine the depth of penetration, h, into an interior wall
and the wall thickness required to stop the same fragment 50%
of the time. Interior wallboard materials are usually 0.5 in.
thick and are used on both sides of an interior wall.

GIVEN: V = striking velocity (ft/s)
$\bar{A}$ = fragment impact area (in.^{2})
W_f = weight of fragment (lb)
wall material = strawboard

FIND: h   REFERENCE

SOLUTION: 1. Ballistic limit equation.

$$V = 59,010 \ (h\bar{A})^{-0.606}(7000W_f)^{-0.674}$$ Eq. (6.59)

2. Rearrange to solve for h.

$$\frac{V}{59,010 \ \bar{A}^{-0.606}(7000W_f)^{-0.674}} = h^{0.606}$$

$$h = \left[\frac{V}{59,010 \ \bar{A}^{-0.606}(7000W_f)^{-0.674}}\right]^{1/0.606}$$

CALCULATION

GIVEN: V = 2000 ft/s
$\bar{A}$ = 0.207 in.
W_f = 0.02 lb

FIND: h

SOLUTION: 1. $h = \left[\dfrac{V}{59,010 \ \bar{A}^{-0.606}(7000W_f)^{-0.674}}\right]^{1/0.606}$

2. $h = \left[\dfrac{2000}{59,010(0.207)^{0.606}(7000 \times 0.02)^{-0.674}}\right]^{1/0.606}$

h = 4.42 in.

Since interior walls usually have a sheet of wallboard
material on each side of the wall (combined thickness
of 1.0 in.), the fragment should easily perforate the
interior wall.

*When using Equations (6.59) and (6.60) the actual fragment impact area
should be used for $\bar{A}$ if it is known. Otherwise, the estimated presented
area of the fragment should be used.

6.4.4 Impacts on Roofing Materials

An analysis for impact upon metal targets leads one to believe
that the important projectile property is momentum. Until more information
is obtained, it must be assumed that momentum is also important in
impact upon roofing materials. [The following discussion is based upon
data by Greenfield (Ref. 6.44) in which synthetic hailstones were
projected at roofing-material targets. The velocities in the tests
correspond to the terminal fall velocities of hailstones of the particular
sizes used.]

Because of the many kinds of roofing and the scarcity of data on
fragment impact upon roofing materials, this discussion will be kept as
general as possible, presenting only the lower limits of damage for
groupings of roofing materials, with the understanding that these are
not known very accurately.

The roofing materials can be separated into three categories:
asphalt shingles, built-up roofs (alternate layers of bitumen and rein-
forcing membranes, often topped with pebbles or crushed stone), and
miscellaneous materials (asbestos cement shingles, slate, cedar shingles,
clay tile, and sheet metal). Lower limits of fragment momentum for serious
damage to common roofing materials are given in Table 6.15. Portions of
the data given in Table 6.15 are presented in Figure 6.30. Figure 6.30
can be readily used to obtain the striking velocity which a fragment of
known mass (M) must have to exceed the minimum fragment momentum required
to produce serious damage.

In general, any fragment which strikes a roofing material will
probably exceed the momentum required to produce serious damage. This
is true because most of the fragments will be large, drag-type fragments,
experiencing little or no lift which might allow it to "settle" on the
roof. To determine the vertical component of the striking velocity V_{y_f}
for the simple case where $y_o = y_f$ and V_{y_o} is greater than 0, the following
equation may be used:

$$V_{y_f} = -\sqrt{Mg/K_y} \, \sin\left[\tan^{-1}\left(V_{Y_o} \, \sqrt{K_y/Mg}\right)\right] \tag{6.61}$$

where M = fragment mass
  g = gravity constant
  V_{y_o} = initial vertical component of velocity
  K_y = $C_D A_D \rho/2$
        where C_D = drag coefficient
            A_D = area presented in the vertical direction
            ρ_o = density of air

Table 6.15 Fragment Impact Damage for Roofing Materials
(Greenfield, Ref. 6.44)

Minimum Fragment Momentum (mV)
for Serious Damage

Roofing Material	lb-sec	Comments
Asphalt shingles	0.159	crack shingle
	1.37	damage deck
Built-up roof	<0.159	crack tar flood coat
	0.451	crack surface of conventional built-up roof without top layer of stones
	>0.991	with a 2.867 lb/ft^2 top layer of slag, there was no damage up to 0.991 ft/sec, which was the maximum momentum of the test

Miscellaneous

1/8-inch asbestos cement shingles	0.159	
1/4-inch asbestos cement shingles	0.285	
1/4-inch green slate	0.285	
1/4-inch grey slate	0.159	
1/2-inch cedar shingles	0.159	
3/4-inch red clay tile	0.285	
Standing seam terne metal	0.991	plywood deck cracked
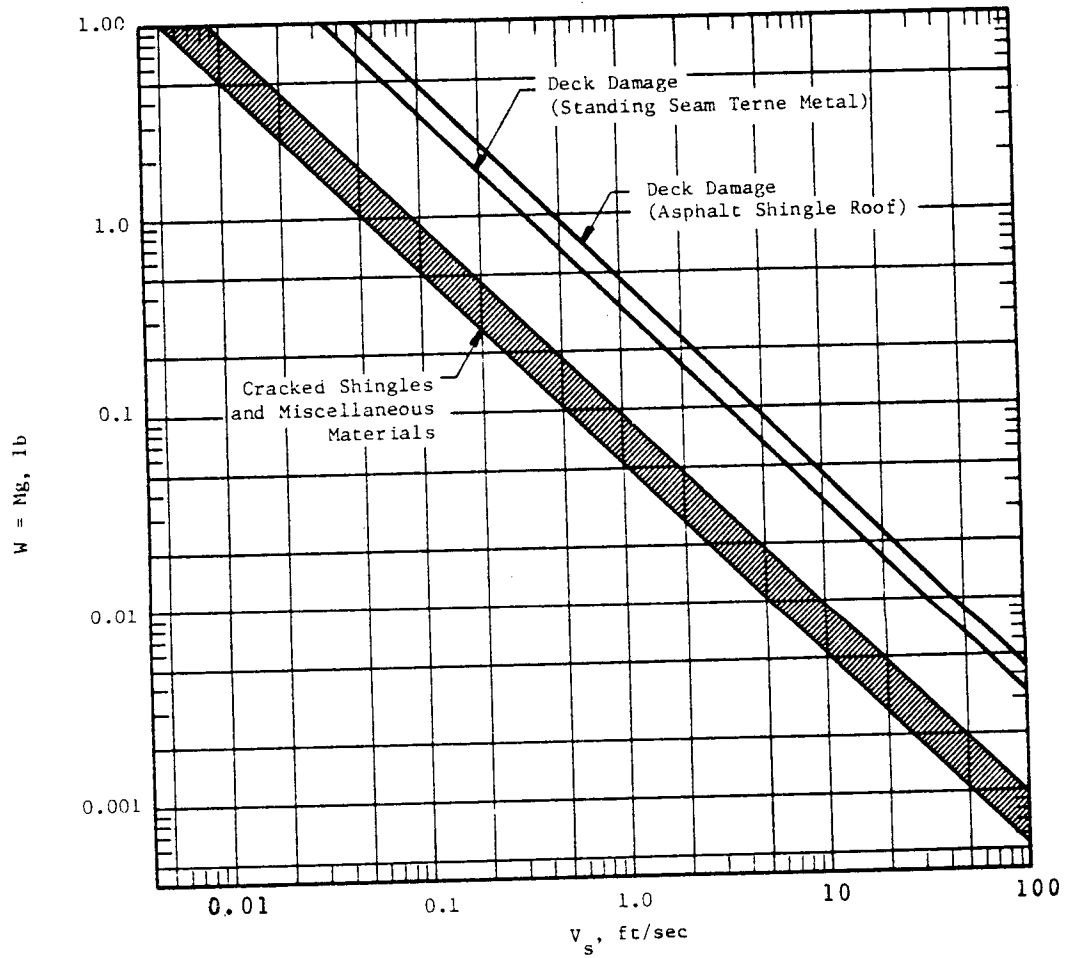
Figure 6.30   Fragment Mass versus Striking Velocity for
Specific Damage to Roofing Materials

Impact conditions for other cases may be estimated using numerical approximations to solve the equations of motion.

6.4.5 Fragment Penetration

This section is divided into three subsections: Cohesive Soil Penetration; Sand Penetration; and Penetration of Miscellaneous Materials. The need for this division arises because different methods are used to derive the equations for predicting penetrations in these materials.

6.4.5.1 Cohesive Soil Penetration*

In this section, the results of a combined analytical and experimental evaluation of penetration in cohesive soils is presented (Ref. 6.45). The development of both fundamental (Ref. 6.45) and empirical (Ref. 6.46) penetration equations are based on Newton's equation of motion. The gravitational force term and the mass of the soil translated by the projectile are assumed to be negligible, resulting in the following form of Newton's equation (Ref. 6.45):

$$dx = M(VdV/F) \qquad (6.62)$$

where V = velocity of projectile
F = force resisting movement
M = mass of the projectile
x = depth of penetration
(NOTE: VdV/dx is acceleration)

Empirically derived equations evolved from the assumption that soil is a single-phase medium (Ref. 6.45 and Section 5.2.1). The functions included here utilize a resisting force which also accounts for pore air and water pressure within the voids between the soil grains. Note that granular soils are not covered by these functions as they have a significant strength variation with depth caused by gravitational effects and are much more dependent on the void ratio (Ref. 6.45).

The final set of equations which will be presented are simplified by substituting the following symbols for recurring groups of parameters (Ref. 6.45):**

$$\bar{x} = \frac{2\beta\rho Ax}{MN} \qquad (6.63a)$$

$$V_{oo} = \left(1 - \frac{\gamma A^{3/2}\rho}{MN^2}\right) V_o \qquad (6.63b)$$

---

*This topic is also discussed in Chapter 7, Section 7.3.

** When using Equations (6.63a-e) one must use a self-consistent set of units. Symbols with a bar over them are dimensionless. V_{oo} has dimensions of length/time, t_{oo} of the time/length and σ_{oo} of length squared/time squared.

6-123

$$t_{oo} = \frac{\beta \rho A t}{MN} \qquad (6.63c)$$

$$\sigma_{oo} = \frac{\sigma_y}{\rho}\left(\frac{\alpha}{\beta}\right) + \frac{P_o}{\rho}\left(\frac{\delta}{\beta}\right) + \frac{P_o}{\rho}\left(\frac{\varepsilon-\delta}{2\beta}\right)\left(1 - \cos\frac{\pi S}{100}\right) \qquad (6.63d)$$

$$\bar{F} = \frac{FN}{\beta \rho V_{oo}^2} \qquad (6.63e)$$

where M = projectile mass

A = projectile cross-sectional area

N = projectile nose shape factor

ρ = soil mass density

x = depth of penetration

V_o = projectile impact velocity

σ_y = unconfined compressive strength of the soil

S = degree of saturation

P_o = ambient atmospheric pressure

t = time

$\left.\begin{array}{l} \alpha = 58.27 \\ \beta = 0.75 \\ \gamma = 0.031 \\ \delta = 93.06 \\ \varepsilon = -35.24 \end{array}\right\}$ These coefficients were determined by curve fitting theoretical equations to experimental data. They do not vary with different-shaped projectiles or different cohesive soil conditions (Ref. 6.45).

Notice that the preceeding five-parameter groups have physical significance: x is an effective displacement x; V_{oo} is an effective velocity of impact V_o; t_{oo} is an effective time t; σ_{oo} is an effective resisting soil stress related to total stress divided by soil density; and $\bar{F}$ is an effective force F.

The parameter N is a nondimensional nose shape factor proportional to C. W. Young's (Ref. 6.46) nose performance coefficient. Values of N for various penetrator shapes are given in Table 6.16 and were determined by Westine (Ref. 6.45).

Having defined $\bar{x}$, V_{oo}, t_{oo}, σ_{oo}, and $\bar{F}$, the equations for transient motion can be presented. Transient displacement is given by:

$$\bar{x} = \left(\ln\ 1 + \frac{\sigma_{oo}}{V_{oo}^2}\right) - \ln\left[\frac{\sigma_{oo}}{V_{oo}^2} + \left\{\frac{1 - \frac{\sigma_{oo}^{1/2}}{V_{oo}}\tan(\sigma_{oo}^{1/2}t_{oo})}{1 + \frac{V_{oo}}{\sigma_{oo}}\tan(\sigma_{oo}^{1/2}t_{oo})}\right\}^2\right]^* \qquad (6.64)$$

---

*The limitations on the various nondimensional groups are the maximum and minimum values of the curves in Figures 6.31, 6.32 and 6.33.

Table 6.16 Nose Shape Factors

(Ref. 6.45)

Shape Penetrator	N Coefficient
Flat Nose	1.00
2.2 CRH* Tangent Ogive	1.47
6.0 CRH Tangent Ogive	1.79
9.25 CRH Tangent Ogive	1.99
12.5 CRH Tangent Ogive	2.16
Cone, $\ell/d^\dagger = 2$	1.93
Cone, $\ell/d = 3$	2.36
Conic Step, Cone Plus Cylinder Plus Cone	2.29
Biconic, $\ell/d = 3$	2.34
Short Inverse Ogive, $\ell/d = 2$	1.84
Inverse Ogive, $\ell/d = 3$	2.36

* Caliber radius head

† ℓ/d is the nose length divided by the projectile major diameter

The transient velocity V is given by:

$$\frac{V}{V_{oo}} = \frac{1 - \dfrac{\sigma_{oo}^{1/2}}{V_{oo}} \tan (\sigma_{oo}^{1/2} t_{oo})}{1 + \dfrac{V_{oo}}{\sigma_{oo}^{1/2}} \tan (\sigma_{oo}^{1/2} t_{oo})} \quad * \tag{6.65}$$

The transient force is given by:

$$\bar{F} = \frac{\sigma_{oo}}{V_{oo}^2} + \left[\frac{1 - \left(\dfrac{\sigma_{oo}}{V_{oo}^2}\right)^{1/2} \tan (\sigma_{oo}^{1/2} t_{oo})}{1 + \left(\dfrac{V_{oo}^2}{\sigma_{oo}}\right)^{1/2} \tan (\sigma_{oo}^{1/2} t_{oo})} \right]^2 \quad * \tag{6.66}$$

Equations (6.64), (6.65), and (6.66) are presented in Figures 6.31, 6.32, and 6.33. The contours of constant V_{oo}^2/σ_{oo} present graphically the transient response for a given impact velocity into a given soil (Ref. 6.47). Note that the time axis $\sigma_{oo}^{1/2} t_{oo}$ has been divided by $(V_{oo}^2/\sigma_{oo})^{1/4}$ in Figures 6.31 through 6.33.

In addition to the transient solutions, equations are presented for predicting residual response. The nondimensional maximum residual penetration $\bar{x}_{max}$ is given by:

$$\bar{x}_{max} = \ln \left(1 + \frac{V_{oo}^2}{\sigma_{oo}}\right)^* \tag{6.67}$$

Motion stops when the velocity V in Equation (6.65) equals zero. The time t_f associated with this event is given by:

$$\tan (\sigma_{oo}^{1/2} t_f) = \left(\frac{V_{oo}^2}{\sigma_{oo}}\right)^{1/2} \quad * \tag{6.68}$$

---

*The limitations on the various nondimensional groups are the maximum and minimum values of the curves in Figures 6.31, 6.32 and 6.33.
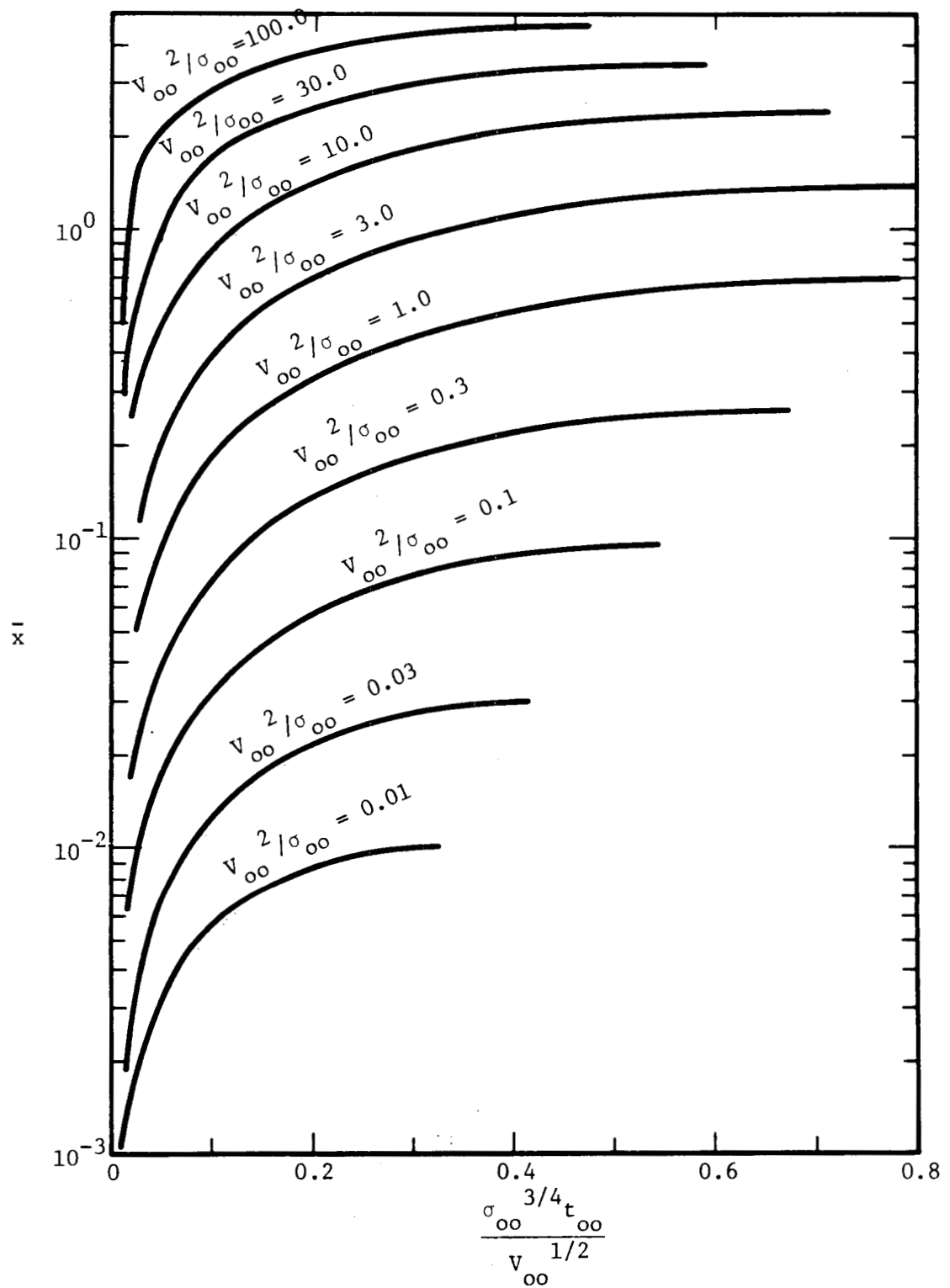
Figure 6.31 Normalized Solution for Transient Displacements
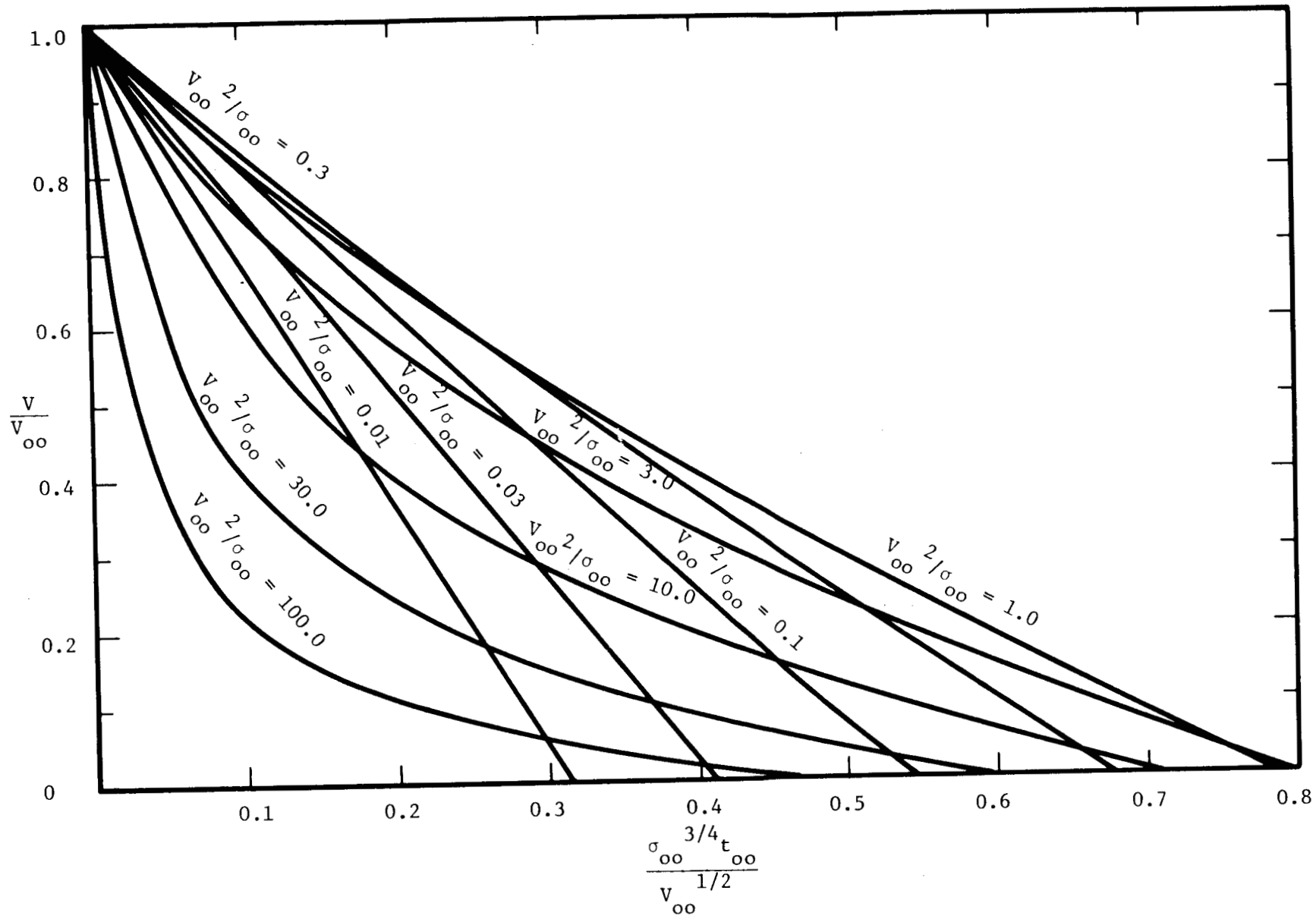
Figure 6.32 Normalized Solution for Transient Velocity
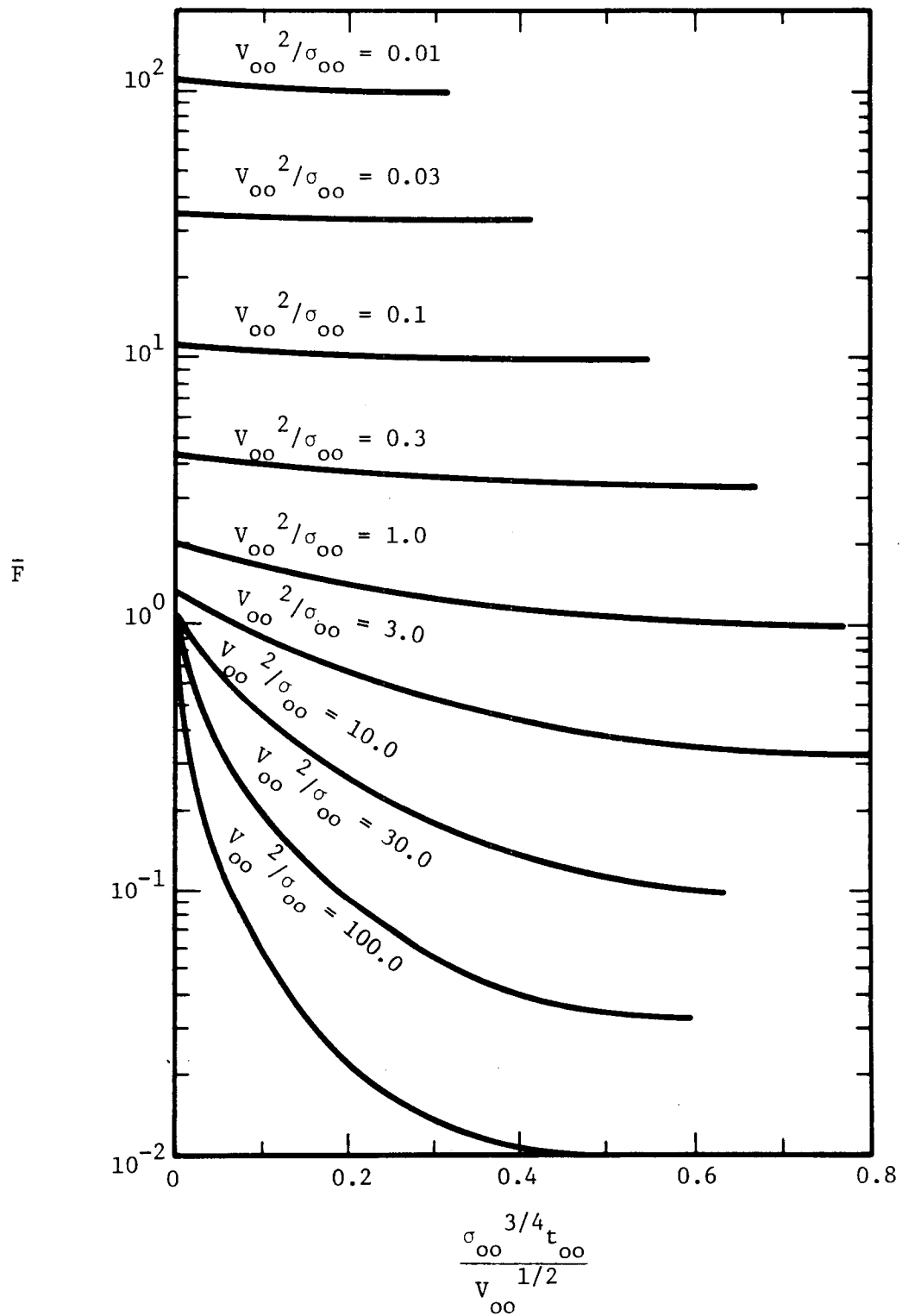
Figure 6.33   Normalized Solution for Transient Retarding Force

The maximum force $\bar{F}_{max}$ occurs at time $t = 0$ and equals:

$$\bar{F}_{max} = \left(1 + \frac{\sigma_{oo}}{V_{oo}^2}\right) \tag{6.69}$$

This force decays until it reaches $\bar{F}_f$ an instant before motion stops. $\bar{F}_f$ is given by:

$$\bar{F}_f = \frac{\sigma_{oo}}{V_{oo}^2} \tag{6.70}$$

The maximum penetration [Equation (6.67)] is presented in Figures 6.34 and 6.35.

6.4.5.2 Sand Penetration

A number of reports have been published describing the relationship between the depth of penetration in sand and the fragment striking velocity (Ref. 6.6, 6.7, 6.14, and 6.48). Unfortunately, the non-homogeneous nature of sand makes the results extremely dependent on the density, compaction, saturation, and grain size (Ref. 6.7). As a result, there is much discrepancy in the predicted depths of penetration (Ref. 6.7). A penetration equation which represents an average of the results of several experiments is Reference 6.7:

$$Z = 19D \ \ell n\left(1 + 2160 \ V_s^2\right) \tag{6.71}$$

where V_s = striking velocity (kfps)

   Z = depth of penetration in projectile diameters
   D = fragment caliber density (lb/in.^{3})

Figure 6.36 contains a plot of this equation for a range of fragment weights and striking velocities for the caliber density 0.186 lb/in.^{3}. This corresponds to the standard design fragment shown in Figure 6.37.

In the event that the sand layer is completely perforated, the residual fragment velocity can be conservatively determined from the following:

$$V_r/V_s = (1 - t/t_s)^{0.555} * \tag{6.72}$$

---

*Figures 6.36 and 6.38 indicate the valid range of Equations (6.71) and (6.72).
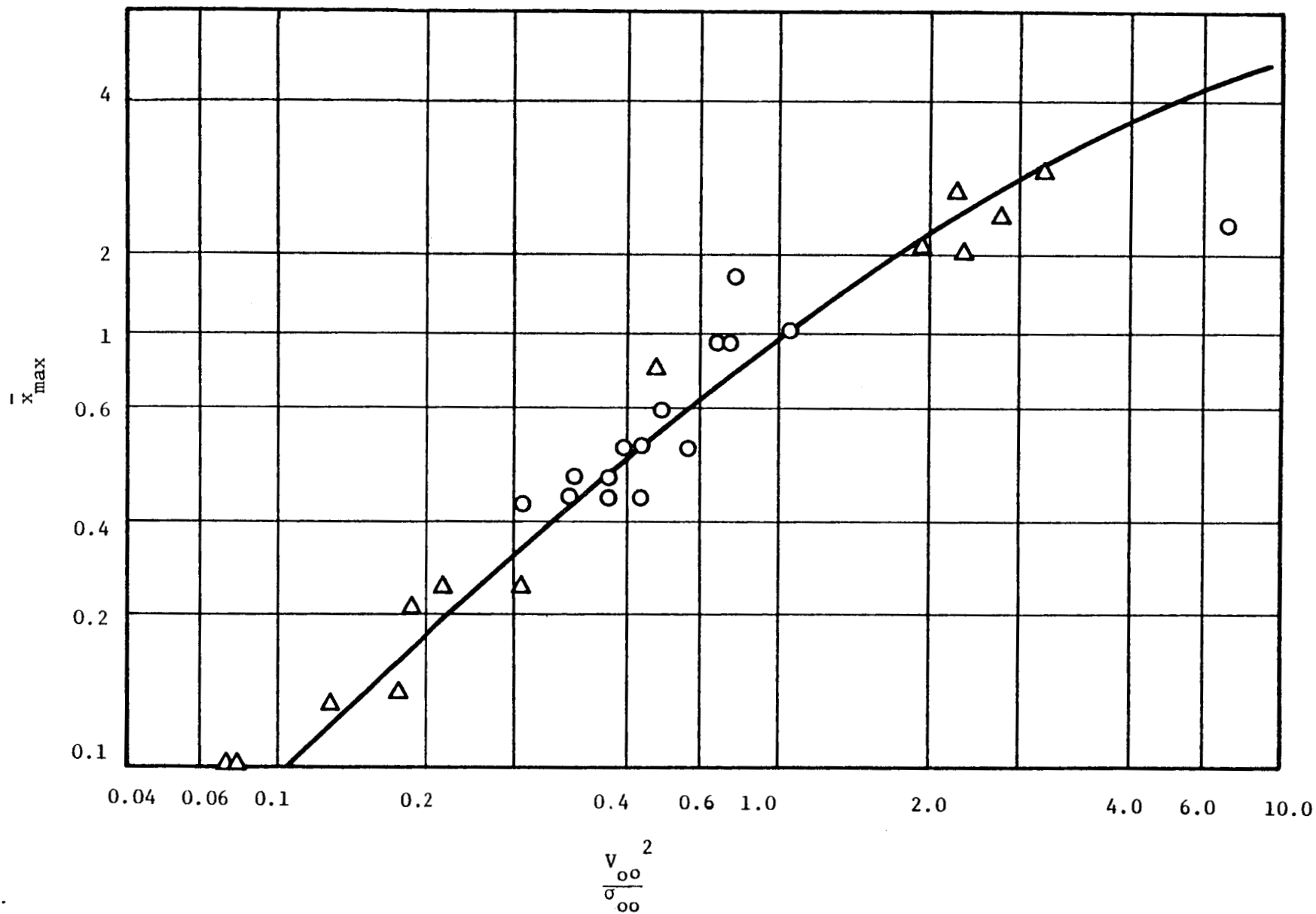
Figure 6. 34. Scaled Maximum Penetration for Flat-Nosed Penetrators
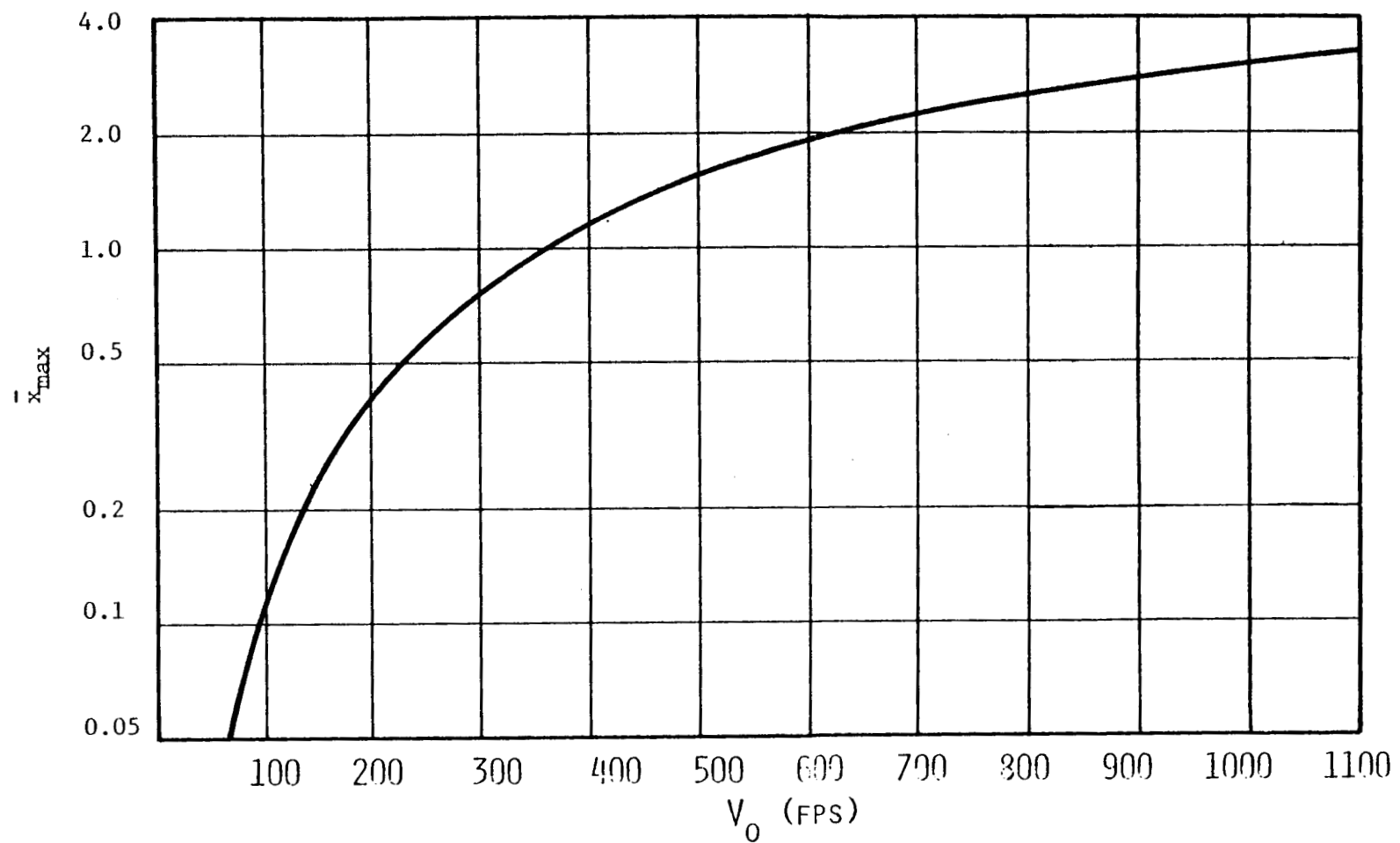
Figure 6.35 Depth of Pointed Projectile Penetration in Soil
(Reference 6.43 & 6.44)
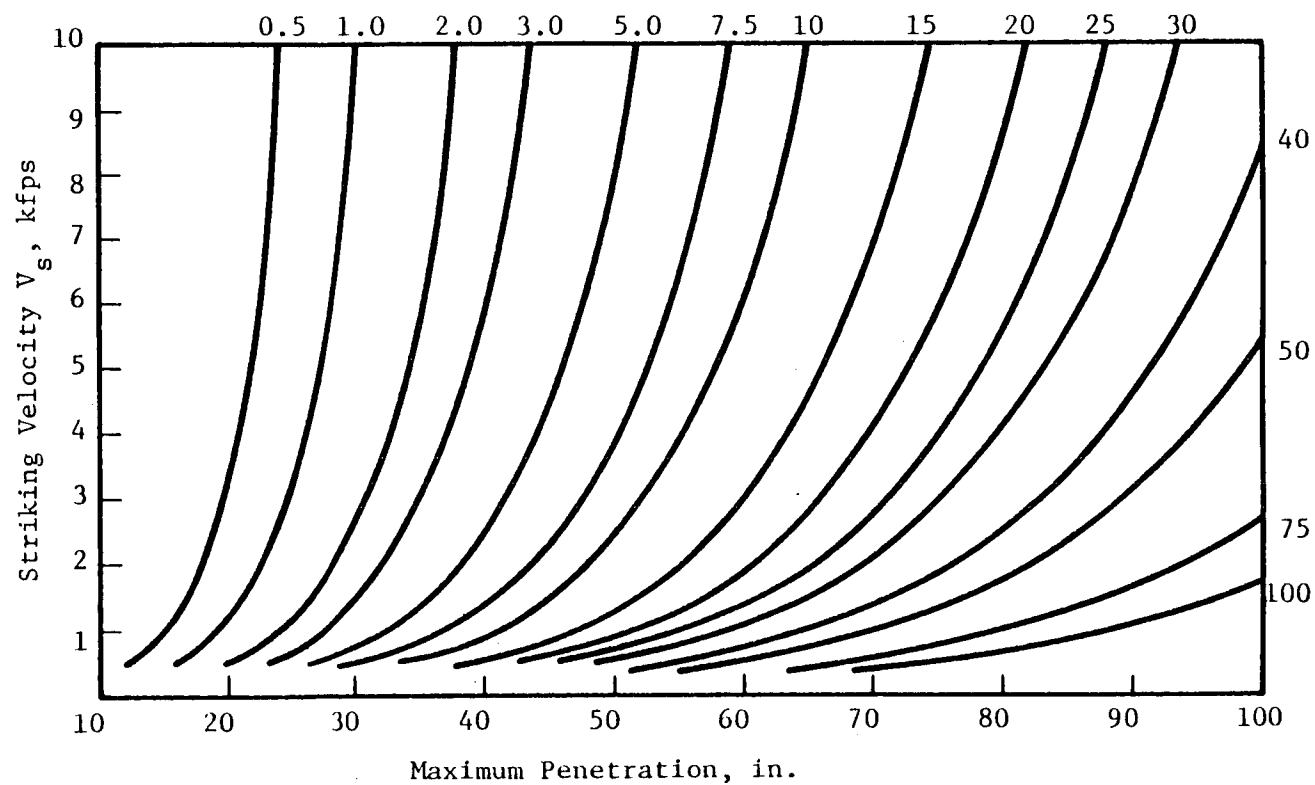
Note: Numbers next to curves indicate fragment weight (oz)

Figure 6.36   Depth of Penetration into Sand by
Standard Primary Fragment
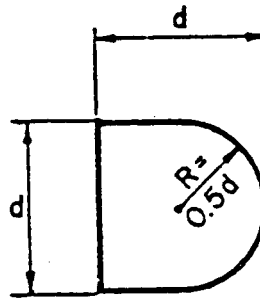
(a) Standard Fragment Shape
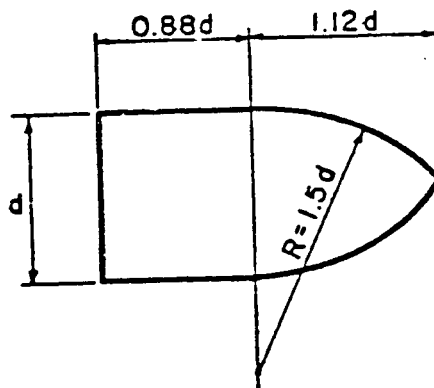
(b) Alternate Fragment Shape

Figure 6.37   Primary Fragment Shapes

where t = depth of penetration (in.) calculated from Equation (6.71) or
obtained from Figure 6.36

t_s = actual thickness of sand layer (in.)

Figure 6.38 contains a plot of Equation (6.72).

6.4.5.3 Penetration in Miscellaneous Materials

The materials included in this section have military significance,
but they do not necessarily constitute primary targets (Refs. 6.43 and
6.49). The equations which will be presented in this section have been
constructed empirically. They are founded on the assumption that the
resistance of a material to perforation by steel fragments can be related
to the losses in weight and velocity sustained by the fragment during
penetration (Ref. 6.43). The data base used in developing these equations
was limited to cases where perforation was achieved, and the residual
velocity and residual weight were recorded. These measurements refer
to the largest piece of the original fragment which perforates the
target material (Ref. 6.43 and 6.49).

The empirical THOR equations, based on a large series of tests
performed over 29 years ago, were presented for metallic target materials
in 1961 (Ref. 6.50) and for nonmetallic materials in 1963 (Ref. 6.43).
Greenspon (Ref. 6.49) summarized the results of the THOR reports and put
the data in nondimensional graphical form in 1976. The most extensively
used of the THOR equations are those for ballistic limit velocity,
residual velocity, and residual mass. The ballistic limit velocity,
V_{ℓ}, is the minimum velocity that a fragment must have to perforate a
target plate of given material and thickness. The THOR equation given
for ballistic velocity is as follows:

$$V_{\ell} = 10^{C_1}(hA)^{\alpha_1}(7000W_s)^{\beta_1} (\sec \theta)^{\gamma_1} \qquad (6.73)$$

where V_{ℓ} = ballistic limit velocity in ft/s

h = target plate thickness in in.

A = average impact area of the fragment in in.^{2}

W_s = weight of the original fragment in lb

θ = angle between the trajectory of the fragment and the normal
to the target

$C_1, \alpha_1, \beta_1, \gamma_1$ = empirical constants which are dependent on the
plate material to be perforated (Refs. 6.50, 6.43,
and 6.49) (see Table 6.17)

The THOR equation for residual velocity is

$$V_r = V_s - 10^C(hA)^{\alpha}(7000W_s)^{\beta}(\sec \theta)^{\gamma}V_s^{\lambda} \qquad (6.74)$$
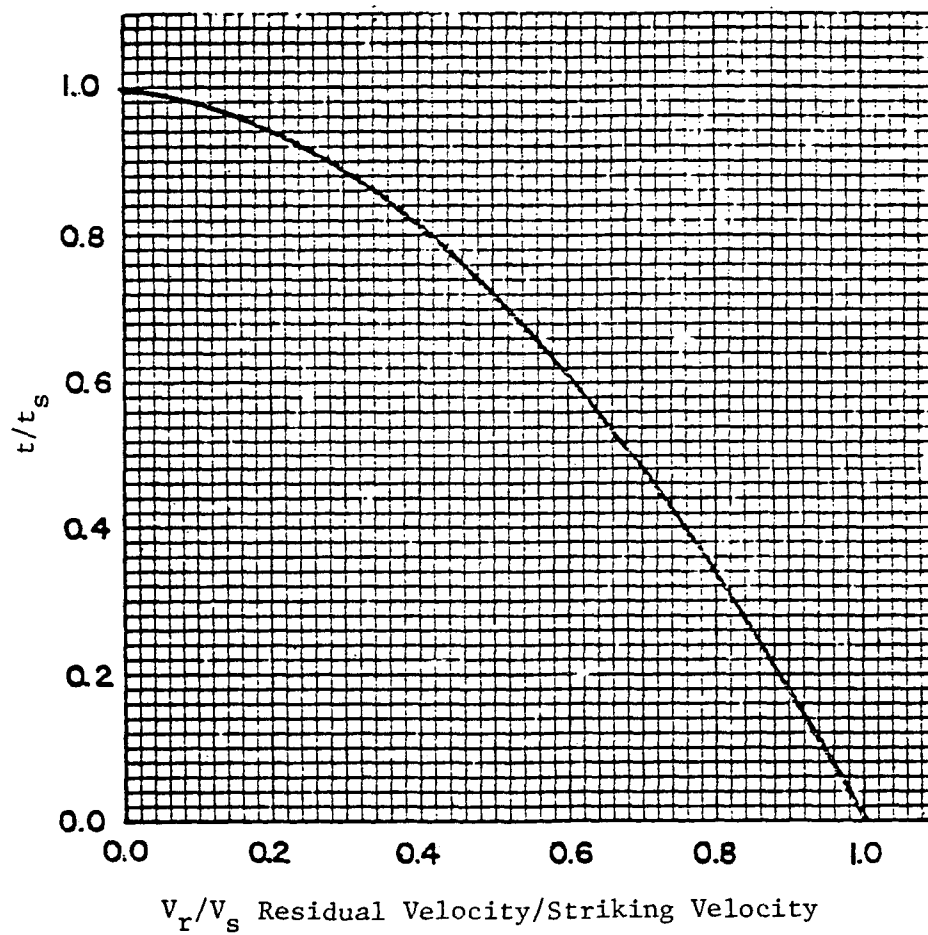
Figure 6.38 Residual Fragment Velocity Upon
Perforation of Sand Layers

where V_r = residual velocity of the fragment (in ft/sec after perforation of the target occurs

V_s = initial velocity of the fragment before perforating the target (in ft/sec)

t, A, W_s, θ = parameters given above

$c, \alpha, \beta, \gamma, \lambda$ = empirical constants similar to those defined for ballistic limit velocity (Refs. 6.50, 6.43 and 6.49) (see Table 6.17).

The THOR equation for residual weight is

$$(7000W_r) = (7000W_s) - 10^{C_2}(hA)^{\alpha_2}(7000W_s)^{\beta_2}(\sec \theta)^{\gamma_2}V_s^{\lambda_2} \qquad (6.75)$$

where $(7000W_r)$ = residual weight of the largest piece of fragment, (in grains) after perforation of the target occurs

t, A, W_s, θ, V_s = parameters given above

$C_2, \alpha_2, \beta_2, \gamma_2, \lambda_2$ = empirical constants similar to those defined for ballistic and residual velocity (Refs. 6.50, 6.43, and 6.49) (see Table 6.17)

The values of the constants in Equations (6.73), (6.74), and (6.75) are given in Table 6.17. The ranges of variables for each material is given in Table 6.18. The constants which appear in Table 6.17 are for no particular fragment shape. Greenspon's (Ref. 6.49) nondimensionalized forms are not included here since they are in graphical form and would require a much larger number of pages to present.

Table 6.17 THOR Constants
(Reference 6.51)

	C	α	β	γ	λ	C_1	α_1	β_1	γ_1	C_2	α_2	β_2	γ_2	λ_2
Magnesium	6.904	1.092	-1.170	1.050	-0.087	6.349	1.004	-1.076	.966	-5.945	0.285	0.803	-0.172	1.519
Aluminum (2024T-3)	7.047	1.029	-1.072	1.251	-0.139	6.185	0.903	-0.941	1.098	-6.663	0.227	0.694	-0.361	1.901
Cast Iron	4.840	1.042	-1.051	1.028	0.523	10.153	2.186	-2.204	2.156	-9.703	0.162	0.673	2.091	2.710
Titanium	6.292	1.103	-1.095	1.369	0.167	7.552	1.325	-1.314	1.643	-2.318	1.086	0.748	1.327	0.459
Face Hard. Steel	4.356	0.674	-0.791	0.989	0.434	7.694	1.191	-1.397	1.747	-1.195	0.234	0.744	0.469	0.483
Mild Homog. Steel	6.399	0.889	-0.945	1.262	0.019	6.523	0.906	-0.963	1.286	-2.507	0.138	0.835	0.143	0.761
Hard Homog. Steel	6.475	0.889	-0.945	1.262	0.019	6.601	0.906	-0.963	1.286	-2.264	0.346	0.629	0.327	0.880
Copper	2.785	0.678	-0.730	0.846	0.802	14.065	3.476	-3.687	4.270	-5.489	0.340	0.568	1.422	1.650
Lead	1.999	0.499	-0.502	0.655	0.818	10.955	2.735	-2.753	3.590	-1.856	0.506	0.350	0.777	0.934
Tuballoy	2.537	0.583	-0.603	0.865	0.828	14.773	3.393	-3.510	5.037	-3.379	0.560	0.447	0.640	1.381
Unbonded Nylon *	5.816	0.835	-0.654	0.990	-0.162	5.006	0.719	-0.563	-.852	-7.538	-0.067	0.903	-0.351	1.717
Bonded Nylon *	4.672	1.144	-0.968	0.743	0.392	7.689	1.883	-1.593	1.222	-13.601	0.035	0.775	0.045	3.451
Lexan	2.908	0.720	-0.657	0.773	0.603	7.329	1.814	-1.652	1.948	-6.275	0.480	0.465	1.171	1.765
Plexiglas as Cast	5.243	1.044	-1.035	1.073	0.242	6.913	1.377	-1.364	1.415	-2.342	1.402	-0.137	0.674	1.324
Stretched Plexiglas	3.605	1.112	-0.903	0.715	0.686	11.468	3.537	-2.871	2.274	-5.344	0.437	0.169	0.620	1.683
Doron	7.600	1.021	-1.014	0.917	-0.362	5.581	0.750	-0.745	0.673	-10.404	0.215	0.343	0.706	2.906
Bullet Resistant Glass	3.743	0.705	-0.723	0.690	0.465	6.991	1.316	-1.351	1.289	-5.926	0.305	0.429	0.747	1.819

* Within the ranges given in Table 6.22, this material did not cause the steel fragments to break up considerably upon impact. Higher striking velocities than those now obtainable in the laboratory would be required to produce the necessary information to establish a satisfactory set of constants for the m_r equations for this material.

Table 6.18
Range of Variables in Equations (6.69), (6.70), (6.71)
[References (6.50 and 6.52)]

Target Material	Target Thickness Range h (in.)	Areal Density Range w (lb/ft^2)	Obliquity Range θ (degrees)	Striking Velocity Range V_s (fps)	Fragment Size Range W_s (lb)
Magnesium Alloys	0.05-3.00	0.5-28	0-80	500-10500	$1.5 \times 10^1 - 2.40 \times 10^2$
Aluminum (2024T-3	0.02-2.00	0.3-29	0-80	1200-11000	$5.0 \times 10^0 - 2.40 \times 10^2$
Titanium Alloys	0.04-1.20	1.0-28	0-80	700-10400	$3.0 \times 10^1 - 2.40 \times 10^2$
Cast Iron	0.19-0.56	7.0-21	0-45	1099-6100	$1.5 \times 10^1 - 2.40 \times 10^2$
Face-Hardened Steel	0.14-0.50	5.0-20	0-70	2500-9800	$1.5 \times 10^1 - 2.40 \times 10^2$
Homogeneous Steel	0.03-1.00	1.0-40	0-70	600-12000	$5.0 \times 10^0 - 8.25 \times 10^2$
Copper	0.06-1.00	3.0-46	0-70	1100-11400	$1.5 \times 10^1 - 2.40 \times 10^2$
Lead	0.07-1.00	4.0-57	0-70	500-10400	$1.5 \times 10^1 - 2.40 \times 10^2$
Tuballoy	0.10-0.20	10-19	0-60	4500-10100	$3.0 \times 10^1 - 4.75 \times 10^2$
Unbonded Nylon	0.02-3.0	0.1-12.5	0-70	300-10000	$7.14 \times 10^{-4} - 2.96 \times 10^{-2}$
Bonded Nylon	0.43-2.0	2.1-9.7	0-70	1000-12000	$7.14 \times 10^{-4} - 1.18 \times 10^{-1}$
Lexan	0.125-1.0	0.8-6.2	0-70	1000-11500	$7.14 \times 10^{-4} - 3.43 \times 10^{-2}$
Plexiglas as Cast	0.20-1.1	1.2-6.7	0-70	200-9500	$7.14 \times 10^{-4} - 6.79 \times 10^{-2}$
Stretched Plexiglas	0.05.1.0	0.3-6.4	0-70	500-11000	$7.14 \times 10^{-4} - 6.79 \times 10^{-2}$
Doron	0.05-1.5	0.5-15.6	0-70	500-11000	$3.57 \times 10^{-4} - 8.57 \times 10^{-2}$
Bullet-Resistant Glass	0.20-1.65	2.6-21.2	0-70	200-10000	$2.14 \times 10^{-3} - 6.79 \times 10^{-2}$

<u>EXAMPLE PROBLEM 6.22</u>

<u>PROBLEM</u> – Determine fragment penetration x into cohesive soil. For illustrative purposes, assume that a steel rod is hurled into an earth barrier.

<u>GIVEN</u>: M = fragment mass

A = fragment presented area

σ_y = unconfined compressive strength of soil (σ_y has to be measured or assumed)

ρ = soil mass density

V_o = impact velocity

s = degree of saturation

P_o = ambient atmospheric pressure

Fragment shape

(or use any self-consistent set of units)

<u>FIND</u>: x   <u>REFERENCE</u>

<u>SOLUTION</u>: 1. a) Nose shape factor N   Table 6.16
                    b) γ, β, α, δ, ϵ Eq. (6.63a-e)

2. Calculate effective velocity.

$$V_{oo} = \left(1 - \frac{\gamma A^{3/2} \rho}{MN^2}\right) V_o$$ Eq. (6.63b)

3. Calculate effective resisting soil stress.

$$\sigma_{oo} = \frac{\sigma_y}{\rho}\left(\frac{\alpha}{\beta}\right) + \frac{P_o}{\rho}\left(\frac{\delta}{\beta}\right) + \frac{P_o}{\rho}\left(\frac{\epsilon-\delta}{2\beta}\right)\left(1 - \cos\frac{\pi s}{100}\right)$$ Eq. (6.63d)

4. Calculate maximum effective penetration.

$$\bar{x}_{max} = \ln\left(1 + \frac{V_{oo}^2}{\sigma_{oo}}\right)$$ Eq. (6.67)

5. Calculate actual penetration.

$$x = \bar{x}_{max}\frac{MN}{2\beta\rho A}$$ Eq. (6.63a)

<u>CALCULATION</u>

<u>GIVEN</u>: M = 0.016 lb-sec^2/ft

A = 0.01 ft^2

σ_y = 288 lb/ft^2

ρ = 3.1 lb-sec^2/ft^4

V_o = 1500 ft/sec

s = 0.5

P_o = 2120 lb/ft^2

Flat nose fragment (The fragment is a flat-faced cylinder with a diameter of 1.33 in. and a length of 1.2 in.)

FIND: x

SOLUTION: 1. $N = 1.00$
$\alpha = 58.27$, $\beta = 0.75$, $\gamma = 0.031$, $\delta = 93.06$
$\epsilon = -35.24$

2. $V_{oo} = \left(1 - \dfrac{\gamma A^{3/2} \rho}{MN^2}\right) V_o$

$= \left[1 - \dfrac{(0.031)(0.01)^{3/2}(3.1)}{(0.016)(1)^2}\right] (1500)$

$V_{oo} = 1490$ ft/s

3. $\sigma_{oo} = \dfrac{\sigma_y}{\rho}\left(\dfrac{\alpha}{\beta}\right) + \dfrac{P_o}{\rho}\left(\dfrac{\delta}{\beta}\right) + \dfrac{P_o}{\rho}\left(\dfrac{\epsilon - \delta}{2\beta}\right)$

$\sigma_{oo} = \left(\dfrac{288}{3.1}\right)\left(\dfrac{58.27}{0.75}\right) + \left(\dfrac{2120}{3.1}\right)\left(\dfrac{93.06}{0.75}\right) + \left(\dfrac{2120}{3.1}\right)\left[\dfrac{(-35.24)-(93.06)}{(2)(0.75)}\right]$

$= 33600$ ft^2/sec^2

4. $\overline{x}_{max} = \ell n \left(1 + \dfrac{v_{oo}^2}{\sigma_{oo}}\right)$

$= \ell n \left[1 + \dfrac{(1490)^2}{(33600)}\right]$

$= 4.21$

5. $x = \overline{x}_{max} \dfrac{MN}{2\beta \rho A}$

$x = (4.21) \dfrac{(0.016)(1.00)}{(2)(0.75)(3.1)(0.01)}$

$x = \underline{1.45 \text{ ft}}$

EXAMPLE PROBLEM 6.23

PROBLEM – Determine fragment penetration, x, into sand. For illustrative purposes, assume a steel fragment with "standard" fragment shape strikes a sand barrier.

GIVEN: W_f = fragment weight (1b)

V_s = striking velocity (kft/sec)

Fragment shape [in diameter (d)] (in.)

FIND: x

SOLUTION: 1. Calculate caliber density.   REFERENCE

$$D = W_f/d^3$$ Fig. 6.5

2. Calculate caliber penetration.

$$Z = 19D \ln(1 + 2160 \, V_s^2)$$ Eq. (6.71)

3. Calculate actual penetration (x).

$$x = Z \cdot d$$

CALCULATION

GIVEN: W_f = 2 lb

V_s = 1.2 kft/sec

d = 3 in.

FIND: x

SOLUTION: 1. $D = W_f/d^3$

$$= \frac{(2)}{(3)^3} = 0.0741 \text{ lb/in.}^3$$

2. $Z = 19D \ln(1 + 2160 \, V_s^2)$

$$= (19)(0.0741) \ln[1 + (2160)(1.2)^2]$$
$$= 11.32$$

3. $x = Z \cdot d$
$$x = (11.32)(3)$$
$$x = \underline{34 \text{ in.}}$$

EXAMPLE PROBLEM 6.24

PROBLEM – Determine the thickness, h, of aluminum (2024T-3) required to stop a steel fragment.

GIVEN: V_s = striking velocity (ft/sec) (In this problem $V_s = V^{\ell}$.)

A = fragment impact area (in.)

W_s = weight of fragment (lb)

θ = angle between the trajectory of the fragment and the normal to the target

FIND: h   REFERENCE

SOLUTION: 1. Determine the penetration constants for aluminum (2024T-3).

C_1, α_1, β_1, γ_1 Table 6.17

2. Solve for thickness h required to prevent
penetration.

$$V_\ell = 10^{C_1} (hA)^{\alpha_1} (7000W_s)^{\beta_1} (\sec \theta)^{\gamma_1}$$

$$h = \frac{1}{A} \left[\frac{V_\ell}{10^{C_1} (7000W_s)^{\beta_1} (\sec \theta)^{\gamma_1}} \right]^{1/\alpha_1}$$

CALCULATION

GIVEN: $V_s = V_\ell = 2000$ ft/sec

$A = 0.11$ in.^{2}

$W_s = 0.01$ lb

$\theta = 0°$

Note that for this problem, the steel fragment can be any shape.
For illustrative purposes, we chose a cubical fragment with a
weight of 0.01 lb and an edge length of 0.33 in. The fragment
impacts the plate face forward with an impact area of 0.11 in.^{2}
(0.33 in. x 0.33 in.).

FIND: h

SOLUTION: 1. $C_1 = 6.85$

$\alpha_1 = 0.903$

$\beta_1 = -0.941$

$\gamma_1 = 1.098$

2. $h = \frac{1}{A} \left[\frac{V_\ell}{10^{C_1} (7000W_s)^{\beta_1} (\sec \theta)^{\gamma_1}} \right]^{1/\alpha_1}$

$$h = \frac{1}{(0.11)} \left\{ \frac{(2000)}{10^{6.185} [(7000)(0.01)]^{-0.941} [\sec(0°)]^{1.098}} \right\}^{1/0.903}$$

$h = \underline{0.49 \text{ in.}}$

6.5 HAZARDS TO PERSONNEL FROM FRAGMENTS

Injuries to personnel due to fragment impact can be divided into two categories, primary fragment and secondary fragment injuries. Primary fragments are normally small, high-speed fragments which cause injury by penetration and perforation of vital areas of the body. Secondary fragments are normally larger and have less velocity upon impact and can cause nonpenetrating blunt trauma. Both of these injury categories are discussed below.

6.5.1 Primary Fragment Injuries

A great deal of research has been conducted to produce classified wound ballistics equations for the military. Although thorough unclassified equations of this type do not exist, some publicly available body penetration data have been accumulated in recent times and some relatively simple analyses have been performed. More reliable damage criteria will undoubtedly be produced as the state of the art improves.

Sperrazza and Kokinakis (Ref. 6.51) concerned themselves with a ballistic limit velocity V_{50} for animal targets. The V_{50} velocity is the striking velocity at which one expects half the impacting missiles to perforate an object. They found that this velocity depended on the area to weight ratio, that is

$$V_{50} \propto \frac{A}{W_f} \tag{6.76}$$

where A is cross-sectional area of the projectile along the trajectory, and w_f is the weight of the projectile. They fired steel cubes, spheres and cylinders of various masses up to 0.033 lb into 0.118-in. thick isolated skin (human and goat) to establish a ballistic limit. One of their assumptions was that, if the projectile penetrates the skin, its residual velocity would be sufficient to cause severe damage. This cautious assumption is appropriate for establishing a certain margin of safety in the calculation. Their conclusions were that, in the range of their data for steel cubes, spheres and cylinders, V_{50} depended linearly on projectile A/W_f ratio. Specifically,

$$V_{50} = 836 \frac{lb}{ft-sec}\left(\frac{A}{W_f}\right) + 72.3 \text{ ft/sec} \tag{6.77}$$

for $A/W_f \leq 0.44$ ft^2/lb and for $W_f \leq 0.033$ lb, where V_{50} is in ft/sec

Kokinakis (Ref. 6.52) fired plastic sabots end-on into 20 percent gelatin that was 0.4-in. thick. The sabots were fired end-on since this represents the worst case, and 20 percent gelatin was used because this ballistically simulates isolated human skin. The linear relation of V_{50} versus A/W_f formulated by Sperrazza and Kokinakis (Ref. 6.51) is plotted in Figure 6.39. The average values for these experiments are located on this graph. Circles on the figure represent the initial
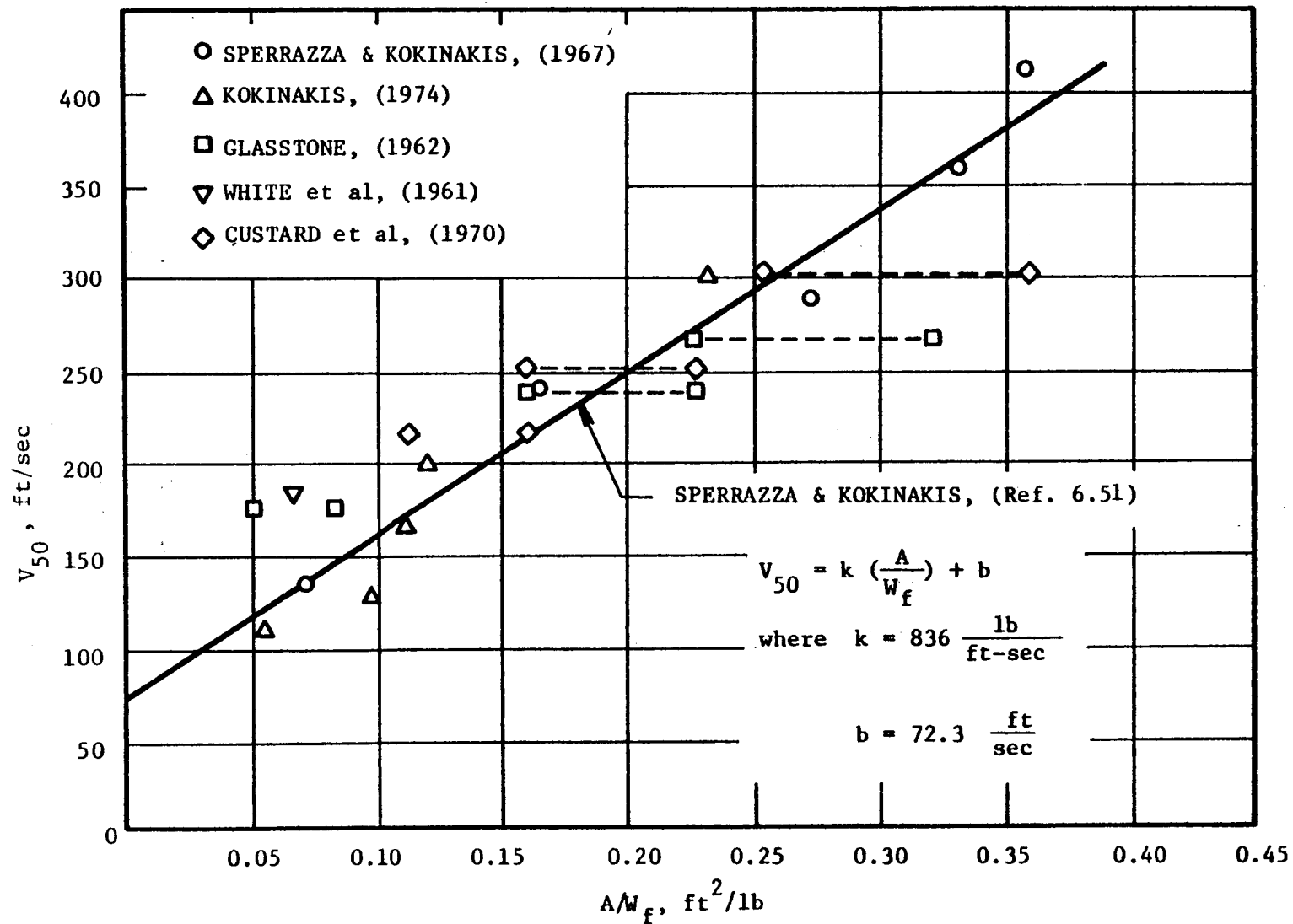
Figure 6.39. Ballistic Limit (V_{50}) versus Fragment Area/Weight
for Isolated Human and Goat Skin

experiments using steel cubes, spheres and cylinders weighing up to
0.033 lb and each average value represents as many as 30 data points.
The line drawn on the graph is a least squares fit to these average
values. Upward pointed triangles represent the average values for the
subsequent experiments with end-on plastic sabots. These average values
also lie near the line drawn for the prior study, thus adding a degree
of confidence in the analysis.

Unfortunately, other authors have not presented their penetration
data in the same form as Sperrazza and Kokinakis. Glasstone (Ref. 6.53)
expressed the probability of glass fragments penetrating the abdominal
cavity in terms of the mass of the glass fragments. To compare Glasstone's
conclusions with that of Sperrazza and Kokinakis, it is necessary to make
a few assumptions. The first assumption is that the glass fragment
velocity for 50 percent probability of penetration of the abdominal cavity
is biologically equivalent to the ballistic limit velocity V_{50} for penetrating
isolated human skin. Glasstone only specifies the mass of the glass
required for penetration and does not give its cross-sectional area,
thickness or density. For the purpose of comparing the conclusions of
Glasstone with those of Sperrazza and Kokinakis it was assumed that
glass fragments are propelled edge-on, which is probably the worst case,
and that they are square with thicknesses of 1/8 in. to 1/4 in. It
was assumed that the glass fragments have an average specific weight of
154.3 lb/ft^3 (Ref. 6.54). With these assumptions, it is not difficult to
calculate A/W_f. If the glass fragment has a thickness, t, and edge length
y, then for volume

$$V = y^2 t \qquad (6.78)$$

where V = volume of the fragment
      y = edge length
      t = thickness

Thus, the weight W_f of the fragment is

$$W_f = \gamma y^2 t \qquad (6.79)$$

where γ is the specific weight of the glass. Rearranging Equation (6.79)
gives the edge length,

$$y = \sqrt{\frac{W_f}{\gamma t}} \qquad (6.80)$$

The area-to-weight ratio A/W_f, assuming edge-on impact, is

$$\frac{A}{W_f} = \frac{ty}{W_f} \qquad (6.81)$$

or from Equations (6.79), (6.80) and (6.81),

$$\frac{A}{W_f} = \sqrt{\frac{t}{\rho W_f}} \qquad (6.82)$$

Glasstone's criteria for 50 percent probability of glass fragments pene-
trating the abdominal cavity are shown in Table 6.19. This table also contains
the estimates for A/W_f for glass thicknesses of 1/8 in. and 1/4 in. The
velocity values and calculated values for A/W_f which fall in the range
of values used by Sperrazza and Kokinakis are plotted as squares in
Figures 6.39. The dashed lines indicate a range of A/W_f values for
thickness values from 1/8 in. to 1/4 in. Even with the crude assumptions
mentioned above, the calculated points fall very near the line drawn
on Figure 6.39.

White (Ref. 6.55) also related skin penetration velocity to
the masses of impacting fragments. He concluded that slight skin
laceration occurred when spherical bullets with weight 0.0191 lb were
propelled into the body at 190 ft/sec. Assuming that the specific weight
of steel is 495 lb/ft^3, the A/W_f ratio can be calculated from

$$\frac{A}{W_f} = \frac{\pi r^2}{W_f}$$
(6.83)

where r is the radius of the spherical penetrator, or

$$\frac{A}{W_f} = \frac{\pi}{W_f} \left(\frac{3M}{4\pi\rho}\right)^{2/3}$$
(6.84)

Using Equation (6.84) and the mass and density mentioned above, A/W_f
becomes 0.0723 ft^2/lb. The velocity value given above (190 ft/sec)
and the calculated value for A/W_f are plotted on Figure 6.39 as a downward
pointed triangle. This point appears to be a little higher than expected,
especially since only slight skin laceration is expected at these velocities
instead of 50 percent penetration.

Custard (Ref. 6.56), like Glasstone, specifies velocity as a
function of mass only for 50 percent penetration. Making the assumptions
that the thickness of the glass can vary from 1/8 in. to 1/4 in., that the
fragments travel edge-on and are square, and that the density of glass
is 154.3 lb/ft^3, A/W_f was calculated from Equation (6.84). The results
are plotted on Figure 6.39 as diamonds and agree fairly well with the
conclusions of Sperrazza and Kokinakis. Thus, for values of A/W_f up to
0.44 ft^2/lb and values of W_f up to 0.033 lb, the functional relationship
expressed in Equation (6.84) and drawn as a solid line in Figure 6.39
is an adequate representation of 50 percent probability of skin penetration
by a projectile that can result in serious wounds.

6.5.2 Secondary Fragment Injuries

Very limited information for body damage from nonpenetrating
objects is contained in Table 6.20. It should be noted that according
to the table, damage is dependent on fragment mass and velocity only.
The table also only contains one fragment mass value. One can logically

Table 6.19 50 Percent Probability of Glass Fragments
Penetrating Abdominal Cavity
(Glasstone, (Ref. 6.55)

Weight of Glass Fragment lb	Impact Velocity ft/sec	A/W_f 1/8 in. thick ft^2/lb	A/Wf 1/4 in. thick ft^2/lb
2×10^{-4}	410	0.555	0.783
$1 \times 10{-3}$	275	0.248	0.350
2×10^{-3}	245	0.175	0.248
2×10^{-2}	180	0.0552	0.0781

Table 6.20 Tentative Criteria for Indirect Blast Effects
from Nonpenetrating Fragments
(Ahlers, Ref. 6.57; Clemedson, Ref. 6.58; White, Ref. 6.59)

Weight	Event	Extent of Damage	Impact Velocity
10 lb	Cerebral Concussion	Mostly "safe"	10 ft/sec
		Threshold	15 ft/sec
	Skull Fracture	Mostly "safe"	10 ft/sec
		Threshold	15 ft/sec
		Near 100%	23 ft/sec

assume that larger weights propelled at the same velocities shown in the table will produce more damage than the 10 lb weight presented in the table.

Figures 6.40 and 6.41 contain personnel fragment impact damage criteria as presented by Ahlers (Ref. 6.57). For fragment weights greater than 10 lb, the criteria for threshold head impact injuries are slightly lower (more conservative) than those of Table 6.20. The percentage next to a particular curve in Figure 6.40 denotes the percent of people (for a large sample) that would die if subjected to any of the impact conditions detailed by the curve. The serious injury threshold curves on Figures 6.40 and 6.41 specify the debris velocity and weight combinations below which no serious injuries are expected to occur.
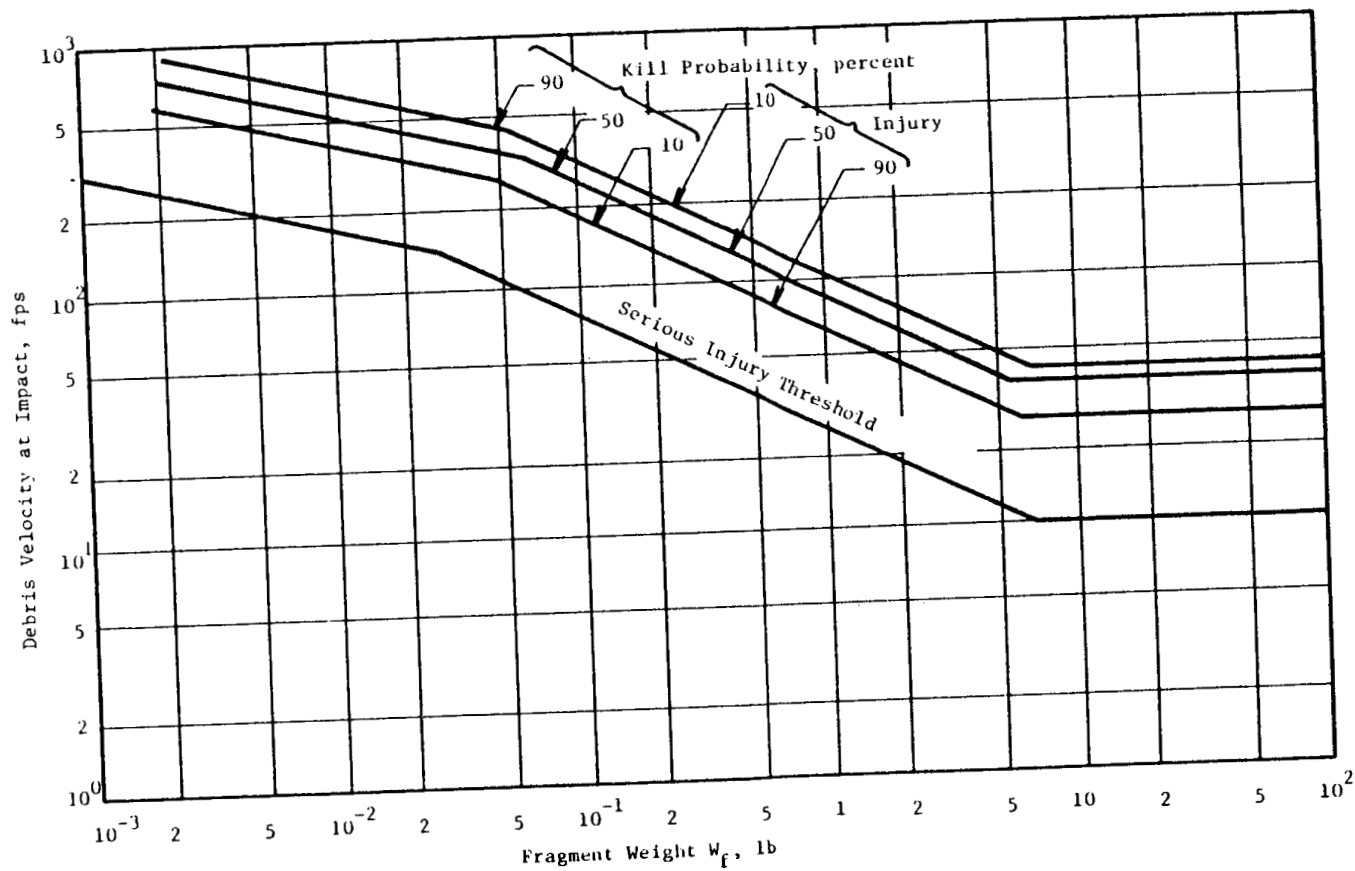
Figure 6.40   Personnel Response to Fragment Impact (Abdomen and Limbs)
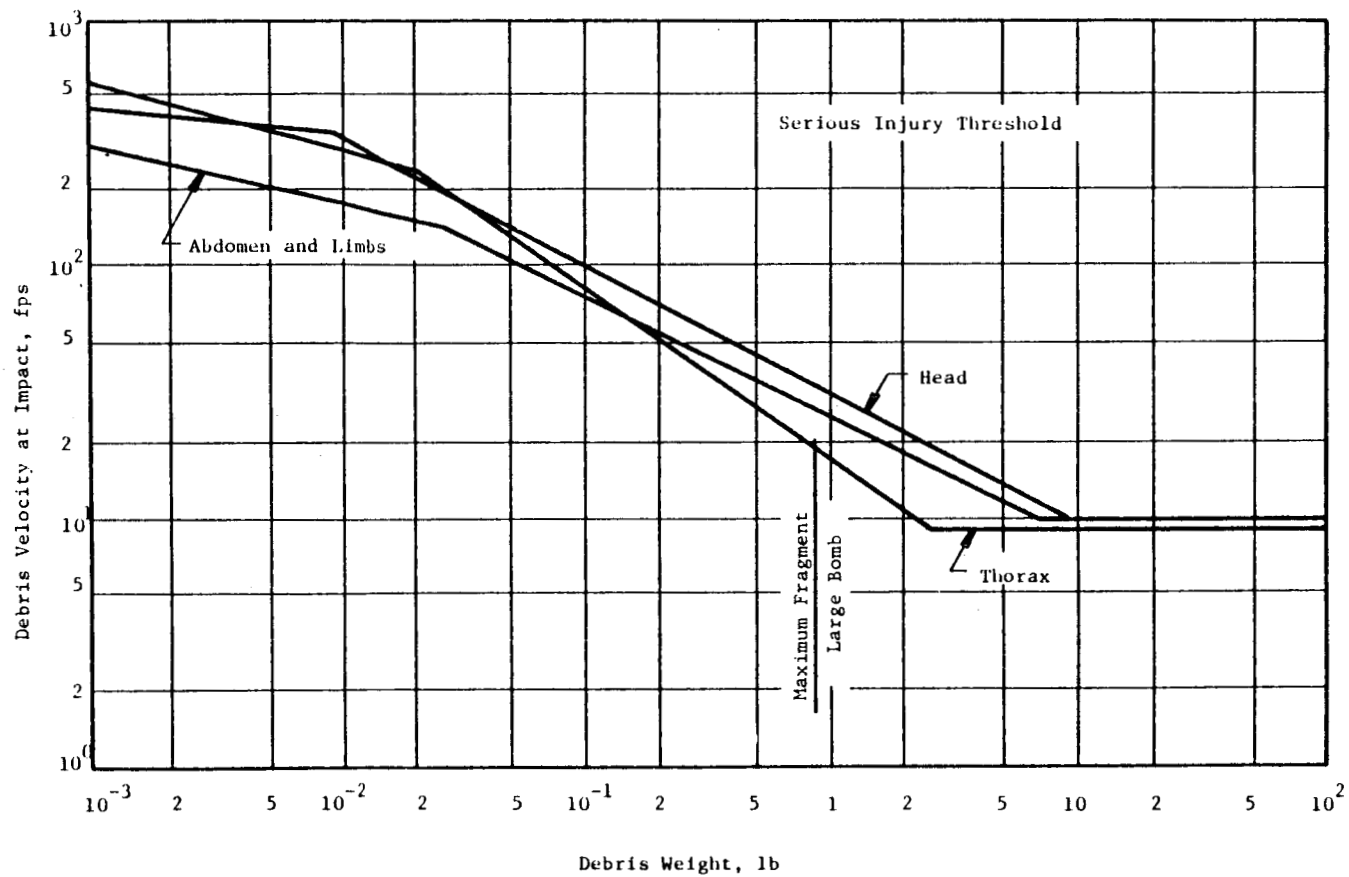
Figure 6.41 Personnel Response to Fragment Impact
(Serious Injury Threshold)

EXAMPLE PROBLEM 6.25

PROBLEM – Determine the velocity at which a fragment of a given size
(defined by a ratio of area to weight) will penetrate human skin
50% of the time and cause serious injury.

GIVEN: A/W_f = area to weight ratio of fragment (ft^2/lb)

FIND: V_{50} REFERENCE

SOLUTION: 1. Determine estimated V_{50} by locating appropriate
A/W_f ratio on graph, or by calculation using the
V_{50} equation fitted by Sperrazza and Kokinakis.

$$V_{50} = k(A/W_f) + b$$ Fig. 6.39

where k = 836 lb /ft-sec

b = 72.3 ft/sec

CALCULATION

GIVEN: A piece of a steel lathe tool which is 5 in. long and 1/2 in.
square on end. Assume it flies off edge-on, i.e., the
cross-sectional area of the fragment along its trajectory is
2.5 in.^{2}. The fragment weighs 0.35 lb.

$$\frac{A}{W_f} = \frac{0.017 \ ft^2}{0.35 \ lb} = 0.050 \ ft^2/lb$$

FIND: V_{50}

SOLUTION: 1. V_{50} = (836 lb/ft-sec)(0.050 ft^2/lb) + 72.3 ft/sec

V_{50} = _114 ft/sec_

EXAMPLE PROBLEM 6.26

PROBLEM – Determine the extent of human head injury resulting from impact
by a 10 lb non-penetrating fragment traveling at a given velocity

GIVEN: V = fragment velocity (fps)
W_f = fragment weight (lb)

FIND: Probability of human head injury   REFERENCE

SOLUTION: 1. Determine the extent of a cerebral concussion   Table 6.20
which would result.
2. Determine the extent of skull fracture.   Table 6.20

CALCULATION

  GIVEN: V = 14 ft/sec
          W_f = 10 lb

  FIND: Probability of human head injury

  SOLUTION: 1. A fragment with an impact velocity of 14 ft/sec would
               be just under the threshold for causing cerebral
               concussion. According to the data, it would not cause
               cerebral concussion.
            2. Again, the velocity is near the threshold, but one would
               conclude that skull fracture would probably not occur.

EXAMPLE PROBLEM 6.27

PROBLEM - Determine the percent of people in a large group who would die
          if subjected to impact by a fragment of particular weight
          impacting at a given velocity (in the area of the abdomen
          or limbs).

  GIVEN: W_f = weight of fragment (lb)
          V = debris velocity (fps)

  FIND: Probability of injury   REFERENCE

  SOLUTION: 1. Locate point on graph defined by the weight   Fig. 6.40
               of the fragment and the debris velocity.
               Estimate kill probability or injury from
               curves given.

CALCULATION

  GIVEN: W_f = 1 lb
          V = 50 fps

  FIND: Probability of injury

  SOLUTION: 1. The point lies near the 10% kill/90% injury probability
               line. Less than 10% of the sample of people would die,
               but greater than 90% would be seriously injured by
               the impact of a 1-lb fragment at 50 fps.

EXAMPLE PROBLEM 6.28

PROBLEM - Determine the impact velocity, V, below which no serious
          head injuries will occur from impact of a particular weight
          of debris.   .

GIVEN: W_f = debris weight (lb)

FIND: V

SOLUTION: 1. Locate point on appropriate curve correspond-   Fig. 6.41
ing to desired debris weight. Read debris
velocity from vertical scale.

CALCULATION

GIVEN: W_f = 2 lb

FIND: V

SOLUTION: 1. Below 24 ft/sec no serious head injuries would result
from impact of a 2-lb fragment.

6.6 EXPLOSIVE INITIATION BY FRAGMENTS

Most severe accidental explosions involving high explosives are escalated from explosions of a single piece of explosive or single explosive component in a weapon or munition by the subsequent impact of high-speed fragments on other pieces of explosive or weapons which are located nearby. Thus, the literature contains many reports of safety-related studies which give test results for initiation of bare and cased explosive charges by high-speed projectiles which stimulate fragments. To collate this mass of data and generate prediction equations, we have reviewed the data from these references which contain enough raw data, calculated values of impact velocities which have a 50 percent probability of causing explosive initiation (V_{50}), and conducted a similitude analysis to scale the data and determine appropriate dimensionless scaling factors for correlating data from different sources. We were able to obtain firm or tentative correlations for several types of bare explosives, lightly cased explosives, and heavily cased explosives. Data are limited, however, to steel-cased explosives and steel simulated fragments. Within the scaled data limits, some prediction curves were developed which can be used for prediction of V_{50} values for a variety of fragment masses, for several types of bare explosives, and for cased explosives having a wide range of scaled casing thicknesses. The results are reported in Reference 6.60, which is the basis for prediction methods given in this section.

6.6.1 Bare Explosive

Test data for explosive initiation of Tetryl and Composition B explosives were obtained by Slade and Dewey (Ref. 6.61), using gun-launched, steel and brass flat-faced projectiles to simulate fragments. Later McLean and Allan (Ref. 6.62) used an explosive projection technique to launch steel rectangular parallelopiped simulated fragments into Pentolite and Cyclotol bare explosive receptors. Finally, Petino and Leondi (Ref. 6.63) report data using the same explosive launch method and steel fragments for Amatex explosive. Time delays after impact for detonation of bare explosives are very short, of the order of microseconds.

All of these data are reduced to obtain mean values of V_{50} and standard deviations for each data set, and are reported in Reference 6.62. The scaling and scaled data correlation in that reference showed good correlations between several scaled parameters, when plotted as functions of scaled mass per unit area of the projectiles,

$$\bar{M}_p = \frac{M_p}{\rho_p A^{3/2}} \tag{6.85}$$

where M_p = projectile mass

ρ_p = density of projectile material

A = frontal area of the flat-faced fragment simulator.

The parameters which correlated were

$$\bar{V}_{50} = \frac{V_{50}}{a_p} \tag{6.86}$$

$$\bar{I} = \bar{M}_p \, \bar{V}_{50} \tag{6.87}$$

and

$$\bar{E} = \frac{\bar{M}_p \, \bar{V}_{50}^2}{2} \tag{6.88}$$

where a_p = sound velocity in projectile material

$\bar{I}$ = scaled impact momentum

$\bar{E}$ = scaled impact kinetic energy.

Plots of $\bar{I}$ and $\bar{V}_{50}$ versus $\bar{M}_p$ are given in Figures 6.42 and 6.43. Prediction curves are drawn in these figures, with Tetryl and Pentolite forming one group, Comp B and Cyclotol another group, and Amatex a third group. The Amatex curve is shown in Figure 6.42; however, the data spread was insufficient for conclusions for a $\bar{V}_{50}$ versus $\bar{M}_p$ curve and hence is not shown in Figure 6.43. Error bands for individual groups of tests are shown in Figure 6.43.

6.6.2 Encased Explosives

The study reported in Reference 6.60 showed that heavily encased* explosives, such as artillery projectiles (shells) react differently to fragment impact than more lightly cased or confined explosives.

Explosives which were tested with simple cover plates on the impacted side, or with weak containers which would rupture under low internal pressures seemed to be initiated in somewhat the same manner as bare explosives, i.e., probably primarily by shock transmission. Perforation of the cover plate was necessary before initiation could occur, so thresholds were somewhat raised. Test data were not as extensive as for bare explosives, consisting of limited series by Slade and Dewey (Ref. 6.61) on Tetryl, Petino et al. (Ref. 6.64) on Composition B, Petino and Leondi (Ref. 6.63) on Amatex, and Frey et al. (Ref. 6.65) on Composition B and Octol. Variations were small in the independent scaled parameter

---

*"Cased" explosive and "encased" explosive are used interchangeably.

$$\bar{h} = h/A^{1/2} \qquad\qquad (6.89)$$

where h is steel casing thickness. Best data correlation was achieved by $\bar{V}_{50}$, which is shown plotted against $\bar{h}$ in Figure 6.44. Tentative ranges for values of $\bar{V}_{50}$ for Comp B and Amatex, and for Tetryl and Octol as two separate groups are shown in the figure. There is a lack of variation of $\bar{h}$ in the test data, and additional tests are needed. Whenever initiations occurred in these tests, time delays were also relatively short, tens of microseconds.

For heavily encased explosives, initiation of violent reactions which would fragment the casing often occurred with long delays (seconds), below velocities which would shock initiate. Test data were from two sources, Reeves (Ref. 6.66) and the Tera Group report (Ref. 6.67), with both using right circular cylindrical fragment simulators gun launched against Composition B loaded artillery shells. In these tests, initiation often seemed to correlate well with ballistic limit (V_{50}) values for the casing alone, although this criterion seemed to fail for low values of $\bar{h}$. The comparisons for this class of testing in Reference 6.48 are shown in Figures 6.45 and 6.46. Either set of curves, V_{50} or $\bar{I}/\bar{h}$ versus $\bar{h}$, can be used for prediction of critical scaled impact conditions. For the latter criterions, values are relatively constant for $\bar{h} > 0.7$. Data scatter shown in these curves indicate confidence limits for the predictions.

Very little or no data exist for fragment impact initiation for many of the pressed explosives present in the Pantex plant, so tests on these explosives are definitely needed to supplement the prediction curves given here.
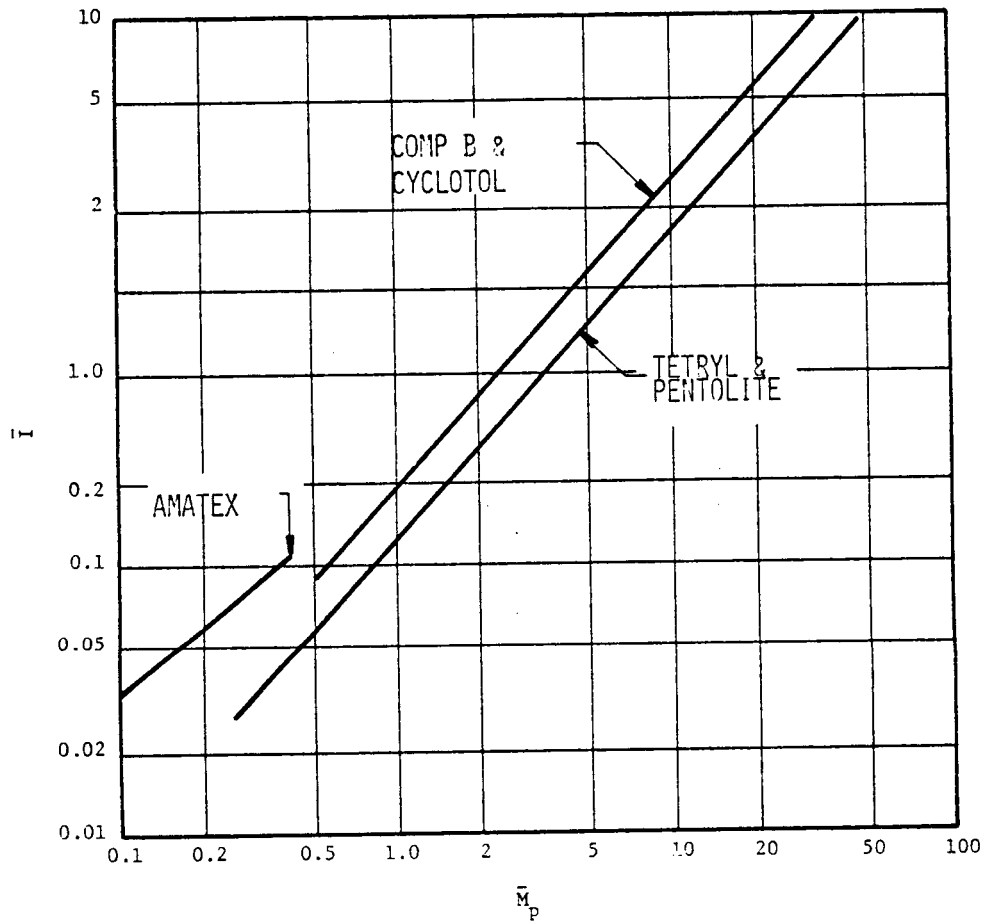
Figure 6.42 $\bar{I}$ versus $\bar{M}_p$ for Bare Explosives
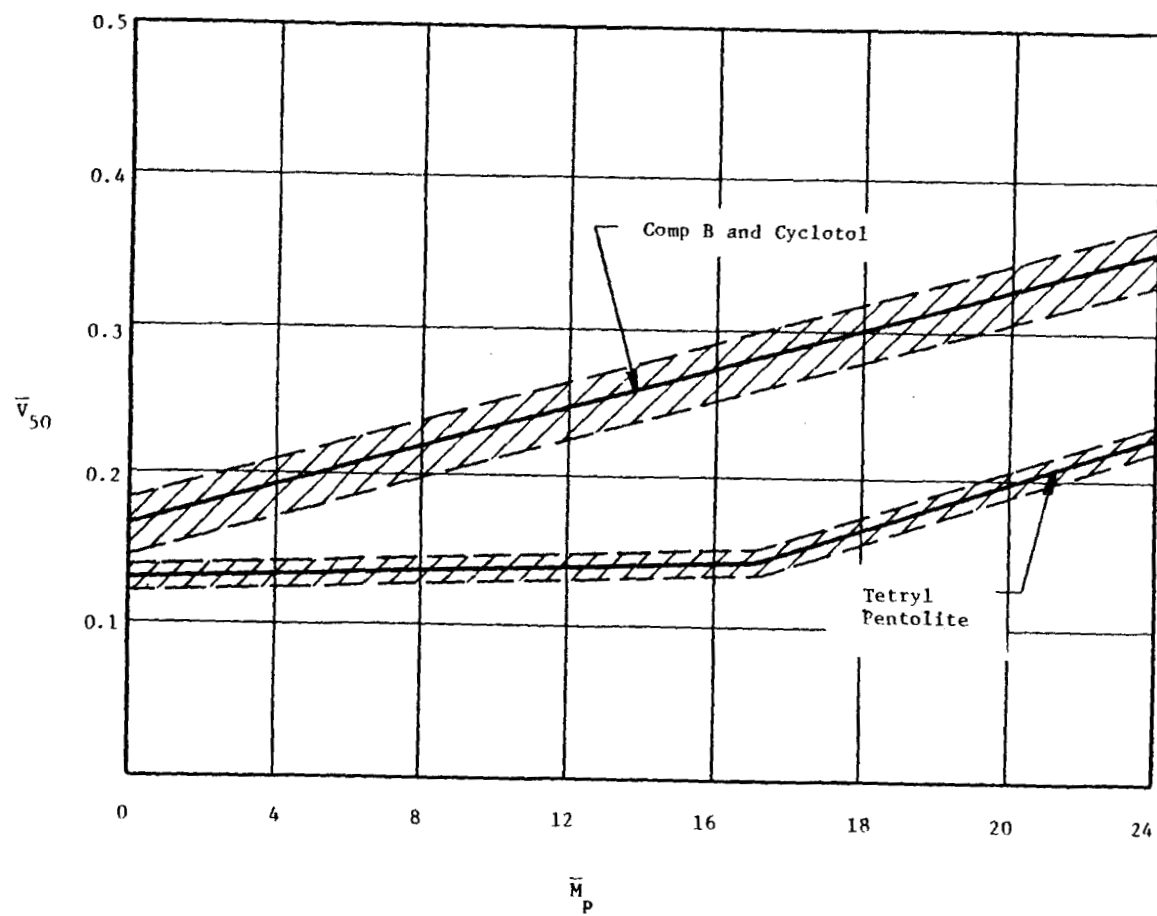
Figure 6.43 $\bar{V}_{50}$ versus $\bar{M}_p$ for Bare Explosives Including 1σ Error Bands
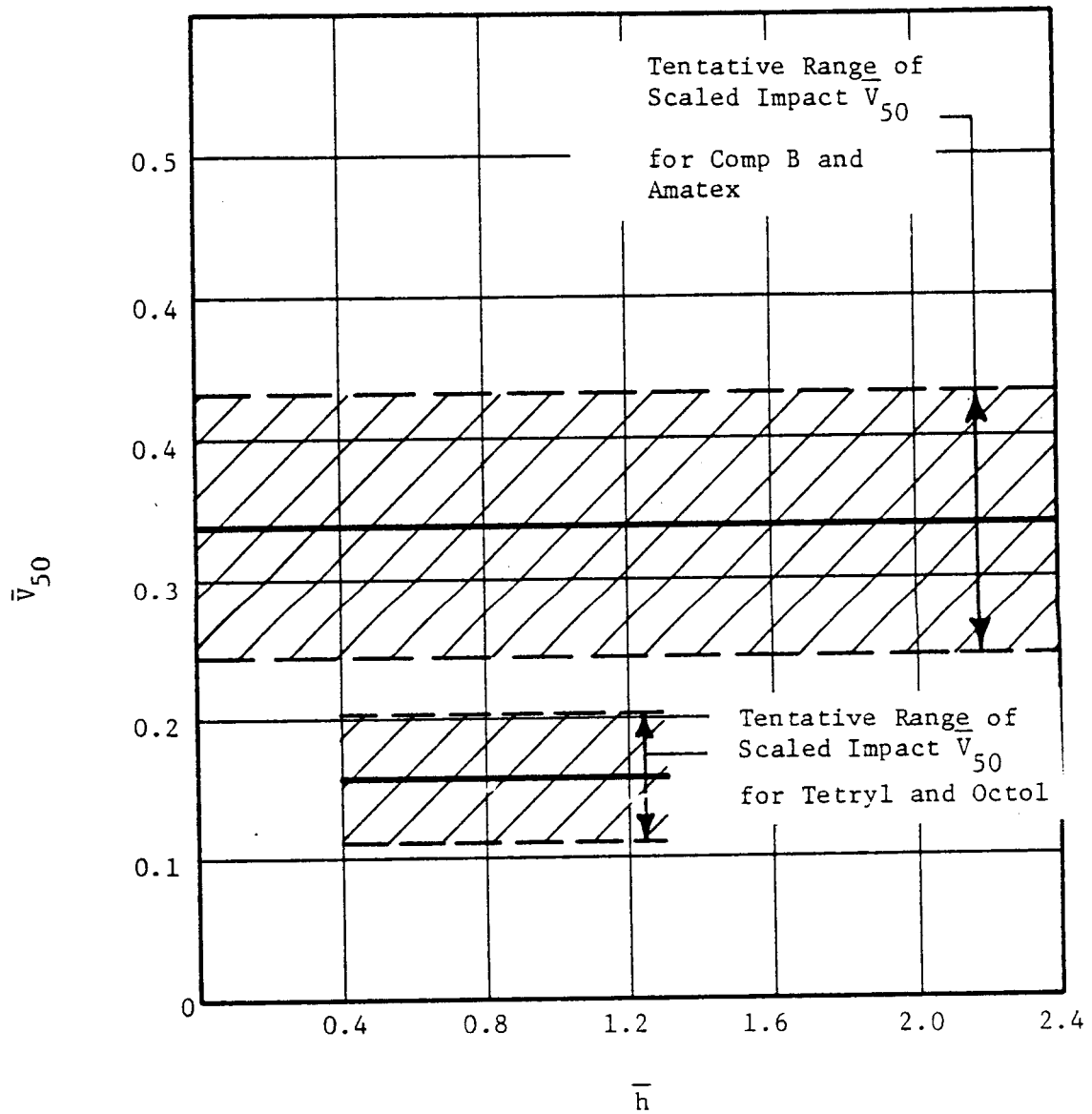
Figure 6.44 $\bar{V}_{50}$ versus $\bar{h}$ Light Explosive Confinement Including
1σ Error Bands

6-160
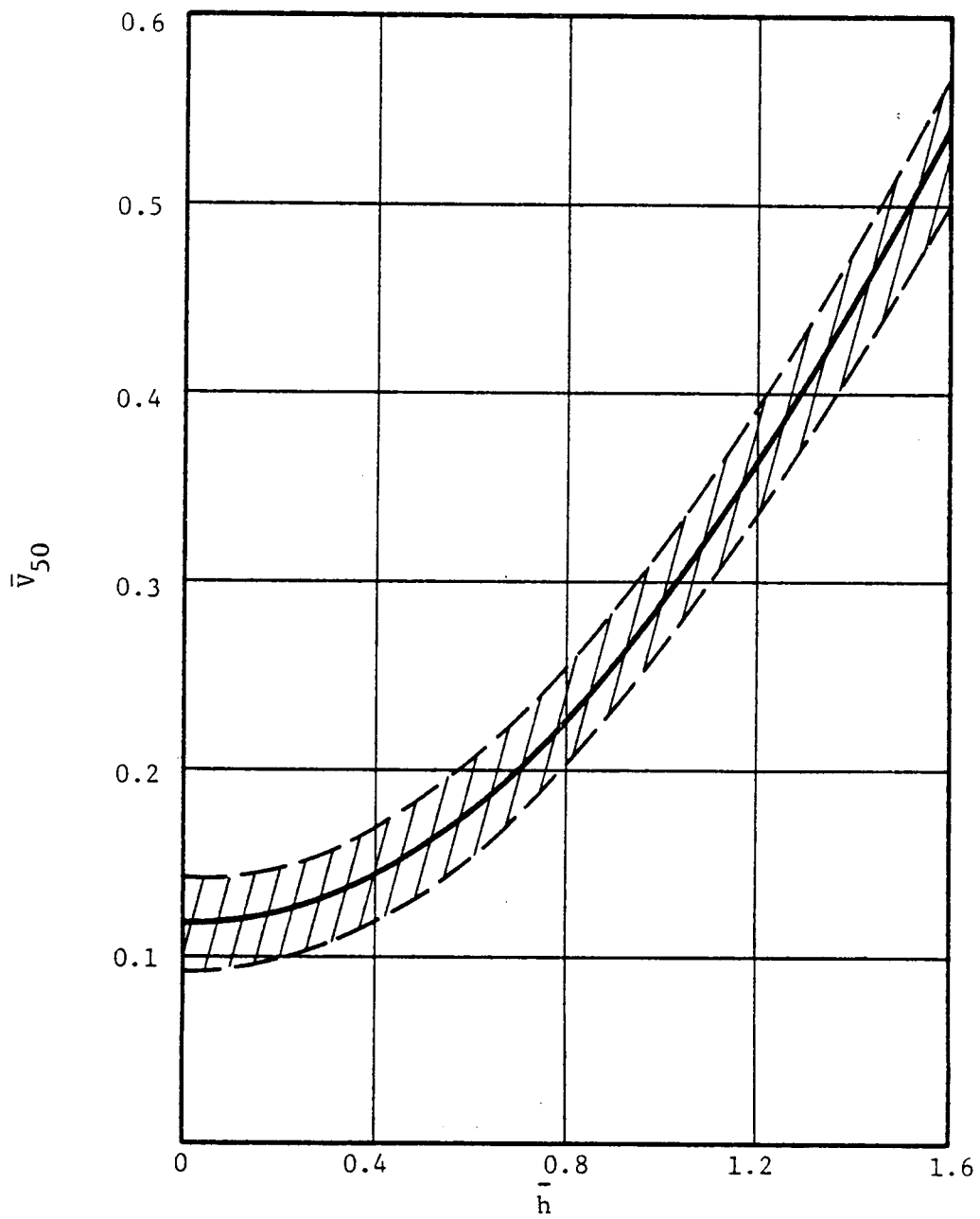
Figure 6.45 $\bar{V}_{50}$ versus $\bar{h}$, Heavy Explosive Confinement
Including 1σ Error Bands
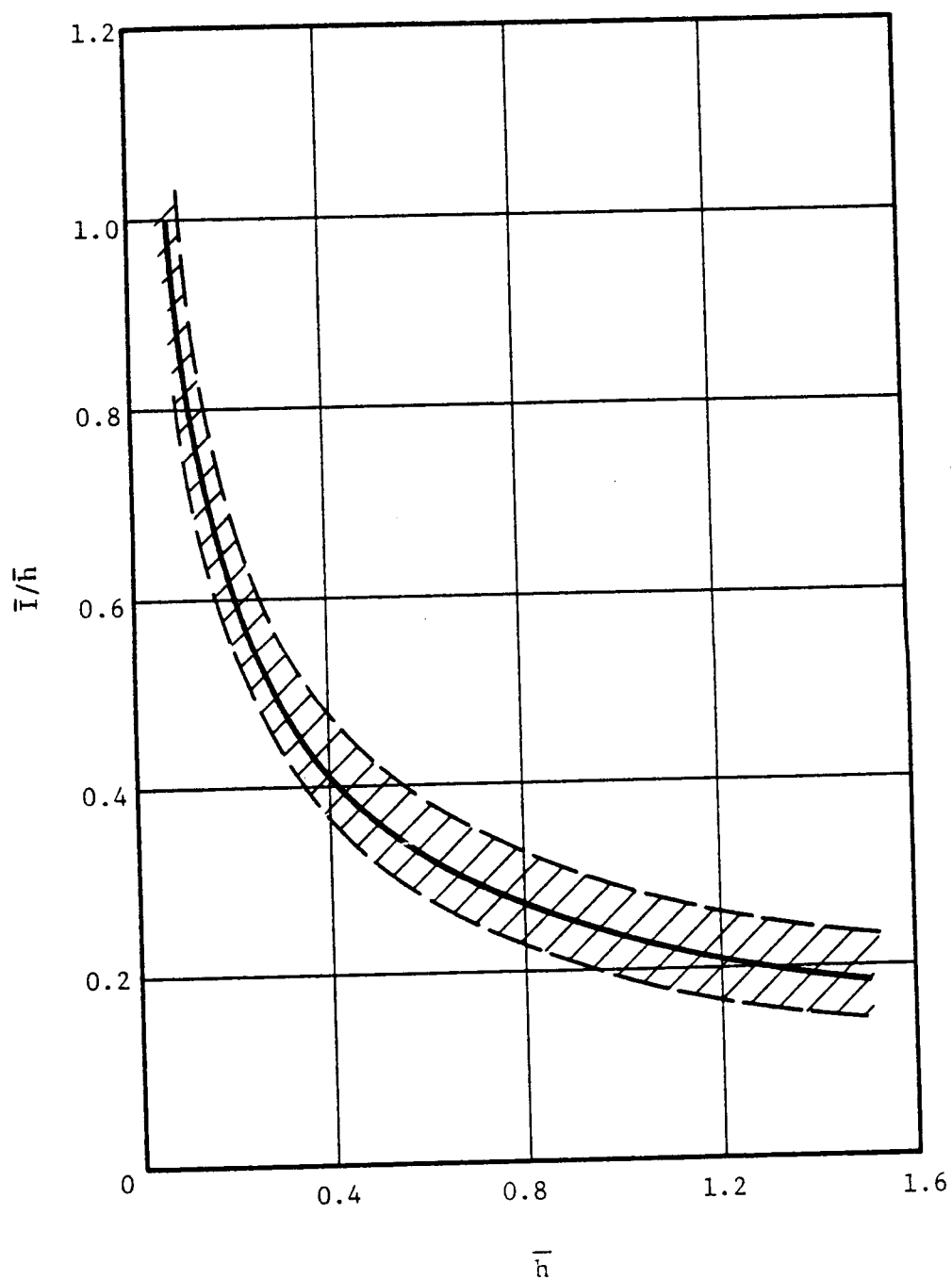
Figure 6.46 $\bar{I}/\bar{h}$ versus $\bar{h}$, Heavy Explosive Confinement Including
1σ Error Bands

EXAMPLE PROBLEM 6.29

PROBLEM – Determine if a fragment of specified dimensions, mass, and
velocity can cause initiation of HE in light explosive
confinement, heavy explosive confinement and for bare explosive.

GIVEN: A = presented fragment area
ρ = density of fragment
M_p = mass of projectile
V = fragment velocity
a_p = speed of sound in projectile
h = casing thickness
Explosive type

FIND: Probability of explosive initiation   REFERENCE

SOLUTION: 1. Calculate the various nondimensional terms   Eq. (6.85),
required to use Figures 6.42, 6.43, 6.44,   (6.86),
6.45, and 6.46. The terms are $\bar{M}_p$, $\bar{V}$, $\bar{I}$,   (6.87),
and $\bar{h}$. Use the same equations for V_{50} but   (6.88),
use V given.   (6.89)
2. Use Figures 6.42, 6.43, 6.44, 6.45, and
6.46 to determine comparison with $\bar{V}_{50}$ curves   Fig. 6.42,
and use judgment to determine if initiation   6.46
will occur.

CALCULATION

GIVEN: Explosive type: Comp B
Fragment type: steel
$A = 1$ in.^{2}
$\rho = 7.36 \times 10^{-4}$ lb-sec^2/in.^{4}
$M_p = 7.36 \times 10^{-4}$ lb-sec^2/in.
$V = 1000$ ft/sec $= 12000$ in./sec
$a_p = 2.00 \times 10^5$ in./sec

Consider three cases:
$h = 0$ in. for uncased
$h_1 = 0.25$ in. for light cased
$h_2 = 1.2$ in. for heavy cased

FIND: Probability of explosive initiation

SOLUTION: 1. $\bar{M}_p = \dfrac{M_p}{\rho_p A^{3/2}} = \dfrac{7.36 \times 10^{-4}}{7.36 \times 10^{-4}(1)^{3/2}} = 1$

$$\bar{V} = \frac{V}{a} = \frac{12000}{2.00 \times 10^5} = 6.0 \times 10^{-2}$$

$$\bar{I} = \bar{M}_p \bar{V} = (1)(6.0 \times 10^{-2}) = 6.0 \times 10^{-2}$$
$$\bar{M} \bar{V}$$

Light Cased
$$\bar{h}_1 = \frac{0.25}{1} = 0.25$$

Heavy Cased
$$\bar{h}_2 = \frac{1.2}{1} = 1.2, \text{ also } \frac{\bar{I}}{\bar{h}_2} = \frac{6.0 \times 10^{-2}}{1.2} = 5 \times 10^{-2}$$

for bare explosive, of course, no $\bar{h}$ exists.

2. Using Figures 6.42 – 6.46, the following is noted:

Bare HE

Figure 6.42 – The point $(\bar{M}_p, \bar{I})$ or $(1, 6.0 \times 10^{-2})$ is below Comp B $\bar{I}$ line and has a low but unknown probability of exploding.

Figure 6.43 – Point $(\bar{M}_p, \bar{V})$ or $(1, 6.0 \times 10^{-2})$ is below the Comp B isoline.

Light Explosive Confinement

Figure 6.44 – Point $(\bar{h}, \bar{V})$ or $(0.25, 6.0 \times 10^{-2})$ is below the $\bar{V}_{50}$ line.

Heavy Explosive Confinement

Figure 6.45 – Point $(\bar{h}_2, \bar{V})$ or $(1.2, 6.0 \times 10^{-2})$ is below the $\bar{V}_{50}$ line.

Figure 6.46 – Point $(\bar{h}_2, \bar{I}/\bar{h}_2)$ or $(1.2, 5 \times 10^{-2})$ is below the curve.

In summary, the probability of an explosion is always very low.

EXAMPLE PROBLEM 6.30

PROBLEM – Rework Example Problem 6.29 using another value for impact velocity.

CALCULATION

GIVEN: This same problem is now reworked with V = 4000 ft/sec = 48,000 in./sec.

FIND: Probability of explosive initiation

SOLUTION: 1. $\bar{M}_p = \dfrac{M_p}{\rho_p A^{3/2}} = 1$

$\bar{V} = \dfrac{V}{a} = \dfrac{48,000}{2.0 \times 10^5} = 0.24$

$\bar{I} = \bar{M}_p \bar{V} = (1)(0.24) = 0.24$

$\bar{E} = \dfrac{\bar{M}_p \bar{V}}{2} = \dfrac{(1)(0.24)}{2} = 0.12$

Light Cased
$\bar{h}_1 = 0.25$

Heavy Cased
$\bar{h}_2 = 1.2$ also $\dfrac{\bar{I}}{\bar{h}_2} = \dfrac{0.24}{1.2} = 0.2$

For bare explosive, of course, no $\bar{h}$ exists.

2. Using Figures 6.44 - 6.48, the following is noted:
Bare HE
   Figure 6.42 - Point $(\bar{M}_p, \bar{I})$ or (1, 0.24) is above
   the Comp B isoline and, therefore, the HE has a greater
   than 0.5 probability of detonating.

   Figure 6.43 - Point $(\bar{M}_p, \bar{V})$ or (1, 0.24) is above
   the Comp B isoline.

Light Explosive Confinement
   Figure 6.44 - Point $(\bar{h}_1, \bar{V})$ or (0.25, 0.24) is near
   or within the 1σ error band of the Comp B region and
   thus HE detonation is likely.

Heavy Explosive Confinement
   Figure 6.45 - The point $(\bar{h}_2, \bar{V})$ or (1.2, 0.24) is
   below the curve and outside the 1σ error band.

   Figure 6.46 - The point $(\bar{h}_2, \bar{I}/\bar{h}_2)$ or (1.2, 0.2) falls
   at the $\bar{I}/\bar{h}_2$ curve and hence predicts a 0.50 probability
   of detonation occurrence.

In summary, the probability of the bare explosive detonating is high (75%). Detonation of the lightly cased explosive also has a probability of about 50%, because it lies within the 1σ error band for this probability. The results for a heavily confined charge are inconclusive, because the two initiation criteria give different answers. To be safe, one should assume the more dangerous result, i.e., that, in this case, the explosive also has a 50% probability of detonating.

6.6.3 Crush, Impact, and Skid Initiation

A number of tests have been conducted on explosive materials to determine their sensitivity to specific initiation methods (Ref. 6.70). Unfortunately, these tests have failed to yield a workable data base on explosive sensitivity. Inconsistencies in the test procedures and a lack of reporting on pertinent variables are two reasons why attempts to develop functional relationships between the various tests have so far been unsuccessful. Therefore, the results of sensitivity tests (see Appendix A, Properties of Explosives) should be used only as a determination of the relative sensitivities of explosives to specific initiation methods. Do not attempt to estimate the results of one test from the results of another; i.e., the results of the skid initiation test cannot be predicted based on the results of the drop-weight test.

6.7 ASSESSMENT OF CONFIDENCE IN PREDICTION METHODS

Because of limited information from accidents and experiments, the accuracy of the prediction methods will be affected. Specific limitations on the use of the prediction methods have been discussed in the respective sections of this chapter. The sections which follow, however, will give an overview, in general terms, of the assumptions and uncertainties in the prediction methods and will list recommended tests and analyses to validate assumptions or reduce uncertainties.

6.7.1 Identification of Assumptions and Uncertainties

This section describes, in general terms, the assumptions and uncertainties in the fragment damage scenario presented in this chapter.

Velocity Prediction of Primary Fragments (Section 6.2.1.1)

Calculation of velocities of primary fragments is based on the Gurney Method. This method, which gives maximum velocities, was developed for cases where an HE completely fills the inside of a cylinder of uniform wall thickness and a few other geometries. There are also limits on the types of explosives for which the Gurney energy was determined. Velocities for containers of different shapes and approximations of Gurney energies for different explosives should be used with appropriate reservation.

Mass Distribution (Section 6.2.1.2)

Calculation of the mass distribution using the Mott equations can only be accurately made for uniform cylinders, completely filled with HE.

Primary Fragment Shape (Section 6.2.1.3)

Choice of fragment shape is somewhat arbitrary. The standard and alternate fragment shapes represent conservative worst-case fragments.

Secondary Fragment Shape (Section 6.2.2)

With the current state of the art, it is necessary for the AE to make an engineering assessment of the manner in which a piece of machinery or equipment will break apart. Because of uncertainty in determining the actual breakup pattern, it is beneficial for the AE to consider all reasonable breakup patterns.

Velocity Prediction of Secondary Fragments (Section 6.2.2.1)

The analytical solution for determining the velocity of unconstrained objects _far_ from the explosive charge should be fairly accurate for many object shapes. Irregular object shapes will have to be evaluated by approximating them by the object shapes mentioned in the section. When this is done, it is best to examine the variance in unconstrained object velocity with changes in drag coefficient and object dimensions. Experimental data for determining the velocity of unconstrained objects _near_ the explosive charge are limited but accurate. Estimation of velocities for other object shapes will vary dependent on the shape factor and area used. The shape factors in Figure 6.11 vary by as much as 50 percent. Since velocity is directly proportional to the shape factor, a choice of an intermediate shape factor for an irregular object could produce an error in calculated velocity of about 25 percent. The experiments were also performed using spherical and cylindrical Comp B charges. Other shapes of types of explosives will yield uncertain results. However, adjustment of an actual HE charge to an equivalent Comp B charge using the heat of detonation of the explosives should yield accurate results.

(Section 6.2.2.2)

Calculation of constrained object velocities _near_ an explosive charge is limited to cantilever and clamped-clamped boundary conditions and uniform beams. Velocity is not too dependent on the type of failure. Thus, velocity calculations are accurate for these two conditions.

Building Fragments (Section 6.2.3)

Building fragmentation depends on a number of factors and can vary significantly from one building type to another. Because of limited information on this subject, the AE will be forced to make numerous engineering assessments. In some cases, it will be necessary to produce alternate scenarios in order to assure an adequate amount of conservatism in design.

Fragment Range and Impact Conditions (Section 6.2.4)

Fragment range for individual fragments is dependent on initial conditions and fragment characteristics. Once these are known, maximum range calculations for a "chunky" fragment should have an accuracy of within 10 percent.

(Section 6.2.4.2)

Impact mass and range distribution functions for fragmenting buildings have a high degree of credibility from a statistical point of view. If similar buildings and explosive charge energies are being considered, a statistically accurate missile map can be constructed. If other building types are being considered, the use of these data may yield inaccurate predictions. If the building characteristics are the same but the charge energy varies, some degree of accuracy can be maintained through interpolation within the energy range in the figures. Extrapolation outside the energy range shown in the figures is not recommended.

(Section 6.2.4.3)

Size of building fragments can be approximated from the mass distribution and knowledge of the type of building materials. Since statistical distribution functions are involved, average sizes are more relevant than sizes of individual fragments.

(Section 6.2.4.4)

Due to the mass of building fragments and the range over which they travel, impact kinetic energies will be high and cause a large amount of damage to objects which they strike. Of more importance are the mass and range distributions of building fragments which are discussed in previous sections.

(Section 6.3.1)

Missile dispersion equations should be used for buildings of similar size and construction and HE charges of similar energies to those used in the analysis. Correlation coefficients for the curve fits to the data are discussed in the text.

Impact Damage (Section 6.4.1)

Impact damage to metal structures is well defined for the conditions specified in this section. The equations and curves are based on experimental data and represent a best-fit to the data.

6-168

(Section 6.4.2)

Within the range of the data, penetration of fragments into concrete and masonry structures is quite accurate.

(Section 6.4.3)

Very limited but accurate penetration characteristics are included for strawboard and fiberboard. The data are limited to a small range of fragment masses and velocities. Extrapolation outside the range of the data is not recommended.

(Section 6.4.4)

It is difficult to know with a high degree of confidence what fragment impact momentum will be without running a trajectory code program. The impact damage criteria, however, provide a good indication of fragment momentum required for damage. Also, the velocity direction provides a useful indication of how velocity varies with drop height.

(Section 6.4.5)

Fragment penetration into cohesive soils and sand is based on experimental studies and should provide good results when used in the range of the data. When determining penetration of fragments into other materials as discussed in this section, there are restrictions to steel fragments, small fragment sizes, and specific types of targets. The equations were empirically developed for military applications and naturally provide limited information for explosion accidents.

(Section 6.5.1)

Primary fragment injury criteria were experimentally derived and provide accurate results within the range of the data.

(Section 6.5.2)

Secondary fragment injury criteria are also experimentally derived and provide accurate results within the range of the data.

Explosive Initiation (Section 6.6.1)

A model analysis and an analysis of test data were performed to develop the criteria for explosive initiation of bare explosives by fragment impact. The criteria are accurate within the range of data but cannot be extrapolated with a predictable degree of accuracy.

(Section 6.6.2)

The criteria for explosive initiation of encased explosives by fragment impact are accurate within the confines of the data.

(Section 6.6.3)

Very little objective explosive sensitivity information can be derived from the crush, impact, and skid initiation tests. These tests provide a subjective comparison between explosives.

6.7.2 Recommended Tests and/or Analyses to Validate Assumptions or Reduce Uncertainties

The subjects of fragmentation and impact damage are extremely broad and may never be fully understood. Fragmentation heavily depends upon the type of loading, positions of loaded objects relative to the source and other objects, material properties, construction design, etc. Fragment impact damage depends on the characteristics of the projectile (material properties, mass, shape, velocity, impact angle, etc.) and of the target (material properties, thickness, constraints, etc.). Because of the large number of parameters involved, it is not difficult to develop an untenable number of subproblems. There are, however, a number of areas which could be examined which would provide major advances in understanding and dealing with the whole problem of fragmentation and impact damage. Some fruitful areas for future work are:

- Studies of fragmentation patterns of HE process machinery and measurement of fragment velocities.

- Translation velocities of unconstrained and constrained objects of various shapes and materials subjected to blast loads from HE charges of several types, shapes and configurations.

- Fragment patterns for structures, similar to those at the Pantex facility, subjected to internal or external HE explosions. Carefully planned model tests would be appropriate.

- Missile maps of fragments from structures, similar to those at the Pantex facility, subjected to internal explosions.

- Measurements of impact velocities of fragments from structures subjected to internal explosions.

- Fragment penetration of building materials and panels. These include at least concrete fragments impacting earth fill and composite building panels, fiberboard, etc.; and steel or other

metal fragments impacting some of the same materials and brick, clay tile, and masonry.

● Explosive initiation due to impact from large, crushing objects.

6.8   PROCEDURE FOR PERFORMING A FRAGMENTATION ANALYSIS

This chapter discusses many different aspects of a fragmentation analysis. Throughout the chapter, we have included illustrative examples of various fragmentation subproblems. To aid the analyst in performing a fragmentation analysis, we have developed the flowcharts contained in Figures 6.47a and 6.47b. To use the flowcharts, one begins at the top of Figure 6.47a and follows the arrows through the appropriate Yes-No answers and analysis blocks (note that Figure 6.47a is linked to Figure 6.47b through the "A" connector). Each analysis block refers to some subsection in this chapter of the manual where an analysis procedure and an example problem can be found. Since many fragments usually need to be considered in a fragmentation analysis, Figure 6.47b leads back to the start of the flowchart in Figure 6.47a. Thus, one iterates through Figures 6.47a and 6.47b until the fragmentation analysis is complete. Figure 6.47a distinguishes between non-building secondary fragments and building fragments. Non-building secondary fragments include pieces of machinery, furniture, tools, and miscellaneous objects near the explosion source. Building fragments are pieces from the structure itself, such as portions of walls and ceilings.
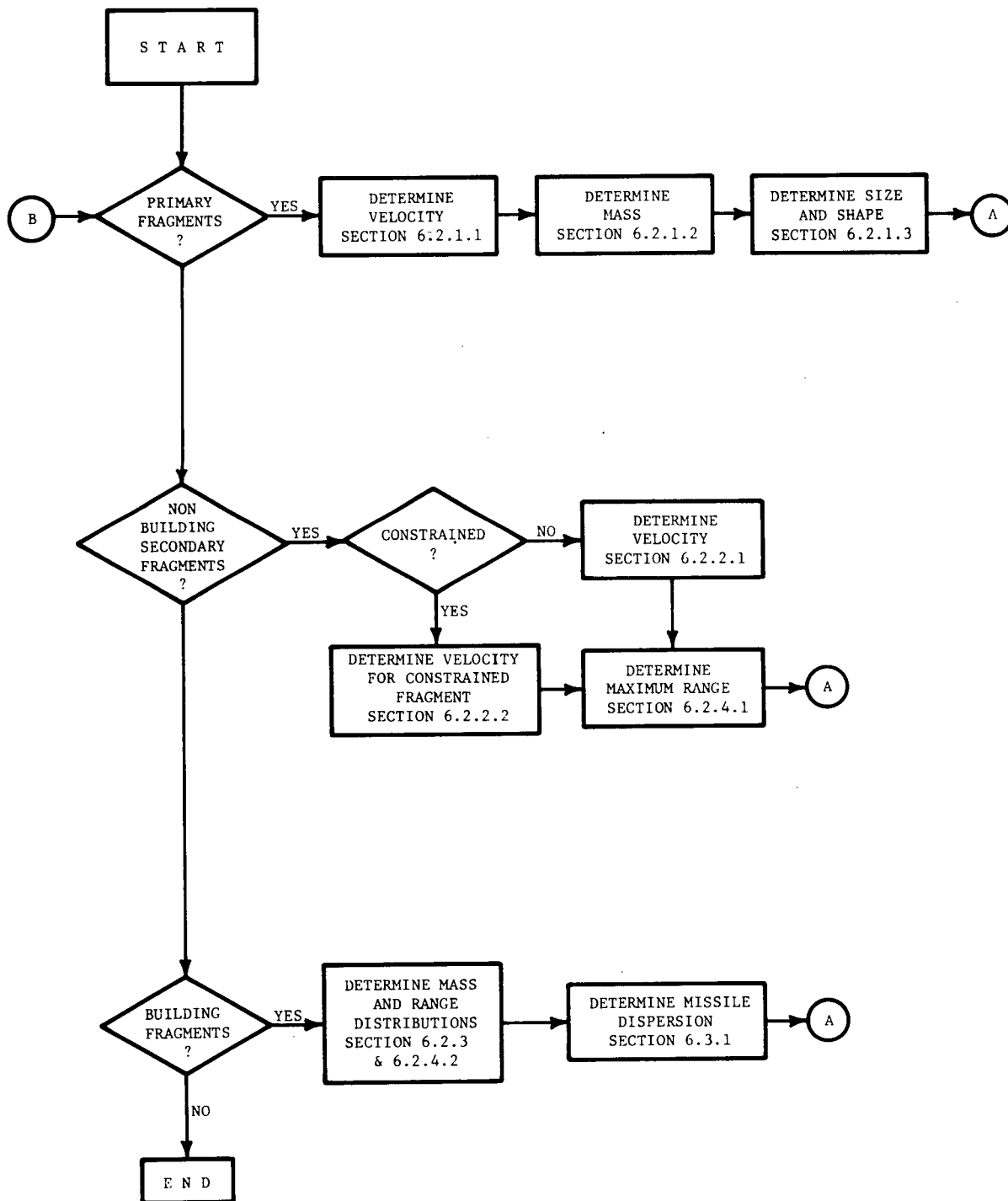
Figure 6.47a   Flow Chart
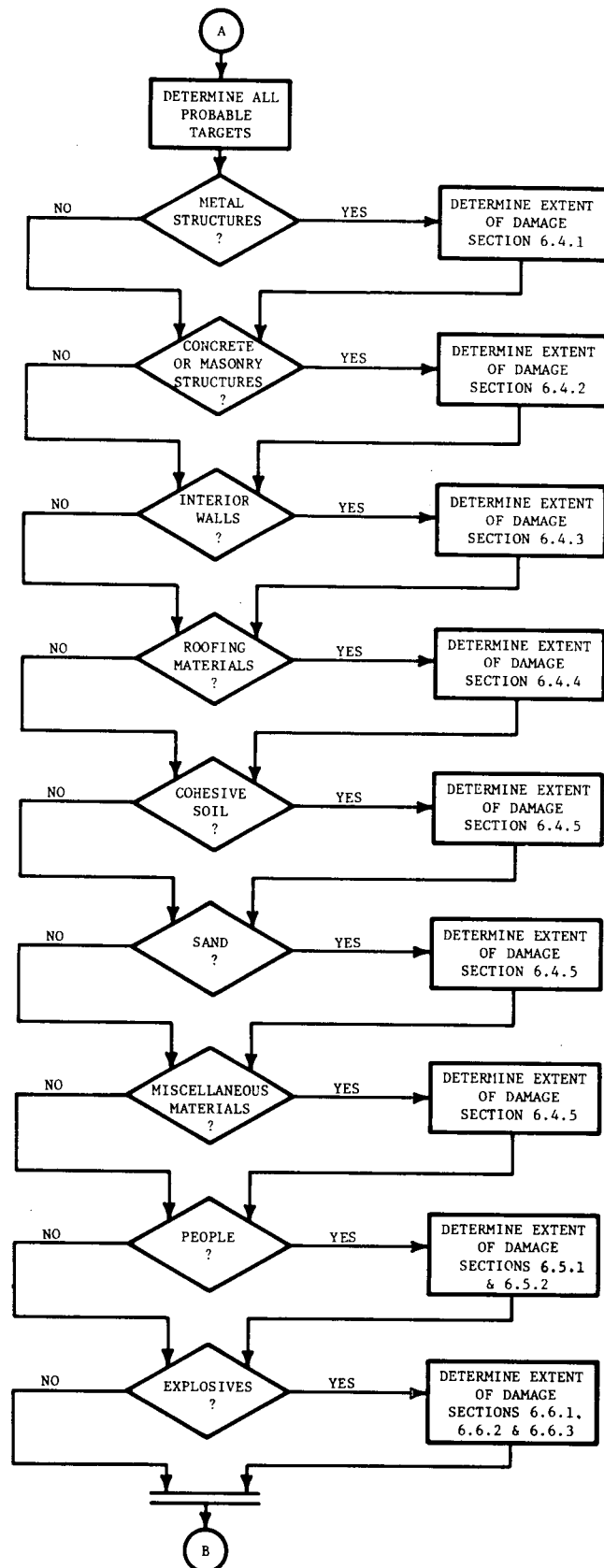
Figure 6.47b Flow Chart (Continued)

6-173

6.9 LIST OF SYMBOLS

A 　　　　presented area for use in striking velocity determinations; presented area of an object exposed to a blast wave; cross-sectional area of a beam; projectile cross-sectional area; fragment average presented area; average fragment impact area; cross-sectional area of projectile along its trajectory; frontal area of flat-faced fragment simulator

A_D 　　　　drag area

A_i 　　　　area of ring defined by the range interval R_i

A_o 　　　　empirical constant for predicting compact fragment limit velocity for mild steel targets

A_p 　　　　fragment area presented to plate

$\bar{A}$ 　　　　estimated average impact area of fragment

a 　　　　radius of fragment; empirical constant for predicting compact fragment residual velocity for mild steel target; speed of sound in target material

a_o 　　　　velocity of sound in air

a_p 　　　　sound velocity in projectile material

a_0 　　　　constant in fragment density equation

a_1 　　　　constant in fragment density equation; speed of sound in fragment material

a_2 　　　　constant in fragment density equation; speed of sound in target material

B 　　　　explosive constant

b 　　　　empirical constant for predicting compact fragment residual velocity for mild steel targets

C 　　　　constant; target material constant for steel fragment penetration

CL 　　　　confidence level

C_D 　　　　drag coefficient

C_L 　　　　lift coefficient

C_s 　　　　dilatational velocity

C_1 　　　　target material constant for steel fragment penetration

C_2 constant for maximum penetration in concrete of metal fragments other than armor-piercing; target material constant for steel fragment penetration

C' fragment distribution constant

c empirical constant for predicting compact fragment residual velocity for mild steel targets; constant in penetration equation; target material constant for steel fragment penetration

c_p sonic velocity of target plate

D diameter; fragment caliber density

d fragment diameter; diameter of rod projectile

d_{co} diameter of a steel core inside an HE containment shell

d_i outside diameter of HE containment shell; average inside diameter of casing

d_p diameter of perforations in a target plate

d_1 impact diameter of fragment

E_c modulus of elasticity for concrete

$\bar{E}$ nondimensional energy; scaled impact kinetic energy

$E*$ areal density of target

E' Gurney energy

F face resisting movement

F_D drag force

F_L lift force

$\bar{F}$ effective force F

$f(t)$ function of time t

$f'c$ static unconfined compressive strength of concrete

g gravity constant

H minimum transverse dimension of mean presented area of object

h steel casing thickness; thickness of a beam; thickness of target

h_p	average center-to-center distance between perforations in a target plate
h_2	target thickness
$\bar{h}$	scaled steel casing thickness; dimensionless target thickness
I	impulse imparted to a target
I_d	total drag and diffraction impulse
I_s	incident specific impulse
I_{st}	impulse absorbed by a deforming target
$\bar{I}$	nondimensional side-on specific impulse; scaled impact momentum
i	specific acquired impulse; specific impulse imparted to a target from an impacting rod missile
K	constant
K_y	constant for free-falling body
k_v	velocity decay coefficient
KE	kinetic energy of an impacting projectile
L	length
ℓ	length of a beam; length of rod projectile; length of pipe missile
ℓ_e	length of explosive line
ℓ_1	length of fragment
M	Mott parameter; mass of an object; mass of projectile
M_A	fragment distribution parameter
M_a	average mass of a fragment
M_B	total destroyed mass of a building
M_i	a particular mass of building fragments
M_p	projecile mass

$\bar{M}_p$	scaled mass per unit area of a projectile
m	empirical constant for predicting compact fragment limit velocity for mild steel targets
N	projectile nose shape factor
N_f	total number of fragments
N_{f_i}	number of fragments in a particular range increment
N_{R_k}	number of fragments of a particular mass in the range interval R_k
N_T	total number of fragments
N_x	number of fragments with weight greater than W_f
n	caliber radius of the tangent ogive of the assumed fragment nose; empirical constant for predicting compact fragment limit velocity for mild steel targets
P	peak contact pressure of rod missile
P_j	ambient atmospheric pressure
P_o	atmospheric pressure
P_r	maximum peak reflected pressure
P_s	peak incident overpressure
$\bar{P}$	nondimensional side-on overpressure
$p(t)$	net transverse pressure
Q	peak dynamic pressure
R	distance from the center of detonation; standoff distance; range; perforation factor
R_e	radius of the explosive
R_{eff}	effective spherical radius of explosive
R_i	a particular range interval
R_{i_1}	lower bound of a particular range interval

R_{i_2} upper bound of a particular range interval

R_k a particular range interval

R_t target radius

$\bar{R}$ nondimensional range

R' effective spherical radius of explosive

r radius of a spherical penetrator

S elastic section modulus; degree of saturation

T toughness

T_C thickness of concrete element

T_1 time of maximum peak reflected pressure

T_2 time at which reflected pressure falls to drag pressure

T_3 time at which ambient pressure is reached after passage of a blast wave

t thickness of fragment; depth of penetration; time; plate thickness

t_a time of arrival

t_c average casing thickness

t_s actual thickness of sand layer

t_w wall thickness of pipe missile

$\bar{t}$ effective time t

U strain energy

u particle velocity of blast wave

V velocity; ballistic limit velocity; velocity of projectile

V_{co} correlation velocity

V_{cr} critical velocity

V_i initial velocity

V_ℓ	ballistic limit velocity
V_o	initial fragment velocity; projectile impact velocity
V_p	impact velocity of projectile
V_r	fragment residual velocity; residual velocity of fragment as it leaves concrete element
V_s	striking velocity; fragment striking velocity
V_{y_f}	vertical component of striking velocity
V_{y_o}	initial vertical component of velocity
V_{50}	ballistic limit velocity; fragment impact velocity which has a 50% probability of causing explosive initiation
$\bar{V}$	nondimensional velocity; effective velocity of impact V_o
$\bar{V}_{50}$	dimensionless limit velocity
W	weight of explosive; a type of statistical distribution function
W_c	weight of HE containment shell
W_{co}	weight of steel core inside an HE containment shell
W_{c1}	weight of one side of a metal plate sandwich containing HE
W_{c2}	weight of one side of a metal plate sandwich containing HE
W_f	fragment weight
W_r	residual weight of the fragment
W_s	fragment striking weight
w	areal density of target (density x thickness)
X	distance from front of object to location of its largest cross-sectional area
$\dot{X}$	horizontal velocity
$\ddot{X}$	horizontal acceleration
X_f	maximum penetration of armor-piercing fragment

X_f' maximum penetration in concrete of metal fragments other than armor-piercing

$\bar{X}$ effective displacement X

x displacement of an object; dispersion angle in fragment density equation; depth of penetration

$\dot{x}$ velocity of an object

$\ddot{x}$ acceleration of an object

$\dot{Y}$ vertical velocity

$\ddot{Y}$ vertical acceleration

y edge length of fragment; distance in fragment density equation

y_f vertical impact height

y_o vertical drop height

Z plastic section modulus; caliber penetration

z fragment density

α trajectory angle; constant in penetration equation; constant for cohesive soil penetration; target material constant for steel fragment penetration

α_e vent area ratio

α_i initial trajectory angle

α_1 target material constant for steel fragment penetration

β nondimensional shape factor; penetration parameter; constant in penetration equation; constant for cohesive soil penetration; target material constant for steel fragment penetration

β_1 target material constant for steel fragment penetration

β_2 target material constant for steel fragment penetration

γ specific weight; constant for cohesive soil penetration; target material constant for steel fragment penetration

γ_1 target material constant for steel fragment penetration

γ_2	target material constant for steel fragment penetration
γ_c	specific weight of concrete
γ_o	specific weight of air
ΔH	heat of detonation
δ	permanent deflection of target at point of impact; constant for cohesive soil penetration
$\bar{\delta}$	dimensionless deflection
ϵ	constant for cohesive soil penetration
θ	subtended angle of a sector; angle between line of flight of fragment and normal to plate surface
λ	target material constant for steel fragment penetration
λ_2	target material constant for steel fragment penetration
ν	Poisson's ratio
ν_{xz}	partial correlation coefficient between fragment density and dispersion angle
ν_{yz}	partial correlation coefficient between fragment density and distance
ρ	density; peak density of blast wave; soil mass density
$\rho_{Comp\ B}$	density of Comp B explosive
ρ_c	weight density of concrete
ρ_{expl}	density of explosive
ρ_i	average fragment density over a range interval
ρ_o	density of air
ρ_p	density of fragment (projectile)
ρ_s	density of a constrained object
ρ_t	density of target
ρ_1	density of fragment material
ρ_2	density of target material

σ ultimate strength of target material

σ_t yield stress of target material

σ_y cohesive yield strength of soil

$\bar{\sigma}$ effective resisting soils stress related to total stress divided by soil density

ϕ least angle between any flat fragment surface and the plate surface

ϕ_c critical orientation angle for shatter

6.10 REFERENCES

6.1   Zaker, T. A., "Fragment and Debris Hazards," Technical Paper
      No. 12, Dept. of Defense Explosives Safety Board, July 1975, AD
      A013 634.

6.2   Zaker, T. A., "Computer Program for Predicting Casualties
      and Damage from Accidental Explosions," Technical Paper No. 11,
      Dept. of Defense Explosives Safety Board, May 1975, AD A012 847.

6.3   Baker, W. E., Kulesz, J. J., Ricker, R. E., Bessey, R. L., Westine,
      P. S., Parr, V. B. and Oldham, G. A., "Workbook for Predicting
      Pressure Wave and Fragment Effects of Exploding Propellant Tanks
      and Gas Storage Vessels," NASA CR-134906, NASA Lewis Research
      Center, September 1977.

6.4   Rinehart, J. S., Stress Transients in Solids, Hyperdynamics,
      Santa Fe, NM.

6.5   Baker, W. E., Hokanson, J. C. and Cervantes, R. A., Model
      Tests of Industrial Missiles," Final Report, SwRI Project 02-9153-
      001, Southwest Research Institute, San Antonio, TX, May 1976.

6.6   Structures to Resist the Effects of Accidental Explosions ,
      Dept. of the Army Technical Manual TM 5-1300, Dept. of the Navy
      Publication NAVFAC P-397, Dept. of the Air Force Manual AFM 88-22,
      Dept. of the Army, the Navy, and the Air Force, June 1979.

6.7   Healey, J., Werner, H., Weissman, S., Dobbs, N., Price, P.,
      "Primary Fragment Characteristics and Impact Effects on Protective
      Barriers," Picatinny Arsenal Technical Report No. 4093, Amman and
      Whitney, Consulting Engineers, New York, NY, December 1975.

6.8   Thomas, L. H., "Computing the Effect of Distance on Damage by
      Fragments," Report No. 468, BRL, Aberdeen Proving Ground, MD,
      May 1944.

6.9   Gurney, R. W., "The Initial Velocities of Fragments from Bombs,
      Shells and Grenades," Report No. 648, Ballistic Research Laboratory,
      Aberdeen Proving Ground, MD, September 1947.

6.10 Henry, I. G., "The Gurney Formula and Related Approximations for
      High-Explosive Deployment of Fragments," Report No. PUB-189,
      Hughes Aircraft Co., Culver City, CA, 1967, Ad 813 398.

6.11 "Behavior and Utilization of Explosives in Engineering Design and
      Biomechanical Principles Applied to Chemical Medicine," Proceedings
      of the 12th Annual Symposium American Society of Mechanical Engineers,
      March 1972.

6.12 Kury, J. W. et al., "Metal Acceleration by Chemical Explosives," _Fourth Symposium (International) on Detonation_, ONR ACR-126, January 13, 1965.

6.13 Kennedy, J. E., "Gurney Energy of Explosives: Estimation of the Velocity and Impulse Imparted to Driven Metal," Sandia Report SC-PR-70-790, December 1970.

6.14 "Effects of Impact and Explosion," Vol. 1, Office of Scientific Research and Development, National Defense Research Committee, Washington, DC, 1946.

6.15 Johnson, C. and Moseley, J. W., "Preliminary Warhead Terminal Ballistic Handbook, Part 1, Terminal Ballistic Effects," NAVWEPS Report No. 7673, U. S. Naval Weapons Laboratory, Dahlgren, VA, March 1964.

6.16 Baker, W. E., Kulesz, J. J., Ricker, R. E., Westine, P. S., Parr, V. B., Vargas, L. M., and Moseley, P. K., "Workbook for Estimating the Effects of Accidental Explosions in Propellant Handling Systems," NASA Contractor Report 3023, Contract NAS 3-20497, NASA Lewis Research Center, August 1978.

6.17 U. S. Energy Research and Development Administration Albuquerque Operation Office, "Report of Investigation of the Explosion with Fatal Injuries in Bldg. 11-14A on March 30, 1977 at the Pantex Plant - Amarillo, Texas," June 28, 1977.

6.18 Hoerner, S. F. _Fluid-Dynamic Drag_, Midland Park, NJ, 1958.

6.19 Westine, P. S. and Kineke, J. H. Jr. (1978), "Prediction of Constrained Secondary Fragment Velocities," _The Shock and Vibration Bulletin 48_, Part 2, Isolation and Damping, Impact, Blast, A publication of the Shock and Vibration Information Center, Naval Research Laboratory, Washington, DC, September 1978.

6.20 Kineke, J. H. Jr., "Secondary Fragment Speed with Unconfined Explosives: Model and Validation," _Minutes of the Seventeenth Explosives Safety Seminar_, Vol. II, September 1976.

6.21 Baker, W. E., "Prediction and Scaling of Reflected Impulse from Strong Blast Waves," _Int. Jour. Mech. Sci._, 9, 1967, pp. 45-51.

6.22 Weals, F. H., "Tests to Determine Separation Distances of Earth-Covered Magazines," _Annals of the New York Academy of Sciences_, Vol. 152, Art. 1, October 1968.

6.23   Bergman, S. G. A., "Swedish Protective Structures for Manufacturing Units Constituting Explosion Hazard in the Range 1 - 2,000 Pounds of TNT," Annals of the New York Academy of Sciences, Vol. 152, Art. 1, October 1968.

6.24   Hahn, G. J. and Shapiro, S. S., Statistical Methods in Engineering, John Wiley and Sons, Inc., New York, NY, 1967.

6.25   Kulesz, J. J., Moseley, P. K., and Parr, V. B., "Prediction of Weight and Range Distributions from Accidental Explosions Inside Buildings," to be presented at the Nineteenth DoD Explosives Safety Seminar, September 9-11, 1980.

6.26   Baker, W. E., Westine, P. S., and Dodge, F. T., Similarity Methods in Engineering Dynamics: Theory and Practice of Scale Modeling, Spartan Brooks, Rochelle Part, NJ.

6.27   McNaughtan, I. I. and Chisman, S. W., "A Study of Hail Impact at High Speed on Light Alloy Plates," Proceedings of the Ninth Annual National Conference on Environmental Effects on Aircraft and Propulsion Systems, Naval Air Propulsion Test Center, October 7-9, 1969, pp. 16-19.

6.28   "Suppressive Shields Structural Design and Analysis Handbook," HNDM-1110-1-2, U. S. Army Corps of Engineers, Huntsville Division, Huntsville, AL, November 1977.

6.29   Ricchiazzai, A. J. and Barb, J. C., "A Tentative Model for Predicting the Terminal Ballistic Effects of Blunt Fragments Against Single and Spaced Targets: A Comparison of Predicted and Experimental Test Results," BRL MR 2578, Aberdeen Proving Ground, MD, January 1976.

6.30   Vassallo, F. A., "Missile Impact Testing of Reinforced Concrete Panels," Calspan Report No. HC-5609-D-1, Final Report, Buffalo, NY, January 1975.

6.31   Stephenson, A. E., "Full-Scale Tornado-Missile Impact Tests," EPRI-NP-440, Project 399, Final Report, Electric Power Research Institute, Palo Algo, CA July 1977.

6.32   Stephenson, A. E., Sliter, G. and Burdette, E., "Full-Scale Tornado-Missile Impact Tests Using a Rocket Launcher," Second ASCE Specialty Conf. on Structural Design of Nuclear Plant Facilities, Vol. 1-A, New Orleans, LA, December 1975, pp. 611-636.

6.33   Jankov, Z. D., Shananhan, J. A., and White, M. P., "Missile Tests of Quarter Scale Reinforced Concrete Barriers," Proceedings of the Symposium on Tornadoes, Assessment of Knowledge and Implications for Man, Texas Tech University, June 22-24, 1976, pp. 608-622.

6.34 Rotz, J. V., "Results of Missile Impact Tests on Reinforced Concrete Panels," Second ASCE Specialty Conf. on Structural Design of Nuclear Plant Facilities, Vol. 1-A, New Orleans, LA, December 1975, pp. 720-738.

6.35 Ting, R. M. L., "Non-Composite and Composite Steel Panels for Tornado Missile Barrier Walls," Second ASCE Specialty Conf. on Structural Design of Nuclear Plant Facilities, Vol. 1A, New Orleans, LA, December 1975, pp. 663-687.

6.36 Barber, R. B., "Steel Rod/Concrete Slab Impact Test (Experimental Simulation)," Technical Development Program, Final Report, Job No. 90142, Scientific Development, Bechtel Corp., October 1973.

6.37 Gueraud, R., Sokolovsky, A., Kavyrchine, M. and Astruc, M., "Study of the Perforation of Reinforced Concrete Slabs by Rigid Missiles - General Introduction and Experimental Study, Part I," Nuclear Engineering and Design, No. 41, 1977, pp. 97-102.

6.38 Fiquet, G. and Dacquet, S., "Study of the Perforation of Reinforced Concrete by Rigid Missiles - Experimental Study, Part II," Nuclear Engineering and Design, No. 41, 1977, pp. 103-120.

6.39 Goldstein, S. and Berriaud, C., "Study of the Perforation of Reinforced Concrete Slabs by Rigid Missiles - Experimental Study, Part III," Nuclear Engineering and Design, No. 41, 1977, pp. 121-128.

6.40 Westine, P. S. and Vargas, L. M., "Design Guide for Armoring Critical Aircraft Components to Protect From High-Explosive Projectiles," Final Report, Contract F33615-77-C-3006, U. S. Air Force Flight Dynamics Laboratory, August 1978.

6.41 Baker, W. E., Cox, P. A., Westine, P. S., Kulesz, J. J., and Strehlow, R. A., A Short Course on Explosion Hazards Evaluation, Copyright 1978, Southwest Research Institute, San Antonio, TX.

6.42 "A Comparison of Various Materials in Their Resistance to Perforation by Steel Fragments, Empirical Relationships," TR#25, Ballistics Research Laboratory, Aberdeen Proving Ground, MD, July 1956.

6.43 "The Resistance of Various Non-Metallic Materials to Perforation by Steel Fragments, Empirical Relationships for Fragment Residual Velocity and Residual Weight," TR#51, Ballistics Research Laboratory, Aberdeen Proving Ground, MD, April 1963.

6.44 Greenfield, S. H., "Hail Resistance of Roofing Products," U. S. Dept. of Commerce, National Bureau of Standards, Building Science Series 23, August, 1969.

6.45 Westine, P. S., "Prediction of Fragment Displacement Velocity and Force on Projectiles Penetrating Cohesive Soils," Journal of Terra Mechanics, Vol. 12, No. 3/4, December 1975, pp. 149-170.

6.46 Young, C. W., "The Development of Empirical Equations for Predicting Depth of an Earth-Penetrating Projectile," Report No. SC-DR-67-60, Sandia Laboratory, May 1967.

6.47 Thompson, L. J., Ferguson, G. H. III, Murff, V. D., and Cetiner, A., "The Effects of Soil Parameters on Earth Penetration of Projectiles," Texas A&M Research Foundation Report No. PB 186074, for Sandia Corp., July 1969.

6.48 Butler, D. K., "Development of a High-Velocity Powder Gun and Analysis of Fragment Penetration Tests into Sand," Miscellaneous Paper S-75-27, ADA 017056, Soils and Pavements Laboratory, U. S. Army Engineer Waterways Experiment Station, Vicksburg, MI, October 1975.

6.49 Greenspon, J. E., "An Approximate Nondimensional Representation of the THOR Equations," U. S. Army Materiel Systems Analysis Activity, TR#173, October 1976.

6.50 Ballistic Analysis Laboratory, Johns Hopkins University,"The Resistance of Various Metallic Materials to Perforation by Steel Fragments; Empirical Relationships for Fragment Residual Velocity and Residual Weight," Institute tor Cooperative Research, Project THOR Technical Report No. 47, April 1961.

6.51 Sperrazza, J. and Kokinakis, W., "Ballistic Limits of Tissue and Clothing," Technical Note No. 1645, Army Ballistic Research Laboratories, RDT&E Project No. 1P025601A027, Ballistic Research Laboartories, January 1967.

6.52 Kokinakis, W., "A New Methodology for Wounding and Safety Criteria," Proceedings of the 16th Explosive Safety Seminar, September 1974, pp. 1209-1226.

6.53 Glasstone, S. , The Effects of Nuclear Weapons, U. S. Government Printing Office Revised Edition, April 1962.

6.54 Fletcher, E. R., "A Model to Simulate Thoracic Responses to Air Blast and to Impact," Aerospace Medical Research Laboratory, Paper No. 1, Wright-Patterson Air Force Base, Ohio, AD 740-438, December 1971.

6.55 White, C. S., Bowen, I. G., Richmond, D. R., and Corsbie, R. L. "Comparative Nuclear Effect of Biomedical Interest," CEX-58.8, Civil Effects Study, U. S. Atomic Energy Commission, January 1961.

6.56 Custard, G. H. and Thayer, J. R., "Evaluation of Explosive Storage Safety Criteria," Falcon Research and Development Co., Contract DAHC 04-69-C-0095, March 1970; also "Target Response to Explosive Blast," September 1970.

6.57 Ahlers, E. B., "Fragment Hazard Study," Minutes of the Eleventh Explosives Safety Seminar, Vol. 1, Armed Services Explosives Safety Board, Washington, DC, September 1969.

6.58 Clemedson, C. J., Hellstrom, G., and Lingren, S., "The Relative Tolerance of the Head, Thorax, and Abdomen to Blunt Trauma," Annals of the New York Academy of Sciences, Vol. 152, Art. 1, pp. 187+, October 1968.

6.59 White, C. S., "The Nature of the Problems Involved in Estimating the Immediate Casualties from Nuclear Explosions," CEX-71.1, Civil Effects Study, U. S. Atomic Energy Commission, DR-1886, July 1971.

6.60 Baker, W. E., Whitney, M. G., and Parr, V. B., "Scaling of Initiation of Explosives by Fragment Impact," (submitted to 50th Shock and Vibration Symposium).

6.61 Slade, D. C. and Dewey, J., "High Order Initiation of Two Military Explosives by Projectile Impact," BRL Report No. 1021, Aberdeen Proving Ground, MD, July 1957, AD 145868.

6.62 McLean, D. G. and Allan, D. S., "An Experimental Program to Determine the Sensitivity of Explosive Materials to Impact by Regular Fragments," Final Report, Contract DA-19-020-ORD-5617, Picatinny Arsenal, December 29, 1965, AD 477875.

6.63 Petino, G. Jr. and Leondi, M. F., "Sensitivity of Molten and Solid Amatex Charges to Impact by Primary Steel Fragments," ARLDC-CR 78011, ARRADCOM, Dover, NJ, April 1978.

6.64 Petino, G. Jr., Demella, D., and Rindner, R. M., "Sensitivity of Cased Charges of Molten and Solid Composition B to Impact by Primary Steel Fragments," PA-TR-4975, Picatinny Arsenal, Dover, NJ, June 1976.

6.65 Frey, R. B., Howe, P. M., Trimble, J., and Melani, G., "Initiation of Explosives by Projectile Impact," Draft Technical Report, USA BRL, June 1979.

6.66 Reeves, H. J., "An Empirically Based Analysis on the Response of HE Munitions to Impact by Steel Fragments," BRL MR 2031, U. S. Army Ballistic Research Laboratory, March 1970, AD 508607.

6.67   TERA Group, New Mexico Institute of Mining and Technology,
       "Vulnerability of 105 mm HE Projectiles to Fragment Impact,"
       Final Report for Contract No. DAAD05-76-C-0789, U. S. Ballistic
       Research Laboratory, August 1978.

6.68   Dobratz, B. M., "Properties of Chemical Explosives and Explosive
       Simulants," University of California, Livermore, CA, July 1974
       (UCRL-51319).

CHAPTER 7

DYNAMIC PROPERTIES OF MATERIALS

7.1 INTRODUCTION

It is well known that materials behave differently under dynamic loading than under static conditions. For most materials, the deformation during loading is not only a function of the amplitude of the applied force but also the rate of application and duration of the force. Optimized design of structures and utilization of materials requires an adequate description and understanding of the material properties at the appropriate rates of loading (or rates of deformation, i.e., strain rates).

Various procedures have been developed to study and quantify the response of materials to dynamic (or impulsive) loads. The principal variables measured in these tests include the stresses and strains produced during loading and the energy absorbed by the specimen. These tests divide naturally into two diverse groups since the stress and strain measurements may be considered properties of the material being studied whereas the energy measurements are related to the geometry of the specimen as well as a variety of the specimen's material properties.

The main purpose of this chapter is to present a review of the material properties which are of interest to the structural engineer, with special emphasis on those which vary with the rate of loading. This information is given in Section 7.2. In Section 7.3, a discussion is given of various measures of a material's ability to absorb energy under dynamic loading. Pertinent material properties are considered. Finally, properties of the materials commonly used in construction are tabulated in Section 7.4. Included in these properties are those dynamic values based on rates of loading applicable to design of structures for blast loads.

Under dynamic loads associated with explosion, strain rates in materials may be in the range of 1 to 100 in./in./sec. If the actual strain rate is known, increases in the material strength can be obtained using the dynamic relationships given in Section 7.2. These relationships are especially useful in conjunction with numerical methods. If the actual rate of strain is not known, the dynamic properties must be based on some average or minimum value of strain rate. Section 7.4, which tabulates properties of various structural materials, includes minimum values of dynamic strength for strain rates of 1 and 100 in./in./sec.

For the design of structures subject to blast loading, engineers typically use a dynamic increase factor (DIF) to account for the dynamic behavior of materials. Values of DIF for various materials used in

facility construction are given in authoritative design manuals or codes. Since this manual is not intended as an independent design guide for DIF, engineers should consult these applicable design manuals or codes for the selection of appropriate DIFs for their design.

7.2 PROPERTIES OF MATERIALS OF CONSTRUCTION UNDER DYNAMIC LOADING

A variety of materials is used in the construction of typical blast-resistant structures. These include: (1) the structural metals, steel and aluminum; (2) concrete and masonry, including reinforced concrete, clay tile block, and brick; (3) woods, such as Southern yellow pine and Douglas fir; and (4) weak, brittle materials, such as insulating roof panels and wallboard. Each of these types of materials displays strain-rate sensitivity in its response to loading. For that reason, a review of each material type is presented in this section. A general review will be made of material properties which are of interest to the structural designer along with a brief discussion of those properties which may vary with the rate of loading.

The material properties most commonly used in design are obtained from "static" uniaxial tension and compression tests. [So-called static strain rates are commonly on the order of 0.0001 in./in./sec (10^{-4} sec^{-1})]. It is customary to plot the results in the form of a stress-strain diagram, such as the one shown in Figure 7.1a. Various properties can be seen in this figure. An initial region is shown in which the stress is linearly proportional to strain. The material behaves in an essentially elastic manner in this region, and the slope of the stress-strain curve is called the modulus of elasticity, E. The termination of the elastic regime is impossible to obtain experimentally since the measurement of slight amounts of plasticity would require perfect instrumentation. The beginning of plastic flow is more practically defined in terms of the stress required to cause some measurable amount of plastic strain. The yield strength, σ_y, is defined often as the stress at which material exhibits a specified deviation from the proportionality of stress to strain. In Figure 7.1a, the yield strength is taken to be the stress at which the strain is offset 0.2 percent from the proportional strain. The ultimate stress, σ_u, is the maximum stress sustained by the material. The elongation, e, is the strain sustained by the material at failure.

The existence of an elastic region varies with materials. Figure 7.1b shows the uniaxial compression curve for materials such as wood and concrete in which little or no proportional region is detectable. For these materials, various definitions are used for modulus of elasticity, including: (1) the tangent modulus, E_T, which is the slope of the stress-strain curve at a given stress, normally the origin; (2) the
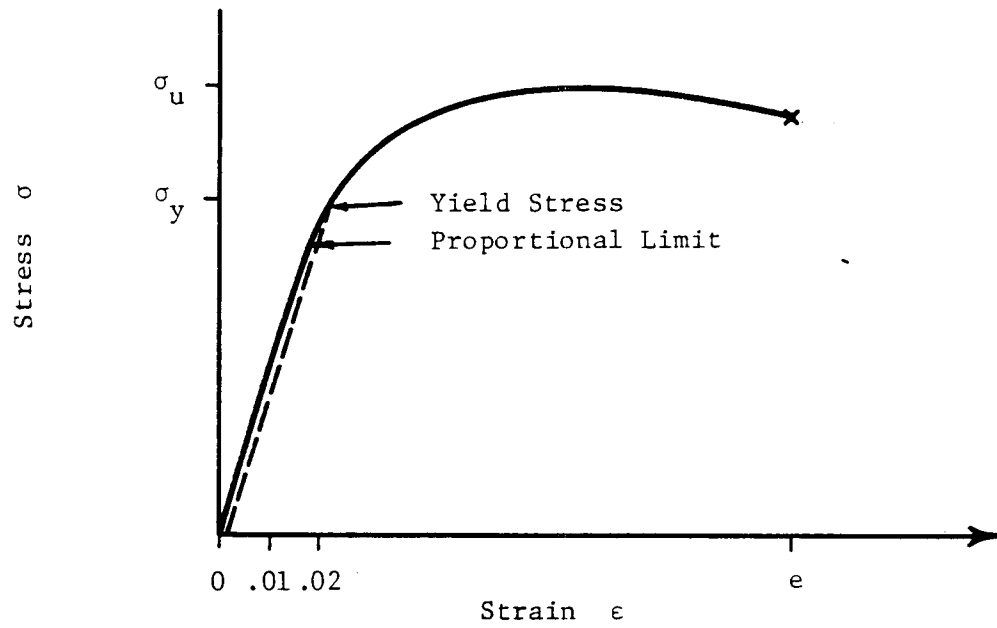
a) General Stress-Strain Curve
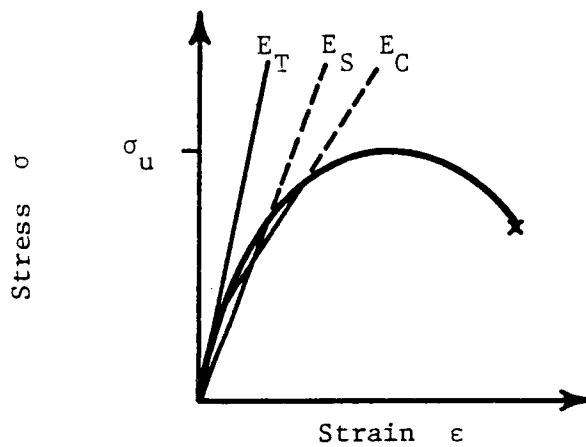
b) Typical Curve for Wood or
    Concrete
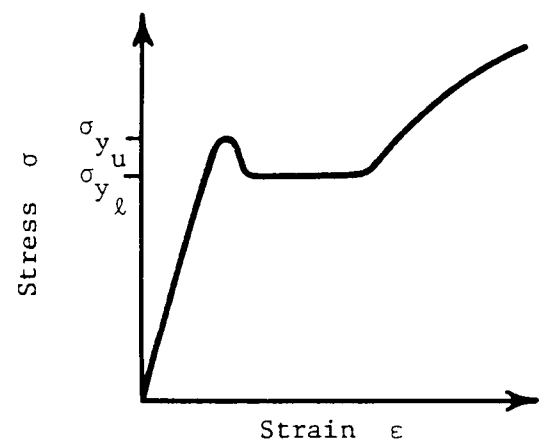
c) Typical Curve for Low-Carbon,
    Structural Steel

Figure 7.1. Typical Stress-Strain Curves for Engineering Materials

secant modulus E_s, which is the slope of the secant drawn from the origin to any specified point on the stress-strain curve; and (3) the chord modulus, E_c, which is the slope of the chord drawn between any two specified points on the stress-strain curve.

For a few materials, notably the low carbon structural steels, a region exists after initial yield in which the amount of stress required to attain a unit increase in strain actually decreases. This behavior, shown in Figure 7.1c, results in the existence of an upper-yield stress, σ_{y_u}, and a lower-yield stress, σ_{y_ℓ}. Subsequent to this behavior, the stress-strain curve rises to an ultimate stress which is substantially greater than either yield stress.

For brittle materials, sporadic results often occur in uniaxial tension tests. For materials such as wood or concrete, it is very difficult to clamp typical design tensile specimens. Therefore, tensile properties for these materials are often obtained from standard flexural or bend tests. In these tests, the specimen is supported at two points and loaded at a third point. Loading is continued until failure occurs. The specimens are designed so that they will fail in tension at the outer surface. Based on the various dimensions of the specimen and test setup and the load required to cause failure, several material properties are determined. The modulus of rupture, R, is calculated using the relation

$$R = \frac{MC}{I} \qquad (7.1)$$

where M = maximum bending moment due to the load
     C = one-half the depth of the beam
     I = moment of inertia of the cross section

The exact significance of this parameter is not clear. Equation (7.1) is the equation for calculating the outer fiber tensile stress in an elastic beam under load. If the stress-strain relationship of the specimen were linear to the point of failure, R would correspond to the ultimate tensile stress. However, most of the materials tested in this fashion display a stress-strain curve similar to Figure 7.1b in which little or no proportionality exists. For this reason, the modulus of rupture should be used more as a qualitative measure of a material's ductility or brittleness than as a quantitative number to be used directly in design.

The material properties which are normally sensitive to the rate of loading are the material strengths and the total elongation at failure. The property most often studied is the yield stress of the material. It is not uncommon for the yield stress to be double the static value for strain rates of 100 sec^{-1}. An increase in ultimate stress often occurs, although not as dramatically as for the yield stress.

Measurements of the total elongation to failure are very hard to obtain for very high rates of loading, i.e., strain rates greater than 1 sec^{-1}. Thus, some reported values of elongation or toughness (area under the stress-strain curve) may be questionable for these high rates of loading. These values will only be given in this section for those cases where there is a high confidence in the accuracy of these data.

7.2.1 Properties of Metals

In the construction of blast-resistant structures, steel and aluminum are the only metals normally used. Various grades of steel are utilized based on the application. A discussion of both the static and dynamic properties of these grades of steel is given in this section. Information on aluminum 6061 is also provided.

7.2.1.1 Static Behavior

The shape of the static stress-strain curve for a steel depends upon the exact alloy content and the stress and temperature history. Stress-strain curves of typical alloy steels are given in Figure 7.2. The curves for the low carbon steels display upper and lower yield points. For design purposes, the lower yield point is considered to represent the practical yield strength. The heat-treated steels do not display these double yield points.

The low carbon steels are preferred for use in construction because of their high ductility. For many years the most common steel used was a low-carbon steel designated by ASTM Specification A7. This was the predominant steel used in the construction of buildings. This steel has now been supplanted by ASTM A36 as the all-purpose construction steel. There are, however, 13 ASTM specifications for structural steels currently approved for use in building construction (Ref. 7.1).

Of these 13, those most commonly used in the construction of buildings are ASTM A36, ASTM A529 structural carbon steel, ASTM A440 high-strength structural steel, ASTM A570 hot-rolled carbon steel sheet and strip, ASTM A441 and A572 high-strength low-alloy structural steels, ASTM A242 and A588 corrosion-resistant high-strength low-alloy structural steels, and ASTM A514 quenched and tempered alloy structural steel plate.

The standard specifications for J-Series and H-Series open-web steel joists (Ref. 7.1) states that the manufacture of chord and web sections shall conform to one of the previously mentioned ASTM specifications or to ASTM A611, Type 2, cold-rolled carbon sheet. The steel used for J-Series joists shall have a minimum yield point of 36,000 psi in the hot-rolled condition prior to forming or fabrication. The design of chord sections for H-Series joists shall be based on a yield point of 50,000 psi. The design of web sections for H-Series joists shall be based on a yield point of either 36,000 psi or 50,000 psi.
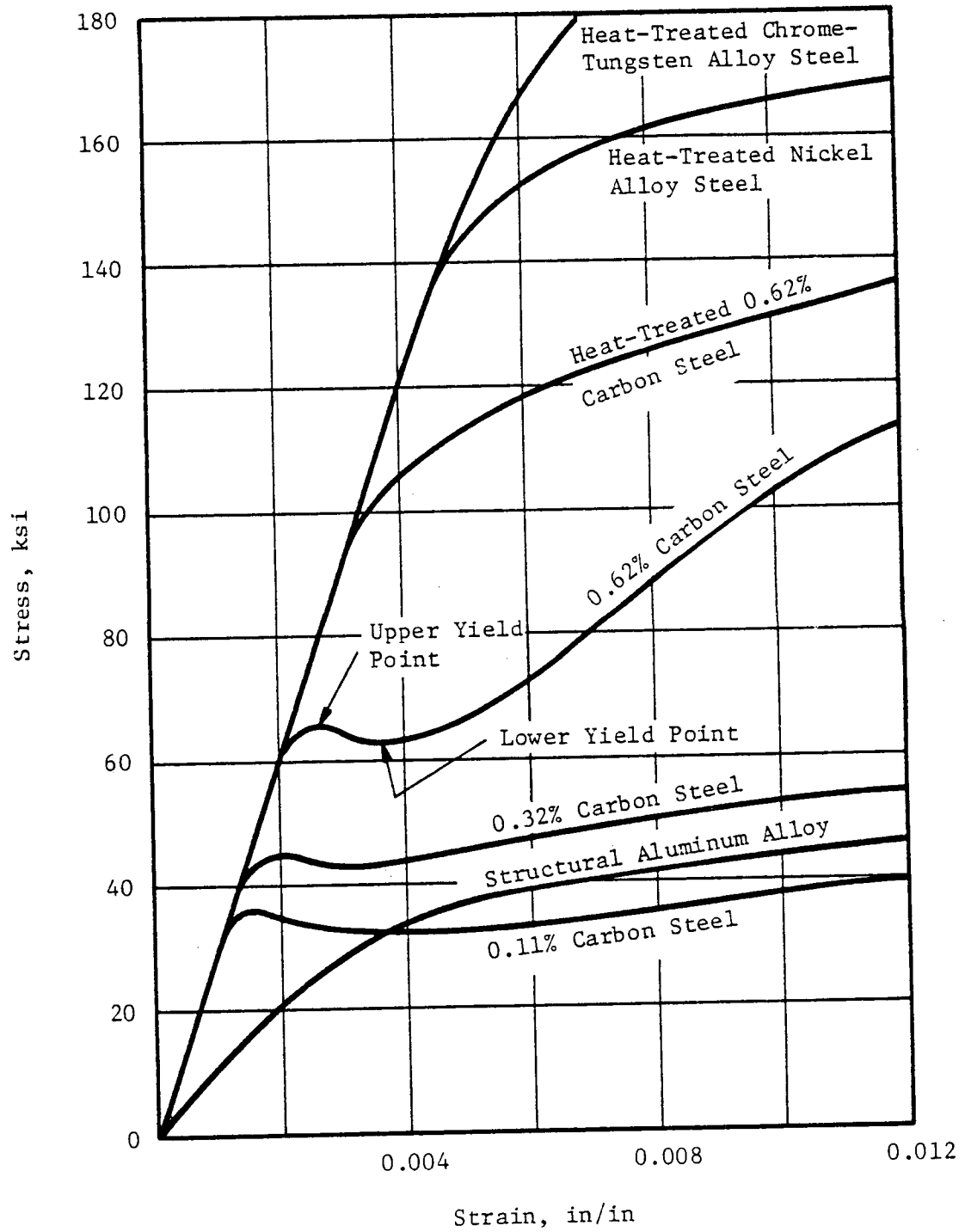
Figure 7.2. Stress-Strain Curves of Typical
Alloy Steels and Structural Aluminum

In the reinforcement of concrete, ASTM A615 deformed and plain billet-steel bars are used. Grade 40 has a minimum yield strength of 40,000 psi and Grade 60 a minimum yield strength of 60,000 psi.

Aluminum 6061 combines good strength with relatively good ductility. It is usually used in a heat-treated condition designated by T4, with a minimum ultimate tensile stress of 30 ksi and T6, with a minimum tensile ultimate stress of 42 ksi.

The minimum static tensile properties for both the structural steels and aluminum are given in Section 7.4.

7.2.1.2 Dynamic Behavior

Under dynamic loading conditions, the strength properties of many structural steels will be altered. In general, the yield strengths and ultimate tensile strengths are higher under the high strain rates associated with blast loads ($\dot{\varepsilon}$ = 1 to 100 sec^{-1}) than under slowly applied "static" loads. In view of the uncertainties involved in determining the blast response of structures, however, great precision in evaluation of strain rate effects is not normally justified. It is generally accepted that strain rate effects resulting from air blast loading can be estimated to increase the static tensile yield strength of structural steels by a minimum of 10 percent (Ref. 7.2). Under certain conditions the increase in yield strength may be much greater. The higher strength steels ($\sigma_y > 60,000$ psi), without definite yield points and pronounced plastic ranges, have not been found to exhibit as high an increase as other structural steels. Unless the actual strain rates can be determined, it is recommended that the dynamic yield strengths of high strength steels be taken equal to their static values. Similarly, without knowledge of actual strain rates, the dynamic ultimate strengths for all steels should be taken equal to their static values. The dynamic shear yield strengths for all steels are normally taken equal to 0.55 times the dynamic tensile yield strengths. The modulus of elasticity is effectively unchanged with rate of strain.

If the actual strain rates in a structure can be accurately determined, more accurate estimates can be made of the material strengths for purposes of design. To this end, relationships between the rate of strain and the strengths of various structural steels will now be given.

A large amount of high-rate testing has been conducted on low carbon steels (Refs. 7.3, 7.4, 7.5, and 7.6) and should be applicable to many of the structural steels. A typical set of data is shown in Figure 7.3. A review of all data on low carbon steels results in the

following relationship between the dynamic yield stress and the strain rate:

$$\frac{\sigma_{dy}}{\sigma_y} = 1.3 + 0.25 \log \dot{\epsilon} \quad (1 < \dot{\epsilon} < 100 \text{ sec}^{-1})* \qquad (7.2)$$

where the dynamic yield stress is denoted by σ_{dy} and the static value by σ_y. This equation is a conservative estimate of the data given in Reference 7.5 and results in yield strength ratios, σ_{dy}/σ_y of 1.3 for $\dot{\epsilon} = 1$ sec^{-1} and 1.8 for $\dot{\epsilon} = 100$ sec^{-1}. There is much less dramatic effect on the ultimate tensile strength. The relationship between ultimate tensile strength and strain rate may be expressed:

$$\frac{\sigma_{dT}}{\sigma_T} = 1.10 + 0.1 \log \dot{\epsilon} \quad (1 < \dot{\epsilon} < 100 \text{ sec}^{-1}) \qquad (7.3)$$

which gives tensile strength ratios, σ_{dT}/σ_T, of 1.10 for $\dot{\epsilon} = 1$ sec^{-1} and 1.30 for $\dot{\epsilon} = 100$ sec^{-1}. In the work by Winlock (Ref. 7.4), the total deformation in a compression test was seen to increase with strain rate. However, this increase was small and it is not clear that it would occur during a tensile test. For these reasons, it is recommended that the total elongation be assumed independent of strain rate.

These relationships were developed for data of annealed low-carbon steels and should be applicable for ASTM A7, A36, A529, A440, A570, and A615. However, A611 Grade E is a cold-rolled steel with a minimum yield strength of 80 ksi. Based on studies of two similar materials (Ref. 7.3), a conservative estimate of the relationship for A611, Grade E may be written:

$$\frac{\sigma_{dy}}{\sigma_y} = 1.0 + 0.1 \log \dot{\epsilon} \quad (1 < \dot{\epsilon} < 100 \text{ sec}^{-1}) \qquad (7.4)$$

No data were given on the variation of tensile strength with strain rate.

Although most of the structural steels are low-carbon steels, several are low-alloy steels, including ASTM A242, A441, A572, A588, and A514. Of this group, tests have been conducted on A242 (Ref. 7.3). In these tests, the yield strength ratio was seen to fit the relationship most closely.

$$\frac{\sigma_{dy}}{\sigma_y} = 1.2 + 0.2 \log \dot{\epsilon} \quad (1 < \dot{\epsilon} < 100 \text{ sec}^{-1}) \qquad (7.5)$$

No data were given for the variation of tensile strength with strain rate.

---

*In this text, log A denotes $\log_{10} A$.
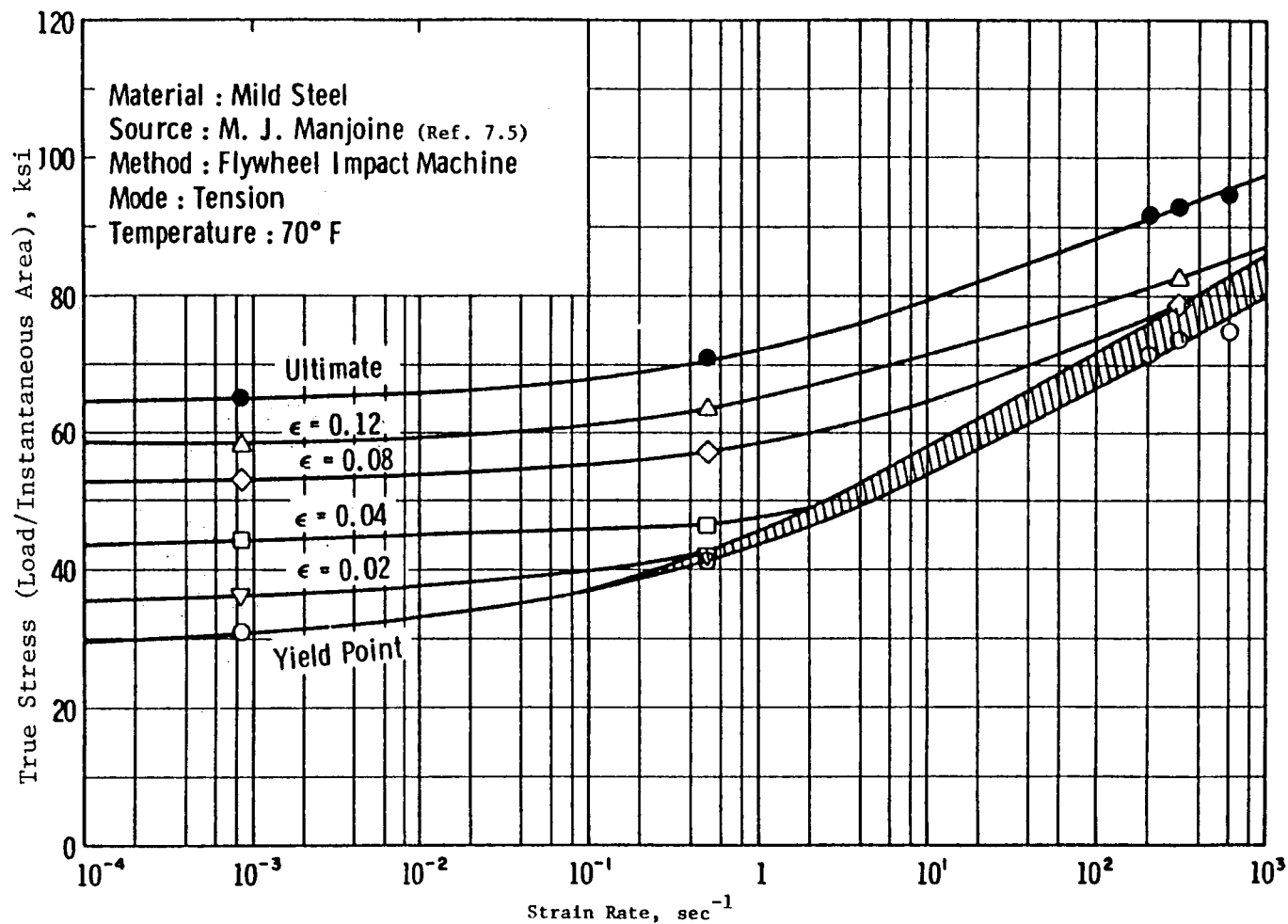
Figure 7.3 Stress-Strain Properties of Mild Steel at Various Strain Rates

No other data for the low-alloy steels have been found. However, a review of the literature (Ref. 7.7) has shown that alloying tends to decrease the rate sensitivity of steel, as was seen for A242 relative to the low-carbon steels. For this reason, a conservative estimate of the variation of strength with strain rate must be used. For A441, A572, and A588 which have minimum yield stresses varying from 42 to 65 ksi, the yield strength ratio will be assumed to have the form:

$$\frac{\sigma_{dy}}{\sigma_y} = 1.1 + 0.1 \log \dot{\varepsilon} \quad (1 < \dot{\varepsilon} < 100 \text{ sec}^{-1}) \qquad (7.6)$$

The ultimate tensile strength for these steels will be assumed independent of strain rate. For A514 with a minimum yield strength of 100 ksi, both strengths should be assumed independent of strain rate.

Because of its extensive use in aircraft and spacecraft construction, a great deal of research has been conducted on the strain rate sensitivity of aluminum. Extensive work on Aluminum 1100, summarized in Reference 7.6, has demonstrated moderate strain rate sensitivity. Similar studies (Ref. 7.8) of annealed 6061 (-0 condition) have demonstrated a very slight increase of yield stress for strain rates above 1 sec^{-1}. However, for structural grades of 6061 (-T4, -T451, -T6, -T651), numerous studies (Refs. 7.8, 7.9, and 7.10) have indicated that the yield stress increases less than 5 percent over the range of strain rates of 10^{-4} sec^{-1} to 10^2 sec^{-1}. Thus, properties of these structural grades of aluminum should be considered independent of strain rate.

7.2.2 Properties of Concrete and Masonry

Concrete may be considered to be a particulate reinforced composite material made up of fine and coarse stone aggregate in a matrix material made from portland cement and water. Its physical properties depend upon many factors, including such things as the properties of the cement and the aggregate portions of each, the size and distribution of aggregate, amount of water used, amount and quality of mixing, and age. Since it is often hard to control each of these when fabricating a structure, it may not be possible to predetermine the exact properties of the concrete. In the design process, the designer must assume some realistic values for the properties and make an effort to assure that the design properties are attained. In the fabrication process, samples of concrete must be taken to make test specimens for later determination of actual static properties.

7.2.2.1 Static Behavior

The most commonly used property of concrete is its compressive strength, f_c', which is measured in compression tests of standard cylinders. Since concrete gains strength as it ages, a time of 28 days has been established as the standard duration of aging prior to test. Typical data from compression testing are given in Figure 7.4. Maximum compressive strength is seen to occur at a strain of about 0.2 percent, and failure occurs near 0.4 percent. The effects of aging on the stress-strain curve can be seen very explicitly in Figure 7.5.

It should be noted in Figure 7.4 that the slope of the stress-strain curve is continually decreasing from initial loading up to the ultimate stress. Concrete has neither a definite proportional limit nor an elastic limit. Thus, various definitions have been given for the modulus of elasticity, as was explained in the introduction to Section 7.2. Various forms of the modulus were displayed in Figure 7.1b, including the tangent modulus, the secant modulus, and the chord modulus.

In compression testing, the only ASTM standard test methods for static modulus of elasticity of concrete, C469, stipulates the use of a chord modulus, with the lower point on the curve near the origin ($\varepsilon = 0.00005$) and the upper point corresponding to a stress equalling 40 percent of the strength of the concrete at the time of loading. The lower point is close to the origin but far enough removed to be free of possible irregularities in the strain readings caused by seating of the test machine plotters and strain measuring devices. The upper point is taken near the upper end of the working stress range assumed in design.

For concretes commonly employed in construction, the compressive strength, f_c', is normally in the range of 2,000 to 5,000 psi. For structural lightweight concrete, typical values for the modulus of elasticity measured in compression range from 1 to 3×10^6 psi and for normal weight concretes, the values range from 2 to 5×10^6 psi. A modulus of elasticity for concrete with unit weight of 90 to 155 pounds per cubic foot can be estimated with the empirical relationship (Ref. 7.12)

$$E_c = 33w^{1.5} \sqrt{f_c'} \text{ psi} \tag{7.7}$$

where w = unit weight of concrete, lb/ft^3

f_c' = specified compressive strength of conctete, psi

Since structural concrete is designed principally to be loaded in compression, very little emphasis has been placed on determining the response of concrete to uniaxial tensile loading. There is no standard test technique for attaining these data. The normal tension test used with metals does not work well due to difficulties in holding the test
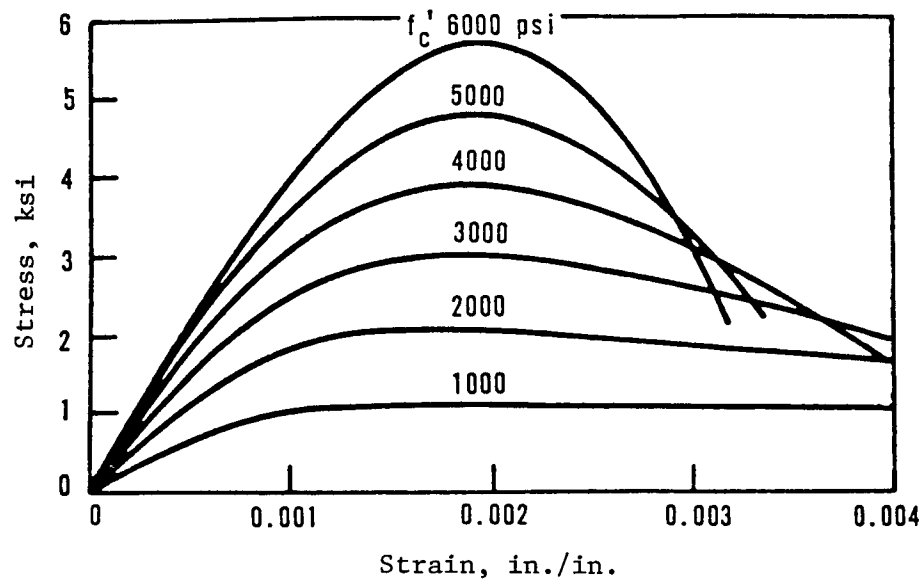
Figure 7.4. Typical Stress-Strain Curves for Concrete
(Ref. 7.11)
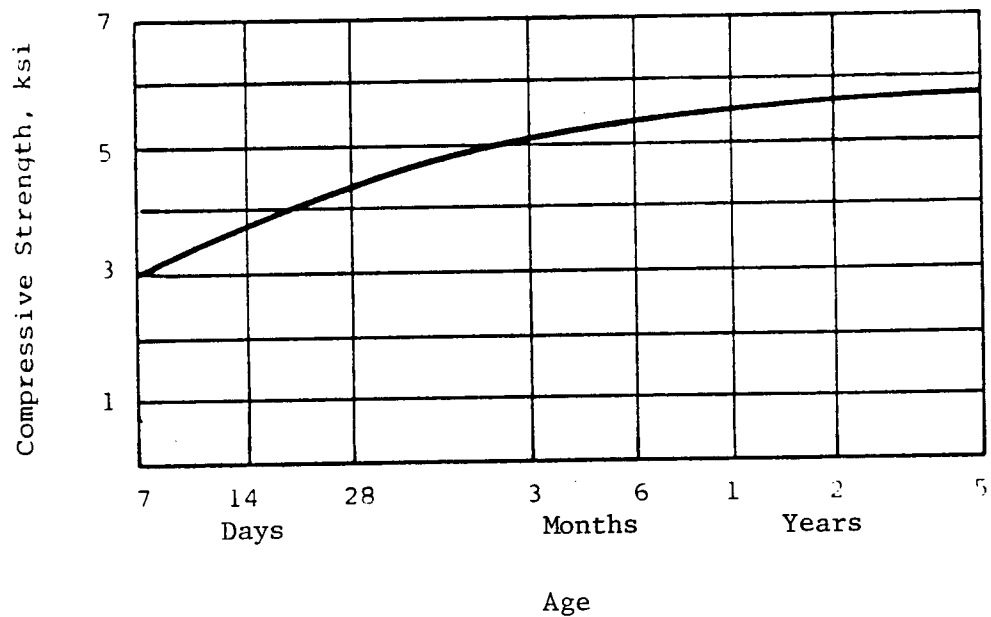
Figure 7.5. Effect of Age on Concrete Compressive
Strength f_c' (Ref. 7.11)

specimen, which may result in failure at the attachments or a nonuniform state of stress in the specimen. The most common method used to obtain tensile data is the three-point bend test, from which the modulus of rupture (tensile strength in flexure) is computed. An explanation of the modulus of rupture is given in the introduction to Section 7.2. Tests have shown that the values obtained for the modulus of rupture are substantially larger than those obtained from uniaxial tension tests. This discrepancy may be due to the incorrect assumption of stress linearity over the cross-sectional area of the beam used in the three-point bend test. As a rule, the modulus of rupture is roughly 10 to 15 percent of the compressive strength (Ref. 7.13).

7.2.2.2 Dynamic Behavior

Concrete possesses a rather high sensitivity to the rate of load application. Thus, the properties of concrete depend strongly on the strain rate. For those cases of design for which the rate of strain is not known, the generally accepted practice is to assume a 25 percent increase in the unconfined compressive strength of concrete due to rapid loading (Ref. 7.13). Similarly, a 10 percent increase is recommended in the direct shear strength of members due to rapid loading.

It is recommended that no increase in diagonal tension or bond strength be allowed for rapid loading. Table 7.1 summarizes dynamic increase factors (DIF) for stresses in concrete members for rapid loading.

Table 7.1 Dynamic Increase Factors for Concrete (Ref. 7.12)

Stress	Dynamic Increase Factor
Compression	1.25
Tension	1.0
Diagonal Tension	1.0
Direct Shear	1.1
Bond	1.0

If the actual strain rates in the structure can be accurately determined, more accurate estimates can be made of the material strengths for purposes of design. To this end, a discussion will now be presented of the relationships between the rate of strain and various properties of concrete.

A survey of the effects of loading rate on mechanical properties (Ref. 7.14) found a considerable increase in compressive strength, modulus of elasticity, and modulus of rupture. Figure 7.6 presents a compilation of data demonstrating the increase of compressive strength with rate of stressing.
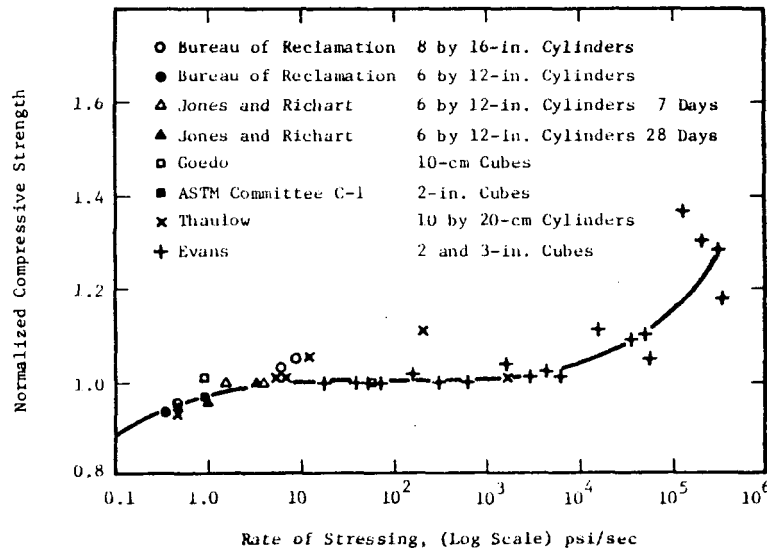
Figure 7.6 Increase of Compressive Strength, f_c', with Rate of Loading for Concrete (Normalized Relative to a Loading Rate of 30 psi/sec) (Reference 7.14)

The work by Watstein (Ref. 7.15) appears to be the most complete and informative program conducted on concrete. His work covered a wide range of strain rates and considered several properties of concrete. In his study, Watstein considered two concretes having approximate compressive strengths of 2500 and 6500 psi. The maximum ratio of dynamic to static compressive strengths was about 1.8 for rates of strain of 10 sec^{-1}. The values of the secant moduli of elasticity increased significantly with the rate of application of load; the maximum ratio of dynamic to static modulus was 1.47 for the "weak" concrete and 1.33 for the "strong" concrete. Resistance of the concrete to impact as measured by its ability to absorb strain energy also increased with strain rate. Figure 7.7 is a plot of compressive strength, f_c', and secant modulus of elasticity, E_s, as a function of strain rate. Typical stress-strain curves for static and dynamic tests are given in Figures 7.8 and 7.9 (data recording ceased after the compressive strength was reached). In Figure 7.8, results are given for static tests (strain rate of 10^{-6} sec^{-1}) and dynamic tests (10.0 sec^{-1}) of the "weak" concrete and in Figure 7.9, results are given for the static tests (10^{-6} sec^{-1}) and dynamic tests (6.69 sec^{-1}) of the "strong" concrete. Watstein also compared the increase in the secant modulus of elasticity with the corresponding increase in compressive strength. These data are presented in Figure 7.10. Watstein commented
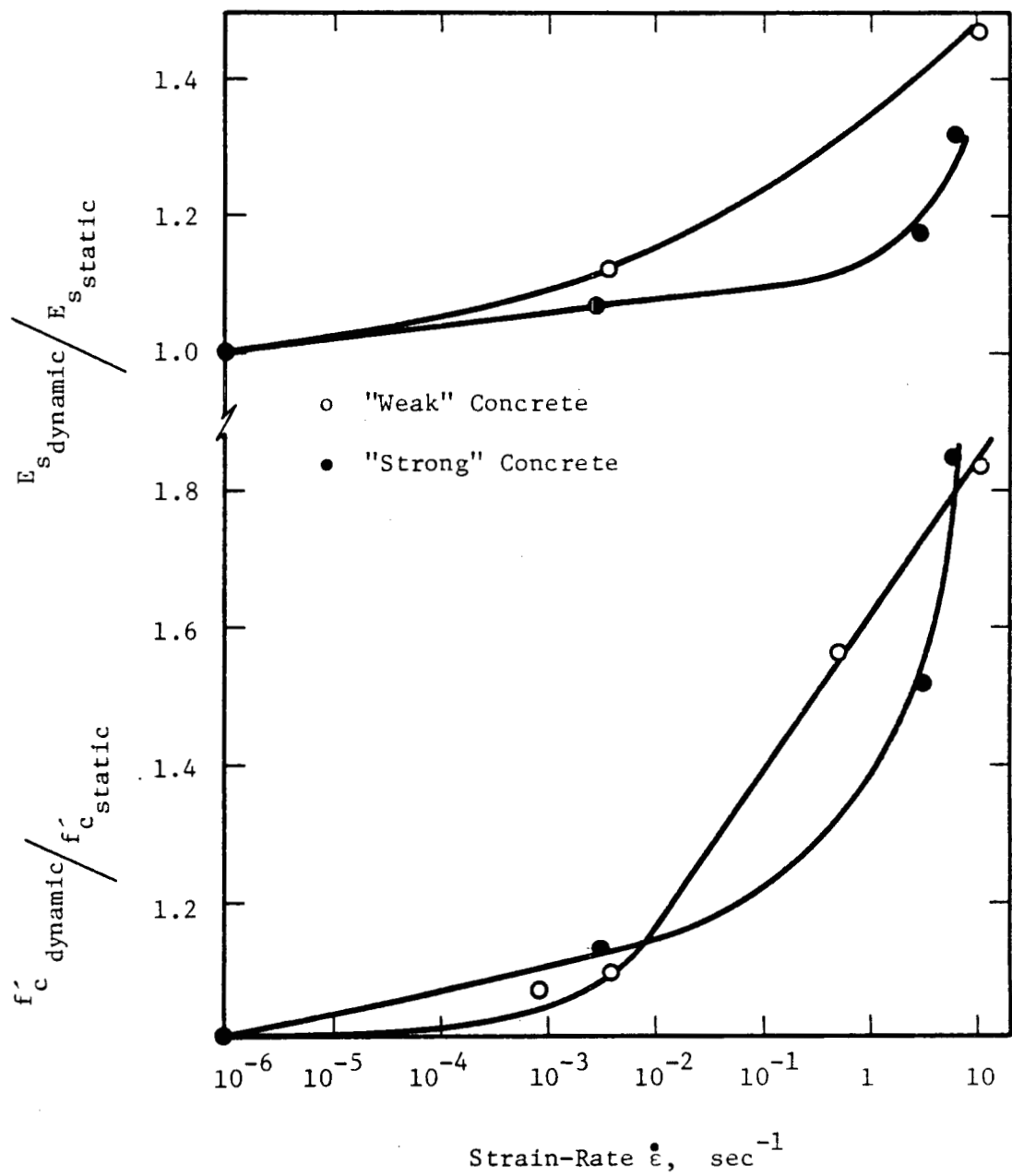
Figure 7.7   Increase of Compressive Strength with Rate
              of Strain for Concrete (Ref. 7.15)
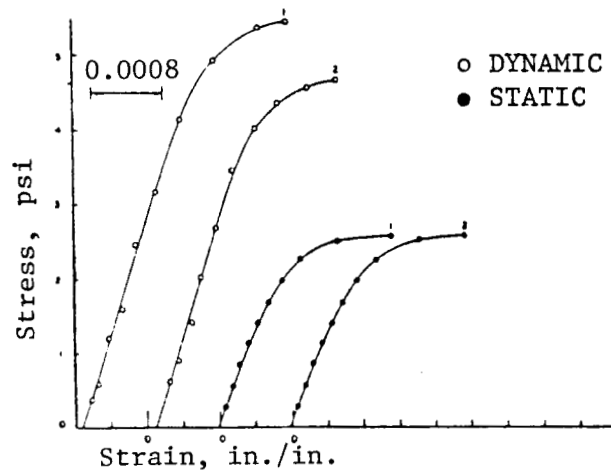
Figure 7.8. Typical Stress-Strain Curves for "Weak" Concrete, $\dot{\varepsilon} = 10.1$ sec^{-1} (Ref. 7.15)
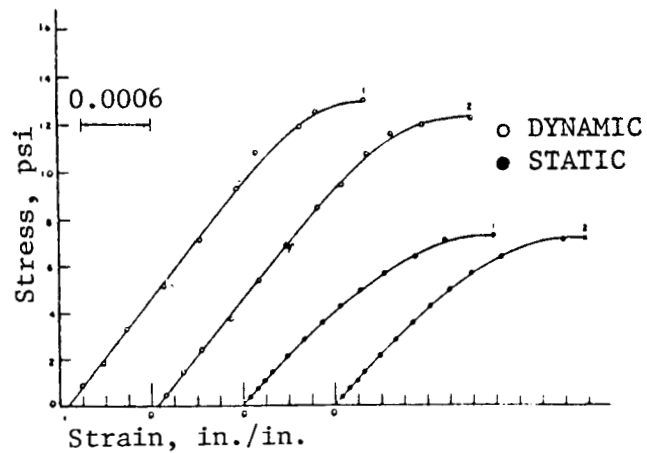
Figure 7.9. Typical Stress-Strain Curves for "Strong" Concrete, $\dot{\varepsilon} = 6.7$ sec^{-1} (Ref. 7.15)

that there was no significant difference in the manner of failure of the concrete test specimens in the dynamic and static tests.

It is apparent from Figures 7.8 and 7.9 that maximum stress occurs at comparable strains for both the static and dynamic tests. The obvious conclusion from this fact is that the strain energy to failure (area under the stress-strain curve up to the maximum stress) is much greater for the dynamic case. This point is shown in Figure 7.11 in which Watstein plots the ratio of the dynamic to static strain energy, W, versus the ratio of the dynamic to static strength ratio. In this figure, an increase in the strain energy on the order of 2.2 was recorded for both the high-strength and low-strength concretes at strain rates on the order of 10 sec^{-1}.

In general, it appears that the properties of various-strength concretes are affected similarly by an increase in strain rate. A good approximation of the increase in compressive strength with strain rate can be given by the relation:

$$\frac{f'_{dc}}{f'_c} = 1.5 + 0.2 \log \dot{\epsilon} \quad (10^{-2} < \dot{\epsilon} < 10^2 \ sec^{-1}) \tag{7.8}$$

A conservative estimate of the increase in modulus of elasticity can be obtained from the relation:

$$\frac{E_d}{E} = 1.1 + 0.1 \log \dot{\epsilon} \quad (10^{-6} < \dot{\epsilon} < 10^2 \ sec^{-1}) \tag{7.9}$$

The increase in strain energy, W, can be approximated by the relation:

$$\frac{W_d}{W} = 1.7 + 0.4 \log \dot{\epsilon} \quad (1 < \dot{\epsilon} < 100 \ sec^{-1}) \tag{7.10}$$

As stated earlier, it is very difficult to obtain true tensile data for concrete. It is almost impossible to measure the dynamic tensile properties directly. Initial efforts to measure the tensile properties are given in Reference 7.16. In this program, the dynamic tensile strength was obtained from impact tests in which the spall threshold was determined. The reported dynamic tensile strength was about ten times the usual static tensile strength; the dynamic shear and compaction strengths were about double the static values. The results are somewhat questionable because of the inherent assumptions made in reducing the data. It is recommended that the values given in Table 7.1 be used until further studies have been conducted on the dynamic tensile properties of concrete.
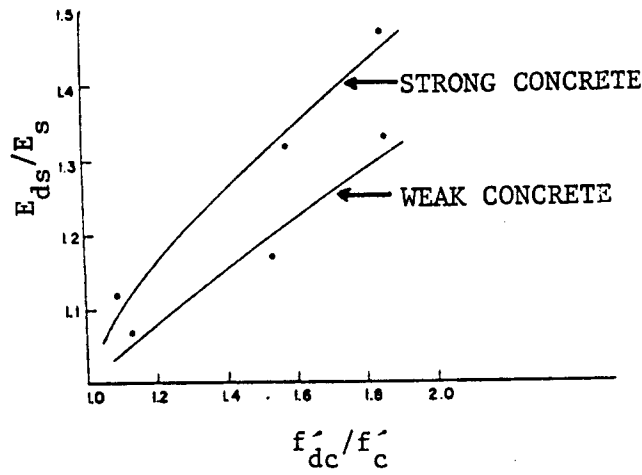
Figure 7.10. Variation of Dynamic Secant Modulus with
Dynamic Compressive Strength for Concrete
(Ref. 7.15)
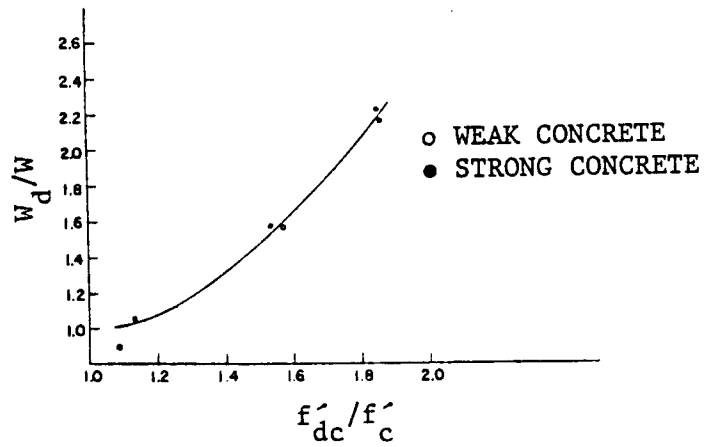
Figure 7.11. Variation of Dynamic Strain Energy with
The Dynamic Strength for Concrete
(Ref. 7.15)

Because of the difficulties inherent in the generation of dynamic material properties in general, high strain rate testing has been limited to only a few classes of materials. For this reason, high strain rate data do not exist for such materials as prestressed concrete, masonry, hollow clay tile block and brick.

7.2.3 Properties of Woods

Wood is used extensively in construction because of its relative low cost, availability, high strength to weight, and good insulating characteristics. Its use in construction is dominated by the anisotropy of its properties; that is, it has unique and independent mechanical properties in three orthogonal (perpendicular) directions--longitudinal, radial, and tangential. The longitudinal direction is along the axis of the fibers (along the grain), the radial direction is perpendicular to the grain in the radial (outward) direction, and the tangential direction is perpendicular to the grain and tangent to the growth rings. These axes are shown in Figure 7.12.
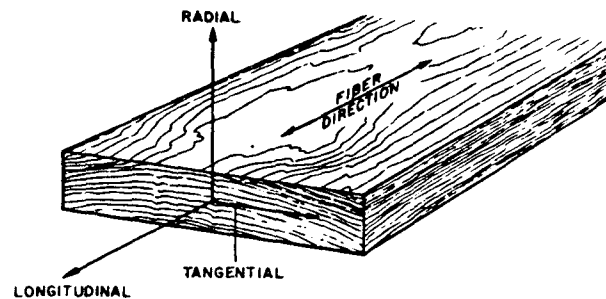
Figure 7.12. The Three Principal Axes of Wood with Respect to Grain Direction and Growth Rings

Mechanical properties of woods are obtained from tests of small pieces of wood termed "clear" and "straight grained." These specimens do not contain "inhomogeneous" characteristics such as knots, cross grain, checks or splits. An extensive presentation of the mechanical properties of various species of wood is given in Reference 7.17. This reference also includes the influence of growth characteristics such as knots, and moisture content on the properties.

7.2.3.1 Static Behavior

The material properties of wood of most interest to the designer are the compressive strength, the tensile strength (or modulus of rupture), the modulus of elasticity and the shear strength. Since wood is an anisotropic material, these properties vary with the direction of loading.

The compressive strength of most importance is obtained from compression parallel to the grain (longitudinal direction) and is reported in terms of the maximum crushing strength, σ_c. This property varies for seasoned woods from 4,000 to 10,000 psi. The compressive strength perpendicular to the grain is reported in terms of the fiber stress at proportional limit and varies from 300 to 2000 psi.

Because of difficulties in measuring the tensile strengths of wood specimens, as discussed in the introduction, the modulus of rupture, R, is often substituted for the tensile strength in the longitudinal direction. This property represents the maximum load-carrying capacity of the member and is proportional to the maximum moment borne by the specimen. Typical values for seasoned wood range from 6,000 to 20,000 psi. When these values are substituted for the tensile strength, they can be considered as conservative or low estimates. Of the small amount of longitudinal tensile data which does exist, values run 10 to 40 percent higher than the corresponding modulus of rupture. The modulus of elasticity, E, is also measured in bending and ranges in value from 0.8 to 2.3 million psi. (Values of the modulus of elasticity which are measured in bending must be increased by 10 percent to correct for the effect of shear deflection.)

It should be pointed out that many of the properties of wood, when measured along the grain axis, compared very favorably with all other structural materials, including structural steel and aluminum. For example, the stiffness to weight of a structural member made from Southern pine is approximately equal to that of a member made from steel, based on the ratio of the modulus of elasticity to the density. The strength-to-weight ratio of the Southern pine is several times greater than that of structural steel, based on both the crushing strength and modulus of rupture of pine relative to the ultimate strength of A36 steel.

7.2.3.2 Dynamic Behavior

It has long been known that the stress-strain relationship for wood is sensitive to the rate of strain. However, except for one recent study, the properties of wood have not been studied at the rates of strain which occur during explosions. Typical of past test programs was an extensive study conducted by Markwardt and Liska (Ref. 7.18) in which two softwood and two hardwood species were included in investigations made to evaluate the effect of "rapid" loading on the compressive and flexural strength properties of wood. Of most importance were their studies of Sitka spruce and maple which they tested in compression parallel to the grain. Typical curves from these tests were given in Figure 7.13. The strain rates observed in these tests were: (a) Sitka spruce, $\dot{\varepsilon} = 1.3 \times 10^{-5}$ sec^{-1} for the standard compression test, and
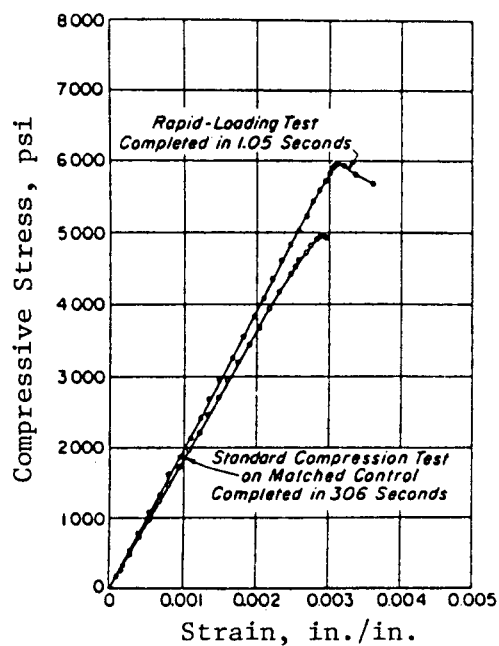
Figure 7.13a. Typical Stress-Strain Curves for
Two Matched Sitka Spruce Specimens
(Ref. 7.18)
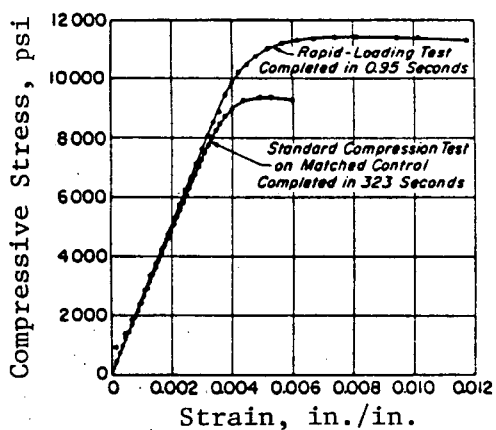
Figure 7.13b. Typical Stress-Strain Curves for
Two Matched Maple Specimens
(Ref. 7.18)

$\dot{\varepsilon}$ = 3.6 x 10^{-3} sec^{-1} for the "rapid" loading test; and (b) maple,
$\dot{\varepsilon}$ = 1.3 x 10^{-5} sec^{-1} and $\dot{\varepsilon}$ = 5.6 x 10^{-3} sec^{-1}. Several features
of these tests can be seen in Figure 7.13. Although the modulus of elasticity
varied little with the increase in strain rate, the ultimate (crush)
strength increased dramatically. Similar results were found in the bending
tests conducted on Douglas fir and birch specimens (Ref. 7.18) in which
a substantial increase in the modulus of rupture was observed.

Recently, studies have been conducted in Australia by Ferguson
and Yew (Ref. 7.19) at strain rates exceeding 100 sec^{-1}. This study
was the first to be reported with data useful for design of blast-
resistant structures. However, the woods tested were from Australia,
so that the data are not directly related to structural woods used in
the United States. In this study, the ultimate crush strength was seen
to increase with strain rate in a fashion similar to that seen in Figures
7.13a and 7.13b.

Figure 7.14 displays data for a variety of Australian pine tested
with varying moisture content. Data for strain rates above $\dot{\varepsilon}$ = 1 sec^{-1}
should probably be ignored due to probable errors caused by inertial
effects during testing.
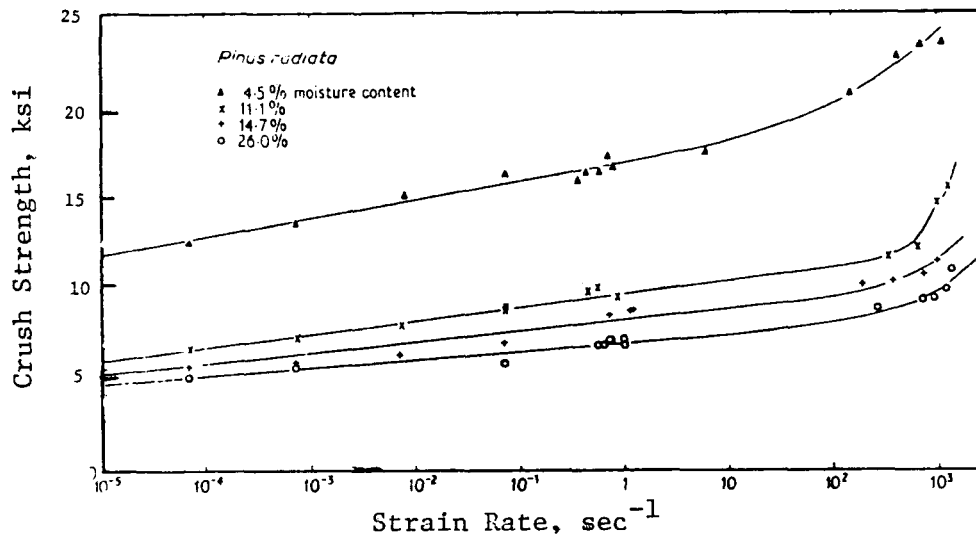
Figure 7.14. Variation of Crush Strength with Rate of Strain (Ref. 7.19)

In Figure 7.15 the data from References 7.18 and 7.19 are compiled
for comparison. Each specimen has a moisture content of 11 to 12 percent.
The curves represent a best fit to the data and extend over the range of
strain rates tested. It is evident that each of these curves can be
fit by an equation of the form:
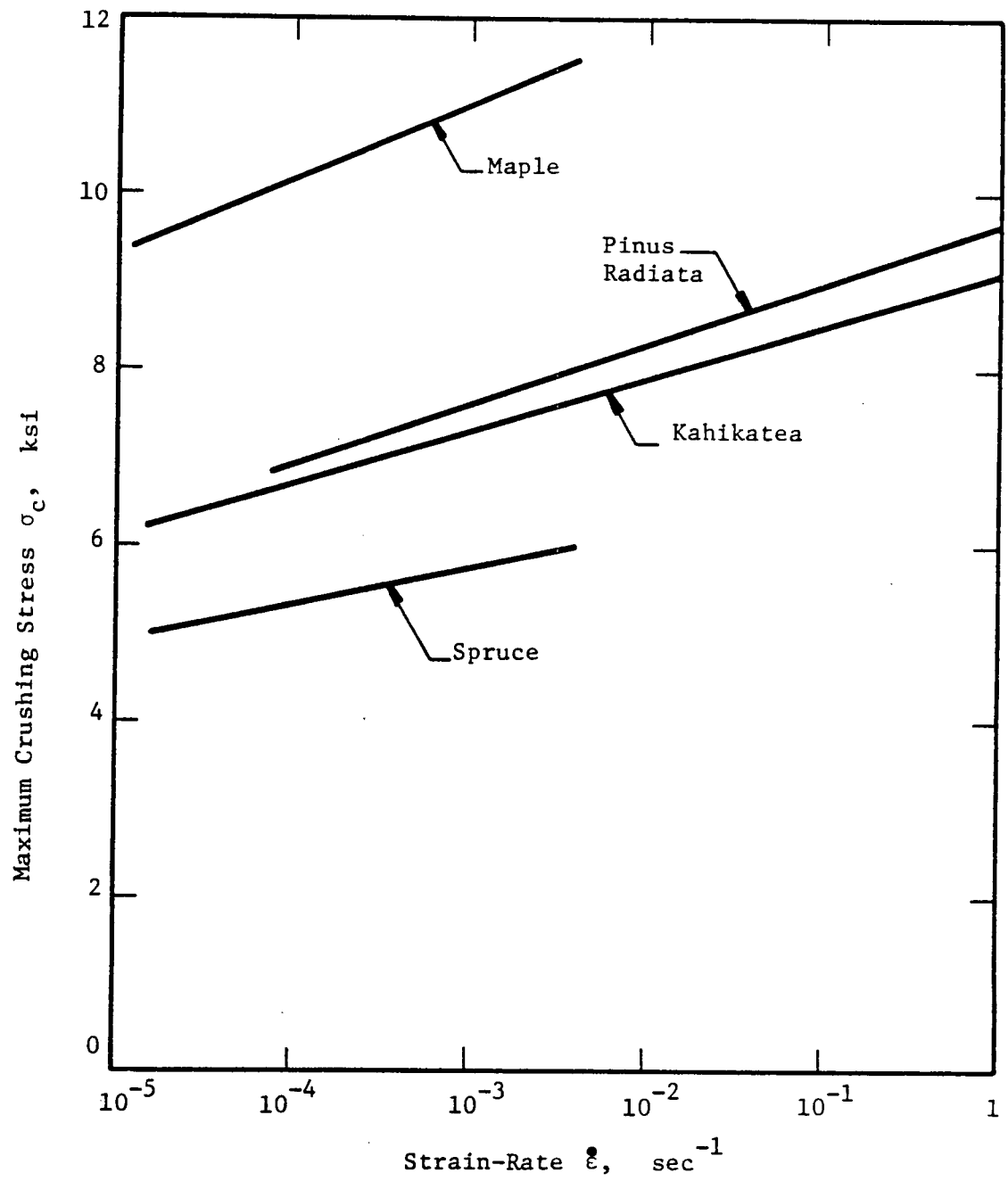
Figure 7.15 Variation of Maximum Crush Strength of Various Woods with Strain-Rate

$$\frac{\sigma_{dc}}{\sigma_c} = K_1 + K_2 \log \dot{\epsilon} \qquad (7.11)$$

. which is similar to that used earlier for steel and concrete.

Because of the limitation of available data, the data in Figure 6.15 must be generalized to cover the entire wood family. For design purposes, the upper and lower bound values of the crush strength should be taken as:

$$\text{Lower Bound} \quad \frac{\sigma_{dc}}{\sigma_c} = 1.35 + 0.080 \log \dot{\epsilon} \qquad (7.12)$$

$$\text{Upper Bound} \quad \frac{\sigma_{dc}}{\sigma_c} = 1.50 + 0.115 \log \dot{\epsilon} \qquad (7.13)$$

These values should be conservative estimates of the crush strength for typical structural woods, such as Douglas fir and yellow pine. The lower bound relationship should be used when designing to prevent failure, whereas the upper bound relationship should be used when failure is desired.

As noted earlier, there is no apparent increase in modulus of elasticity with strain rate. There are also insufficient data available to determine the rate sensitivity of the tensile strength for wood.

7.2.4 Properties of Frangible Materials*

In the construction of the Pantex facility, various frangible materials have been used. These include roof and wall board materials such as Cemesto, Thermo-Bord, gypsum board (Sheetrock) and insulating roof panels. Since these materials are often used in the design of structures which may be subjected to blast loads, the response of these materials to high rates of loading is of interest. To our knowledge, no studies have been conducted on the rate sensitivity of these materials. However, some relevant comments can be made for frangible materials in general.

In the use of frangible materials as blow-out panels, the designer is interested in the toughness of the material as a measure of its ability to absorb blast energy prior to failure. In static testing, frangible materials have high strength but low ductility, resulting in little toughness (or strain energy to failure). It is clear that under high rates of loading associated with blast, the material strength may be increased with no increase in ductility. Thus, the toughness of a frangible material may increase by a factor of two or three. It should

---

*In this context, frangible materials refers to materials used in frangible construction, as defined in the glossary of TM 5-1300 (Ref. 7.12).

be noted that the dynamic toughness, though large relative to static toughness, is still small relative to that for more ductile materials.

An example of this type of behavior is the response of glass to high strain rates. It has been reported (for example, Ref. 7.20) that the strength of glass may increase by as much as a factor of three or more under dynamic loads. In both the static and dynamic case, the strain is essentially elastic until failure, implying a similar increase of three or more in the failure strain under dynamic loads. Thus, the toughness of glass at high rates may be greater by a factor of ten or more. For typical glass, this results in a toughness on the order of 30 to 3,000 psi, which is well below that of the more ductile building materials, such as steel, which has toughness values on the order of 10,000 psi.

For this reason, the increase in toughness of frangible materials due to high rates of loading, though large, is relatively unimportant in the design of blast-resistant structures, and should be ignored by the designer.

7.3 ENERGY-ABSORBING PROPERTIES OF MATERIALS

Impact properties of materials and structures need not be limited to the influence of rate of loading on their constitutive relations or stress-strain response. A common objective in all impact testing is to determine the energy absorbed in fracturing a particular test piece under high-speed loading. The energy of rupture is considered a measure of the impact strength of a material. Actually, the strain energy per unit volume required for complete rupture of a material is termed the "toughness" and is given by the area under the stress-strain curve. As a result, a variety of testing techniques has been developed to characterize qualitatively the response of materials and structures to impact loading.

In this section, a discussion will be presented of the various test techniques used to assess a material's energy absorption capability. Tests will be described which are commonly used to assess steels, woods, plastics, etc. This discussion is oriented to help the designer determine the usefulness of these tests and their results in the design process. An effort is also made to describe the information currently available to the designer for the determination of a structure's ability to absorb energy or to prevent fragment perforation.

In general, the essential features of an impact test are: (a) a suitable specimen; (b) a support system on which the test specimen is placed to receive the blow of a moving mass; (c) a moving mass of known kinetic energy sufficient to deflect (and normally to break) the specimen

placed in its path; and (d) a device to measure the residual energy in the moving mass. Falling weight, Charpy and Izod impact tests are typical of this type of measurement. However, there are a host of other dynamic testing devices which have been developed for certain unique materials, structures or environments.

In the tensile impact test, either a variable speed flywheel or a pendulum delivers an impact loading to a smooth specimen similar to a tensile specimen or to a similar specimen with a circumferential notch. A test of this nature permits the study of impact strength of a material under a uniaxial stress condition. The specimen shape may be controlled to produce additional effects. A short specimen will have a high strain rate and produce a brittle fracture. Longer gage lengths at the same impact velocity will result in lower rates of strain and possibly ductile failures (Ref. 7.21).

Charpy and Izod tests are considered to be bending impact tests. Unfortunately, due to the presence of a stress raising notch or keyway, this test is more of a measure of notch sensitivity than material impact strength or energy absorbing capability. One of the most significant uses of the Charpy and Izod impact tests is in the determination of the transition temperature. If the mode of failure is observed, the transition temperature is that temperature where the mode of failure changes from ductile to brittle. Since this does not occur abruptly, an arbitrary value (15 ft-lb) may be used to establish transition (Ref. 7.22). Some of the many other definitions of transition temperature currently being used are: (a) the lowest temperature at which the specimen exhibits 100 percent fibrous fracture; (b) the temperature where the fracture shows a 50 percent crystalline and a 50 percent fibrous appearance; and (c) the temperature corresponding to the energy value 50 percent of the difference between values obtained at 100 percent and 0 percent fibrous fracture (Ref. 7.24). It should be pointed out that the energies measured in these impact tests are actually related to the failure of a particular specimen geometry subjected to a particular condition of loading. Therefore, although different materials are not compared to each other regarding their energy-absorbing capability, the effects of heat treatments and alloying elements on a given material may be evaluated.

The Charpy impact test is a simply supported rectangular or circular beam containing a backward facing keyway, V-notch, slot or sawcut (Ref. 7.23). The striking edge of the moving mass is attached to a pendulum and positioned to strike the beam directly in the center. The procedure is used not only for metallic materials but also plastics and electrical insulating materials (Ref. 7.24).

The Izod impact test is a cantilevered beam with either a rectangular or circular cross section. A variety of standard notches are used and may be tested as either forward facing or backward facing depending on the impact resistance. As in the case of the Charpy test, this is more

parallel to perpendicular to the fibers can be approximated using a Hankinson-type formula:

$$\frac{N}{P} = \frac{Q/P}{\sin^n\theta + Q/P \cos^n\theta} \qquad (7.17)$$

in which N represents the impact bending strength at an angle θ from the fiber direction, Q is the strength across the grain, P is the strength parallel to the grain, and n is an empirically determined constant. It has been found experimentally that the impact bending values fall close to the curve for $Q/P = 0.05$ and $n = 1.5$. This equation is shown in Figure 7.17 along with data tabulated in Reference 7.17.

Woods are used to form structures such as floors, roofs and walls. The energy-absorbing characteristics of whole structures may be evaluated by using the standard testing techniques described in ASTM E72 (Ref. 7.26). In this particular test, the initial and residual energies are used to determine the energy absorbed by a particular panel, either vertical or horizontal. Unfortunately, the resulting value of energy absorbed is unique to the particular panel tested and to the particular technique of loading. Extension of these data for engineering design is not recommended.

Based on the review just given, it should be apparent that the results from the various impact tests are of questionable value to the designer. It is recommended that the design be based on established procedures using the dynamic values of the strength discussed in Sections 7.2 and 7.4.

The fragment penetration resistance of wood is so low that it is not normally considered in design studies. For this reason, no ballistic penetration data exist for the various woods. The only data available have been developed for materials frequently used in the collection of fragments in arena tests and residual projectiles in ballistic perforation tests. These include celotex and strawboard, for which empirical penetration equations are given in Chapter 6. For design purposes, it is recommended that the penetration resistance of wood be ignored.

7.3.3 Plastic and Metallic Foams

Cellular structures possess a great capacity for energy absorption through the collapse of the cells which comprise the structure. The crush strength, f_{cr}, may be engineered with some precision over a wide range of values and may be either directional or isotropic. Materials used in such systems may vary from paper and plastic to metallic-expanded material or foam. In each case, the objective of the designer is to produce a medium which will have some desirable force-deflection characteristics. A constant force versus displacement characteristic
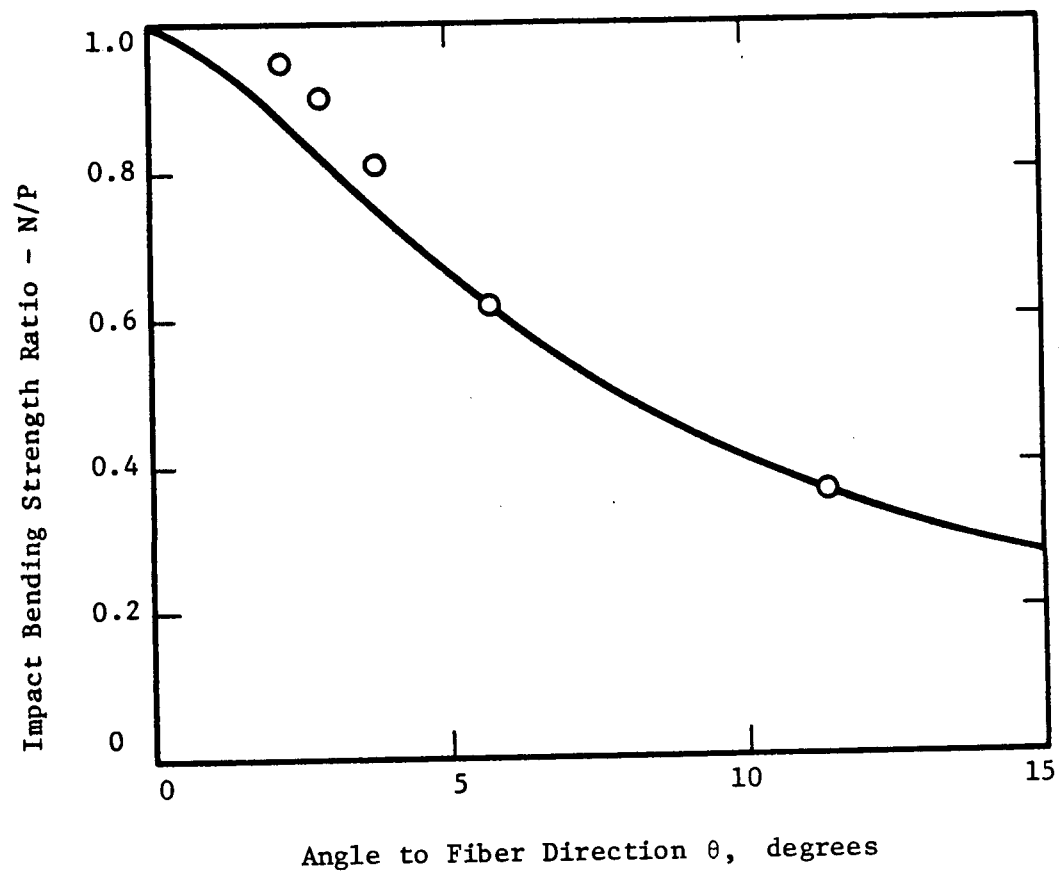
Figure 7.17 Impact Bending Strength versus Wood Fiber Direction

of a measure of notch sensitivity and is commonly used to identify the transition temperature of a material. The energy values determined are quantitative comparisons on a selected specimen but cannot be converted into energy values that would serve for engineering design calculations. The results from this type of test are sensitive to the notch size and shape, specimen size, testing conditions (particularly temperature), and the velocity of straining.

A similar test on block-type insulating materials utilizes an unmatched specimen to determine the "apparent impact strength" (Ref. 7.25). In this case, however, the "equivalent impact strength" is defined as a unit impact strength and can be used to compare the strengths of a material when the dimensions differ by a modest amount.

A variety of other impact tests has been defined by ASTM for a variety of special applications. Although the testing of panels for building construction (Ref. 7.26) is typical, the ASTM currently lists Standard Methods for 14 drop tests and over 30 impact tests to verify the specifications of a variety of specimens from football headgear to railway axles.

7.3.1 Soil or Sand Fill

The ability of soil or sand to absorb energy is of utmost importance in the design of structures to absorb the energy of a blast wave or to stop a penetrating fragment. Design for these cases is based on various empirical relationships described elsewhere in this manual. A review of these relationships will now be presented along with those properties of soil which must be obtained for use in these relationships.

In Section 6.4, the equations developed by Westine (Ref. 7.27) for predicting transient and residual displacements and velocities of projectiles penetrating cohesive soils were presented. The soil properties which must be considered in these equations are: the soil mass density; the cohesive yield strength of the soil; and the degree of saturation. In addition, the ambient atmospheric pressure is required to account for the pore air and water pressures within the voids between the soil particles.

Note that granular soils are not covered by these equations as they have a significant strength variation with depth caused by gravitational effects and are much more dependent on the void ratio relative to the critical void ratio (Westine, Ref. 7.27). The critical void ratio is defined as the ratio at which no net change in the void volume occurs during missile penetration. The only exceptions would be horizontal penetration through a vertical barricade or penetration through a sloped mound in which the penetration path is parallel to the surface. In

these cases, the gravitational dependence is eliminated by maintaining a constant overburden.

For the case of projectile penetration into sand, equations have been developed empirically assuming the form proposed by Poncelet (Ref. 7.28). Poncelet assumed that the resisting force on a projectile is:

$$F = C_0 + C_2 v^2 \tag{7.14}$$

where the coefficients C_0 and C_2 are functions of A, the presented area (Ref. 7.27). By substituting Equation (7.14) into Newton's equation of motion:

$$dx = m \frac{v}{F} dv \tag{7.15}$$

and integrating x from the surface of the soil at x = 0 to the maximum depth of penetration x_{max} and v from the impact velocity V_o to rest at v = 0 yields:

$$x_{max} = \frac{m}{2C_2} \ln \left[1 + \frac{C_2 V_o^2}{C_0} \right] \tag{7.16}$$

where m = mass of projectile

V_o = impact velocity

C_0, C_2 = empirical constants

This procedure assumes that gravitational force, the mass of the soil accompanying the projectile, and the pore air and water pressures are negligible (Ref. 7.27).

The penetration equation for sand presented in Section 6.4 represents an average of the Poncelet results obtained for a number of tests (Ref. 7.28). This average was calculated making the further assumption that depth of penetration is equal to the total curved length of the missile path (Ref. 7.28). As a result of these allowances, the equation presented in Chapter 6 may be considered conservative for safety in virtually every case, and tests within a candidate sand should, therefore, be conducted before utilizing it as a fragment barricade.

Additionally, any use of soils or sands to absorb the energy in a blast wave should be based on the mass of the material. Designs based on the tensile strength of the material would be overly dependent on the degree of saturation, the internal angle of friction, grain size, compaction, and other physical properties which may vary with age, weather, and cylic loading.

Because of the variability of soil and sand properties with location
and depth, no properties will be given in this section. It is important
that the designer obtain properties for the specific material to be used.
Section 5.2 discusses the soil mechanics in more detail.

7.3.2 Wood

The everyday use of timber in its multitudinous forms has led to
the establishment of standard methods of testing selected specimens of
wood. The technique for testing is documented as ASTM D143 (Ref. 7.29)
and the results tabulated in the Wood Handbook (Ref. 7.17). Two proper-
ties of interest which merit discussion are: (a) the "work to maximum
load in bending"; and (b) the "impact bending strength."

The work to maximum load is a measure of the energy absorbed by a
specimen as it is slowly loaded to failure. Under these conditions, state
of stress is not uniform and the failure of the specimen will depend
on the distribution of stress. Therefore, the energy absorbed cannot be
considered to be a property of the material but more of a qualitative
measure of different materials when subjected to similar forms of static
bending.

The impact bending strength is related to the energy absorbed
when subjected to a rapid or falling load. The data take the form of
the height of drop in a carefully controlled test onto a standard specimen.
Again, the results are a qualitative measure of the response of a
particular specimen and cannot be used as a material property in engineer-
ing design. The specimen is 2 x 2 x 30 in., supported so as to have a
span of 28 in. and positioned to receive a load at center span in a Hatt-
Turner or similar impact machine. A 50-lb hammer is dropped and the height
to cause complete failure or a 6-in. deflection of the specimen is recorded.

The impact bending strength obtained as described above has a
"coefficient of variation" of 25 percent (Ref. 7.17) regardless of
moisture content. This characteristic of wood is a function of many
parameters, both geometric and environmental. The most significant
environmental conditions are moisture content and temperature. For this
reason, impact bending strength is tabulated under standard conditions
of 12 percent moisture content and 68°F. Data are not available on the
variation of this particular property; however, the influence of moisture
and temperature on modulus of elasticity is shown in Figure 7.16.
Similar variations would be expected for modulus of rupture and probably
impact bending strength.

The geometric parameter which is of primary significance is the
direction of the grain (or natural axis of the fiber) relative to the
direction of the stress. Strength properties in directions ranging from
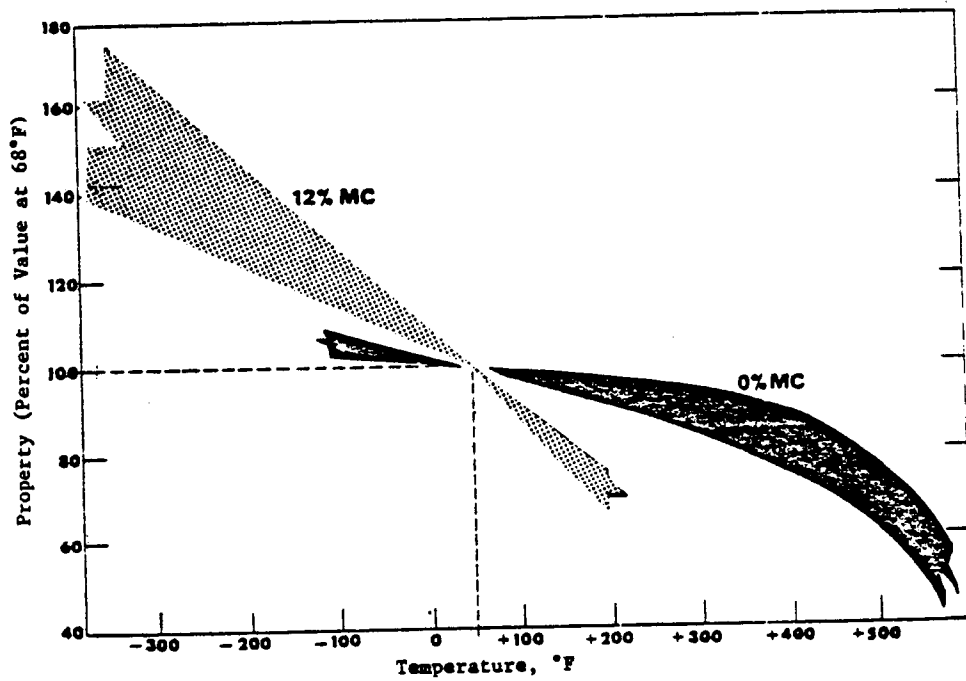
Figure 7.16 The Immediate Effect of Temperature on the Modulus of Elasticity of Wood Relative to the Value at 68°F

is very attractive since it maximizes the energy dissipated for a given rate of deceleration. However, an increasing force with displacement will produce even greater energy dissipation per pound of material, provided deceleration rate is not critical.

The design of a suitable energy-absorbing system is relatively straightforward. The energy to be absorbed must be specified along with the area and distance available to accomplish the event (Ref. 7.30). This information is sufficient to establish the necessary crush strength of the material. In order to prevent "bottoming out" of the energy-absorbing system, it is customary to assume that only 70 percent of the thickness is available for energy dissipation. Standard honeycomb materials are available in a variety of strengths, densities and cell sizes (Ref. 7.31) as shown in the Figure 7.18. Likewise, plastics in the form of low-density rigid foams, such as polystyrene, may be used as a core material to form a cellular structure capable of energy absorption. The force exerted by a rigid plastic foam is limited by either the critical stress for collapse of the cells or the yield stress of the polymer itself (Ref. 7.32). As in the case of expanded honeycombs, the crush strength is a function of the density of the foam which is determined from the density of the polymer as well as the cell size. For very low-density foams this may be approximated by the expression:

$$f_{cr} = \frac{8\pi^2 E_p}{6(1-\nu_p^2)} \frac{(\alpha - 1)^3}{\alpha} \tag{7.18}$$

where

$$\alpha = \left(1 - \frac{\rho_f}{\rho_p}\right)^{-1/3}$$

Here the subscripts f and p refer to the foam and polymer, respectively, while E and ν are Young's modulus and Poisson's ratio. It should be noted that Young's modulus of the polymer, E_p, is a function of the foam density.

Metal matrix cellular materials may also be used as an energy-absorbing medium. The size, shape and size distribution of the open cells in the structure can be controlled with precision and the scope for alloy selection covers a wide range of materials. The material is manufactured by the infiltration of a porous substance with molten metal. For light alloys a suitably graded aggregate of rock salt (NaCℓ) is sintered into the metal. After solidification, the soluble component is removed by leaching and the cellular metal structure remains (Ref. 7.33). Materials manufactured in this manner have been tested to determine their energy-absorbing characteristics which are shown in Table 7.2. The specific energy, $\bar{E}$, may be considered to be a material property and defined as:

$$\bar{E} = \frac{1}{\rho} \int_0^{0.40} \sigma d\varepsilon \tag{7.19}$$
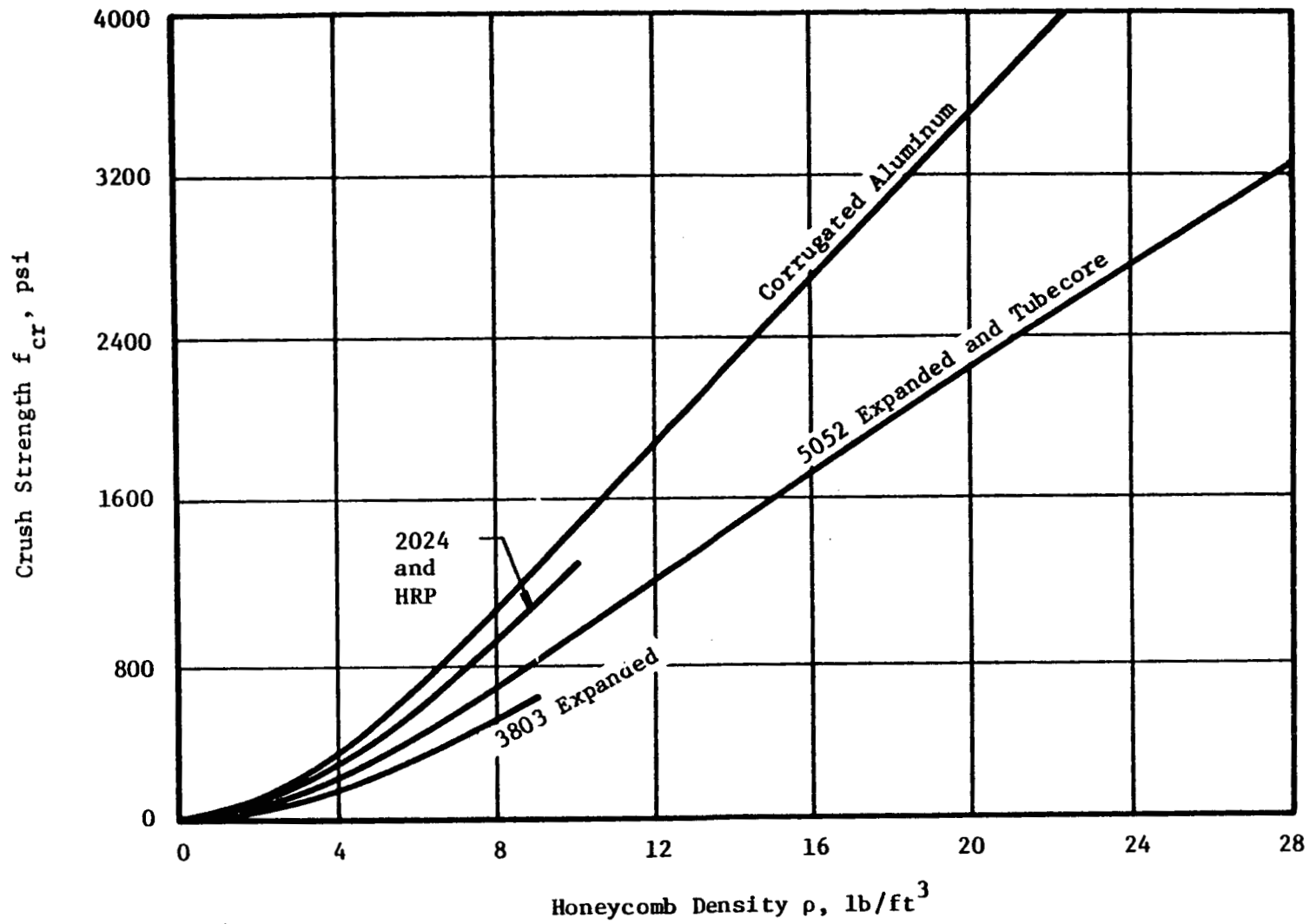
Figure 7.18 Honeycomb Crush Strength versus Density for Standard
Honeycomb Material (Reference 7.31)

Table 7.2. Properties of Energy Dissipation Materials
at 40 Percent Deformation (Ref. 7.33)

Material		Specific Energy at 40% Deformation (ft-lb/lb)	Loading Ratio[a]
Alloy	Cell Structure		
7075-T6	Std distr	7,600	2.06
7075-T6	Mixed[b]	3,000	1.66
2024-T6	Std distr	6,800	2.15
195-T62	Std distr	5,800	2.85
195-T62	Mixed[b]	1,750	4.00
220-T4	Std distr	5,600	4.00
220-T4	Mixed[b]	3,500	4.00
122-T6	Mixed[b]	3,000	2.00
43[c]	20 mesh	3,000	1.66
Al[c]	20 mesh	2,850	2.30

[a]Load (40% Def)/Load (Initial Yielding)
[b]Equal parts by weight of 6, 8, 10, 20, 30, and 48 mesh
[c]Kanamite filled

Inherent in this relationship is the fact that bottoming out of the energy absorbing system occurs for deflections greater than 40 percent. (Ref. 7.33).

The most efficient material shown is 7075-T6 aluminum alloy matrix with a standard cell structure. This indicates that 7,600 ft-lb is achievable with cellular aluminum which is comparable to the efficiency of commercially available aluminum honeycombs.

Design of a cellular structure to prevent penetration of projectiles is relatively straightforward. Inherent in the use of a cellular material is the fact that the projected area of the projectile onto the structure must be large relative to the cell size. Thus, it is recommended that the cell size chosen for the structure be at least five times smaller than that of the expected projectile. The thickness of cellular material required to stop a projectile may be calculated by equating the energy per unit projected area of the projectile to the energy absorption capability of the cellular material per unit area. For the honeycomb material given in Figure 7.18 or the plastic foam described by Equation (7.18), the energy absorption, capability, E_a, is simply the work required to crush the material over the available thickness, t_a, i.e.,

$$E_a = \int_o^{t_a} f_{cr} \, dt \qquad (7.20)$$

For the honeycomb materials and the plastic foams, the crush strength, f_{cr}, is approximately constant through the crushing process, so that Equation (7.20) becomes

$$E_a = f_{cr} \, t_a \qquad (7.21)$$

If f_{cr} is given in terms of psi, then the E_a is the available energy absorption capability per square inch. Equating the kinetic energy of the projectile to energy absorption capability of the cellular material

$$\frac{KE}{A_p} = E_a = f_{cr} \, t_a \qquad (7.22)$$

where A_p is the projected area of the projectile onto the material. From this relation, the required material thickness can be obtained

$$t_a = \frac{KE}{f_{cr} \, A_p} \qquad (7.23)$$

For the metallic foams discussed, the energy absorption capability per unit area is obtained from the relation

$$E_a = \rho \, \bar{E} \, t_a \qquad\qquad (7.24)$$

and the required thickness to stop a projectile is

$$t_a = \frac{KE}{\rho \, \bar{E} \, A_p} \qquad\qquad (7.25)$$

Pressure attenuation data are not available for these materials.

7.3.4 Composite Material

Composite constructions, both in buildings and in barricades, are often designed to absorb energy and to prevent ballistic perforation. This design process uses accepted design practices and the properties of the various construction materials used. The properties of the materials most often used have been discussed in other portions of this section. For the sake of completeness, we will briefly review the design of composite structures.

Composite construction of buildings or barricades utilizing layering of materials (i.e., steel-concrete-soil) may be treated sequentially to evaluate penetration resistance. The procedure required that a fragment be traced through the media, calculating its residual velocity at each interface and assuming that this is the striking velocity into the next medium. Conservatively, the fragment should be considered to remain intact, experiencing no loss of mass.

Contrary to the case of fragment penetration, determination of the energy absorption capabilities of a composite material must consider any synergistic "properties" which may develop. This is particularly noticeable in "reinforced earth." Reinforced earth is a composite material of earth and reinforcements, the latter generally consisting of metal strips arranged horizontally and capable of withstanding high tensile stresses (Ref. 7.34).

The principal phenomenon in reinforced earth is the transmission of stresses which develop in the earth to the reinforcements. The reinforcements are thereby placed in tension, and the composite material develops a pseudocohesive strength which is directly proportional to the tensile strength of the reinforcements and acts in the direction of their placements (Ref. 7.35).

The design or analysis of reinforced earth structures consists of considering the local equilibrium between the facing elements and the reinforcing strips under the assumption that the reinforced volume is in a state of limit equilibrium and that the principal directions of the stresses are vertical and horizontal (Ref. 7.35). Unlike a retaining

wall anchored with tie rods, the tensile stress in the layer of reinforcements is not a maximum at the face. The distribution of stresses at a given level have the following characteristics (Ref. 7.34):

a) The traction force on the flexible, vertical face is a fraction (usually small) of the maximum traction force in the reinforcement. Therefore, the face plays only a local mechanical role.

b) The points of maximum tension in the different layers of reinforcement lie on a parabolic curve which separates the mass into two zones as shown in Figure 7.19: (1) an active zone located near the face in which the tangential stress exerted by the earth on the reinforcement is directly toward the face; and (2) a resistant or passive zone in which the tangential stress is directed inward. In this zone, the earth tends to retain the reinforcements, analogous to the anchoring zone in the case of a tie rod.

c) The tangential component, τ, of the stress exerted by the earth on each face of a reinforcement is:

$$\tau = \frac{1}{2b} \frac{dT}{d\ell} \qquad (7.26)$$

where b = length of reinforcement
T = tensile stress in the reinforcement
ℓ = abscissa of the point considered along the reinforcement

It is therby directly proportional to the slope of the curve of stress distribution in the reinforcement.

d) The coefficient, $f^* = \tau/\sigma$, of friction mobilized along a reinforcement in the active zone is close to the value of the coefficient of friction, f, between earth and reinforcement. In the passive zone, its value varies along the reinforcement and depends primarily on the length of the reinforcement in this zone. This is called the adherence length: the shorter it is, the greater the mean friction mobilized. The active zone, which can be equated to a thrust wedge, is of smaller dimensions that the thrust wedge which would be mobilized behind a retaining wall in a nonreinforced fill of the same geometry and characteristics (Ref. 7.34).

In general, the use of a composite material as an energy-absorbing medium will require that model testing and analysis of the structure be conducted prior to full-scale implementation. Conservatively, the AE
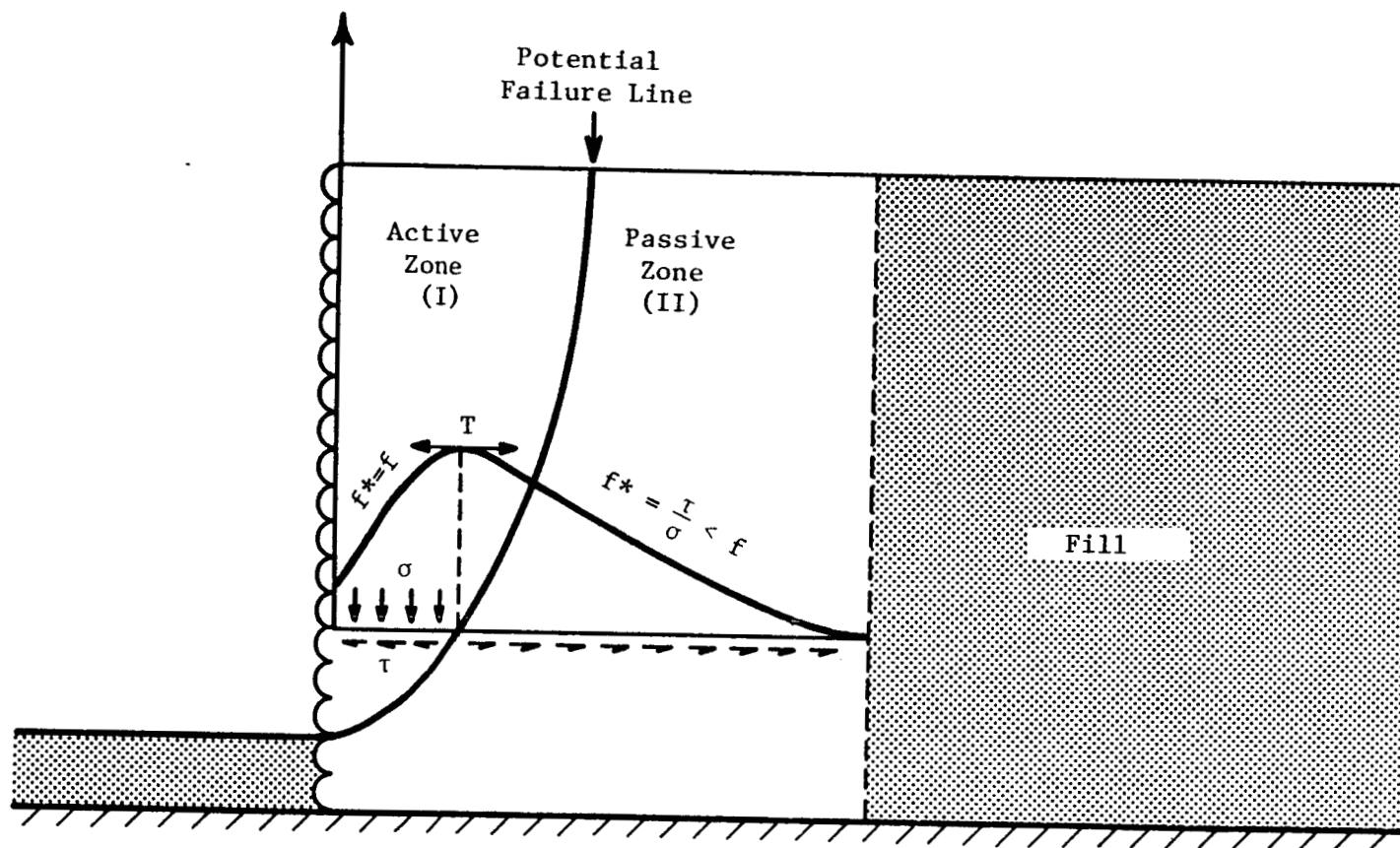
Figure 7.19   Tension Distribution Along Reinforcements

may initially assume that no composite properties develop to enhance the energy-absorbing capabilities of the structure. However, since the move to composite materials is often made for economy and efficiency, this approach may be inadequate to achieve a final design.

The pressure attenuation characteristics of composite structures are not known.

7.3.5 Discussion

A large number of dynamic impact tests have been developed for the materials of interest. However, the results of these tests are of limited usefulness to the designer. This is due to the fact that the results of these tests are normally a function of the geometry of the specimen used, the state of stress in the specimen, and the details of the impact load. In general, a designer must conduct a structural analysis using the material properties given in Table 7.2 in order to determine a structure's ability to absorb energy. For soil and sand, the material properties are so variable from one location to the next that they must be measured for the exact soil or sand to be used.

A discussion was presented of projectile penetration into soil and sand and plastic and metallic foams. For the case of wood, no data exist for projectile penetration, and the recommendation was made that the penetration resistance of wood be neglected.

7.4 TABLES OF DYNAMIC MATERIAL PROPERTIES

The mechanical properties of various structural steels, 6061 aluminum, and structural woods are presented in this section. Those properties most useful to the designer are given, including those values which differ under high rates of loading.

7.4.1 Mechanical Properties of Structural Metals

Table 7.3 lists the mechanical properties of all structural types of steel commonly used in the construction of an explosives facility. All properties given are for plate, thickness $\leq$ 3/4 in., or bar, diameter $\leq$ 3/4 in. Values for other thicknesses and diameters can be obtained in the Annual ASTM Standards, Part 4 (Ref. 7.36). The properties given are the minimum values designated by ASTM.

Table 7.4 lists the mechanical properties of 6061 aluminum (Ref. 7.37). As noted in Section 7.2.1, these properties are assumed independent of strain rate.

Table 7.3. Mechanical Properties of Steel (Ref. 7.36, Part 4)

ASTM Type	Grade	Type Steel	Tensile Yield Stress - σ_y (Minimum)			Tensile Ultimate Stress - σ_T or σ_u (Minimum*)			Percent Elongation e (Minimum)	
			Static 10^3psi	$\dot{\epsilon} = 1$ sec^{-1} 10^3psi	$\dot{\epsilon} = 100$ sec^{-1} 10^3psi	Static 10^3psi	$\dot{\epsilon} = 1$ sec^{-1} 10^3psi	$\dot{\epsilon} = 100$ sec^{-1} 10^3psi	in 8 in.	in 2 in.
A7		Low Carbon	33	42.9	59.4					
A36		Low Carbon	36	46.8	64.8	58-80	63.8-88.0	75.4-114.4	20	23
A529		Low Carbon	42	54.6	75.6	60-85	66.0-93.5	78.0-110.5	19	-
A440**		Low Carbon	50	65.0	90.0	70	77.0	91.0	18	21
A570	30	Low Carbon	30	39.0	54.0	49	53.9	63.7	19	25
	33	Low Carbon	33	42.9	59.4	52	57.2	67.6	18	23
	36	Low Carbon	36	46.8	64.8	53	58.3	68.9	17	22
	40	Low Carbon	40	52.0	72.0	55	60.5	71.5	16	21
	45	Low Carbon	45	58.5	81.0	60	66.0	78.0	14	18
	50	Low Carbon	50	65.0	90.0	65	71.5	84.5	12	17
A611	A	Low Carbon	25	32.5	45.0	42	46.2	54.6	-	26
	B	Low Carbon	30	39.0	54.0	45	49.5	58.5	-	24
	C	Low Carbon	33	42.9	59.4	48	52.8	62.4	-	22
	D	Low Carbon	40	52.0	72.0	52	57.2	67.6	-	20
	E	Low Carbon	80	80.0	96.0	82	82.0	96.0	-	-
A242		Low Alloy	50	60.0	80.0	70	70.0	70.0	18	-
A441		Low Alloy	50	55.0	65.0	70	70.0	70.0	18	-
A572	42	Low Alloy	42	56.2	54.6	60	60.0	60.0	20	24
	45	Low Alloy	45	49.5	58.5	60	60.0	60.0	19	22
	50	Low Alloy	50	55.0	65.0	65	65.0	65.0	18	21
	55	Low Alloy	55	60.5	71.5	70	70.0	70.0	17	20
	60	Low Alloy	60	66.0	78.0	75	75.0	75.0	16	18
	65	Low Alloy	65	71.5	84.5	80	80.0	80.0	15	17
A588		Low Alloy	50	55.0	65.0	70	70.0	70.0	18	21
A514		Low Alloy	100	100.0	100.0	110-130	110-130	110-130	-	18
A615	40	Low Carbon	40	52.0	72.0	70	77.0	91.0	12	-
	60	Low Carbon	60	78.0	108.0	90	99.0	117.0	9	-
A616	50	Low Carbon	50	65.0	90.0	80	88.0	104.0	6	-
	60	Low Carbon	60	78.0	108.0	90	99.0	117.0	6	-
A617	40	Low Carbon	40	52.0	72.0	70	77.0	91.0	12	-
	60	Low Carbon	60	78.0	108.0	90	99.0	117.0	8	-

*All values for tensile ultimate are minimum values except A36, A529, and A514 for which the acceptable range of values are given.

**Discontinued in 1979

Table 7.4. Mechanical Properties of 6061 Aluminum
Alloy Sheet and Plate (Ref. 7.37)

Condition	Thickness in.	Yield Stress σ_y (minimum) psi	Ultimate Stress σ_T (minimum) psi	Percent Elongation in 2 in. e (minimum)
T4	0.010-0.020	16	30	14
	0.021-0.249	16	30	16
T451	0.250-1.000	16	30	18
	1.001-2.000	16	30	16
	2.001-3.000	16	30	16
T6	0.010-0.020	35	42	8
	0.021-0.499	35	42	10
T651	0.500-1.000	35	42	9
	1.001-2.000	35	42	8
	2.001-3.000	35	42	6
	3.001-4.000	35	42	6
	4.001-6.000	35	40	6

Modulus of Elasticity $E = 9.9 \times 10^6$ psi
Density $\rho = 0.098$ lb/in.^{3}

T4   - Solution heat treated
T451 - Solution heat treated and stress relieved
T6   - Solution heat treated and artificially aged
T651 - Solution heat treated, stress relieved, and artificially aged

7.4.2 Mechanical Properties of Structural Woods

Lumber of any species and size, as it is sawed from the log, is quite variable in its mechanical properties. Pieces may differ in strength by several hundred percent. For simplicity and economy in use, pieces of lumber of similar mechanical properties are placed in a single class called a stress grade. Explanations of the stress grading process and the derivation of mechanical properties for visually graded lumber are given in the Wood Handbook (Ref. 7.17).

The derivation of mechanical properties of visually graded lumber is based on clear wood properties and on the lumber characteristics allowed by the visual sorting criteria. The influence of the sorting criteria is handled with "strength ratios" for the strength properties of wood and with "quality factors" for the modulus of elasticity.

From piece to piece, there is variation both in the clear wood properties and in the occurrence of the property-modifying character- istics. The influence of this variability on lumber properties is handled differently for strength than for modulus of elasticity.

Once the clear wood properties have been modified for the in- fluence of sorting criteria and variability, additional modifications for size, moisture content, and load duration are applied. The composite of these adjustments is an "allowable property."

Each strength property of a piece of lumber is derived from the product of the clear wood strength for the species and the limiting strength ratio. The strength ratio is the hypothetical ratio of the strength of a piece of lumber with visible strength-reducing charac- teristics to its strength if those characteristics were absent.

Strength ratios for all knots, shakes, checks, and splits are derived using similar concepts. Strength ratio formulas are given in ASTM D-245 (Ref. 7.36, Part 22). The same reference contains rules for measuring the various growth characteristics.

The range of strength ratios in a grade, and the natural variation in clear wood strength, give rise to variation in strength between pieces in the grade. To account for this variation, and provide for safety in design, it is intended that any strength property associated with a grade be less than the actual strength of at least 95 percent of the pieces in the grade. In visual grading according to ASTM D-245, this is handled by using a near-minimum clear wood strength value, and multiplying it by the minimum strength ratio permitted in the grade to obtain the grade strength property. The near-minimum value is called the 5 percent exclusion limit. ASTM D-2555 (Ref. 7.36, Part 22) provides clear wood strength data and gives a method for estimating the 5 percent exclusion limit.

Table 7.5 Clear Wood Strength Values: Unadjusted for Sorting Criteria
and Variability, Size, Moisture Content, and Load Duration
(ASTM D-2555, Ref. 7.36, Part 22)

Species or Re-tion, or Both	Modulus of Rupture[a]			Modulus of Elasticity[b]			Compression Parallel to Grain, crushing strength, max.			Shear Strength			Compression, Perpendicular to Grain;[c] Fiber Stress at Proportional Limit		Specific Gravity		
	Avg., psi	Varia-bility Index	Stan-dard Devia-tion, psi	Avg., 1000 psi	Varia-bility Index	Stan-dard Devia-tion, 1000 psi	Avg., psi	Varia-bility Index	Stan-dard Devia-tion, psi	Avg., psi	Varia-bility Index	Stan-dard Devia-tion, psi	Avg., psi	Stan-dard Devia-tion, psi	Avg., psi	Varia-bility Index	Stan-dard Devia-tion
Douglas fir																	
Coast	7665	1.05	1317	1560	1.05	315	3784	1.05	734	904	1.03	131	382	107	0.45	...	0.057
Interior West	7713	1.03	1322	1513	1.04	324	3872	1.04	799	936	1.02	137	418	117	0.46	...	0.058
Interior North	7438	1.04	1163	1409	1.04	274	3469	1.04	602	947	1.03	126	356	100	0.45	...	0.049
Interior South	6784	1.01	908	1162	1.00	200	3113	1.01	489	953	1.00	153	337	94	0.43	...	0.045
Southern Pine																	
Loblolly	7300	1.08	1199	1402	1.08	321	3511	1.09	612	863	1.05	112	389	109	0.47	1.06	0.057
Longleaf	8538	1.07	1305	1586	1.07	295	4321	1.07	707	1041	1.05	120	479	134	0.54	1.05	0.069
Shortleaf	7435	1.04	1167	1388	1.04	268	3527	1.05	564	905	1.05	125	353	99	0.47	1.05	0.052
Slash	8692	1.09	1127	1532	1.08	295	3823	1.07	547	964	1.05	128	529	148	0.54	1.09	0.062

[a]Modulus of rupture values are applicable to material 2 in. in depth.

[b]Modulus of elasticity values are applicable at a ratio of shear span to depth of 14.

[c]All maximum crushing strength perpendicular to grain values are based on standard test data only.

The method for determining the modulus of elasticity of a piece of wood is also described in ASTM D-245.

Woods are also stress graded mechanically. Mechanical stress grading is based on an observed relation between modulus of elasticity and bending strength, tensile strength, or compressive strength parallel to the grain. The modulus of elasticity of lumber thus is the sorting criterion used in this method of grading. The mechanical properties associated with lumber quality, for the stress grading method, are adjusted to give allowable unit stresses and an allowable modulus of elasticity suitable for most engineering uses. Adjustments are made to each strength property to account for the effects of size, moisture, and duration of load. The specific adjustments are described in ASTM D-245.

For a given design application, ASTM D-245 and D-2555 should be consulted to determine the static strength and elastic modulus for the wood to be used. The strengths should be increased for dynamic applications according to the discussion in Section 7.2.3. Table 7.5 provides the clear wood strength data given in ASTM D-2555.

7.4.3 Additional References

Since this manual is not intended as an independent design guide, engineers should consult the various design handbooks and manuals for further information on appropriate design practices. References 7.38 – 7.44 cover most of the materials of interest.

7.5 LIST OF SYMBOLS

A_p projected area

b length of reinforcement

C_0, C_2 empirical constants in Poncelet's Equation

c one-half the depth of a span

E modulus of elasticity under near static loading

E_a energy absorption capability

E_c chord modulus

E_d dynamic modulus of elasticity under near static loading

E_s secant modulus

E_T tangent modulus

$\bar{E}$ specific energy

e maximum elongation

F force

f coefficient of friction

f_{cr} static ultimate strength of a material in compression (crush strength)

f_c' static compressive strength of concrete

f_{dc}' dynamic compressive strength of concrete

I moment of inertia of a cross section

K, K_1, K_2 material constants for wood

ℓ abscissa of the point considered along the reinforcement

M maximum bending moment due to a load

m mass of projectile

N impact bending strength of a wood specimen

n	empirically determined constants
P	strength parallel to the grain
Q	strength across the grain
R	modulus of rupture
T	tensile stress in reinforcement
t_a	thickness of material available for crushing (energy absorption)
v	velocity
V_o	initial impact velocity
W	static strain energy of a material
W_d	dynamic strain energy of a material
α	empirical constant
ε	strain
$\dot{\varepsilon}$	rate of strain
θ	angle from the fiber direction
ν	Poisson's ratio
ρ	density
σ	stress
σ_c	ultimate strength of a material in compression (crush strength)
σ_{dc}	dynamic crush strength
σ_{dT}	dynamic ultimate strength of a material in tension
σ_{du}	dynamic ultimate strength of a material
σ_{dy}	dynamic yield strength of a material
σ_o	strength of a material at a strain rate of $1 \ sec^{-1}$
σ_T	static ultimate strength of a material in tension
σ_u	static ultimate strength of a material

σ_y static yield strength of a material

σ_{y_ℓ} lower yield stress

σ_{y_u} upper yield stress

τ tangential component of stress exerted on reinforcement

7.6   REFERENCES

7.1   AISC Specification for the Design, Fabrication and Erection of
       Structural Steel for Buildings, American Institute of Steel
       Construction, New York, NY, February 1969.

7.2   "Suppressive Shields Structural Design and Analysis Handbook,"
       U. S. Army Corps of Engineers, Huntsville Division, HNDM-1110-1-2,
       November 1977.

7.3   Symonds, P. S., "Survey of Methods of Analysis for Plastic Deforma-
       tion of Structures under Dynamic Loading," Final Report to Naval
       Ship Research and Development Center, No. BU/NSRDC/1-67, Contract
       No. 3248, June 1967.

7.4   Winlock, J., "The Influence of the Rate of Deformation on the
       Tensile Properties of Some Plain Carbon Sheet Steels, Transactions,
       AIME, Journal of Metals, Volume 197, pp. 797-803, June 1953.

7.5   Manjoine, M. J., "Influence of Rate of Strain and Temperature on
       Yield Stresses of Mild Steel," Journal of Applied Mechanics,
       pp. A211-A218, December 1944.

7.6   Lindholm, U. S. and Bessey, R. L., "A Survey of Rate Dependent
       Strength Properties of Materials," Final Report to Air Force
       Materials Laboratory, AFML-TR-69-119, April 1969.

7.7   Kraft, J. M., "Correlation of Plane Strain Crack Toughness with
       Strain Hardening Characteristics of a Low, a Medium, and a High
       Strength Steel," Applied Materials Research, Vol. 3, p. 88, 1964.

7.8   Holt, D. L., Babcock, S. G., Green, S. J., and Maiden, C. J.,
       "The Strain-Rate Dependence of the Flow Stress of Some Aluminum
       Alloys," Transactions of the American Society of Metals, Vol. 60,
       p. 152, 1967.

7.9   Steidel, R. F. and Makerou, C. E., "The Tensile Properties of Some
       Engineering Materials at Moderate Rates of Strain," ASTM Bulletin,
       pp. 57-64, July 1960.

7.10   Lindholm, U. S. and Yeakley, L. M., "High Strain-Rate Testing:
       Tension and Compression," Experimental Mechanics, Vol. 8, p. 1,
       1968.

7.11   "Systems Applications of Nuclear Technology: Effects of Air Blast
       Cratering, Ground Shock and Radiation on Hardened Structures,"
       AFSC Manual 500-8, Department of the Air Force, Chapter 8, January
       1976.

7.12 Structures to Resist the Effects of Accidental Explosions (1969), Dept. of the Army Technical Manual TM 5-1300, Dept. of the Navy Publication NAVFAC P-397, Dept. of the Air Force Manual AFM 88-22, Dept. of the Army, Navy, and Air Force, June 1979.

7.13 American Concrete Institute Building Code Requirements for Reinforced Concrete (ACI 318-77) Section 10.2.

7.14 McHenry, D. and Shideler, J. J., "Review of Data on Effect of Speed in Mechanical Testing of Concrete," Symposium on Speed of Testing of Non-Metallic Materials, Atlantic City, NJ, (ASTM Special Technical Publication No. 185), pp. 72-82, June 29, 1955.

7.15 Watstein, D., "Effect of Straining Rate on the Compressive Strength and Elastic Properties of Concrete," Journal of the American Concrete Institute, pp. 729-744, April 1953.

7.16 Gupta, Y. M. and Seaman. L., "Local Response of Reinforced Concrete to Missile Impact," EPRI NP-1217, Research Project 393-1, Final Report, October 1979.

7.17 U. S. Forest Products Laboratory, Wood Handbook: Wood as an Engineering Material, U. S. Department of Agriculture, Agriculture Handbook No. 72, 1974.

7.18 Markwardt, L. J. and Liska, J. A., "The Influence of Rate of Loading on the Strength of Wood and Wood-Base Materials," Symposium on Speed of Testing of Non-Metallic Materials, Atlantic City, NJ (ASTM Special Technical Publication No. 185), pp. 3-17, June 29, 1955.

7.19 Ferguson, W. G. and Yew, F. K., "The Application of the Rate Theory of Deformation to the Yield Behavior of Wood," Journal of Materials Sciences.

7.20 Ritland, H. N., "The Effect of Speed of Testing on Glass," Symposium on Speed of Testing of Non-Metallic Materials, Atlantic City, NJ (ASTM Special Tehcnical Publication No. 185), pp. 19-29, June 29, 1955.

7.21 Tensile-Impact Energy to Break Plastics and Electrical Insulating Materials," ANSI/ASTM D 1822-68.

7.22 Smith, C. O., The Science of Engineering Materials, Second Edition, Prentice Hall, Inc., p. 187, 1977.

7.23 "Notched Bar Impact Testing of Metallic Materials, ASTM E23-72.

7.24 "Impact Resistance of Plastics and Electrical Insulating Materials," ANSI/ASTM D256-78.

7.25 "Apparent Impact Strength of Preformed Block-Type Insulating Materials," ANSI/ASTM C 589-68, (Reapproved 1975).

7.26 "Conducting Strength Tests of Panels for Building Construction," ANSI/ASTM E 72-77.

7.27 Westine, P. S., "Prediction of Transient Displacement, Velocity. and Force on Projectiles Penetrating Cohesive Soils," Journal of Terramechanics, 12 3/4, pp. 149-170, December 1975.

7.28 Healey, J., Werner, H., Weissman, S., Dobbs, N., Price, P., "Primary Fragment Characteristics and Impact Effects on Protective Barriers," Picatinny Arsenal Technical Report No. 4903, Amman and Whitney, Consulting Engineers, New York, NY, December 1975.

7.29 "Small Clear Specimens of Timber," ASTM D 143-52 (Reapproved 1972).

7.30 "Design Data for the Preliminary Selection of Honeycomb Energy Absorption Systems," TSB 122, HEXCEL, 1964.

7.31 "Mechanical Properties of Hexcel Honeycomb Materials," TSB 120, HEXCEL, Winter 1979 Revision.

7.32 Matonis, V. A., "Elastic Behavior of Low-Density Rigid Foams in Structural Applications," Society of Plastics Engineering Journal, pp. 1024-1030, September 1964.

7.33 Lipson, S., "Cellular Aluminum for Use in Energy Dissipation Systems," NASA CR-93, September 1964.

7.34 "Recent Results in Trench Research on Reinforced Earth," Francois Schlosser and Nguyen-Thank Long, Journal of the Construction Division ASCE, September 1974.

7.35 "Tests on the Effects of Explosive Charges on Reinforced Earth Walls," Victor Elias, Minutes of the Eighteenth Explosives Safety Seminar, Vol. 1, September 1978.

7.36 Annual Book of ASTM Standards, American Society for Testing and Materials, Parts 1-48, Race Street, Philadelphia, PA, 19103, 1978.

7.37 Metallic Materials and Elements for Aerospace Vehicle Structures:
      Military Standardization Handbook, MIL-HDBK-5C, 15 September 1976.

7.38 ACI Manual of Concrete Practices, Parts 1, 2, and 3, American
      Concrete Institute, Detroit, MI (Current Edition).

7.39 Aluminum Standards and Data, The Aluminum Association, New York,
      NY (Current Edition).

7.40 PCI Design Handbook: Precast, Prestressed Concrete, Prestressed
      Concrete Institute, Chicago, IL (Current Edition).

7.41 Specifications for the Design of Cold Formed Steel Structural
      Members, American Iron and Steel Institute, Washington, DC (Current
      Edition).

7.42 Standard Specifications and Load Tables, Steel Joist Institute,
      Arlington, VA (Current Edition).

7.43 Concrete Masonry Handbook, Portland Cement Association, Chicago,
      IL (Current Edition).

7.44 Masonry Design Manual, Masonry Industrial Advancement Committee,
      Masonry Institute of America, Los Angeles, CA (Current Edition).

CHAPTER 8

STRUCTURAL DESIGN

8.1 INTRODUCTION

The contents of this Chapter are intended for use in understanding design
philosophy; the contents are not intended to replace existing design sources.
The purpose of this Chapter is to provide general guidance in the application
of analysis methods for the design of structures to resist the effects of dy-
namic loads. The aim is to increase the analyst's understanding of dynamic
response and make him aware of analysis methods from which he can select a
method that is appropriate for his design problem.

In general terms the steps that are taken when designing a building for
blast resistance are:

1. Establish siting, general building layout, and the design criteria.

2. Size members for static loads.

3. Determine potential sources of accidental explosions and establish
    their location and magnitude.

4. Calculate the blast loads on the building.

5. Define the fragments for which the building must be designed.

6. Calculate loading from fragment impact.

7. Calculate the loading from earth ejecta if cratering throws earth
    against the building.

8. Define the ground shock at the building site.

9. Perform a preliminary analysis to size the structure for the blast
    loads.

10. Perform an analysis using either simplified or numerical methods.

11. Redesign or resize the structure as required to meet the design
    criteria.

Design of a building usually involves interaction between several disciplines.
An architect engineer (AE) is usually responsible for the siting and general
layout of the building. The AE may also size structural members of the build-
ing to resist conventional loads. Conventional loads will include dead weight,

equipment operating loads, and loads associated with natural phenomena such as tornado, fire, and earthquake. Safety and process engineers may define the location and energy of potential explosions that will produce overpressures, fragments, and ground shock for which the building must be designed.

Using Chapter 4 of the handbook, the designer can, knowing the location and energy in an explosion, predict the blast loading (p(t) or P and i) for which the building must be designed. Also, using Chapters 5 and 6 of the handbook, the designer can estimate ground shock and fragments that may strike the building.

Once the building has been designed for conventional loads and the blast loads on the building have been established, the analyst is ready to apply Chapters 7 and 8 with existing design aids to evaluate the strength of the building for these loads. Chapter 7 gives the material properties that the designer and analyst should use in sizing the members. Usually some allowance can be taken for the fact that dynamic loading will cause the building to respond with a strain rate that is high enough to increase the material yield strength. Using the appropriate material properties and load, this chapter provides the analyst with guidance on how to analyze the structure and set the dimensions (sizes) of structural members in the building. Because analytical methods for structural design have already been developed and documented, this chapter identifies applicable methods and provides some guidance for a choice of method and for its application.

Analysis methods described here have been divided into two general categories: simplified methods and numerical methods. In this discussion the definitions will be:

Simplified Methods: Refers to single or two-degree-of-freedom approximations to the dynamic behavior of structural elements. Most often the solution is presented in graphical or in closed form, but numerical integration is used to obtain solutions in some cases.

Numerical Methods: Refers to sophisticated multi-degree-of-freedom solutions for the response of structural elements or of complex structural systems. A digital computer is required for these solutions, and the cost can be high if plasticity is included and a dynamic solution is obtained.

Typical "simplified methods" for the design of structures to resist dynamic loads are contained in manuals such as TM5-1300, "Structures to Resist the Effects of Accidental Explosions" (Ref. 8.1), in books such as Introduction to Structural Dynamics by Biggs (Ref. 8.2), and in papers such as "Energy Solutions for Predicting Deformations in Blast Loaded Structures" by Westine and Baker (Ref. 8.3). Numerical methods are characterized by large multi-purpose finite element (F.E.) computer programs such as ADINA (Ref. 8.4), ANSYS (Ref. 8.5), MARC (Ref. 8.6), and a limited number of special purpose

codes (both finite element and finite difference) such as **DYNFA (Ref. 8.7) and**
PETROS 4 (Ref. 8.8). Additional explanation and some comparisons between the
various methods are included in Sections 8.3.1 and 8.3.2.

8.2 ELEMENTS OF DYNAMIC RESPONSE ANALYSIS

8.2.1 Transient and Quasi-Static Loads

By their very nature, accidental explosions produce transient loads on
buildings. To design for blast resistance, the effect of these transient
loads on the response of the building must be determined; however, what seems
to be very brief to the observer in real time can be quite long in terms of
the vibration periods of a structure so that the loads are classified as short
(impulsive), or long (quasi-static) relative to the structural vibration per-
iods. The intermediate region between impulsive and quasi-static, where per-
iods are about the same as loading times, is called the pressure-time region.

The types of loads considered herein that can be produced on a build-
ing by an explosion are:

* overpressures produced by the blast wave

* a long term gas pressure if the explosion is confined

* ground shock

* fragment impact

* impact from soil if cratering occurs

The most important load in design is usually the overpressure produced by the
blast wave. This load will always occur unless the explosion is confined and
no venting is produced. Ground shock will also occur unless the explosion is
confined and isolated from the ground; however, ground shock is usually of
secondary importance. The increase in long term pressure occurs only when there
is confinement, and the creation of fragments or soil ejecta will depend upon
the position of the explosion relative to the ground and adjacent structure.

Each of these loads can be classified as impulsive, pressure-time, or
quasi-static relative to a specific structural component. If the period of
the fundamental vibration of the component is very short, all of the loads
may be quasi-static (long duration relative to the structural period). If
the period of vibration is long (low frequency), then all of the loads may
be impulsive for that component. Even so, for most building structures, im-
pact loads produced by fragments and earth ejecta are idealized as an im-
pulse or initial velocity and the gas pressure increase is usually quasi-
static. It is easy to see that the same load may be classified differently
for different components in a building.

The way a load affects the structure depends not only upon its duration but upon its rise time and general shape as well. An example of the effect of different load pulse shapes for an elastic oscillator is given in Figure 8.1. This figure gives the dynamic load factor (DLF) and the time (t_m) at which the maximum response occurs for a rectangular force, a triangular force with zero rise time, and a ramp function to a constant load. Notice that the maximum DLF is always a function of the ratio between some characteristic time of the loading (t_d or t_r) and the fundamental period (T) of the one-degree-of-freedom oscillator. $(DLF)_{max}$ is the ratio of the maximum response of the structure (maximum deflection, stress, etc.) relative to the maximum response produced by a static load of the same magnitude. Notice that all of the forces give about the same peak value of DLF (approximately 2.0). For the rectangular and triangular force pulses, this occurs when the duration is long (both have zero rise times), and for the ramp function to a constant load it occurs when the rise time is short. These cases all equal or approach the DLF for a step function to a constant load. It is well known that DLF = 2.0 for a step function with $t_d/T > 5.0$ (Ref. 8.2).

Loading from a blast wave from high explosive (HE) charges can be closely approximated by the triangular pulse with zero rise time. If the explosion is produced by vapor or dust clouds, very different forcing functions can occur as explained in Section 8.2.3. Curve shapes for quasi-static pressure loadings are closely approximated by the ramp function to a constant value or, conservatively, by using long duration rectangular or triangular force pulses with zero rise time.

When the forces on the building are either impulsive or quasi-static, simplifications in the analysis are possible. Impulsive loads can be replaced by an initial velocity imparted to the structure. As explained in Chapter 4 of Ref. 8.9, this is done by equating the total impulse to the change in momentum of the structure. From the initial velocity, the initial kinetic energy is obtained. Equating the initial kinetic energy to the strain energy absorbed by the structure during deformation (elastic or plastic) will give the impulsive asymptote for the structure. For many structural components, equations can be derived to give this asymptote.

When the forces are quasi-static then, for elastic behavior, a static analysis can be used. This is strictly true only for very slowly applied loads; however, for suddenly applied constant loads (step function), the results of the static analysis, multiplied by two, are also valid. If the material deforms plastically, the quasi-static asymptote can be obtained by equating the work done by the load as the structure deforms to the strain energy of deformation. As for impulsive loads, simple formulas that give the quasi-static asymptote can be derived for many structural components. Figure 8.2 from Reference 8.9 gives a P-i (pressure-impulse) diagram for beams. The ordinate and abscissa are nondimensional terms so that the results are applicable to beams of different geometry. In this example the curves are for different values of maximum strain in the beam. Note that four different boundary conditions are permitted by the proper choice of the constants ψ.
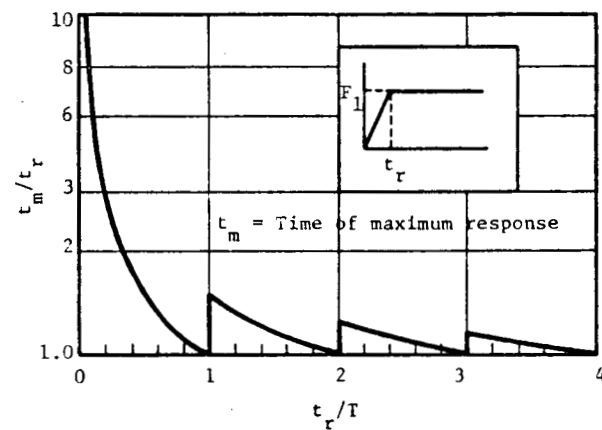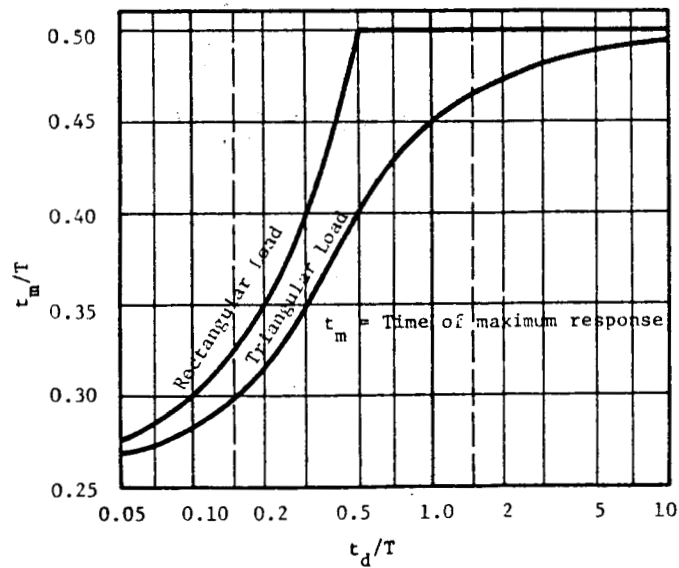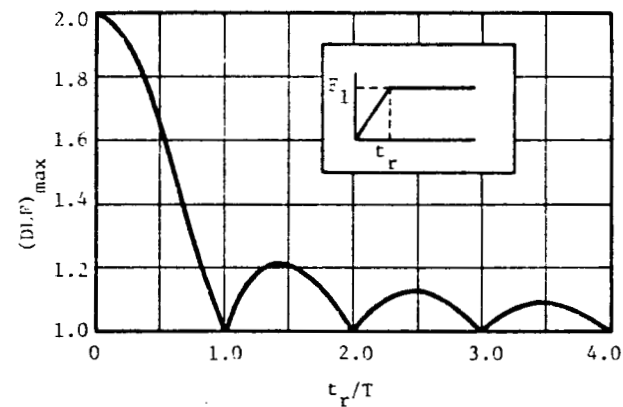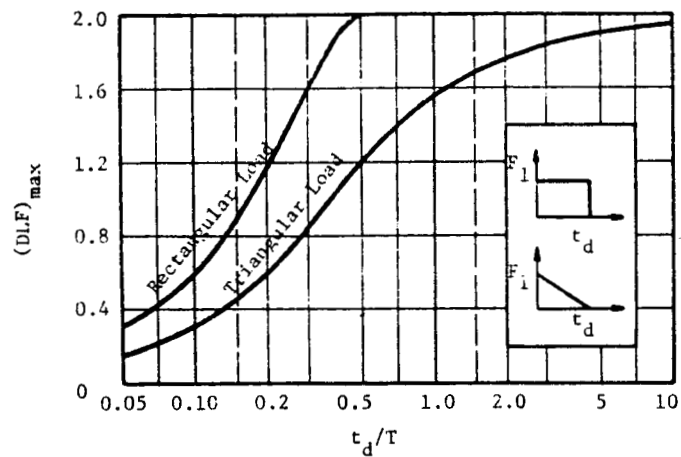
(a) Triangular and rectangular force pulses with zero rise time

(b) Constant force with finite rise time

Figure 8.1 Dynamic Load Factors (DLF) and Time to Maximum Response (t_m) for Different F(t)'s

BOUNDARY CONDITIONS	ψ_p	ψ_i	ψ_ϵ	ψ_{w_o}
SIMPLE SUPPORT	10.00	0.913	1.250	0.2083
CLAMPED - CLAMPED	23.10	0.861	1.925	0.0625
CLAMPED - PINNED	15.83	0.885	1.979	0.0867
CANTILEVER	3.333	0.577	1.000	0.5000

$$\frac{H\,w_o}{\ell^2\,\epsilon_{max}} = \psi_{w_o}$$

Vertical axis: $\dfrac{\psi_i \sqrt{pA}\,\sigma_y\,Z}{i b \sqrt{EI}}$

Right axis: $\dfrac{IE\epsilon_{max}}{\psi_\epsilon\,HZ\sigma_y}$

Horizontal axis: $\dfrac{pb\,\ell^2}{\psi_p\,\sigma_y\,Z}$
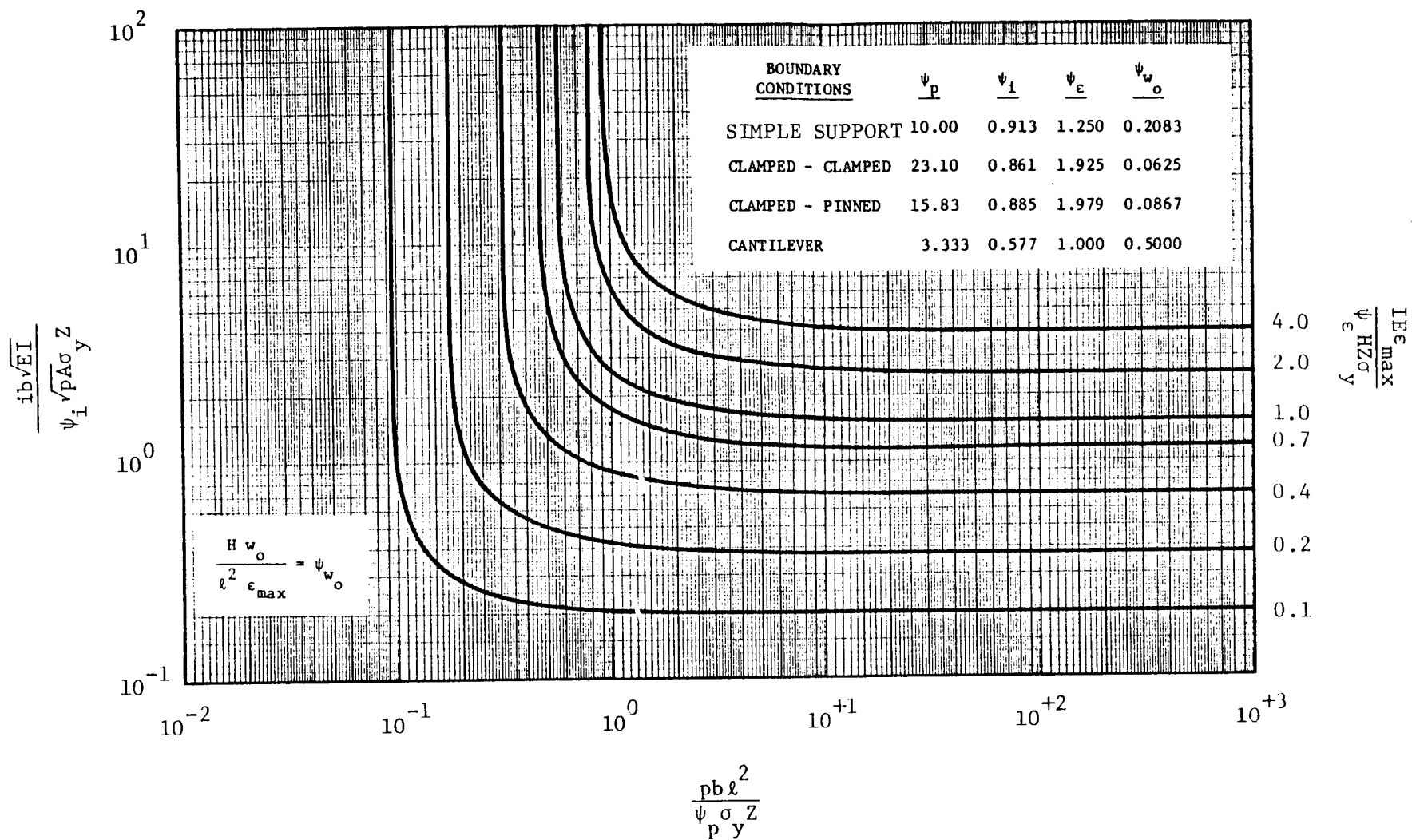
Figure 8.2 Elastic-Plastic Solution for Bending of Blast-Loaded Beams (Ref. 8.9)

In Figure 8.2 the vertical asymptote is the quasi-static one. Increasing the impulse (load duration) along this asymptote does not change the result. Only a change in pressure will increase the strain. Likewise, the horizontal asymptote is for impulse. Increasing the pressure along this asymptote does not change the result. The intermediate, curved portion of the curve is called the dynamic realm. Here the beam response is a function of both pressure and impulse, and the problem must be solved dynamically.

To enter Figure 8.2, the nondimensional terms on the ordinate and abscissa are evaluated from the load parameters (p & i), the beam material properties and the beam geometry. These coordinates will fall on or near a curve which gives the value of the nondimensional group for maximum strain. From this value, ε_{max} can be determined. Using ε_{max}, the center displacement can be found from the equation in the lower left-hand corner of Figure 8.2.

Ground shock produced by an explosion is difficult to define. For linear problems it can be represented by a response spectrum. Approximate methods of defining such a spectrum are discussed in paragraph 5.6.1, Chapter 5 of this manual, and in Reference 5.36 and Reference 8.2. In nonlinear response problems, ground shock is most conveniently represented as a displacement-time history that is applied to the base of the building.

8.2.2 Material Behavior

Under dynamic loads associated with explosions, strain rates in materials will be in the range of 1 to 100 in./in./sec. These rates are high enough to increase the yield strength of some structural materials above static values. Data on strain rate effects in structural steels, concrete, and other materials are given in Chapter 7.

When using numerical methods, continuous variations in strain rate that occur in the materials can be included in the analysis. In such cases the approximate formulas given in Chapter 7 that relate yield stress to strain rate are useful; however, when using simplified methods, a simpler way of accounting for strain rate is required. Norris, et al. (Ref. 8.10), suggests that some average value be used which is based upon the time required to reach the yield stress. Following this approach, the authors cite average strain rates of 0.02 to 0.2 in./in./sec, and for ASTM A7 structural steel recommend an increase in the yield stress from about 38,000 psi to 41,600 psi. A similar increase is probably warranted for other structural steels, but a choice for any material can be made if the strain rate data are available and if 0.2 in./in./sec is accepted as a reasonable average for structural response to blast loads.

Numerical results reported by Cox, et al. (Ref. 8.11), showed that strain rate is very important for rings that are subjected to uniform dynamic internal pressures. Including the effect of strain rate reduces peak strains to about one-third. For beams in the same structure, strain rates had very

little effect on calculated peak strains, but the peak strains in the beam were only slightly above yield, and in bending only the surface experiences the maximum strain rates. For rings, the rate of straining is uniform over the total cross section of the component; high strain rates significantly increase the total yield loads and, thus, significantly reduce the total strain.

Strain rate effects should be included in numerical methods if it can be done conveniently, particularly when membrane action (significant stretching of the material at the neutral axis) is predominant in the response. For simplified methods, some increase in the yield stress above static values is also warranted. Of course, ignoring strain rate entirely leads to conservative results.

Material damping (the hysteresis which occurs in the stress-strain diagram when a material is subjected to cyclic loads) is small and can be ignored in blast related response problems. Only the first few cycles of response are of interest and the effect of material damping will be insignificant. Overall structural damping will be higher, but it too will be small compared to the damping effects of structural plasticity. Thus, for transient response problems involving material plasticity, ignoring damping will lead to a slightly conservative result.

8.2.3 Structural Behavior

This section will give a brief overview of the behavior of structures when subjected to transient loading. It covers the effects of such things as plasticity, load history, and damping on structural behavior and discusses single and multiple degree-of-freedom solutions.

8.2.3.1 Elastic-Plastic Behavior

Normal operating loads for a building are far below those which can be produced by an accidental explosion. Loads from the explosion can be thought of as overloads, and if the building is designed for elastic behavior at these overload conditions, then a massive, overdesigned structure can be the result. It is acceptable design practice to permit some permanent deformation in the building at overload. If the amount of permanent deformation is small, the building can be reused after the accident. If large permanent deformation occurs, the building cannot be reused.

For a one-degree-of-freedom system, the effect of plasticity has been demonstrated by Baker, et al. (Ref. 8.9). Figure 8.3 compares two systems with equal stiffness, but one is 33 percent stronger than the other. The displacement-time history for the stronger system is not shown but it oscillated about zero with an amplitude equal to that given by the dashed line labeled "elastic solution." Under equal dynamic loads, the strong spring is stressed just to yield (elastic solution) and the weaker spring yields, as shown by the displacements. The significant point is that the peak deformation of the weaker spring was very nearly the same as for the stronger spring (elastic solution).
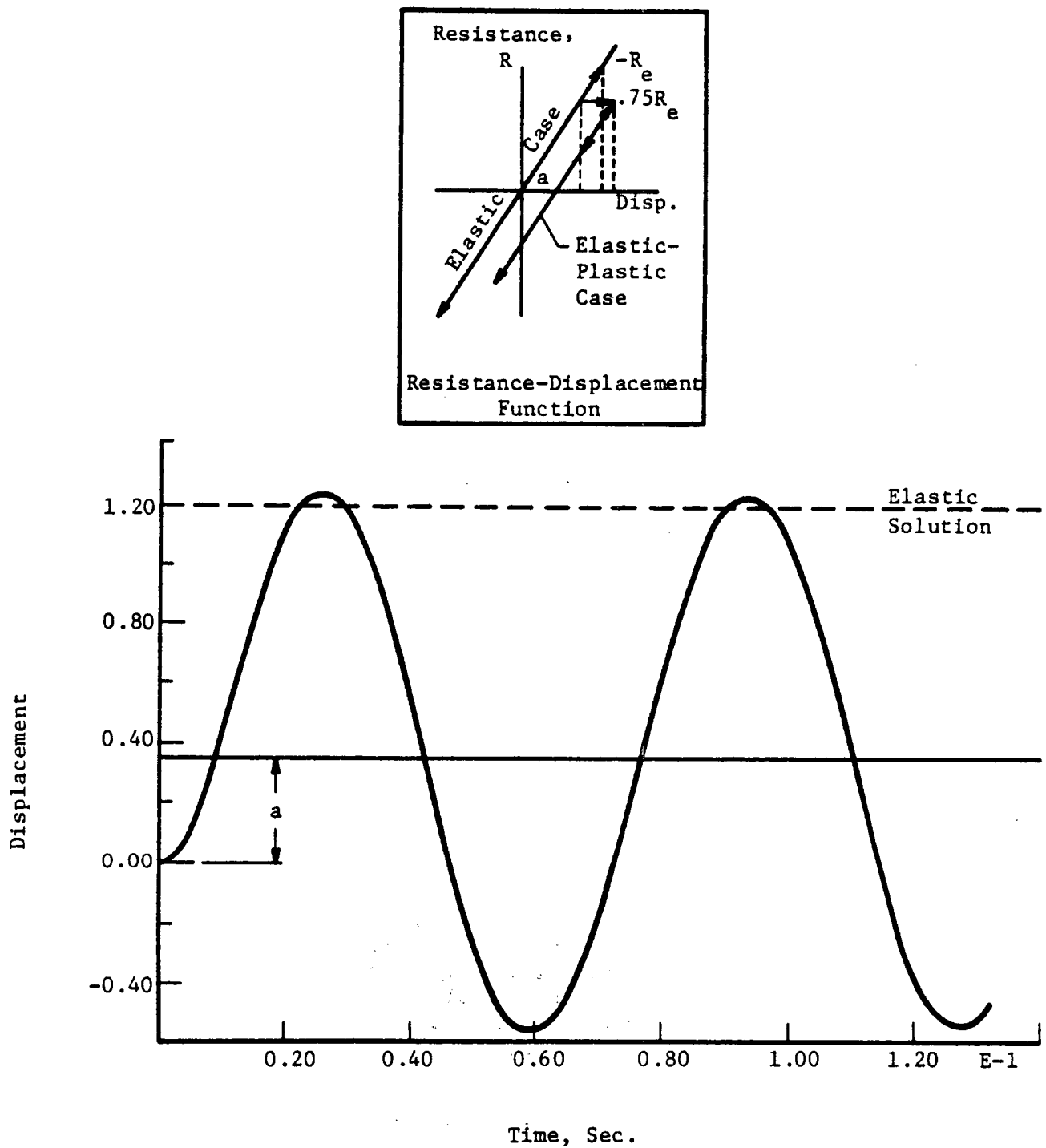
Figure 8.3   Displacements of One-Degree-of-Freedom System with a
Bi-Linear Resistance Function (Ref. 8.9)

This occurs because only a slight increase in deformation is required in the weaker system to equal the strain energy in the stronger system. The ductility ratio, μ, is a common criterion for evaluating plastic behavior in structures (Refs. 8.1, 8.2 and 8.3). It is the total deformation divided by the deformation at which yielding occurs. For the weak spring this ratio is

$$\mu = 1.35$$

A ductility ratio of three generally is acceptable for reusable structures, if other criteria such as hinge rotations and lateral sway are met. [See Refs. 8.17 and 8.19 for a discussion of design criteria for steel construction and Refs. 8.1 and 8.10 for a discussion of design criteria for concrete construction.] Thus, it is apparent that a substantial reduction in strength still produces an acceptable design for peak overloads when even modest plasticity is permitted.

The effect of plasticity on the response of a two-degree-of-freedom model (simulating a two-story frame building) subjected to sinusoidal ground motions has been demonstrated by Biggs (Ref. 8.2). In this example, the strength of the building was reduced to 50 percent of the peak force experienced by the structure for elastic behavior. The stiffness was unchanged. Figure 8.4 repeated from Ref. 8.2 work, shows that the peak deformations in both the first and second stories of the building are reduced when plasticity is permitted. This behavior is somewhat unusual, but can occur because plasticity prevents the resonance that can occur in a structure under sinusoidal excitation.

From these simple examples, one cannot predict what might happen in every problem, but, in general, the designer will find that economies in design will result when modest plasticity is permitted, and only small increases in the deformation, relative to an elastic system, will occur.

8.2.3.2 Effect of Loading History on Structural Response

The effects of three different load pulses on the response of a single-degree-of-freedom oscillator were shown in Figure 8.1. These pulse shapes can be used to approximate "conventional" types of blast loads such as that produced by shock waves from a high explosive or a change in ambient pressure within a confined volume. In this section the effects of load histories that characterize vapor and dust explosions and bursting pressure vessels are shown.

a. Gas or Dust Explosions. Gas and dust explosions are not normally a problem at Pantex but the phenomena are discussed herein for completeness. The loadings on a structure or structural element caused by an internal gas or dust explosion are in many cases different from the loadings produced by condensed explosives. Overpressures produced by condensed explosives

50 psf

I = 4000 in.^{4}

I = 240 in.^{4}

80 psf

I = 5000 in.^{4}

Walls 20 psf

I = 450 in.^{4}

12'

15'

25' Bent spacing

50'

(a) two story frame

U_2

M_2=0.177 kip-sec^2/in.

U_1

M_1=0.294 kip-sec^2/in.

y_s

(b) two-degree-of-freedom model

y_s

$\frac{1}{2}$"

$\frac{1}{2}$"

t

0.5 sec

$y_s = y_{so} \sin \Omega t$

$= 0.5 \sin 4 \pi t$ in.
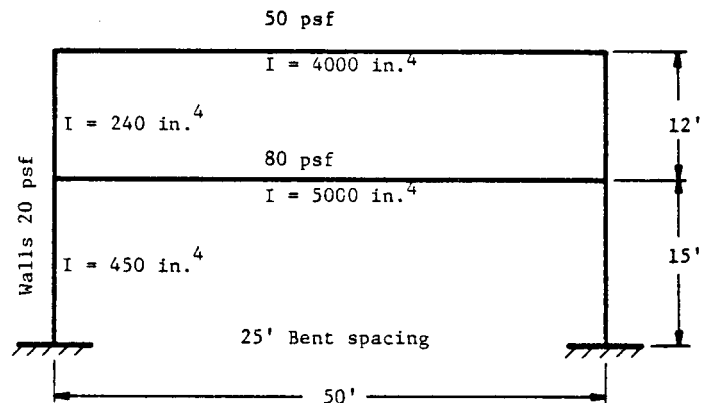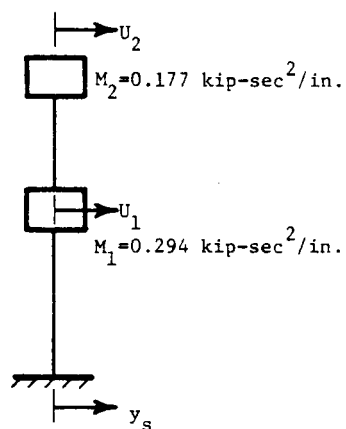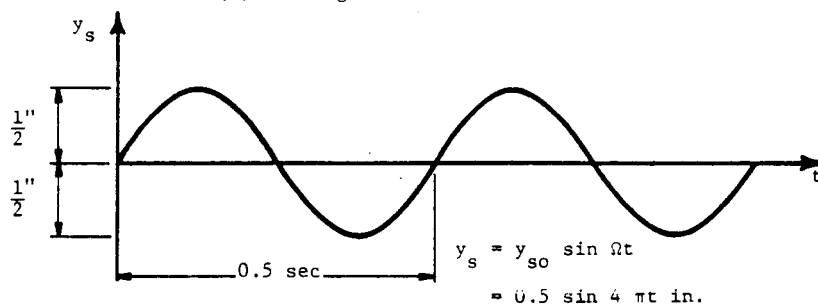
(c) support motion

Figure 8.4 Elastic and Inelastic Responses of Two Story Building Frame Subjected to Sinusoidal Support Motions (Ref. 8.2)
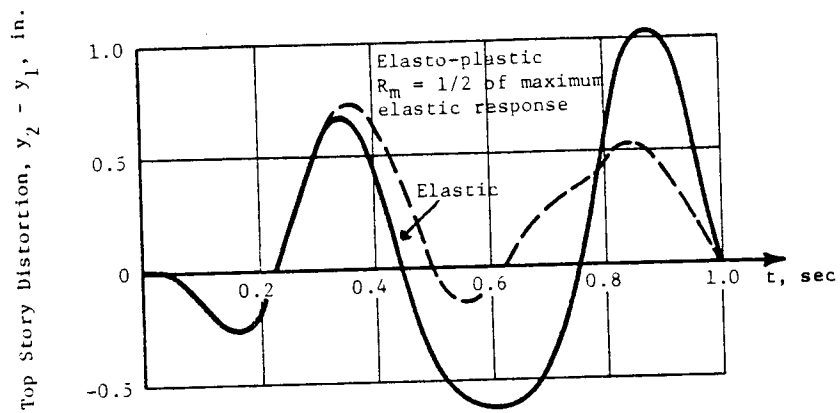
(d) top story
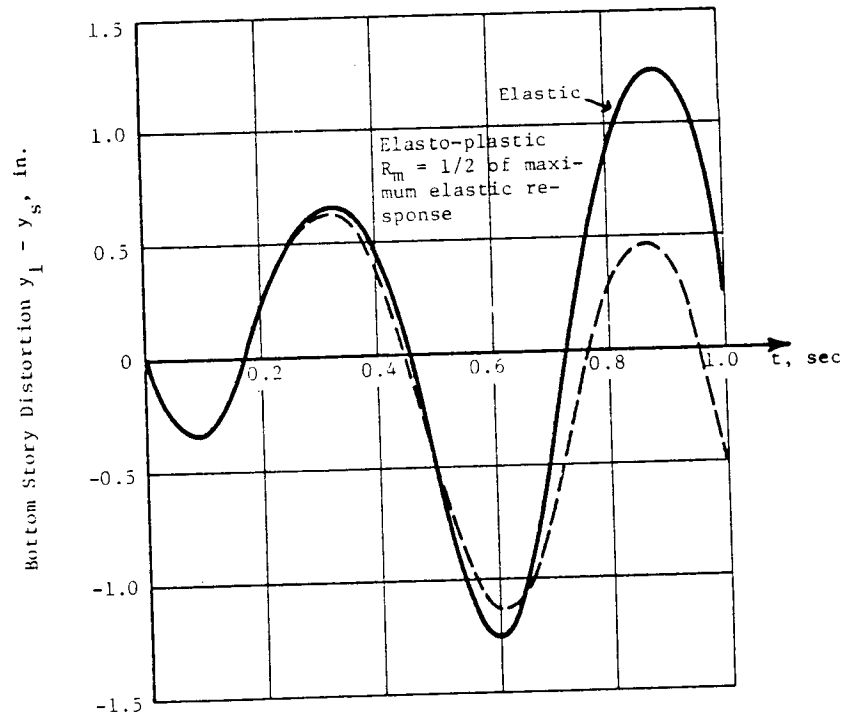
(e) bottom story

Figure 8.4 (Continued)

are characterized by very short rise times and exponential decay. Often a triangular approximation is assumed. For vapors or dust explosions, the loading is characterized by a finite rise time and a different shape. In fact, many researchers performing gas or dust explosion experiments give, as their results, the peak value of the overpressure, P_m, a rate of pressure rise, dp/dt, and, in case of venting, some duration, t_d, (see Figure 8.5).
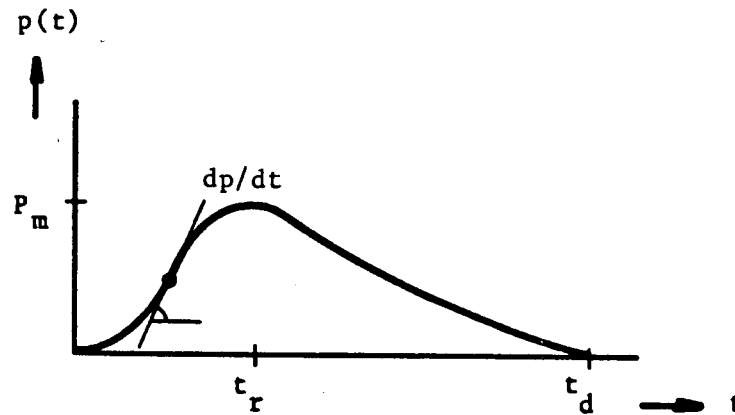
Figure 8.5 Schematic Overpressure-Time History in
Confined Gas or Dust Explosions

The loading can be described approximately by the following formula:

$$p(t) = P_m \left[t/t_r - \frac{1}{2\pi} \sin \frac{2\pi t}{t_r} \right] \qquad t \leq t_r \qquad (8.1)$$

$$= P_m \left(1 - \frac{t - t_r}{t_d - t_r} \right) e^{-\left(t - t_r / t_d - t_r \right)} \quad t_r \leq t \leq t_d \qquad (8.2)$$

The pressure rate defined as the slope at $t = t_r/2$ will then be:

$$\frac{dP}{dt} \left(t = \frac{t_r}{2} \right) = \frac{2 P_m}{t_r} \qquad (8.3)$$

For this loading, the influence of the finite rise time and the shape of the loading on structural response were investigated using a one-degree-of-freedom elastic-plastic mass-spring system as a calculation model for the structural response. The calculated P-I diagram is given in Figure 8.6. For comparison, the P-I curve for exponential decay ($P = P_{max} e^{-t/T_1}$) is also shown.
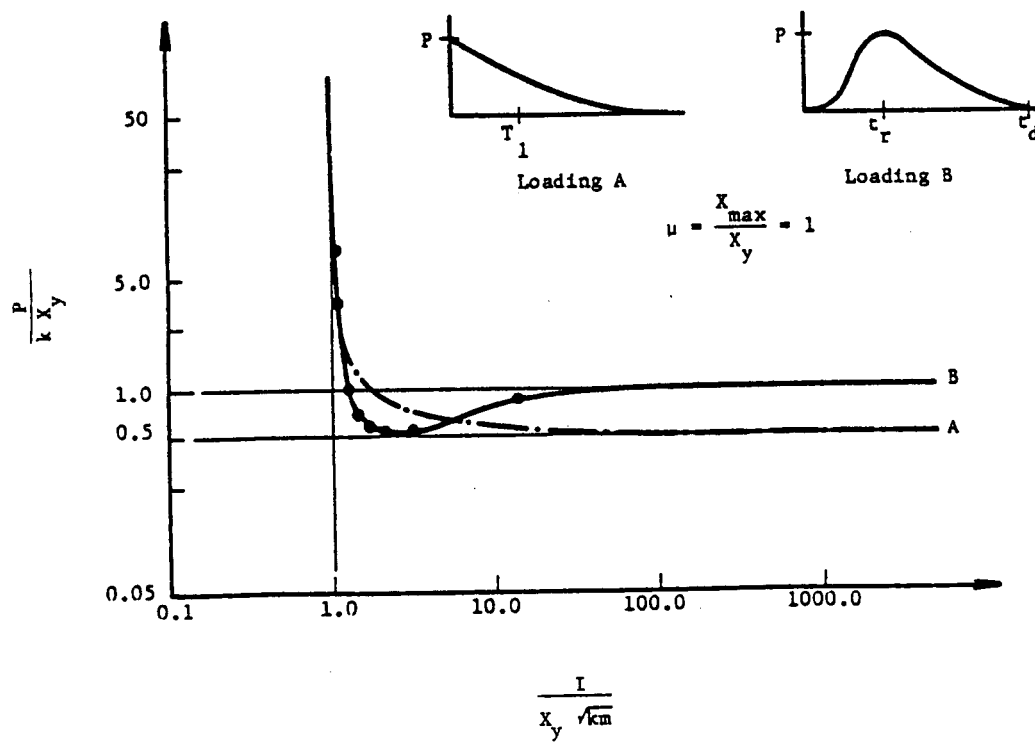
Figure 8.6 Comparison of Zero and Finite Rise Times on the P-i Diagram

Two important observations can be made from these results:

(1) The pressure asymptote for a finite rise time loading is 1.0 (equivalent to a static loading), whereas the pressure asymptote for a loading with zero rise time is 0.50 (equivalent to twice the static loading).

(2) In the region $1.15 < \dfrac{I}{X_{max} \sqrt{km}} < 5.5$, the loading with finite rise time is more severe than the loading with zero rise time. This behavior is produced by resonance between the loading rate and the structural frequency.

Results differ only slightly if the ratio of t_r/t_d is shifted within reasonable limits. This is shown in Figure 8.7 where the curve in Figure 8.6 ($t_r/t_d = 0.40$) is compared to a loading width of $t_r/t_d = 0.20$.

Influence of the ductility ratio is shown in Figure 8.8. Here the loading is identical to A in Figure 8.7, but in one case, the structure responds elastically, and in the other the structure experiences significant plasticity. The effect of the plasticity is to damp the dynamic overshoot that occurs elastically and to shift the curve to the right. The shift occurs because it takes more energy to deform the structure plastically. Note that elastic, perfectly plastic behavior was assumed.

b. <u>Pressure Vessel Burst</u>. The loading on a structure or structural element caused by a pressure vessel burst is somewhat different from that associated with a high explosive (Loading A, Figure 8.6) or with dust or gaseous vapor explosions (Loading B, Figure 8.6). The principal difference is that a large, long duration negative pressure (the so-called negative phase) occurs in vessel bursts, and there are usually multiple shock waves. Figure 8.9 gives an actual recorded pressure-time history from a vessel burst, taken from Esparza and Baker (Ref. 8.12).

In order to investigate the influence of this different type of loading, the loading is approximated as in Figure 8.10. Using this schematization of the loading, the data from Ref. 8.13 are well approximated when $\alpha = 0.24$, $\beta = 0.76$, $\gamma = -0.85$, and $\delta = 0.8$.

The response of structures to this kind of loading can now be examined and compared to the usual loading types. As for dust and vapor explosions, this was done by replacing the structure with a one-degree-of-freedom elastic-plastic spring mass system. Results are given in Figure 8.11. As can be seen from the graph, there is a region of t_{d1}/T where the triangular approximation based on the first positive pressure pulse greatly underestimates the true loading. This region is approximately bounded by $0.05 < t_{d1}/T < 10.0$. The contribution of the negative phase of the loading is important in this region, as well as the presence of the second positive peak. The contribution of the negative pressure can be explained by the fact that the mass
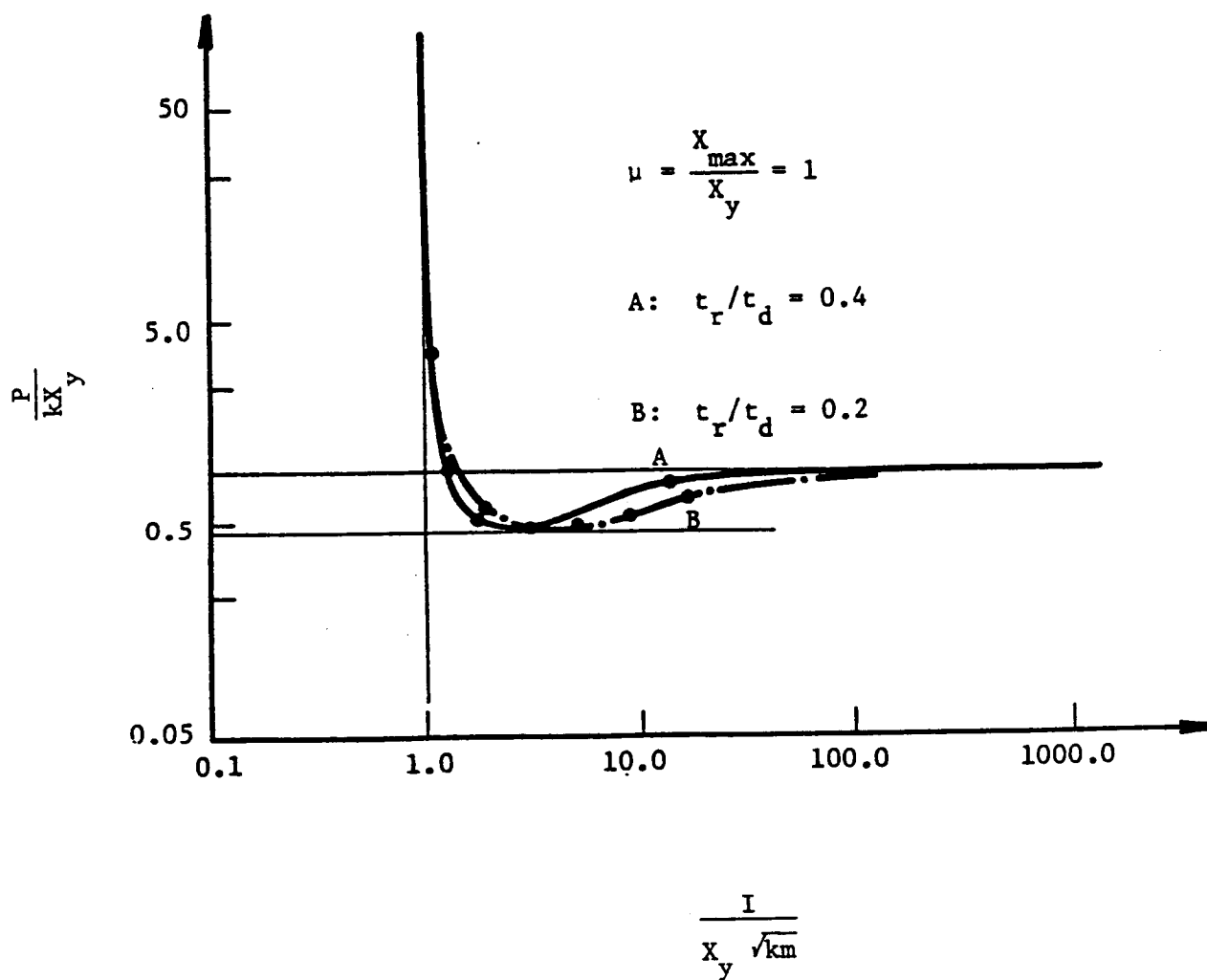
Figure 8.7 Effect of Change in t_r/t_d For Finite Rise Time Loading
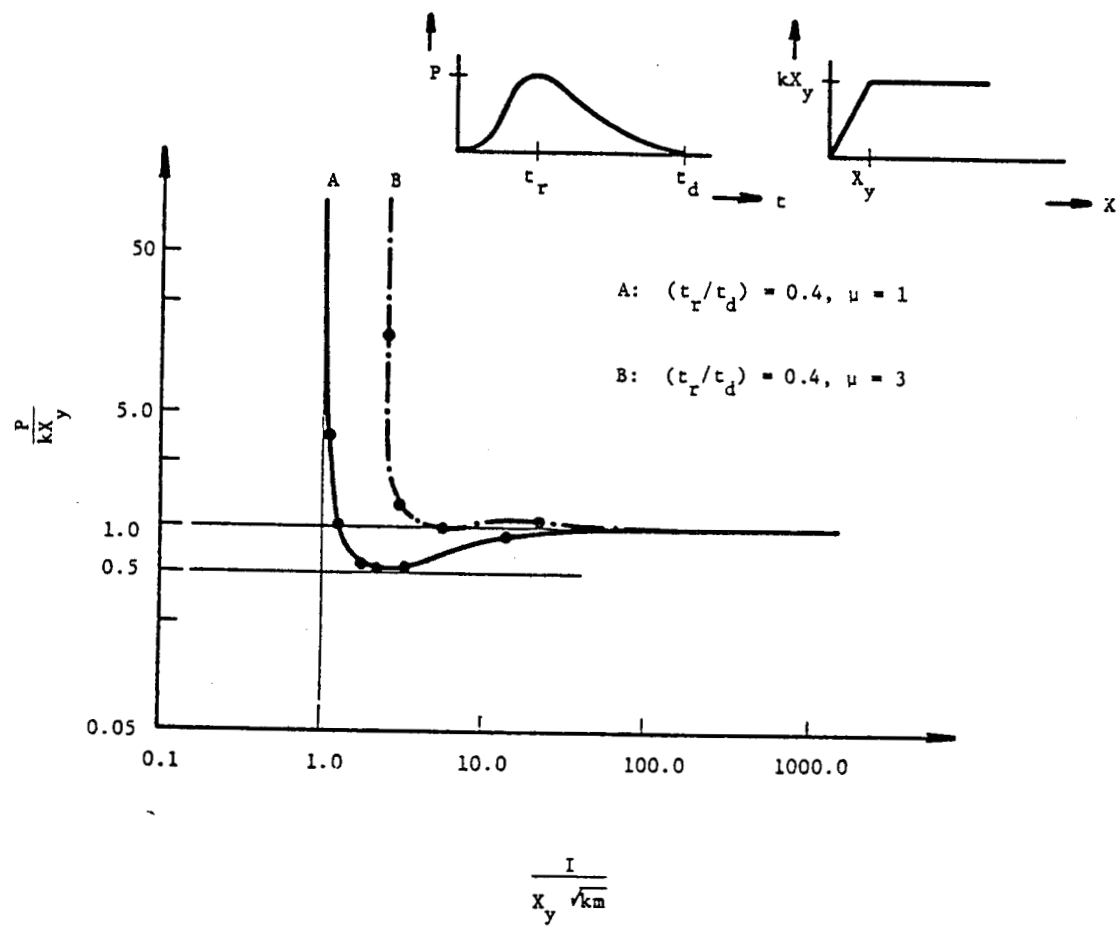
Figure 8.8 Effect of Plasticity
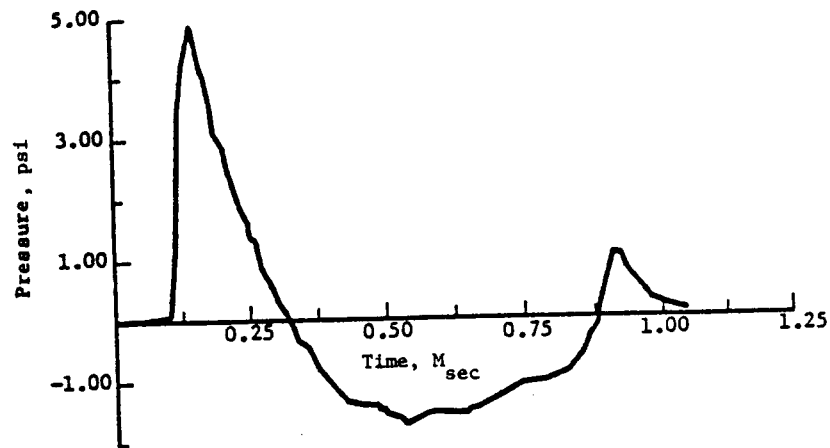
Figure 8.9   Recorded Pressure-Time Histories from Bursting Spheres
(Ref. 8.12)

$$t \le t_{d1}: \ p(t) = P_m \left(1 - \frac{t}{t_{d1}} \right)$$

$$t_{d1} < t < t_{d2}: \ = \gamma P_m \sin \left[\left(\frac{t - t_{d1}}{t_{d2} - t_{d1}} \right) \right] \pi$$

$$t_{d2} < t \le t_{d3}: \ = \delta P_m \left(1 - \frac{t - t_{d2}}{t_{d3} - t_{d2}} \right)$$

where $t_{d1} = \alpha \ t_{d3}$ and $t_{d2} = \beta \ t_{d3} = \frac{\beta}{\alpha} \ t_{d1}$
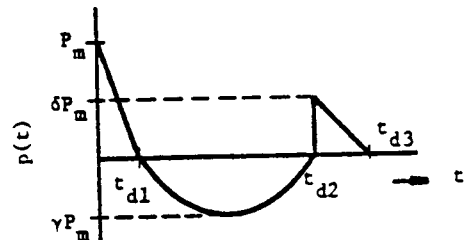
Figure 8.10   Schematic of Blast Loading from Vessel Burst

8-18
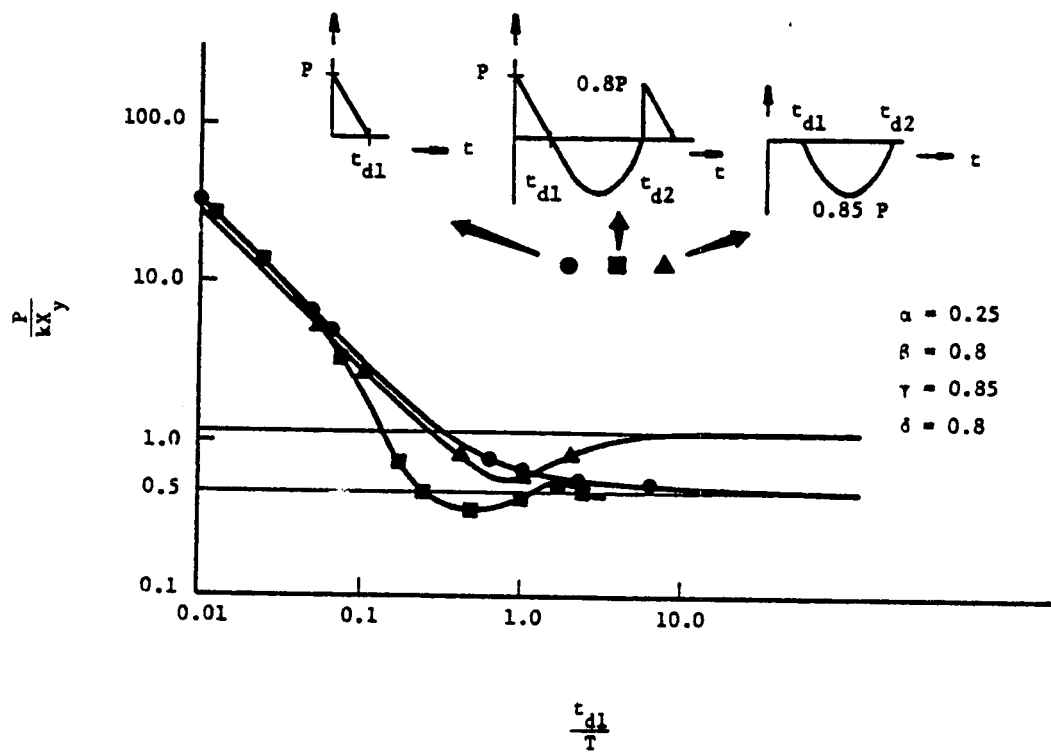
Figure 8.11 Effects of Loading which Characterize a Bursting Vessel

has a negative velocity, acceleration or both at the time the negative load-
ing phase starts. Assuming the first response to be impulsive, it appears
that:

$$\text{velocity } v < 0 \longrightarrow t \geq T/4$$

$$\text{acceleration } a < 0 \longrightarrow t \geq T/8$$

$$\text{both } < 0 \longrightarrow T/4 \leq t \leq T/2$$

We conclude from these values and the P-I diagram that the influence of the
negative phase is the worst when $1/4 \leq t_{d1}/T \leq 1/2$ for the stated values of
α, β, γ and δ, and only for the extremes in t_{d1}/T can the blast loading from
a vessel burst be accurately modeled by single triangular pressure pulse.

8.2.3.3 Structural Response to Ground Shock

The response of a two-story building frame to ground displacement, as
given in Section 8.2.3.2, shows the effect of plasticity on building displace-
ments when the base is excited by two cycles of sinusoidal motion. Displace-
ments were obtained by numerical integration of the two-degree-of-freedom
model in Figure 8.4. This is the only practical approach for solving non-
linear problems with ground motion. Graphical solutions, such as those ob-
tained for the elastic-plastic behavior of simple systems under direct loading
(See Section 8.2.3.8), have not been developed for ground shock. For simple
models, the numerical integration procedure in Ref. 8.2 can be followed. For
more complex problems, multi-degree-of-freedom numerical methods that have
provisions for time-displacement boundary conditions are available (See Sec-
tion 8.3.2).

With elastic behavior, the dynamic load factors, DLF, such as pre-
sented in Section 8.2.1, can be used if the ground shock is specified as a
time-dependent acceleration. For one-degree-of-freedom models, the forcing
function is simply the mass multiplied by the base acceleration. Note that
the time history of the acceleration must match that of the force in order to
use the DLF. All other parameters are unchanged. In a multi-degree-of-
freedom model, the modal contributions can be found from the DLF's and com-
bined as explained in Section 8.3.3.6. This is equivalent to using a shock
spectrum to obtain the modal contributions. Many of the numerical methods
described in Section 8.3.2 have provisions for elastic solutions to shock
spectra by modal superposition.

8.2.3.4 Effect of Damping

The effect of material damping was discussed in Section 8.2.1. For
inelastic behavior, it was concluded that material damping and even total
structural damping can be ignored without significantly affecting the re-
sults. For elastic behavior, damping is more significant. Baker, et al.
(Ref. 8.9), show that for a simple elastic oscillator, excited by a short

duration transient load, 10 percent critical damping attenuates the peak response by 14 percent and rebound by 37 percent. Typically, shock spectra and earthquake spectra are given for different levels of damping, and 2 to 5 percent of critical damping is a reasonable range to use for most blast-resistant buildings. When damping is ignored, a conservative result is obtained.

8.2.3.5 Coupling in Multi-Degree-Of-Freedom Systems

When a simple model is used to represent a complex structure, some coupling that can occur in the structure is usually ignored. For example, when a roof joist is analyzed, the loading is applied to the joist through flexible roofing and the joist is supported by a flexible beam that rests on beam columns. Each of these systems is coupled together, and for dynamic conditions, this coupling can affect the load transfer through the structure and the response of each component. Conceptually, multi-degree-of-freedom numerical methods can treat this problem with sufficient accuracy to account for all of the coupling that occurs; however, practically it may not be economical to perform such an analysis. Certainly when one-degree-of-freedom approximations for various components are used, then the coupling must be ignored. For this case, one usually assumes that the load is transferred, undiminished, through the structure and that each component is rigidly supported.

Baker, et al. (Ref. 8.9), give an example that illustrates the effect that coupling can have on structural response. Using simple models, the effect of the support on the response of the supported structure and also the effect of the supported structure upon the response of the support are shown. The results, given in Figures 8.12a and 8.12b were obtained using spring mass systems in which the spring constants were varied to change the period ratios. Masses were constant at 16 lb-sec^2/in. In Figures 8.12a and 8.12b, K_2 was 140,000 lb/in and K_1 was varied. A triangular force pulse with zero rise time and a duration of T_L was used in the calculations. T_1 and T_2 are the uncoupled frequencies of the systems.

Results in Figure 8.12a show that as the support stiffness increases, the response of the supported structure approaches that which is obtained when rigid support is assumed, i.e., the displacement ratio approaches 1. The dip at $T_2/T_1 = 0.8$ corresponds to a 3 to 1 ratio of the frequencies in the coupled system. Figure 8.12b shows that the load transfer is a maximum over a range that bounds $T_2/T_1 = 1.0$. It also shows that the load transfer is higher for long duration loads and that the load can be "amplified," but this effect is small.

These results are not general, but they do give some guidance when treating single-degree-of-freedom approximations. Generally, it will be conservative to neglect flexibility in the support when analyzing secondary structure and to assume full undistorted load transfer from secondary structure when analyzing the supports.
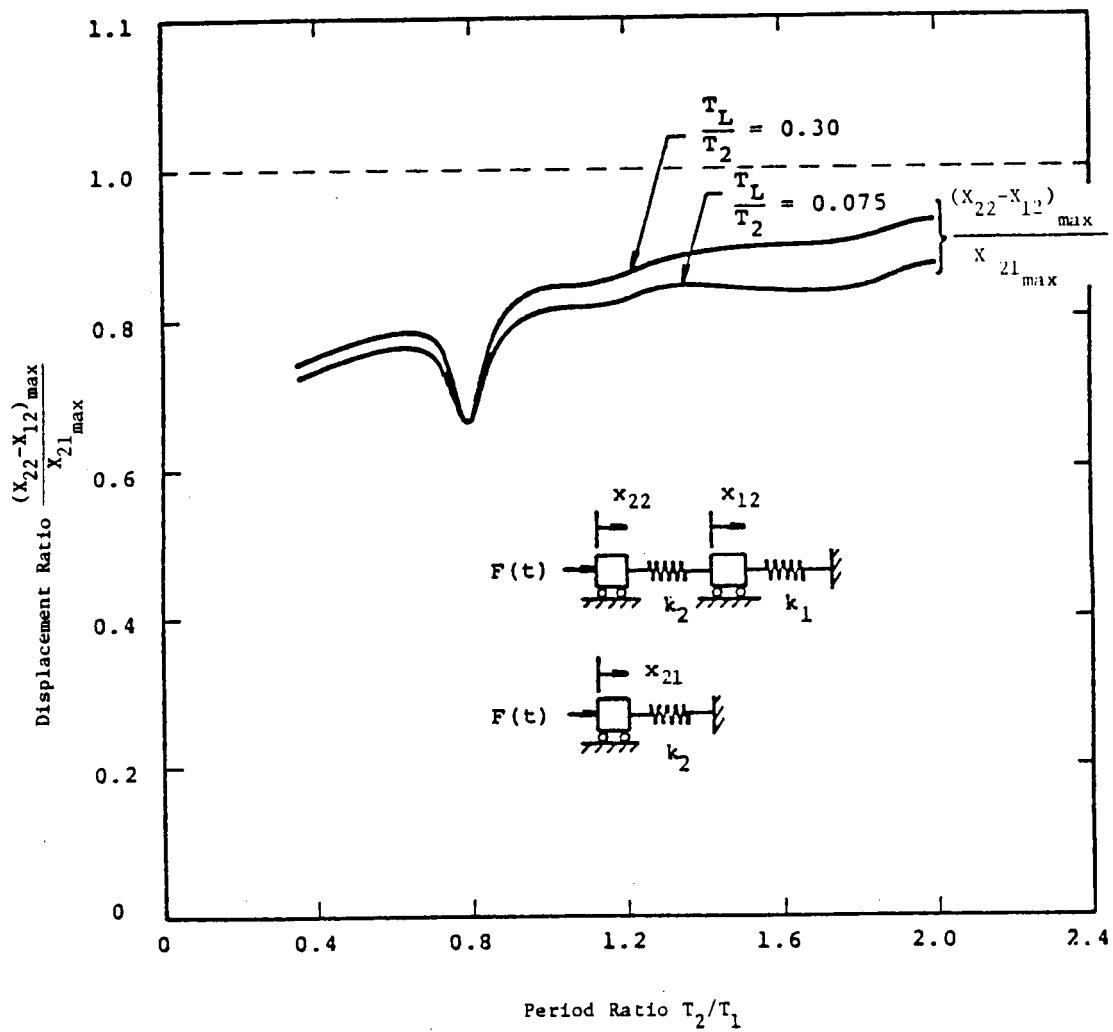
Figure 8.12a Effect of Support Stiffness on
Maximum Displacements (Ref. 8.9)
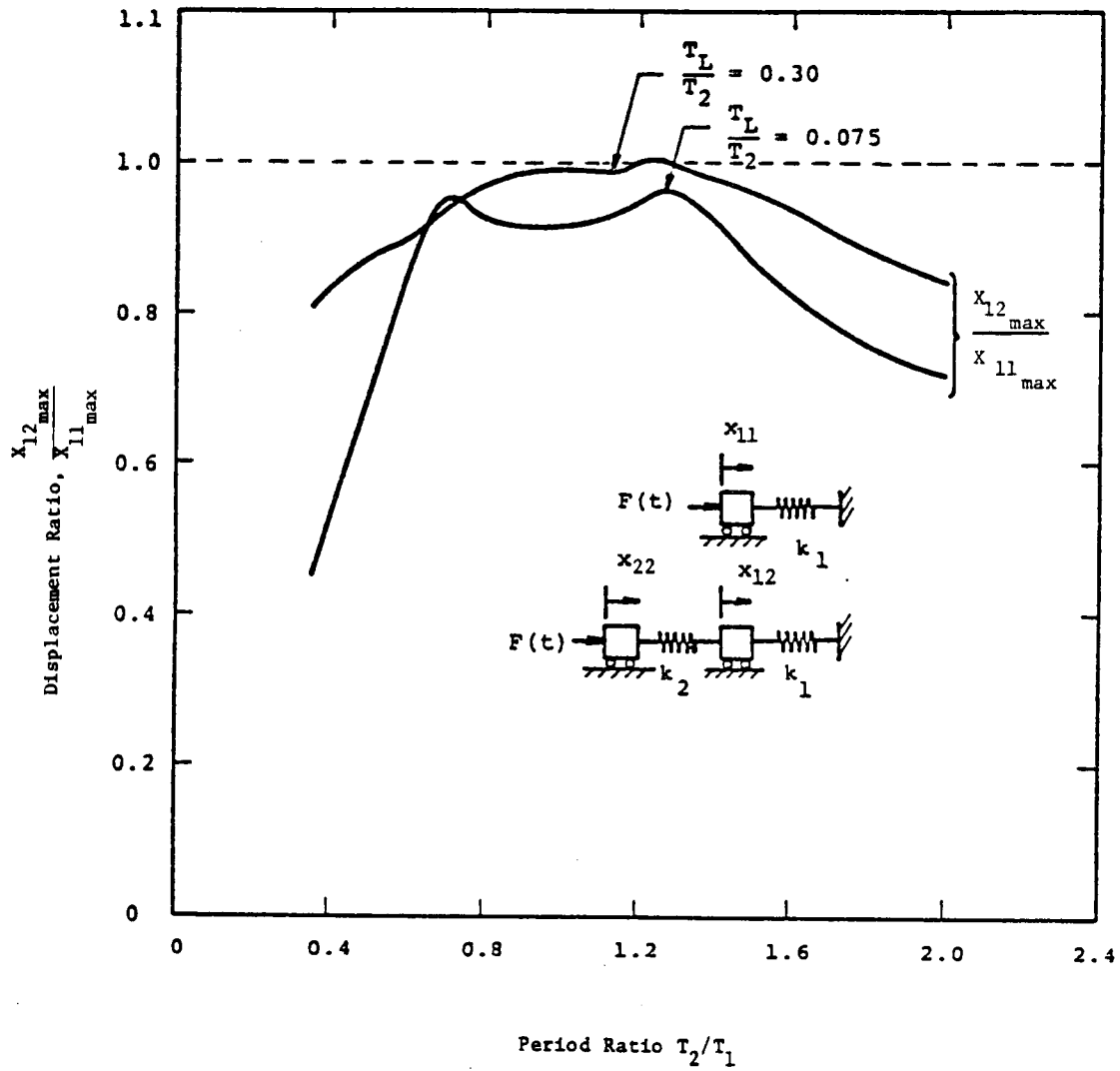
Figure 8.12b   Load Transfer Through Flexible
Structure (Ref. 8.9)

8.2.3.6 Approximate Modal Solutions

Approximate modal solutions provide good estimates of peak response when only elastic behavior is considered. This method permits the analyst to use a shock spectrum or dynamic load factors to make response calculations for multi-degree-of-freedom models. This method is possible because in mode superposition analysis, each normal mode responds to the loading independently as a one-degree-of-freedom system. The general procedure for an applied force is given in Reference 8.2.

8.2.3.7 One-Degree-Of-Freedom Equivalent System

To derive one-degree-of-freedom "equivalent" systems for what are normally regarded as multi-degree-of-freedom structural elements, deformation patterns must be assumed for the elements. With this assumption, displacements, velocities, and accelerations at all points in the structural element can be defined in terms of the displacement, at a single point. Various choices for the deformation pattern can be made, e.g., the fundamental mode shape, the static deformed shape for the load distribution of the dynamic loading, or simply some approximate shape which resembles the fundamental mode or static deformed shape and matches the appropriate boundary conditions.

One-degree-of-freedom approximations have been derived for many different structural elements and for different loading conditions. For example, in Reference 8.1, 8.2, 8.10, and 8.16 approximations can be found for

- simply supported beams

- clamped beams

- propped cantilevers

- one-and two-way slabs

- two-way slabs with interior column supports

Because the one-degree-of-freedom approximations have been derived on the basis of kinetic similarity, the maximum displacement computed by this method is accurate. Moments, shears and strains, which depend upon derivatives of the assumed deformation pattern, are less accurate. Reference 8.10 gives some comparisons between one-degree-of-freedom results and multi-degree-of-freedom results for a simply supported beam. To obtain better approximations, particularly for strains and shears, requires the use of multi-degree-of-freedom models.

8.2.3.8 Transient Solutions

Transient solutions for one-degree-of-freedom equivalent systems can be obtained by integrating the equations of motion numerically, or by seeking

closed-form solutions if the behavior is elastic. If nonlinearities are present, then numerical integration is preferred. For a one-degree-of-freedom system the numerical integration is very straightforward (as explained in Refs. 8.2 and 8.9) and can be done easily by hand calculations or solved on any programmable calculator. Equations for one-degree-of-freedom approximations have been solved and the results presented graphically in References 8.1, 8.2, 8.10, 8.16, and 8.18; however, because these graphical solutions apply to both elastic and plastic behavior for many different structural components, a further approximation is introduced when both elastic and plastic behavior occurs. For this case the transformation factors which define the one-degree-of-freedom approximation must be chosen as some average of those given for elastic behavior and those given for plastic behavior. The only advantage to a transient solution for the one-degree-of-freedom equivalent system is that the transformation factors do not have to be approximated when both elastic and plastic behavior is occurring.

For multi-degree-of-freedom systems with dynamic loads and nonlinear behavior, a transient solution is required. These solutions are performed in much the same way as for a one-degree-of-freedom system; however, the solution time increases rapidly as the number of degrees of freedom increases. Many of the numerical methods described in Section 8.3.2 have provisions for solving the equations for nonlinear transient behavior. Results from these calculations will be displacements, strains, and reactions in the structures at many points in time during the transient solution.

8.3 AVAILABLE METHODS FOR DYNAMIC RESPONSE

8.3.1 Simplified Methods

The basis for all simplified methods is an assumption about how the structure will deform when subjected to blast loading. Two basic approaches have been taken in the development of these methods. One approach, described in Section 8.2.3.7, is based upon the derivation of a one-degree-of-freedom approximation which is kinetically equivalent to the real structure. This equivalent system is then solved (numerically or in closed form) to give the time-history of the displacement. From such solutions, graphs have been developed that give peak displacements for selected force pulses. These solutions include both elastic and plastic behavior and apply for any one-degree-of-freedom equivalent system. Some additional approximation is involved in the use of the graphs. This approximation arises because changes in the transformation factors when yielding occurs are different for different components, yet the graphs are applied to all components.

Once the peak displacement has been obtained, strains can be calculated from this displacement and the assumed deformation pattern. Strains involve the second derivative of the deformation pattern and are much less accurate than displacements. Note also that shears can be calculated for elastic behavior by taking the third derivative of the displacements, but,

again, accuracy is poor. Separate expressions (derived from a free body diagram) are given for the peak reactions which occur. These expressions provide reasonable accuracy when the duration of the loading is greater than the fundamental period of the structure. For short duration loads, the error is high. This approach to blast resistant design is used in References 8.1, 8.2, 8.10, and 8.15 through 8.20. Specific comments on selected references are given in the annotated bibliography.

The other approach used to derive simplified methods is based upon the development of P-i (pressure-impulse) diagrams for the structural component. As shown in References 8.3 and 8.19, fairly simple relationships can be obtained to define the pressure and impulsive asymptotes of the structure. Behavior in the intermediate (dynamic) realm between the two asymptotes is approximated or determined numerically as explained by Baker, et al., in Ref. 8.9. An example of this type of solution was given in Figure 8.2.

Often it is unnecessary to determine the complete P-i diagram. If the loading is impulsive, then only the impulsive asymptote is required. Similarly, if the loading is quasi-static, only the quasi-static asymptote is needed. Combinations of impulsive and quasi-static loads, applied simultaneously, can also be treated in this way. Equations which include impulsive plus quasi-static loads are given in Refs. 8.11 and 8.16.

Using this approach to develop one-degree-of-freedom approximations, the displacement history is not obtained. The peak displacement is given directly or, in a P-i diagram, a fail/no-fail result can be obtained. As in the other approach, strains and shears (for elastic behavior) can be calculated from the peak displacements and assumed deformations patterns. Again, accuracy of these values is poor. Applications of this approach for blast resistant design are explained in References 8.3, 8.9, 8.11, and 8.21 through 8.23. Comments on selected references are given in the annotated bibliography.

Two-degree-of-freedom methods have also been derived using each of these two approaches. Westine has derived two-degree-of-freedom equivalent systems for the elastic behavior of two-story frames (Ref. 8.11) and for the elastic behavior of plates supported by beams (Ref. 8.24). Because these methods are for elastic behavior only, its use is limited for blast resistant design. A two-degree-of-freedom solution for rigid-plastic behavior is also given by Cox, et al. (Ref. 8.11) and applied to the problems of beams supported by rings and plates supported by beams. These rigid-plastic solutions were compared to experimental and finite element results and were found to give good estimates of residual strains.

8.3.2 Numerical Methods

Numerical methods described here refer to computer programs that utilize finite element methods, finite difference methods, or some combination of

the two. Most finite element programs use finite elements for spatial representation of the structure and finite differences in time. Finite difference codes use finite differences in both space and time.

A very large number of structural mechanics computer programs exist, as evidenced in the summaries by Fenves, et al. (Ref. 8.25), Pilkey, et al. (Ref. 8.26), and by Perrone and Pilkey (Refs. 8.27 and 8.28). Here, only the most general and readily available computer programs will be discussed along with a few programs that appear to be particularly well suited to blast resistant design.

Fourteen widely used finite element computer programs that include provisions for static and dynamic structural behavior are listed in Table 8.1. Of these, the first seven permit metal plasticity and five of these permit a nonlinear transient solution to be performed. This is the type of analysis that is needed for the most general type of calculation for blast loaded structures. Three of the codes that permit a nonlinear transient solution also permit time dependent boundary displacements. This feature is required for the nonlinear analysis of structures subjected to ground shock. Thus, these three codes permit a nonlinear calculation to be performed for combined blast loading, fragment impact, and ground shock.

Additional features of the four most general programs, ADINA, ANSYS, MARC, and NASTRAN, are given in Table 8.2. Additional information on these four codes is found in References 8.4, 8.5, 8.6, and 8.29.

Four other programs, which offer unique capabilities for nonlinear analysis, are included in this review. These programs were developed specifically for nonlinear behavior, but they are not as well known and widely distributed as the codes above. The four codes are:

- AGGIE I

- DEPROSS

- DYNFA

- PETROS 4

Of these four codes, AGGIE I is the most general. The other codes were developed for the response of specific types of structures to transient loads.

AGGIE I (Refs. 8.30 and 8.31). This finite element code is an extension to the SAP and NONSAP codes included in Table 8.1. It includes provisions for a nonlinear transient solution with all elements. Nonlinearities include material and large displacements. Element types include a three-dimensional truss, two-dimensional isoparametric solid, and a three-dimensional isoparametric solid. The three-dimensional isoparametric solid can represent a thick shell. Time dependent displacements are not now permitted.

Table 8.1 Comparison of Capabilities of General Purpose Computer Programs

CAPABILITIES \ PROGRAM	ADINA	ANSYS	ASKA III-1,2	MARC	NASTRAN	NEPSAP	NONSAP	STARDYNE	SUPERB	SAP IV	NISA	DANUTA	SDRC	STRUDL II
STATIC	X	X	X	X	X	X	X	X	X	X	X	X	X	X
DYNAMIC	X	X	X	X	X	X	X	X	X	X	X	X	X	X
NONLINEAR TRANSIENT	X	X	O	X	X^2	X	X^3	O	O	O	X	O	X	O
ELEMENTS 1-D	X	X	X	X	X	X	X	X	X	X	X	X	X	X
ELEMENTS 2-D	X	X	X	X	X	X	X	X	X	X	X	X	X	X
ELEMENTS 3-D	X	X	X	X	X	X	X	X	X	X	X	X	X	O
SHELLS — SHELLS OF REVOLUTION	O	X	X	X	X	X	X	X	X	X	X	X	X	X
SHELLS — ARBITRARY	O	X	X	X	X	X	X	X	X	X	X	X	X	X
THERMAL LOADINGS	X	X	X	X	X	X	O	X	X	X	X	X	X	X
CREEP	X	X	X	CREEP & RELAXATION	O	X	O	O	O	O	O	O	O	O
TIME DEPENDENT BOUNDARY DISPLACEMENT	O	X	O	X	X	O	O	X	O	O	O	O	O	O
TEMPERATURE DEPENDENT MATERIAL PROPERTIES	X	X	X	X	O	X	O	O	O	O	O	O	X	O
GEOMETRIC NONLINEARITIES	X	X	X	X	X	X	X	O	O	O	O	O	X	X
LARGE STRAINS	X	X	O	X	O	X	X	O	O	O	O	O	X	X
MATERIAL MODEL — METAL PLASTICITY	X	X	X	X	X^2	X	X	O	O	O	O	O	O	O
MATERIAL MODEL — SOILS/ROCKS	O	O	O	X	O	O	O	O	O	O	O	O	O	O
MATERIAL SYMMETRY — ISOTROPIC	X	X	X	X	X	X	X	X	X	X	X	X	X	X
MATERIAL SYMMETRY — ANISOTROPIC	X	X	X	X	X	X	X	O	O	X	O	O	O	X
CRACK (3-D)	O	X	O	X	O	O	O	O	O	O	O	O	O	O
GEOMETRY PLOTTINGS	O	X	O	X	X	O	O	X	X	O	X	X	X	O

1   COMMERCIAL VERSION (PROPRIETARY)
X = YES
O = NO
2   1-D ELEMENTS ONLY
3   2-D ELEMENTS ONLY

Table 8.2 Additional Features of the Most Suitable Programs for Elastic-Plastic Behavior

FEATURE OF PROGRAM \ PROGRAM	ANSYS	ADINA	MARC	NEFSAP
ELEMENT LIBRARY	GENERAL	GENERAL	GENERAL	GENERAL
MATERIAL TREATMENT	GENERAL	MODERATELY GENERAL	GENERAL	GENERAL
PLASTICITY THEORY	ISOTROPIC HARDENING, KINEMATIC HARDENING, RAMBERG-OSGOOD OR ANY OTHER POWER-LAW REPRESENTATION	ISOTROPIC HARDENING, KINEMATIC HARDENING	ISOTROPIC HARDENING, KINEMATIC HARDENING	ISOTROPIC HARDENING, KINEMATIC HARDENING
METHOD OF SOLVING LINEAR EQUATIONS	WAVE FRONT	PARTITIONING	GAUSIAN ELIMINATION	SKYLINE
EASE OF USE	EASY	EASY	MODERATE	MODERATE
DOCUMENTATION	EXTENSIVE	EXTENSIVE	EXTENSIVE	LIMITED
RESTART	X	X	X	X
SUBSTRUCTURING	X	X	O	O
MULTIPOINT CONSTRAINTS (TYING MODES)	X	O	X	X
PRE- AND POST-PROCESSORS	X	X	X	X
EQUILIBRIUM CHECKS	O	X	X	X
METHOD OF 3-D CRACK ANALYSIS	SINGULARITY ELEMENT FORMULATION	O	SINGULARITY ELEMENT FORMULATION	O
AUTOMATIC MESH GENERATORS	X	O	X	X
NODE NUMBERING	DOES NOT RENUMBER NODES INTERNALLY		REQUIRES PRE-PROCESSOR	
COST OF RUN	AVERAGE	AVERAGE	EXPENSIVE	AVERAGE
PROPRIETARY	X	X	X	X

X: AVAILABLE OR YES
O: NOT AVAILABLE OR NO

DEPROSS (Ref. 8.32). These programs calculate the elastic-plastic re-
sponse of impulsively loaded, simple structures. The structures are repre-
sented by discrete masses connected by massless lengths. Extensional deforma-
tion is distributed in the lengths, and bending deformation is concentrated
at the joints (mass points). The beam cross sections are further idealized
by a number of flanges separated by material that carries only shear and no
axial stresses. The equations of motions of the mass points are cast in fi-
nite difference form, and the time history of the response is found by a step-
wise integration process. Material behavior is inelastic strain hardening,
and strain rate effects can be included. Brief descriptions of the three pro-
grams are given below.

DEPROSS 1 - This program calculates the dynamic response of beams and
circular rings that are subjected to axisymmetric impulsive loading. Beams
can be simply supported or clamped and rings clamped or free. The program re-
quires that the cross sections be rectangular and uniform.

DEPROSS 2 - The dynamic response of unbonded, concentric circular rings
is calculated by this program. As for DEPROSS 1 the ring section must be rec-
tangular and uniform, and the impulse loading must be axisymmetric. The con-
centric rings may consist of different materials and have different thick-
nesses but must be the same width. In addition, the two rings must be ini-
tially concentric but not necessarily in contact.

DEPROSS 3 - This program is similar to DEPROSS 1 but applies to circu-
lar plates and spherical shells. Plates can be simply supported and clamped.
Shells must be clamped. Again the thickness of the plates or shells must be
uniform, and the impulse loading must be axisymmetric.

DYNFA (Ref. 8.7). This program was designed specifically for the anal-
ysis of frame structures subjected to blast loading. The program is based
upon standard matrix methods of structural analysis and a lumped parameter
representation of the frame. Numerical integration by the linear acceleration
method is used to solve for frame displacements. Inelastic behavior of the
frame members is included by the formation of plastic hinges at the nodes
whenever the combined axial load and bending moment capacity of a member is
exceeded. The recommended modeling procedure is to include nodes at the quar-
ter points of a beam or column member, resulting in five nodes and four ele-
ments per member. Although the program is limited to two-dimensional frames,
the use of four elements per member can result in a fairly large number of
elements and degrees-of-freedom, even for fairly simple frames; however, such
a representation is necessary in order to study the combined effect of local
beam and column response (to local handling) and gross frame motions. In
addition to metal plasticity, nonlinear effects which are accounted for in
the program include the P-Δ effect produced by large sway of axially loaded
members. This effect is accounted for by the addition of a shear couple to
the loading.

PETROS 4 (Ref. 8.8). The PETROS 4 program was developed to predict the arbitrarily large deflection, elastic-plastic transient responses of arbitrary initial shape, thin, multilayer, variable thickness shells, with temperature distributions, undergoing various types of deformation in response to arbitrary initial velocity distributions, transient loads, and temperature histories. Strain-hardening and strain-rate sensitive material behavior are taken into account.

The program is based upon a finite-difference solution to the governing shell equations. Displacement boundary conditions can be very general and include time-dependent translations. Applied forces can vary arbitrarily in both space and time. Up to nine different types of shells can be analyzed by PETROS 4, including shells with variable thickness, multilayer, multimaterial shells, with hard or soft bonding, and shells whose thicknesses vary with time.

8.4 ANALYSIS AND DESIGN PROCEDURES

There are many steps in the procedure which must be followed to design buildings for blast resistance. The steps can be loosely divided into five major areas:

1. Design requirements

2. Structural configuration

3. Preliminary sizing for dynamic loads

4. Dynamic analysis

5. Design iterations

The important points to consider in each of these five areas are described in the following sections; however, the emphasis of this chapter is on the analysis of structures for blast loading and not the establishment of design requirements, the layout and siting of a building, or the design for static loads. Results of these tasks are provided as input to the analyst. Of course, interaction should take place between all parties involved in the building design. Interaction early in the design stage may alter the building location, orientation, and structural configuration in ways that improve its blast resistance.

Flow charts are provided in Section 8.4.6 that show the important steps in the design/analysis procedure. These steps cover all important areas in the design process, but they are not specifically keyed to the five major areas listed above. The flow charts are substantially more detailed in some of the areas than in others. An explanation of each block in the charts is also given.

8-31

8.4.1 Design Requirements

Design requirements for the structure are usually established by the safety engineer, architectural engineer, or by some procuring agency. Often very extensive facility design requirements are established. As a minimum, the design requirements should include:

- A complete description of the accidental explosion for which the structure is to be designed. This description must be in sufficient detail so that blast wave overpressures, fragment impacts, earth ejecta, and ground shock that affect the building can be determined. Alternately, the design loads (pressures, impulse, fragment impacts, etc.) can just be specified for the analyst.

- The level of protection and serviceability of the building after the design accident must be specified. This information will allow the analyst to determine whether or not

  - glass breakage is permitted

  - siding or sheathing must remain in place

  - fragment penetration is permitted

  - the primary structure is to be reusable after the "design" accident

8.4.2 Structural Configuration

For many buildings, the location, orientation, and basic structural configuration will be set by the operational functions that it must perform. These will be dictated principally by architects and production personnel. In certain cases, such as for containment vessels, the primary function is blast containment, and here the design configuration may be dictated by the designer/analyst. Regardless of whether this information is provided by others or is determined by the analyst, it should include:

- building location and orientation

- identification of surrounding terrain and neighboring structures

- type of structure, i.e., above ground, buried, steel panel and frame, steel shell, reinforced concrete

- general building layout

- details of primary and secondary structural members designed for static loads

8.4.3 Preliminary Sizing for Dynamic Loads

Before detailed analyses are performed on the structure, it is usually advantageous to establish preliminary sizes of the main structural members for the dynamic loads. For frame structures, this is most easily done by performing a two-dimensional mechanism analysis.

A mechanism analysis requires that the dynamic load factor be estimated for the loads acting on the building. Usually only the air blast loads (the primary loads) are considered because dynamic load factors are difficult to establish for ground shock or fragment impact. Once the equivalent load has been determined, different collapse mechanisms are checked to find the one that governs the design of the frame. In the analysis, work of the external loads (product of force and distance) is equated to strain energy (products of the plastic moments and hinge rotations). The procedures for mechanism analysis, such as given in Ref. 8.7, provide guidance for the choice of a mechanism that will produce an economical design. A mechanism analysis will establish the minimum required plastic yield moment in the frame members from which the member dimensions can be established.

Mechanism analyses for dynamic loads are usually limited to single-story frames. The reason is that an equivalent static loading is difficult to establish for two-story buildings. Mechanism analyses for two-story frames under static loads are described in Ref. 8.34.

After a mechanism analysis has been performed, dynamic one-degree-of-freedom analyses and/or numerical methods can be used to check and refine the structural members. If numerical methods are used, it is recommended that the members' sizes first be determined as accurately as possible using simplified methods. This includes the use of a mechanism analysis, one-degree-of-freedom dynamic analyses, and even small multi-degree-of-freedom numerical models. The purpose is to reduce the design iterations (number of analyses) required with the more sophisticated numerical model. These analyses are very costly, and the number of cases run should be minimized.

Before a non-linear transient analysis is performed, it is suggested that an estimate of the cost for such a calculation be made. A good source of cost information is the code developer. The developer is usually aware of similar problems which have been solved with the code (although nonlinear transient solutions are not common place) and he knows the code operations which are required for a solution. Thus, after the analyst has selected a code to be used for the calculations and has formulated the problem in specific terms, he should contact the code developer for data on which to base the estimate. It is also possible that the developer can put the analyst in touch with users who have solved similar problems, even though the developer can seldom release information directly. We further suggest that a small test problem, with only a few degrees-of-freedom but which uses all of the code features which will be required in the calculations, first be solved to check the cost-estimating procedure and confirm the estimate.

8.4.4 Dynamic Analysis

Both simplified methods and more sophisticated numerical methods for performing nonlinear dynamic analyses were described in Section 8.3. With numerical methods, the analyst can usually treat all loads and even secondary effects readily. With simplified methods, secondary effects must be approximated or ignored, and it is often difficult to treat multiple loads simultaneously.

Some questions that must be considered when analyzing buildings for blast loads are:

How are dead loads treated?

What is the effect of combined axial and bending loads in beam-columns?

Is it good practice to use shear walls and bracing in blast-resistant design?

The answers to these questions depend to a large extent upon the type of analysis performed; however, some general guidelines can be given.

8.4.4.1 Dead Loads

Dead loads are often ignored in blast-resistant design. There are three main reasons for neglecting their effects. One is that the dead loads are usually small relative to the loads produced by an explosion. Thus, if the dead loads do reduce the strength of the structure, the percentage reduction will be small. Another reason is that dead loads are almost always associated with mass that is placed on or in the building. This additional mass can be beneficial to the structure for dynamic loads if it is well attached. This effect tends to offset initial stresses associated with their weight. The third reason is that if the mass is not attached, but is free to move, its true effect is very difficult to evaluate.

If dead loads are important in the blast-resistant design, and they can be for multi-story buildings or buildings designed for low overpressures, then their effect should be included. For simplified analyses, the common way of treating dead loads is to account for their effect on the bending capacity of the structural members. This is done by reducing the allowable plastic moments because of the initial static moments and axial loads. If numerical methods are being used, then the dead loads should be included as added masses or concentrated forces. If masses, representing equipment, etc., are free to move relative to the building, then they can be approximated by fixed (or moving forces) and their mass ignored in the response calculations.

8.4.4.2 Effect of Axial Loads

As discussed above, static axial loads will reduce the allowable plastic moments in beam-columns. Because the dead loads are usually small, this effect should be small also, but it is sometimes used as a convenient way of including the effect of dead loads in simplified analyses. In nonlinear numerical analyses, the effect of axial loads is included directly because a stress criterion is used to predict the onset of yielding.

Dynamic axial loads will also occur in the members. This effect is ignored in simplified analyses. Because the axial response of beam-columns usually occurs at much higher frequencies than the lateral or bending response, neglecting the effect of dynamic axial loads is justified. In nonlinear numerical methods the effect of dynamic axial forces on the members is automatically included unless this mode of behavior is eliminated (by node coupling, etc.).

8.4.4.3 Bracing and Shear Walls

Shear walls and bracing, when properly used, can result in efficient structures for resisting blast loads; however, there are two principal objections to these components that keep them from being used frequently. One objection is that they can be subjected to lateral loads (braces are often combined with a wall panel) that may cause premature failure or at least reduce the "in-plane" strength. Another objection is that, when these components fail, the failure tends to be sudden and catastrophic, not gradual and progressive. If these components are used, the designer must take care to assure that these components do not fail.

When designing with shear walls or cross bracing, the designer/analyst must recognize that these components are very stiff relative to most other components in the building for loads applied in their plane. Thus, all lateral loads on the building, which act parallel to the shear wall or plane of the bracing, tend to be reacted by these components. This concentrates the loads on the component and upon connections to the remainder of the structure. The designer must assure that these components and the attachments can react the total lateral loads with a high margin of safety and also take steps to protect them from blast loads normal to their surface.

The designer/analyst should also be aware that buildings with shear walls or bracing are difficult to treat with simplified methods. The main difficulty is in the calculation of vibration periods. Formulas are not available for estimating frequencies in the plane of these components, and numerical methods are required for accurate calculation. Thus, numerical methods are needed for good design calculations. If simplified methods must be used, then a conservative approach would be to design the braced panels or shear walls for twice the total load on the building or bay as appropriate; however, because of the uncertainty in load transfer through the structure, a multi-degree-of-freedom model is recommended.

8.4.5 Design Iteration

In order to assure that the design requirements are met, the designer/ analyst must set criteria or design allowables for the structure. These criteria may include maximum allowable stress, strain, deformation, or joint rotation. Recommended criteria for blast-resistant design are given in References 8.1, 8.7, and 8.9. The criteria are seldom met on the first attempt, and so design iterations are required. Iterations should be performed using simplified methods such as a mechanism analysis or one-degree-of-freedom equivalent system. Design iterations with complex numerical methods should be avoided, if possible. Guidance for changing the resistance of the structure must be obtained by examining the results of previous response calculations.

8.4.6 Flow Charts

The flow charts in Figures 8.13 and 8.14 outline procedures for the blast-resistant design of a building or structure. Figure 8.13 applies to buildings that are subjected to external loads. Figure 8.14 applies to buildings that are subjected to internal loads. Information in these flow charts is intended to give the AE guidance in the design of blast-resistant structures and not to supplant other design manuals.

As noted earlier, external loads that can be produced from an accidental explosion are:

- overpressures from the blast wave

- ground shock

- impact from soil if cratering occurs

- impacts from fragments

When the explosion occurs internally, additional loads are produced by an increase in the ambient pressure, but ground shock and cratering are not usually significant loads. All of these loads may act independently or they may occur in combination, depending upon the nature of the accident and the position of the building relative to the explosion. Treatment of multiple loads acting on the structure is covered in the procedure.

Nomenclature used in Figures 8.13 and 8.14 is equally applicable to steel frame and reinforced concrete structures. Dashed lines are used to suggest optional feedback loops or information exchange that should occur. Phantom lines enclose blocks that are not active tasks, but that contain comments, instructions, or conclusions.

Each block in the flow charts is identified and specific comments on each block are given in Sections 8.4.6.1 and 8.4.6.2. When it is suggested that an analysis be performed using numerical methods, a nonlinear transient
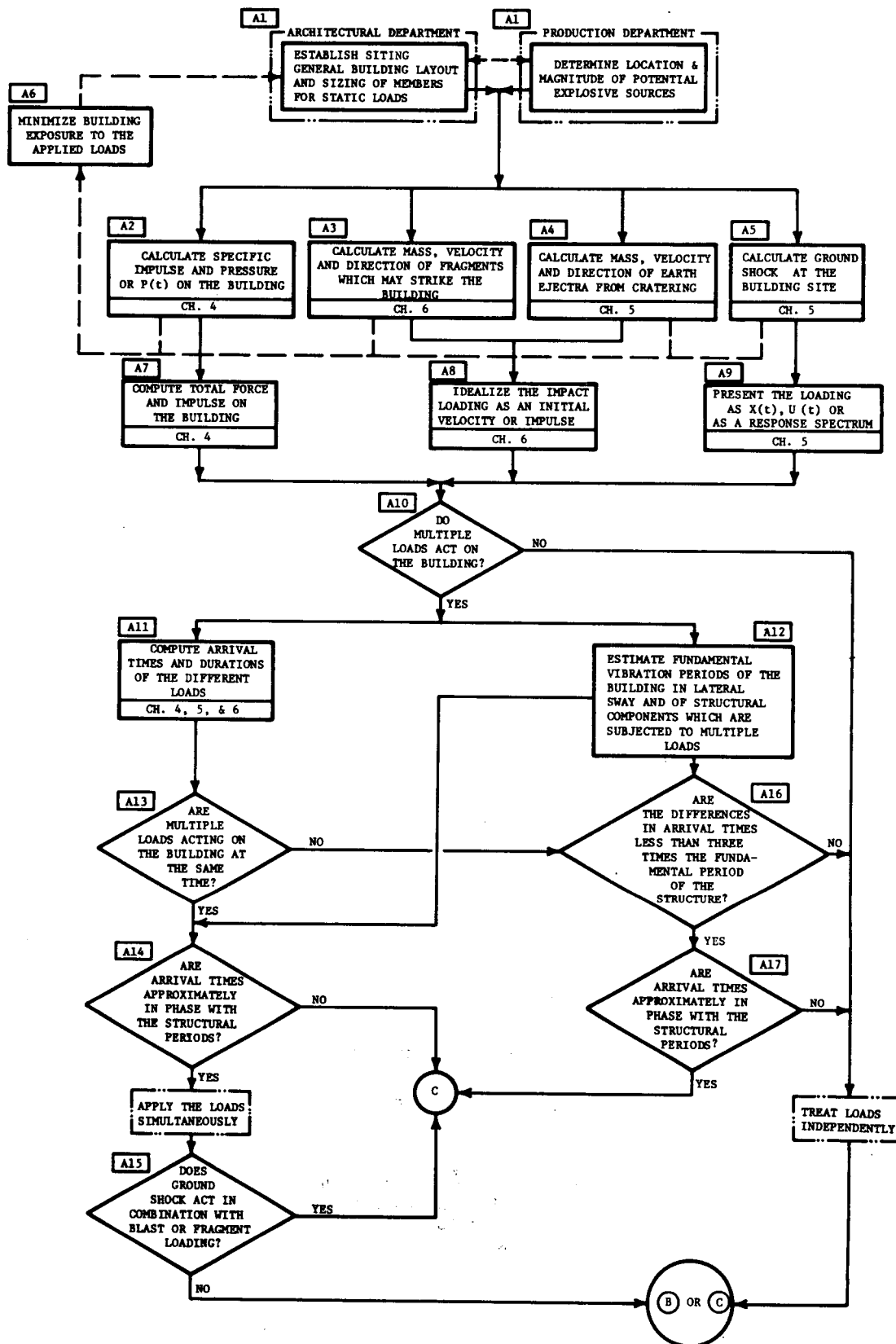
Figure 8.13 Design for External Explosions

8-37
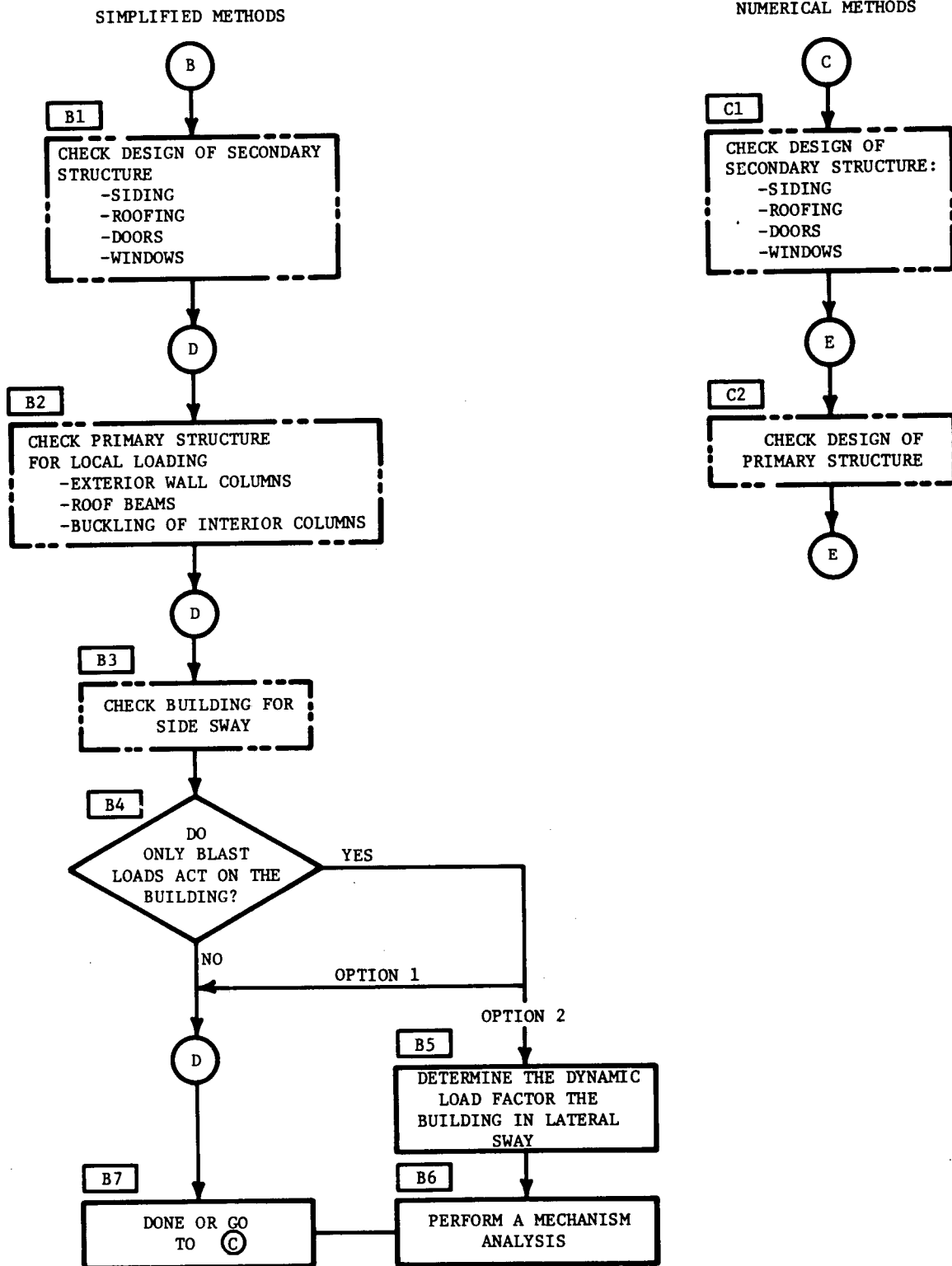
Figure 8.13 Design for External Explosions (Con't)
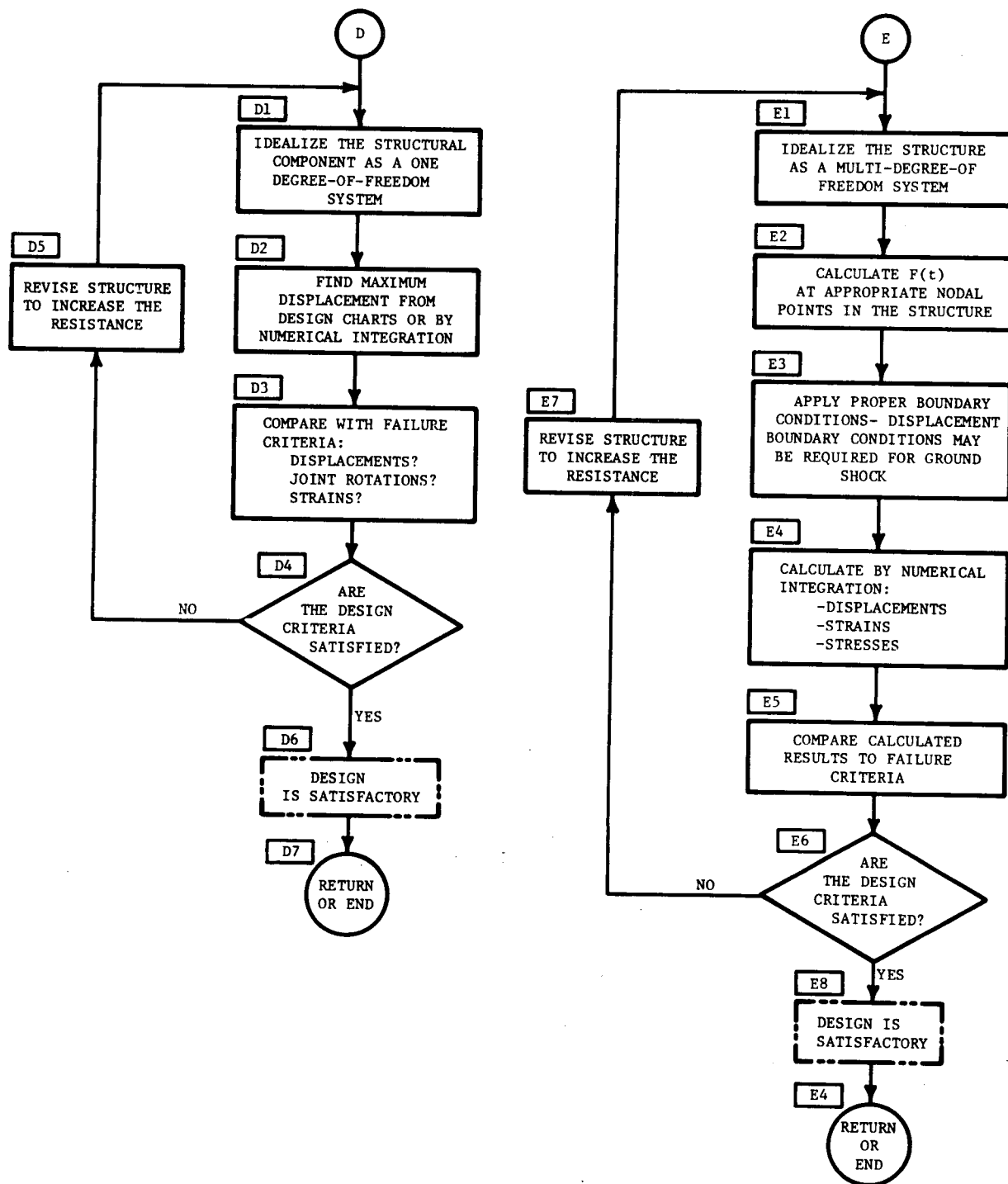
Figure 8.13   Design for External Explosions (Con't)
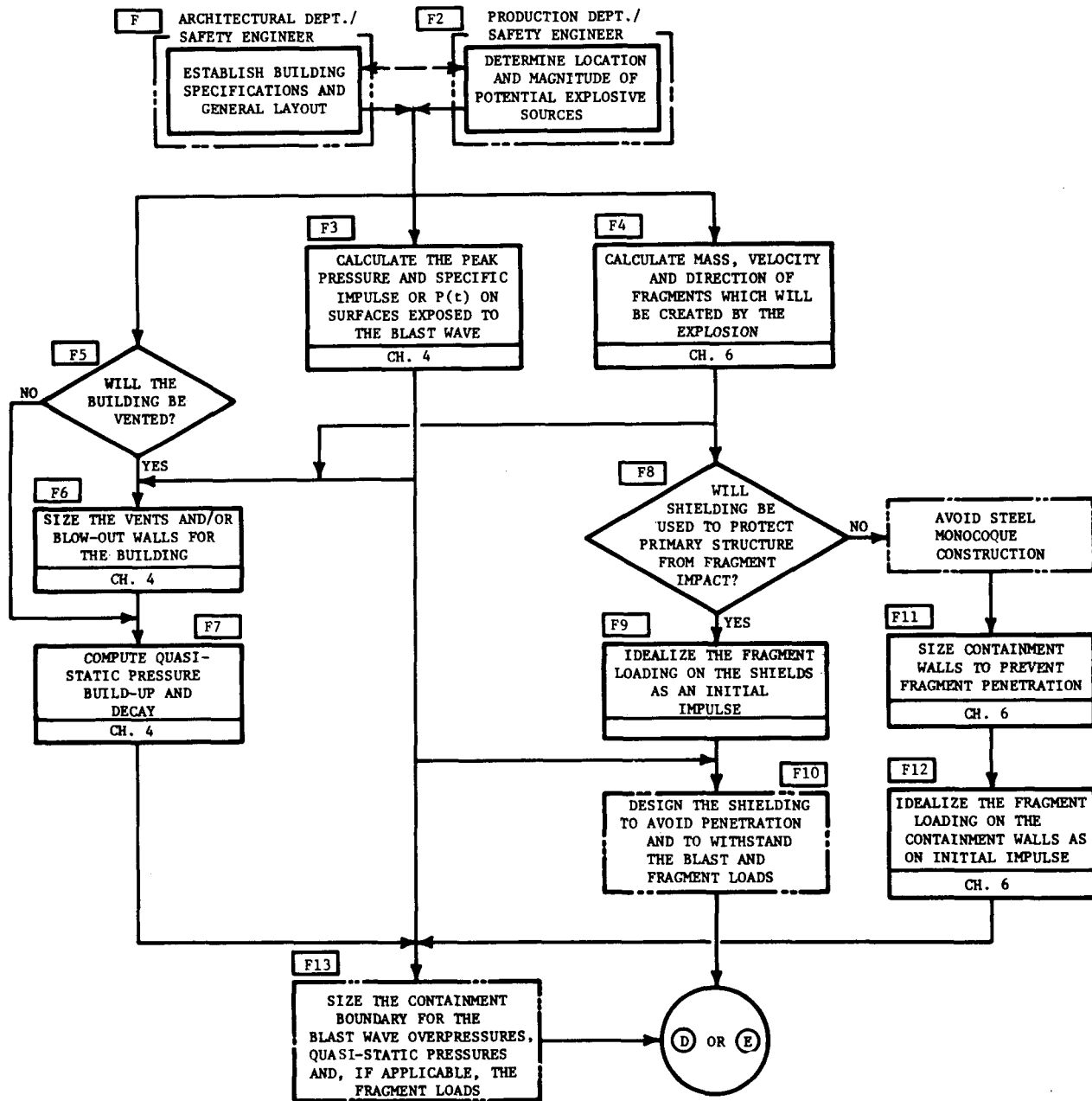
Figure 8.14 Design for Internal Explosions

type of calculation is intended. Simplified methods can be nonlinear transients or other types of approximations.

8.4.6.1 <u>Design for External Loads (Figure 8.13)</u>

  $\boxed{A1}$ These two blocks are considered as basic input to the analyst or designer/analyst who will be responsible for assuring that the building meets the requirements for blast resistance that have been placed upon it. Although the source of these input data will vary within each organization, for purposes of the flow chart it has been assumed that it is provided by the architectural and production departments in consultation with the safety engineer. Within some companies, a single design department may perform the entire job, but the architectural engineering work and the prediction of probable accidents are not covered in this handbook. Data provided to the analyst should include:

- position and orientation of the building relative to other facilities

- building plan and elevation drawings that give exterior dimensions

- detail drawings giving the primary and secondary structural members that have been sized to meet the static design loads

- location and magnitude of the energy release in postulated accidents which the building must be designed to withstand

- level of protection and post-accident service that the building must provide

  $\boxed{A2}$ Overpressures and specific impulse on the building can be calculated by knowing the energy release in the accident, whether detonation or deflagration occurs, and the distance from the accident to the loaded face of the building. Ground reflection at the accident location and local blast wave reflection on the building must be considered in the calculations. Note that each surface of the building may have a different p(t) and that both the reflected shock wave and the "wind" behind the shock will impart loads to the building.

  $\boxed{A3}$ Procedures for calculating the distribution and energy in fragments that may occur in an accidental explosion are covered in Chapter 6. To avoid penetration, the "worst case" fragment that can strike the building must be determined. To account for the loading on the building, i.e., the force-time or impulse that the fragments can impart to the building, the total energy in the fragments (mass, velocity, and number) that strike the building must be known. Usually the energy imparted to a building by fragments is small relative to the energy imparted to the building by overpressures; however, for individual building components it may be a significant part of the applied load.

A4 A nearby explosion at or below ground level can cause earth ejecta to be thrown against the building. This loading can be a significant part of the total load on the building and perhaps the major load for some building components. In this case, individual fragments are usually not important, but the total mass and velocity of the soil impacting the building must be known. Means of estimating the loading produced by earth ejecta from cratering are provided in Chapter 5.

A5 Ground shock occurs in every explosion, whether it is above or below the ground surface, but usually the effect of the shock is small compared to the effect of the air blast; however, for some explosions this will not be the case, particularly for subsurface ones. Also, some buildings may be underground and only subjected to the ground shock loads.

A6 Siting and orientation influence the loads on the building and, if possible, these two factors should be selected to reduce the loads on the building to some minimum value. Feedback between load estimates and the building placement and orientation is necessary to accomplish this objective.

A7 From the overpressure and specific impulse, the total forces and impulses on the different faces of the building and for various structural components can be calculated. For lateral sway of the building, it is customary to neglect the pressures on the side of the building opposite the explosion, but these pressures can easily be included when using numerical methods. Depending upon the frequency of the response of the building and the arrival times of the loads, the "back side" pressure can increase, but it usually decreases, the response.

A8 Loading from both the fragment impacts and the earth ejecta thrown against the building can be idealized as an impulse or as an initial velocity imparted to the building. These estimates are based upon change in momentum, and when penetration occurs, residual fragment velocities can be taken as the final velocity if the fragment does not strike another part of the building. It is conservative and customary to neglect the residual velocity.

A9 It is often difficult to determine the displacement, d(t), or acceleration, a(t), produced at the building by ground shock. When these values are not well known, a good approximation of a shock spectrum can still be obtained as explained in Reference 8.2. A shock spectrum is adequate for calculating the elastic response of the building using mode superposition; however, for a nonlinear dynamic analysis, the ground displacement must be applied.

A10 A single accident will very likely produce air blast, fragments, and ground shock, all of which can excite the structure. It is necessary to consider multiple loads from either a single or multiple explosion and to decide how they must be applied to the structure for design purposes.

[A11] Arrival times and durations of the different loads that act on the building must be determined. Data are readily available to make this calculation for air blast, but only estimates are available for ground shock and fragments. Because fragment loads are treated as an initial impulse, their duration is zero.

[A12] To determine the effect of multiple loads on the building, the fundamental period of vibration must be estimated for the building in lateral sway and for building components that are subjected to multiple loads. References 8.1, 8.2, 8.14, and any vibration textbook contain formulas for computing fundamental periods of vibration for structural components.

[A13] If multiple loads act on the building at the same time, then simplified methods may not be appropriate. Because impact loads are represented as an impulse, they have no duration. If the arrival times of two separate loads, one of which is an impact load, are within one half-period of the fundamental mode of vibration of the structure, then the loads should be treated as acting at the same time.

[A14] If multiple loads are acting at the same time and the arrival times are approximately in phase with the fundamental periods of vibration, then the loading can be idealized as acting simultaneously for purposes of performing a simplified analysis (see Chapter 4). If they are not approximately in phase, then numerical methods must be applied to compute the structural response of the building (see Ref. 8.2).

[A15] Even if the loads act together and the arrival times are approximately in phase with the vibration period of the structure, there is no simple method of combining ground shock and fragment or air blast loading. For this combination of loads, numerical methods are again recommended (we know of no structures designed for these combined loads to date).

[A16] Even if the loads are not acting at the same time, the loads should be treated together if loads after the first are applied while the structure is still vibrating. A separation time of three times the fundamental vibration period has been chosen as a criterion for deciding whether or not to treat the loads together or separately. After three periods of vibration have passed, damping has reduced the amplitude substantially, particularly if plastic straining has occurred, and treating the loads separately will permit a simplified analysis to be performed and should give a good estimate of the maximum response.

[A17] At this point it has been determined that the loads do not act together; yet loads after the first are applied within a time equal to three times the fundamental vibration period of the structure. If the arrival times are approximately in phase with the period of the structure, then the loads should be applied together. For this case numerical methods are recommended so that proper phasing of the loads can be accounted for. If the arrival times are not in phase with the structural period, then it is usually safe to

treat the loads independently and use simplified methods of analysis (see Chapter 4 and Refs. 8.2 and 8.18).

[B] Simplified Methods. When using simplified methods, individual components of the building and the building itself are idealized as a one- (or possibly two-) degree-of-freedom system. The response of each one-degree-of-freedom system is then found for the assumption that coupling between the various parts of the structure does not occur, i.e., the support for each component is treated as rigid and no alteration of the loading occurs as it passes through the structure. This approach usually yields conservative results.

Because the procedure of idealizing the parts of the structure as a one-degree-of-freedom is repeated many times for different parts of the building, it has been treated in a separate flow diagram and referred to as [D]. This part of the flow chart functions as a subroutine that is entered and used, and it then returns control back to the location from which it was entered. Contents are described under Subroutine [D].

[B1] As the first step in the simplified analysis of a building, the secondary structure is analyzed and sized for blast and fragment loads. Design of secondary structure is performed first because its mass must be included in frequency calculations for the primary structure. Only significant changes, such as changes in frame spacing, which may occur subsequently during the analysis of the primary structure, will require redesign of the secondary structure. When the secondary structure is analyzed first, it is also possible to compute boundary reactions and apply them as loads to the primary structure. This approach is not recommended for simplified analysis because the boundary reactions cannot be determined accurately.

Secondary structure includes wall panels, roofing, windows, and doors. Wall panels are usually constructed with siding, girts, and purlins. Each component must be analyzed for the applied loads. Roofing includes both the decking and roof joists, and each of these components must be checked also. Doors and windows that are blast resistant require strong supports so the frames also must be checked for adequate strength.

[B2] After the secondary structure has been designed, the primary structure should be checked for local loads. This includes:

- exterior columns

- interior columns

- roof beams

- wall panels that are part of the primary structure

If the building is first designed for adequate strength in lateral sway, then any increase in the above members for local loading will result in some over-

design of the building. However, if the above members are first sized for local loads, then any additional strength that may be required for these loads will also contribute to the strength of the building in lateral sway.

[B3] At this point in the analysis, the building is checked for side sway. If one axis of the building is oriented along the direction from the building to the explosion, then side sway in only one direction may need to be checked. If this is not the case or if the building is irregular in shape, then side sway must be checked in two perpendicular directions. When biaxial bending of the columns occur, the bending capacity in each direction must be reduced accordingly. Reference 8.7 gives formulas for the reduction of bending capacity under these conditions. Columns can also be subjected to combined axial and lateral loads; however, the frequency of the column response in compression is much higher than the response of the building in lateral sway so coupling for these loads can be neglected. Even so, Reference 8.7 gives formulas for reducing the allowable fully plastic bending moment for combined bending and axial loads.

[B4] If only air blast loads are acting on the building, side sway can be checked using either a mechanism analysis or by one-degree-of-freedom methods. Impulsive loads from fragment impact cannot be easily treated in a mechanism analysis because it requires that a dynamic load factor be established for the applied load. Such a load factor is difficult to obtain for impact loading.

[B5], [B6] Option 1 is to use one-degree-of-freedom methods and proceed to [D]; Option 2 is to perform a mechanism analysis. A mechanism analysis is also an iterative process, but this is inherent in the method and so no looping to increase the resistance is shown. As the first step in the analysis, dynamic load factors must be determined for the roof loads and for lateral loads. These loads are a function of the structural frequencies and the nature of the loading. Reference 8.7 gives guidance for determining the dynamic load factors and for performing the mechanism analysis.

[B7] If only simplified methods are being used, then the analysis is complete. If numerical methods will also be used to confirm or refine the design, then the results obtained from the amplified methods will be used as input for the more exact analyses. Preliminary sizing by simplified methods is always recommended before undertaking a more complex and expensive numerical analysis.

[C] Numerical Methods. The flow chart for numerical methods includes a section (identified as [E]) that is utilized more than once, and so it has been separated from the main flow diagram. Section [E] outlines, in general terms, the process of performing a multi-degree-of-freedom analysis of a structure or structural component. This section is referred to twice because it is suggested in the flow diagram that the primary and secondary structures of the building be analyzed separately. The reason for performing separate analyses is to minimize the degree-of-freedom that must be included

in the model. If one attempts to analyze an entire structure with one model, the model size (degree-of-freedom, number of elements, etc.) would be large and the analysis might not be economically feasible. The primary structure alone can be represented by a model of reasonable size. Models of individual components would be used to analyze the secondary structure. Alternately, some combination of numerical and simplified methods can be used. For example, the primary structure can be analyzed with numerical methods and secondary structure with simplified methods. Regardless of which approach is used, it is recommended that, before numerical methods are used to analyze a structure or structural component, preliminary sizing of the structure be made using simplified methods.

[C1] As for simplified methods, analysis and sizing of secondary structure have been placed ahead of the analysis of the primary structure. Secondary structure is analyzed first so that the mass of these components will be known and so that the boundary reactions can be used as the applied loads for the primary structure. This approach has merit when numerical methods are used because the boundary reactions are more accurate than those obtained with simplified methods; however, even with numerical methods the reactions are still approximate because flexibility of the primary structure is neglected in the analysis. Thus, this approach is optional and the approach taken with simplified methods can be used, whereby flexibility of the secondary structure is ignored when loads for the primary structure are computed. Refer to paragraph [B1] under Simplified Methods for additional comments. The steps in setting up a multi-degree-of-freedom model and computing the transient response of a structure are covered in Subsection [E].

[C2] Primary structure of the building can be analyzed in total using multi-degree-of-freedom methods or it can be analyzed in parts. How the structure is analyzed will depend upon the structural symmetry and the symmetry of the loading. For example, a multi-frame structure with a loading direction parallel to the plane of the framework can be analyzed by treating individual frames. This assumes that the frames are identical except for the outside ones, or have small variations. For non-symmetric structures with loading from arbitrary directions, a three-dimensional analysis is required. Loading on the primary structure is often transferred through secondary structure. The exceptions are concrete slab or cylindrical structures where the walls provide the strength and the covering. When the loading is transferred through secondary structure, the analyst has three choices: (1) analyze the coupled problem (include primary and secondary structure in the model), (2) use support reactions from separate analyses of the secondary structure, or (3) assume that the loading is unaltered by the secondary structure. The simplest choice is (3) and it most often results in conservative results (see Figure 8.12). In the most general case, the loading on the structure will not be uniform or simultaneous. Variations in the magnitude, arrival time, and duration of the loads can be readily treated with numerical methods but computing the loading at multiple points on the structure is tedious. Note that when the third approach is used, the secondary structure is represented as an added mass on the primary structure. When the second approach is chosen, the mass of the secondary structure is ignored in the model.

$\boxed{D}$ One Degree-of-Freedom Analysis. This part of the flow chart functions like a subroutine in a FORTRAN program in that it is entered from different parts of the flow chart and returns control to the position from which it was entered. This part of the flow chart is entered from $\boxed{B}$, Simplified Methods (Figure 8.13) and from Figure 8.14.

$\boxed{D1}$, $\boxed{D2}$ References 8.1, 8.2, 8.10, and 8.15 through 8.18 contain transformation factors for deriving one-degree-of-freedom approximations for distributed systems. Factors are generally given for beams and plates with different boundary conditions and different loads. Solutions for elastic-plastic behavior are contained in design charts such as Figure 2.25 of Reference 8.2 or they can be obtained by numerical integration procedures that are outlined for tabular solution in References 8.2, 8.16, and others. Derivation of the transformation factors is explained briefly in Section 8.2.3.7 and described more fully in Reference 8.9.

References 8.21 through 8.23 use a similar, but slightly different approach for finding a one-degree-of-freedom solution. This approach gives solutions for the asymptotes of the response for quasi-static and impulsive loads and also gives procedures for approximating the intermediate (dynamic) region of response. The result is a P-i (pressure-impulse) diagram for the one-degree-of-freedom system. If the deformation pattern (or failure mode) assumed is the same for the two methods, very similar results are obtained. Asymptotes of the response are expressed in equation form so that graphical or numerical methods are not required to obtain a solution; however, as a consequence, no information on the transient nature of the response is obtained. Solutions for the simultaneous application of a long duration pressure pulse and an impulse are given in References 8.11 and 8.16.

$\boxed{D3}$ One-degree-of-freedom equivalent systems are developed to give displacements that are the same as the maximum displacement in the distributed system. Thus, the most reliable information that can be obtained is the displacement. This displacement can be compared to the displacement at which yielding occurs in the structure and a value for the ductility ratio, μ, which is the ratio of the maximum deflection to the deflection at yield, can be computed. This is one suitable criterion for design, and recommended design values are given in References 8.1 and 8.9. From the assumed deformation pattern and the maximum displacement, additional information can be obtained, such as the maximum strain and joint rotations. These too can be used as design criteria, but the values obtained from the one-degree-of-freedom approximation are less reliable than the displacements.

Accurate values for the maximum reactions at supports are difficult to obtain from these simple methods; however, estimates are given in References 8.2 and 8.15 for the maximum reaction at the support as a function of the applied load and the system resistance. These estimates are good for

loads of long duration relative to the fundamental period of the structure, but can be nonconservative for loads of very short duration and high intensity.

[D4] If the design criteria are not satisfied at this stage, then design modification of the structure is necessary. A logical step is to increase the resistance of the structure. Alternatives to increasing the resistance would be to reduce the loading or relax the criteria, but it is assumed at this point in the design that these values are set.

[D5] Increasing the resistance of the structure to satisfy the design criteria is an iterative process; however, the previous calculation and response charts (if they are being used) provide guidance for selecting a new resistance. Because the frequency changes with changes to the structure, estimates of the proper resistance to provide a given ductility ratio are only approximate, but do provide good estimates. From the resistance chosen, values of the yield moment, etc., and thus the size of the structural member, can be obtained.

[D6], [D7] When the design criteria are met, the design is satisfactory and, if the analyses of all components have been completed, the job is ended; otherwise, the analyst returns to the position in the flow diagrams from which the subroutine was entered.

[E] Multi-Degree-Of-Freedom Analysis. This part of the flow chart is entered repeatedly from different points in Figures 8.13 and 8.14. Return is to the point in the flow chart from which it was entered. It outlines the steps in setting up and performing a multi-degree-of-freedom analysis.

[E1] To perform a multi-degree-of-freedom numerical analysis, the structure or component to be analyzed must first be represented by an analytical model, just as for simplified methods. In this case the model can be much more detailed and represent the structure more accurately. Every model will be a compromise between accuracy and cost. When designing structures to resist accidental explosions, plasticity is usually permitted (so that a more efficient structure is obtained), and, because the loading is dynamic, a nonlinear transient solution is required. This type of analysis is very costly in terms of computer time, and so it is extremely important that large models be avoided. Also, a detailed (fine mesh) model should be avoided for this type of analysis because flow rules for metal plasticity are not exact, and uncertainty exists in the loads which are applied to the structure.

Modeling structures for multi-degree-of-freedom analyses must be learned by experience. To keep the model small, the analyst must take advantage of symmetry in the structure and in the loading. If one plane of symmetry exists in the structure and if the loading is also symmetric about this plane, then only one-half of the structure need be included in the model. If this same condition exists for two planes of symmetry, then only one-fourth of the structure need be modeled. This condition can easily occur for structures loaded internally, but will seldom occur for external loads.

Because of the complexity and expense associated with a nonlinear dynamic analysis, three-dimensional problems are often treated in only two dimensions. Reference 8.7 provides guidance for the modeling of frame type structures in two dimensions when using the program DYNFA. This program is suitable for two-dimensional frame structures acted on by a general blast loading. Finite element programs, such as MARC (Ref. 8.6) and ANSYS (Ref. 8.5), can be used for modeling more general configurations and for three-dimensional problems. Example problems have been solved using these programs, and the problem manuals should be consulted before attempting to prepare a model for either code. The user is again cautioned to keep models as small as practical and also to solve a very small sample problem first, using the features of the program that will be required in the analysis, before attempting to solve the actual problem.

[E2] The applied forces, which will be a function of time, must be calculated and applied at selected nodal points on the model. If the blast wave travels perpendicular to the wall, normal reflection will occur and reflected values of pressure and/or impulse must be used when computing the forces. For surfaces loaded by normal blast waves, the loading is applied simultaneously to all nodes and will have the same duration. For surfaces loaded by oblique blast waves or side-on blast waves that sweep across the surface (such as the roof), the loads arrive at different times at different nodes. These loads will also have slightly different magnitudes and durations. An adequate approximation is to assume a linear variation of arrival times, durations, and pressure magnitudes over the building surfaces. Chapter 4 provides the analyst with sufficient information to calculate side-on and reflected values of pressure and impulse, arrival times, durations, and the drag phase of the loading.

Impulsive loads associated with fragment or soil impact should be applied as an initial velocity or as an impulse. An alternative way of applying an impulse is with a very short duration, but high intensity load. The load duration should be shorter than about one-fourth of the shortest period in the model. Shock loads will be applied as a displacement-time history at the base of the building for a nonlinear analysis.

[E3] Normal boundary conditions are specified by setting to zero those displacements on the model that are fixed (do not move) in the building or structural component. These will usually be points where the building is attached to the foundation. If the foundation is included in the model, then some points on the foundation must either be fixed or it must be attached to points in the soil which are in turn attached at some point in the model. As a minimum, sufficient displacements must be set to zero to prevent rigid body motions of the model in translation and rotation.

When planes of symmetry in the structure (refer to [E1]) are used to reduce the size of the model, then the symmetry boundary conditions

must be applied at these model boundaries. As an example, if the plane of symmetry is the X-Y plane, then the boundary conditions require that no translations occur in the Z-direction and no rotations occur about the X- and Y-axes.

Ground shock is applied to the model as a displacement-time history at points corresponding to the building foundation. These will be vertical or lateral displacements or a combination of both. Without ground shock, these points would normally be fixed points in the structure.

[E4] When analyzing structures with numerical methods, a computer program is used that solves the analytical model based upon the input data provided. With such a code, detailed procedures are followed in the preparation and coding of input data for the multi-degree-of-freedom model developed in [E1]. Instructions are provided in the user's manual for the program.

Once the input data have been coded, the load case is run to obtain displacements, strains, and stresses. To obtain the solution for a nonlinear transient problem, a numerical integration in time is performed with a specified time step, and, when yielding occurs, iterations to obtain convergence are sometimes required within the time step. These elaborate integration and convergence procedures require substantial computation time. Specification of the integration time step is the choice of the user, but guidance is provided in the user's manual. Again, some compromise between accuracy and cost is often sought. If the integration time step is too large, excessive numerical damping or instability can result. If the integration time step is too small, costs can be excessive. A few trial runs with different time steps may be required before the correct choice can be made. Because each program uses a somewhat different approach to numerical integration, recommendations in the user's manual should be followed.

From the numerical results, displacements, strain, and stresses are obtained at points within elements or a nodal point in the model. Many programs offer graphical output of data that are very valuable in evaluating the results, which are often voluminous.

[E5] Results from the numerical solution are compared to preset criteria to determine whether or not the design is satisfactory. For elastic-plastic structures, these will usually be maximum allowable strains, translations, rotations, or boundary reactions at points of attachment.

[E6] If the design criteria are not satisfied, then an iteration is required with a modified design.

[E7] If the design criteria are not satisfied, it is necessary to increase the resistance of the structure, alter the loading or change the design criteria. It is assumed that the latter two possibilities have been properly treated earlier in the solution and are not considered here. Increasing the strength or resistance also changes stiffness and frequency.

For elastic structures, increasing frequency will sometimes offset an increase in strength because the load amplification is increased by the increase in frequency. For elastic-plastic behavior, this factor is not so important because of the substantial damping produced by structural yielding. Little guidance can be offered the analyst in selecting ways to increase the resistance. It depends upon the type of structure and the type of "failure." The analyst must depend upon the results of the previous analysis in order to select the best alteration to increase the structural resistance. In some situations (with simple models), it may be helpful to consider the additional energy that must be absorbed within a specified strain or displacement in order to determine how much the resistance should be increased.

$\boxed{\text{E8}}$, $\boxed{\text{E9}}$ When the design criteria have been satisfied, then the design is satisfactory and control is returned to the main flow diagram at the point from which $\boxed{\text{E}}$ was entered. If the primary structure has been analyzed, then the design for blast resistance is complete.

8.4.6.2 Design for Internal Explosions

The flow diagram of Figure 8.14 pertains primarily to containment type structures. It references parts of the flow chart in Figure 8.13. In this design procedure, it is assumed that the structure is designed to contain fragments that may be generated by the accident; however, this may not always be the case for structures with blow-out walls. It is also assumed that the foundation will be designed to contain the explosion and prevent cratering. No reference is made to secondary and primary structures in the design for internal explosions. All structure in the containment boundary is considered to be primary structure.

$\boxed{\text{F1}}$, $\boxed{\text{F2}}$ It is assumed that general building layout and design specifications have been provided the AE. If a factor of safety is to be included in the design of the building, it will be included in the Design Criteria.

$\boxed{\text{F3}}$ If the explosion involves high explosives, then data are readily available for determining the peak pressures, specific impulse, and arrival times, both at standard atmospheric conditions and for reduced pressures. It is only necessary to know the energy release, the distance from the explosion, the angle of incidence of the surface exposed to the blast wave, and the ambient pressure. If the explosion is not produced by a high explosive, the HE data can still be used once an equivalent amount of HE is defined for the accident. For vapors or dusts, different conditions exist inside the dust or vapor cloud. Chapter 4 explains how the overpressures and impulses are determined for vapor and dust explosions. If detonation does not occur, then only a low intensity shock or none at all may occur. In this case a quasi-static pressure buildup can still occur from the burning process.

$\boxed{\text{F4}}$ Fragments may be created by the accident if machines or other structures are located near the explosion. Chapter 6 gives guidance and

information necessary to determine the mass, velocity, directions, and distribution of these fragments.

| F5 | If venting occurs in the structure, it will affect the decay time and peak value of the quasi-static pressure produced in the enclosure. Predictions for vented gas pressures, with and without vent closures, are given in Chapter 4.

| F6 | If venting does occur, then the vent areas and blow-out walls must be properly designed. The rate at which the vent opens (for blow-out walls) and the total effective vent area are the important parameters, and are covered in Chapter 4. Venting is most effective for deflagration processes such as with burning propellant. For these relatively slow processes, both the peak pressure produced in the enclosure and the decay time can be significantly reduced. For high explosives, the chemical reactions are very fast and very large vent areas, without covers, are required to attenuate the peak pressure. The decay time can be shortened, however, and this can be important in the design of some types of structures. In general, initial shock and peak quasi-static pressure loads on the structure cannot be significantly reduced by venting when the explosion is produced by a high explosive charge.

| F7 | The quasi-static pressure in a confined volume is produced by the heating of the air and the release of explosive products. It is affected by venting and by the availability of sufficient oxygen for complete combustion. Graphical solutions are provided in Chapter 4 for the maximum pressure and the decay time for HE explosions in enclosures with small vents. For other explosives, the maximum pressure is estimated from the products of the chemical reaction. Graphical solutions are also provided for vent times with and without blow-out walls. These data were generated by a computer program that is described and documented.

| F8 | Sometimes it is more economical to provide fragment shields in some locations than to design a large containment boundary to avoid fragment penetration. Also, some types of containment structures should not be used to both contain the explosive and stop the fragments. This applies primarily to single skin steel structures where stress risers produced by fragment impact can cause fracture of the stressed steel skin at lower than normal design stresses. Reinforced concrete, layered steel, or frame and panel construction is recommended when the primary containment boundary must resist both the blast loads and fragment impacts.

| F9 | Loading on the shields from fragment impacts can be idealized as an initial impulse for design purposes. When the fragments are stopped by the shield, their momentum is converted to an impulse on the structure. This approach assumes the inelastic impact occurs and that the fragment is fully arrested by the shield. If the fragment imbeds in the shield, then its mass should be included when computing the initial shield velocity. If fragment rebound occurs, then an initial shield velocity can be estimated by considering elastic impact with a low coefficient of restitution.

[F10] The shields must be designed, not only to avoid penetration, but also to remain in place when the explosion occurs. (They must not become fragments themselves.) Thus, the penetration resistance of the shields must be designed for the worst case fragment and the shield support must be designed to resist the blast and fragment loads. Either simplified methods or numerical methods can be used for this design analysis.

[F11] If shielding is not used and if the fragments are to be contained, then it is necessary to size the walls and ceiling of the structure to prevent fragment penetration. The thickness required to prevent penetration can be calculated for various materials from the equations in Chapter 6. The thickness set by penetration requirements may be larger or smaller than that required to resist the blast and fragment loading.

[F12] As for the shields, the fragment loads on the walls and ceiling are idealized as an initial impulse for the conditions of inelastic impact and no residual fragment velocity.

[F13] Once the fragment penetration criteria have been satisfied, the primary containment boundary is designed to withstand the blast loading (pressure and impulses from the blast wave and the quasi-static pressure) and the fragment loads. For internal explosions, multiple reflections of the blast wave are usually assumed as explained in Chapter 4. For HE charges, the quasi-static pressure reaches its peak very quickly and can be assumed to occur simultaneously with the blast wave. This is particularly convenient for simplified analysis. For numerical analyses this assumption is not necessary. Dead loads are usually small relative to the blast loading and can be omitted in the analysis.

Arrival times of the blast wave and fragments can be calculated to establish their phasing; however, it is acceptable for simplified analyses to apply them simultaneously. It is often found that the fragment loads are small relative to the blast and quasi-static loads and can be neglected.

Either simplified or numerical methods can be used to analyze the structure. Symmetric shell and concrete slab structures can usually be analyzed conveniently with one-degree-of-freedom models. The analysis of penetrations through the boundary of shell structures can be difficult, and off-the-shelf door designs should be used when possible (if it has been established that they can withstand the applied loads). Penetrations through the boundary are more straight-forward for reinforced concrete or frame and panel construction.

8.5 LIST OF SYMBOLS

A	beam cross-sectional area
b	beam width
$DLF, (DLF)_{MAX}$	dynamic load factor, maximum dynamic load factor
E	elastic modulus
F_1	magnitude of the total load applied to the structural component
$F(t)$	time-dependent force
H	beam depth
I	moment of inertia of the beam cross-sectional area
i	specific impulse
k, K_1, K_2	spring stiffness
ℓ, L	beam length
m	mass of single-degree-of-freedom system; total mass of the structural component
P, p	peak pressure
R	resistance of the structural component
R_e	resistance of the equivalent system
R_m	maximum resistance of the structural component
T	fundamental period of elastic vibration
t	time
t_d	duration of the applied load
t_m	time at which the maximum displacement is reached
t_r	rise time of the applied load

w	lateral displacement
w_o	lateral displacement at some location on the structural component, usually at the point of maximum displacement
X	position along the beam
X_1, X_2	displacements of single-degree-of-freedom systems
$X_{1_{MAX}}, X_{2_{MAX}}$	maximum displacements of systems 1 and 2
X_y	displacement at which yielding occurs
y	displacement of a structural component or single-degree-of-freedom system
y_{el}	displacement at which yielding occurs
y_{max}	maximum displacement
Z	plastic section modulus of a beam
$\alpha, \beta, \gamma, \delta$	constants used to characterize blast waves from bursting pressure vessels
ε_{MAX}	maximum strain in the beam
μ	ductility ratio (y_{MAX}/y_{el})
ρ	mass density
σ_y	yield stress
$\psi_P, \psi_i, \psi_\varepsilon, \psi_{wo}$	constants defined for beams with different boundary conditions

8.6 ANNOTATED REFERENCES

- Design of Structure...   U. S. Army Corps of Engineers
  (Ref. 8.15)

  This volume of a multi-volume design manual was one of the first to
  present simplified dynamic design procedures for plastically deforming
  structures. It was prepared by staff at MIT. The methods reported in
  this manual reappear in many later manuals, with no or minimal change.

- Norris, et al. (Ref. 8.10)

  This book first appeared as a set of course notes for a short course
  taught by MIT staff. Procedures carry over directly from an earlier
  U. S. Army Corps of Engineers manual. As with the Army manual, these
  methods reappear in many later manuals.

- Biggs (Ref. 8.2)

  This is an excellent introductory text for any engineer engaged in
  dynamic structural design. Biggs is one of the authors of the earlier
  Army Corps of Engineers manual, and Norris, et al. (Ref. 8.10). This
  book draws heavily on the earlier work, but adds considerable material.
  Presentation is very clear and understandable.

- Structures to Resist....   TM 5-1300 (Ref. 8.1)

  This design manual is the "Bible" for most structural engineers in-
  volved in blast-resistant design in reinforced concrete. Its strengths
  are in presentation of detailed procedures for estimating blast loading
  for internal explosions, failure modes for reinforced concrete, struc-
  tural elements, and design of reinforcing. Some of the blast loading
  and fragment impact data in this manual are, however, now outdated and
  should be supplanted by later information. Basic structural design
  procedures are identical to those presented earlier by MIT authors.

- Suppressive Shields....   (Ref. 8.18)

  Chapter 5 in this manual is directed primarily to simplified methods
  for dynamic elastic and elastic-plastic design of steel structures
  subjected to internal blast loading. The primary methods are those
  previously developed by the MIT staff and by Newmark, but special
  attention is paid to response to loading pulses for initial shock loads
  and gas venting pressures for the structures with small or no venting
  which typify suppressive shields. More sophisticated dynamic design
  methods are identified, but not used.

- Baker (Ref. 8.35), Baker (Ref. 8.36), Lee & Martin (Ref. 8.37), Kaliszky (Ref. 8.38), Symonds (Ref. 8.39), Symonds & Chon (Ref. 8.40), Symonds & Chon (Ref. 8.41)

  These are all survey papers that discuss approximate methods for dynamic plastic deformations of impulsively loaded structures. The methods are not always applicable to blast-loaded structures because not all such structures respond impulsively. But, these papers should give the reader a good grasp of the open literature on this topic, throughout the world.

- Greenspon (Ref. 8.23), Westine & Baker (Refs. 8.42 and 8.43), Westine & Cox (Ref. 8.21)

  A number of dynamic structural design equations and graphs for quick estimation of response to blast loads have been developed in recent years. The referenced reports are the principal original references. All use the scaled P-i (pressure-impulse) concept for relating response to loading and give predictions for beams, plates, shells, and other structural elements. Many of the results are collected and discussed in Baker, Cox, et al. (Ref. 8.9), which also covers Biggs/Newmark's simplified methods for structural response.

8.7 REFERENCES

8.1 Structures to Resist the Effects of Accidental Explosions, Department of the Army Technical Manual TM5-1300, Department of the Navy Publication NAVFAC P-397, Department of the Air Force Manual AFM 88-22, June 1969.

8.2 Biggs, J. M., Introduction to Structural Dynamics, McGraw-Hill Book Company, New York, 1964.

8.3 Westine, P. S. and Baker, W. E., "Energy Solutions for Predicting Deformations in Blast Loaded Structures," Minutes of 16th Annual Explosion Safety Seminar, Department of Defense Safety Board, 1974.

8.4 Bathe, K. J., "ADINA, A Finite Element Program for Automatic Dynamic Incremental Nonlinear Analysis," Report 82448-1, Acoustics and Vibration Lab, Med. Eng. Dept., MIT, 1976.

8.5 DeSalvo, G. J. and Swanson, J. A., ANSYS Engineering Analysis Systems, User's Manual, Swanson Analysis Systems, Inc., Houston, PA, 1979.

8.6 Nonlinear Finite Element Analysis Program Volume I: Users Information Manual, MARC Analysis Corporation and Control Data Corporation, 1975.

8.7 Stea, W., Tseng, G., Kossover, D., Price, P., and Caltagirone, Jr., "Nonlinear Analysis of Frame Structures Subjected to Blast Overpressures," Contractor Report ARLCD-CR-77008, U. S. Army Armament Research & Development Command, Large Caliber Weapon Systems Laboratory, Dover, NJ, May 1977.

8.8 Pirotin, S. D., Berg, B. A., and Witmer, E. A., "PETROS 4: New Developments and Program Manual for the Finite-Difference Calculation of Large Elastic-Plastic, and/or Viscoelastic Transient Deformations of Multilayer Variable-Thickness (1) Hard-Bonded, (2) Moderately-Thick Hard-Bonded, or (3) Thin Soft-Bonded Shells," BRL Contract Report No. 316, MIT, September 1976.

8.9 Baker, W. E,, Cox, P. A., Westine, P. S., Kulesz, J. J., and Strehlow, R. A., A Short Course on Explosion Hazards Evaluation, Southwest Research Institute, San Antonio, TX, 1978.

8.10 Norris, C. H., Hansen, R. J., Holley, M. J., Jr., Biggs, J. M., Namyet, S., and Minami, J. K., Structural Design for Dynamic Loads, McGraw-Hill Book Company, New York, 1959.

8.11 Cox, P. A., Westine, P. S., Kulesz, J. J., and Esparza, E. D., "Analysis and Evaluation of Suppressive Shields," Final Technical Report, Edgewood Arsenal Contractor Report, ARCFL-CR-77028, Report No. 10, January 1978.

8.12 Esparza, E. D. and Baker, W. E., "Measurement of Blast Waves from Bursting Frangible Spheres Pressurized with Flash-Evaporating Vapor or Liquid," NASA Contractor Report 2811, Contract NSG-3008, National Aeronautics and Space Administration, November 1977.

8.13 Nuclear Regulatory Commission, Regulation Guide 1.92.

8.14 Den Hartog, J. P., Mechanical Vibrations, 3rd Edition, McGraw-Hill Book Company, New York, 1947.

8.15 Design of Structures to Resist the Effects of Atomic Weapons, TM 5-856, 1 through 9, Department of the Army, U. S. Army AG Publications Center, 1655 Woodson Road, St. Louis, MO 63114, March 1965. [This is an updated version of the U. S. Army COE Manual EM110-345-415, March 1957.]

8.16 "Shelter Design and Analysis, Volume 4, Protective Construction for Shelters," Defense Civil Preparedness Agency, TR-20, (Reviewer's Draft), July 1972.

8.17 Crawford, R. E., Higgins, C. J., and Bultmann, E. H., The Air Force Manual for Design and Analysis of Hardened Structures, AFWL-TR-75-102, Air Force Weapons Lab., Kirtland AFB, NM, October 1974.

8.18 Suppressive Shields Structural Design and Analysis Handbook, HNDM-1110-1-2, U. S. Army Corps of Engineers, Huntsville Division, November 1977.

8.19 Healey, J., Ammar, A., Vellozzi, J., Pecone, G., Weissman, S., Dobbs, N., and Price, P., "Design of Steel Structures to Resist the Effects of HE Explosions," Technical Report 4837, Picatinny Arsenal, Dover, NJ, August 1975.

8.20 Tseng, G., Weissman, S., Dobbs, N., and Price, P., "Design Charts for Cold-Formed Steel Panels and Wide-Flange Beams Subjected to Blast Loading," Technical Report 4838, Picatinny Arsenal, Dover, NJ, August 1975.

8.21 Westine, P. S. and Cox, P. A., "Additional Energy Solutions for Predicting Structural Deformations," Edgewood Arsenal Contractor Report EM-CR-76031, Report No. 4, Southwest Research Institute, November 1975.

8.22 Westine, P. S., "R-W Plane Analysis for Vulnerability of Targets to Air Blast," The Shock & Vibration Bulletin, Bulletin 42, Part 5, pp. 173-183, January 1972.

8.23 Greenspon, J. E., "Energy Approaches to Structural Vulnerability with Application of the New Bell Stress-Strain Laws," BRL Contract Report No. 291, Aberdeen Proving Ground, MD, March 1976.

8.24 Baker, W. E., Cox, P. A., Esparza, E. D., and Westine, P. S., "Design Study of a Suppressive Structure for a Melt Loading Operation," Edgewood Arsenal Contractor Report EM-CR-76043, Report No. 9, December 1975.

8.25 Fenves, S. J., Perrone, N., Robinson, A. R., and Schnobrich, W. C. (Editors), Numerical and Computer Methods in Structural Mechanics, Academic Press, New York, 1973.

8.26 Pilkey, W., Saczalski, K., and Schaeffer, H. (Editors), Structural Mechanics Computer Programs, University Press of Virginia, Charlottesville, VA, 1974.

8.27 Perrone, N. and Pilkey, W. (Editors), Structural Mechanics Software Series, Volume I, University Press of Virginia, Charlottesville, VA, 1977.

8.28 Perrone, N. and Pilkey, W. (Editors), Structural Mechanics Software Series, Volume II, University Press of Virginia, Charlottesville, VA, 1978.

8.29 McCormick, C. W. (Editor), "MSC/NASTRAN User's Manual," MSR-39, The MacNeal-Schwendler Corporation, 7442 North Figueroa Street, Los Angeles, CA, May 1976.

8.30 Haisler, W. E., "AGGIE I – A Finite Element Program for Nonlinear Structural Analysis," Report TEES-3275-77-1, Aerospace Engineering Department, Texas A&M University, June 1977.

8.31 Haisler, W. E., "Status Report of AGGIE I Computer Program," Technical Report No. 3275-78-2, Aerospace Engineering Department, Texas A&M University, April 1978.

8.32 Wu, R. W-H and Witmer, E. A., "Finite Element Analysis of Large Transient Elastic-Plastic Deformations of Simple Structures, with Application to the Engine Rotor Fragment Containment/Deflection Program," NASA CR-120886, ASRL TR 154-4, Aeroelastic and Structures Research Laboratory, MIT, Cambridge, MA, January 1972.

8.33 Neal, B. G., Plastic Methods of Structural Analysis, Chapman & Hall, London, England, 1977.

8.34 Baker, W. E., "Approximate Techniques for Plastic Deformation of Structures Under Impulsive Loading," Shock and Vibration Digest, 7, (7), pp. 107-117, 1975.

8.35 Baker, W. E., "Approximate Techniques for Plastic Deformation of Structures Under Impulsive Loading, II," Shock and Vibration Digest, 11, (7), pp. 19-24, 1979.

8.36 Lee, L. S. S. and Martin, J. B., "Approximate Solutions of Impulsively Loaded Structures of a Rate Sensitive Material," Z. Agnew. Math. Phys., 21, pp. 1011-1032, 1970.

8.37 Kaliszky, S., "Approximate Solutions for Impulsively Loaded Inelastic Structures and Continua," Intl. J. Nonlin. Mech., 5, pp. 143-158, 1970.

8.38 Symonds, P. S., "Approximation Techniques for Impulsively Loaded Structures of Rate Sensitive Plastic Behavior," SIAM J. Appl. Math., 25, (3), pp. 462-473, 1973.

8.39 Symonds, P. S. and Chon, C. T., "Bounds for Finite-Deflections of Impulsively Loaded Structures with Time-Dependent Plastic Behavior," Intl. J. Solids Struc., 11, pp. 403-425, 1975.

8.40 Symonds, P. S. and Chon, C. T., "Approximation Techniques for Impulsive Loading of Structures of Time-Dependent Plastic Behavior with Finite-Deflections," Mechanical Properties at High Rates of Strain, J. Harding, Ed., Inst. Physics (London), Conf. Ser. No. 21, pp. 299-316, 1974.

8.41 Westine, P. S. and Baker, W. E., "Energy Solutions for Predicting Deformations in Blast-Loaded Structures," Edgewood Arsenal Contractor Report EM-CR-76027, Report No. 6, Southwest Research Institute, November 1975.

8.42 Westine, P. S. and Baker, W. E., "Energy Solutions for Predicting Deformations in Blast Loaded Structures," Minutes of 16th Annual Explosion Safety Seminar, Department of Defense Safety Board, 1974.

APPENDIX A

PROPERTIES OF EXPLOSIVES

This appendix includes various properties of explosives which are or could be present or used in various facilities of the Pantex Plant. Separate tables are given for:

- Physical Properties of Explosives

- Chemical Properties of Explosives

- Sensitivity of Explosives

- Hugoniots for Unreacted HE's

- Thermal Properties of Explosives

- Performance of Explosives

Blanks in the tables indicate that we were unable to find the specific property for the listed explosive. Common abbreviations or contractions are used to identify each explosive. Explosives are listed in alphabetical order in each table.

REFERENCES

1. Properties of Chemical Explosives and Explosive Simulants, Brigitta M. Dobratz, 1974.

2. Engineering Design Handbook; Explosives Series; Properties of Explosives of Military Interest, 1971.

Table 1(a)   Physical Properties of Explosives[a]

COMMON NAME	CHEMICAL NAME	FORMULATION	COLOR	PHYSICAL STATE	THEORETICAL MAXIMUM SPECIFIC WEIGHT		NOMINAL SPECIFIC WEIGHT	
					Mg/m^3	lb/in^3	Mg/m^3	lb/in^3
BARATOL		TNT – 24% $Ba(NO_3)_2$ – 76%		Solid	2.63	9.50×10^{-2}	2.60 – 2.61	9.39×10^{-2} – 9.42×10^{-2}
BORACITOL		TNT – 40% Boric Acid – 60%		Solid	1.52	5.49×10^{-2}	1.53 – 1.54	5.53×10^{-2} – 5.56×10^{-2}
BTF	Benzotrifuroxab Hexanitrosobenzene	$C_6N_6O_6$	Buff	Solid	1.901	6.87×10^{-2}	1.87	6.76×10^{-2}
COMP B		RDX – 60% TNT – 40%	Yellow-Brown	Solid	1.74	6.29×10^{-2}	1.71	6.18×10^{-2}
COMP C-4		RDX – 91% Plasticizer – 9%	Varies Yellow, White	Putty-like			1.59	5.74×10^{-2}
CYCLOTOL 75/25		RDX – 75% TNT – 25%	Yellow[b] Buff	Solid	1.77	6.39×10^{-2}	1.75 – 1.76	6.32×10^{-2} – 6.36×10^{-2}
DATNB/DATB	Diamino Trinitrobenzene	$C_6H_5N_5O_6$	Yellow	Crystal[b]	1.837	6.64×10^{-2}	1.79	6.47×10^{-2}
DIPAM	3,3' – Diamino-2,2', 4,4', 6,6' – Hexanitrobiphenyl	$C_{12}H_6N_8O_{12}$		Solid	1.79	6.47×10^{-2}		
DNPA	2,2' – Dinitro-Propylacrylate	$C_6H_8N_2O_6$	Off-White	Solid	1.47	5.31×10^{-2}		
EDNP	Ethyl – 4,4' – Dinitropentanoate	$C_7H_{12}N_2O_6$	Yellow	Liquid	1.28	4.62×10^{-2}		
FEFO	Bis (2,2' – Dinitro – 2 – Flouro-Ethyl)	$C_5H_6N_4O_{10}F_2$	Straw	Liquid	1.607	5.81×10^{-2}		
HMX	Cyclotetramethyl-Enotetranitramine	$C_4H_8N_4(NO_2)_4$	White	Solid	1.90	6.86×10^{-2}	1.89	6.83×10^{-2}
HNAB	2,2', 4,4', 6,6' – Hexanitroazobenzene	$C_{12}H_4N_8O_{12}$	Orange	Solid	1.799	6.50×10^{-2}		
HNS	2,2', 4,4', 6,6' – Hexanitrostilbene	$C_{14}H_6N_6O_{12}$	Yellow	Solid	1.74	6.29×10^{-2}	1.72	6.21×10^{-2}

Table 1(a) Physical Properties of Explosives[a] (Con't)

COMMON NAME	CHEMICAL NAME	FORMULATION	COLOR	PHYSICAL STATE	THEORETICAL MAXIMUM SPECIFIC WEIGHT		NOMINAL SPECIFIC WEIGHT	
					Mg/m^3	lb/in^3	Mg/m^3	lb/in^3
LX-01		NM - 51.7% TNM - 33.2% 1 - Nitropropane - 15.1%	Clear	Liquid	1.23	4.44×10^{-2}		
LX-02-1		PETN - 73.5% Butyl Rubber - 17.6% Acetyltributyl Citrate - 6.9% CAB-O-Sil - 2%	Buff	Putty-like Solid	1.44	5.20×10^{-2}	1.43 - 1.44	5.17×10^{-2} - 5.20×10^{-2}
LX-04		HMX - 85% Viton A - 15%	Yellow	Solid	1.889	6.82×10^{-2}	1.86 - 1.87	6.72×10^{-2} - 6.76×10^{-2}
LX-07		HMX - 90% Viton A - 10%	Orange	Solid	1.892	6.84×10^{-2}	1.86 - 1.87	6.72×10^{-2} - 6.76×10^{-2}
LX-08		PETN - 63.7% Sylgard - 34.3% CAB-O-Sil - 2%	Blue	Putty-like	1.439	5.20×10^{-2}	≥ 1.42	$\geq 5.13 \times 10^{-2}$
LX-09-0		HMX - 93% PDNPA - 4.6% FEFO - 2.4%	Purple	Solid	1.867	6.74×10^{-2}	1.837 - 1.845	6.64×10^{-2} - 6.67×10^{-2}
LX-10-0		HMX - 95% Viton A - 5%	Blue-Green Spots on White	Solid	1.896	6.85×10^{-2}	1.858 - 1.868	6.71×10^{-2} - 6.75×10^{-2}
LX-11		HMX - 80% Viton A - 20%	White	Solid			1.87 - 1.876	6.76×10^{-2} - 6.78×10^{-2}
LX-14		HMX - 95.5% Estane 5702 F-1 - 4.5%	Violet Spots on White	Solid	1.849	6.68×10^{-2}	1.834	6.62×10^{-2}
NG	1, 2, 3 - Propanetriol-Trinitrate	$C_3H_5N_3O_9$	Clear	Liquid	1.59	5.74×10^{-2}		
NQ	Nitroguanidine	$C_1H_4N_4O_2$	White	Solid	1.72	6.21×10^{-2}	1.55	5.60×10^{-2}

Table 1(a) Physical Properties of Explosives[a] (Con't)

COMMON NAME	CHEMICAL NAME	FORMULATION	COLOR	PHYSICAL STATE	THEORETICAL MAXIMUM SPECIFIC WEIGHT		NOMINAL SPECIFIC WEIGHT	
					Mg/m^3	lb/in^3	Mg/m^3	lb/in^3
OCTOL 75/25		HMX - 75% TNT - 25%	Buff	Solid	1.83	6.61×10^{-2}	1.80 - 1.82	6.50×10^{-2} - 6.57×10^{-2}
PBX-9007		RDX - 90% Rosin - 0.4% Polystyrene - 9.1% Di-2-Ethylexyl- phthalate - 0.5%	White or Gray	Solid	1.697	6.13×10^{-2}	1.66	6.00×10^{-2}
PBX-9010		RDX - 90% KEL F - 10%	White	Solid	1.822	6.58×10^{-2}	1.789	6.46×10^{-2}
PBX-9011		RDX - 90% Estane - 10%	Off- White	Solid	1.795	6.48×10^{-2}	1.770	6.39×10^{-2}
PBX-9205		RDX - 92% Polystyrene - 6% Di-2-Ethylhexyl- phthalate - 2%	White	Solid	1.72	6.21×10^{-2}	1.68	6.07×10^{-2}
PBX-9404		HMX - 94% NC - 3% Tris-B-Chloro- ethylphosphate - 3%	White or Blue	Solid	1.865	6.74×10^{-2}	1.831 - 1.844	6.61×10^{-2} - 6.66×10^{-2}
PBX-9407		HMX - 94% Exon 461 - 6%	White or Black	Solid	1.81	6.54×10^{-2}	1.60 - 1.62	5.78×10^{-2} - 5.85×10^{-2}
PBX-9501		HMX - 95% Estane - 2.5% BDNPA - 1.25% BDNPF - 1.25%	White	Solid	1.855	6.70×10^{-2}	1.843	6.73×10^{-2}
PENTOLITE 50/50		PETN - 50% TNT - 50%		Solid	1.71	6.18×10^{-2}	1.67	6.03×10^{-2}
PETN	Pentaerythritol Tetranitrate	$C_5H_8(NO_3)_4$	White	Solid	1.77	6.39×10^{-2}	1.76	6.36×10^{-2}
RDX	Cyclotrimethylene Trinitramine	$C_3H_6N_3(NO_2)_3$	White	Solid	1.806	6.52×10^{-2}		

Table 1(a) Physical Properties of Explosives[a] (Con't)

COMMON NAME	CHEMICAL NAME	FORMULATION	COLOR	PHYSICAL STATE	THEORETICAL MAXIMUM SPECIFIC WEIGHT		NOMINAL SPECIFIC WEIGHT	
					Mg/m^3	lb/in^3	Mg/m^3	lb/in^3
TATB	1, 3, 5 - , Triamino - 2, 4, 6 - Trinitrobenzene	$C_6H_6N_6O_6$	Yellow	Solid	1.94	7.01×10^{-2}	1.88	6.79×10^{-2}
TETRYL	Trinitrophenyl- Methylnitramine	$C_7H_5N(NO_2)_4$	Yellow	Solid	1.73	6.25×10^{-2}	1.71	6.18×10^{-2}
TNETB	2, 2, 2 - Trinitroethyl - 4, 4, 4 - Trinitrobutyrate	$C_6H_6N_6O_{14}$	Color- less	Crystal			1.78^b	6.43×10^{-2}
TNT	Trinitrotoluene	$C_7H_5N_3O_6$	Buff	Solid	1.654	5.98×10^{-2}	Cast 1.55 Pressed 1.635	Cast 5.60×10^{-2} Pressed 5.91×10^{-2}

a. Taken from Properties of Chemical Explosives and Explosive Simulants by Brigitta M. Dobraty, 1974, unless otherwise indicated.

b. Taken from Engineering Design Handbook; Explosives Series; Properties of Explosives of Military Interest, 1971.

c. Molecular weight of mixture calculated based on:

$$MW_T = \sum_{i=1}^{N} \frac{a_N}{100} \ MW_N$$

where MW_T = total molecular weight of mixture;

MW_N = molecular weight of Nth constituent; and

a_N = weight percentage of the Nth constituent.

* Calculated Values

Table 1(b) Physical Properties of Explosives[a]

COMMON NAME	MOLECULAR WEIGHT		MELTING POINT		VAPOR PRESSURE				TOXICITY
	Amu	kg	°C	°F	Pa	lb/in^2	°C	°F	
BARATOL	253.0[c]	4.20×10^{-25}	79.0 - 80.0	174.2 - 176.0	13.3	1.93×10^{-3}	100	212.0	
BORACITOL	117.0[c]	1.94×10^{-25}	79.0 - 80.0	174.2 - 176.0					
BTF	252.1	4.18×10^{-25}	198.0 - 200.0	388.4 - 392.0					
COMP B	224.0[c]	3.72×10^{-25}	78.0 - 80.0	172.4[b] - 176.0					
COMP C-4	∿222.0[c]	3.69×10^{-25}							Moderate
CYCLOTOL 75/25	223.4[c]	3.71×10^{-25}	79.0 - 80.0	174.2 - 176.0	13.3	1.93×10^{-3}	100	212.0	
DATNB/DATB	243.0	4.03×10^{-25}	286.0 - 290.0	546.8 - 554.0					
DIPAM	454.1	7.54×10^{-25}	304.0	579.2					Moderate
DNPA	204.1	3.39×10^{-25}							
EDNP	220.2	3.66×10^{-25}	-6.0	21.2					
FEFO	320.1	5.31×10^{-25}	11.3 - 12.9	52.34 - 55.22	0.02854	4.14×10^{-6}	25	77.0	High
HMX	296.2	4.92×10^{-25}	285.0 - 287.0	545.0 - 548.6	4.00×10^{-7}	5.80×10^{-11}	100	212.0	Slight
HNAB	452.21	7.51×10^{-25}	215.0 - 216.0	419.0 - 420.8	1.33×10^{-5}	1.93×10^{-9}	100	212.0	Slight
HNS	450.3	7.47×10^{-25}	313.0	595.4	1.33×10^{-7}	1.93×10^{-11}	100	212.0	Slight
LX-01			-54.0	65.2	3.87×10^{3}	5.61×10^{-1}	25	77.0	
LX-02-1									
LX-04	279.8[c]	4.64×10^{-25}	Decomposes > 250.0	Decomposes > 482.0					
LX-07	285.3[c]	4.74×10^{-25}	Decomposes > 250.0	Decomposes > 482.0					
LX-08	228.0[c]	3.78×10^{-25}	Decomposes 129.0 - 135.0	Decomposes 264.2 - 275.0					
LX-09-0			Decomposes > 280.0	Decomposes > 536.0					
LX-10-0	291.0[c]	4.83×10^{-25}	Decomposes > 250.0	Decomposes > 482.0					

Table 1(b) Physical Properties of Explosives[a] (Con't)

COMMON NAME	MOLECULAR WEIGHT		MELTING POINT		VAPOR PRESSURE				TOXICITY
	Amu	kg	°C	°F	Pa	lb/in²	°C	°F	
LX-11	274.4^c	4.56×10^{-25}	Decomposes > 250.0	Decomposes > 482.0					
LX-14			Decomposes > 270.0	Decomposes > 518.0					
NG	227.1	3.77×10^{-25}	13.2	55.76	0.2	1.40×10^{-5}	20	68.0	Very High
NQ	104.1	1.73×10^{-25}	Decomposes 246.0 - 247.0	Decomposes 474.8 - 476.6					Slight
OCTOL 75/25	275.5^c	4.57×10^{-25}	79.0 - 80.0	174.2 - 176.0	13.3	1.93×10^{-3}	100	212.0	
PBX-9007			Decomposes > 200.0	Decomposes > 392.0					
PBX-9010	211.5^c	7.51×10^{-25}	Decomposes > 200.0	Decomposes > 392.0					
PBX-9011			Decomposes > 250.0	Decomposes > 482.0					
PBX-9205			Decomposes > 200.0	Decomposes > 392.0					
PBX-9404			Decomposes > 250.0	Decomposes > 482.0					
PBX-9407	341.3^c	5.67×10^{-25}	Decomposes > 200.0	Decomposes > 392.0					
PBX-9501			Decomposes > 240.0	Decomposes > 464.0					
PENTOLITE 50/50	271.7^c	4.51×10^{-25}	76.0	168.8	13.3	1.93×10^{-3}	100	212.0	
PETN	316.2	5.25×10^{-25}	139.0 - 142.0	282.2 - 287.6	1.10×10^{-3}	1.55×10^{-7}	100	212.0	High
RDX	222.1	3.69×10^{-25}	205.0	401.0	0.87	1.26×10^{-4}	111	231.8	Slight
TATB	258.2	4.28×10^{-25}	Decomposes > 325.0	Decomposes > 617.0					
TETRYL	287.0	4.77×10^{-25}	130.0	266.0					High
TNETB	386.0^b	6.41×10^{-25}	93.0	199.4^b	3.07 18.6	4.45×10^{-5} 2.70×10^{-4}	100 120	212.0 248.0	

Table 1(b)   Physical Properties of Explosives[a] (Con't)

COMMON NAME	MOLECULAR WEIGHT		MELTING POINT		VAPOR PRESSURE				TOXICITY
	Amu	kg	°C	°F	Pa	lb/in^2	°C	°F	
TNT	227.1	3.77×10^{-25}	80.9	177.62	14.13	2.05×10^{-3}	100	212.0	Moderate

a. Taken from Properties of Chemical Explosives and Explosive Simulants by Brigitta M. Dobratz, 1974, unless otherwise indicated.

b. Taken from Engineering Design Handbook; Explosives Series; Properties of Explosives of Military Interest, 1971.

c. Molecular weight of mixture calculated based on:

$$MW_T = \sum_{i=1}^{N} \frac{a_N}{100} MW_N$$

where MW_T = total molecular weight of mixture;

MW_N = molecular weight of Nth constituent; and

a_N = weight percentage of the Nth constituent.

* Calculated Values

A-8

Table 2 Chemical Properties of Explosives[a]

COMMON NAME	HEAT OF FORMATION (SEE NOTE 1)		HEAT OF DETONATION (SEE NOTE 2)		HEAT OF COMBUSTION	
	kJ/kg	ft-lb/lb	MJ/kg	ft-lb/lb	MJ/kg	ft-lb/lb
BARATOL	-2.952×10^3	-9.876×10^5	3.10	1.04×10^6		
BORACITOL	-1.076×10^4	-3.600×10^6	1.67	5.59×10^5		
BTF	2.399×10^3	8.026×10^5	7.07	2.37×10^6		
COMP B	5.78×10^1	1.94×10^4	6.44	2.15×10^6	1.17×10^1 b	3.91×10^6 b
COMP C-4	1.39×10^2	4.65×10^4	6.65	2.22×10^6		
CYCLOTOL 75/25	1.38×10^2	4.62×10^4	6.57	2.20×10^6	1.10×10^1 b	3.68×10^6 b
DATB/DATNB	-5.03×10^2	-1.68×10^5	5.27	1.76×10^6		
DIPAM	-1.85×10^2	-6.19×10^4	5.65	1.89×10^6		
DNPA	-2.255×10^3	-7.544×10^5	4.44	1.48×10^6		
EDNP	-2.660×10^3	-8.899×10^5	5.15	1.72×10^6		
FEFO	-2.320×10^3	-7.762×10^5	6.07	2.03×10^6		
HMX	2.53×10^2	8.46×10^4	6.78	2.27×10^6	9.88 b	3.31×10^6 b
HNAB	5.35×10^2	1.79×10^5	6.15	2.06×10^6		
HNS	1.29×10^2	4.32×10^4	5.94	1.99×10^6		
LX-01	-1.152×10^3	-3.854×10^5	7.20	2.41×10^6		
LX-02-1	-2.053×10^3	-6.869×10^5	5.94	1.99×10^6		
LX-04	-9.01×10^2	-3.01×10^5	5.94	1.99×10^6		
LX-07	-5.17×10^2	-1.73×10^5	6.23	2.08×10^6		
LX-08	-1.859×10^3	-6.219×10^5	8.27	2.77×10^6		
LX-09-0	7.61×10^1	2.55×10^4	6.69	2.24×10^6		
LX-10-0	-1.31×10^2	-4.38×10^4	6.49	2.17×10^6		
LX-11	-1.286×10^3	-4.302×10^5	5.77	1.72×10^6		
LX-14	6.28×10^1	2.10×10^4	6.59	2.20×10^6		

Table 2 Chemical Properties of Explosives[a] (Con't)

COMMON NAME	HEAT OF FORMATION (SEE NOTE 1)		HEAT OF DETONATION (SEE NOTE 2)		HEAT OF COMBUSTION	
	kJ/kg	ft-lb/lb	MJ/kg	ft-lb/lb	MJ/kg	ft-lb/lb
NG	-1.673×10^3	-5.597×10^5	6.65	2.22×10^6	6.76	2.26×10^6
NQ	-9.49×10^2	-3.17×10^5	4.44	1.49×10^6 b	8.35	2.79×10^6
OCTOL 70/30	1.19×10^2	3.98×10^4	6.57	2.20×10^6	1.14×10^1 b	3.81×10^6 b
PBX-9007	2.98×10^2	9.97×10^4	6.53	2.18×10^6		
PBX-9010	-3.29×10^2	-1.10×10^5	6.15	2.06×10^6		
PBX-9011	-1.70×10^2	-5.69×10^4	6.40	2.14×10^6		
PBX-9205	2.43×10^2	8.13×10^4	6.11	2.04×10^6		
PBX-9404	3.31	1.11×10^3	6.53	2.18×10^6		
PBX-9407	4.84×10^2	1.62×10^5	6.69	2.24×10^6		
PBX-9501	9.54×10^1	3.19×10^4	6.65	2.22×10^6		
PENTOLITE 50/50	-9.937×10^2	-3.32×10^5	6.40	2.14×10^6		
PETN	-1.702×10^3	-5.69×10^5	6.90	2.31×10^6	8.20 b	2.70×10^6 b
RDX	2.771×10^2	9.27×10^4	6.78	2.27×10^6	9.56 b	3.20×10^6 b
TETRYL	6.66×10^1	2.23×10^4	6.32	2.11×10^6	1.22×10^1 b	4.08×10^6 b
TNETB	-1.28×10^3	-4.28×10^5 b			6.99 b	2.34×10^6 b
TNT	-2.84×10^2	-9.50×10^4	5.90	1.97×10^6	1.51×10^1 b	5.05×10^6 b

a.   See Table 1.
b.   See Table 1.

NOTE 1:   Heat of formation values taken from the Engineering Design Handbook Explosive Series Properties of Explosives have been multiplied by (-1) to retain the sign convention that ΔH_f is negative when the reaction is exothermic.

NOTE 2:   Heat of detonation values are calculated maximum values for reactions ending in liquid phase water. For a more complete description, see Dobratz, 1974.

A-10

Table 3(a)   Sensitivity of Explosives[a]

COMMON NAME	DROP WEIGHT TEST				SKID TEST			FRICTION PENDULUM TEST	
	SAMPLE		HEIGHT		HEIGHT		ANGLE OF IMPACT DEG	STEEL SHOE	FIBER SHOE
	Mass, kg	Weight, lb	m	in	m	in			
BARATOL	5.0	11.0	0.950	37.4					
BORACITOL	5.0	11.0	> 1.770	> 69.68					
BTF	5.0	11.0	0.110	4.33					
COMP B	5.0	11.0	0.450	17.72					
COMP C-4								unaffected	unaffected
CYCLOTOL 75/25	5.0	11.0	0.330	12.99				unaffected	unaffected
DATB/DATNB	5.0	11.0	> 1.770	> 69.68				unaffected	unaffected
DIPAM	5.0	11.0	0.950	37.4					
DNPA	5.0	11.0	> 1.770	> 69.68					
EDNP									
FEFO	5.0	11.0	0.280	11.024					
HMX	5.0	11.0	0.330	12.99					
HNAB									
HNS									
LX-01									
LX-02-1	4.99	11.0	0.800	31.5					
LX-04	4.99	11.0	0.410	16.14	4.30 / 1.52	169.3 / 59.8	14 Low Order / 45 (Mild)		
LX-07	4.99	11.0	0.380	14.96	0.760 / 2.160	29.9 / 85.0	14 Explodes / 45 Explodes		
LX-08									
LX-09-0	4.99	11.0	0.320	12.6	0.38 / 1.52	15.0 / 59.8	14 Explodes / 45 Explodes		

Table 3(a) Sensitivity of Explosives[a] (Con't)

COMMON NAME	DROP WEIGHT TEST				SKID TEST			FRICTION PENDULUM TEST	
	SAMPLE		HEIGHT		HEIGHT		ANGLE OF IMPACT DEG	STEEL SHOE	FIBER SHOE
	Mass, kg	Weight, lb	m	in	m	in			
LX-10-0	4.99	11.0	0.350	13.78	1.07	42.1	45 Explodes		
LX-11			0.590	23.23					
LX-14								explodes	
NG	2.0	4.4	0.150	5.91				unaffected	unaffected
NQ	4.99	11.0	> 1.770	> 69.68				unaffected	unaffected
OCTOL 75/25	4.99	11.0	0.410	16.14					
PBX-9007	4.99	11.0	0.350	13.78					
PBX-9010	4.99	11.0	0.300	11.81	0.381	14.0	14 Explodes		
PBX-9011	4.99	11.0	0.440	17.32	6.10	240.2	14 Puff		
					6.10	240.2	45 No Reaction		
PBX-9205	4.99	11.0	0.420	16.54	0.381	15.0	14 Puff		
					0.760	29.9	45 Low Order		
PBX-9404	4.99	11.0	0.340	13.39	0.381	15.0	14 Explodes		
					1.07	42.1	45 Explodes		
PBX-9407	4.99	11.0	0.330	12.99					
PBX-9501	4.99	11.0	0.440	17.32	3.05	120.1	14 Low Order		
					3.05	120.1	45 Nothing		
PENTOLITE 50/50	4.99	11.0	0.350	13.78				unaffected	unaffected
PETN	4.99	11.0	0.110	4.331				crackles	unaffected
RDX	4.99	11.0	0.280	11.02				explodes	unaffected
TATB									
TETRYL	4.99	11.0	0.280	11.02				crackles	unaffected
TNETB									
TNT	4.99	11.0	0.800	31.496				unaffected	unaffected

Table 3(b)   Sensitivity of Explosives[a]

COMMON NAME	EXPLOSION TEMPERATURE (5 SEC)		RIFLE BULLET IMPACT TEST			SUSAN TEST			GAP TEST	
			EXPLODE (%)	PARTIAL (%)	BURN (%)	THRESHOLD VEL.		PROBABILITY OF REACTION		
	°C	°F				km/sec	ft/sec		m	in
BARATOL	Ignites 385	Ignites 725.0							Failed at 0	Failed at 0
BORACITOL										
BTF										
COMP B	Decomposes 278	Decomposes 532.4 b	3	13	4				4.06×10^{-4} – 6.60×10^{-4}	0.016 – 0.026
COMP C-4	290	554.0 b			20					
CYCLOTOL 75/25			30	40		0.055	180.5	High	2.54×10^{-4} – 4.06×10^{-4}	0.010 – 0.016
DATB/DATNB										
DIPAM										
DNPA										
EDNP										
FEFO										
HMX	327	620.6							7.06×10^{-2}	2.78
HNAB										
HNS										
LX-01										
LX-02-1										
LX-04						0.154 .0430 – .0460	505.0 140 – 150	Low Some Geometries High		
LX-07						0.038	125.0	Moderate	1.80×10^{-3} – 2.30×10^{-3}	0.071 – 0.091
LX-08										

Table 3(b)   Sensitivity of Explosives[a]   (Con't)

COMMON NAME	EXPLOSION TEMPERATURE (5 SEC)		RIFLE BULLET IMPACT TEST			SUSAN TEST			GAP TEST	
	°C	°F	EXPLODE (%)	PARTIAL (%)	BURN (%)	THRESHOLD VEL.		PROBABILITY OF REACTION		
						km/sec	ft/sec		m	in
LX-09-0						0.034	110.0	High	1.91×10^{-3} – 2.70×10^{-3}	0.075 - 0.106
LX-10-0						0.037	120.0	High	2.00×10^{-3} 2.49×10^{-3}	0.079 - 0.098
LX-11						0.053	174.0	Low	1.09×10^{-3} 1.70×10^{-2}	0.043 - 0.669
LX-14						0.048	158.0	Low	1.50×10^{-3} 2.01×10^{-3}	0.059 - 0.079
NG	Explodes 222	Explodes 431.6	100							
NQ	Decomposes 275	Decomposes 527.0								
OCTOL 75/25	Flames Erratically 335	Flames Erratically 635.0				0.055	180.0	High	5.60×10^{-4} – 7.10×10^{-4}	0.022 - 0.028
PBX-9007									1.09×10^{-3} – 1.40×10^{-3}	0.043 - 0.055
PBX-9010						0.034	110.0	High	1.91×10^{-3} – 2.39×10^{-3}	0.075 - 0.094
PBX-9011						0.050	165.0	Low	1.40×10^{-3} – 1.80×10^{-3}	0.055 - 0.071
PBX-9205						0.037	120.0	Moderate	6.35×10^{-4} – 8.89×10^{-4}	0.025 - 0.035
PBX-9404						0.032	105.0	High	2.21×10^{-3} – 2.69×10^{-3}	0.087 - 0.106
PBX-9407									2.31×10^{-3} – 3.10×10^{-3}	0.091 - 0.122
PBX-9501						0.061	200.0	High	1.30×10^{-3} – 1.80×10^{-3}	0.051 - 0.071

A-14

Table 3(b) Sensitivity of Explosives[a] (Con't)

COMMON NAME	EXPLOSION TEMPERATURE (5 SEC)		RIFLE BULLET IMPACT TEST			SUSAN TEST			GAP TEST	
	°C	°F	EXPLODE (%)	PARTIAL (%)	BURN (%)	THRESHOLD VEL.		PROBABILITY OF REACTION		
						km/sec	ft/sec		m	in
PENTOLITE 50/50	Decomposes 220	Decomposes 428.0	72	20					Cast 7.62 X 10^{-4} - 9.65 X 10^{-4} Hot Pressed 2.70 X 10^{-3} - 3.61 X 10^{-3}	Cast 0.030 - 0.038 Hot Pressed 0.106 - 0.142
PETN	Decomposes 225	Decomposes 437.0	100							
RDX	Decomposes 260	Decomposes 500.0	100							
TATB						1.000	> 3281.0		5.00 X 10^{-5} - 2.00 X 10^{-4}	2.320 - 0.100
TETRYL	Ignites 257	Ignites 494.6 b	13	54	10					
TNETB	225	437.0								
TNT	Decomposes 475	Decomposes 887.0	40			0.072	235.0		2.12 X 10^{-4} - 4.10 X 10^{-4}	7.90 X 10^{-3} - 1.60 X 10^{-2}

a. See Table 1.

b. See Table 1.

Table 4 Hugoniots for Unreacted HE's

COMMON NAME	HUGONIOT DATA					HUGONIOT INTERCEPT	
	S	DENSITY		RANGE		km/sec	ft/sec
		Mg/m^3	lb/in^3	km/sec	ft/sec		
BARATOL	1.66 2.16			$c_o \leq u_s \leq 3.66$ $3.66 \leq u_s \leq 4.00$	$c_o \leq u_s \leq 12008$ $12008 \leq u_s \leq 13123$	2.4 1.5	7.87 X 10^3 4.92 X 10^3
BORACITOL							
BTF							9.68 X 10^3
COMP B	1.58^b 2.81	1.7 1.71	0.061 0.062	$4.40 \leq u_s \leq 5.04$	$14436 \leq u_s \leq 16535$	2.95 1.20	3.94 X 10^3
COMP C-4							
CYCLOTOL 75/25	2.36^b	1.729	0.062	$4.67 \leq u_s \leq 5.22$	$15322 \leq u_s \leq 17126$	2.02 c_o = 2.74	6.63 X 10^3 c_o=8989
DATNB/DATB	1.89	1.78	0.064	$3.16 \leq u_s \leq 4.49$	$10367 \leq u_s \leq 14731$	2.45 c_e = 2.66	8.038 X 10^3 c_e=8727
DIPAM							
DNPA							
EDNP							
FEFO							
HMX							
HNAB							
HNS	2.77^b 3.21	1.38 1.57	0.050 0.057	$1.44 \leq u_s \leq 2.00$ $1.00 \leq u_s \leq 3.18$	$4725 \leq u_s \leq 6562$ $3281 \leq u_s \leq 10434$	0.61 c_o = 1.00 1.00	2.001 X 10^3 c_o=3281 3.2808 X 10^3
LX-01							
LX-02-1							7.740 X 10^3
LX-04-1	2.43^b	1.86 - 1.863	0.067	$2.61 \leq u_s \leq 3.24$	$8563 \leq u_s \leq 10630$	2.36	

Table 4 Hugoniots for Unreacted HE's (Con't)

COMMON NAME	HUGONIOT DATA					HUGONIOT INTERCEPT	
	S	DENSITY		RANGE		km/sec	ft/sec
		Hg/m^3	lb/in^3	km/sec	ft/sec		
LX-07-2							
LX-08							
LX-09-1	2.90^b	1.839	0.066			2.43	7.97×10^3
LX-10-0							
LX-11-0							
LX-14							
NG							
NQ							
OCTOL 70/30	1.72^b	1.8	0.065			3.01	9.88×10^3
	2.51	1.803	0.065	$3.24 \leq u_s \leq 4.97$	$10630 \leq u_s \leq 16307$	2.31	7.58×10^3
PBX-9007							
PBX-9010							
PBX-9011	2.64	1.79	0.065	$4.10 \leq u_s \leq 6.10$	$13452 \leq u_s \leq 20014$	2.22	7.28×10^3
PBX-9205							
PBX-9404	1.57	1.72	0.062	$2.40 \leq u_p \leq 3.70$	$7874 \leq u_p \leq 12140$	1.89	6.201×10^3
	2.09	1.84	0.066	$2.90 \leq u_s \leq 6.70$	$9515 \leq u_s \leq 21983$	2.49	8.18×10^3
	2.77	1.84	0.066	$u_s \leq 3.20$	$u_s \leq 10499$	$2.31\ c_o = 2.31$	$7.58 \times 10^3\ c_o=7579$
	2.48	1.84	0.066	$2.45 \leq u_s \leq 6.05$	$8038 \leq u_s \leq 19850$	$2.45\ c_o = 2.60$	$8.04 \times 10^3\ c_o=8531$
PBX-9407	1.99	1.60	0.058	$2.11 \leq u_s \leq 3.18$	$6923 \leq u_s \leq 10434$	1.33	4.36×10^3
PBX-9501	1.91	1.844	0.067	$2.90 \leq u_s \leq 14436$	$9515 \leq u_s \leq 14436$	2.68	8.80×10^3
PENTOLITE 50/50	1.91	1.67	0.060	$4.52 \leq u_s \leq 5.25$	$1480 \leq u_s \leq 17225$	2.83	9.29×10^3
	3.20	1.676	0.061			0.89	2.90×10^3

Table 4 Hugoniots for Unreacted HE's (Con't)

COMMON NAME	HUGONIOT DATA					HUGONIOT INTERCEPT	
	S	DENSITY		RANGE		km/sec	ft/sec
		Mg/m³	lb/in³	km/sec	ft/sec		
PETN	2.18	1.59		$1.40 \leq u_s \leq 2.14$	$4593 \leq u_s \leq 7021$	$1.33 \, c_o = 2.45$	$4.36 \times 10^3 \, c_o = 8038$
	4.19			$1.86 \leq u_s \leq 2.65$	$6103 \leq u_s \leq 8695$	$0.06 \, c_o = 2.45$	$1.96 \times 10^2 \, c_o = 8038$
	2.58	1.60		$1.89 \leq u_s \leq 2.56$	$6201 \leq u_s \leq 8399$	1.32	4.33×10^3
RDX	0.67	1.64		$2.00 \leq u_s \leq 2.16$	$6562 \leq u_s \leq 7087$	$1.93 \, c_o = 2.8$	$6.33 \times 10^3 \, c_o = 9187$
	4.11			$2.14 \leq u_s \leq 2.63$	$7021 \leq u_s \leq 8629$	$0.70 \, c_o = 2.8$	$2.30 \times 10^3 \, c_o = 9187$
	1.61	1.8		$4.21 \leq u_s \leq 5.45$	$13812 \leq u_s \leq 17881$	2.87	9.42×10^3
TATB							
TETRYL	1.43	1.30		$2.58 \leq u_s \leq 4.16$	$8465 \leq u_s \leq 13649$	$2.16 \, c_e = 1.10$	$7.09 \times 10^3 \, c_e = 3609$
	1.97	1.40		$2.20 \leq u_s \leq 4.07$	$7218 \leq u_s \leq 13354$	$1.61 \, c_e = 1.13$	$5.29 \times 10^3 \, c_e = 3708$
	1.62	1.50		$2.63 \leq u_s \leq 4.17$	$8629 \leq u_s \leq 13682$	$2.17 \, c_e = 1.36$	$7.11 \times 10^3 \, c_e = 4462$
	1.53	1.60		$2.86 \leq u_s \leq 4.25$	$9384 \leq u_s \leq 13944$	$2.36 \, c_e = 1.66$	$7.75 \times 10^3 \, c_e = 5446$
	1.42	1.70		$3.08 \leq u_s \leq 4.17$	$10106 \leq u_s \leq 13682$	$2.47 \, c_e = 2.04$	$8.12 \times 10^3 \, c_e = 6677$
TNETB							
TNT	2.65	1.62		$u_s \leq 3.70$	$u_s \leq 12140$	2.27	$7.461 \times 10^3 \, c_e = 7536$
	1.36			$u_s \leq 3.70$	$u_s \leq 12140$	$2.99 \, c_e = 2.3$	9.800×10^3
	2.05	1.614		$3.03 \leq u_s \leq 5.41$	$9955 \leq u_s \leq 17763$	$2.39 \, c_o = 2.57$	$7.84 \times 10^3 \, c_o = 8439$
	1.88	1.63		$4.46 \leq u_s \leq 4.89$		$2.57 \, c_e = 2.57$	
	1.69	1.582		$4.17 \leq u_s \leq 5.22$	$14633 \leq u_s \leq 16044$	$2.52 \, c_e = 2.57$	8.268×10^3
	1.29	1.62		$2.78 \leq u_s \leq$	$13485 \leq u_s \leq 17327$	3.09	1.0×10^4
	2.16	1.693 - 1.648		$2.35 \leq u_s \leq 3.38$	$9121 \leq u_s$	$2.37 \, c_o = 2.3$	7.782×10^3

Table 5(a)   Thermal Properties of Explosives[a]

COMMON NAME	THERMAL CONDUCTIVITY		LINEAR THERMAL EXPANSION COEFFICIENT	
	ft-lb/hr-ft-°F	W/m-K	$(10^{-6}$ in/in-°F)	$(10^{-6}$ cm/cm-°C)
BARATOL	2.227×10^2	0.495	28.38 + .144T @ -40° → 60.8°F 25.94 @ -.4° → 60.8°F	33 + .26T @ -40° → 16° 46.69 @ -18° → 16°
BORACITOL				
BTF				
COMP B	1.17×10^2	0.260		
COMP C-4				
CYCLOTOL 75/25	1.13×10^2	0.251	17.78 - 25.56° @ 68° 28.86 - 36.67° @ 185°	32.00 @ 20° 52.00 - 66.01 @ 85°
DATB/DATNB				
DIPAM				
DNPA				
EDND				
FEFO			28 @ -65.2° → 165.2°	50.40 @ -54° → 74°
HMX			44.44	80.0
HNAB			51.11	92.0
HNS				
LX-01			71.60 @ -20.2° → 122°	129.00 @ -29° → 50°
LX-02-1	1.74×10^2	0.387	28.50 @ -65.2° → -18.4° 39.50 @ -18.4° → -165.2°	51.30 @ -54° → -28° 71.10 @ -28° → -109.5°
LX-04	1.79×10^2	0.398	26.67 @ -65.2° → -18.4° 35.00 @ -18.4° → 163.4°	48.0 @ -54° → -28° 63.00 @ -28° → 73°
LX-07			104.33	188.00
LX-08	1.943×10^2	0.432	27.11 @ -64.0° → -18.4° 31.00 @ -18.4° → 165.2°	48.80 @ -53° → -28° 55.80 @ -28° → 74°
LX-09-0				44.60 @ -54° → -18° 46.98 @ -18° → 74°
LX-10-0	1.943×10^2	0.432	24.78 @ -65.2° → -.4° 26.10 @ -.4° → -165.2°	

Table 5(a)   Thermal Properties of Explosives[a] (Con't)

COMMON NAME	THERMAL CONDUCTIVITY		LINEAR THERMAL EXPANSION COEFFICIENT	
	ft-lb/hr-ft-°F	W/m-K	$(10^{-6}$ in/in-°F)	$(10^{-6}$ cm/cm-°C)
LX-11	1.633×10^2	0.363	31.11 @ -65.2° → -11.2° 46.11 @ 10.4° → 165.2°	56.00 @ -54° → -24° 83.00 @ -12° → 74°
LX-14			26.94 @ < -29.2° 31.00 @ > -29.2°	48.50 @ < -34° 55.80 @ > -34°
NG				
NQ				
OCTOL 70/30				
PBX-9007				
PBX-9010	9.667×10^1	0.215	36.67	66.00
PBX-9011	1.88×10^2	0.418	28.72 @ -65.2° → -40° 37.28 @ -31.0° → 165.2°	51.70 @ -54° → -40° 67.10 @ -35° → 74°
PBX-9205				
PBX-9404	1.900×10^2	0.422	28.11 @ -65.2° → -31° 32.20 @ -11.2° → 165.2°	50.60 @ -54° → -35° 58.00 @ -24° → 74°
PBX-9407				
PBX-9501	2.032×10^2	0.452	30.61 @ -79.6° → 159.8°	55.10 @ -62° → 71°
PENTOLITE 50/50				
PETN			42.5 - 49.9 (-20.2° - 194°)	83.0 (-29° - 90°)
RDX	1.300×10^6 ρ=1.263 Mg/m³ 1.313×10^6 ρ=1.533 Mg/m³	0.289 0.292	35.33 @ 68°	63.6 @ 20°
TATB				
TETRYL	1.093×10^6 ρ=1.394 Mg/m³ 1.285×10^6 ρ=1.528 Mg/m³	0.243 0.286		
TNETB				
TNT	1.053×10^6 ρ=1.54 Mg/m³ 1.166×10^6 ρ=1.6 Mg/m³ 2.297×10^6 ρ=1.67 Mg/m³	0.234 0.260 0.511	30.00 @ -40.0° → 140° b	54.00 @ -40° → 60°

Table 5(b)   Thermal Properties of Explosives[a]

COMMON NAME	VOLUME THERMAL EXPANSION COEFFICIENT		SPECIFIC HEAT				THERMAL STABILITY	
	$(10^{-6}\ in^3/in^3-°F)$	$(10^{-6}\ cm^3/cm^3-°C)$	ft-lb/lb /°F	J/kg/°K	°F	°C	in^3 at STP	m^3 at STP
BARATOL			122.09 156.31 313.40 149.31	657 841 169 803	86 122 158 181-212	30 50 70 83-100	.00092 - .0012	1.5×10^{-8} - 2.0×10^{-8}
BORACITOL							.0147 - .0245	
BTF								2.4×10^{-7} - 4.0×10^{-7}
COMP B			182.75 b 171.09 194.42 292.40 242.63	983 920 1046 1573 1305	-103 32 77 167 212	-75 0 25 75 100	.00312	5.1×10^{-8}
COMP C-4							.00159	2.6×10^{-8}
CYCLOTOL 75/25			171.09 174.97 197.53 273.74 272.96	920 941 1063 1473 1469	-103 32 77 167 212	-75 0 25 75 100	.000857 - .00245	1.4×10^{-8} - 4.0×10^{-8}
DATB/DATNB							< .00184	$< 3.015 \times 10^{-8}$
DIPAM								
DNPA							.00245 - .00367	4.015×10^{-8} - 6.014×10^{-8}
EDND								
FEFO			194.42 279.957 365.500	1046 1506 1966	-99.4 77 260.6	-73 25 127	.00245 - .006124	4.015×10^{-8} - 1.004×10^{-7}
HMX	90.19 @ -22° → 158°	162.50 @ -30° → 70°	177.31 206.86 229.41 244.96	954 1113 1234 1318	32 b 122 212 302	0 50 100 150	< .0006124	$< 1.004 \times 10^{-8}$
HNAB								
HNS			311.06	1674	68	20	.000612	1.003×10^{-8}
LX-01							.101 @ 176°	1.80×10^{-6} @ 80°

Table 5(b)   Thermal Properties of Explosives[a] (Con't)

COMMON NAME	VOLUME THERMAL EXPANSION COEFFICIENT		SPECIFIC HEAT				THERMAL STABILITY	
	$(10^{-6}$ in^3/in^3-°F)	$(10^{-6}$ cm^3/cm^3-°C)	ft-lb/lb /°F	J/kg/°K	°F	°C	in^3 at STP	m^3 at STP
LX-02-1	213.89 @ -22.0°→ 158°	385.00 @ -30°→ 70°	225.52	1213		20	.018 - .037	3.0 X 10^{-7} - 6.0 X 10^{-7}
LX-04	126.78 @ -18.4°→ 163.4°	228.20 @ -30°→ 70°	233.30	1255		20	.00612 - .0024	1.003 X 10^{-8} - 4.0 X 10^{-8}
LX-07	101.61 @ -20.2°→ 158°	182.90 @ -29°→ 70°	225.52	1213		20		
LX-08	313.89	565.00	217.74	1172		20		
LX-09-0			209.97	1130	68	20	.0018 - .0024	3.0 X 10^{-8} - 7.0 X 10^{-8}
LX-10-0			217.74	1172	68	20	.00122	1.999 X 10^{-8}
LX-11			241.08	1297	68	20	.00612 - .00294	1.0 X 10^{-8} - 4.0 X 10^{-8}
LX-14			209.97	1130	68	20	.00122	2.0 X 10^{-8}
NC			276.85	1490	95-392	35-200		
NQ							.00122 - .00306	2.0 X 10^{-8} - 5.0 X 10^{-8}
OCTOL 70/30			209.97	1130	68	20		
PBX-9007			217.75	1172	68	20	.0018 - .0043	3.0 X 10^{-8} - 7.0 X 10^{-8}
PBX-9010			209.97	1130	68	20	.0012 - .0024	2.0 X 10^{-8} - 4.0 X 10^{-8}
PBX-9011			209.97	1130	68	20	.00147	2.409 X 10^{-8}
PBX-9205			217.75	1172	68	20	.00153	2.507 X 10^{-8}
PBX-9404			209.97	1130	68	20	.022 - .0245	3.605 X 10^{-7} - 4.015 X 10^{-7}
PBX-9407			209.97	1130	68	20	.00367	6.0
PBX-9501			209.97	1130	68	20	.00429	7.030 X 10^{-8}
PENTOLITE 50/50			202.19	1088	68	20		
PETN	138.44 @ -22.0°→ 158°	249.19 @ -30°→ 70°	202.19	1088	68	20	.006124 - .00857	1.004 X 10^{-7} - 1.404 X 10^{-7}
RDX	106.11 @ 680°	191.00 @ 20°	213.08	1146	68	20	.00122 - .00153	2.0 X 10^{-8} - 2.50 X 10^{-8}
			221.64	1192	122	50		
			224.75	1209	158	70		
			227.86	1226	212	110		
TATB								

Table 5(b) Thermal Properties of Explosives[a] (Con't)

COMMON NAME	VOLUME THERMAL EXPANSION COEFFICIENT		SPECIFIC HEAT				THERMAL STABILITY	
	$(10^{-6}\ in^3/in^3-°F)$	$(10^{-6}\ cm^3/cm^3-°C)$	ft-lb/lb /°F	J/kg/°K	°F	°C	in^3 at STP	m^3 at STP
TETRYL			155.532	837	-58 b	-50	.0022	3.60×10^{-8}
			164.864	887	32	0		
			173.418	933	122	50		
			183.528	987	140	100		
TNETB								
TNT	88.89 @ 80.6°→ 176° b	160.00 @ 27°→ 80°	240.30	1293	32	0	0. - .00073	$0. - 1.2 \times 10^{-8}$
			255.07	1372	68	20		
			274.51	1477	122	50		
			290.85	1565	176	80		

a. See Table 1.

Table 6 Performance of Explosives[a]

COMMON NAME	DETONATION VELOCITY		CHAPMAN-JOUGET DETONATION PRESSURE		TNT EQUIVALENT WEIGHT*	CRITICAL ENERGY	
	ft/sec	km/sec	lb/in^2	MPa		ft-lb/ft^2	J/m^2
BARATOL	15,978	4.87	2.03 X 10^6	1.40 X 10^4	0.525		
BORACITOL	15,945	4.86			0.283		
BTF	27,838	8.48	4.26 X 10^6*	2.94 X 10^4*	1.198		
COMP B	26,214	7.99	4.28 X 10^6	2.95 X 10^4	1.092	1.03 X 10^5	1.50 X 10^6
COMP C-4	26,378	8.04	3.73 X 10^6*	2.57 X 10^4*	1.129		
CYCLOTOL 75/25	27,231	8.30	4.58 X 10^6	3.15 X 10^4	1.115		
DATB/DATNB	24,672	6.85	3.76 X 10^6	2.59 X 10^4	0.893		
DIPAM	24,278	7.52			0.959		
DNPA	20,013 *	6.10 *			0.752		
EDNP	20,669 *	6.30 *			0.874		
FEFO	23,622 *	7.20 *			1.149		
HMX	29,888	9.11	5.61 X 10^6	3.87 X 10^4	1.042		
HNAB	24,934	7.60			1.044		
HNS	22,966	7.00			1.009	9.73 X 10^4 @ p=1.555	1.42 X 10^6 @ p=1.555
LX-01	22,441	6.84	2.26 X 10^6	1.56 X 10^4	1.222		
LX-02-1	24,180	7.37			1.009		
LX-04	27,756	8.46	4.08 X 10^6	3.50 X 10^4	1.007	7.47 X 10^4	1.09 X 10^6
LX-07	28,346	8.64	5.02 X 10^6*	3.46 X 10^4*	1.058		
LX-08	21,522	6.56			1.406		
LX-09-1	28,904	8.81	5.47 X 10^6	3.77 X 10^4	1.136	6.59 X 10^4	9.62 X 10^5
LX-10-0	28,937	8.82	5.44 X 10^6	3.75 X 10^4	1.101		
LX-11-0	27,296	8.32	4.50 X 10^6*	3.10 X 10^4*	0.874		
LX-14	28,992	8.84	5.37 X 10^6	3.70 X 10^4	1.119		

*Values are based on calculated heats of detonation

Table 6   Performance of Explosives[a] (Con't)

COMMON NAME	DETONATION VELOCITY		CHAPMAN-JOUGET DETONATION PRESSURE		TNT EQUIVALENT WEIGHT †	CRITICAL ENERGY	
	ft/sec	km/sec	lb/in^2	MPa		$ft-lb/ft^2$	J/m^2
NG	25,262	7.70	3.67×10^6	2.53×10^4	1.136		
NQ	25,098	7.65			0.752		
OCTOL 70/30	27,821	8.48	4.96×10^6	3.42×10^4	1.113		
PBX-9007	26,542	8.09	3.84×10^6	2.65×10^4	1.108		
PBX-9010	27,460	8.37	4.76×10^6	3.28×10^4	1.044		
PBX-9011	27,887	8.50	4.70×10^6	3.20×10^4	1.087		
PBX-9205	26,804	8.17	4.18×10^6 *	2.88×10^4 *	1.037		
PBX-9404	28,871	8.80	5.44×10^6	3.75×10^4	1.108		
PBX-9407	25,951	7.91	4.16×10^6	2.87×10^4	1.136		
PBX-9501	28,970	8.83			1.129		
PENTOLITE 50/50	24,508	7.47	4.06×10^6 *	2.80×10^4 *	1.085		
PETN	27,099	8.26	4.93×10^6	3.40×10^4	1.169	$\sim 1.14 \times 10^4$	1.67×10^5
RDX	28,543	8.70	4.90×10^6	3.40×10^4	1.149		
TATB						6.10×10^5	9.50×10^6
TETRYL	25,754	7.85	3.77×10^6	2.60×10^4	1.071	2.88×10^4 @ p=1.655	4.20×10^5
TNETB	22,736	8.29	2.76×10^6	1.90×10^4			
TNT	27,198	6.93			1.0	2.88×10^4 Cast 9.73×10^4 Pressed	4.20×10^6 Cast 1.42×10^6 Pressed

a.   See Table 1.

*   Calculated

†   Values are based on calculated heats of detonation

APPENDIX B

BIBLIOGRAPHY

The references cited in this appendix were acquired from a number of sources. Journal articles were usually copied from the journals in a technical library. The majority of the references were U. S. Government technical reports, and these were ordered from National Technical Information Services (NTIS), using accession numbers listed in the NTIS catalogs. In some instances, the accession numbers are missing from our citations because we are on the mailing lists for explosives safety and explosives effects reports for a number of government agencies and obtained these reports directly. Reports and standards for materials, structural member properties, and codes were obtained from the appropriate industrial associations. General Department of Energy codes and regulations, and those specific for the Pantex Plant, were obtained from Amarillo Area Office, Department of Energy. U. S. Army Corps of Engineers, Huntsville Division, furnished a number of reference reports and design manuals. Some reports giving results of related work in Europe were obtained through our contacts with the appropriate European laboratory or agency.

If an AE needs to obtain specific references from the Bibliography, he should use the sources noted above.

Abbott, P. A., "Hand Solution of One-Dimensional Inelastic Wave Propagation Problems," The Eric H. Wang Civil Engineering Research Facility, University of New Mexico, AFWL-TR-67-69, Air Force Weapons Laboratory, October 1967.

Abrahamsson, Eddy, "Blast Loaded Windows," 18th Explosive Safety Seminar sponsored by the Department of Defense Explosive Safety Board, Swedish Publication SAI Report Dnr 605/7131-75, Solna, Sweden, October 1978.

Abrahamsson, Eddy, "Dome Action in Slabs with Special Reference to Blast-Loaded Concrete Slabs," Stockholm, Sweden, 1967.

Abrahamsson, Eddy, "Operation Block," Report No. 119:5, Royal Swedish Fortifications Administration, Stockholm 80, Sweden, 1974.

Abrahamson, G. R., and Lindberg, H. E., "Peak Load-Impulse Characterization of Critical Pulse Loads in Structural Dynamics," Stanford Research Institute, Menlo Park, California, Nuclear Engineering and Design, Vol. 37, January 1976 pp 35-46.

ACI Manual of Concrete Practices, Parts 1, 2, and 3, American Concrete Institute, P. O. Box 19150, Redford Station, Detroit, Michigan (current edition).

"A Comparison of Various Materials in Their Resistance to Perforation by Steel Fragments, Empirical Relationships," Technical Report No. 25, U. S. Army Ballistic Research Laboratory, Aberdeen Proving Ground, Md, July 1956.

Adams, Channing L., Sarmousakis, James, N., and Sperrazza, Joseph, "Comparison of the Blast From Explosive Charges of Different Shapes," Ballistic Research Laboratories, Aberdeen Proving Ground, Md., Report No. 681, January 1949.

Ahlers, E. B., "Fragment Hazard Study," Minutes of the Eleventh Explosives Safety Seminar, Vol. 1, Armed Services Explosives Safety Board, Washington, D. C., September 1969.

Ahrens, T. J., "Stress Wave Propagation in a Prestressed Medium," Report No. AFCRL-67-0529, Stanford Research Institute, Poulter Laboratory for High Pressure Research, Menlo Park, California, October 1967.

AISC Specification for the Design, Fabrication and Erection of Structural Steel for Buildings, American Institute of Steel Construction, New York, NY, February 1969.

Albright, G. H., Beck, E. J., LeDoux, J. C., and Mitchell, R. A., "Evaluation of Buried Corrugated-Steel Arch Structures and Associated Components, Operation Plumbbob-Project 3.3," Headquarters, Field Command Defense Atomic Support Agency, Sandia Base, Albuquerque, New Mexico, February 1961.

Albritton, G. E., "Deep Slabs Subjected to Static and Blast Loading," Journal of the Structural Division, Proceedings of the American Society of Civil Engineers, Vol. 95, No. ST11, November 1969, pp 2449-2462.

Altman, F. D., "Model Studies of Explosive Storage Cubicles," Report No. 1917, Warhead and Terminal Ballistics Laboratory, May 1964.

Aluminum Standards and Data, The Aluminum Association, 750 Third Avenue, New York, NY 10017, (current edition).

Building Code Requirements for Reinforced Concrete, ACI 318-77, Section 10.2, The American Concrete Institute.

Anderson, J. H. B., "A Study of the Flow Field Induced by an Explosion Near The Ground," PCN-21K01, Defense Research Establishment, Suffield, Ralston, Alberta, Canada, April 1978.

Anderson, J. H. B., "A Study of the Flow Field Induced by an Explosion Near the Ground," Paper presented at the 5th International Symposium on the Military Applications of Blast Simulation, Stockholm, Sweden, May 23-26, 1977.

Annual Book of ASTM Standards, American Society for Testing and Materials, Parts 1-48, American Society for Testing and Materials, 1916 Race Street, Philadelphia, Pa, 19103.

Anon. "Effects of Airblast, Cratering, Ground Shock and Radiation on Hardened Structures," AFSCM 500-8, Air Force Systems Command Manual, January 1976.

Anon. "Hardness Program Non-EMP, Subsystem Hardness Assurance Report for Safeguard Ground Facilities, Vol. 1, Executive Summary," HNDDSP-72-156-ED-R, U. S. Army Corps of Engineers, Huntsville Division, June 1975.

Anon. "Hardness Program Non-EMP, Subsystem Hardness Assurance Report for Safeguard Ground Facilities, Vol. 2, Final Report," HNDDSP-72-156-ED-R, U. S. Army Corps of Engineers, Huntsville Division, June 1975.

Anon. "Overpressure Effects on Structures," HNDTR-75-23-ED-SR, U. S. Army Corps of Engineers, Huntsville Division, February 1976.

Anon., Seismic Hazard and Building Structure Behavior at the Pantex Facility, URS/John Blume and Associates, April 1976.

"Apparent Impact Strength of Preformed Block-Type Insulating Materials," ANSI/ASTM C 589-68, (reapproved 1975).

Armendt, B. F., Hippensteel, R. G., Hoffman, A. J., and Keefer, J. H., " Project White Tribe: Air Blast from Simultaneously Detonated Large Scale Explosive Charges," BRL Report No. 1145, U. S. Army Ballistic Research Laboratories, Aberdeen Proving Ground, Md., 1961.

Armendt, B. G., Hippensteel, R. G., Hoffman, A. J. and Kingery, C. N., "The Air Blast from Simultaneously Detonated Explosive Spheres," BRL Report No. 1294, U. S. Army Ballistic Research Laboratories, Aberdeen Proving Ground, Md., 1960.

Armendt, B. F., Hippensteel, R. G., Hoffman, A. J. and Schlueter, S. D., "The Air Blast from Simultaneously Detonated Explosive Spheres: Part II-Optimization," BRL Memorandum Report No. 1384, U. S. Army Ballistic Research Laboratories, Aberdeen Proving Ground, Md., January 1962.

Army-Navy Explosives Safety Board, "The Missile Hazard from Explosions," Technical Paper No. 2, December 1945.

Arvidsson, T. and Eriksson, L., "Fragmentation, Structure and Mechanical Properties of Some Steels and Pure Aluminum After Shock Loading," Forsvarets Forskningsanstalt (FOA), National Defence Research Institute, Stockholm, Sweden, 1974.

Arya, R., Ammar, A., Dobbs, H., Weissman, S. and Price, P., "Blast Capacity Evaluation of Below-ground Structures," Ammann & Whitney Report No. ARLCD-CR-77006 for U. S. Army Armament Research and Development Command Large Caliber Weapon Systems Laboratory, Dover, New Jersey, May 1977.

Ashcraft, R. W., "Mathematical Analysis of HE Data," MHSMP-73-43R, Development Division, Mason & Hanger, Silas Mason Co., Inc., July-September 1973.

Assheton, R., History of Explosions on Which the American Table of Distances Was Based, Including Other Explosions of Large Quantities of Explosives, The Institute of Makers of Explosives, 1930.

Bach, G. G. and Lee, J. H. S., "An Analytic Solution for Blast Waves," AIAA Journal, Vol. 8, 1970, pp 271-75.

Bach, G. G. and Lee, J. H. S., "Higher Order Perturbation Solutions for Blast Waves," AIAA Journal, Vol. 7 No. 4, April 1969, pp 742-744.

Bacigalupi, C. M., "Design of a Maze Structure to Attenuate Blast Waves," UCRL-52921, Lawrence Livermore Laboratory, Livermore, CA, March 1980.

Baker, C. F. and Mullins, R. K., "Design of a Building Wall Subject to Blast Loading," Lawrence Livermore Laboratory, UCID-16275, University of California, Livermore, California, June 1973.

Baker, E. J., Garza, L. R. and Westine, P. S., "Development of A Design of a Relocatable Command and Control Bunker," CR N-77-1, Waterways Experiment Station, March 1977.

Baker, W. E., "Approximate Techniques for Plastic Deformation of Structures Under Impulsive Loading," Shock and Vibration Digest, Vol. 7 No. 7, 1975, pp 107-117.

Baker, W. E., "Approximate Techniques for Plastic Deformation of Structures Under Impulsive Loading, II," Shock and Vibration Digest, Vol. 11, No. 7, 1979, pp 19-24.

Baker, W. E., Explosions in Air, University of Texas Press, Austin, Texas, 1973.

Baker, W. E., "Prediction and Scaling of Reflected Impulse from Strong Blast Waves," International Journal of Mechnical Science, Vol. 9, 1967, pp 45-51.

Baker, W. E., "Scale Model Tests for Evaluating Outer Containment Structures for Nuclear Reactors," Proceedings of the Second International Conference on the Peaceful Uses of Atomic Energy, United Nations, Geneva, Vol. II, 1958, pp 79-84.

Baker, W. E., "The Elastic-Plastic Response of Thin Spherical Shells to Internal Blast Loading, Journal of Applied Mechanics, Vol. 27, Series E, 1, March 1960, pp 139-144.

Baker, W. E. and Oldham, G. A., "Estimates of Blowdown of Quasistatic Pressures in Vented Chambers," EM-CR-76029, Edgewood Arsenal, Aberdeen Proving Ground, Md., November 1975.

Baker, W. E. and Westine, P. S., "Methods of Predicting Loading and Blast Field Outside Suppressive Structures," Minutes of the 16th Annual Safety Seminar, Department of the Defense Explosives Safety Board, 1974.

Baker, W. E. and Westine, P. S., "Methods of Predicting Blast Loads Inside and Outside Suppressive Structures," EM-CR-76026, Report No. 5, Edgewood Arsenal, Aberdeen Proving Ground, Md., 1975.

Baker, W. E., Cox, P. A., Esparza, E. D. and Westine, P. S., "Design Study of a Suppressive Structure for a Melt Loading Operation," EM-CR-76043, Report No. 9, Edgewood Arsenal, Aberdeen Proving Ground, Md., December 1975.

Baker, W. E., Cox, P. A., Westine, P. S., Kulesz, J. J. and Strehlow, R. A., A Short Course on Explosion Hazards Evaluation, Southwest Research Institute, San Antonio, Texas, Copyright 1978.

Baker, W. E., Esparza, E. D., and Kulesz, J. J., "Venting of Chemical Explosions and Reactions," Proceedings of 2nd International Symposium on Loss Prevention and Safety Promotion in the Process Industries, Heidelberg, Germany, September 1977.

Baker, W. E., Hokanson, J. C. and Cervantes, R. A., "Model Tests of Industrial Missiles," Final Report SwRI Project 02-9153, Southwest Research Institute, San Antonio, Texas, May 1976.

Baker, W. E. Hu, W. C. L., and Jackson, T. R., "Elastic Response of Thin Spherical Shells to Axisymmetric Blast Loading," Journal of Applied Mechanics, Vol. 33, Series E, 4, December 1966, pp 800-806.

Baker, W. E., Kulesz, J. J., Ricker, R. E., Bessey, R. L., Westine, P. S., Parr, V. B., and Oldham, G. A., "Workbook for Predicting Pressure Wave and Fragment Effects of Exploding Propellant Tanks and Gas Storage Vessels," NASA CR-134 906, NASA Lewis Research Center, September 1977.

Baker, W. E. Kulesz, J. J., Ricker, R. E., Westine, P. S., Parr, V. B., Vargas, L. M. and Moseley, P. K., "Workbook for Estimating the Effects of Accidental Explosions in Propellant Handling Systems," NASA CR 3023, NASA Lewis Research Center, August 1978.

Baker, W. E., Parr, V. B., Bessey, R. L. and Cox, P. A., "Assembly and Analysis of Fragmentation Data for Liquid Propellant Vessels," Minutes of the 15th Explosives Safety Seminar, Department of Defense Explosives Safety Board, Washington, D. C., Vol. II, September 1973, pp 1171-1203.

Baker, W. E., Parr, V. B., Bessey, R. L., and Cox, P. A., "Assembly and Analysis of Fragmentation Data for Liquid Propellant Vessels," NASA CR 134538, NASA Lewis Research Center, Cleveland, Ohio, January 1974.

Baker, W. E., Silverman, S., Cox, P. A., and Young, D., "Methods of Computing Structural Response of Helicopters to Weapons' Muzzle and Breech Blast," The Shock and Vibration Bulletin, Bulletin 40, Part 2, pp 227-241, December 1969.

Baker, W. E., Westine, P. S. and Cox, P. A., "Methods for Prediction of Damage to Structures from Accidental Explosions," Proceedings of the 2nd International Symposium on Loss Prevention and Safety Promotion in the Process Industries, Heidelberg, Germany, September 1977.

Baker, W. E., Westine, P. S., and Dodge, F. T., Similarity Methods in Engineering Dynamics: Theory and Practice of Scale Modeling, Spartan Books, Rochelle Park, NJ, 1973.

Baker, W. E., Whitney, M. G. and Parr, V. B., "Scaling of Initiation of Explosives by Fragment Impact," (submitted to 50th Shock and Vibration Symposium).

Baladi, E. Y., et al., "Ground Shock Calculation Parameter Study, Report 3, Influence of Type of Constitutive Model on Ground Motion Calculations," Army Engineer Waterways Experiment Station, Vicksburg, Mississippi, April 1974.

Baladi, G. Y., Zelasko, J. S., George, M. E. and Wehl, R. E., "Effects of Depth of Burst and Geology on Calculated SMB Peak Stress Environments," Soils and Pavements Laboratory, U. S. Army Engineer Waterways Experiment Station, Vicksburg, Miss., September 1976.

Balemans, A. W. M., and van de Putte, T., "Guideline for Explosion-resistant Control Buildings in the Chemical Process Industry," 2nd International Symposium on Loss Prevention and Safety Promotion in the Process Industries, Heidelberg, Germany, September 1977, pp 215-222.

Barber, R. B., "Steel Rod/Concrete Slab Impact Test (Experimental Simulation)," Technical Development Program, Final Report, Job No. 90142, Scientific Development, Bechtel Corp., October 1973.

Barkan, D. D., Dynamics of Bases and Foundations, McGraw Hill Book Co., New York, NY, 1962.

Barnard, A. J. and Sharman, P. W., "The-Elasto-Plastic and Large-Displacement Response of Plates to Blast Loading," Loughborough University of Technology, England, October 1973.

Barnard, A. J. and Sharman, P. W., "Elasto-Plastic Response of Plates to Blast Loading," European Research Office, United States Army, London W.1., England, September 1972.

Barnett, R. L., Costello, J. F. and Feinstein, D. I., "Debris Formation and Translation," IIT Research Institute, Technology Center, Chicago, Illinois, November 1966.

Bartknecht, W., "Explosion Pressure Relief," CEP 73, 9, September 1977, pp 45-53.

Bartknecht, W., "Report of Investigations on the Problem of Venting Explosions of Flammable Dusts in Vessels," Central Safety Service TS 3, February 10, 1974, (translated by H. Burg).

Basler & Hofmann Ingenieure and Planer, A. G., "Modellversuche Fuer Die Projektierte Laborieranlage Der Eidgenoessischen Munitionsfabrik Altdorf, B877-2, Zurich, Switzerland, June 1978.

Basler & Hofmann Ingenieure and Planer, A. G., "Modellversuche Fuer Unterflurmagazine, Teil I, Konzeption and Durchfuhrung Der Modellversuche," B726-1, Zurich, Switzerland, May 1976.

Basler & Hofmann Ingenieure and Planer, A. G., "Modellversuche Fuer Unterflurmagazine, Teil III, Ausvertung der Daten," B555.2-35, B726-6, Zurich, Switzerland, November 1976.

Basler & Hofmann A. G. Inguenieure and Planer, A. G., "Modellversuche Fuer Unterflurmagazine, Teil II, Versuchsdaten," B726-2, Zurich, Switzerland, June 1976.

Batchelder, F. E., et al., "Hardness Program, Non-EMP, Hardness Program Plan for Safeguard Ground Facilties, Vol. 1, Management and Technical Plan," U. S. Army Corps of Engineers, Huntsville Division, August 1974.

Bathe, K. J., "ADINA, A Finite Element Program for Automatic Dynamic Incremental Nonlinear Analysis," Report 82448-1, Acoustics and Vibration Lab, Med. Eng. Department, Massachusetts Institute of Technology, 1976.

Bdzil, J. B. and Davis, W. C., "Time-Dependent Detonations," LA-5926-MS, Los Alamos Scientific Laboratory, Los Alamos, New Mexico, June 1975.

"Behavior and Utilization of Explosives in Engineering Design and Biomechanical Principles Applied to Chemical Medicine," Proceedings of the 12th Annual Symposium of the American Society of Mechanical Engineers, March 1972.

Benedick, W. B. and Daniel, C. J., "Explosion Containment Device," United States Patent 4,055,247, October 1977.

Bergman, S. G. A., "Swedish Protective Structures for Manufacturing Units Constituting Explosion Hazard in the Range 1 - 2,000 Pounds of TNT," Annals of the New York Academy of Sciences, Vol. 152, Art. 1, October 1968.

Bertrand, B. P., "Suppressive Shielding: Scenario Definition," BRL Memorandum Report No. 2704. U. S. Army Ballistic Research Laboratories, Aberdeen Proving Ground, Md., December 1976.

Bethe, H. A., Fuchs, K. Hirschfelder, H. O., Magee, J. L., Perierls, R. E., and vonNeumann, J., "Blast Wave," LASL 2000, Los Alamos Scientific Laboratory, August 1947.

Bethe, H. A., Fuchs, K., vonNeumann, J.,Perierls, R., and Penny, W. G., "Shock Hydrodynamics and Blast Waves," AECD 2860, October 1944.

Biggs, J. M., Introduction to Structural Dynamics, McGraw-Hill Book Company, New York, NY, 1964.

Black, J. F., Brandt, R. F., and McArdle, K. T., "The Design and Characterization of an Aluminum Fragment Projector," AFATL-TR-76-44, Air Force Armament Laboratory, Eglin Air Force Base, Florida, April 1976.

Boger, R. C. and Waldman, G. D., "Blast Wave Interactions from Multiple Explosions," Paper #XII, Proceedings of the Conference on Mechanisms of Explosion and Blast Waves, J. Alstor, Editor, sponsored by the Joint Technical Coordinating Group for Air Launched Non-Nuclear Ordnance Working Party for Explosives, November 1973.

Booker Associates, Inc., "Title I Design Analysis, Volume I of II, Replacement of High Explosives Machining Facility," Pantex Plant, Amarillo, Texas, January 1979.

Booker Associates, Inc., "Title II Design Analysis, Volume II of IV, Structural Calculations. Replacement of High Explosives Machining Facility," Pantex Plant, Amarillo, Texas, September 1979.

Booker Associates, Inc., "Title II Design Analysis, Volume III of IV, More Structural Calculations. Replacement of High Explosives Machining Facility," Pantex Plant, Amarillo, Texas September 1979.

Bowen, I. G., Fletcher, E. R. and Richmond, D. R., "Estimate of Man's Tolerance to the Direct Effects of Air Blast," Technical Report to Defense Atomic Support Agency, DASA 2113, Lovelace Foundation for Medical Education and Research, October 1968.

Bowen, I. G., Fletcher, E. R., Richmond, D. R., Hirsch, F. G. and White, C. S., "Biophysical Mechanisms and Scaling Procedures Applicable in Assessing Responses of the Thorax Energized by Air-Blast Overpressures or by Non-Penetrating Missiles," Contract No. DA-49-146-XZ-372, Lovelace Foundation for Medical Education and Research, Albuquerque, New Mexico, November 1966.

Bradley, D. and Mitcheson, A., "The Venting of Gaseous Explosions in Spherical Vessels. I- Theory," Combustion and Flame, Vol. 32, 1978, pp 221-236.

Bradley, D. and Mitcheson, A., "The Venting of Gaseous Explosions in Spherical Vessels, II. Theory and Experiment," Combustion and Flame, Vol. 32, 1978, pp 237-255.

Brinkley, S. R. and Kirkwood, J. G., "Theory of the Propagation of Shock Waves," Phys. Rev., Vol. 71, 1947, p. 606.

Brinn, L. G., "A Select Bibliography on Explosions in Industrial Plant with Particular Reference to Design Aspects of Explosion Containment and Relief," SM/BIB/851, British Steel Corporation, 1974.

Brode, H. L., "Blast Wave From a Spherical Charge," Physics of Fluids, Vol. 2, 1959, 217.

Brode, H. L., :Numerical Solutions of Spherical Blast Waves," Journal of Applied Physics, Vol. 26, 1955, pp 766-775.

Brode, H. L., "Quick Estimates of Peak Overpressure from Two Simultaneous Blast Waves," Final Report for Defense Nuclear Agency, DNA4503T, R&D Associates, RDA-TR-107006-008, Marina Del Rey, California, December 1977.

Brogan, J. T. and Murrell, D. W., "Shock Isolation By Discontinuities," Paper No. N-68-6, U. S. Army Engineer Waterways Experiment Station, Corps of Engineers, Vicksburg, MI., November 1968.

Bronowicki, A. J., and Evensen, D. A., "Modeling the Dynamic Response of Slabs to Overpressure," Final Report No. 4535F for Defense Nuclear Agency, J. H. Wiggins Company, Redondo Beach, California, December 1977.

Brooks, W. B., "Transient Pressures Induced on a Slender Body Under Oblique Blast Wave Interception," Aeroelastic and Structures Research Laboratory, Department of Aeronautics and Astronautics, Massachusetts Institute of Technology, Cambridge, Massachusetts, July 1967.

Brown, C. J. and Ricchiazzi, A. J., "Fragment Penetration Estimates for the 81mm Suppressive Shield," Minutes of the Sixteenth Explosives Safety Seminar, Vol. II, September 1974.

Brown, J. A. and Collins, M., "Explosion Phenomena Intermediate Between Deflagration and Detonations," Esso Research and Engineering Company, Linden, New Jersey, October 1967.

Brown, J. W., "Response of Selected Materials to High-Speed Fragment Impact," U. S. Army Engineer Waterways Experiment Station, Vicksburg, MI, 1970.

Bucci, D. R. and Mlakar, P. F., "Design of Earth-Covered Structures to Defeat Contact Burst Rounds," Technical Report N-76-7, U. S. Army Engineer Waterways Experiment Station, Vicksburg, MI, June 1976.

Burenin, P. I., "Effect of Shock Waves," Final Report on Contract NASA-2485, Techtran Corporation, March 1974.

Bureau of Explosives, "Hazardous Materials Regulations of the Department of Transportation by Air, Rail, Highway, Water and Military Explosives by Water Including Specifications for Shipping Containers," R. M. Graziano's Tariff No. 31, Association of American Railroads, Washington, D. C., March 1, 1977.

Butler, D. K., "Development of a High-Velocity Powder Gun and Analysis of Fragment Penetration Tests into Sand," Miscellaneous Paper S-75-27, Soils and Pavements Laboratory, U. S. Army Engineer Waterways Experiment Station, Vicksburg, MI, October 1975.

Butlin, R. N., "Estimation of Maximum Explosion Pressure from Damage to Surrounding Buildings. Explosion at Mersey House, Bootle-28 August, 1975," Fire Research Note No. 1054, Fire Research Station, England, July 1976.

Butlin, R. N., "A Review of Information on Experiments Concerning the Venting of Gas Explosions in Buildings," Fire Research Note No. 1026, Fire Research Station, England, February 1975.

Butlin, R. N. and Tonkin, P. S., "Pressures Produced by Gas Explosions in a Vented Compartment," Fire Research Note No. 1019, Fire Research Station, England, September 1974.

Caggiano, T., "Calculation of TNT Air-Blast Equivalencies for Surface Bursts," AD-775-422, Picatinny Arsenal, Dover, New Jersey, December 1973.

Carder, D. S. and Cloud, W. K., "Surface Motion from Large Underground Explosions," Journal Geophysical Research, Vol. 64, 1959, pp 1471-1487.

Carmichael, J. B. and von Gierke, H. E., "Biodynamic Applications Regarding Isolation of Humans from Shock and Vibration," Aerospace Medical Research Laboratory, AD 770-316, Wright-Patterson Air Force Base, Ohio, September 1973.

Carpenter, H. J., "On Nuclear Height-of-Burst Airblast at High Overpressure," Final Report for Defense Nuclear Agency, Contract DNA001-75-C-0057, R&D Associates, January 1975.

Carpuchin, I. A. and Bobolev,V. K., "The Law Governing the Generation of Impact Explosion of Solid Explosive Mixtures," Report No. FTD-MT-24-0138-73, Air Force Systems Command, U. S. Air Force, Wright Patterson AFB, OH., 1970.

Cassen, B. and Stanton, J. S., "The Decay of Shock Waves," Report No. 1011, U. S. Naval Ordnance Test Station, Inyokern, California, March 29, 1948.

Chabai, A. J., "Crater Scaling Laws for Desert Alluvium," SC-4391, Sandia Corporation, Albuquerque, New Mexico, December 1965.

Char, W. T., "Simplified Approach for Design of Buildings Containing Accidental Explosions," 18th Explosive Safety Seminar, U. S. Army Corps of Engineers, Huntsville Division, September 1978.

Chawla, M. S. and Frey, R. B., "A Numerical Study of Projectile Impact on Explosives," BRL Report No. 2741, U. S. Army Ballistic Research Laboratory, Aberdeen Proving Ground, MD, April 1977.

Cherry, J. T., Barker, T. G., Day, S. M. and Coleman, P. L., "Seismic Ground Motion from Free-Field and Underburied Explosive Sources," ARPA Order No. 2551, AD A 055 141, Advanced Research Projects Agency, La Jolla, California, July 1977.

Chiu, K., Lee, J., and Knystautas, R., "The Blast Waves from Asymmetrical Explosions," Department of Mechanical Engineering, McGill University, Montreal, Canada, 1976.

Chou, P. C., Karpp, R. R. and Huang, S. L., "Numerical Calculation of Blast Waves by the Method of Characteristics," AIAA Journal, Vol. 5, 1967, pp 618-723.

Christoffersen, Oivind, "Investigation of Underground Explosions with Model Tests System Description and Jcrue Implementation Details," Teknisk Notat S-498, Torsvarets Torkingsinstitutt, Norwegian Defence Research Establishment, Kjeller, Norway, February 1978.

Clear, A. J., "Standard Laboratory Procedures for Determining Sensitivity, Brisance, and Stability of Explosives," Report No. 3278, Propellants Laboratory, Feltman Research Laboratories, Picatinny Arsenal, Dover, New Jersey, April 1970.

Clemedson, C. J., Hellstrom, G. and Lingren, S., "The Relative Tolerance of the Head, Thorax, and Abdomen to Blunt Trauma," Annals of the New York Academy of Sciences, Vol. 152, Art. 1, October 1968, p 187.

Cohen, E. and Dobbs, N., "Supporting Studies to Establish Safety Design Criteria for Storage and Processing of Explosive Materials," Contract No. DA-28-017-AMC-423A, Ammann & Whitney, New York, NY, June 1965.

Cohen, E. and Saffian, L. W., "Prevention of and Protection Against Accidental Explosion of Munitions, Fuels and Other Hazardous Mixtures," Annals of the New York Academy of Sciences, Vol. 152, Art. 1, October 1968, pp 1-913.

Coleburn, N. L., "Chapman-Jouguet Pressures of Several Pure and Mixed Explosives," NOLTR-64-58, U. S. Naval Ordnance Laboratory, White Oak, MD., June 1964.

Collett, R. W., "Half-Scale Tests for Containment of a Fragmenting Projectile," Technical Memorandum 2206, Picatinny Arsenal, Dover, New Jersey, July 1976.

Colton, J. D., "Measurement of Pressure, Impulse, and Detonation Velocity for Detasheet L Explosive," AFWL-TR-71-23, Stanford Research Institute, April 1971.

Concrete Masonry Handbook, Portland Cement Association, 33 West Grand Avenue, Chicago, Ill. (current edition).

"Conducting Strength Tests of Panels for Building Construction," ANSI/ASTM E, pp 72-77.

Constance, J. D., "Pressure Ventilate for Explosion Protection," Chemical Engineering, September 1971.

Coulter, G. A., "Translation and Impingement of Furniture Debris in a Model Apartment House Shelter," Report No. ARBRL-MR-02835, U. S. Army Ballistic Research Laboratory, Aberdeen Proving Ground, MD., May 1978.

Cowan, M., "Measurements from Gravel Gertie Tests," SC-R-64-127, Health and Safety TID-4500 (31st edition), Sandia Corporation, July 1964.

Cox, P. A. and Esparza, E. D., "Design of a Suppressive Structure for a Melt Loading Operation," Minutes of the 16th Annual Explosion Safety Seminar, Department of the Defense Safety Board, 1974.

Cox, P. A., Westine, P. S., Kulesz, J. J. and Esparza, E. D., "Analysis and Evaluation of Suppressive Shields," Edgewood Arsenal Contractor Report ARCFL-CR-77028, Report No. 10, Contract No. DAAA15-75-C-0083, Edgewood Arsenal, Aberdeen Proving Ground, MD., January 1978.

Crandell, F. J., "Ground Vibrations Due to Blasting and Its Effect Upon Structures," Journal Boston Society of Civil Engineers, Vol. 36, 1949, p. 245.

Crandell, F. J., "Transmission Coefficient for Ground Vibrations Due to Blasting," Journal Boston Society of Civil Engineers, Vol. 47, 1960, pp 152-168.

Cranz, C., Lehrbuch der Ballistik, Springer-Verlag, Berlin, 1926.

Crawford, R. E., Higgins, C. J. and Bultmann, E. H., "The Air Force Manual for Design and Analysis of Hardened Structures," Report No. AFWL-TR-74-102, Civil Nuclear Systems Corporation, Albuquerque, New Mexico, October 1974. (second printing October 1976).

Criswell, M. E., "Design and Testing of a Blast-Resistant Reinforced Concrete Slab System," Technical Report No. N-72-10, U. S. Army Engineer Waterways Experiment Station, Vicksburg, MI, November 1972.

Criswell, M. E., "Strength and Behavior of Reinforced Concrete Slab-Column Connections Subjected to Static and Dynamic Loadings," Technical Report N-70-1, U. S. Army Engineer Waterways Experiment Station, Vicksburg, MI, December 1970.

Crocker, M. J. and Hudson, R. R., "Structural Response to Sonic Booms," _Journal of Sound and Vibrations_, Vol. 9, 1969, pp 454-468.

Cubbage, P. A. and Marshall, M. R., "Chemical Process Hazards with Special Reference to Plant Design, Vol. I,"_Chemical Engineering Symposium Series_ No. 39, 1-15, Institute of Chemical Engineers, London, England.

Custard, G. H. and Thayer, J. R., "Evaluation of Explosive Storage Safety Criteria," Contract DAHC-04-69-C-0095, Falcon Research and Development Company, March 1970.

Custard, G. H. and Thayer, J. R., "Target Response to Explosive Blast," Falcon Research and Development Company, September 1970.

Damon, E. G., Henderson, E. A. and Jones, R. K., "The Effects of Intermittent Positive Pressure Respiration on Occurrence of Air Embolism and Mortality Following Primary Blast Injury," Final Report to the Defense Nuclear Agency, DNA 2989F, Lovelace Foundation for Medical Education and Research, Albuquerque, New Mexico, January 1973.

Damon, E. G., Richmond, D. R., Fletcher, E. R. and Jones, R. K., "The Tolerance of Birds to Airblast," Final Report to Defense Nuclear Agency, DNA 3314F, Lovelace Foundation for Medical Education and Research, Albuquerque, New Mexico, July 1974.

Damon, E. G., Yelverton, J. T., Luft, U. C., and Jones, R. K., "Recovery of the Respiratory System Following Blast Injury," Technical Progress Report to Defense Atomic Support Agency, DASA 2580, Lovelace Foundation for Medical Education and Research, Albuquerque, New Mexico, October 1970.

Damon,E. G., Yelverton, J. T., Luft, U. C., Mitchell, K., and Jones, R. K., "The Acute Effects of Air Blast on Pulmonary Function in Dogs and Sheep," Technical Progress Report to Defense Atomic Support Agency, DASA 2461, Lovelace Foundation for Medical Education and Research, Albuquerque, New Mexico, March 1970.

Den Hartog, J. P., _Mechnical Vibrations_, McGraw-Hill Book Co., Inc. New York, NY, 1956.

Department of Defense Explosives Safety Board, "Fragment and Debris Hazards," Technical Paper No. 12, Washington, D.C., July 1975.

DeSalvo, G. J. and Swanson, J. A., "ANSYS Engineering Analysis System User's Manual," Swanson Analysis System, Inc., Elizabeth, PA., March 1977.

"Design Data for the Preliminary Selection of Honeycomb Energy Absorption Systems," TSB 122, HEXCEL, 1964.

"Design Manual for Tornado Resistant Structures at the Pantex Plant Site," Department of Civil Engineering, Texas Tech University, Lubbock, Texas, November 1974.

Design of Structures to Resist the Effects of Atomic Weapons, TM 5-856, 1 through 9, Department of the Army, U. S. Army AG Publications Center, St. Louis, MO., March 1965. (This is an updated version of the U. S. Army COE Manual EM110-345-415, March 1957).

"Development of Design Basis Tornadoes and Design Manual for Pantex Plant Site," Department of Civil Engineering, Texas Tech University, Lubbock, Texas, August 1975.

Dewey, J. M. and Sperrazza, J., "The Effect of Atmospheric Pressure and Temperature on Air Shock," BRL Report No. 721, U. S. Army Ballistic Research Laboratories, Aberdeen Proving Ground, MD., 1950.

Dewey, J. M., Johnson, O. T., and Patterson, J. D., "Some Effects of Light Surrounds and Casings on the Blast From Explosives," BRL Report No. 1218, U. S. Army Ballistic Laboratories, Aberdeen Proving Ground, MD., September 1963.

Dewey, J. M., Johnson, O. T., and Patterson, J. D., "Mechanical Impulse Measurements Close to Explosive Charges," BRL Report No. 1182, U. S. Army Ballistic Research Laboratories, Aberdeen Proving Ground, MD., November 1962.

Diepold, W., Pfortner, H., and Hommel, H., "Safety Distances in the Storage and Handling of Explosive Matters," Explosivstoffe, Vol. 18, No. 2, 1970, pp 25-39.

Dishon, J. F. III, "Investigation of Intermediate and Maximum Range Missiles Produced by Cratering Experiments," Report No. MP E-74-2, Army Engineer Waterways Experiment Station, Livermore, California, March 1974.

Dobbs, N., Ammar, A., Weissman, S. and Price, P., "Blast Capacity Evaluation of Single Revetted Barricades," DAAA-21-76-C-0125, Ammann & Whitney Final Report for Picatinny Arsenal, Manufacturing Technology Directorate, Dover, New Jersey, November 1976.

Dobbyn, R. C., Bruchey, W. J., Jr., and Shubin, L. D., "An Evaluation of Police Handgun Ammunition: Summary Report," Law Enforcement Standards Program Report No. LESP-RPT-0101.01, National Institute of Law Enforcement and Criminal Justice, Law Enforcement Assistance Administration, U. S. Department of Justice, August 1975.

Dobratz, Brigitta, M., "Properties of Chemical Explosions and Explosive Simulants," UCRL-51319, Rev. 1, U. S. Atomic Energy Commission Contract No. W-7405-Eng-48, Lawrence Livermore Laboratory, University of California, July 1974.

Doering, W. and Burkhardt, G., "Contributions to the Theory of Detonation," Translation from the German as Technical Report No. F-TS-1227-IA, Headquarters, Air Material Command, Wright Patterson Air Force Base, OH., Mary 1949.

Dolling, J. C., "Fragmentation of Underground Metallic Silos Subjected to Internal Blast," United States Patent 3,404,797, October 1968.

Donahue, J. D., "Evaluation of Explosives Storage Criteria," Falcon Research and Development Company, Denver, Colorado, March 1970.

Doughty, Capt. Jerry S., "An Investigation of Airblast Diffraction Loading on Simple Structural Shapes," Air Force Weapons Laboratory, Kirtland, AFB, New Mexico, January 1976.

Dow Chemical Company, "Fire and Explosion, Dow's Safety and Loss Prevention Guide, Hazard Classification and Protection," prepared by the Editors of Chemical Engineering Progress, American Institute of Chemical Engineering, New York, 1973.

Doyle, W. H., "Estimating Losses," paper presented at CSSCI Meeting in Houston, Texas, April 1970.

Doyle, W. H., "Industrial Explosions and Insurance," Loss Prevention, Vol. 3, pp. 11-17.

Draper, E. and Watson, R. R., "Collated Data on Fragments From Stacks of High Explosive Projectiles, " Report No. TM 2/70, Directorate of Safety (Army), London, England, March 1970.

Dutton, S. R. and Katsanis, D. J., "Computer-Aided Design of Suppressive Shields," EM-CR-76080, AAI Corporation, Baltimore, Md., report for Edgewood Arsenal, Aberdeen Proving Ground, MD., June 1976.

Duvall, W. I. and Fogelson, D. E.,"Review of Criteria for Estimating Damage to Residences from Blasting Vibrations,"Bureau of Mines Report of Investigation 5968, 1962.

Dvorak, A., "Seismic Effects of Blasting on Brick Houses," Proce geofyrikeniha Ustance Ceskoslavenski Akademie, Vol. 169, Geofysikalni Sbornik, 1962, pp 189-202.

DYNO Industrier A. S., "Double-Walled Steel Houses as Production Buildings for Explosives Factories," June 1978.

Edwards, A. T. and Northwood, T. D., "Experimental Studies of the Effects of Blasting on Structures," The Engineer, Vol. 210, September 1960, pp 538-546.

"Effects of Impact and Explosion," Vol. 1. Office of Scientific Research and Development, National Defense Research Committee, Washington, D. C., 1946.

Eichler, T. V. and Napadensky, H. S., "Accidental Vapor Phase Explosions on Transportation Routes Near Nuclear Plants," IITRI Final Report J6405, Argonne National Laboratory, April 1977.

Enig, J., and Metcalf, F. T., "Theoretical Calculations on the Shock Intiation of Solid Explosives," NOLTR 62-160, United States Naval Ordnance Laboratory, White Oak, Maryland, August 1962.

Enig, J. W. and Petrone, F. J., "On Equations of State in Shock Initiation Problems," Report No. NOLTR 64-182, U. S. Naval Ordnance Laboratory, White Oak, Silver Spring, Maryland, May 1965.

Esparza, E. D., "Estimating External Blast Loads from Suppressive Structures," Edgewood Arsenal Contract Report EM-CR-76030, Report No. 3, Edgewood Arsenal, Aberdeen Proving Ground, Md., November 1975.

Esparza, E. D., and Baker, W. E., "Measurement of Blast Waves From Bursting Frangible Spheres Pressurized with Flash-Evaporating Vapor or Liquid," NASA Contractor Report 2811, Contract NSG-3008, National Aeronautics and Space Administration, November 1977.

Esparza, E. D., Baker, W. E. and Oldham, G. A., "Blast Pressures Inside and Outside Suppressive Structures," Edgewood Arsenal Contractor Report EM-CR-76042, Report No. 8, Edgewood Arsenal, Aberdeen Proving Ground, Md., December 1975.

Ethridge, N. H., "Blast Diffraction Loading on the Front and Rear Surfaces of a Rectangular Parallelopiped,"BRL Memorandum Report No. 2784, U. S. Army Ballistic Research Laboratories, Aberdeen Proving Ground, Maryland, September 1977.

Eubanks, R. A. and Juskie, B. R., "Shock Hardening of Equipment," Shock and Vibration Bulletin, No. 32, Part III, December 1973.

"Explosives Accident/Incident Abstracts," Armed Services Explosives Safety Board, Washington D. C., October 1967.

"Explosives Hazard Classification Procedures," Department of the Army Technical Bulletin TB 700-2, Department of the Navy Publication NavOrd 8020.3, Department of the Air Force Technical Order TO 11A-1-47, Defense Supply Agency Reg. DASR 8220.1, May 1967.

"Facilities General Design Criteria," Energy Research and Development Administration, Division of Construction Planning and Support, ERDA Manual Appendix 6301, March 1977.

Feinstein, D. I., "Fragmentation Hazard Evaluations and Experimental Verification," Minutes of the 14th Explosives Safety Seminar, New Orleans, 8-10 November 1972, Department of Defense Explosives Safety Board, pp 1099-1116.

Feinstien, D. I., "Fragment Hazard Study: Grading and Analysis of 15mm Yma Test Fragments," IIT Research Institute, Chicago, Ill,,October 1972.

Feinstein, D. I. and Nagaoka, H. H., "Fragmentation Hazard Study Phase III: Fragment Hazards from Detonation of Multiple Munitions in Open Stores," IIT Report No. J-6176, IIT Research Institute, Chicago, Ill., August 1971.

Fenves, S. J., Perrone, N., Robinson, A. R. and Schnobrich, W. C., (Editors), Numerical and Computer Methods in Structural Mechanics, Academic Press, New York, NY, 1973.

Ferguson, W. G. and Yew, F. K., "The Application of the Rate Theory of Deformation to the Yield Behavior of Wood," Journal of Materials Sciences.

Ferritto, J. M., "Explosive Tests of Blast Cell, Naval Torpedo Station, Bangor Annex," No. TR-823, Civil Engineering Laboratory, Naval Construction Battalion Center, Port Hueneme, CA, May 1975.

Ferritto, J. M., "Optimum Dynamic Design of Nonlinear Plates Under Blast Loading," Technical Note No. N-1518, Naval Construction Battalion Center, Port Hueneme, CA, March 1978.

Ferritto, J. M., "Optimum Dynamic Design of Reinforced Concrete Slabs Under Blast Loading," Technical Note No. N-1494, Civil Engineering Laboratory, Naval Facilities Engineering Center, Port Hueneme, CA, July 1977.

Ferritto, J. M. and Forrest J. B., "Ground Motion from Pacific Cratering Experiments 1,000 Pound Explosive Shots: Data Supplement," Report R 8085, Naval Civil Engineering Laboratory, January 1975.

Filler, W. S., "The Effect of a Case on Airblast Measurements, Part 1, Friable Inert Cases," NOLTR 74-62, Naval Ordnance Laboratory, White Oak, April 1974.

Filler, W. S., "The Influence of Inert Cases on Airblast: An Experimental Study," The Sixth Symposium (International) on Detonation, Naval Surface Weapons Center, White Oak Laboratory, Silver Spring, Md. August 1976.

Filler, W. S., Rossi, J. M. and Walsh, H. R. J., "Barricade Effectiveness Evaluated From Records of Accidental Explosions," Armed Services Safety Board, Department of Defense, Washington, D. C., July 1966.

Fiquet, G., and Dacquet, S., "Study of the Perforation of Reinforced Concrete By Rigid Missiles-Experimental Study, Part II," Nuclear Engineering and Design, No. 41, 1977, pp 103-120.

Fishburn, Barry D., "Some Aspects of Blast from Fuel-Air Explosives," Acta Astronautica, Vol. 3, April 1976, pp 1049-1065.

Fisher, J. D., Irvine, B. W., Kopenhaver, R. L., and Lunger, W. D., "The Attenuation of Blast Waves by Barricades," School of Engineering, Widener College, Chester, PA.

Fletcher, E. R., "A Model to Simulate Thoracic Responses to Air Blast and To Impact," Aerospace Medical Research Laboratory, Paper No. 1, Wright Patterson Air Force Base, Ohio, December 1971.

Florence, A. L., "Critical Loads for Reinforced Concrete Bunkers," Defense Nuclear Report No. DNA 4469F, Stanford Research International, Menlo Park, CA. November 1977.

Forbes, D. J., "Design of Blast-Resistant Buildings in Petroleum and Chemical Plants," paper presented at API 1976 Autumn Meeting, Subcommittee on Facilities and Maintenance, October 1976.

Ford, M. B., "Correlation of Impact and Explosively Created Ground Shock Phenomena," Report No. N-76-10, Weapons Effects Laboratory, U. S. Army Engineer Waterways Experiment Station, Vicksburg, MI, June 1976.

Fortifikationsfoervaltiningen, Kungliga, "List of Unclassified Reports and Technical Notes Issued by the Research Department of the Royal Swedish Fortifications Administration (RSFA)," September 1973.

Freiwald, D. A. and Axford, R. A., "Approximate Spherical Blast Theory Including Source Mass," Journal of Applied Physics, Vol. 46, No. 3, March 1975, pp 1171-1174.

Freund, H. U. and Geiger, W., "Velocity and Density Fields in Reaction Products of a Detonating Cylindrical Charge," Acta Astronautica, Vol. 1, No. 3-4, March-April 1974, pp 405-416.

Frey, R. B., Howe, P. M., Trimble, J., and Melani, G., "Initiation of Explosives by Projectile Impact," Draft Technical Report, U. S. Army Ballistic Research Laboratory, June 1979.

Fuehrer, H. R. and Keeser, J. W., "Breach of Buried Concrete Structures," AFATL-TR-78-92, Air Force Armament Laboratory Report by Orlando Technology Inc., Orlando, Florida, August 1978.

Fuehrer, H. R. and Keeser, J. W., "Response of Buried Concrete Slabs to Underground Explosions," AFATL-TR-77-115, Orlando Technology, Inc., Orlando, Florida, September 1977.

Fugelso, L. E. and Rathmann, C. E., "Effect of Earth Cover on Far-Field Fragment Distribution," General American Research Division, General American Transportation Corporation, Niles, Ill, December 1973.

Fugelson, L. E., Weiner, L. M. and Schiffman, T. H., "A Computation Aid for Estimating Blast Damage from Accidental Detonation of Stored Munitions," Minutes of the 14th Explosives Safety Seminar, New Orleans 8-10 November 1973, Department of Defense Explosives Safety Board, pp 1139-1166.

Fugelso, L. E., Weiner, L. M. and Schiffman, T. H., "Explosion Effects Computation Aids," Final Report GARD Project No. 1540, General American Research Division, General American Transportation Corporation, June 1972.

Fundamentals of Protection Design (Nonnuclear), Department of the Army Technical Manual, TM5-855-1, Department of the Army, July 1965.

Gabrielsen, B. and Wilton, C., "Shock Tunnel Tests of Arched Wall Panels," Report No. URS 7030-19, Defense Civil Preparedness Agency Contract No. DAHC20-71-C-0223, DCPA Work Unit 11236, URS Research Company, San Mateo, California, December 1974.

Gabrielsen, B. L., "Response of Wall Panels Subjected to Blast Loading," Preprint 1399, ASCE National Structural Engineering Meeting, Baltimore, Maryland, April 19-23, 1971.

Gallagher, R. H., Finite Element Analysis: Fundamentals, Prentice Hall, Englewood Cliffs, New Jersey, 1975.

Gallo, J. G., "Shock Induced Structural Response," ADA 105 387 Naval Postgraduate School, Monterey, California, March 1978.

Gastrich, H. G., Hartlove, C. F. and Schroeder, F. J., "Rotating Product Door and the Sliding Personnel Door in the Category 4 Shield Test Report," Edgewood Arsenal Contractor Report No. EM-CR-76018 ER-8407, September 1975.

Gibson, N. and Harris, G. F. P., "The Calculation of Dust Explosion Vents," Chemical Engineering Progress, November 1976, pp 62-67.

Gill, H. L., "Active Arching of Sand During Dynamic Loading--Results of an Experimental Program and Development of an Analytical Procedure," Report No. R541, Naval Civil Engineering Laboratory, Port Hueneme, California, September 1967.

Glasstone, S., The Effects of Nuclear Weapons, U. S. Government Printing Office Revised Edition, April 1962.

Glasstone, S. and Dolan, P. J., The Effects of Nuclear Weapons, U. S. Government Printing Office, Revised Edition, 1977.

Goldstein, S. and Berriavd, C., "Study of the Perforation of Reinforced Concrete Slabs by Rigid Missiles--Experimental Study, Part III," Nuclear Engineering and Design, No. 41, 1977, pp 121-128.

Goodman, H. J., "Compiled Free Air Blast Data on Bare Spherical Pentolite," BRL Report No. 1092, U. S. Army Ballistics Research Laboratory, Aberdeen Proving Ground, Md., 1960.

Goodman, H. J. and Giglio-Tos, L., "Equivalent Weight Factors for Four Plastic Bonded Explosives: PBX-108, PB-109, AFX-103 and AFX-702," Technical Report ARBRL-TR-02057, U. S. Army Ballistic Research Laboratory, Aberdeen Proving Ground, Md., April 1978.

Gorman, J. W., "Base Fragment Velocities of Service Navy Projectiles," Report No. 1201, Final Report E1551J1, Naval Weapons Laboratory, Dahlgren, VA., 1979.

Grant, R. L., Murphy, J. N. and Bowser, M. L., "Effects of Weather on Sound Transmission from Explosive Shots," Bureau of Mines Report of Investigation 6921, 1967.

"R. M. Graziano's Tariff Publishing Hazardous Materials Regulations of the Department of Transportation Including Specifications for Shipping Containers," Bureau of Explosives, Association of American Railroads, March 1977.

Green, L. G., Nidick, E. J. and Walker, F. E., "Critical Shock Initiation Energy of PBX-9404, A New Approach," UCRL-51522, Lawrence Livermore Laboratory, University of California, January 1974.

Greenfield, S. H., "Hail Resistance of Roofing Products," U. S. Department of Commerce, National Bureau of Standards, Building Sciences Series 23, August 1969.

Greenspon, J. E., "An Approximate Nondimensional Representation of the Thor Equations," U. S. Army Materiel Systems Analysis Activity, October 1976.

Greenspon, J. E., "Energy Approaches to Structural Vulnerability with Application of the New Bell Stress-strain Laws," BRL CR No. 291, U. S. Army Ballistics Research Laboratory, Aberdeen Proving Ground, Md. March 1976.

Gregory, F. H., "Analysis of the Loading and Response of a Suppressive Shield When Subjected to an Internal Explosion," Minutes of the 17th Explosive Safety Seminar, Denver, Colo., September 1976.

Gregory, F. H., "Blast Loading Calculations and Structural Response Analyses of the 1/4 Scale Category I Suppressive Shield," BRL Report No. 2003, U. S. Army Ballistic Research Laboratory, Aberdeen Proving Ground, Md., August 1977.

Gross, A. G., "A Bibliography on Head and Brain Injuries," Protection, Inc., Englewood, California, January 1966.

Gueraud, R., Sokolovsky, A., Kavyrchine, M., and Astruc, M., "Study of the Perforation of Reinforced Concrete Slabs by Rigid Missiles--General Introduction and Experimental Study, Part I," Nuclear Engineering and Design, No. 41, 1977, pp 97-102.

Gupta, Y. M. and Seaman, L., "Local Response of Reinforced Concrete to Missile Impact," EPRI NP-1217, Research Project 393-1, Electric Power Research Institute, October 1979.

Gurke, G., "Experimentelle und theoretische Untersuchungen zur Wechselwirkung von LuftstoBwellen mit querschnittverengenden Einbauten (Drosselstellen) in Kanalen," Ernst-Mach Institut, Freiburg i. Br. Eckerstrabe 4, Bericht Nr. 9/70, November 1970.

Gurney, R. W., "The Initial Velocities of Fragments From Bombs, Shells, and Grenades," Report No. 648, U. S. Army Ballistic Research Laboratory, Aberdeen Proving Ground, Md., September 1947.

Habberjam, G. M. and Whetton, J. T., "On the Relationship Between Seismic Amplitude and Charge of Explosive Fired in Routine Blasting Operations," Geophysics 17, pp 116-128, January 1952.

Hage, K. G., "Dynamic Tensile Strength of Explosive Materials," Lawrence Radiation Laboratory, University of California, Atomic Energy Commission.

Haisler, W. E., "AGGIE I- A Finite Element Program for Nonlinear Structural Analysis," Report TEES-3275-77-1, Aerospace Engineering Department, Texas A&M University, June 1977.

Haisler, W. E., "Status Report of AGGIE I Computer Program," Technical Report No. 3275-78-2, Aerospace Engineering Department, Texas A&M University, April 1978.

Hahn, G. J. and Shapiro, S. S., Statistical Methods in Engineering, John Wiley and Sons, Inc., New York, NY, 1967.

Hanes, L. D., and Canada, C. E., "Unreacted Hugoniots and Detonation Sensitivity of HNS I," MHSMP-75-25, Sandia Laboratories, Albuquerque, New Mexico, April-June 1975.

Hardesty, D. R. and Lysne, P. C., "Shock Initiation and Detonation Properties of Homogeneous Explosives," SLA-74-0165, Sandia Laboratories, 1974.

Harlow, F. H. and Adamsden, A. A., "Fluid Dynamics—An Introductory Text," LA 4100, Los Alamos Scientific Laboratory, University of California, Los Alamos, New Mexico, February 1970.

Harper, M. J., Hawkins, S. J. and Hicks, J. A., "Explosively Generated Air Pressure Waves for Structural Forcing," Journal Sound Vibration, Vol. 11, No. 2, February 1970, pp 217-224.

Harrell, J. D., "HE Pressing," Development Division, Mason & Hanger, Silas Mason Co., Inc. October-December 1973.

Harvey, W., Dishan, J. and Thomas, T., "Near Surface Cratering Experiments," CA AFWL-TR-351, Fort Polk, Louisiana, U. S. Army Waterways Experiment Station, Livermore, CA, November 1975.

Hashmi, M. S. J. and Al-Hassani, S. T. S., "Large-Deflection Response of Square Frames to Concentrated Impulsive Loads," Journal of Mechanical Engineering Science, Vol. 19, No. 6, 1977, pp 243-250.

Hawkins, S. J. and Hicks, J. A., "Acoustic Approximation of Far-Field Blast From Spatially Distributed Explosive Charges," International Congress on Acoustics, 6th, Tokyo, Japan, August 21-28, 1968, pp 201-204.

Hayes, E. B., and Mitchell, D. E., "Shock Sensitivity of Porous HNS Explosive," SAND77-1363, Sandia Laboratories, December 1977.

"Hazardous Materials Regulations of the Department of Transportation by Air, Rail, Highway, Water and Military Explosives By Water Including Specifications for Shipping Containers," Prescribed under the act of September 6, 1970, Department of Transportation, March 1977.

"Hazards of Chemical Rockets and Propellants Handbook, Volume II., Solid Rocket Propellant Processing, Handling, Storage and Transportation," CPIA/194, May 1972.

Healey, J., Ammar, A., Vellozzi, J., Pecone, G., Weissman, S., Dobbs, N., and Price, P., "Design of Steel Structures to Resist the Effects of HE Explosions," Technical Report 4837, Picatinny Arsenal, Dover, New Jersey, August 1975.

Healey, J., Werner, H., Weissman, S., Dobbs, N., and Price, P., "Primary Fragment Characteristics and Impact Effects on Protective Barriers," Picatinny Arsenal Report No. 4093, Ammann & Whitney, Consulting Engineers, New York, NY, December 1975.

Henry, G. A., "Blast Injuries of the Ear," Laryngoscope 55, pp 663-672, 1945.

Henry, I. G., "The Gurney Formula and Related Approximations for High-Explosive Deployment of Fragments," Report No. PUB-189, Hughes Aircraft Co., Culver City, CA., 1967.

Hiesing, C., "Betriebserfehrungen mit dem Entspannungssprengen," Gluckauf, Vol. 114, No. 17, September 1978, pp 754-757.

Highter, W. H., "Comparison of Soil Moduli Obtained from Non-Destructive Dynamic Testing and Constitutive Equations," Department of Civil and Environmental Engineering, Clarkson College of Technology, Potsdam, New York, Final Report Air Force Office of Scientific Research Grant No. AFOSR 77-3364, June 1978.

Hirsch, A. E., "The Tolerance of Man to Impact," Annals of the New York Academy of Sciences, Vol. 152, Art. 1, October 1968, pp 168+.

Hirsch, F. G., "Effects of Overpressure on the Ear--A Review," Annals of the New York Academy of Sciences, Vol. 152, Art. 1, October 1968, pp 147+.

Hodge, D. C. and Garinther, G. R., "Noise and Blast," Human Engineering Laboratory, Aberdeen Proving Ground, Md., June 1973.

Hoerner, S. F., Fluid Dynamic Drag, Midland Park, New Jersey, 1958.

Hokanson, J. C. and Wenzel, A. B., "Reflected Blast Measurements Around Multiple Detonating Charges," Minutes of the Eighteenth Explosives Safety Seminar, Vol. I, September 1978, pp 447-471.

Holt, D. L., Babcock, S. G., Green, S. J. and Maiden, C. J., "The Strain-Rate Dependence of the Flow Stress of Some Aluminum Alloys," Transactions of the American Society of Metals, Vol. 60, 1967, page 152.

Holzer, S. M., Somers, A. E. and Bradshaw, J. C., "Reliability Study of Singer," AFWL-TR-76-192, Vol. 1, Department of Civil Engineering, Virginia Polytechnic Institute and State University, Blacksburg, VA., January 1977.

Hopkinson, B., "British Ordnance Board Minutes 13565," 1915.

Hornberg, H., "State of the Detonation of Products of Solid Explosives," Propellants and Explosives, Vol. 3, No. 3, June 1978, pp 97-106.

Howe, P. M. and Frey, R. B. , "Catastrophic Reaction of Compartmentalized Ammunition--Causes and Preventive Measures," U. S. Army Ballistic Research Laboratory, June 1978.

Huang, S. L. and Chou, P. C.,"Calculations of Expanding Shock Waves and Late-State Equivalence,"Final Report Contract No. DA-18-001-AMC-876, Report 125-12, Drexel Institute of Technology, Philadelphia, PA, April 1968.

Hubich, H. O. and Kachinski, R. L., "Explosive Waste Removal Systems for Suppressive Shields," Edgewood Arsenal Contractor Report No. EM-CR-76002, Edgewood Arsenal, Aberdeen Proving Ground, Md., August 1975.

Hudson, D. E., Alford, J. L. and Iwan, W. D., "Ground Accelerations Caused By Large Quarry Blasts," Bulletin of the Seismic Society, A. 51, 1961, pp 191-202.

Huffington, N. J. Jr., (Ed)., Behavior of Materials Under Dynamic Loading, The American Society of Mechanical Engineers, New York, NY, 1965.

Huffington, N. J. and Robertson, S. R., "Containment Structures Versus Suppressive Structures," Ballistic Research Laboratory Report No. 2597, U. S. Army Ballistic Research Laboratory, Aberdeen Proving Ground, MD., February 1976.

Humphrey, J. R., "LX-10-1: A High-Energy Plastic-Bonded Explosive," Lawrence Livermore Laboratory, University of California, July 1974.

Ichiro, I., "On The Relationship Between Seismic Ground Amplitude and the Quantity of Explosives in Blasting," Reprint from Memoirs of the Faculty of Engineering Kyoto University, 15, 1953, pp 579-87.

"Impact Design Criteria for Blockhouse Subjected to Abortive Launch Environments," Technical Publication, PMR-TR-70-2, Mechanical Research Inc., Pacific Missile Range, Point Mugu, CA, July 1970.

"Impact Resistance of Plastics and Electrical Insulating Materials," ANSI/ASTM D256-78.

Ingard, U., "A Review of the Influence of Meteorological Conditions on Sound Propagation," Journal of the Acoustic Society of America, Vol. 25, pp 405-411.

Ingram, J. K., "Cense Explosion Test Program: Report 2, CENSE 2, Explosions in Soil," U. S. Army Engineer Waterways Experiment Station, Technical Report No. N-77-6, December 1977.

"Interim Safety Criteria for the Design of Production Plant Explosive Facilities," Available from U.S. Department of Energy, Albuquerque Operations Office, Albuquerque, New Mexico.

"Internal Blast Damage Mechanisms Computer Program," JTCG/ME-73-3, April 10, 1973.

Isley, R., "Glass and Plaster Damage from Small Explosions," Armed Services Explosives Safety Board, AD 637 835, March 15, 1950.

Jack, W. H., Jr., "Measurements of Normally Reflected Shock Waves From Explosive Charges," BRL Memorandum Report No. 1499, Aberdeen Proving Ground, Md., July 1963.

Jack W. H., Jr. and Armendt, B. F., Jr., "Measurements of Normally Reflected Shock Parameters Under Simulated High Altitude Conditions," BRL Report No. 1208, Aberdeen Proving Ground, MD., April 1965.

Jackson, R. K., Green, L. G., Barlett, R. H., Hofer, W. W., Kramer, P. E., Lee, R. S., Nidick, E. J., Jr., Shaw, L. L. and Weingart, R. C., "Initiation and Detonation Characteristics of TATB," Lawrence Livermore Laboratory, Livermore California, U. S. Energy Research and Development Administration, 1978.

Jameson, R. L. and Hawkins, A. L., "Detonation Pressure Measurements in TNT and Octol," U. S. Army Ballistic Research Laboratory, Aberdeen Proving Ground, Md., 1970.

Jankov, Z. D., Shananhan, J. A. and White, M. P., "Missile Tests of Quarter Scale Reinforced Concrete Barriers," Proceedings of the Symposium on Tornadoes Assessment of Knowledge and Implications for Man, Texas Tech University, June 22-24, 1976, pp 608-622.

Janzon, B., "Retardation of Fragments in Air," Royal Aircraft Establishment, Forsvarets Forskningsanstalt, Sweden, FOA 2 Report A, 2539-44, Crown Copyright, January 1973.

Jarrett, D. E., "Derivation of British Explosive Safety Distances," Annals of the New York Academy of Science, Vol. 152, Art. 1, October 1968, pp 18-35.

Jezek, B. W., "Suppressive Shielding for Hazardous Munitions Production Operations," Technical Report No. ARCSL-TR-77020, U. S. Army Armament Research and Development Command, Chemical Systems Laboratory, Aberdeen Proving Ground, Md., April 1977.

Johansson, C. H. and Persson, P. A., Detonics of High Explosives, Academic Press, London and New York, 1970.

Johnson, C. and Moseley, J. W., "Preliminary Warhead Terminal Ballistic Handbook, Part 1, Terminal Ballistic Effects," NAVWEPS Report No. 7673, U. S. Naval Weapons Laboratory, Dahlgren, VA., March 1964.

Johnson, H. D., "Mechanical Properties of High Explosives," MHSMP-74-19-D, SANL No. 260-009, April-June 1974.

Johnson, O. T., "A Blast-damage Relationship," BRL Report No. 1389, U. S. Army Ballistic Research Laboratory, Aberdeen Proving Ground, Md., September 1967.

Johnson, O. T., Patterson, J. D. and Olson, W. C., "A Simple Mechanical Method for Measuring the Reflected Impulse of Air Blast Waves," BRL Report No. 1099, Aberdeen Proving Ground, Md., July 1957.

Jones, O. E., "Metal Response Under Explosive Loading," 12th Annual Symposium of Behavior and Utilization of Explosives in Engineering Design, Sandia Laboratories, Albuquerque, New Mexico, March 1972, pp 125-148.

Kachinski, R. L., Schnepfe, R. W., Hom, W. R., Russell, K., and Kineke, J. H., "Technical Feasibility of Suppressive Shields for Improved Hawk Launch Sites," Edgewood Arsenal Contractor Report No. EM-CR-76057, February 1976.

Kaleps, I. and von Gierke, H. E., "A Five-Degree-of-Freedom Mathematical Model of the Body," Aerospace Medical Research Laboratory, Paper No. 8, Wright-Patterson Air Force Base, OH, 1971.

Kaliszky, S., "Approximate Solutions for Impulsively Loaded Inelastic Structures and Continua," International Journal of Nonlinear Mechanics, Vol. 5, 1970, pp 143-158.

Kalkbrenner, D. K. and Swider, E., "Secondary Fragment Impact Sensitivity of Various Munitions," Engineering Research Division, Report No. J6375, IIT Research Institute, Chicago, IL., December 1977.

Kangas, P., "Hailstone Impact Tests on Aircraft Structural Components," Civil Aeronautics Administration Technical Development and Evaluation Center Report No. 124, Indianapolis, In., September 1950.

Kaplan, K., "Dangers of Secondary Missiles," Minutes of the Seventeenth Explosives Safety Seminar, Vol. II, September 1976.

Katona, M. G., Thompson, R. and Smith, J., "Efficiency Study of Implicit and Explicit Time Integration Operators for Finite Element Applications," Technical Report No. R-856, Civil Engineering Laboratory, Naval Construction Battalion Center, Port Hueneme, CA., July 1977.

Katsanis, D. J., "Safety Approval of Suppressive Shields," Edgewood Arsenal Technical Report No. EM-TR-76088, Edgewood Arsenal, Aberdeen Proving Ground, Md., August 1976.

Katsanis, D. J. and Jezek, B. W., "Suppressive Shielding of Hazardous Ammunition Production Operations," Technical Report No. EM-TR-76015, Edgewood Arsenal, Aberdeen Proving Ground, MD., December 1975.

Keefer, J. H. and Reisler, R. E., "Multiburst Environment--Simultaneous Detonations Project Dipole West," BRL Report No. 1766, U. S. Army Ballistic Research Laboratory, Aberdeen Proving Ground, Md., March 1975.

Keenan, W. A., "Strength and Behavior of Laced Reinforced Concrete Slabs Under Static and Dynamic Load," Naval Civil Engineering Laboratory Technical Report No. R-620, Port Hueneme, CA., April 1969.

Keenan, W. A. and Tancreto, J. E., "Effects of Venting and Frangibility of Blast Environment from Explosions in Cubicles," Minutes of the 14th Explosives Safety Seminar, New Orleans, November 1972, pp 125-162.

Keenan, W. A. and Tancreto, J. E., "Blast Environment from Fully and Partially Vented Explosions in Cubicles," Technical Report 51-027, Civil Engineering Laboratory, Naval Construction Battalion Center, Port Hueneme, CA., February 1974.

Kennedy, J. E., "Explosive Output for Driving Metal," 12th Annual Symposium of Behavior and Utilization of Explosives in Engineering Design, Sandia Laboratories, Albuquerque, New Mexico, March 1972, pp 109-124.

Kennedy, J. E., "Gurney Energy of Explosives: Estimation of the Velocity and Impulse Imparted to Driven Metal," Sandia Report SC-PR-70-790, December 1970.

Kennedy, J. E. and Schwarz, A. C., "Detonation Transfer By Flyer Plate Impact," Document No. SLA-74-5073, Sandia Laboratories, Albuquerque, New Mexico, 1974.

Kennedy, W. D., "Explosions and Explosives in Air," Effects of Impact and Explosion, M. T. White (Ed.), Summary Technical Report of Division 2, NDRC, Vol I, Washington, D. C., 1946.

Kiger, S. A. and Balsara, J. P., "Response of Shallow-Buried Structures to Blast Loads," Waterways Experiment Station, Vicksburg, MI., June 1978.

Kimberly, F. V., "Experimental Investigation of Initial Surface Particle Motion Resulting from Small Subsurface Explosions in Dry Ottowa Sand," Air Force Institute of Technology, School of Engineering, Wright-Patterson Air Force Base, OH, June 1972.

Kineke, J. H. Jr., "Secondary Fragment Speed with Unconfined Explosives: Model and Validation," Minutes of the 17th Explosives Safety Seminar, Vol. II, September 1976.

Kingery, C. N., "Air Blast Parameters Versus Distance for Hemispherical TNT Surface Bursts," BRL Report No. 1344, Aberdeen Proving Ground, Md. September 1966.

Kingery, C. N., "Blast Loading on Model Earth Covered Magazines," Technical Report No. ARBRL-TR-02092, U. S. Army Ballistic Research Laboratory, Aberdeen Proving Ground, Md., August 1978.

Kingery, C. N., "Parametric Analysis of Sub-Kiloton Nuclear and High Explosive Air Blast," BRL Report No. 1393, Aberdeen Proving Ground, Md., February 1968.

Kingery, C. N. and Coulter, G., "Shock Wave Attenuation by Single Perforated Plates," BRL Memorandum Report No. 2664, U. S. Army Ballistic Research Laboratory, Aberdeen Proving Ground, Md., August 1976.

Kingery, C. N. Coulter, G. and Pearson, R., "Venting of Pressure Through Perforated Plates," Technical Report No. ARBRL-TR-02105, U. S. Army Ballistic Research Laboratory, Aberdeen Proving Ground, Md., September 1978.

Kingery, C. N., Coulter, G. and Watson, G. T., "Blast Parameters From Explosions in Model Earth Covered Magazines," BRL Memorandum Report No. 2680, U. S. Army Ballistic Research Laboratory, Aberdeen Proving Ground, Md., September 1976.

Kingery, C. N., Pearson, R. and Coulter, G., "Shock Wave Attenuation by Perforated Plates with Various Hole Sizes," BRL Memorandum Report No. 2757, U. S. Army Materiel Development and Readiness Command, Alexandria, VA. June 1977.

Kingery, C. N., Schumacher, R., and Ewing, W., "Internal Pressure from Explosions in Suppressive Structures," BRL Memorandum Report No. ARBRL-MR-02848, U. S. Army Armament Research and Development Command, Aberdeen Proving Ground, Md., June 1978.

Kinney, G. F., "Engineering Elements of Explosions," NWC TP4654, Naval Weapons Center, China Lake, CA, November 1968.

Kinney, G. F., Explosive Shocks in Air, MacMillian, New York, NY, 1962.

Kinney, G. F. and Sewell, R. G. S., "Venting of Explosions," NWC Technical Memorandum 2448, Naval Weapons Center, China Lake, CA., July 1974.

Kokinakis, W., "A New Methodology for Wounding and Safety Criteria," Proceedings of the 16th Explosive Safety Seminar, September 1974, pp 1209-1226.

Korobeinikiv, V. P., Mil'nikova, N. S. and Ryazanov, Y. V., The Theory of Point Explosion, Fizmatgiz, Moscow, 1961; English Translation, U. S. Department of Commerce, JPRS: 14,334, Washington, D. C., 1962.

Kot, C. A., "Spalling of Concrete Walls Under Blast Load," Components Technology Division, Argonne National Laboratory, Argonne, IL.

Kot, C. A. and Turula, P., "Air Blast Effect on Concrete Walls," Technical Memorandum ANL-CT-76-50, Argonne National Laboratory, Argonne, IL., July 1976.

Kot, C. A., Valentin, R. A., McLennon, D. A. and Turula, P., "Effects of Air Blast on Power Plant Structures and Components," NUREG/CR-0442, ANL-CT-78-41, R5, Argonne National Laboratory, Argonne, IL., October 1978.

Kraft, J. M., "Correlation of Plane Strain Crack Toughness with Strain Hardening Characteristics of a Low, a Medium and a High Strength Steel," Applied Materials Research, Vol. 3, page 88, 1964.

Kramer, P. E., "Sensitivity and Performance Testing of HE," Mason & Hanger, Silas Mason Co., Inc., Development Division, Endeavor No. 231, MHSMP-75-40S, July-Sept. 1975.

Kramer, P. E., "Sensitivity & Performance Testing of High Explosives," Development Division, Mason & Hanger-Silas Mason Company, Inc., Endeavor No. 216, April-June 1974.

Kramer, P. E. and Ashcraft, R. W., "Reduction of C-J Pressure Test Data," Development Division, Mason & Hanger, Silas Mason Co., Inc., December 1972.

Krantz, F. M., "Structure for Atomic Blast Resistance," U. S. Patent No. 3,266,203, Patented August 16, 1966, (filed May 3, 1966).

Krauklis, P. and Bedford, A. J., "Fragmentation Data Analysis, I. Computer Program for Mass and Number Distributions and Effects of Errors on Mass Distributions," Australian Defence Scientific Service, Materials Research Laboratory, Report No. 549, Maribyrnong, Victoria, Australia, November 1974.

Kulesz, J. J. and Friesenhahn, G. J., "Explosion Venting in Buildings," <u>Minutes of the 19th Explosives Safety Seminar</u>, (to be published).

Kulesz, J. J., Moseley, P. K. and Baker, W. E., "Fragment and Blast Hazards From Explosions in a Tender Torpedo Workshop," Vol. 1, Final Report Prepared for the David Taylor Naval Ship Research and Development Center, November 1978.

Kulesz, J. J., Moseley, P. K. and Parr, V. B., "Prediction of Weight and Range Distributions from Accidental Explosions Inside Buildings," to be presented at the 1980 Explosive Safety Seminar, 1980.

Kury, J. W., "Metal Acceleration by Chemical Explosives," <u>Fourth Symposium International on Detonation</u>, ONR ACR-126, January 13, 1965.

Kusher, A. S., Giltrud, M. E., Lehto, D. L. and Ward, J. M., "Recommended Design and Analysis Procedures for Suppressive Shield Structures," Technical Report No. NSWC/WOL/TR 76-112, Naval Surface Weapons Center, White Oak Laboratory, White Oak, Silber Spring, Md., March 1977.

Kvammen, A., Pichumani, R. and Dick, J. L.,"Pavement Cratering Studies," University of New Mexico, Eric H. Wang Research Facility Report for Air Force Weapons Laboratory, 1973.

Ladegaard-Pederson, A. and Dally, J. W., "A Review of Factors Affecting Damage In Blasting," Mechanical Engineering Department, University of Maryland, College Park, Maryland, January 1975.

Lamb, H., "On the Propagation of Tremors Over the Surface of an Elastic Solid," <u>Philosophical Transactions of Royal Society London</u>, Series A, Volume 203, September 1904.

Langefors, U., Kihlstron, B. and Westerberg, H., "Ground Vibrations in Blasting," <u>Water Power</u>, February 1958, pp 335-338, 390-395 and 421-424.

Laporte, O. and Chang, T. S., "Exact Expressions for Curved Characteristics Behind Strong Blast Waves," North Carolina State University, Report No. TSC-70-3, November 1970.

Lawrence, W. and Johnson, E., "Design for Limiting Explosion Damage," <u>Chemical Engineering</u>, January 1974.

Lee, J. H., Knystautas, R. and Bach, G. G., "Theory of Explosions," Department of Mechanical Engineering, McGill University, Report 69-3090, 1969.

Lee, L. S. S. and Martin, J. B., "Approximate Solutions of Impulsively Loaded Structures of a Rate Sensitive Material," <u>Z. Agnew. Math. Phys.</u>, 21, 1970, pp 1011-1032.

Lehto, D. L. and Larson, R. A., "Long Range Propagation of Spherical Shock Waves from Explosions in Air," NOLTR 69-88, Naval Ordnance Laboratory, White Oak, Md., 1969.

Leigh, B. R., "Lifetime Concept of Plaster Panels Subjected to Sonic Boom," UTIAS Technical Note 91, Institute for Space Studies, University of Toronto, July 1974.

Leondi, M. F., "Dynamic Modeling of the Post Failure Conditions of Reinforced Concrete Elements Subjected to Blast Overpressure," ARRADCOM, LCWSL, MTD, STB, Dover, New Jersey.

Levy, S., "An Imrpoved Computer Program to Calculate the Average Blast Impulse Loads Acting on a Wall of a Cubicle," Ammunition Engineering, Picatinny Arsenal, Dover, New Jersey, May 1970.

Lewis, B. and von Elbe, G., Combustion, Flames and Explosions of Gases, Academic Press, New York, NY, 1961.

Liebman, I., Corry, J. and Richmond, J. K., "Pressure Sensitive Explosion Barrier," U. S. Patent No. 3,958,644, May 1976.

Liepmann, H. W. and Roshko, A., Elements of Gasdynamics, John Wiley and Sons, Inc., New York, NY., 1967.

T. Y. Lin and Associates, "Ferro Cement Panels," Consulting Engineers, Van Nuys, CA, November 1968.

Lindberg, H. E., Anderson, D. L., Firth, R. D. and Parker, L. V., "Response of Reentry Vehicle-Type Shells to Blast Loads, Final Report SRI Project FGD-5228, P. O. 24-14517, Stanford Research Institute, Menlo Park, CA., September 1965.

Lindholm, U. S. and Bessey, R. L., "A Survey of Rate Dependent Strength Properties of Materials," Final Report to Air Force Materials Laboratory, April 1969.

Lindholm, U. S. and Yeakley, L. M., "High Stain Rate Testing: Tension and Compression," Experimental Mechanics, Vol. 8, 1968, page 1.

Lipson, S., "Cellular Aluminum for Use in Energy Dissipation Systems," NASA CR-93, September 1964.

Livesley, R. K., Matrix Methods of Structural Analysis, Pergamon and MacMillan, 1964.

Loxley, T. E., "Large Scale Sample Drop Testing of Castable Plastic Bonded Explosives," AD 350 648-L, U. S. Naval Weapons Laboratory, Dahlgren, VA., June 1964.

Lutsky, M., "Theoretical Versus Experimental Results for Air Blast From One-Pound Spherical TNT and Pentolite Charges at Sea Level Conditions," Report No. NOLTR 65-57, U. S. Naval Ordnance Laboratory, White Oak, Silver Spring, Md., September 1965.

McCormick, C. W. (Ed.), "MSC/NASTRAN User's Manual," MSR-39, The Mac-Neal
Schwendler Corporation, Los Angeles,CA, May 1976.

McGuire, W. and Leyendecker, E. V., "Analysis of Non-Reinforced Masonary
Building Response to Abnormal Loading and Resistance to Progressive Collapse,"
National Bureau of Standards, November 1974.

McHenry, D. and Shideler, J. J., "Review of Data on Effect of Speed in Mechanical
Testing of Concrete," Symposium on Speed of Testing of Non-Metallic Materials,
Atlantic City, NJ, (ASTM Special Technical Publication No. 185), June 1955,
pp 72-82.

McIntyre, F. L., McKown, G. L. and Koger, D. M., "Mound Laboratory Pyrotechnic
Transport Container," National Space Technology Laboratories, Computer Sciences
Corporation Engineering and Science Services Laboratory, NSTL Station, MI,
June 1978.

McKown, G. L., "Near Field Blast Effects From Bare Charges," Edgewood Arsenal
Technical Report No. EM-TR-77002, Edgewood Arsenal, Aberdeen Proving Ground,
Maryland, January 1977.

McKown, G. L., McIntyre, F. L. and Price, P., "TNT Equivalency of Composition
A-5," Contract No. MIPR 816B602101F4W5, Manufacturing Technology Directorate,
Picatinny Arsenal, Dover, New Jersey, June 1976.

McLean, D. G. and Allan, D. S., "An Experimental Program to Determine the Sensi-
tivity of Explosive Materials to Impact by Regular Fragments," Final Report
Contract DA-19-020-ORD-5617, Picatinny Arsenal, December 1965.

McNamara, J. F., "Solution Scheme for Problems of Non-Linear Structural Dynamics,"
Paper No. 74-PVP. 30, Journal of Pressure Vessel Technology, American Society
of Mechanical Engineers, 1975.

McNaughtan, I. I. and Chisman, S. W., "A Study of Hail Impact at High Speed on
Light Alloy Plates," Proceedings of the Ninth Annual National Conference on
Environmental Effects on Aircraft and Propulsion Systems, Naval Air Propulsion
Test Center, October 7-9, 1969, p 16.

Macek, A.,"Sensitivity of Explosives," Chem. Rev. 62, pp 41-62.

Mach, E. and Sommer, J., "Uber die Fortpflanzunggeshwindigkeit von Explosion-
schallwellen," Akademie Der Wissenschaften, Sitzangberichte der Wiener, 74,
1977.

Mackenzie, A., Dalrymple, E. W. and Schwartz, F., "Design of Pressure Vessels
for Confining Explosives," Picatinny Arsenal, Dover, New Jersey, July 1965.

Makino, R. C. and Goodman, J. J., "Air Blast Data on Bare Explosives of Different
Shapes and Compositions," BRL Report No. 1015, U. S. Army Ballistic Research
Laboratory, Aberdeen Proving Ground, Md., 1956.

Mainstone, R. J., "The Breakage of Glass Windows by Gas Explosions," Building Research Establishment Current Paper CP 26/71, Building Research Establishment, September 1971.

Mainstone, R. J., "The Hazard of Explosion, Impact and Other Random Loadings on Tall Buildings," Building Research Establishment Current Paper CP 64/74, Building Research Establishment, June 1974.

Mainstone, R. J., "The Hazard of Internal Blast in Buildings," Building Research Establishment Current Paper CP 11/73, Building Research Establishment, April 1973.

Mainstone, R. J., "The Response of Buildings to Accidental Explosions," Building Research Establishment Current Paper 24/76, Building Research Establishment, Garston, Watford, England, April 1976.

Majid, K. I., Non-Linear Structures, Wiley-Interscience, A Division of John Wiley and Sons, Inc., New York, NY, 1972.

Makino, R., "The Kirkwood-Brinkley Theory of Propagation of Spherical Shock Waves and Its Comparison with Experiment," BRL Report No. 750, April 1951.

Manjoine, M. J., "Influence of Rate of Strain and Temperature on Yield Stresses of Mild Steel," Journal of Applied Mechanics, December 1944, pp A-211-A-218.

MARC Analysis Corporation and Control Data Corporation, "Non-Linear Finite Element Analysis Program Volume I: Users Information Manual," 1975.

Markwardt, L. J. and Liska, J. A., "The Influence of Rate of Loading on the Strength of Wood and Wood-Base Materials," Symposium on Speed of Testing of Non-Metallic Materials, Atlantic City, New Jersey, (ASTM Special Technical Publication No. 185), June 1955, pp 3-17.

"Masonry Design Manual," Masonry Industrial Advancement Committee, Masonry Institute of America, Los Angeles, CA., (current edition).

Matonis, V. A., "Elastic Behavior of Low-Density Rigid Foams in Structural Applications," Society of Plastics Engineering Journal, September 1964, pp 1024-1030.

"Mechanical Properties of Hexcel Honeycomb Materials," TSB 120, Hexcel, Winter 1979, Revision.

Medearis, K., "Rational Damage Criteria for Low-Rise Structures Subjected to Blasting Vibrations," Proceedings of the Institute of Civil Engineers, Part 2, No. 65, November 1978, pp 611-621.

Medenica, W. V., "Blast Shields Testing," NASA TN D-4894, November 1968.

Meireis, E. C. and Wright, A. R., "Hardness Program-Non-EMP Hardness Program Plan for Safeguard Ground Facilities, Vol. 2, Safeguard Structures and TSE Descriptions," U. S. Army Corps of Engineers, Huntsville Division, November 1973.

Mellsen, S. B., "Drag on Free Flight Cylinders in a Blast Wave," Defence Research Establishment, Suffield, Ralston, Alberta, Canada.

Mente, L. J., and Lee, W. M., "DEPROP- A Digital Computer Program for Predicting Dynamic Elastic-Plastic Response of Panels to Blast Loading," Kaman AviDyne, A Division of Kaman Sciences Corp., Burlington, MA., June 1976.

Metallic Materials and Elements for Aerospace Vehicle Structures: Military Standardization Handbook," MIL-HDBK-SC, September 1976.

Meyer, R., Explosives, Verlag Chemie, Weinheim, New York, 1977.

Ministry of Labour, "Guide to the Use of Flame Arresters and Explosion Reliefs," Safety, Health and Welfare Series No. 34, Her Majesty's Stationery Office, London, 1965.

Minutes of the Eleventh Explosives Safety Seminar, Vol. I, Conducted by the Armed Services Explosives Safety Board, September 9-10, 1969.

Minutes of the Fourteenth Explosives Safety Seminar, Vol. II, Department of Defense Explosives Safety Board, November 8-10, 1972.

Minutes of the Thirteenth Annual Explosives Safety Seminar, The Armed Services Explosives Safety Board, September 14-16, 1971.

Moore, C. V., "The Design of Barricades for Hazardous Pressure Systems," Nuclear Engineering and Design, Vol. 5, 1967, pp 81-97.

Morales, W. J., "Displacement Bounds for Blast Loaded Structures," Journal of the Engineering Mechanics Division, Proceedings of the American Society of Civil Engineers, Vol. 98, No. EM4, August 1972, pp 965-974.

Morris, G., "The Reduction of Ground Vibrations from Blasting Operations," Engineering, April 1950, pp 430-433.

Murphey, B. F., "Particle Motions Near Explosions in Halite," Journal of Geophysical Research, Vol. 66, No. 3, March 1961, pp 947-958.

Murrell, D.W. , "Earth Motion and Stress Measurements, Project LN 302, Operation DIAL PACK," Army Engineer Waterways Experiment Station Technical Report N-74-3, U. S. Army Corps of Engineers, Vicksburg, MI, April 1974.

Napadensky, H. S., Swatosh, J. J., and Morita, D. R., "TNT Equivalency Studies," Minutes of the 14th Explosives Safety Seminar, New Orleans, November 8-10, 1972, pp 289-312.

Nara, H. R. and Dennington, R. J., "Ricochet and Penetration of Steel Spheres in Clay and Sand Soils," TM-E7, Case Institute of Technology, Project DOAN Brook, October 1954.

National Fire Protection Association, "Explosion Prevention Systems," NFPA No. 69, 1973.

National Fire Protection Association, "Guide for Explosion Venting," NFPA No. 68, National Fire Codes, Vol. 13, 1975.

National Oceanic and Atmospheric Administration, U. S. Standard Atmosphere, NOAA-S/T, 76-1562, U. S. Government Printing Office, October 1976.

Neal, B. G, The Plastic Methods of Structural Analysis, Chapman and Hall, London, England, 1977.

Nelson, K. P., "Spherical Shields for the Containment of Explosions," Edgewood Arsenal Technical Report No. EM-TR-76096, Edgewood Arsenal, Aberdeen Proving Ground, Md., March 1977.

Nelson, K. P., "The Economics of Applying Suppressive Shielding to the M483A1 Improved Conventional Munition Loading, Assembling, and Packing Facility," Technical Report No. EM-TR-76087, Edgewood Arsenal, Aberdeen Proving Ground, Md., January 1977.

Newmark, N. M., "A Method of Computation for Structural Dynamics," The Office of Naval Research, Department of the Navy, Journal of the Engineering Mechanics Division, Proceedings of the American Society of Civil Engineers, July 1959, pp 67-94.

Nicholls, R. W., Johnson, C. F., and Duvall, W. I., "Blast Vibrations and Their Effects on Structures," Bureau of Mines Bulletin 656, p. 105, 1971.

NMAB Committee, "Response of Metals and Metallic Structures to Dynamic Loading," NMAB-341, National Materials Advisory Board, National Academy of Sciences, Washington, D. C., May 1978.

Nonaka, T., "Shear and Bending Response of a Rigid-Plastic Beam to Blast-Type Loading," Ingenieur-Archiv 46, S.35-52, 1977.

Norrie, H. and de Vries, G., The Finite Element Method: Fundamentals and Applications, Academic Press, New York, NY, 1973.

Norris, C. H., Hansen, R. J., Holley, M. J., Biggs, J. M., Namyet, S. and Minami, J. V., Structural Design for Dynamic Loads, McGraw-Hill Book Co., New York, NY, 1959.

"Notched Bar Impact Testing of Metallic Materials," ASTM E23-72.

Nuclear Regulatory Commission, Regulation Guide 1.92.

O'Brien, J., "U. S. Regulatory Requirements for Blast Effects from Accidental Explosions," Nuclear Engineering and Design, Vol. 46, 1978, pp 145-150.

Odello, R. and Price, P., "Ground Shock Effects from Accidental Explosions," Picatinny Arsenal Technical Report 4995, Picatinny Arsenal, Dover, New Jersey, November 1976.

Oertel, F. H., "Evaluation of Simple Models for the Attenuation of Shock Waves by Vented Plates," BRL Report No. 1906, U. S. Army Ballistic Research Laboratory, Aberdeen Proving Ground, Md., August 1976.

Office of Scientific Research and Development, "Effects of Impact and Explosion," National Defense Research Committee, Division 2, Washington, D. C., AD 221 586, 1946.

Olson, J. J., and Flecher, L. R., "Airblast-Overpressure Levels From Confined Underground Production Blasts," Bureau of Mines Report of Investigation BM-RI-7574, 1971.

Oppenheim, A. K., Introduction to Gas Dynamics of Explosions, Course Lecture Notes #48, CISM, Udine, Italy, Springer-Verlag, New York, NY, 1972, p. 43.

Oppenheim, A. K., Lundstrom, E. A., Kuhl, A. L. and Kamel, M. M., "A Systematic Exposition of the Conservation Equations for Blast Waves," Journal of Applied Mechanics, December 1971, pp 783-794.

Osborn, A. G. and Stallings, T. L., "PBX Processing," Development Division, Mason & Hanger, Silas Mason Co. Inc., SANL 260-002, October-December 1973.

Owczarek, J. A. Fundamentals of Gas Dynamics, Int. Textbook Co., Scranton, PA.

Palmer, K. N., Dust Explosions and Fires, Chapman and Hall, Ltd., London.

Palmer, K. N., "Loss Prevention: Relief Venting of Dust Explosions," Chemical Engineering Progress, Vol. 70 No. 4, April 1974, pp 57-61.

Pei, R., "A Design Aid and Cost Estimate Model for Suppressive Shielding Sturctures," Department of Safety Engineering, USAMC Intern Training Center, Report No. YTC-02-08-76-413, Red River Army Depot, Texarkana, Texas, December 1975.

Penny, W. G., Samuels, D. E. J. and Scorgie, G. C., "The Nuclear Explosive Yields at Hiroshima and Nagasaki," Phil. Trans. Royal Society, 266, 1970, p. 357.

Perret, W. R. and Bass, R. C., "Free-Field Ground Motion Induced By Underground Explosions," Sandia Laboratories, Albuquerque, New Mexico, November 1975.

PCI Design Handbook: Precast, Prestressed Concrete, Prestressed Concrete Institute, Chicago, Ill., (current edition).

Perrone, N. and Pilkey, W. (eds.), Structural Mechanics Software Series, Vol. I, University Press of Virginia, Charlottesville, VA., 1977.

Perrone, N. and Pilkey, W., (eds.), Structural Mechanics Software Series, Vol. II, University Press of Virginia, Charlottesville, VA, 1978.

Perkins, B. J. and Jackson, W. F., "Handbook for Prediction of Air Blast Focusing," BRL Report No. 1240, U. S. Army Ballistic Research Laboratory, Aberdeen Proving Ground, Md., 1964, p. 100.

Perry, G. L. E., Hudson, C. C. and Loring, B. P., "Analysis of Ground Motion Data and Prediction Techniques from the Pre-Dice Throw II Events," Contract No. DNA001-750C-0023, and DNA001-76-C-0376, General Electric Company, TEMPO, Albuquerque, New Mexico, March 1977.

Peterson, F. H., Lemont, C. J. and Vergnolle, R. R., "High Explosive Storage Test," Air Force Weapons Laboratory Technical Report No. AFWL-TR-67-132, Air Force Weapons Laboratory, Kirtland AFB, Mew Mexico, May 1968.

Peterson, F., Lemont, C. J. and Vergnolle, R. R., "High Explosive Storage Test Big Papa," Technical Report No. AFWL-TR-67-132, Air Force Weapons Laboratory, Air Force Systems Command, Kirtland Air Force Base, New Mexico, May 1968.

Petino, G., and Leondi, M. F., "Sensitivity of Molten and Solid Amatex Charges to Impact by Primary Steel Fragments," ARLCD-CR-78011, ARRADCOM, Dover, New Jersey, April 1978.

Petino, G., DeMella, D. and Rindner, R. M., "Sensitivity of Cased Charges of Molten and Solid Composition B to Impact by Primary Steel Fragments," PA-TR-4975, Picatinny Arsenal, Dover, New Jersey, June 1976.

Pilkey, W., Saczalski, K. and Schaeffer, H., (eds.) Structural Mechanics Computer Programs, University Press of Virginia, Charlottesville, VA., 1974.

Pinney, E., "The Early Effect of an Explosion in a Multi-layered Medium," University of California, NONR-222-04, 1965.

Pirotin, S. D., Berg, B. A. and Witmer, E. A., "PETROS 4: New Developments and Program Manual for the Finite-Difference Calculation of Large Elastic-Plastic, and/or Viscoelastic Transient Deformations of Multilayer Variable Thickness, (1) Thin Hard-Bonded, (2) Moderately-Thick Hard-Bonded, or (3) Thick Soft-Bonded Shells," ASRL TR 152-6, BRL Contract Report No. 316, prepared by MIT Aeroelastic and Structures Research Laboratory, Cambridge, MA, September 1976.

Plooster, M. N., "Blast Front Pressure from Cylindrical Charges of High Explosives," Naval Weapons Center Technical Memorandum No. 3631, Denver Research Institute, Denver, Colorado, September 1978.

Potapov, V. A., "Investigation of the Explosion-Induced Vibration of Buildings," Translated from Osnovaniya, Fundamenty i Mekhanika Gruntov, No. 3, May-June 1974, pp 18-20.

Potter, R. and Jarvis, C. V., "An Experimental Study of the Shock Wave in Free Air from Spherical Charges of TNT and 60/40 RDX/TNT," AWRE Report No. 0 1/73, United Kingdom Atomic Energy Authority, 1973.

"Prediction of Ground Motion Characteristics of Underground Nuclear Detonations," Environmental Research Corporation, NVO-1163-239, Las Vegas, Nevada, March 1974.

"Problems of Explosions Inside Containment Vessels," CONF-710903-3, paper presented at First International Conference on Structural Mechanics in Reactor Technology held in Berlin, Germany, September 1971.

Proceedings of the Army Symposium on Solid Mechanics, 1978-Case Studies on Structural Integrity and Reliability, Army Materials and Mechanics Research Center, Watertown, Mass, September 1978.

Proctor, J. F. and Filler, W. S., "A Computerized Technique for Blast Loads from Confined Explosions, Minutes of the 14th Annual Explosives Safety Seminar, New Orleans, Louisiana, 8-10 November 1972, pp 99-124.

Proctor, J. F., "Internal Blast Damage Mechanisms Computer Program," JTCG/ME Report No. 61, JTCG/ME-73-3, April 1973.

Przemieniecki, J. S., Theory of Matrix Structured Analysis, McGraw-Hill, Inc. New York, NY, 1968.

Raghavan, K. S. and Sundararajan, V., "Transient Nonlinear Response of Beam Columns," Indian Institute of Technology, Kanpur, India, Noise, Shock and Vibration Conference, Monash University, Melbourne, Victoria, Australia, 1974.

Ramsey, R. T., Powell, J. G. and Smith, W. D., "Fragment Hazard Investigation Program," NSWC/DL TR-3664, Naval Surface Weapons Center, October 1978.

Raouf, Z. A., Al-Hassani, S. T. S. and Simpson, J. W., "Explosive Testing of Fiber-Reinforced Cement Composites," Department of Building and the Department of Mechanical Engineering at UMIST.

Rasbash and Rogowski, Explosion Relief, Institute of Chemical Engineering, Vol. 1, p 58-68, 1961.

Rausch, E., Maschinenfundamente Und Andere Dynamische Bauaufgaben, Vertrieb VDE, Verlag G.M.B.H., Berlin, Germany, 1943.

"RDX, HMX and Explosive Compositions," Holston Army Ammunition Plant, April 1965.

Recht, R. F., "Containing Ballistic Fragments," Engineering Solids Under Pressure, H. Pugh (ed.), 1970, pp. 51-60.

Reed, J. W., "Distant Blast Predictions for Explosions," Minutes of the 15th Explosives Safety Seminar, Department of Defense Explosives Safety Board, Washington, D. C., 1973.

Reed, J. W., Minor, J. C. and DeHart, R. C., "Evaluation of Window Pane Damage Intensity in San Antonio Resulting from Medina Facility Explosion on November 13, 1963," Annals of the New York Academy of Science, Vol. 152, I, 1968, pp. 565-584.

Reeves, H. J., "An Empirically Based Analysis on the Response of HE Munitions to Impact By Steel Fragments," BRL MR 2031, U. S. Army Ballistic Research Laboratory, Aberdeen Proving Ground, Md., March 1970.

Reiher, H. and Meister, F. J., "Die Empfindlichkeit der Menschen gegen Erschutterungen," Forsch Gebiete Ingenieur wesen, Vol. 2 No. 11, 1931, pp 381-386.

Reisler, R. C., "Explosive Yield Criteria," Minutes of the 14th Explosives Safety Seminar, New Orleans, November 8-10, 1972, pp 271-288.

Reisler, R. E. and Kennedy, L. W., "Air Blast Dynamic Pressures From Silmultaneous and Non-Simultaneous Multiburst Detonations," BRL Report No. ARBRL-TR-02043, U. S. Army Ballistic Research Laboratory, Aberdeen Proving Ground, Md., Feb. 1978.

Reisler, R. E., Kennedy, L. W. and Keefer, J. H., "High Explosive Multiburst Airblast Phenomena (Simultaneous and Non-Simultaneous Detonations)," BRL Technical Report No. ARBRL-TR-02142, U. S. Army Ballistic Research Laboratory, Aberdeen Proving Ground, Md., February 1979.

Reisler, R. E. and Pettit, B. A., "Project Dipole West-Multiburst Environment (Non-Simultaneous Detonations)," BRL Report No. 1921, U. S. Army Ballistic Research Laboratory, Aberdeen Proving Ground, Md., September 1976.

Ribovich, J. and Watson, R. W., "Active List of Permissible Explosives and Blasting Devices Approved Before December 31, 1972," Bureau of Mines Information Circular 8597, June 1973.

Ribovich, J., Watson, R. and Gibson, F., "Instrumented Card-Gap Test," AIAA Journal Vol. 6, No. 7, 1968, pp 1260-1263.

Ricchiazzi, A. J. and Barb, J. C., "Test Results for 608 Gram Fragments Against Category I Suppressive Structures," BRL Memorandum Report No. 2592, U. S. Army Ballistic Research Laboratory, Aberdeen Proving Ground, Md., February 1976.

Richart, F. E., Hall, J. R. and Woods, R. D., Vibrations of Soils and Foundations, Prentice-Hall, Inc., Englewood Cliffs, New Jersey, 1970.

Richmond, D. R., Damon, E. G., Fletcher, E. R., Bowen, I. G. and White, C. S., "The Relationship Between Selected Blast Wave Parameters and the Response of Mammals Exposed to Air Blast," Annals of the New York Academy of Sciences, Vol. 152, Art. 1, October 1968, pp 103-121.

Ricker, N., "The Form and Nature of Seismic Waves and the Structure of Seismograms," Geophysics, Vol. 5, 1940, p 348-366.

Rindner, R., Cohen, E. and Dobbs, N., "Description and Utilization of a Versatile Slab-Support Test Facility, Report No. 7, Establishment of Safety Design Criteria for Use in Engineering of Explosive Facilities and Operations," Report No. 3445, Picatinny Arsenal, Dover, New Jersey, October 1966.

Rindner, R.M. and Schwartz, A. H., "Establishment of Safety Design Criteria for Use in Engineering of Explosive Facilities and Operations," Technical Report No. 3267, Armed Services Explosives Safety Board, Picatinny Arsenal, Dover, New Jersey, June 1965.

Rindner, R. M., Stanley, W. and Saffian, L. W., "Establishment of Safety Design Criteria for Use in Engineering of Explosive Facilities and Operations," Technical Report No. 11, Armed Services Explosive Safety Board, Technical Report 3712, Picatinny Arsenal, Dover, New Jersey, September 1968.

Rinehart, J. S., Stress Transients in Solids, Hyperdynamics, Santa Fe, New Mexico, 1975.

Rinehart, J. S. and Pearson, J., "Behavior of Metals Under Impulsive Loads," The American Society of Metals, Cleveland, Oh., 1954.

Ritland, H. N., "The Effect of Speed on Testing on Glass," Symposium on Speed of Testing of Non-Metallic Materials, Atlantic City, New Jersey, (ASTM Special Technical Publication No. 185), June 1955, pp 19-29.

Robani, B., "Fragment and Projectile Penetration Resistance of Soils; Report 2, High-Velocity Fragment Penetration into Laboratory-Prepared Soil Targets," Miscellaneous Paper S-71-12, U. S. Army Engineer Waterways Experiment Station, Vicksburg, MI, June 1973.

Robinson, C. S., Explosions, Their Anatomy and Destructiveness, McGraw-Hill Book Co., New York, NY, 1944.

Robinson, D. N., "A Displacement Bound Principle for Elastic-Plastic Structures Subjected to Blast Loading," Journal of Mech. Phys. Solids, Vol. 18, 1970, pp 65-80.

Rollvik, S. and Vigstad, M., "Investigation of Underground Explosions With Model Tests," Intern Rapport VM-61, Torsvarets Torskingsinstitutt, Norwegian Defence Research Establishment, Kjeller, Norway, August 1978.

Rollvik, S. and Vigstad, M., "Investigation of Underground Explosions With Model Tests: Measurements in the Tube," Intern Rapport VM-60, Forsvarets Forskning Sinstitutt, Norwegian Defence Research Establishment, Kjeller, Norway, March 1978.

Rooke, A. D., "Essex-Diamond Ore Research Program, Apparent Crater Measurements for Simulated, Low Yield Nuclear Explosions Project Essex I, Phase 1 and 2," Waterways Experiment Station, WES MP N-78-3, Vicksburg, MI., March 1978.

Rooke, A. D. and Davis, L. K., "Project Pre-Buggy Emplacement and Firing of High Explosive Charges and Crater Measurements," Paper No. 1-663, U. S. Army Engineer Waterways Experiment Station, Corps of Engineers, Vicksburg, MI, February 1965.

Ross, R., "Criteria for Assessing Hearing Damage Risk from Impulse-Noise Exposure," AD 666-206, Human Engineering Laboratory, Aberdeen Proving Ground, Md., August 1967.

Ross, C. A., Sterakowski, R. L., Ebcioglu, I. K., Schauble, C. C. and Yen, C. F., "Studies on the Failure of Stiffened Cylindrical Shells Subjected to Dynamic Loads," AFOSR-TR-78-0697, University of Florida, U. S. Air Force Office of Scientific Research, December 1977.

Ross, C. A., Sterakowski, R. L. and Hoover, J. W., "Studies on the Failure of Metal Mechanical Joints Subjected to Dynamic Loads," AFOSR-TR-78-0078, U. S. Office of Scientific Research, Eglin AFB, FL., September 1977.

Rossi, B. D. and Pozdnyakov, Z. G., "Commercial Explosives and Initiators---A Handbook," Promyshlennyye Vzryvchatyye Veshchestva i Sredstva Vzryvaniya---Spravochnik, Moscow, "Nedra" Press, Report No. FSTC-HT-23-587-73, October 1973.

Rotz, J. V., "Results of Missile Impact Tests on Reinforced Concrete Panels," Second ASCE Specialty Conference on Structural Design of Nuclear Plant Facilties, Vl. 1-A, New Orleans, La., December 1975, pp 720-738.

Rudlin, L., "On the Origin of Shockwaves from Condensed Explosives in Air, Part 2, Measurements of Air Shock Pressures from 8-lb TNT Spheres of Various Densities at Ambient Pressures," NOLTR 63-13, DASA-1360, Naval Ordnance Laboratory, Air-Ground Explosions Division, Explosion Research Department, October 1963.

Runes, E., "Explosion Venting," Loss Prevention, Vol. 6, pp 63-67.

Sachs, R. G., "The Dependence of Blast on Ambient Pressure and Temperature," BRL Report 466, U. S. Army Ballistic Research Laboratory, Aberdeen Proving Ground, Md., 1944.

Safety Manual, Chemical Propulsion Information Agency, AMCR 385-100, Headquarters, U. S. Army Material Command.

Sakurai, A., "Blast Wave Theory," Basic Developments in Fluid Mechanics, Vol. I, Morris Holt (ed.), Academic Press, New York, NY, pp 309-375.

Saucier, K. L., "Dynamic Properties of Mass Concrete," WES-MP-C-77-6, CTIAC Report No. 18, U. S. Army Engineer Waterways Experiment Station, Concrete Laboratory, Vicksburg, MI, June 1977.

Schlenker, G., "Economic Systems Perspective Applied to Explosive Hazards," Report No. SAO Note 20, U. S. Army Armament Command, Systems Analysis Office, Rock Island, Ill., March 1975.

Schlosser, F., and Nguyen-Thank, L., "Recent Results in Trench Research On Reinforced Earth," Journal of the Construction Division ASCE, September 1974.

Schomer, P. D., Goff, R. J., and Little, L. M., "The Statistics of Amplitude and Spectrum of Blasts Propagated in the Atmosphere," Vol. I, Construction Engineering Research Laboratory, Report No. N-13, November 1976.

Schomer, P. D., Goff, R. J. and Little, L. M., "The Statistics of Amplitude and Spectrum of Blasts Propagated in the Atmopshere," Vol. II, Appendices C through E, Construction Engineering Research Laboratory, Report No. N-13, November 1976.

Schroeder, F.J., Kachinski, R. L., Schnepfe, R. W., Koger, D. M., McKivrigan, J. L., and Jezek, B. W., "Engineering Design Guidelines, Drawings and Specifications for Support Engineering of Suppressive Shields," Edgewood Arsenal Contractor Report No. EM-CR-76097, Edgewood Arsenal, Aberdeen Proving Ground, Md., December 1976.

Schumacher, R. N., "Air Blast and Structural Response Testing of a Prototype Category III Suppressive Shield," BRL Memorandum Report No. 2701, U. S. Army Ballistic Research Laboratory, Aberdeen Proving Ground, Md., November 1976.

Schumacher, R. N. and Ewing, W. O., "Blast Attenuation Outside Cubical Enclosures Made Up of Selected Suppressive Structures Panel Configurations," BRL Memorandum Report No. 2537, U. S. Army Ballistic Research Laboratory, Aberdeen Proving Ground, Md., September, 1975.

Schumacher, R. N., Kingery, C. N. and Ewing, W. O., "Air Blast and Structural Response Testing of a 1/4 Scale Category I Suppressive Shield," BRL Memorandum Report No. 2623, U. S. Army Ballistic Research Laboratory, Aberdeen Proving Ground, Md., May 1976.

Schuring, D. J., Scale Models in Engineering, Fundamentals and Applications, Pergmon Press, Oxford, England, 1977.

Schwartz, A., Cohen, E. and Dobbs, N., "Test of 1/10 Scale Bay Structure, Report No. 5, Establishment of Safety Design Criteria for Use in Engineering of Explosive Facilities and Operations," Report No. 3439, Picatinny Arsenal, Dover, New Jersey, July 1966.

Settles, J. E., "Deficiencies in the Testing and Classification of Dangerous Materials," Annals of the New York Academy of Sciences, Vol. 152, Art. 1, October 1968, pp 199+.

Sewell, R. G. S., and Kinney, G. F., "Internal Explosions in Vented and Unvented Chambers," Minutes of the 14th Explosives Safety Seminar, New Orleans, November 8-10, November 1973, pp 87-98.

Sewell, R. G. S. and Kinney, G. F., "Response of Structures to Blast: A New Criterion," Annals of New York Academy of Sciences, Vol. 152, Art. 1, October 1968, pp 532-547.

Sharma, S. K., "Dynamic Response of Reinforced Concrete Structures," Construction Engineering Research Laboratory, Champaign, IL, July 1978.

Shear, R. E., "Incident and Reflected Blast Pressures for Pentolite," BRL Report No. 2162, U. S. Army Ballistic Research Laboratory, Aberdeen Proving Ground, Md., September 1964.

Shear, R. E. and Arbuckle, A. L., "Calculated Explosive and Blast Properties for Selected Explosives," Annex of the Explosive Steering Committee, NOL 61-JTCG/ME-70-10, 1971.

Shear, R. E. and Wright, E., "Calculated Peak Pressure---Distance Curves for Pentolite and TNT," BRL Memorandum Report No. 1423, U. S. Army Ballistic Research Laboratory, Aberdeen Proving Ground, Md., August 1962.

"Shelter Design and Analysis, Vol. 4, Protective Construction for Shelters," Defense Civil Preparedness Agency, TR-20, July 1972.

Shumacher, R. N., Kingery, C. N. and Ewing, W. O., "Air Blast and Structural Response Testing of a 1/4 Scale Category I Supressive Shield," BRL Memorandum Report No. 2623, U. S. Army Ballistic Research Laboratory, Aberdeen Proving Ground, Md., May 1976.

Simmons and Cubbage, "Explosion Relief," Institution of Chemical Engineering, Vol. 1, 1961, pp 69-77.

Sisemore, C. J., "Analyzing of Surface-Motion Data from Old Reliable Mine Blast," Lawrence Livermore Laboratory, University of California, Livermore, CA, July 1973.

Siskind, D. E., "Ground and Air Vibrations from Blasting, Subsection 11.8," SME and Mining Engineering Handbook, A. B. Cummings and I. A. Given, (eds.), Soc. of Mining Engineering of the American Institute of Mining and Metallurgy and Petroleum Engineering Inc., New York, NY, pp 11-112.

Siskind, D. E. and Summers, C. R., "Blast Noise Standards and Instrumentation," Bureau of Mines Environmental Research Program, Technical Report No. 78, U. S. Department of the Interior, May 1974.

Skjeltorp, A. T., Hegdahl, T. and Jennsen, A., "Underground Ammunition Storage, Blast Propagation in the Tunnel System Report V A., Connected Chamber Storage Blast Load on Doors in Three Sites," NOTAT 83-72, Forsvarets Bygningstjeneste, July 1976.

Slade, D. C. and Dewey, J., "High Order Initiation of Two Military Explosives by Projectile Impact," BRL Report No. 1021, U. S. Army Ballistic Research Laboratory, Aberdeen Proving Ground, Md., July 1957.

"Small Clear Specimens of Timber," ASTM D 143-52, (reapproved 1972).

Smith, C. O., The Science of Engineering Materials, Second Edition, Prentice Hall, Inc., 1977, p. 187.

"Specifications for the Design of Cold Formed Steel Structural Members," American Iron and Steel Institute, Washington, D. C., (current edition).

Spencer, A. F. and McKivrigan, J. L., "Preliminary Design Procedures for Suppressive Shields," Technical Report No. EM-TR-76089, Edgewood Arsenal, Aberdeen Proving Ground, Maryland, December 1976.

Sperrazza, J., "Modeling of Air Blast," Use of Modeling and Scaling in Shock and Vibration, (W. E. Baker, ed.), ASME, New York, NY, November 1963, pp 65-78.

Sperrazza, J. and Kokinakis, W., "Ballistic Limits of Tissue and Clothing," Technical Note No. 1645, U. S. Army Ballistic Research Laboratory, Aberdeen Proving Ground, Md., January 1967.

"Standard Specifications and Load Tables," Steel Joist Institute, Arlington, VA. (current edition).

Stea, W., Tseng, G., Kossover, D., Price, P. and Caltagirone, J., "Nonlinear Analysis of Frame Structures Subjected to Blast Overpressures," ARLCD-CR-77008, U. S. Army Armament Research and Development Command, Large Caliber Weapons Systems Laboratory, Dover, New Jersey, May 1977.

Steffens, R. J., "The Assessment of Vibration Intensity and Its Application to the Study of Building Vibrations," National Building Studies Special Report No. 19, Department of Scientific and Ind. Research, Building Research Station, London, England, 1952.

Steidel, R. F. and Makerou, C. E., "The Tensile Properties of Some Engineering Materials at Moderate Rates of Strain," ASTM Bulletin, July 1960, pp 57-64.

Stephenson, A. E., "Full-Scale Tornado-Missile Impact Tests," EPRI-NP-148, Project 399, Interim Report, Electric Power Research Institute, Palo Alto, CA., April 1976.

Stephenson, A. E., Sliter, G. and Burdette, E., "Full-Scale Tornado-Missile Impact Tests Using a Rocket Launcher," Second ASCE Specialty Conference on Structural Design of Nuclear Plant Facilities, Vol. 1-A, New Orleans, LA., December, 1975, pp 611-636.

Stevenson, J. D. and Havers, J. A., "Entranceways and Exits for Blast-Resistant Fully-Buried Personnel Shelters," IIT Research Institute, Technology Center, Chicago, IL, September 1965.

Stirrat, W. M., "Minimum Nonpropagation Distance of Open Rubber Buckets Containing Explosive Composition A5," Report No. ARLCD-TR-78045, U. S. Army Armament Research and Development Command, Large Caliber Weapons Laboratory, Dover, New Jersey, August 1978.

Stirrat, W. M. and Rindner, R. M., "Critical Depth Tests of Bulk TNT Flake Explosive," U. S. Army Armament Research and Development Command, Large Caliber Weapons Laboratory, Dover, New Jersey, January 1978.

Strehlow, R. A., Fundamentals of Combustion, International Textbook Co., Scranton, PA., reprinted by Robert E. Krieger Publishing Co., Box 542, Huntington, NY, 1968.

Strehlow, R. A. and Adamczyk, A. A., "On The Nature of Non-Ideal Blast Waves," Technical Report AAE 74-2, UILU-ENG-740502, University of Illinois, Urbana, IL., 1974.

Strehlow, R. A. and Baker, W. E., "The Characterization and Evaluation of Accidental Explosions," NASA CR 134779, NASA Lewis Research Center, Cleveland, OH., June 1975.

Strehlow, R. A. and Baker, W. E., "The Characterization and Evaluation of Accidental Explosions," Progress in Energy and Combustion Science, Vol. 2 No. 1, 1976, pp 27-60.

Stricklin, J. A. and Haisler, W. E., "Survey of Solution Procedures for Nonlinear Static and Dynamic Analysis," Proceedings SAE International Conference on Vehicle Structural Mechanics, Detroit, MI, March 1974.

Structures to Resist the Effects of Accidental Explosions, Department of the Army Technical Manual TM5-1300, Department of the Navy Publication NAVFAC P-397, Department of the Air Force Manual AFM 88-22, Department of the Army, the Navy and the Air Force, June 1969.

Stubbs, I. R. and Benuska, K. L., "A Computer Program for the Dynamic Blast Response of Box-Type Structures," T. Y. Lin and Associates, Consulting Engineers, December 1966.

Stull, D. R., Fundamentals of Fire and Explosion, AIChE Monograph Series, 73, 10, 1977, p. 124.

Suko, M. and Adams, P. F., "Dynamic Analysis of Multibay Multistory Frames," Journal of the Structural Division, Proceedings of the American Society of Civil Engineers, Vol. 97, No. ST10, October 1971, pp 2519-2533.

Sullivan, B. R. and Bombich, A. A., "Evaluation of Methods of Attenuating Blast Pressures on Walls," No. 6-856, U. S. Army Engineer Waterways Experiment Station, Corps of Engineers, Vicksburg, MI., November 1966.

"Suppressive Shielding," AAI Corporation, Cockeysville, Md., DAAA15-75-C-0120, U. S. Army Armament Research and Development Command, Chemical Systems Laboratory, Aberdeen Proving Ground, Md., April 1977.

"Suppressive Shields Structural Design and Analysis Handbook," HNDM-1110-1-2, U. S. Army Corps of Engineers, Huntsville Division, Huntsville, Ala., November 1977.

Swihart, G. R., "Study to Determine the Optimum Section of Reinforced Concrete Beams Subjected to Blast Loads," Naval Civil Engineering Laboratory, Port Hueneme, CA., February 1959.

Swisdak, M. M., "Explosion Effects and Properties: Part I--Explosion Effects in Air," NSWC/WOL/TR 75-116, Naval Surface Weapons Center, White Oak, Silver Spring, Md., October 1975.

Symonds, P. S., "Approximation Techniques for Impulsively Loaded Structures of Rate Sensitive Plastic Behavior," SIAM Journal Applied Mathematics, Vol. 25, No. 3, 1973, pp 462-473.

Symonds, P. S., "Survey of Methods of Analysis for Plastic Deformation of Structures under Dynamic Loading," BU/NSRDC/1-67, Naval Ship Research and Development Center, June 1967.

Symonds, P. S. and Chon, C. T., "Approximation Techniques for Impulsive Loadind of Structures of Time-Dependent Plastic Behavior with Finite-Deflections," Mechanical Properties at High Rates of Strain, J. Harding, Ed., Institute of Physics, London, Conf. Ser. No. 21, pp 299-316, 1974.

Symonds, P. S. and Chon, C. T., "Bounds for Finite-Deflections of Impulsively Loaded Structures with Time-Dependent Plastic Behavior," International Journal Solids Structures, Vol. 11, pp 403-425, 1975.

"Systems Applications of Nuclear Technology: Effects of Airblast, Cratering, Ground Shock and Radiation on Hardened Structures," AFSC Manual 500-8, Department of the Air Force, Chapter 8, January 1976.

Tami, T. M., "Analysis of Ground-Motion Peak Particle Velocities from Cratering Experiments at Trinidad, Colorado," U. S. Army Engineer Waterways Experiment Station, Explosive Excavation Research Laboratory, Livermore, California, May 1972.

Tancreto, J. E., "Effects of Charge Composition and Surface Conditions on Blast Environment," Civil Engineering Laboratory, Port Hueneme, California.

Taylor, D. B. and Price, C. F., "Velocities of Fragment From Bursting Gas Reservoirs," ASME Transactions, Journal of Engineering for Industry, 93B, 1971, pp 981-985.

Taylor, G. I., "The Formation of a Blast Wave by a Very Intense Explosion," Proceedings Royal Society, A201, 1950, p. 159.

Taylor, N. and Alexander, S. J., "Structural Damage in Buildings Caused by Gaseous Explosions and Other Accidental Loadings," Building Research Establishment Current Paper CP 45/74, Building Research Establishment, March 1974.

Teichmann, G. A. and Westwater, R., "Blasting and Associated Vibrations," Engineering, April 1957, pp 460-465.

"Tensile-Impact Energy to Break Plastics and Electrical Insulating Materials," ANSI/ASTM D 1822-68.

TERA Group, New Mexico Institute of Mining and Technology, "Vulnerability of 105 mm HE Projectiles to Fragment Impacts," U. S. Army Ballistic Research Laboratory, Aberdeen Proving Ground, Md., August 1978.

"Tests on the Effects of Explosive Charges on Reinforced Earth Walls, Minutes of the Eighteenth Explosives Safety Seminar, Vol. 1, September 1978.

"The Resistance of Various Metallic Materials to Perforation by Steel Fragments; Empirical Relationships for Fragment Residual Velocity and Residual Weight," Institute for Cooperative Research, Project Thor Technical Report No. 47, April 1961.

"The Resistance of Various Non-Metallic Materials to Perforation by Steel Fragments; Empirical Relationships for Fragment Residual Velocity and Residual Weight," BRL Technical Report No. 51, Project THOR, U. S. Army Ballistic Research Laboratory, Aberdeen Proving Ground, Md., April 1963.

Thoenen, J. R. and Windes, S. L., "Seismic Effects of Quarry Blasting," Bureau of Mines Bulletin No. 442, 83, 1942.

Thomas, L. H., "Computing the Effect of Distance on Damage by Fragments," Report No. 468, U. S. Army Ballistic Research Laboratory, Aberdeen Proving Ground, Md., May 1944.

Thomas, L. R., "Theory of the Explosion of Cased Charges of Simple Shape," BRL Report No. 475, U. S. Army Ballistic Research Laboratory, Aberdeen Proving Ground, Md., July 1944.

Thomson, W. T., Mechanical Vibrations, Prentice-Hall, New York, NY, 1948.

Thompson, L. J., Ferguson, G. H., Murff, V. D. and Cetiner, A., "The Effects of Soil Parameters on Earth Penetration of Projectiles," Texas A&M Research Foundation Report No. PB 186074, July 1969.

Thornhill, C. K., "Explosions in Air," ARDE Memo (B) 57/60, Armament Research and Development Establishment, England, 1960.

Timoshenko, S., Vibration Problems in Engineering, D. Van Nostrand Company, Inc., New York, NY, 1928.

Ting, R. M. L., "Non-composite and Composite Steel Panels for Tornado Missile Barrier Walls," Second ASCE Specialty Conference on Structural Design of Nuclear Plant Facilities, Vol. 1A, New Orleans, LA., December 1975, pp 663-687.

Trott, B. D. and White, J. J., "Design of Ammunition Storage Compartments," Battelle Columbus Laboratories, paper presented at the Fourth Symposium on Vulnerability and Survivability, March 1979.

Ts'ao, H-S., Reddy, D. P. and Dowdy, R. W., "Magazine Headwall Response to Explosive Blast," Agbabian Associates, El Segundo, CA., January 1974.

Tseng, G., Weissman, S., Dobbs, N., and Price, P., "Design Charts for Cold-Formed Steel Panels and Wide-Flange Beams Subjected to Blast Loading," Technical Report 4838, Picatinny Arsenal, Dover, New Jersey, August 1975.

Tyler, L. D., "Numerical Results of Blast Wave Propagation in Tunnel Intersections," SC-RR-68-430, Sandia Laboratories, Albuquerque, New Mexico, September 1968.

Uemura, S., "Explosion-Resistant Construction Designs," University of Tokyo, Japan, 1965.

United States Army Materiel Command, "Safety-Safety Manual," DARCOM C3, AMCR-385-100 DARCOM Change No. 3, Department of the Army, Headquarters, U. S. Army Materiel Development and Readiness Command, Alexandria, VA., January 1977.

URS/John A. Blume and Associates, "Seismic Hazard and Building Structure Behavior at the Pantex Facility," April 1976.

URS/John A. Blume and Associates, "Seismic Design of Building and Sprinkler System for the Pantex Facility," April 1976.

U. S. Army Corps of Engineers, "Suppressive Shields Structural Design and Analysis Handbook," Huntsville Division, Huntsville, Alabama, November 1977.

U. S. Army Corps of Engineers, "Design of Structures to Resist the Effects of Atomic Weapons," EM 1110-345-415, 1975.

U. S. Army Corps of Engineers, "Overpressure Effects on Structures," HNDTR-75-23-ED-SR, Huntsville Division, Huntsville, Alabama, February 1976.

U. S. Army Material Command, "Engineering Design Handbook: Explosions in Air, Part I," AMC Phamphlet No. 706-181, Department of the Army, Headquarters, United States Army Material Command, Alexandria, VA., July 1974.

U. S. Army Material Command, "Engineering Design Handbook: Explosives Series, Properties of Explosives of Military Interest," AMCP 706-177, Headquarters, Department of the Army, Alexandria, VA., January 1971.

U. S. Army Material Command, "Engineering Design Handbook: Principles of Explosive Behavior," AMC Pamphlet 706-180, Headquarters, Department of the Army, Alexandria, VA., 1972.

U. S. Energy Research and Development Administration, Albuquerque Operations Office, "Report of Investigation of the Explosion with Fatal Injuries in Building 11-14A on March 30, 1977 at the Pantex Plant-Amarillo, Texas," June 28, 1977.

U. S. Forest Products Laboratory, Wood Handbook: Wood as an Engineering Material, U. S. Department of Agriculture, Agriculture Handbook No. 72, 1974.

Vadala, A. J., "Effects of Gun Explosions on the Ear and Hearing Mechanism," Milit Surg. Vol. 66, 1930, pp 710-822.

Van Dolah, R. W., Gibson, F. C. and Murphy, J. N., "Further Studies on Sympathetic Detonation," Report of Investigation No. 6903, United States Department of the Interior, Bureau of Mines, 1966.

Vassallo, F. A., "Missile Impact Testing of Reinforced Concrete Panels," Calspan Report No. HC-5609-D-1, Calspan, Buffalo, NY, January 1975.

Venable, D., Taylor, R. W. and Rogers, B. T., "Method for Mitigating Blast and Shock Transmission Within a Confined Volume," United States Patent 3,804,017, April 1974.

Vigstad, M. and Skarbovik, K., "Investigation of Underground Explosions with Model Tests, The Experimental Set-up," Teknisk Notat VM-309, Forsvarets Forskning-Sinstitutt, Norwegian Defense Research Establishment, Norway, April 1978.

Voight, H. W., Gulbierz, J. and Yearwood, C., "Blast Shield for Explosive Devices Including Linear Shaped Charges," United States Patent 3,712,221, January 1973.

von Gierke, H. E., "Biodynamic Models and Their Applications," Aerospace Medical Research Laboratory, Wright-Patterson Air Force Base, Ohio, 1971.

von Gierke, H. E., "Dynamic Characteristics of the Human Body," Aerospace Medical Research Laboratory, Wright-Patterson Air Force Base, Ohio, 1973.

von Gierke, H. E., "Man to Model or Model to Man," Aerospace Medical Research Laboratory, Wright-Patterson Air Force Base, Ohio, 1973.

von Gierke, H. E., "Medical Behavior of Biological Systems," Aerospace Medical Research Laboratory, Wright-Patterson Air Force Base, Ohio, September 1967.

von Gierke, H. E., "On The Dynamics of Some Head Injury Mechanisms," Aerospace Medical Research Laboratory, Wright-Patterson Air Force Base, Ohio, 1971.

von Neumann, J., and Goldstein, H., "Blast Wave Calculation," Communication on Pure Applied Mathematics, Vol. 8, pp 327-353, reprinted in John von Neumann Collected Works, (A. H. Taub, ed.), Vol. VI, Pergamon Press, New York, NY, pp 386-412.

Vortman, L. J., "Airblast From Project Trinidad Detonations," SC-RR-710056, TID 4500 UC-35, Nuclear Explosions, Peaceful Applications, Underground Physics Division, Sandia Laboratories, Albuquerque, New Mexico, June 1971.

Wallace, J. G. and Fowler, J., "Fundamental Experiments in Ground Shock Phenomenology," U. S. Army Engineer Waterways Experiment Station, Vicksburg, MI, Paper No. N-73-2, March 1973.

Warren, A., "Blast Pressures from Distant Explosions," ARDE Memo 18-58, 1958.

Watson, J. and Huestis, E., "A Method for Evaluating the Performance of Very Long Explosive Charges," Suffield Memorandum 60/67, DRB Project No. D52-99-10-40, Defense Research Establishment, Suffield, February 1968.

Watson, R. W. and Hay, J. E., "Continuous Explosive Fragmentation Techniques," U. S. Bureau of Mines, Pittsburgh Mining and Safety Research Center, Pittsburgh, PA, February 1974.

Watstein, D., "Effect of Straining Rate on the Compressive Strength and Elastic Properties of Concrete," Journal of the American Concrete Institute, April 1953, pp 729-744.

Weals, F. H., "Tests to Determine Separation Distance of Earth-Covered Magazines," Annals of the New York Academy of Sciences, Vol. 152, Art. 1, October 1968.

Weibull, H. R. W., "Pressures Recorded in Partially Closed Chambers at Explosion of TNT Charges," Annals of the New York Academy of Sciences, Vol. 152, Art. 1, October 1968, pp 256-361.

Weissman, S., Dobbs, N., Stea, W., and Price, P., "Blast Capacity Evaluation of Glass Windows and Aluminum Window Frames," Ammann and Whitney, Consulting Engineers, June 1978.

Wenograd, J., "Sensitivity of Explosives IV-The Correlation of the Impact Sensitivity of Organic High Explosives with Their Thermal Decomposition Rates," Chemistry Research Department, U. S. Naval Ordnance Laboratory, White Oak, Md., September 1957.

Wenzel, A. B. and Bessey, R. L., "Barricaded and Unbarricaded Blast Measurements," Contract No. DAHC04-69-C-0028, Subcontract 1-OU-431, Southwest Research Institute, San Antonio, Texas, 1969.

Wenzel, A. B. and Esparza, E. D., "Measurements of Pressures and Impulses at Close Distances from Explosive Charges Buried and in Air," Final Report on Contract No. DAAK 02-71-C-0393, U. S. Army MERDC, Ft. Belvoir, VA., 1972.

West, G. T., "Classification of Explosives," Development Division, Mason and Hanger, Silas Mason Co., Inc., Endeavor No. 216, January-March 1976.

Westine, P. S., "Bomb Crater Damage to Runways," Southwest Research Institute, Contract F29601-72-C-0053, Air Force Weapons Laboratory, February 1973.

Westine, P. S., "Explosive Cratering," Journal of Terramechanics, VII, 2, 1970, pp 9-19.

Westine, P. S., "Ground Shock from the Detonation of Buried Explosives," Journal of Terramechanics, Vol. 15, No. 2, 1978, pp 69-79.

Westine, P. S., "Prediction of Transient Displacement, Velocity and Force on Projectiles Penetrating Cohesive Soils," Journal of Terramechanics, Vol. 12, No. 3-4, December 1975, pp 149-170.

Westine, P. S., "R-W Plane Analysis for Vulnerability of Targets to Air Blast," The Shock and Vibration Bulletin, Bulletin 42, Part 5, January 1972, pp 173-183.

Westine, P. S. and Baker, W. E., "Energy Solutions for Predicting Deformations in Blast Loaded Structures," Minutes of the 16th Annual Explosives Safety Seminar, Department of the Defense Safety Board, 1974.

Westine, P. S. and Baker, W. E., "Energy Solutions for Predicting Deformations in Blast-Loaded Structures," Edgewood Arsenal Contractor Report EM-CR-76027, Report No. 6, Edgewood Arsenal, Aberdeen Proving Ground, Md., November 1975.

Westine, P. S. and Cox, P. A., "Additional Energy Solutions for Predicting Structural Deformations," Edgewood Arsenal Contract Report No. EM-CR-76031, Report No. 4, Edgewood Arsenal, Aberdeen Proving Ground, Md., November 1975.

Westine, P. S. and Esparza, E. D., "Analysis and Testing of Pipe Response to Buried Explosive Detonations," Interim Report, 1976 Annual Report, Southwest Research Institute Project No. 02-4300 for the American Gas Association, January 1977.

Westine, P. S. and Kineke, J. H., "Prediction of Constrained Secondary Fragment Velocities," The Shock and Vibration Bulletin, Part 2. Isolation and Damping, Impact, Blast, Bulletin 48, September 1978.

Westine, P. S. and Vargas, L. M., "Design Guide for Armoring Critical Aircraft Components to Protect From High Explosive Projectiles," Final Report, Contract No. F33615-77-C-3006, U. S. Air Force Flight Dynamics Laboratory, Wright-Patterson Air Force Base, Ohio, August 1978.

Westine, P. S., Esparza, E. D. and Wenzel, A. B., "Analysis and Testing of Pipe Response to Buried Explosive Detonations," SwRI Final Report for the American Gas Association, July 1978.

White, C. S., "The Nature of the Problems Involved in Estimating the Immediate Casualties from Nuclear Explosions," CEX71.1, Civil Effects Study, U. S. Atomic Energy Commission, DR-1886, July 1971.

White, C. S. ,"The Scope of Blast and Shock Biology and Problem Areas in Relating Physical and Biological Parameters," Annals of the New York Academy of Sciences, Vol. 152, Art. 1, October 1968, pp 89-102.

White, C. S., Bowen, I. G. and Richmond, D. R., "The Relation Between Eardrum Failure and Blast-Induced Pressure Variations," Lovelace Foundation for Medical Education and Research, Report No. DASA-2064, Albuquerque, New Mexico, August 1967.

White, C. S., Bowen, I. G., Richmond, D. R. and Corsbie, R. L., "Comparative Nuclear Effect of Biomedical Interest," CEX 58.8, Civil Effects Study, U. S. Atomic Energy Commission, January 1961.

White, C. S., Jones, R. K., Damon, E. G., Fletcher, E. R. and Richmond, D. R., "The Biodynamics of Airblast," Technical Report to Defense Nuclear Agency, DNA 2738T, Lovelace Foundation for Medical Education and Research, Albuquerque, New Mexico, July 1971.

Whitham, G. B., "The Propagation of Spherical Blast," Proc. Royal Society, A203, pp 571-581.

Wiehle, C. K., "Summary of Shelter Entranceways and Openings," Public Works Systems, Stanford Research Institute, Menlo Park, CA., September 1967.

Willis, D. E. and Wilson, J. T., "Maximum Vertical Ground Displacement of Seismic Waves Generated By Explosive Blasts," Bulletin of the Seismic Society of America, Vol. 50, pp 455-459, 1960.

Willoughby, A. B., Wilton, C., Grabrielsen, B. L. and Zaccor, J. V., "A Study of Loading, Structural Response, and Debris Characteristics of Wall Panels," Office of Civil Defense Contract No. 11618, OCD Work Unit 1123D, URS Research Company, Burlingame, CA., July 1969.

Wilton, C. and Gabrielson, B., "House Damage Assessment," Minutes of the 14th Explosives Safety Seminar, New Orleans, LA., November 1972.

Wilton, C., Gabrielsen, B., Edmunds, J., and Bechtel, S., "Loading and Structural Response of Wall Panels," URS Research Company, San Mateo, CA, November 1969.

Winlock, J., 'The Influence of the Rate of Deformation on the Tensile Properties of Some Plain Sheet Steels," Transactions, AIME, Journal of Metals, Vol. 197, June 1953, pp 797-803.

Wisotski, J. and Snyer, W. H., "Characteristics of Blast Waves Obtained From Cylindrical High Explosive Charges," University of Denver, Denver Research Institute, U. S. Naval Ordnance Laboratory, Air Ground Explosions Division, November 1965.

Woods, R. D., "Screening of Surface Waves in Soils," Journal of Soil Mechanics and Foundations Division, American Society of Civil Engineers, Vol. 94, No. SM4, July 1968, pp 951-979.

Wu, R. W-H., and Witmer, E. A., "Finite Element Analysis of Large Transient Elastic-Plastic Deformations of Simple Structures with Application to the Engine Rotor Fragment Containment/Deflection Program," NASA CR-120886, ASRL TR 154-4, Aeroelastic and Structures Research Laboratory, Massachusetts Institute of Technology, Cambridge, MA., January 1972.

Wu, J. H. T., Archer, R. D. and Moelder, S. M., "Shock Propagation in a Two-Dimensional Symmetric Logarithmic Spiral Channel," International Shock Tube Symposium, 9th, Proceedings, Stanford University, CA., pp 604-612.

Yamada, Y., Kawai, T. and Yoshimura, N., Proceedings of the 2nd Conference on Matrix Methods in Structural Mechanics, AFFDL-TR-68-150, 1968.

Yang, L. C. and Menichelli, V. J., "Laser Initiation of Insensitive High Explosives," The Sixth Symposium (International) on Detonation, California Institute of Technology, Pasadena, CA., August 1976.

Yao, C., "Explosion Venting of Low-Strength Equipment and Structures," Loss Prevention, Vol. 8, American Institute of Chemical Engineers, New York, NY, 1974.

Yeager, H. H., "Investigation of Possible Kevlar Utilization in Explosion Protection Structures Applications," Department of Safety Engineering, USAMC Intern Training Center, Red River Army Depot, Texarkana, TX., December 1975.

York, E. N., Holze, D. H. and Malone, E., "Industrial Plant Hardness Phase II," Defense Nuclear Agency Report No. DNA 4549F, Boeing Aerospace Company, P. O. Box 3999, Seattle, Washington, April 1978.

Young, C. W., "The Development of Empirical Equations for Predicting Depth of an Earth-Penetrating Projectile," Report No. SC-DR-67-60, Sandia Laboratory, May 1967.

Zaker, T. A., "Blast Pressures From Sequential Explosions," IIT Research Institute, Chicago, ILL, March 1969.

Zaker, T. A., "Computer Program for Predicting Casualties and Damage from Accidental Explosions," Technical Paper No. 11, Department of Defense Explosives Safety Board, May 1975.

Zaker, T. A., "Fragment and Debris Hazards," Technical Paper No. 12, Department of Defense Explosives Safety Board, July 1975.

Zenkiewicz, O. C., The Finite Element Method in Engineering Science, McGraw-Hill, London, England, 1971.

Zilliacus, S., Phyillaier, W. E. and Shorrow, P. K., "The Reponse of Clamped Circular Plates to Confined Explosive Loadings," NSRDC, Bethesda, MD., February 1974.

APPENDIX C

UNIT CONVERSION TABLES

Conversions are given from English (customary)
units to SI. To convert from SI to English,
<u>divide</u> by conversion factors, rather than
multiply. Dimensions in a mass, length, angle,
time (M, L, Θ, T) system are also given, as
are common abbreviations. Exponential nota-
tion is used, e.g., E -02 means multiply by
10^{-2}.

Acceleration

To Convert From	To	Multiply by	
Angular (θ/T^2):			
degree per second squared	radian per second squared (rad/s^2)	1.745 329	E-02
revolution per minute squared (r/min^2)	radian per second squared (rad/s^2)	1.745 329	E-03
revolution per second squared (r/s^2)	radian per second squared (rad/s^2)	6.283 185	
Linear (L/T^2):			
centimeter per second squared (cm/s^2)	meter per second squared (m/s^2)	*1.000	E-02
foot per second squared (ft/s^2)	meter per second squared (m/s^2)	*3.048	E-01
gravity, standard free fall (G or g)	meter per second squared (m/s^2)	*9.806 650	
inch per second squared (in/s^2)	meter per second squared (m/s^2)	*2.540	E-02

Area (L^2)

square centimeter (cm^2)	square meter (m^2)	*1.000	E-04
square foot [U.S. survey] (ft^2)	square meter (m^2)	9.290 341	E-02
square inch (in^2)	square meter (m^2)	*6.451 600	E-04
square kilometer (km^2)	square meter (m^2)	*1.000	E+06
square yard (yd^2)	square meter (m^2)	8.361 274	E-01

* Exact conversion

Density (M/L^3)

To Convert From	To	Multiply by	
gram per cubic centimeter (g/cm^3)	kilogram per cubic meter (kg/m^3)	*1.000	E+03
pound per cubic inch (lb/in^3)	kilogram per cubic meter (kg/m^3)	2.767 990	E+04
pound per cubic foot (lb/ft^3)	kilogram per cubic meter (kg/m^3)	1.601 846	E+01
slug per cubic foot (slug/ft^3)	kilogram per cubic meter (kg/m^3)	5.153 788	E+02

Energy: Work – Thermal – Electrical (ML/T^2)

British thermal unit [mean] (Btu$_m$)	joule (J)	1.055 870	E+03
calorie [IT] (cal$_{IT}$)	joule (J)	*4.186 800	
erg	joule (J)	*1.000	E-07
foot-pound force (ft·lbf)	joule (J)	1.355 818	
foot-poundal (ft·pdl)	joule (J)	4.214 011	E-02
kilowatt hour (kW·h)	joule (J)	*3.600	E+06
ton [TNT equivalent]	joule (J)	4.184	E+09
watt hour (W·h)	joule (J)	*3.600	E+03
watt second (W·s)	joule (J)	*1.000	

Force (ML/T^2)

dyne (dyn)	newton (N)	*1.000	E-05
kilogram force (kgf)	newton (N)	*9.806 650	
kilopond	newton (N)	*9.806 650	
kip	newton (N)	4.448 222	E+03
pound force (lbf)	newton (N)	4.448 222	
poundal (pdl)	newton (N)	1.382 550	E-01
ton force	newton (N)	8.896 444	E+03

* Exact conversion

Inertia		
To Convert From	To	Multiply by

Area (L^4):

inch^4 (in^4)	meter^4 (m^4)	4.162 314 E-08
foot^4 (ft^4)	meter^4 (m^4)	8.630 975 E-03
millimeter^4 (mm^4)	meter^4 (m^4)	*1.000 E-12

Line (L^3):

inch cubed (in^3)	meter cubed (m^3)	1.638 706 E-05
foot cubed (ft^3)	meter cubed (m^3)	2.831 685 E-02
millimeter cubed (mm^3)	meter cubed (m^3)	*1.000 E-09

Mass (ML^2):

pound foot squared (lb·ft^2)	kilogram meter squared (kg·m^2)	4.214 011 E-02
pound inch squared (lb·in^2)	kilogram meter squared (kg·m^2)	2.926 397 E-04
slug foot squared (slug·ft^2)	kilogram meter squared (kg·m^2)	1.355 818

Length (L)		
centimeter (cm)	meter (m)	*1.000 E-02
foot [international] (ft)	meter (m)	*3.048 E-01
inch (in)	meter (m)	*2.540 E-02
kilometer (km)	meter (m)	*1.000 E+03
microinch (µin)	meter (m)	*2.540 E-08
micrometer (µm)	meter (m)	*1.000 E-06
micron [obsolete, replaced by micrometer]	meter (m)	*1.000 E-06
mil (mil)	meter (m)	*2.540 E-05
mile [international] (mi)	meter (m)	1.609 344 E+03

* Exact conversion

Mass (M)

To Convert From	To	Multiply by
grain	kilogram (kg)	6.479 891 E-05
gram (g)	kilogram (kg)	*1.000 E-03
kilogram force-second squared per meter (kgf·s^2/m)	kilogram (kg)	*9.806 650
megagram (Mg)	kilogram (kg)	*1.000 E+03
metric ton (t)	kilogram (kg)	*1.000 E+03
milligram (mg)	kilogram (kg)	*1.000 E-03
pound [avoirdupois] (lb)	kilogram (kg)	4.535 924 E-01
slug	kilogram (kg)	1.459 390 E+01
ton [short]	kilogram (kg)	9.071 847 E+02
tonne (t)	kilogram (kg)	*1.000 E+03

Pressure - Stress (M/LT^2)

To Convert From	To	Multiply by
atmosphere [standard] (atm)	pascal (Pa)	1.013 250 E+05
bar	pascal (Pa)	*1.000 E+05
dyne per square centimeter (dyn/cm^2)	pascal (Pa)	*1.000 E-01
foot of water [4°C]	pascal (Pa)	2.988 980 E+03
gram force per square centimeter (gf/cm^2)	pascal (Pa)	*9.806 650 E+01
inch of mercury [0°C]	pascal (Pa)	3.386 380 E+03
inch of mercury [16°C]	pascal (Pa)	3.376 850 E+03
inch of water [4°C]	pascal (Pa)	2.490 817 E+02
inch of water [16°C]	pascal (Pa)	2.488 400 E+02
kip per square inch (kip/in^2)	pascal (Pa)	6.894 757 E+06
kip per square foot (kip/ft^2)	pascal (Pa)	4.788 026 E+04
megapascal (MPa)	pascal (Pa)	*1.000 E+06
millimeter of mercury [0°C] (mm(Hg))	pascal (Pa)	1.333 220 E+02

* Exact conversion

Pressure - Stress (M/LT²) (Continued)

To Convert From	To	Multiply by	
millimeter of water [4°C] (mm(H₂0))	pascal (Pa)	9.806 365	
newton per square meter (N/m²)	pascal (Pa)	*1.000	
pound per square meter (lb/ft²)	pascal (Pa)	4.788 026	E+01
pound per square inch (lb/in²)	pascal (Pa)	6.894 757	E+03
poundal per square foot (pdl/ft²)	pascal (Pa)	1.488 164	

Velocity - Speed

Anuglar (θ/T):			
degree per second	radian per second (rad/s)	1.745 329	E-02
revolution per minute (f/min)	radian per second (rad/s)	1.047 198	E-01
revolution per second (r/s)	radian per second (rad/s)	6.283 185	
Linear (L/T):			
foot per second (ft/s)	meter per second (m/s)	*3.048	E-01
inch per second (in/s)	meter per second (m/s)	*2.540	E-02
kilometer per hour (km/h)	meter per second (m/s)	2.777 778	E-01
knot [nautical miles per hour] (kn)	meter per second (m/s)	5.144 444	E-01
mil per hour (mi/h)	meter per second (m/s)	4.470 400	E-01

Volume - Capacity (L³)

cubic centimeter (cm³)	cubic meter (m³)	*1.000	E-06
cubic foot (ft³)	cubic meter (m³)	2.831 685	E-02
cubic inch (in³)	cubic meter (m³)	1.638 706	E-05
liter (L)	cubic meter (m³)	*1.000	E-03
quart [U.S., liquid]	cubic meter (m³)	9.463 529	E-04

* Exact conversion